EXPERIMENTAL STUDY OF BRIDGE SCOUR IN COHESIVE SOIL

A Dissertation

by

SEUNG JAE OH

Submitted to the Office of Graduate Studies of
Texas A&M University
in partial fulfillment of the requirements for the degree of

DOCTOR OF PHILOSOPHY

December 2009

Major Subject: Civil Engineering

EXPERIMENTAL STUDY OF BRIDGE SCOUR IN COHESIVE SOIL

A Dissertation

by

SEUNG JAE OH

Submitted to the Office of Graduate Studies of
Texas A&M University
in partial fulfillment of the requirements for the degree of

DOCTOR OF PHILOSOPHY

Approved by:

Co-Chairs of Committee,	Jean-Louis Briaud
	Kuang-An Chang
Committee Members,	Hamn-Ching Chen
	Mark Everett
Head of Department,	David V. Rosowsky

December 2009

Major Subject: Civil Engineering

ABSTRACT

Experimental Study of Bridge Scour in Cohesive Soil.

(December 2009)

Seung Jae Oh, B.E., GyeongSang National University, South Korea;

M.S., Pusan National University, South Korea

Co-Chairs of Advisory Committee: Dr. Jean-Louis Briaud
Dr. Kuang-An Chang

The bridge scour depths in cohesive soil have been predicted using the scour equations developed for cohesionless soils due to scarce of studies about cohesive soil. The scour depths predicted by the conventional methods will result in significant errors. For the cost effective design of bridge scour in cohesive soil, the Scour Rate In COhesvie Soil (SRICOS) for the singular circular pier in deep water condition was released in 1999, and has been developed for complex pier and contraction scour.

The present study is the part of SRICOS-EFA method to predict the history of contraction scour, and local scours, such as abutment scour and pier scour. The main objective is to develop the prediction methods for the maximum and the uniform contraction scour depth, the maximum pier scour depth and the maximum abutment using flume test results. The equations are basically composed with the difference between the local Froude number and the critical Froude number. Because the scour happens when the shear stress is bigger than the critical shear stress, which is the

maximum shear stress the channel bed material can resist from the erosion, and continues until the shear stress becomes equal to the critical shear stress.

All results obtained from flume tests for pier scour have been conducted in Texas A&M University from 1997 to 2002 are collected and reanalyzed in this study. Since the original pier scour equation did not include soil properties. The effect of water depth effect, pier spacing, pier shape and flow attack angle for the rectangular pier are studied and correction factors with respect to the circular pier in deep water condition were newly developed in present study.

For the abutment scour, a series of flume tests in large scale was performed in the present study. Two types of channel – rectangular channel, and compound channel – were used. The effect of abutment length, shape and alignment of abutment were studied and the correction factors were developed. The patterns of velocity and of scour were compared, and it was found that the maximum local scour occurred where the maximum turbulence was measured.

For the contraction scour, the results obtained from a series of flume tests performed in 2002 and a series of flume tests for the abutment scour in the present study are analyzed. The methodologies to predict the maximum contraction scour and the uniform contraction scour in the compound channel was developed.

Although all prediction methods developed in the present study are for the cohesive soils, those methods may be applicable to the cohesionless soils because the critical shear stress is included in the methods. All prediction methods were verified by the comparison with the databases obtained from flume test results and field data.

DEDICATION

This dissertation is dedicated to the author's father, to the author's mother, and also to his wife and two daughters. Their support, devotion, love, unselfish sacrifice, and encouragement made this dissertation possible in the end.

ACKNOWLEDGMENTS

TABLE OF CONTENTS

LIST OF FIGURES

FIGURE   Page

LIST OF TABLES

CHAPTER I

INTRODUCTION

1.1 Background

Bridge scour is the aggradation or degradation of the riverbed around the bridge structure. Bridge scour is usually widely divided into general scour, contraction scour and local scour. General scour happens without the existence of bridge. The contraction scour results from the acceleration of the flow due to the constriction of channel, while local scour happens by the turbulence around bridge obstacles such as pier and abutment. Generally the main cause of general scour is the manmade channel straightening of a river inducing the increase of the flow velocity in the river. The main reason of local scour is the existence of bridge abutment and pier which leads high velocity and big turbulence. Pier scour is the removal of the soil around the foundation of pier, abutment scour is the removal of the soil around the abutment which is the structure supporting the bridge deck at the end of embankment, and contraction scour is the removal of the soil by the reason of channel narrowing by the approach embankment.

Bridge scour is the main cause of bridge failure in the United States. Shirhole and Holt (1991) found that around 60 % of bridge failures in the United States were related with bridge scour on the basis of their survey from 1950 to 1990. Studies to predict the depth of bridge scour have been performed since the middle of 20th century, and most methods to predict bridge scour have been developed on the basis of laboratory flume

_____

This dissertation follows the style and format of the *Journal of Hydraulic Engineering*.

test results using cohesionless soil. Those methods have been also used for cohesive soil which has much slower erosion rate than cohesionless soil. It usually takes less than a day for cohesionless soil to reach the maximum scour depth in cohesionless soil under constant flow rate while the scour depth developed in a day maybe less than a percentile of the maximum scour depth in cohesive soil by the reason of its slower erosion rate. The erosion rate of soils has been studied by Briaud et al. (1999(b), 2003) and they found that the scour rate of cohesive soils can be 1000 times slower than that of cohesionless soils. In order to design cost-effective bridge, the time factor should be considered for the scour depth prediction in cohesive soil. Briaud et al. (2003) considered the time effect in bridge scour in cohesive soils for complex pier and contraction scour in the research project NCHRP 24-15. A method to predict the scour depth in cohesive soil in NCHRP 24-15 was called as Scour Rate In COhesive Soils (SRICOS) method. The SRICOS method uses the maximum shear stress and the maximum scour depth to predict the scour with time effect.

In present study as a part of the extension of SRICOS method, a method is developed to solve the problems of abutment scour. In addition, the new method to predict contraction scour and complex pier scour is developed using the data obtained from the laboratory tests in Texas A&M University since 1997.

1.2 Objectives

The specific objectives of this study are:

1. To develop a methodology to predict the maximum complex bridge pier scour with consideration of the critical shear stress of soil and the effect of water depth, attack angle, pier shape and the spacing of piers.

2. To develop a methodology to predict the maximum bridge contraction scour in the compound channel with consideration of the critical shear stress of soil and the effect of contraction length and transition of contraction.

3. To develop a methodology to predict the maximum abutment scour in the compound channel with consideration of the critical shear stress and the effect of abutment shape, transition angle and abutment location.

4. To update the SRICOS-EFA method to predict pier scour, contraction scour, and abutment scour using developed prediction methods.

1.3 Methodology

Scour occurs when the shear stress generated by flow around bridge structure exceeds the critical shear stress of channel bottom soils. The shear stress decreases with scour development and the scour continues until the shear stress acting around the bridge structure equals to the critical shear stress of channel bottom soils. Flume tests results are collected and analyzed to identify the scour patterns.

1.3.1   Flume tests

A series of flume tests was conducted for abutment scour and contraction scour in compound channel composed with cohesive soil. The evolution of channel bottom was measured frequently during every flume test, and the hyperbolic model was used to get the maximum abutment scour and contraction scour depth at the equilibrium condition. The water depth and velocity pattern were measured to find the relationship between the variation of water depth and velocity with scour development.

The flume test results performed by Gudavalli (1997) and Li (2002) are re-analyzed to formulize the relationship between pier scour depth and all parameters including the critical shear stress of soil, hydraulic data and geometry.

In addition, Li's flume test results (2002) are included for the formulation of contraction scour.

1.3.2   Hyperbolic model

The scour rate of clays can be ten thousand times slower than that of sand. It can take several months or years to reach the maximum scour depth because the Porcelain clay is used for channel bottom material in flume tests in this study. In order to get the maximum local scour depths, a hyperbolic model proposed by Briaud et al. (1999(a), 2001(a), 2001(b)), who found that the maximum pier scour depth could be obtained by extrapolation with scour depth versus time, is applied to obtain the maximum scour depths for pier, contraction and abutment scour.

1.3.3 SRICOS-EFA method

The EFA (Erosion Function Apparatus) is a device to get the erosion properties of soil. SRICOS-EFA (Scour Rate In COhesive Soil-Erosion Function Apparatus) is a method to predict the scour depth with the function of time considering the erosion properties of soil. The procedure of SRICOS-EFA is summarized as following;

1. Perform EFA (Erosion Function Apparatus) tests on the samples and obtain the relation of the erosion rate $\dot{z}$ to the hydraulic shear stress τ.

2. Determine the initial maximum bed shear stress τ_{max} around the hydraulic structure before the scour process using the equation obtained from numerical simulations.

3. Obtain the initial scour rate $\dot{z}_i$ corresponding to τ_{max} on the $\dot{z}$-τ curve.

4. Calculate the maximum scour depth y_s.

5. Develop the complete scour depth y_s versus time t curve.

$$y_s(t) = \frac{t}{\dfrac{1}{\dot{z}_i} + \dfrac{t}{y_s}} \qquad (1.1)$$

6. Predict the scour depth at the time corresponding to the duration of the flood by reading the y_s-t curve.

1.4 Outline

This dissertation is written on the basis of flume test results performed since 1997 in Texas A&M University; Gudavalli (1997) conducted flume tests for pier scour in deep water condition with cylindrical pier, but he did not formulize the results with the term

of soil property. Li (2002) conducted flume tests for pier scour and contraction scour. He conducted a series of flume test to find the effect of water depth, pier shape, attack angle and aspect ratio, and another series of flume test for contraction scour in the rectangular channel. A series of flume test have been conducted for abutment scour and contraction scour in compound channel since 2005. In this dissertation all flume test results are used to formulize the results of pier, contraction and abutment scour.

Chapter II is consisted with the overview of the existing knowledge. This chapter presents the literature review of pier scour, contraction scour, and abutment scour for both cohesionless soil and cohesive soil. The summary of SRICOS-EFA method – maximum shear stress for pier scour, contraction scour, and abutment scour, and procedure of SRICOS-EFA - is also overviewed in this chapter.

Experiment setup is presented in Chapter III. This chapter details the test setup, equipment, the properties of soil used in the flume tests, and test procedure.

The flume test results for abutment scour in the compound channel are induced in Chapter IV. The pattern of velocity, the water depth change and the evolution of channel bed are measured. Both the maximum abutment scour and the maximum contraction scour of each test are calculated on the basis of the hyperbolic model. The pattern of velocity and the scour pattern are compared to find the main cause of abutment scour and contraction scour.

The comparison between the measurement during flume tests and one dimensional simulation results are conducted in Chapter V. For one dimensional simulation, HEC-RAS (Hydrologic Engineering Center River Analysis System) is used.

The flume test results for pier scour from Gudavalli (1997) and Li (2002) are reanalyzed in Chapter VI. The data for deep water condition are selected, and the prediction equation of pier scour in deep water condition is proposed. Using the prediction equation in deep water condition, the shallow water effect, abutment shape effect, attack angle effect and group pier effect are studied and several correction factors are presented in this chapter. The pier scour equation is applied to the previous test results for cohesionless soil for the verification.

Chapter VII presents the contraction scour prediction using flume test results from Li (2002) and present study. The maximum contraction scour equation applicable to both compound channel and rectangular channel is proposed. The uniform contraction scour equation is also proposed using the relationship between the maximum contraction scour and the uniform contraction scour, which is proposed by Li (2002). The uniform contraction scour equation is applied to the flume test results conducted by Gill (1981).

Chapter VIII presents the abutment scour prediction using flume test results. The abutment is regarded as the half of the wide pier, and the prediction equation form of abutment scour is same to that of pier scour. The abutment shape effect, the attack angle effect and the abutment location effect in the compound channel are studied with flume test results. The abutment scour equation is applied to the Froehlich's (1989) database and Sturm's (2004) database for the verification. The comparisons with other equations using imaginary condition are conducted in this chapter.

Chapter IX presents newly developed SRICOS-EFA method. The principle of SRICOS-EFA, the procedure of the method, and new version of SRICOS-EFA program is introduced in this chapter.

Chapter X addresses the conclusions of the dissertation and recommendations for future research.

CHAPTER II

LITERATURE REVIEW OF BRIDGE SCOUR

2.1 Introduction

The local bridge scour includes pier scour and abutment scour. Pier scour is the removal of the soil around the foundation of pier, abutment scour is the removal of the soil around the abutment which is the structure supporting the bridge deck at the end of embankment. The contraction scour is the removal of the soil by the reason of channel narrowing by the approach embankment. The local scour can be divided into clear-water scour and live-bed scour with respect of the ratio between the shear stress and the critical shear stress at approach section. The clear-water scour happens without sediment transport from upstream, but the live-bed scour happens with sediment transport from upstream to scour hole. The scour rate of clear-water scour is much slower than that of live-bed scour while the deepest maximum scour depth happens at the threshold condition, which is the borderline between clear-water scour and live-bed scour.

Extensive studies on bridge scour have been performed in the past. In this chapter, the literatures about three local bridge scours - pier, contraction and abutment scour - are summarized in the view of soil type.

2.2 Pier scour

2.2.1 Pier scour in cohesionless soil

A lot of pier scour studies have been conducted since 1950s, and these studies are based on the laboratory test results in cohesionless soil. The followings are the summary of famous studies on pier scour in cohesionless soil.

Laursen and Toch (1956) studied the effect of pier nose shape, attack angle and water depth on pier scour. They presented a basic design curve of pier scour depth in rectangular piers with zero attack angle, which was expressed as:

$$\frac{y_{s(pier)}}{a} = 1.5\left(\frac{y_1}{a}\right)^{0.3} \tag{2.1}$$

where $y_{s(pier)}$ is pier scour depth, y_1 is approach flow depth and a pier width. They found the correction factor for pier nose shape, and the correction factors for the pier scour depth as the function of attack angle and the ratio of pier width to pier length. The correction factors for pier shape and attack angle proposed by the authors are presented in Table 2.1 and Figure 2.1, respectively. Thus pier scour prediction considering pier nose shape and attack angle is:
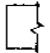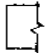
$$\frac{y_{s(pier)}}{a} = K_1 \cdot K_2 \cdot 1.5\left(\frac{y_1}{a}\right)^{0.3} \tag{2.2}$$

where K_1 is the correction factor for pier nose shape, and K_2 is the correction factor for attack angle.

Tison (1961) conducted a series of flume test with 0.7 m wide flume. The flow condition mostly used in flume test was 0.105 m of flow depth and 0.03 m^3/sec of

discharge and mean velocity of 0.41 m/sec. A medium size of sand of $D_{50} = 0.48$ mm was used. He studied the pattern of flow around a bridge and approach section. He showed that the downward velocity generated in front of pier so-called "horseshoe vortex" is main cause of pier scour. He also mentioned that the maximum scour depth occurred at the nose for the rectangular pier, and the length of pier was not important if the flow direction is parallel to the direction of pier length $(\theta = 0°)$ for the rectangular channel.

Table 2.1. Correction factor for pier nose shape (Laursen and Toch (1956))

Shape of pier nose	L/a		K_1
Rectangular			1.0
Semicircular	1:1		0.9
Elliptic	2:1		0.8
	3:1		0.75
Lenticular	2:1		0.8
	3:1		0.7
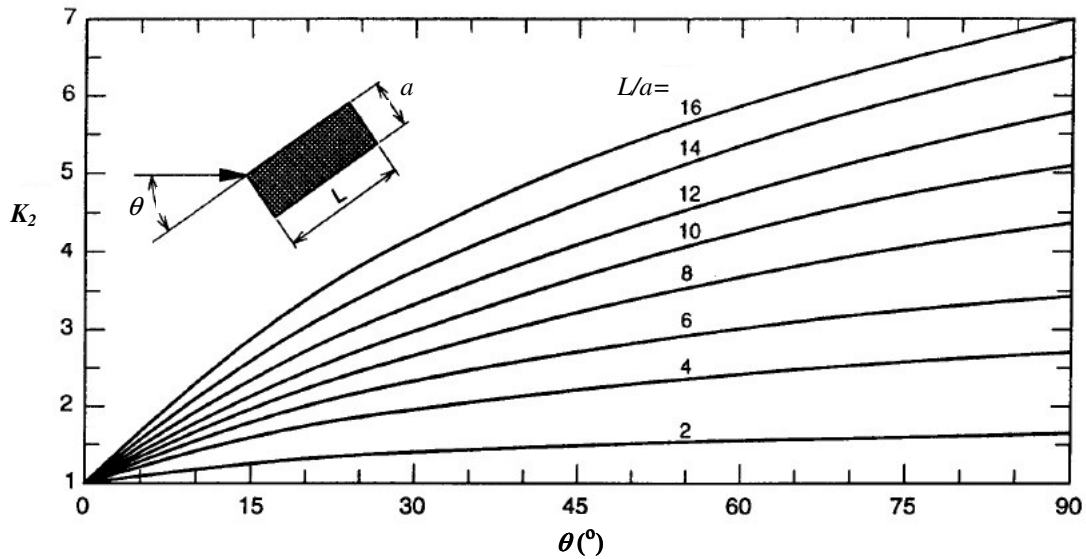
Figure 2.1. Correction factor for attack angle (Lauresen and Toch (1956))

Larras (1963) analyzed Chabert and Engeldinger (1956) data and found the relation of pier scour depth as functions of pier width, pier nose shape and attack angle. The relation suggested by the author is:

$$y_{s(pier)} = K_1 \cdot K_2 \cdot 1.05 \cdot a^{0.75} \tag{2.3}$$

where $y_{s(pier)}$ is pier scour depth in the unit of meter, a is the width of pier in the unit of meter, K_1 is the correction factor for pier nose shape ranging from 0.41 to 1.4, and K_2 is the correction factor for attack angle ranging from 1 to 2.0.

Jain and Fisher (1980) conducted a series of flume tests with tilting flume. Three types of sand, which are fine, medium and coarse sands, were used for soil material. Two circular cylinder piers with diameter of 0.051 m and 0.102 m were used for laboratory tests. The proposed equation is:

$$\frac{y_{s(pier)}}{a} = 1.86 \cdot \left(\frac{y_1}{a}\right)^{0.5} (Fr_1 - Fr_c)^{0.25} \tag{2.4}$$

where Fr_1 is Froude number based on approach water depth and velocity

$\left(Fr_1 = \dfrac{V_1}{\sqrt{g \cdot y_1}}\right)$, and Fr_c is the critical Froude number based on critical velocity and

approach water depth $\left(Fr_c = \dfrac{V_c}{\sqrt{g \cdot y_1}}\right)$.

Melville and Sutherland (1988) analyzed data obtained from lots of previous studies - Chiew (1984), Ettema (1980), Chee (1982), Melville (1975), Shen et al. (1966), and Davoren (1985).

$$\frac{y_{s(pier)}}{a} = K_1 \cdot K_2 \cdot K_I \cdot K_w \cdot K_d \cdot K_\sigma \tag{2.5}$$

where K_I is correction factor for flow intensity, K_w is correction factor for water depth, K_d is correction factor for sediment size ratio, and K_σ is correction factor for sediment gradation. Those correction factors recommended by authors follow:

Authors recommended to select one of reasonable correction factor for pier shape effect among Chabert and Engeldinger (1956), Laursen (1958), Laursen and Toch (1956), Tison (1940) and Venkatadri et al. (1965). The correction factor for attack angle is same with Laursen and Toch (1956) as shown in Figure 2.1.

$$K_I = \begin{cases} 2.4 \left| \dfrac{V - (V_a - V_c)}{V} \right| & , \text{for } \dfrac{V - (V_a - V_c)}{V} < 1.0 \\ 2.4 & , \text{else} \end{cases} \tag{2.6}$$

$$K_w = \begin{bmatrix} 0.78\left(\dfrac{y_1}{a}\right)^{0.255} & \text{, for } \dfrac{y_1}{a} < 2.6 \\ 1.0 & \text{, else} \end{bmatrix} \qquad (2.7)$$

$$K_d = \begin{bmatrix} 1.0 & \text{, for } a/D_{50} > 25 \\ 0.57\log(2.24 \cdot a/D_{50}) & \text{, else} \end{bmatrix} \qquad (2.8)$$

where V_a is the mean velocity of flow at the "armor peak" for nonuniform sediment or critical velocity for uniform sediment.

Melville (1997) found more detail correction factor for water depth effect. It is that the pier scour depth in deep water condition ($y \geq 1.43 \cdot a$) is independent on the water depth as shown in Figure 2.2. This relation is very helpful to analyze Gudavali's data (1997) and Li's (2002) data in present study.
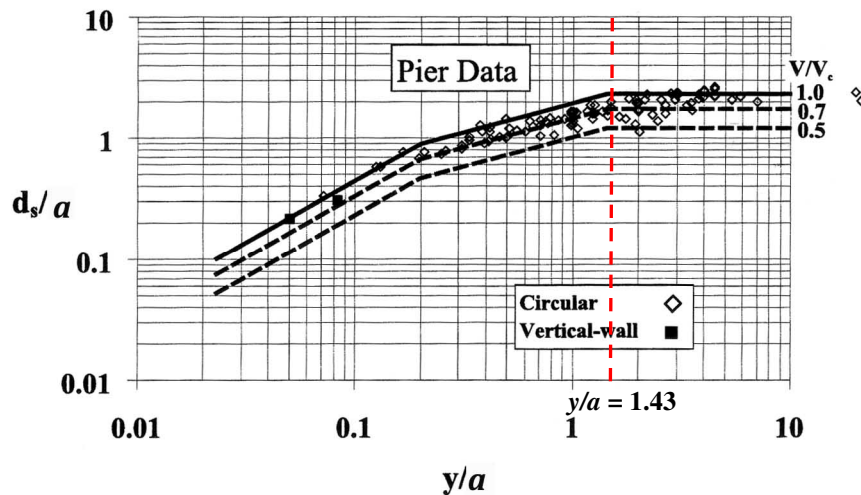
Figure 2.2. The influence of flow shallowness on local scour depth (Melville 1997, Melville and Coleman, 2000)

Abdou (1993) performed experiments to study the effect of sediment gradation on pier scour. The author used six different sediment mixtures with a constant median

diameter. The following relation was proposed on the basis of experimental results and data regression:

$$\text{For } \sigma_g = 1.38 \quad \frac{y_{s(pier)}}{y_1} = 144.5 \cdot Fr^{3.47} \tag{2.9}$$

$$\text{For } \sigma_g = 2.43 \quad \frac{y_{s(pier)}}{y_1} = 38.0 \cdot Fr^{3.03} \tag{2.10}$$

$$\text{For } \sigma_g = 2.43 \quad \frac{y_{s(pier)}}{y_1} = 23.0 \cdot Fr^{3.2} \tag{2.11}$$

$$\frac{y_{s(pier)}}{y_1} = 148 \cdot Fr^{2.93} \cdot \left(\frac{D_{90}}{D_{50}}\right)^{-1.48} \tag{2.12}$$

where $\sigma_g = (D_{84}/D_{16})^{0.5}$ is the geometric standard deviation of the bed material, and D_{16}, D_{50}, D_{84}, and D_{90} are the particle size for 16, 50, 84 and 90 percentile of weight, respectively.

Richardson et al.'s equation (1995, 2001) is recommended for the computation of maximum pier scour for both live-bed and clear-water pier scour in HEC-18. The pier nose shape, attack angle, bed condition and armoring effects are considered in the recommended equation. The equation is:

$$y_{s(pier)} = 2.0 K_1 \cdot K_2 \cdot K_3 \cdot K_4 \cdot a^{0.65} \cdot y_1^{0.35} Fr_1^{0.43} \tag{2.13}$$

where K_3 is the correction factor for bed condition , K_4 is the correction factor for armoring by bed material size. The correction factors from K_1 to K_4 are expressed in following:

Table 2.2. Correction factor for pier nose shape (K_1) proposed by Richardson et al.(2001)

Shape of pier nose	K_1	Shape of pier nose	K_1
Square nose	1.1	Group of cylinders	1.0
Round nose	1.0	Sharp nose	0.9
Circular cylinder	1.0	-	-

$$K_2 = \left(\cos\theta + \frac{L}{a}\sin\theta \right)^{0.65}$$ (2.14)

Note: If the attack angle is bigger than 5 degree, the effect of pier nose shape becomes irrelevant to scour depth. Thus $K_1 \cdot K_2 = K_2 = \left(\cos\theta + \frac{L}{a}\sin\theta \right)^{0.65}$, for $\theta > 5°$.

Table 2.3. Correction factor for bed condition (K_3)

Bed condition	H (m)	K_3
Clear-water scour	N/A	1.1
Plane bed and antidune flow	N/A	1.1
Small dunes	$3 > H \geq 0.6$	1.1
Medium dunes	$9 > H \geq 3$	1.2 to 1.1
Large dunes	$H \geq 9$	1.3

where H is the height of dune.

$$K_4 = 0.4 \cdot V_R^{0.15}$$ (2.15)

where V_R is velocity ratio $\left(V_R = \left[\dfrac{V_1 - V_{i50}}{V_{c50} - V_{i95}} \right] \right)$, V_{i50} is approach velocity to initiate scour at

the pier for grain size D_{50} $\left(V_{i50} = 0.645 \left(\dfrac{D_{50}}{a} \right)^{0.053} V_{c50} \right)$, V_{i95} is approach velocity to

initiate scour at the pier for grain size D_{95} $\left(V_{i95} = 0.645 \left(\dfrac{D_{95}}{a} \right)^{0.053} V_{c95} \right)$, V_{c50} is critical

velocity for grain size D_{50} $\left(V_{c50} = 6.19 \cdot y_1^{1/6} \cdot D_{50}^{1/3} \right)$, and V_{c95} is critical velocity for grain

size D_{95} $\left(V_{c95} = 6.19 \cdot y_1^{1/6} \cdot D_{95}^{1/3} \right)$.

Note that the limits of bed material is $D_{50} \geq 0.002 \text{ m}$ and $D_{95} \geq 0.02 \text{ m}$, and the

minimum value and maximum value of K_4 is 0.4 and 1.0, respectively.

2.2.2 Pier scour in cohesive soil

Pier scour in cohesive soil were investigated through laboratory tests or site observations. Some of the interesting conclusions and predictive equations from those investigations are given in the following:

Hosny (1995) investigated bridge cylindrical pier scour by flume tests in different streambed states, i.e., mixed beds (cohesive and non-cohesive soils), unsaturated cohesive soil and saturated cohesive soil. He found that soil compaction, and initial water content (IWC) could affect local scour depth. The results also indicated that the existence of cohesive soil could reduce the final scour depth, and the time to reach the maximum scour depth in saturated cohesive soils was longer than that in mixed soils.

Hosny recommended the following equations to estimate pier scour depth in cohesive soils through test data regression and dimensional analysis:

For sandy-clayey soil:

$$y_{s(Pier)} = 18.9a\left(\frac{Fr_1}{1+C}\right)^2 \tag{2.16}$$

For unsaturated and saturated cohesive soil:

$$y_{s(Pier)} = 0.9B(IWC)^{-\frac{2}{3}} Fr_1^{\frac{3}{2}} Comp^{-2} \tag{2.17}$$

Scour depth $y_{s(Pier)}$ has relationship with the volume of scour hole V_s as:

$$y_{s(Pier)} = kB\left(\frac{V_s}{a^3}\right)^{k'} \tag{2.18}$$

where $y_{s(Pier)}$ is the maximum scour depth, B is the diameter of pier, C is clay content, *Comp* is degree of compaction (0.58<*Comp*<1), *IWC* is initial water content (0.15<*IWC*<0.5), $Fr = V_1/(gy_1)^{0.5}$ is the Froude number (0.18<*Fr*<0.51), k' is a constant (0.4<k'<0.7), V_s is the volume of scour, V_1 is the approach average velocity and g is the gravitational acceleration.

Annandale (1995) proposed the Erodibility Index Method (EIM) to predict pier scour in erosive rock and other resistant earth materials. The method is based on the comparison between the available stream power and the required stream power. The available stream power is the erosive power of the flowing water, and the required stream power is the critical erosive power necessary to erode the soil away. Scour occurs only at the condition that the available power is larger than the required power; and scour stops when the contrary occurs. Therefore, the maximum scour depth happens

when the available stream power curve and the required stream power curve intersect each other.

The Erodibility Index is identical to Kirsten's Excavatability Index (Kirsten, 1982) used to quantify the relative ability of earth materials to resist erosion, and can be determined as:

$$K = M_s K_b K_d J_s \tag{2.19}$$

where K is the Erodibility Index, M_s is the intact material strength number, K_b is the particle/block size number, K_d is the shear strength number, and J_s is the relative ground structure number. Each parameter can be obtained from tables and equations according to the bed materials. The relationship between the required stream power and erodibility index is given by:

$$P_{required} = \begin{cases} K^{0.75} & K > 0.1 \\ 0.96 K^{0.44} & K < 0.1 \end{cases} \tag{2.20}$$

The available stream power at the base of the piers can be calculated for different types of piers on the method developed by Federal Highway Administration's (FHWA) hydraulic laboratory for granular materials.

Annandale built relationships between the stream power amplification at the base bridge piers P_c/P_a and dimensionless scour depth $y_{s(Pier)} / y_{s(Pier)\_HEC}$ by fitting experimental data for different types of piers.

For round piers

$$\frac{P_c}{P_a} = 3.2997 \left(\frac{y_{s(Pier)}}{y_{s(Pier)\_HEC}} \right)^2 - 9.6589 \left(\frac{y_{s(Pier)}}{y_{s(Pier)\_HEC}} \right) + 7.661 \tag{2.21}$$

For square piers

$$\frac{P_c}{P_a} = -4.0741\ln\left(\frac{y_{s(Pier)}}{y_{s(Pier)\_HEC}}\right) + 1.3186 \tag{2.22}$$

For rectangular piers (0° skew angle)

$$\frac{P_c}{P_a} = 11.643\left(\frac{y_{s(Pier)}}{y_{s(Pier)\_HEC}}\right)^2 - 22.71\left(\frac{y_{s(Pier)}}{y_{s(Pier)\_HEC}}\right) + 12.614 \tag{2.23}$$

For rectangular piers (15 ° skew angle)

$$\frac{P_c}{P_a} = 5.1806\left(\frac{y_{s(Pier)}}{y_{s(Pier)\_HEC}}\right)^2 - 13.212\left(\frac{y_{s(Pier)}}{y_{s(Pier)\_HEC}}\right) + 9.3696 \tag{2.24}$$

For rectangular piers (30 ° skew angle)

$$\frac{P_c}{P_a} = 6.1026\left(\frac{y_{s(Pier)}}{y_{s(Pier)\_HEC}}\right)^2 - 16.998\left(\frac{y_{s(Pier)}}{y_{s(Pier)\_HEC}}\right) + 12.267 \tag{2.25}$$

where $y_{s(Pier)}$ is the maximum scour depth in cohesive soil, $y_{s(Pier)\_HEC}$ is the maximum scour depth calculated using HEC-18, P_c is the stream power at the base of piers (or the available stream power) and P_a is the approach stream power per unit area in the upstream reach and calculated by FHWA equation.

Gudavalli (1997) conducted extensive experimental research on cylindrical pier scour in different soil beds. The results indicated that the existence of cohesive soils has no noticeable influence on scour depth compared to the values predicted by HEC-18, and a relatively simple equation was proposed to predict simple pier scour depth as:

$$y_{s(Pier)} = 0.0018\left(\frac{aV_1}{v}\right)^{0.635} \tag{2.26}$$

where $y_{s(Pier)}$ is the maximum pier scour depth in meter, a is pier diameter, V_1 is the mean approaching velocity, and v is kinematical viscosity of water.

In the study, it was also found that hyperbolic model works well to simulate the time history of scour development and predict the maximum scour depth, especially for scour in cohesive soils where scour depth strongly depends on the scouring time.

Li (2002) assumed that the difference between maximum shear stressaround pier and the critical shear stress of channel bottom soil governs the scour depth. He analyzed the database of scour in Gudavalli (1997), and proposed the pier scour equation in deep water condition as:

$$\frac{y_{s(Pier)}}{a} = 20 \left(\frac{\tau_{max(Pier)} - \tau_c}{\rho g a} \right)^{0.4} \tag{2.27}$$

He conducted a series of flume tests to find the effect of water depth, pier spacing, and pier shape, developed Gudavalli's (1997) equation as:

$$y_{s(Pier)} = 0.0018 \cdot K_w \cdot K_{sp} \cdot K_1 \cdot \left(\frac{a'V}{v} \right)^{0.635} \tag{2.28}$$

where $y_{s(Pier)}$ is the maximum pier scour depth, a is pier diameter, $a' = a \left(\dfrac{L}{a} \sin\theta + \cos\theta \right)$ is the projected pier width for rectangular pier, ρ is the density of water, $\tau_{max(Pier)} = \left[0.094 \rho V_1^2 \left(\dfrac{1}{\log \mathrm{Re}} - 0.1 \right) \right]$ is maximum shear stress around cylindrical pier proposed by Wei et al. (1997), τ_c is the critical shear stress of channel bottom soils, V_1 is approach velocity, $\mathrm{Re} = (V_1 a / v)$ is pier Reynolds number, v is the kinematical

viscosity of water ($10^{-6}\,m^2$/s at 20°C), K_w is the correction factor for water depth effect, K_{sp} is the correction factor for pier spacing effect.

Ivarson (1999) found that the pier scour predictive equation in HEC-18 only restricts to bed materials with particle size $D_{50} > 0.06$m. He proposed a bed material size factor, K_4, for clay beds based on the correlation between the unconfined compressive strength and the critical stress of soil:

$$K_4 = 0.677 \log \left(500 \frac{a}{S_u} \right) \qquad (2.29)$$

where a is the width of pier, S_u is the unconfined compressive strength of clay (lbs/ft^2). In order to apply this correction factor into HEC-18, the unconfined compressive strength (lbs/ft^2) must be greater than 17 times of the pier width (inches).

Molinas et al. (1999) investigated bride pier scour in unsaturated and saturated cohesive soils concerning the effect of clay content, soil compaction, and initial water content (*IWC*). Based upon dimensional analysis and experimental data regression, the scour depth equation using parameters such as compaction, initial water content, and Froude Number was developed as follows.

For unsaturated cohesive soil:

$$\frac{y_{s(Pier)}}{a^{0.66}y^{1.13}} = \begin{cases} 0 & \left(\begin{array}{l} Fr_1 \leq 0.2 \\ Comp \geq 0.85 \end{array}\right) \\ 45.95(IWC)^{-0.36} Fr_1^{1.92} Comp^{1.62} & \left(\begin{array}{l} Fr_1 \leq 0.2 \\ Comp < 0.85 \\ Fr_1 > 0.2 \end{array}\right) \end{cases} \qquad (2.30)$$

For saturated cohesive soil:

$$\frac{y_{s(Pier)}}{y_1} = \begin{cases} 0 & Fr_1 < Fr_i \\ 9.61\left(\dfrac{a}{y_1}\right)^{0.66} (IWC)^{2.62} (Fr_1 - Fr_i)^{0.32} & Fr_1 > Fr_i \end{cases} \qquad (2.31)$$

where $y_{s(Pier)}$ is maximum pier scour depth, y_1 is the depth of approach flow, a is pier width, *Comp* is the degree of compaction, *IWC* is initial water content, $Fr_1 = V_1/(gy_1)^{0.5}$ is the Froude number, $Fr_i = V_i/(gy_1)^{0.5}$ is the scour initiating Froude number, V_1 is the approach average velocity, $V_i = 0.065/(IWC)^{2.92}$ is the scour initiating velocity, and g is the gravitational acceleration.

Kwak (2000) extended Gudavalli's (1997) pier scour research to the condition of multi-floods and layered soils, and resulted in the SRICOS method. In this method, soil erosion functions measured by EFA (Erosion Function Apparatus) and flow conditions are combined in a series of hyperbolas, and these hyperbolas are joined together in a time sequence to simulate the whole time history of scour process.

From the literature on pier scour in cohesive soils, it was found that the influence of soil properties on pier scour has been partially examined in the previous research. The deceleration effect of scour rate due to the existence of clay was clearly addressed and

modeled. Even though arguments still exist, more and more evidences tend to support that clay and sand have different maximum scour depth. Annandale and Molinas made special contributions by independently developing the concept that it is under certain critical values for a given soil that scour initiates and stops. But these boundary conditions were not fully developed in their equations to represent the flow-soil interaction. Also, the proposed methods by them to calculate the critical values are too specific to be applied in general cases.

2.3 Contraction scour

The flow passing through the bridge section gets the higher velocity and the corresponding higher shear stress than approach section. If the increased shear stress is greater than the critical shear stress of the channel bottom soils, the contraction scour happens. Many studies on the contraction scour in cohesionless soils have been conducted since 1930s, and studies on the contraction scour in cohesive soils have been performed recently.

2.3.1 Contraction scour in cohesionless soil

Straub (1934) is a pioneer to develop a methodology to predict the long contraction scour in the live-bed condition. He assumed that the contraction scour would continue until the local transport capacity is equal to the amount of sediment particles supplied from upstream. Many researchers after him have developed long contraction scour prediction method with his approach. Laursen (1963) and Komura (1966) applied Straub's approach (1934) in the live-bed contraction scour to the clear-water contraction

scour. The formulations of long-contraction scour in cohesionless soil are summarized in

Table 2.4.

Table 2.4. Formulations for long contraction scour in cohesionless soil

Reference	Contraction Scour Equation	Notes	Scour Condition
Laursen (1960)	$\dfrac{y_{Cont}}{y_1} = \left(\dfrac{Q_2}{Q_1}\right)^{\frac{6}{7}} \left(\dfrac{L_1}{L_2}\right)^{\frac{6}{7}\frac{2+a}{3+a}} \left(\dfrac{n_2}{n_1}\right)^{\frac{6}{7}\frac{a}{3+a}}$	a depends on the mode of sediment movement	Live-bed
Laursen (1963)	$\dfrac{y_{Cont}}{y_1} = 0.13\left(\dfrac{Q}{D_{50}^{1/3} y_1^{7/6} L_2}\right)^{6/7}$		Clear-water
Komura (1966)	$\dfrac{y_{Cont}}{y_1} = \left(\dfrac{\tau_{c1}}{\tau_{c2}}\right)^{\frac{2}{7}} \left(\dfrac{L_1}{L_2}\right)^{6/7}$	$\tau = \dfrac{\rho g n^2 V^2}{D_{50}^{1/3}}$	Live-bed
Komura (1966)	$\dfrac{y_{Cont}}{y_1} = \left(\dfrac{\tau_{c1}}{\tau_{c2}}\right)^{\frac{2}{7}} \left(\dfrac{L_1}{L_2}\right)^{6/7}$	$\dfrac{\tau_c}{\rho} = ac\left[Gs-1\right]gD$	Clear-water
Gill (1981)	$\dfrac{y_{Cont}}{y_1} = C\left(\dfrac{L_1}{L_2}\right)^{6/7} \left[\left(\dfrac{L_2}{L_1}\right)^{1/m}\left(1-\dfrac{\tau_c}{\tau_1}\right)+\dfrac{\tau_c}{\tau_1}\right]^{-3/7}$	m is a function of sediment transport rate and varies between 1.5 and 3.0	Live-bed
Lim and Cheng (1998 (a))	$\dfrac{y_{Cont}}{y_1} = \left(\dfrac{L_2}{L_1}\right)^{0.75}$		Live-bed

2.3.2 Contraction scour in cohesive soil

Ivarson (1999) developed a clear-water contraction scour formulation in cohesive

soils using similar approach used in Laursen (1963) in cohesionless soil. They used

Flaxman's (1963) relationship between the unconfined compressive strength and the

critical shear stress in clay in order to get the critical shear stress, and the relationship is:

$$\tau_c = \frac{12.11 \log Su - 28.67}{V_2} \tag{2.31}$$

Substituting shear stress at contracted section in Manning's equation for the friction

slope with Flaxman's relationship (equation (2.31)), the total flow depth in the

contracted section is:

$$y_{Cont} = \left[\frac{2.32 q_2^3 n^2}{\log S_u - 2.367} \right]^{3/10} \tag{2.32}$$

where τ_c is the critical shear stress of channel bottom soil (lbs / ft^2), Su is the

unconfined compressive strength of channel bottom soil (lbs / ft^2), V_2 is the average

velocity in the contracted section ($ft / \sec$), y_{Cont} is the total flow depth in the contracted

section, $q_2 = Q / L_2$ is the unit discharge in the contracted section ($ft^3 / \sec / ft$), n is

Manning's roughness coefficient.

Li (2002) conducted 13 contraction scour experiments in the rectangular channel

using Porcelain clay. He varied the approach velocity, contraction ratio, contraction

length and contraction transition angle, and found that the contraction scour depth can be

determined by flow and critical shear stress of soil in contracted section while the

contraction length and contraction transition angle did not affect contraction scour depth. He derived the maximum contraction scour equation and the uniform contraction scour equation, and applied the uniform contraction scour equation to other laboratory test results using sand performed by Gill (1981), Komura (1966) and Rana (1986). He showed that his equation agreed well with those test results. The equations proposed by Li (2002) are:

For maximum contraction scour

$$\frac{y_{s(Cont)}}{y_1} = 1.9\left(1.38 Fr_2 - Fr_c\right) \tag{2.33}$$

For uniform contraction scour

$$\frac{y_{s(uni\_Cont)}}{y_1} = 1.41\left(1.31 Fr_2 - Fr_c\right) \tag{2.34}$$

where $y_{s(Cont)}$ is the maximum contraction scour depth, $y_{s(unif\_Cont)}$ is the uniform contraction scour depth, y_1 is approach water depth, $Fr_2 = \dfrac{V_1(L_1/L_2)}{\sqrt{gy_1}}$ is Froude number in contracted section, $Fr_c = \dfrac{V_c}{\sqrt{gy_1}}$ is the critical Froude number, $V_c = \dfrac{(y_1)^{1/6}}{n} \cdot \sqrt{\dfrac{\tau_c}{\rho \cdot g}}$ is the critical velocity, τ_c is the critical shear stress of channel bottom soil, n is Manning's coefficient, g is gravitational acceleration and ρ is unit mass of water.

2.4 Abutment scour

2.4.1 Abutment scour in cohesionless soil

Laursen (1960) assumed that the depth of abutment scour is a multiple of the depth of long contraction scour. The depth of contraction scour was considered only as a function of the contraction ratio for live-bed scour. The width of the abutment scour hole was assumed to be 2.75 times the abutment scour depth. The relationship for live-bed abutment scour in sand was based on these assumptions and expressed as:

$$\frac{L'}{y_1} = 2.75 \frac{y_{s(Abut)}}{y_1} \left[\left(\frac{1}{11.5} \cdot \frac{y_{s(Abut)}}{y_1} + 1 \right)^{7/6} - 1 \right] \tag{2.35}$$

where L' is the projected length of abutment normal to the flow, y_1 is the water depth in the approach section, and $y_{s(Abut)}$ is the maximum abutment scour depth.

Laursen (1963) used the same approach and developed an equation to predict the depth of abutment scour for clear-water scour. The equation for abutment scour in sand was:

$$\frac{L'}{y_1} = 2.75 \frac{y_{s(Abut)}}{y_1} \left[\frac{\left(\frac{1}{11.5} \cdot \frac{y_{s(Abut)}}{y_1} + 1 \right)^{7/6}}{\left(\frac{\tau_1}{\tau_c} \right)^{1/2}} - 1 \right] \tag{2.36}$$

The scour depth equation (2.36) in the region of $1 \leq L'/y_1 \leq 10$ can be approximated by

$$\frac{y_{s(Abut)}}{y_1} = 0.8 \frac{L'}{y_1} \left(\frac{\tau_1}{\tau_c} \right)^{2/3} \tag{2.37}$$

where L' is the projected length of abutment normal to the flow, y_1 is the water depth in the approach section, and $y_{s(Abut)}$ is the maximum abutment scour depth, τ_1 is the shear stress on the channel bed at the approach section, and τ_c is the critical shear stress on the channel bed.

Garde et al. (1961) conducted a series of experiments in a rectangular channel with various contraction ratio, sediment size of sand, and discharge. The flume used in the experiments was 2 ft wide and 25 ft long. The maximum local scour occurred at the toe of the abutment and the shape of the abutment scour hole was conical. In their findings, the radius of the conical scour hole did not have any correlation with the depth of the abutment scour. This contradicts Laursen's (1960) finding that the radius is 2.75 times the scour depth. They also found that the median size of sediment, contraction ratio (L_2/L_1), and Froude number are crucial parameters that affect abutment scour depth. They suggested an equation for abutment scour in sand as follows:

$$\frac{y_{s(Abut)}}{y_1} = K\left(\frac{L_1}{L_2}\right)Fr_1^{\,n} - 1 \tag{2.38}$$

where K and n are coefficients that are function of the sediment size, L_1 is the width of the channel at the approach section, L_2 is the width of the channel at the contracted section, Fr_1 is the Froude number at the approach section, y_1 is the water depth in the approach section, and $y_{s(Abut)}$ is the maximum abutment scour depth.

Gill (1972) used Straub's (1940) model of long contraction scour to develop a maximum abutment scour model. He stated that the maximum scour occurred when the

channel bed material is under the critical shear stress (i.e., $\tau_1 = \tau_c$). Both fine sand and coarse sand were used as channel material. The scour rate for the fine sand was observed to be much faster than that for the coarser sand. An equation for scour rate was proposed for both fine sand and coarse sand as:

$$\frac{y_{s(Abut)}(t)}{y_{s(Abut)}} = 0.206\log t + 0.310 \qquad \text{for coarse sand}$$

$$\frac{y_{s(Abut)}(t)}{y_{s(Abut)}} = 0.290\log t + 0.375 \qquad \text{for fine sand} \qquad (2.39)$$

where $y_{s(Abut)}(t)$ is the abutment scour depth at time t, t is time in minute, and $y_{s(Abut)}$ is the maximum abutment scour depth. The empirical equation for predicting the maximum abutment scour depth in sand suggested by Gill is:

$$\frac{y_{s(Abut)}}{y_1} = 8.375 \left(\frac{D_{50}}{y_1} \right)^{0.25} \left(\frac{L_1}{L_2} \right)^{6/7} - 1 \qquad (2.40)$$

where D_{50} is the median size of soil particle, L_1 is the width of the channel at the approach section, L_2 is the width of the channel at the contracted section, y_1 is the water depth in the approach section, and $y_{s(Abut)}$ is the maximum abutment scour depth.

Froehlich (1989) performed data regression using a total of 164 clear-water and 170 live-bed abutment scour measurements in sand taken by other researchers in rectangular channels in different laboratories from 1953 to 1985. Froehlich applied multiple linear regression analysis to obtain the relation among the local scour (normalized by the initial water depth at the approach section) and several other

dimensionless parameters. He proposed a live-bed scour and a clear-water scour equation for abutment scour in sand as follows:

Clear-water scour:

$$\frac{y_{s(Abut)}}{y_1} = 0.78 \cdot K_1 \cdot K_2 \cdot \left(\frac{L'}{y_1}\right)^{0.63} \left(\frac{y_1}{D_{50}}\right)^{0.43} Fr_1^{1.16} \sigma_g^{-1.87} \tag{2.41}$$

Live-bed scour

$$\frac{y_{s(Abut)}}{y_1} = 2.27 \cdot K_1 \cdot K_2 \cdot \left(\frac{L'}{y_1}\right)^{0.43} Fr_1^{0.61} \tag{2.42}$$

where $\sigma_g = \left(D_{84}/D_{16}\right)^{0.5}$ is the geometric standard deviation of the bed material, and D_{16}, D_{50}, and D_{84} are the particle size for 16, 50 and 84 percentile of weight, respectively, $Fr_1 = \left(V_1/\sqrt{g \cdot y_1}\right)$ is Froude number based on approach water depth and approach velocity, K_1 is the correction factor for abutment shape that has a value of 1.0, 0.82 and 0.55 for vertical wall, wing-wall, and spill-through abutment, respectively. K_2 is the correction factor for the alignment of the abutment with respect to the flow direction $\left(K_2 = (\theta/90)^{0.13}\right)$ with θ being the angle of abutment alignment (the embankment is skewed downstream if $\theta < 90°$, and skewed upstream if $\theta > 90°$). L' is the average length of abutment ($L' = A_e/y_1$ with A_e being the flow area obstructed by the embankment), y_1 is the water depth in the approach section, and $y_{s(Abut)}$ is the maximum abutment scour depth.

HEC-18 uses equation (2.42) and a 1.0 safety factor for live-bed abutment scour prediction in sand, i.e.:

$$\frac{y_{s(Abut)}}{y_1} = 2.27 \cdot K_1 \cdot K_2 \cdot \left(\frac{L'}{y_1}\right)^{0.43} Fr_1^{0.61} + 1.0 \qquad (2.43)$$

Melville (1992) developed a method to predict the abutment scour depth in sand in a rectangular channel using a large number of experimental results under the clear water scour condition. The ratio between the abutment length and the water depth was found to be very important for the prediction. The method is classified into three conditions: short abutment ($L'/y_1 \leq 1.0$), intermediate abutment ($1.0 < L'/y_1 < 25$), and long abutment ($L'/y_1 \geq 25$). The effect of abutment shape becomes irrelevant as the length of abutment becomes longer. Similarly, the effect of the abutment alignment becomes irrelevant as the length of abutment becomes shorter. Melville proposed the following equations for the abutment scour depth in sand considering the three conditions as:

$$y_{s(Abut)} = 2.0 \cdot K_I \cdot L' \qquad\qquad \text{for } L'/y_1 \leq 1.0$$

$$y_{s(Abut)} = 2.0 \cdot K_I \cdot K_1^* \cdot K_2^* \left(L' \cdot y_1\right)^{0.5} \quad \text{for } 1.0 < L'/y_1 < 25$$

$$y_{s(Abut)} = 10.0 \cdot K_2 \cdot y_1 \qquad\qquad \text{for } L'/y_1 \geq 25 \qquad (2.44)$$

where L' is the projected length of abutment normal to the flow, $y_{s(Abut)}$ is the maximum abutment scour depth, K_I is a correction factor for flow intensity ($K_I = V_1/V_c$ for $V_1/V_c \leq 1.0$ and $K_I = 1.0$ for $V_1/V_c > 1.0$), and K_1 and K_2 are correction factors for abutment shape and abutment alignment to the flow as shown in Table 2.5 and Figure 2.3, respectively. These two correction factors vary with the ratio between the abutment length and the water depth as expressed in the following:

$$K_1^* = K_1 \qquad\qquad\qquad \text{for } L'/y_1 \le 1.0$$

$$K_1^* = K_1 + (1 - K_1)\left(0.1\dfrac{L'}{y_1} - 1.5\right) \qquad\qquad \text{for } 1.0 < L'/y_1 < 25$$

$$K_1^* = 1.0 \qquad\qquad\qquad \text{for } L'/y_1 \ge 25$$

$$K_2^* = K_2 \qquad\qquad\qquad \text{for } L'/y_1 \ge 3.0$$

$$K_2^* = K_2 + (1 - K_2)\left(1.5 - 0.5\dfrac{L'}{y_1}\right) \qquad\qquad \text{for } 1.0 < L'/y_1 < 3.0$$

$$K_2^* = 1.0 \qquad\qquad\qquad \text{for } L'/y_1 \le 1.0$$

Table 2.5. Factor of abutment shape (K_1) (Melville, 1992)

Shape of Abutment		K_1
Vertical wall	narrow wall	1.0
	semicircular end	0.75
Wing-wall	45°	0.75
Spill-through (H:V)	0.5 : 1.0	0.6
	1.0 : 1.0	0.5
	1.5 : 1.0	0.45
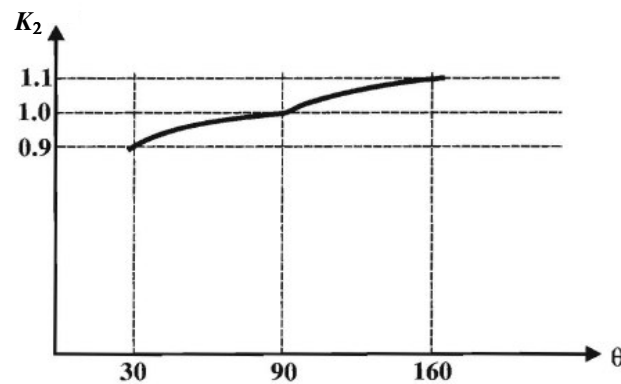
Figure 2.3. Correction factor of abutment alignment (K_2) (Melville, 1992)

Melville (1995) verified the effect of compound channel using Dongol's (1994) experimental results. In his study, only the abutments terminating in the main channel were studied because abutments terminating in the main channel were considered as being in rectangular channels. The correction factor for channel geometry was proposed as:

$$K_G = \frac{y_{s(Abut)}}{y^*_{s(Abut)}}$$

where $y^*_{s(Abut)}$ is the local scour depth at an abutment situated in a compound channel. The correction factor for channel geometry is:

$$K_G = \sqrt{L_e / L'}$$

where $L_e = L' \left\{ 1 - \frac{L_f}{L'} \left(1 - \frac{y_f}{y_m} \right)^{5/3} \frac{n_m}{n_f} \right\}$ in which L is the length, y is the water depth, n is

Manning's roughness coefficient, and the subscripts f and m indicate floodplain and main channel, respectively. Accordingly, Melville (1995) expressed the final form for abutment scour prediction in sand by considering all the conditions as:

$$\frac{y_{s(Abut)}}{\sqrt{L' \cdot y_1}} = 2.0 \cdot K_I \cdot K_G \cdot K_1^* \cdot K_2^* \qquad (2.45)$$

where y_1 is the approach water depth at the line of the toe of the abutment, $y_{s(Abut)}$ is the maximum abutment scour depth, L' is the projected length of abutment normal to the flow, K_I is a correction factor for flow intensity ($K_I = V_1/V_c$ for $V_1/V_c \leq 1.0$ and $K_I = 1.0$ for $V_1/V_c > 1.0$), K_G is the correction factor for channel geometry, K_1^* is the

correction factor for abutment shape, K_2^* is the correction factor for abutment alignment.

Sturm and Janjua (1994) conducted 37 experiments with sand in a compound channel using a vertical wall abutment for abutment scour prediction. The slope of the main channel was vertical and only half of the channel was modeled to maximize the scale. The channel thus was assumed to be symmetrical and the width of flume was one half of the channel width. They showed that the velocity at the approach section, the distribution of the discharge at the contracted section, and the critical velocity are the most important factors affecting the abutment scour depth. Although the ratio of the channel opening in the approach section to the channel opening in the contracted section were used in previous studies, the concept does not work in compound channels because of the difference in velocity distribution between the main channel and the floodplain. Both the contraction ratio in terms of discharge and the contraction ratio in terms of channel opening width were used in the data analysis and evaluated against the experimental results. They found that using the discharge contraction ratio resulted in a better comparison. Their abutment scour equation for sand obtained after data regression is as follows:

$$\frac{y_{s(Abut)}}{y_{f1}} = 7.7 \left[\frac{V_{f1}}{M \cdot V_{fc}} - 0.35 \right] \tag{2.46}$$

where V_{f1} is average approach velocity on the floodplain, V_{fc} is the critical velocity on the floodplain, $y_{s(Abut)}$ is the maximum abutment scour depth, y_{f1} is the approach water depth on the floodplain, and M is the discharge contraction ratio defined as $M = (Q_{total} - Q_{block})/Q_{total}$ with Q_{total} being the total discharge and Q_{block} being the

discharge blocked by the approach embankment.

Sturm (1999, 2004) and Sturm and Janjua (1994) presents the results of flume tests for abutment scour in compound channels using 3 types of cross sections. Various contraction ratio, water depth, and soils were used but only a vertical wall abutment was used. The backwater problem found by some researchers was not found by Sturm and Janjua (1994). The flume used in their study is only 5.18 m long so it may be too short to observe the backwater effect. They developed an equation for vertical abutment scour in sand using the test results without the influence of backwater caused by abutment. It is expressed as:

$$\frac{y_{s(Abut)}}{y_{f0}} = 8.14 \left[\frac{q_{f1}}{C_r \cdot q_{fc0}} - 0.4 \right] \tag{2.47}$$

where $q_{f1}(=V_{f1} \cdot y_{f1})$ is the unit flow rate at the approach section with the effect of backwater induced by the abutment, $q_{fc0}(=V_{fc0} \cdot y_{f0})$ is the critical unit flow rate on the floodplain without the effect of backwater, V_{f1} is the approach average velocity on the floodplain, $V_{fc0} = \left(\frac{1}{k_n} \cdot \sqrt{(Gs-1)\tau_{*c}} D_{50}^{1/3} y_{f0}^{1/6} \right)$ is the critical velocity on the floodplain without backwater effect, Gs is the specific gravity of cohesionless soil, k_n is constant in Strickler-type relationship for Manning's n $\left(n = k_n D_{50}^{1/6} \right)$, τ_{*c} is the critical value of Shields' parameter, D_{50} is the median diameter of sediment, y_{f0} is water depth on floodplain without backwater effect, y_{f1} is the approach water depth on the floodplain and $y_{s(Abut)}$ is the maximum abutment scour depth.

Sturm (2004) found the effect of abutment shape to be negligible $(K_1 = 1.0)$ with the increase of the length of approach embankment. The correction factor associated with the abutment shape for spill-through abutments was calculated based on the ratio between the predicted scour depth using equation (7.13) and that using the vertical abutment. The correction factor for spill-through abutment was suggested as:

$$K_1 = 1.52 \frac{\xi - 0.67}{\xi - 0.4} \qquad \text{for} \quad 0.67 \le \xi \le 1.2 \qquad (2.48)$$

where $\xi = \dfrac{q_{f1}}{M \cdot q_{fc0}}$, $q_{f1}(= V_{f1} \cdot y_{f1})$ is the unit flow rate at the approach section with the effect of backwater induced by the abutment, $q_{fc0}(= V_{fc0} \cdot y_{f0})$ is the critical unit flow rate on the floodplain without the effect of backwater, and M is the discharge contraction ratio defined as $M = (Q_{total} - Q_{block})/Q_{total}$ with Q_{total} being the total discharge and Q_{block} being the discharge blocked by the approach embankment. Note that $K_1 = 1.0$ for $1.2 < \xi$ and $K_1 = 0$ for $\xi < 0.67$. The correction factor is the same for both wing wall abutment and spill-through abutment. Accordingly, the abutment scour depth considering abutment shape becomes:

$$\frac{y_{s(Abut)}}{y_{f0}} = K_1 \cdot 8.14 \left[\frac{q_{f1}}{M \cdot q_{fc0}} - 0.4 \right] \qquad (2.49)$$

Kouchakzadeh and Townsend (1997) used a symmetrical compound channel with 2 types of sand to investigate the lateral momentum transfer on abutment scour. They used 4 types of abutments – vertical wall, wing wall, semi circular vertical wall, and

spill-through. They found the discharge ratio, Q_w/Q_a, is an important factor and developed the following dimensionless function:

$$\frac{y_{s(Abut)}}{y_{f1}} = f\left(\frac{Q_w}{Q_a}, Fr_{f1}, Fr_{fc}, Sh\right) \tag{2.50}$$

Based on multiple data regression, they obtained the following equation:

$$\frac{y_{s(Abut)}}{y_{f1}} = K_1 \cdot 13.5\left(\frac{Q_w}{Q_a}\right)^{3.9} Fr_{f1}^{1.17} \cdot Fr_{fc}^{-0.25} \tag{2.51}$$

where $Fr_{f1}\left(=\dfrac{V_{f1}}{\sqrt{gy_{f1}}}\right)$ is the Froude number in the approach section on the floodplain,

$Fr_{fc}\left(=\dfrac{V_{fc}}{\sqrt{gy_{f1}}}\right)$ is the critical Froude number in the approach section on the floodplain,

Sh is the shape of abutment, Q_w is the floodplain flow beyond the toe of the abutment which converges and accelerates towards the abutment toe, Q_a is the flow intercepted by the abutment, and K_1 is a shape correction factor of abutment with values of 1.25, 1.08, and 0.95, respectively, for vertical wall, wing wall, and spill-through abutment with a side slope of 0.85 (H): 1 (V) , y_{f1} is the approach water depth on the floodplain, and $y_{s(Abut)}$ is the maximum abutment scour depth.

Lim (1997) developed a maximum abutment scour equation for sand based on a semi-empirical analysis for clear water scour. He assumed that only the flow at the approach section with a width corresponding to the length of the abutment and the lateral length of local scour hole could develop the local scour at the toe of abutment. The shear

velocity concept proposed by Rajaratnam and Nwachukwu (1983) was used to derive the equation. Lim's clear water abutment scour depth is given as:

$$\frac{y_{s(Abut)}}{y_1} = K_1 \cdot (0.9X - 2.0) \tag{2.52}$$

where y_1 is the approach water depth, $y_{s(Abut)}$ is the maximum abutment scour depth, K_1 is the correction factor for abutment shape that has a value of 1.0 for vertical wall abutments, and using Melville's (1992) correction factor for other shapes, X in the equation is given as:

$$X = \frac{F_0^{0.75} \left(D_{50} / y_1 \right)^{0.25}}{\theta_c^{0.375} \cdot \left(0.9\sqrt{L'/ y_1} + 1.0 \right)}$$

where $F_0 \left(= V_1 / \sqrt{(Gs-1) \cdot g \cdot D_{50}} \right)$ is the densimetric Froude number at the approach section, $\theta_c \left(= \tau_c / \left[(\rho_s - \rho) g D_{50} \right] \right)$ is Shields' parameter, Gs is the specific gravity of the soil solids, and g is gravitational acceleration, τ_c is the critical shear stress, ρ_s is the density of soil particle, ρ is the density of water, and D_{50} is the median diameter of sediment. He suggested this equation should be used for the case of $X > 2.22$ because $y_{s(Abut)}/y_1 = 0$ for $X = 2.22$.

Lim and Cheng (1998 (b)) derived a maximum abutment scour equation for live bed condition using the same approach as in Lim (1997). The equation to predict abutment scour in sand is given as:

$$\left(1+\frac{y_{s(Abut)}}{2y_1}\right)^{4/3} = K_1 \cdot \frac{1+1.2\sqrt{L'/y_1}}{\sqrt{\left(\frac{u_{*c}}{u_{*1}}\right)^2 + \left(\frac{L'\cdot\tan\phi}{y_{s(Abut)}}+1\right)^{2/3}\cdot\left[1-\left(\frac{u_{*c}}{u_{*1}}\right)^2\right]}} \qquad (2.53)$$

where y_1 is the approach water depth, $y_{s(Abut)}$ is the maximum abutment scour depth, K_1 is the correction factor for abutment shape, u_{*1} is the shear velocity at the approach section, u_{*c} is the critical shear velocity, L' is the length of abutment, and ϕ is the lateral side slope angle of scour hole.

In the clear water scour condition, the term $1-\left(u_{*c}/u_{*1}\right)^2$ in equation (2.53) should be regarded as zero and the equation is reduced to the clear scour equation proposed by Lim (1997). The abutment scour depth equation for sand in the clear water condition is thus:

$$\left(1+\frac{y_{s(Abut)}}{2y_1}\right)^{4/3} = K_1 \cdot \frac{1+1.2\sqrt{L'/y_1}}{u_{*c}/u_{*1}} \qquad (2.54)$$

Chang and Davis (1999(a), 1999(b)) developed a method to predict the abutment scour depth for non-cohesive soil by assuming that abutment scour is a function of contraction scour. Contraction scour was postulated to develop until the shear stress is in the critical state; it was expressed as:

$$V_c = q / y_{Cont} \qquad (2.55)$$

where V_c is the critical velocity, q is the average unit discharge in the approach section, and y_{Cont} is the contraction scour flow depth. They transformed Neill's (1973) critical velocity curve, shown in Figure 2.4, in terms of median diameter of cohesionless soil

and water depth into a set of equations to calculate the clear-water contraction scour flow depth. The clear-water contraction scour flow depth is given in equation (2.56).
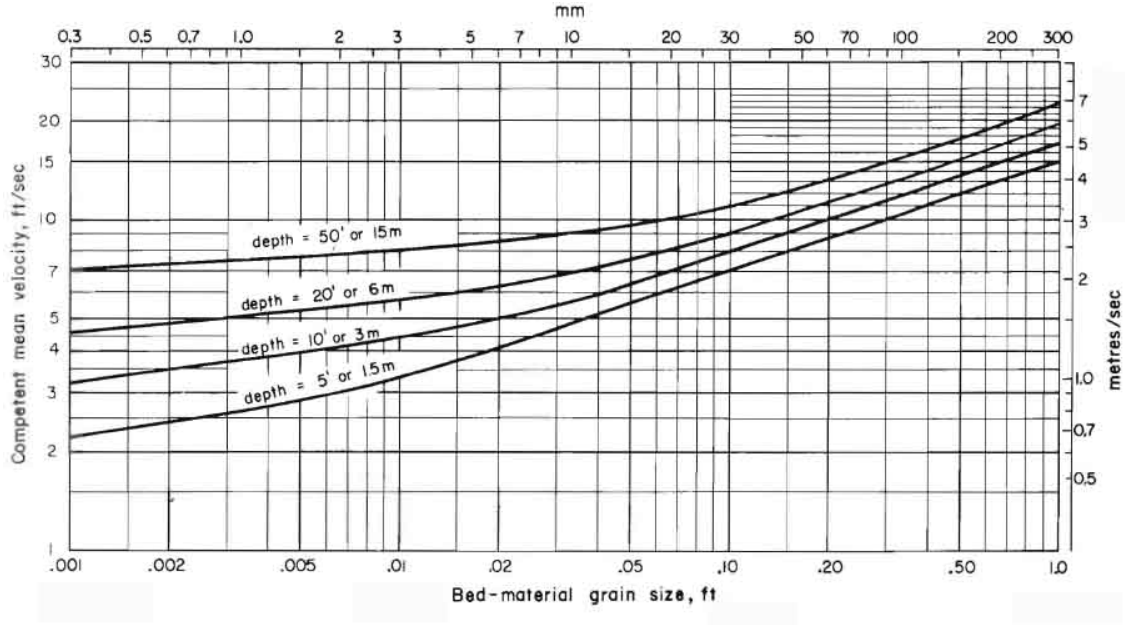
Figure 2.4. Neill's (1973) critical velocity curve in terms of median diameter of cohesionless soil and water depth

$$y_{Cont} = \left(\frac{q_1}{6.35 \cdot D_{50}^{1/3}} \right)^{0.86} \qquad \text{for } D_{50} \geq 0.03\text{m}$$

$$y_{Cont} = \left(\frac{q_1}{4.16 \cdot D_{50}^{1/4}} \right)^{1/(1+0.125/D_{50}^{0.18})} \qquad \text{for } 0.03\text{m} > D_{50} \geq 0.0003\text{m}$$

$$y_{Cont} = 1.49 \cdot q_1^{0.67} \qquad \text{for } 0.0003\text{m} > D_{50} \qquad (2.56)$$

where y_{Cont} is the contraction scour flow depth, q_1 the average unit discharge in the approach section, and D_{50} is the median diameter of sediment. They recommended the use of Laursen's (1960) equation for the calculation of the live-bed contraction scour flow depth. The clear-water contraction scour depth ($y_{s(Cont)}$) is obtained by subtracting

the initial flow depth at the contracted section from the contraction scour flow depth.

The abutment scour depth is always deeper than the contraction scour depth because of the high turbulence around the toe of the abutment. Chang and Davis (1999(a), 1999(b)) proposed an abutment scour equation for vertical wall abutments which uses the flow around the end of abutment:

$$y_{s(Abut)} = K_p \cdot K_f \cdot K_v^{0.857} \cdot y_{Cont} - y_0 \qquad (2.57)$$

where $y_{s(Abut)}$ is the maximum abutment scour depth, y_0 is the initial flow depth at contracted section, y_{Cont} is the contraction scour flow depth, K_p is the correction factor for pressure flow ($K_p = 0.66 Fr_1^{-0.45}$), K_f is the correction factor for spiral flow at the abutment toe ($K_f = 0.1 + 4.5 Fr_1$ for clear water scour and $K_f = 0.35 + 3.2 Fr_1$ for live-bed scour, and it should be between 1.0 and 3.2), and K_v is the ratio of velocity at the abutment toe to the mean velocity in the contracted section ($K_v = 0.8(q_1 / q_2)^{1.5} + 1$ with q_1 being the unit discharge in the approach section and q_2 the unit discharge in the bridge section) .

Subsequently, Chang and Davis studied the effect of abutment shape and presented the results in the Maryland SHA bridge scour program. In addition, the correction factor for spiral flow K_f was updated in the Maryland SHA bridge scour program version 8 (Chang and Davis, 2007), and it is $0.13 + 5.85 Fr_1$ for clear water scour and $0.46 + 4.16 Fr_1$ for live-bed scour in the range between 1.4 and 4.0.

The effect of abutment shape diminishes with an increase of abutment length; the effect becomes negligible if the length of the abutment is ten times greater than the horizontal distance between the toe of abutment and the end of wetted part of abutment at the upstream section. The correction factor for abutment shape is proposed as:

$$K_1 = 0.55 + 0.05(X_2 / X_1 - 1) \quad \text{for spill-through abutment}$$

$$K_1 = 0.82 + 0.02(X_2 / X_1 - 1) \quad \text{for wing-wall abutment}$$

$$K_1 = 1.0 \quad \text{if } K_1 > 1.0 \quad (2.58)$$

where X_1 is the horizontal distance between the toe of abutment and the end of the wetted part of the abutment at the upstream section and X_2 is the length of abutment as shown in Figure 2.5.
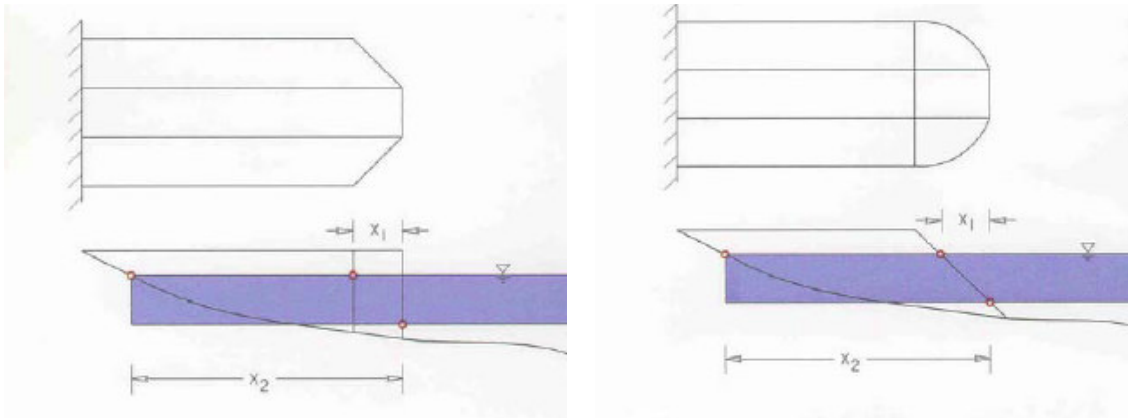
(a) Wing-wall abutment   (b) Spill-through abutment

Figure 2.5. Abutment shape factor measurement (Chang and Davis, 2007)

Finally the abutment scour equation is expressed as:

$$y_{s(Abut)} = K_1 \cdot K_2 \left(K_p \cdot K_f \cdot K_v^{0.857} \cdot y_{Cont} - y_0 \right) \quad (2.59)$$

where $y_{s(Abut)}$ is the maximum abutment scour depth, y_0 is the initial flow depth at

contracted section, y_{Cont} is the contraction scour flow depth, K_p is the correction factor

for pressure flow, K_f is the correction factor for spiral flow at the abutment toe, K_v is

the ratio of velocity at the abutment toe to the mean velocity in the contracted section ,

K_1 is the correction factor of abutment shape, and K_2 is the correction factor for

abutment alignment proposed by Froehlich (1989).

Ettema et al. (2008) categorized abutment scour into three conditions. In condition

A ($L' \geq 0.75 L_f$), the maximum local scour occurs in the main channel. In condition B

($L' < 0.75 L_f$), the maximum local scour occurs on the floodplain. In condition C, the

breach of embankment is fully developed and the abutment columns are exposed like a

bridge pier. The maximum local scour flow depths ($y_{Abut} = y_{s(Abut)} + y_{f1}$ in condition B,

$y_{Abut} = y_{s(Abut)} + y_{m1}$ in condition A) were compared to Laursen's long contraction scour

flow depths ($y_{Cont} = y_{s(Cont)} + y_{f1}$ in condition B, $y_{Cont} = y_{s(Cont)} + y_{m1}$ in condition A). The

scour condition A ($L' \geq 0.75 L_f$) and B ($L' < 0.75 L_f$) were classified as the ratio of the

length of embankment projected normal to the flow (L') to the width of floodplain (L_f),

as shown in Figure 2.6. The ratio (y_{Abut} / y_{cont}) was defined as an amplification factor:

α_A, α_B and α_C for the three scour conditions and discussed below.
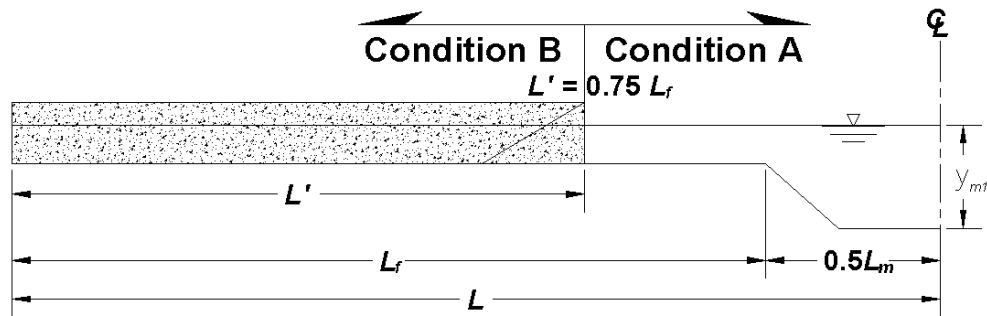
Figure 2.6. Boundary of scour condition A and B with the ratio of abutment length to the width of floodplain (Ettema et al., 2008)

Laursen's live bed contraction scour flow depth was used in condition A. Usually the floodplain is made of less erodible soils while the main channel is made with more erodible soils. Accordingly, live bed contraction scour occurs in the main channel and clear water scour occurs on the floodplain during a flood event. The amplification factor α_A depends on the unit discharge ratio and the abutment shape, as shown as Figure 2.7 (a). In the figure, q_1 is the average unit discharge at the approach section, q_2 is the average unit discharge at the bridge section, q_{f1} is the unit discharge in the floodplain at the approach section, and q_{f2} is the unit discharge in the floodplain at bridge section.

The maximum local scour occurs on the floodplain if the abutment has a long set back on the floodplain or exists in a rectangular channel (condition B). Laursen's clear water scour flow depth was used for condition B because scour on a floodplain is mainly clear water scour during a flood event. The amplification factor α_B displays a relative higher peak than that for condition A. The highest value occurs when the length of abutment is very short as shown as Figure 2.7 (b).

In condition C, embankments were built with the same material as for the channel bottom so the embankments are vulnerable to erosion. Laursen's clear water scour flow depth was used to compare with the maximum local scour flow depth. The amplification factor α_C is less than 1.0 since embankments failed before local scour is fully developed. The foundation of the abutment is exposed to the flow like a pier.

(a) Condition A   (b) Condition B
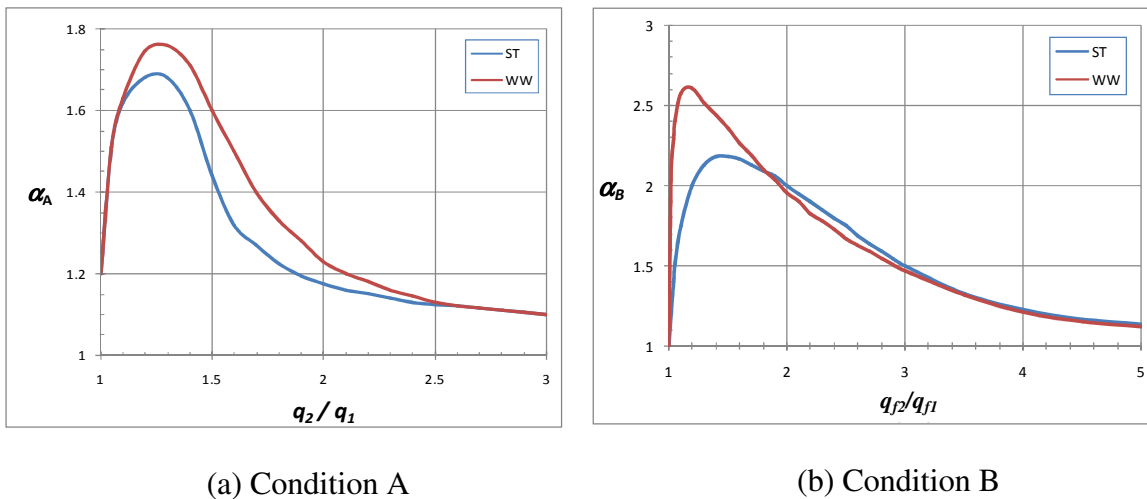
Figure 2.7. Scour amplification factor versus unit discharge ratio (replotted using data from Ettema et al., 2008)

2.4.2 Abutment scour in cohesive soil

Yakoub (1995) varied *WC* (initial water content), *CC* (clay content), *C* (the degree of compaction related to the optimum compaction) and *CT* (clay type) for a series of tests on abutment scour in cohesive material. He compared abutment scour depth in cohesive material with that in sand. He used a constant water depth and the same abutment to examine the effect of clay. A vertical abutment that is 0.116 m (0.38 ft) long and 0.219 m (0.72 ft) wide was used. The medium size and the geometric standard

deviation of the sand were 0.81 mm and 2.41, respectively. The experimental results in cohesive soil were directly compared with that in cohesionless soil with the same test condition. He found that the abutment scour depth in cohesive soil is related to *WC, CC, C*, and *CT* and can be expressed as:

2.4.2.1 Montmorillonite clay

(1) 100 % of Montmorillonite clay

For unsaturated soil

$$\frac{d_{sc}}{d_{ss}} = (2.186 - 5.342 \cdot WC) \cdot \left(15.407 - 52.202 \cdot C + 60.873 \cdot C^2 - 23.512 \cdot C^3\right) \quad (2.60)$$

For saturated soil

$$\frac{d_{sc}}{d_{ss}} = (4.76 - 45.1 \cdot WC + 136.1 \cdot WC^2 - 126 \cdot WC^3) \cdot \left(-0.339 + 1.744 \cdot C\right) \quad (2.61)$$

(2) Effect of clay content

$$\frac{d_{sc}}{d_{ss}} = 1.0 - 0.608 \cdot CC - 4.286 \cdot CC^2 + 10.159 \cdot CC^3 \quad (2.62)$$

where d_{sc} is the abutment scour depth in cohesive material, d_{ss} is the abutment scour depth in sand based on a 0.81 mm D_{50}, *WC* is the initial water content, *CC* is clay content, *C* is the degree of compaction related to the optimum compaction, and *CT* is clay type.

2.4.2.2 Kaolinite clay

(1) 30 % of Kaolinite clay

The degree of compaction has no effect on the scour depth at the sandy soil with a 30% mixture of Kaolinite clay. The effect of initial water content was also found negligible.

(2) Effect of clay content

$$\frac{d_{sc}}{d_{ss}} = 0.988 - 2.788 \cdot CC - 52.56 \cdot CC^2 + 110 \cdot CC^3 \tag{2.63}$$

where d_{sc} is the abutment scour depth in cohesive material, d_{ss} is the abutment scour depth in sand based on a 0.81 mm D_{50}, and CC is clay content.

2.5 SRICOS-EFA method

Since cohesive soils are much more slowly eroded than cohesionless soils, it needs to include the scour rate in the calculations. The SRICOS-EFA (Scour Rate In Cohesive Soils – Erosion Function Apparatus) method (Briaud et al., 1999(a)) was developed to consider the erosion rate for the scour depth prediction.

2.5.1 Procedure of SRICOS-EFA method

The time to reach the maximum scour depth in cohesive soils is much longer than the duration of flood. Thus the time effect should be considered to predict the scour depth. The SRICOS method was proposed in 1999 to predict the single cylindrical pier scour depth with consideration of time. The procedure of SRICOS method (Briaud et al., 1999(a)) is:

1. Collecting Shelby tube samples near the bridge pier,

2. Testing them in the EFA (Erosion Function Apparatus, Briaud et al. 1999(a)) to obtain the erosion rate $\dot{z}$ (mm/hr) versus hydraulic shear stress τ (N/m²) curve,

3. Calculating the maximum hydraulic shear stress τ_{max} around the pier before scour starts,

4. Reading the initial erosion rate $\dot{z}_i$ (mm/hr) corresponding to τ_{max} on the $\dot{z}$ vs. τ curve,

5. Calculating the maximum depth of scour y_s,

6. Constructing the scour depth $y_s(t)$ versus time t curve using a hyperbolic model,

7. Reading the scour depth corresponding to the duration of the flood on the scour depth $y_s(t)$ vs. time t curve.

The hyperbolic model describing the shape of scour depth $y_s(t)$ vs. t curve is:

$$y_s(t) = \frac{t}{\dfrac{1}{\dot{z}_i} + \dfrac{t}{y_s}}$$ (2.64)

The SRICOS-EFA was developed to predict the single cylindrical pier scour, and this method was extended to the complex pier scour, contraction scour and abutment scour.

2.5.2 Maximum shear stress

In order to read the initial erosion rate $\dot{z}_i$ (mm/hr) on the $\dot{z}$ vs. τ curve, the maximum shear stress τ_{max} should be calculated. Since Wei (1997) constructed the maximum shear stress equation for single cylindrical pier, three maximum shear stress equations for different bridge structure have been developed by Nurtjahyo (2003) and

Chen (2008). Maximum shear stress equations after Wei (1997) are summarized in following:

2.5.2.1 Maximum shear stress for single cylindrical pier

Wei (1997) studied the maximum bed shear stress around circular pier on constant depth cannel with 3D simulation. The maximum bed shear stress equation is proposed based on pier Reynolds number rather than the commonly used approach bed shear stress in open channel flow. The maximum bed shear stress is also found independent of water depth when the upstream flow is deeper than twice of the pier diameter.

$$\tau_{max} = 0.094 \rho V^2 \left[\frac{1}{\log \text{Re}} - \frac{1}{10} \right] \tag{2.65}$$

where ρ is the density of water (kg/m^3), V_1 is the approach velocity (m/sec), $\text{Re}(=V_1 a / v)$ is the Reynolds number

2.5.2.2 Maximum shear stress for complex pier

Nurtjahyo (2003) further extended Wei's equation to the complex pier conditions, including the effect of water depth k_w, the effect of pier spacing k_{sp}, the effect of shape k_{sh}, and the effect of attack angle k_θ.

$$\tau_{max(pier)} = k_w k_{sh} k_{sp} k_\theta \cdot 0.094 \rho V_1^2 \left[\frac{1}{\log \text{Re}} - \frac{1}{10} \right] \tag{2.66}$$

where ρ is the density of water (kg/m^3), V_1 is the approach velocity (m/sec), θ is the attack angle (in degree), S is spacing between adjacent two piers (measured center to center), a is width of pier, L is length of pier, y_1 is approach water depth, $\text{Re}(=V_1 a / v)$

is the Reynolds number, k_w the correction factor for the water depth effect, k_{sh} is the correction factor for the pier shape, k_θ is the correction factor for the attack angle effect, and k_{sp} is the correction factor for the pier spacing

$$k_w = 1 + 16\exp(-4y/a)$$

$$k_{sh} = 1.15 + 7\exp(-4L/a)$$

$$k_\theta = 1 + 1.5\left(\theta\middle/90\right)^{0.57}$$

$$k_{sp} = 1 + 5\exp(-1.1S/a)$$

2.5.2.3 Maximum shear stress for contraction scour

Nurtjahyo (2003) numerically studied the maximum bed shear stress at the center of the channel under long contraction. The equation is generated by correcting the open channel flow equation including several correction factors for channel geometry and water depth effect.

$$\tau_{\max(Cont)} = k_R k_{Wa} k_\alpha k_w \rho g n^2 V_1^2 R_h^{-\frac{1}{3}} \tag{2.67}$$

where ρ is the density of water (kg/m^3), V_1 is the approach velocity (m/sec), g is the gravitational acceleration, n is Manning's coefficient, R_h is the hydraulic radius, α is the transition angle (in degree), W_a is the top width of the abutment, L_1 is the channel width at approach section, L_2 is the channel width at bridge section, k_R is the correction factor for the contraction ratio, k_α is the correction factor for the transition angle, k_{wa} is the correction factor for the contraction length, and k_w is the correction factor for the water

depth

$$k_R = 0.62 + 0.38 \left(\frac{L_1}{L_2} \right)^{1.75},$$

$$k_\alpha = 1.0 + 0.9 \left(\frac{\alpha}{90} \right)^{1.5},$$

$$k_{wa} = \begin{bmatrix} 0.77 + 1.36 \left(\frac{W_a}{(L_1 - L_2)} \right) - 1.98 \left(\frac{W_a}{(L_1 - L_2)} \right)^2, & for \ \frac{W_a}{(L_1 - L_2)} \leq 0.35 \\ 1.0 & , \quad for \quad otherwise \end{bmatrix}$$

$$k_w = 1.0$$

2.5.2.4 Maximum shear stress for abutment scour

Chen (2008) numerically studied the maximum bed shear stress around the toe of abutment considering Froude number effect, aspect ratio effect, abutment shape effect, abutment alignment effect, and overtopping flow effect. The maximum shear stress equation around abutment is:

$$\tau_{\max(Abut)} = 12.45 k_{Cr} k_{sh} k_{Fr} k_s k_{sk} k_L k_o \rho V_1^2 \, \text{Re}^{-0.45} \tag{2.68}$$

where ρ is the density of water (kg/m^3), V_1 is the approach velocity (m/sec), $\text{Re} (= V_1 W_a / \nu)$ is the Reynolds number defined with top width of the abutment, q_1 is the unit discharge at approach section, q_2 is the unit discharge at bridge section, d_1 is the distance from the water surface to the low chord of the bridge at upstream face of the bridge, d_{deck} is the thickness of the bridge deck, k_{sh} is the correction factor for the aspect ratio of the approach embankment, k_{Fr} is the correction factor for Froude number, k_s is the correction factor for abutment shape, k_{sk} is the correction factor for abutment

alignment, k_o is the correction factor for overtopping

$$k_c = 3.65\frac{q_2}{q_1} - 2.91$$

$$k_{sh} = 0.85 \times \left(\frac{L'}{W_a}\right)^{-0.24}$$

$$k_{Fr} = \begin{cases} 2.07\,Fr + 0.8 & Fr > 0.1 \\ 1.0 & Fr \leq 0.1 \end{cases}$$

$$k_{sk} = 1.0$$

$$k_s = \begin{cases} 1.0 & \text{vertical-wall abutment} \\ 0.65 & \text{wing-wall abutment} \\ 0.58 & \text{spill-through abutment} \end{cases}$$

$$k_L = \begin{cases} 1.0 & \text{for } \left(L_f - L'\right)/y_f \leq -2 \\ 0.6(L_f - L')/y_f + 1.2 & \text{for } -2 < (L_f - L')/y_f \leq 0 \\ -1.2(L_f - L')/y_f + 1.2 & \text{for } 0 < (L_f - L')/y_f \leq 1 \\ 1.0 & \text{for } 1 \leq (L_f - L')/y_f \end{cases}$$

$$k_o = \begin{cases} 0.92 \cdot \left(d_1/d_{deck}\right) + 1.0 & \text{for } d_1/d_{deck} < 1.0 \\ 0.21\left(d_1/d_{deck}\right)^2 - 1.27\left(d_1/d_{deck}\right) + 2.97 & \text{for } 1.0 \leq d_1/d_{deck} \leq 3.0 \\ 1.0 & \text{for } 3.0 < d_1/d_{deck} \end{cases}$$

CHAPTER III

FLUME TEST SETUP

3.1 Introduction

Gudavalli (1997) used two different flumes located in the Hydromechanics Laboratory at Texas A&M University for singular circular pier scour tests in deep water condition. One is a 0.45 m wide variable slope flume, and the other is a 1.5 m wide concrete flume. Li (2002) used same flumes which Gudavalli used in 1997. Li used a 0.45 m flume for the contraction scour tests in the rectangular channel, and a 1.5 m wide concrete flume for the complex pier scour. Another concrete flume which is 3.6 m wide is used for the abutment scour and the contraction scour located in the Haynes Coastal Laboratory at Texas A&M University. The details of test setup, equipment and test results are described in the following.

3.2 Experiment setup

3.2.1 Flume

Three different flumes have been used for scour experiments in Texas A&M University since 1997. One is a variable flume, which is 0.45 m wide, 36 m long, and 1. 2 m deep with plexiglass side wall. The second flume is a concrete flume, which is 1.52 m wide, 30.48 m long, and 3.48 m deep. Gudavlli (1997) used both flumes for singular pier scour while Li (2002) used the first flume for the contraction scour in the rectangular channel and the second flume for the complex pier scour. A false bottom

made of plywood was installed in the flume. The details of two flumes were described in Gudavalli (1997) and Li (2002).

A concrete flume that is 45.7 m in length, 3.6 m in width and 3.4 m in depth was used to conduct the abutment scour tests. A sediment pit is located around the middle of the flume that has dimensions of 7.5 m in length, 3.7 m in width and 1.5 m in depth. Four recirculation pumps with a combined capacity of 2.21 m^3/s were used to generate the needed flow. A flow straightener was installed at the outlet of recirculation pumps to decrease the magnitude of flow irregularity. The water depth and velocity were controlled by varying the height of a tailgate and the output of the pumps since the slope of the flume is fixed. A false bottom was built and installed to form a compound channel. Figure 3.1 depicts the setup in the flume. Only one half of the channel was modeled in the tests to maximize the scale of the experiments.

Two types of channel were used in the experiments. One is a rectangular channel with a long setback abutment while the other is a compound channel with a short setback. Figure 3.2 shows the cross sectional view of the rectangular channel and compound channel. The rectangular channel was used directly without the installation of a false bottom, while a false bottom was used to induce a smooth flow to the test section and to form the compound channel. The width of floodplain (L_f) was fixed at L_f = 2.4 m for the compound channel, and the false bottom was installed at approach section and downstream section of the abutment. The upstream part is 18.3 m long and 2.4 m wide and the downstream part is 9 m long and 2.4 m wide.

Plane View of Flume

Scour Measurement Section

Rail

Main Channel Slope

Main Channel

Flow Straightener

False Bottom

Rail

Abutment

Flood plain

False Bottom

Collection Tank

Ramp

Ramp

Side View of Flume

Clay

Sand

Tail Gate

Sump

Water Pump
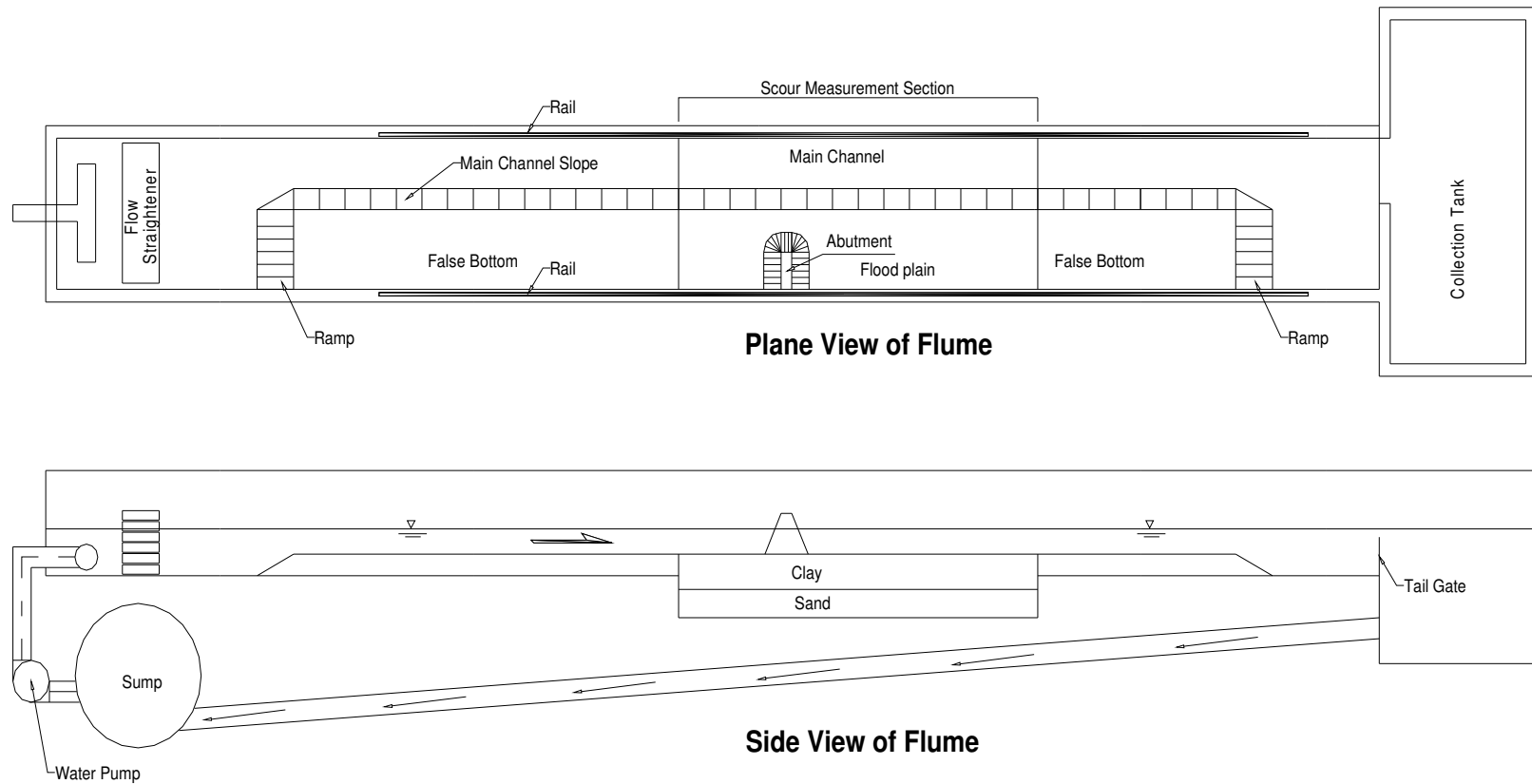
Figure 3.1. Sketch of the flume and experimental setup in Haynes Coastal Laboratory at Texas A&M University (not to scale)

(a)Rectangular Channel

(b)Compound Channel
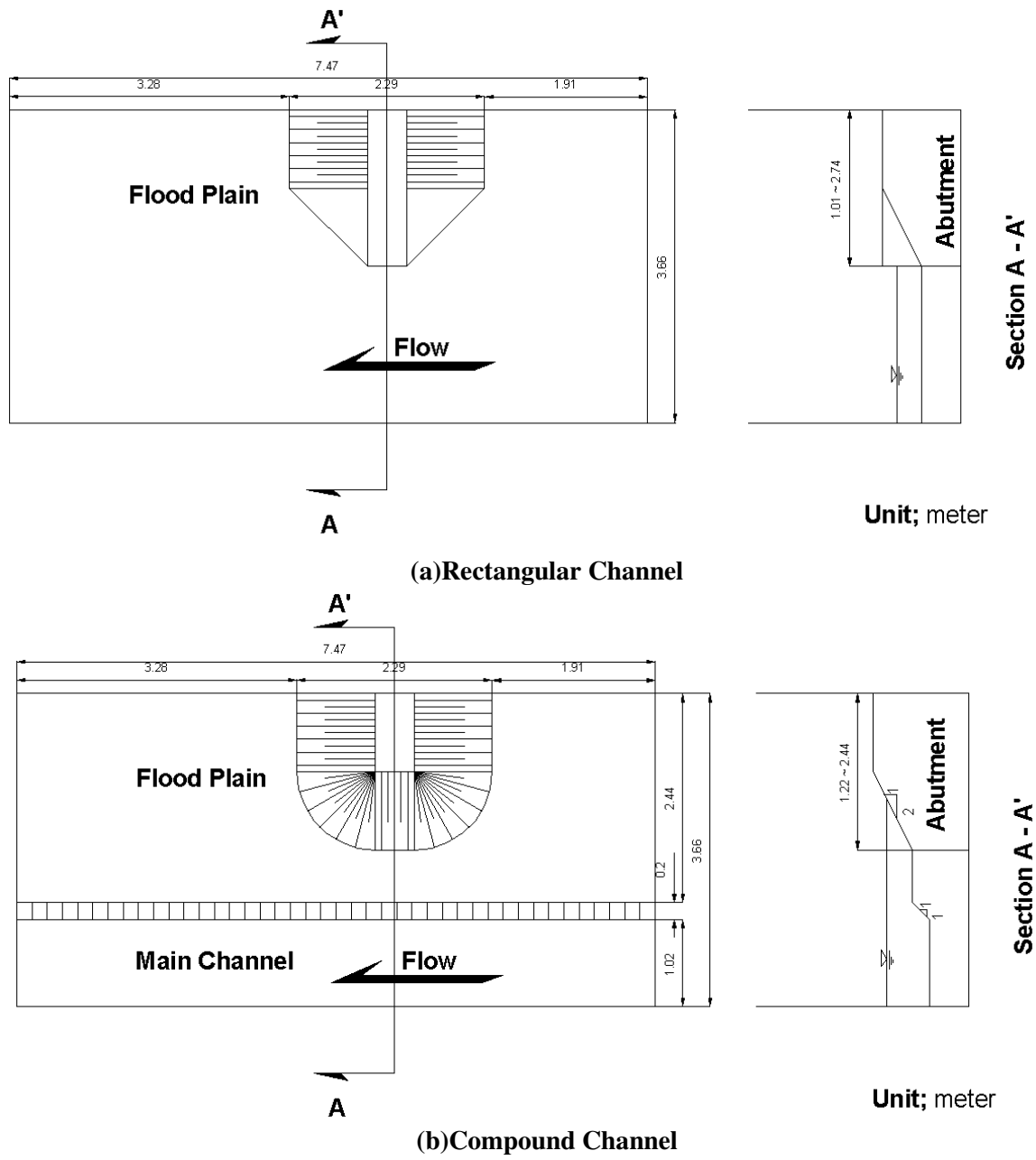
Figure 3.2. Channel configurations for the abutment scour

58

3.2.2 Bridge structure

Gudavalli (1997) used circular piers made of plexiglass. Four piers with 25 mm, 75 mm, 150 mm and 210 mm diameter were used. Li (2002) used circular piers made of PVC pipes for shallow water effect and pier spacing effect, and rectangular piers for pier shape effect and attack angle effect.

Three circular piers with 61 mm, 160 mm and 273 mm diameter, and four rectangular piers with 61 X 61 mm, 61 X 244 mm, 61 X 488 mm and 61 X 732 mm were used. Three types of contraction ratio – L_2/L_1 = 0.25, 0.5 and 0.75 - were made by blocking the flume with wooden structures. The length of contraction and the transition angle were changed to find the effect of those two parameters. The details of pier scour and contraction scour in the rectangular channel can be found in Gudavalli (1997) and Li (2002).

Three types of abutment made of plywood were used in the flume tests for the abutment scour: the first one is of a wing wall shape, the second one is of a spill-through shape with a 2(H):1(V) slope, and the third one is of a spill-through shape with a 3(H):1(V) slope. They are shown in Figure 3.3. The projected length of abutment (*L'*) was adjusted by changing the length of the embankment.

(a) Wing-Wall	(b) Spill-Through	(c) Spill-Through
	(2(H):1(V))	(3 (H): 1(V))
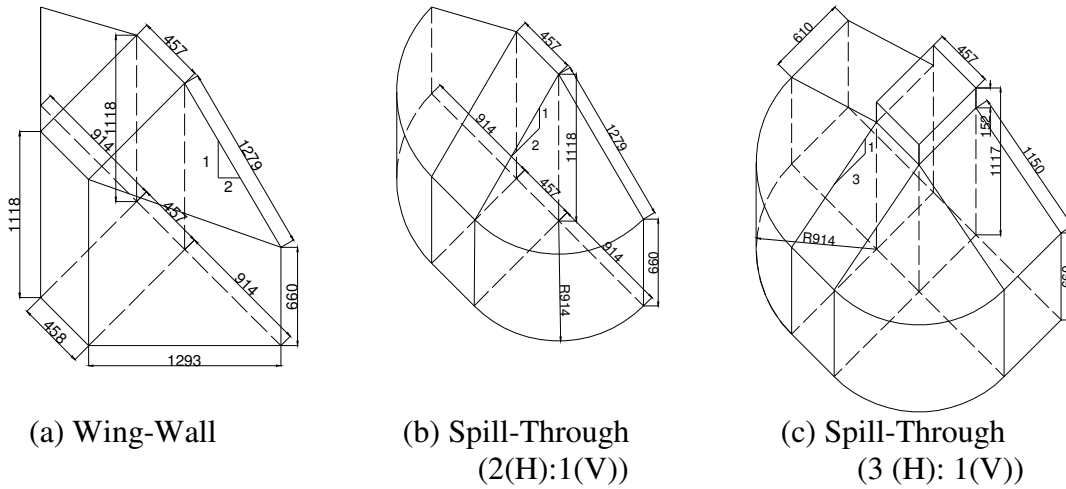
Figure 3.3. Abutment shapes (all dimensions are in mm)

3.2.3 Soils and channel bottom preparation

1. Soils

Five types of soil – 2 types of sand, Porcelain clay, Bentonite and Armstone - were used in Gudavalli (1997). Porcelain clay was used in Li (2002) and present study. The Porcelain clay, Bentonite and Armstone used in the tests were prepared by a supplier. The mineral content, compaction degree, and water content were maintained in the clay. The clay was delivered in individual blocks of 150 mm x 150 mm x 230 mm in size. Each block was sealed in a plastic bag to minimize the change of water content.

Geotechnical tests were conducted according to ASTM (American Society for Testing and Materials) standards. The properties of soil are given in from Table 3.1 to Table 3.3. The grain size distribution of sand used by Gudavalli is shown in Figure 3.4 and of Porcelain clay used in Li (2002) and the study on abutment scour is shown in Figure 3.5.

The erosion properties of the Porcelain clay were obtained by EFA tests (Briaud et al., 2001(a)). After 2 EFA tests in Li (2002) and 11 EFA (Erosion Function Apparatus) tests for the study on the abutment scour, the results of the EFA tests obtained by Li and late 11 tests are given in Figure 3.6 and Figure 3.7, respectively. Based on the tests, the critical shear stress of the Porcelain clay is 0.7 Pa in Li (2002) and 0.8 Pa in the recent tests.

Table 3.1. Geotechnical properties of soils used by Gudavalli (1997)

	Sand A	Sand B	Porcelain clay	Armstone clay	Bentonite clay
D_{50} (mm)	0.6	0.14	-	-	-
Plasticity Index (%)	-	-	14.15	25.81	39.78
Clay content (%)	0	0	100	75	0
Water content (%)	-	-	28.51	26.18	39.28
τ_c (Pa)	0.456	0.107	0.515	0.761	0.7

Table 3.2. Geotechnical properties of Porcelain clay used by Li (2002)

Property	Test 1	Test 2
Liquid Limit (LL) (%)	40.23	37.7
Plastic Limit (PL) (%)	19.17	14.4
Plasticity Index (PI) (%)	21.06	23.3
Water Content (%)	27.35	30.5
Bulk Unit Weight (kN/m^3)	19.65	24.99
Undrained Shear Stress (kPa)	10.7	18.1

Table 3.3. Geotechnical properties of the Porcelain clay used in the study on abutment scour

Property	Test 1	Test 2	Test 3	Test 4
Liquid Limit (LL) (%)	30.9	29.8	31.5	30.7
Plastic Limit (PL) (%)	16.9	17.2	16.0	16.3
Plasticity Index (PI) (%)	14.0	12.6	15.5	14.4
Water Content (%)	25.5	23.25	26.75	24.35
Undrained Shear Stress (kPa)	19.5	21.3	20.7	23.4
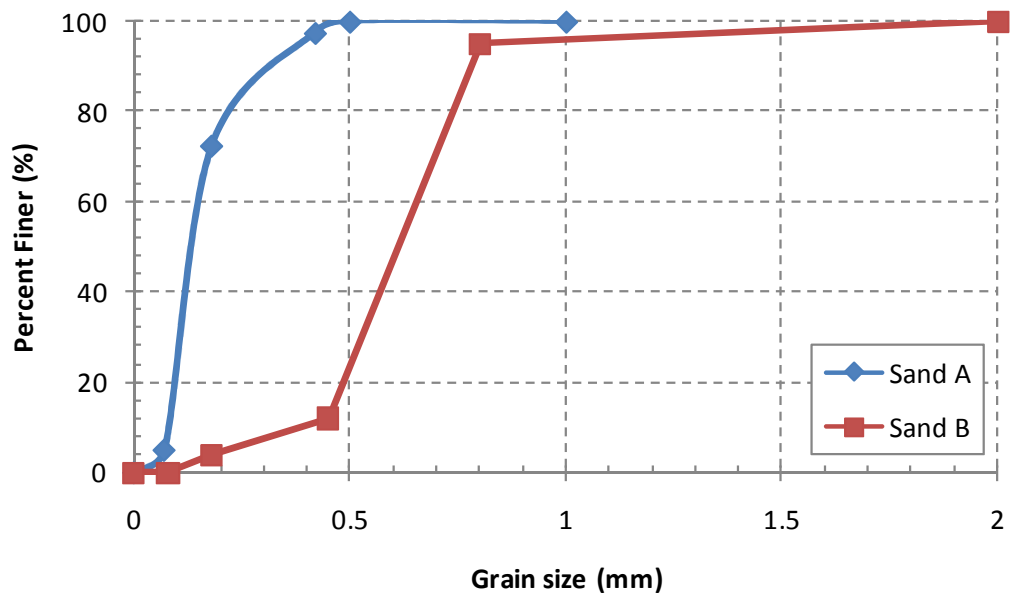
Figure 3.4. Grain size distribution of Sand A and B
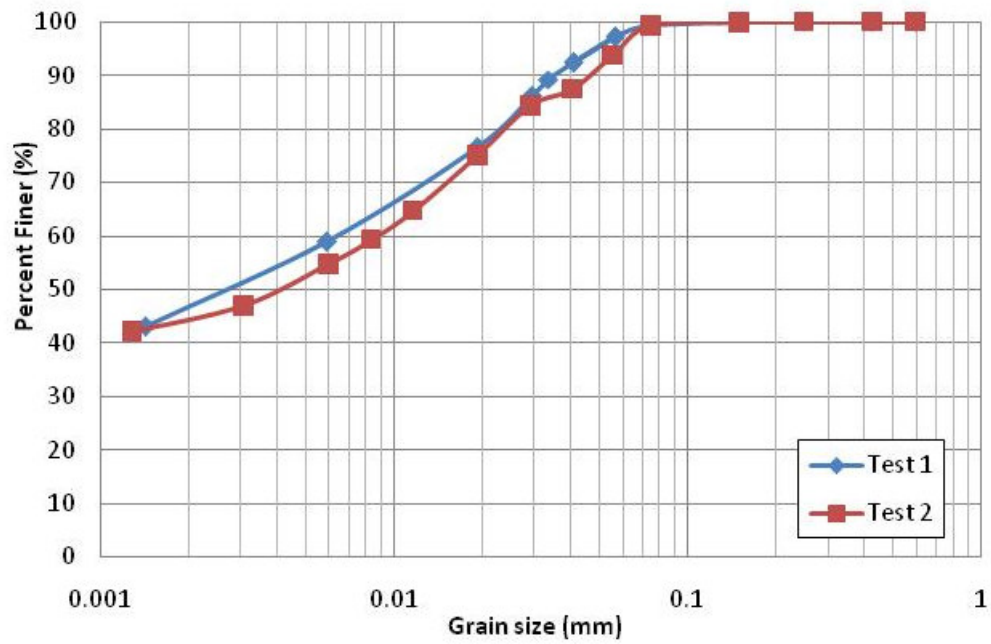
Figure 3.5. Grain size distribution of Porcelain clay
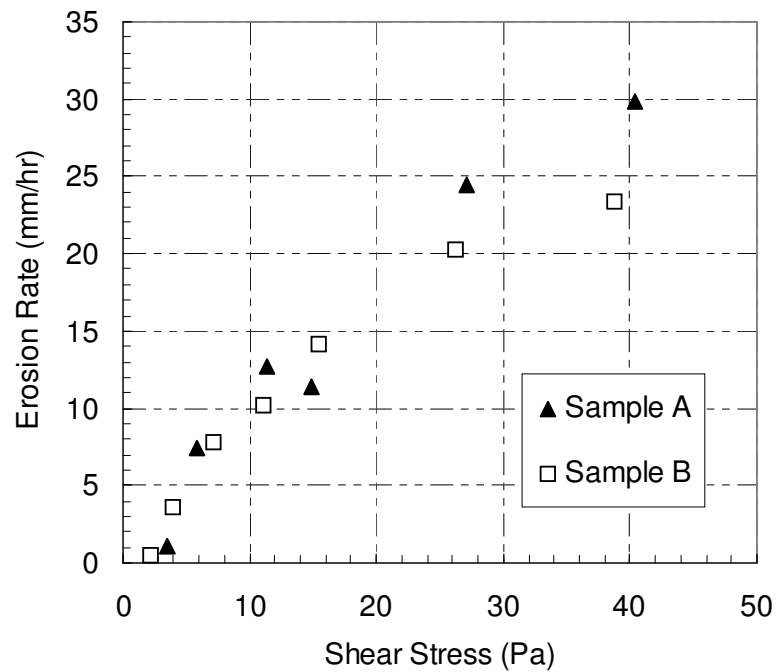
Figure 3.6. Erosion function curves for Porcelain Clay in Li (2002)
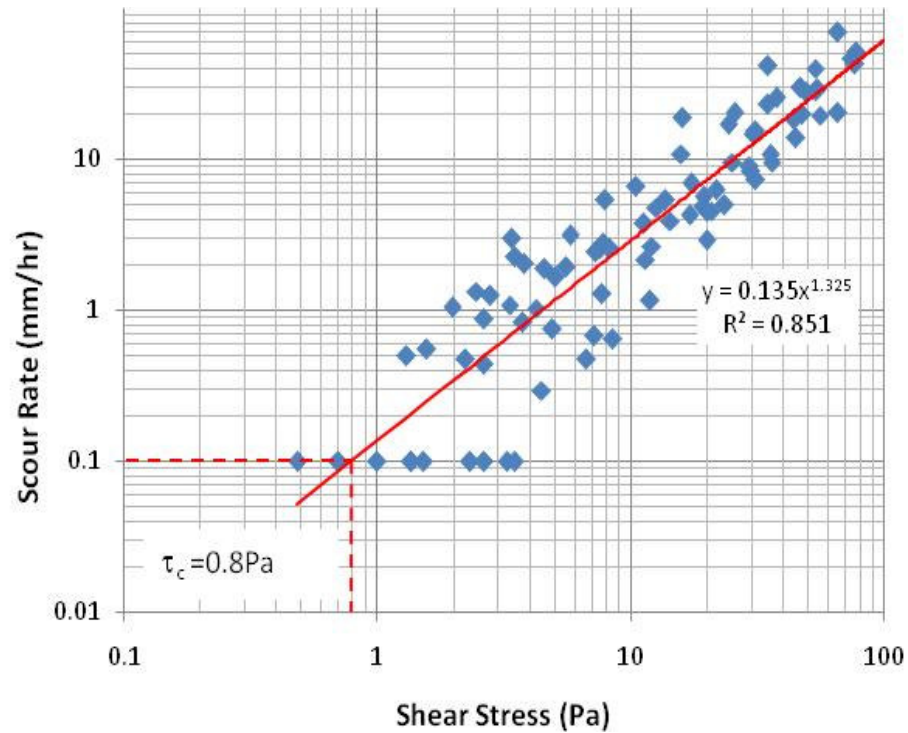
Figure 3.7. Results of 11 EFA tests

2. Channel bottom preparation

For the flume tests, the clay was installed block by block in the sediment pit and compacted with a 254 mm X 254 mm tamper to minimize voids and gaps between the clay blocks. Clay installation and compaction was repeated until the elevation of the clay surface was leveled with the channel bottom. The soil surface was then leveled and smoothened by using trowels. Figure 3.8 shows the clay installation, and Figure 3.9 shows the test section after clay installation for the rectangular channel and the compound channel. After each test, the excessive water was pumped out of the test section, the layer of clay around the scour holes was removed until undisturbed clay was reached, and new clay was used to replace the excavated clay.

(a) Clay compaction

(b) Plaster work

Figure 3.8. Clay installation

(a) Rectangular channel

(b) Compound channel

Figure 3.9. Test area for abutment scour after clay installation

3.2.4 Measurement equipment for the study on the abutment scour

Two side looking three-dimensional ADVs (Acoustic Doppler Velocimetry) were used for point velocity measurements in the study on the abutment scour. One ADV made by Nortek was capable of measuring velocities from 1 mm/s to 4 m/s with a 0.5% error of the measured value. The other ADV made by Sontek was capable of measuring velocity up to 2.5 m/s with a 1% error of the measured value. The sampling rate of the two ADVs was kept constant at 25 Hz. The depth-averaged velocities were approximated by taking measurements at the 60% water depth from the free surface according to open-channel theory. At each point the velocity was averaged over data taken 60 seconds or longer. The velocity measurement was performed to obtain the discharge and velocity pattern from the approach section to the downstream side. The locations of velocity measurement varied with the test condition. Figure 3.10 shows the view of AVD probes used in flume tests. Figure 3.11 shows typical locations of velocity measurement in the tests.

A point gauge was used to measure the water depth and the maximum scour depth. The point gauge is designed based on the differences in electrical conductivity between two different materials: between clay and water and between water and air. The accuracy of the point gauge is 0.1 mm. Figure 3.12 shows the typical locations of water depth measurements in the tests.

A bed profiler was used to scan the channel bottom topography. It was necessary to use a profiler because the flow was very muddy during the tests, and it is impossible to find the location of the deepest scour hole and the pattern of scour without using the

profiler. The profiler consists of 23 sets of pipes. Each set consists of two plastic pipes with a different diameter and length. The bigger and shorter pipes guide the smaller and longer pipes to move only vertically. A ruler is attached to each of the smaller pipes. Each of the 23 sets measures the bed elevation at a given point. There is a 150 mm interval between two adjacent points. The accuracy of the measured profile is 3 mm. The point gauge was used to measure the maximum scour depth after finding the location of maximum scour using the bed profiler. Figure 3.13 shows eleven bed profilers among the twenty-three bed profilers. Figure 3.14 shows typical points of scour measurement using the bed profiler in the experiments.

The ADVs, bed profiler, and point gauge were mounted on the carriage which is allowed to move forward and backward. Figure 3.15 shows the view of carriage and measurement scene.

(a) Nortek side-looking 3D AVD   (b) Sontek side-looking 3D ADV

Figure 3.10. View of ADVs
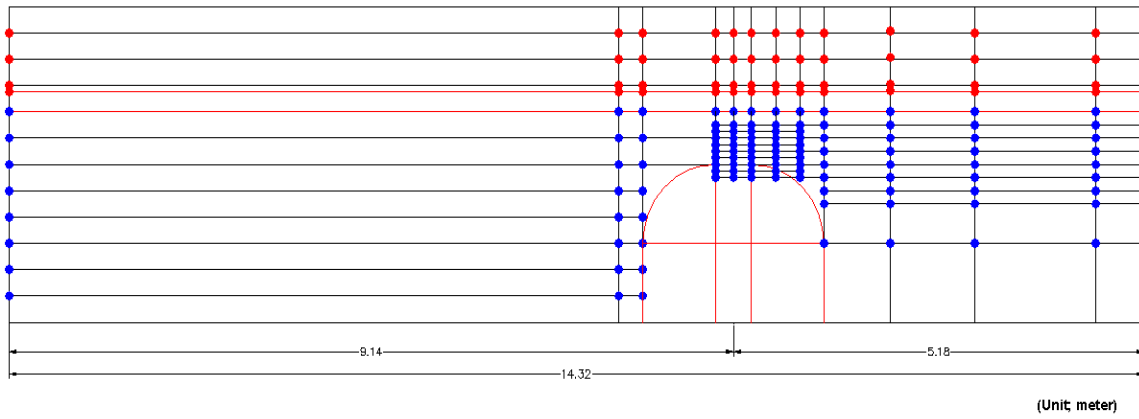
Figure 3.11. Velocity measurement points
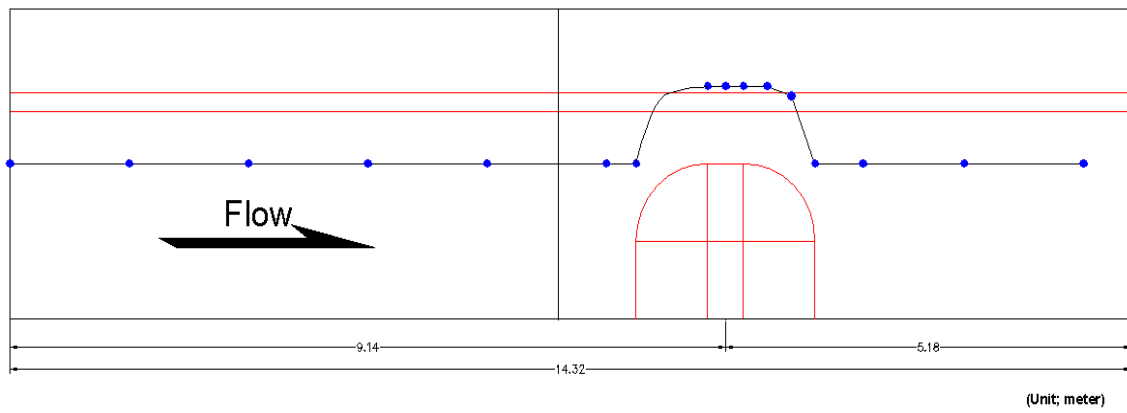
Figure 3.12. Water depth measurement positions
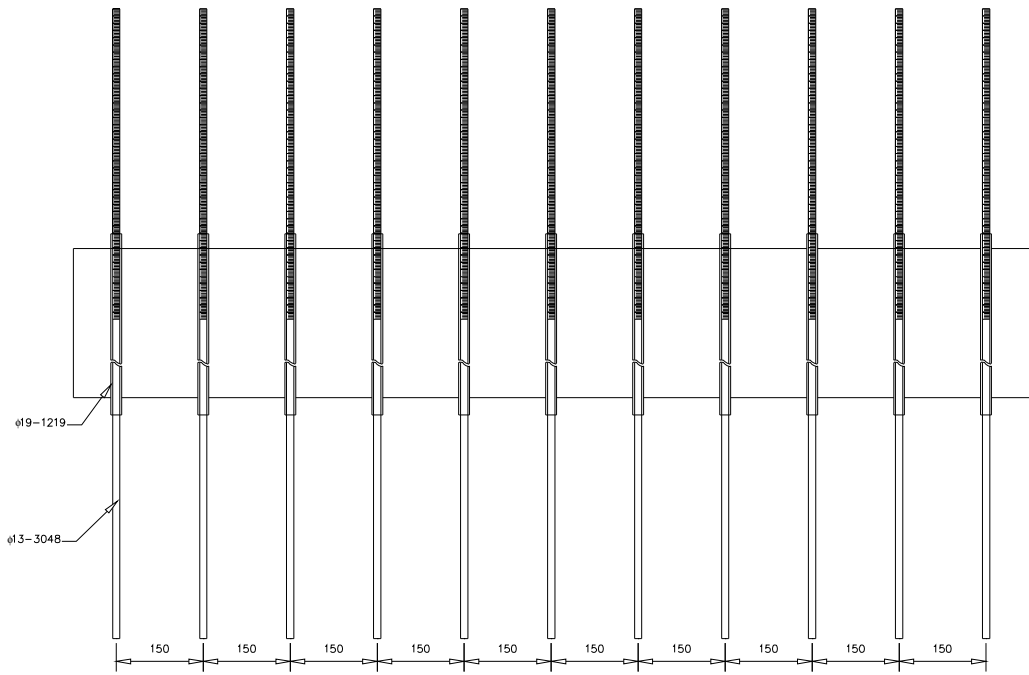
Figure 3.13. Diagram of bed profiler (unit: mm)
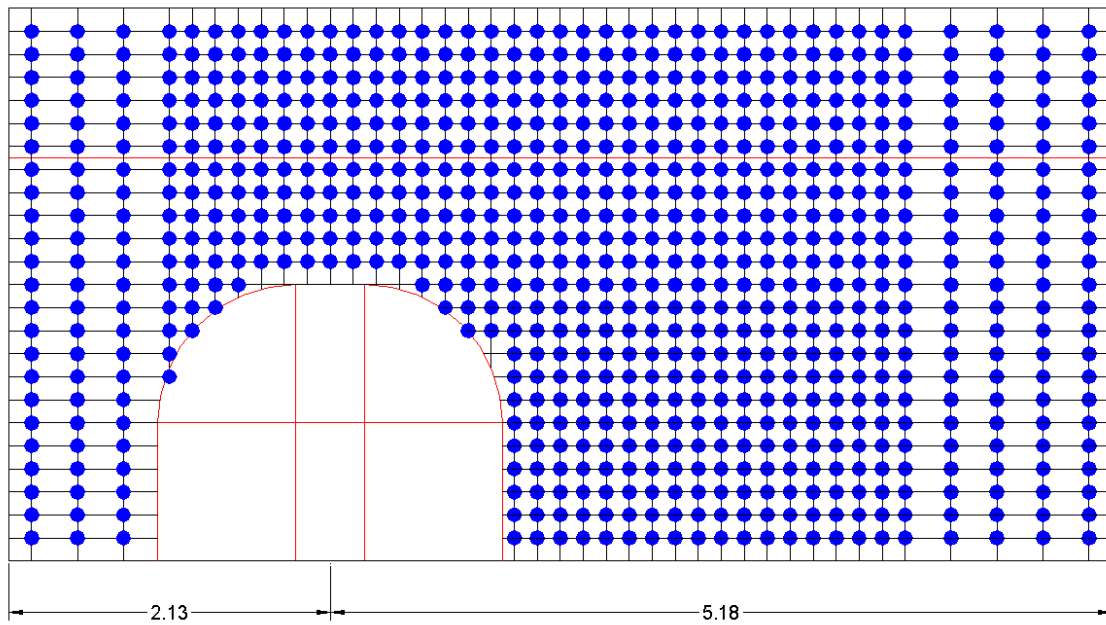
(Unit; meter)

Figure 3.14. Points of scour measurement using the bed profiler

Figure 3.15. View of carriage and measurement scene

CHAPTER IV

FLUME TEST AND MEASUREMENT RESULTS

4.1   Flume test and measurement results for abutment scour

The flume test results for abutment scour are induced in this chapter. The pattern of velocity, the water depth change and the evolution of channel bed are measured. Both the maximum abutment scour and the maximum contraction scour of each test are calculated on the basis of the hyperbolic model. The pattern of velocity and the scour pattern are compared to find the main cause of abutment scour and contraction scour.

4.1.1   Flume test condition

The test matrix for the abutment scour experiments is shown in Table 4.1 and Table 4.2 in dimensionless form and dimensional form, respectively. The definition of variables is illustrated in Figure 4.1. There are 17 experiments in the test matrix plus 2 additional experiments which are case 12B and case 1II. The test condition of case 12B is identical to that of case 12 except the velocity and Froude number. The velocity and Froude number in case 12B at the approach section are 0.635 m/s and 0.31, respectively. Case 1II was performed as a repeatability test; the test condition is identical to that of case 1. In Table 4.1, each dimensionless parameter was varied in the compound channel condition to examine the effect of the parameter. The cases with an even number have a lower value, while the cases with an odd number have a higher value in terms of the dimensionless parameter if compared with case 1.

Table 4.1. Test matrix in dimensionless form

	Case	y_{f1}/L'	F_r	L'/L	$tan(\beta_a)$	$\Theta\,(^o)$
Compound Channel	1	0.16	0.23	0.5	0.5	90
	2	0.1	0.23	0.5	0.5	90
	3	0.22	0.23	0.5	0.5	90
	4	0.16	0.18	0.5	0.5	90
	5	0.16	0.28	0.5	0.5	90
	6	0.16	0.23	0.333	0.5	90
	7	0.16	0.23	0.667	0.5	90
	8	0.16	0.23	0.5	0.3	90
	9	0.16	0.23	0.5	vertical	90
	10	0.16	0.23	0.5	0.5	60
	11	0.16	0.23	0.5	0.5	120
	12	0.16	0.18	0.5	vertical	90
Rectangular Channel	13	0.36	0.18	0.28	vertical	90
	14	0.23	0.18	0.44	vertical	90
	15	0.16	0.18	0.61	vertical	90
	16	0.13	0.18	0.75	vertical	90
	17	0.28	0.18	0.36	vertical	90

Table 4.2. Test conditions in dimensional form

Test No.	Abutment Shape	Channel Type	V_1 (m/s)	y_{f1} (m)	y_{m1} (m)	L (m)	L_f (m)	L' (m)	θ $(^o)$	$tan(\beta_a)$	$0.5Q_{total}$ (m³/s)
Case1	ST (2:1)	Comp.	0.464	0.291	0.494	3.658	2.438	1.829	90	0.5	0.573
Case 1II	ST (2:1)	Comp.	0.456	0.294	0.497	3.658	2.438	1.829	90	0.5	0.562
Case2	ST (2:1)	Comp.	0.377	0.184	0.387	3.658	2.438	1.829	90	0.5	0.320
Case3	ST (2:1)	Comp.	0.496	0.400	0.604	3.658	2.438	1.829	90	0.5	0.813
Case4	ST (2:1)	Comp.	0.358	0.278	0.482	3.658	2.438	1.829	90	0.5	0.442
Case5	ST (2:1)	Comp.	0.546	0.294	0.497	3.658	2.438	1.829	90	0.5	0.662
Case6	ST (2:1)	Comp.	0.432	0.294	0.497	3.658	2.438	1.219	90	0.5	0.561
Case7	ST (2:1)	Comp.	0.472	0.291	0.494	3.658	2.438	2.438	90	0.5	0.564
Case8	ST (3:1)	Comp.	0.456	0.291	0.494	3.658	2.438	1.829	90	0.33	0.570
Case9	WW	Comp.	0.453	0.294	0.497	3.658	2.438	1.829	90	vertical	0.568
Case10	ST (2:1)	Comp.	0.458	0.291	0.494	3.658	2.438	1.829	60	0.5	0.554
Case11	ST (2:1)	Comp.	0.457	0.291	0.494	3.658	2.438	1.829	120	0.5	0.565
Case12	WW	Comp.	0.347	0.294	0.497	3.658	2.438	1.829	90	vertical	0.433
Case12B	WW	Comp.	0.635	0.294	0.497	3.658	2.438	1.829	90	vertical	0.759
Case13	WW	Rect.	0.328	0.366	0.366	3.658	3.658	1.015	90	vertical	0.430
Case14	WW	Rect.	0.326	0.372	0.372	3.658	3.658	1.625	90	vertical	0.433
Case15	WW	Rect.	0.310	0.384	0.384	3.658	3.658	2.234	90	vertical	0.416
Case16	WW	Rect.	0.233	0.347	0.347	3.658	3.658	2.743	90	vertical	0.285
Case17	WW	Rect.	0.364	0.360	0.360	3.658	3.658	1.320	90	vertical	0.485
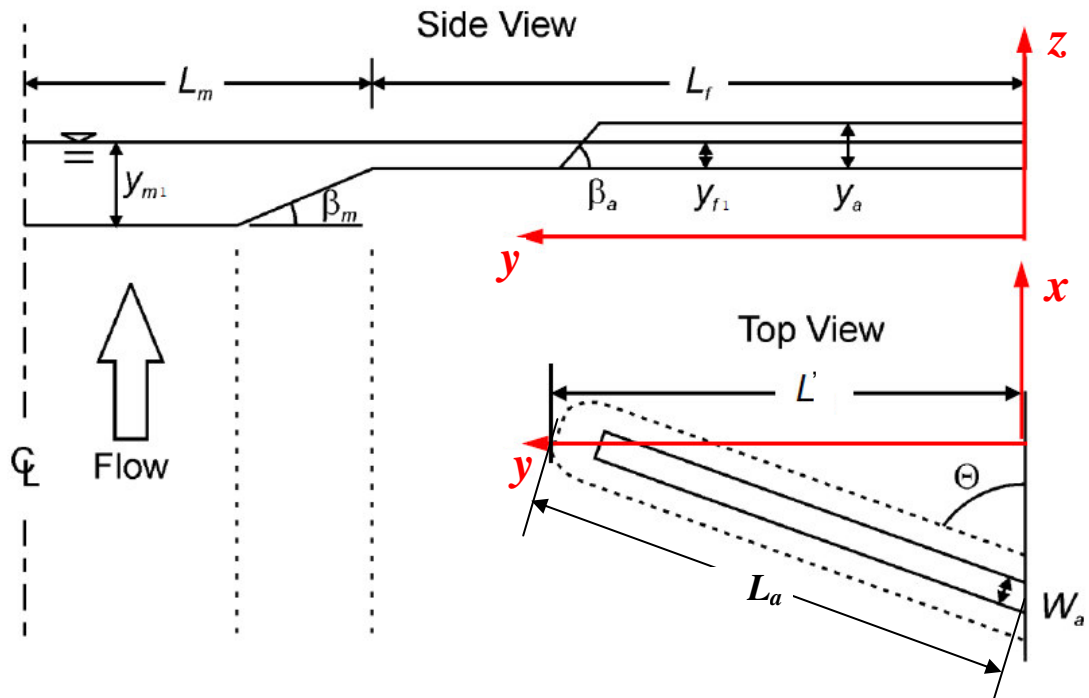
Notes: $\beta_a = 90^o$ for wing-wall shape abutment

where L: half width of channel

L': projected length of embankment normal to flow

L_a: length of embankment

L_f: width of flood plain

L_m: half width of main channel

θ: skew angle of approach embankment

$\tan(\beta_a)$: slope of abutment (V:H)

V_1: approaching average velocity

y_{f1}: water depth at the toe of the abutment estimated as the water depth immediately upstream of the toe of the abutment

y_{m1}: approach water depth at main channel

Figure 4.1. Definition of variables and coordinate system

4.1.2   Water surface profiles

The measured streamwise water surface profiles at the beginning of the experiments are shown in Figure 4.2 for all the tests cases in the present study with a compound channel. Note that the test matrix is shown in Table 4.1and Table 4.2. Case 1 is the reference case while case 1II is a repeat test of case 1. All water surface measurement results in the compound channel are compared with that in case 1 and case 1II. In Figure 4.2, the variation of water surface profile at the approach section is negligible while the profile at the bridge section becomes more prominent with the increase of velocity and abutment length. The water level becomes stable after the bridge section in all the experiments.

In Figure 4.2 (a), the length of abutment was held constant, while both the water depth and velocity were changed to maintain a constant Froude number to study the effect of water depth variation. In Figure 4.2 (b), the length of abutment and approach water depth were kept constant, while the approach velocity was varied to examine the effect of velocity variation. Figure 4.2 (c) shows the water depth profile for different abutment lengths. Figure 4.2 (d) and Figure 4.2(e) show that the abutment shape and abutment alignment do not have a remarkable effect on the water depth variation if the flow conditions are maintained constant.
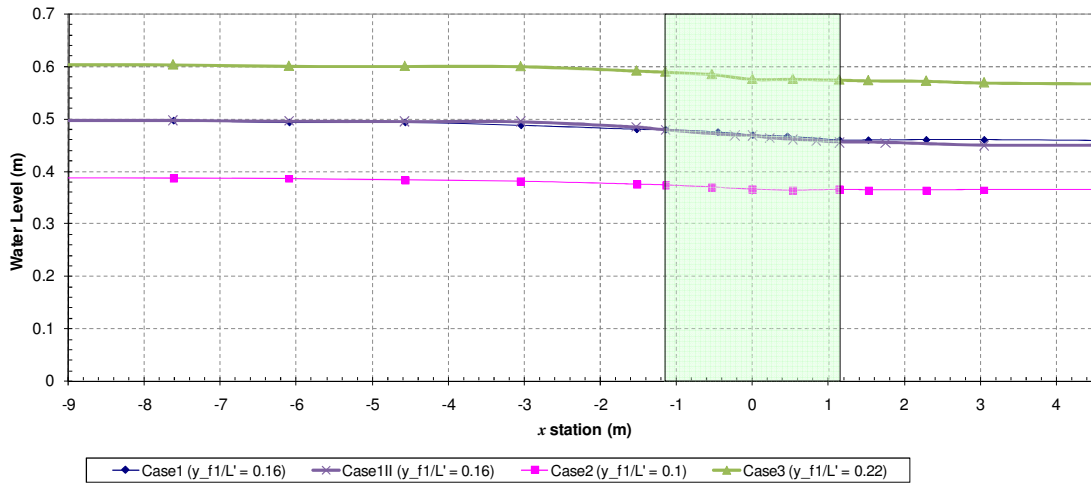
(a) Effect of water depth with the same Froude number and abutment length
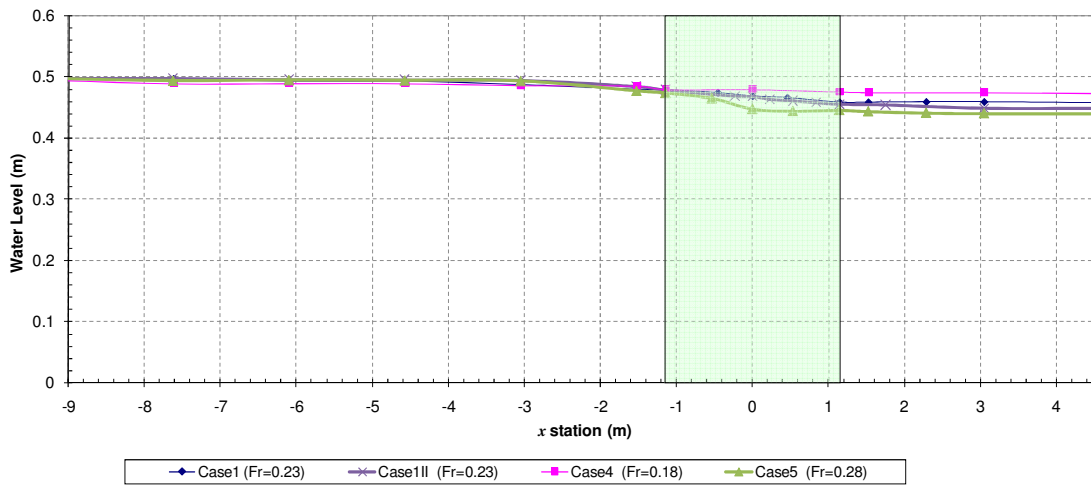
(b) Effect of velocity with the same approach water depth and abutment length

Figure 4.2. Water surface profile in compound channel
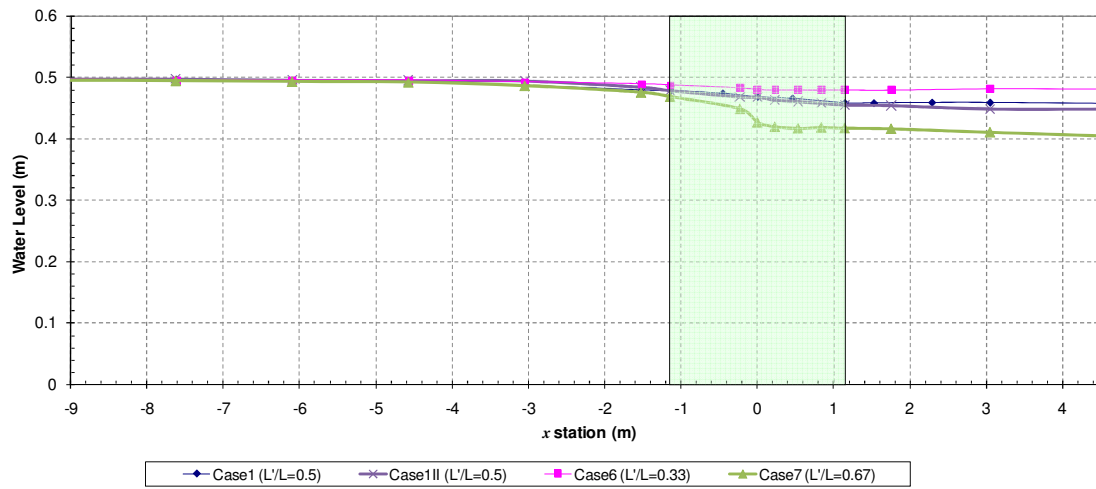
(c) Effect of abutment length with the same flow condition
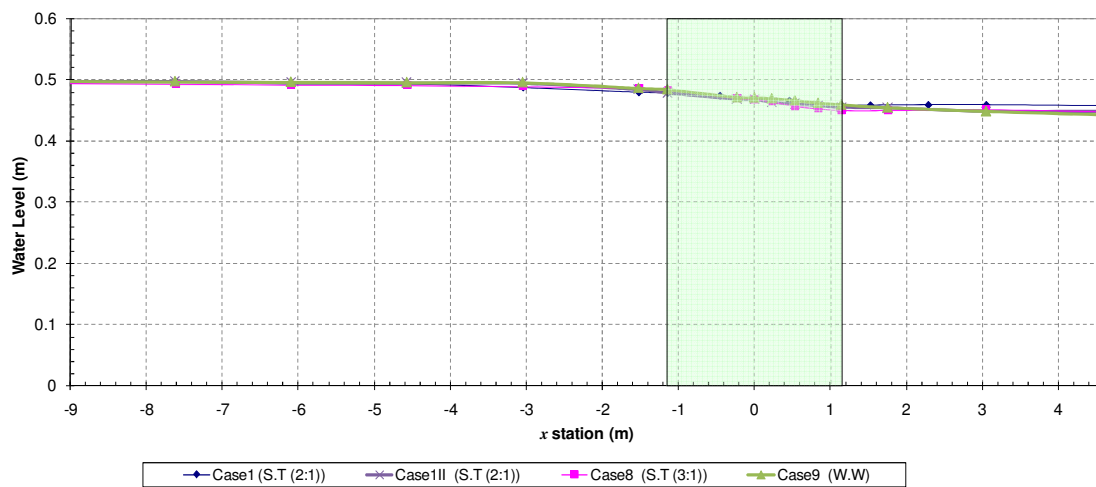
(d) Effect of abutment shape with the same flow condition and abutment length.
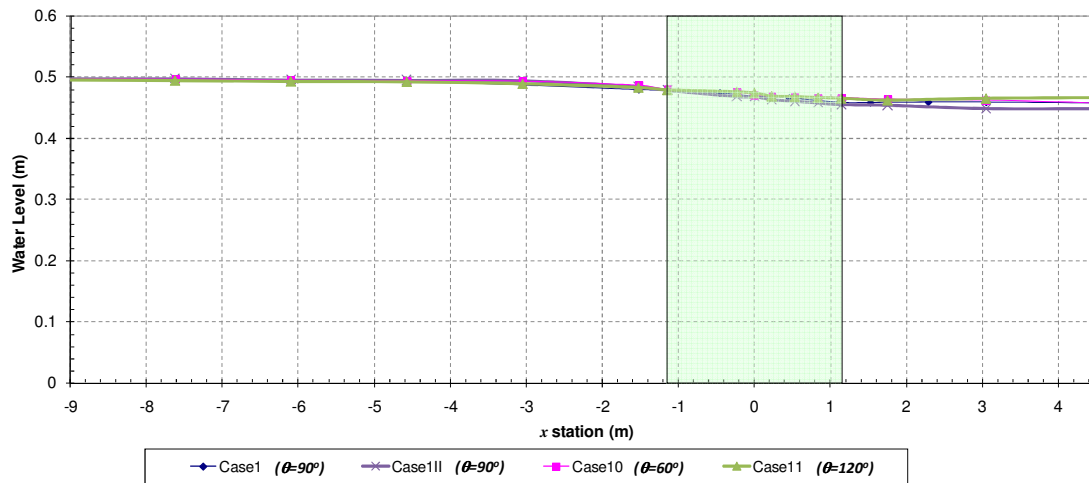
Figure 4.2. (continued)

(e) Effect of abutment alignment with the same flow condition and abutment length

Figure 4.2. (continued)

The water surface profile changes as scour develops. The water surface at the approach section (up to $x = -1.41$ m) was almost constant while scour was progressing, but there were significant changes in the surface elevation after the approach section. The water level after the approach section increased as scour progressed. It finally reached the same level as that of the approach section and reached an equilibrium condition. Figure 4.3 shows the change of water surface profile for case 1II and case 7. The water depth at the approach section seems to be a dominant parameter in evaluating the scour depth. However, the approach water depth in a real channel is not constant through the flow direction while it is nearly constant in the flume test. Thus the water depth immediately upstream of the abutment is used to evaluate the clear water scour depth not only for the laboratory tests but also for the real channel.
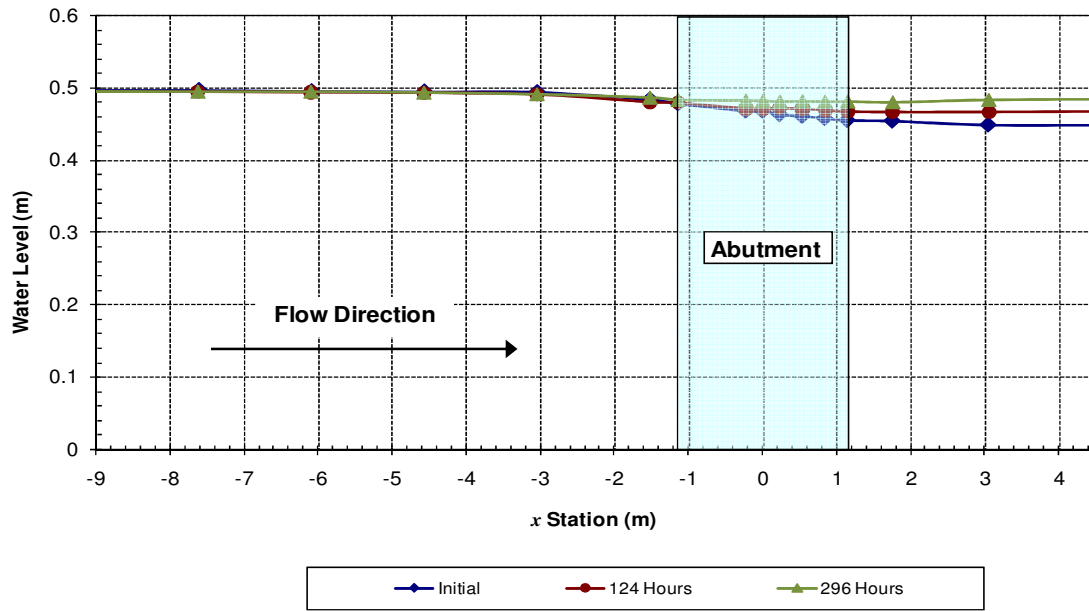
(a) Case 1II
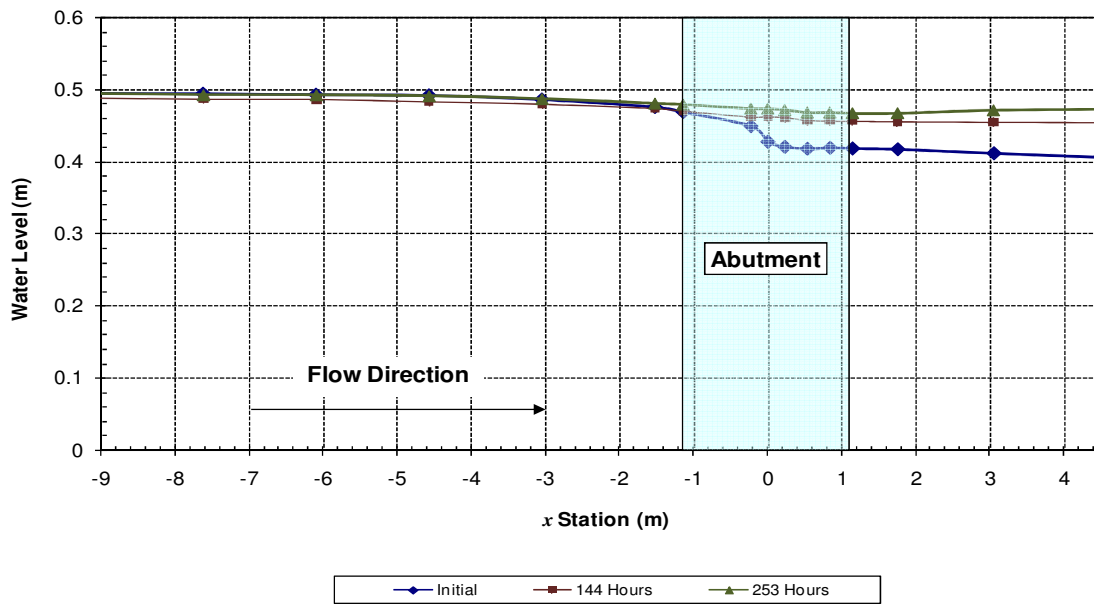
(b) Case 7

Figure 4.3. Change of water surface profile with scour development

4.1.3 Velocity distribution

The streamwise velocity distribution in the approach section at the compound channel is shown in Figure 4.4. The main channel velocities are slightly higher than that on the floodplain, and the maximum difference of streamwise velocity between the floodplain and main channel is less than 10% throughout the experiments.

The streamwise velocity in the contracted section along the abutment centerline is shown in Figure 4.5. The maximum velocity is found to be around the toe of the abutment regardless of the shape, the alignment, and the length of the abutment. The ratio between the maximum streamwise velocity and the average velocity in the main channel is found in the range between 1.04 and 1.17 from the flume test results. Figure 4.6 shows the pattern of time averaged velocity distribution of case 1II. The color indicates the magnitude of the velocity, and the arrows show the direction and magnitude of the velocity (V_x and V_y). The maximum velocity occurs downstream from the abutment and close to the flume wall near the center of the channel (only one-half of the channel is modeled). The downstream velocity decreases with the scour development.

TI (turbulence intensity) is calculated in this study and is expressed as:

$$TI = \sqrt{\sigma_x^2 + \sigma_y^2 + \sigma_z^2}$$

(4.1)

where σ is the standard deviation of the measured velocity and the subscripts *x, y* and *z* are the directions of flow. The coordination system is shown in Figure 4.1.

Figure 4.7 shows the corresponding pattern of turbulence intensity with scour development. The maximum turbulence intensity appears to be around the toe of abutment on the downstream side. The magnitudes of velocity and turbulence intensity

decrease with the scour development. The patterns of velocity and turbulence intensity

for other cases are displayed in Appendix A.
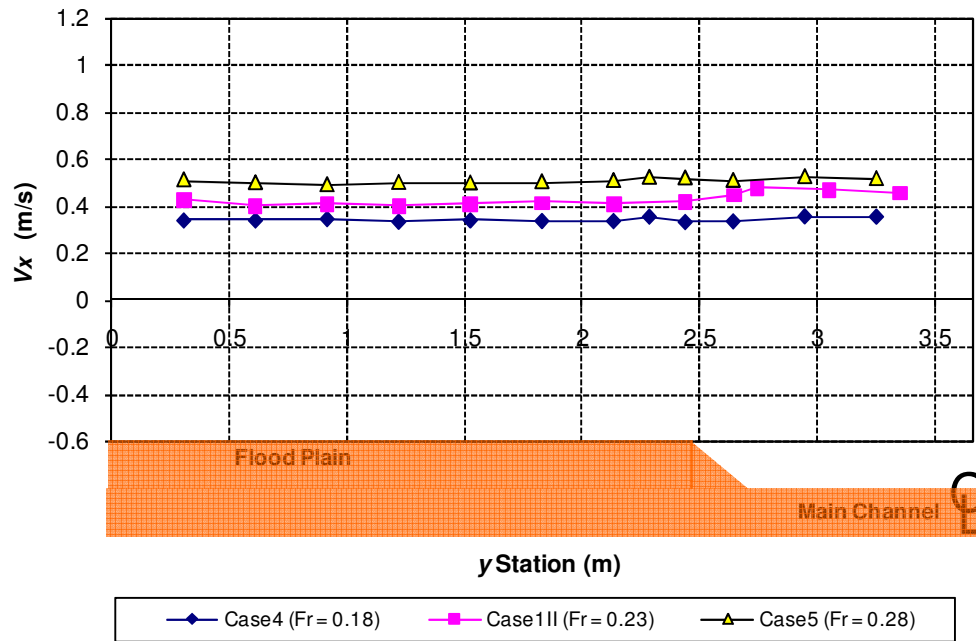
Figure 4.4. Streamwise velocity distribution at approach section
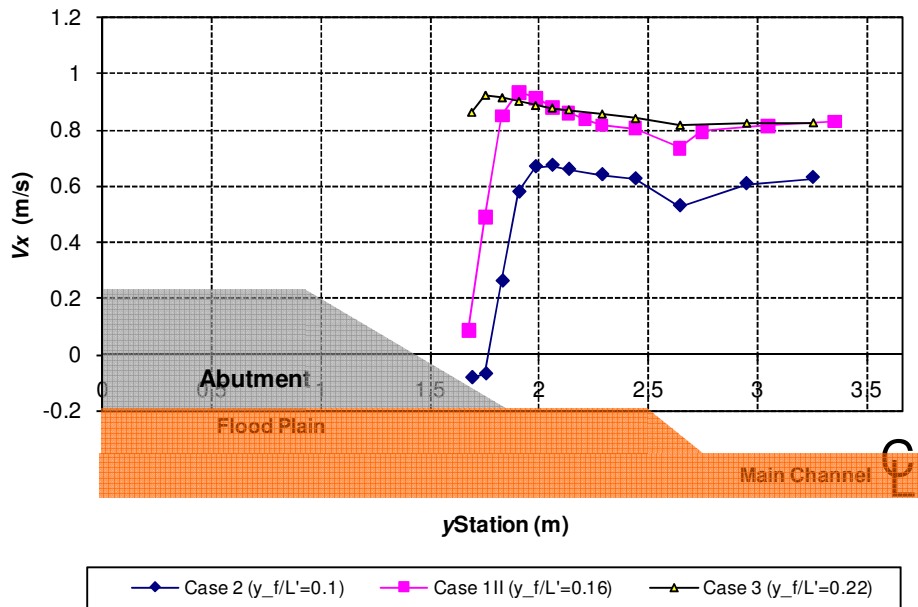
(a) Effect of water depth with the same Froude number and abutment length
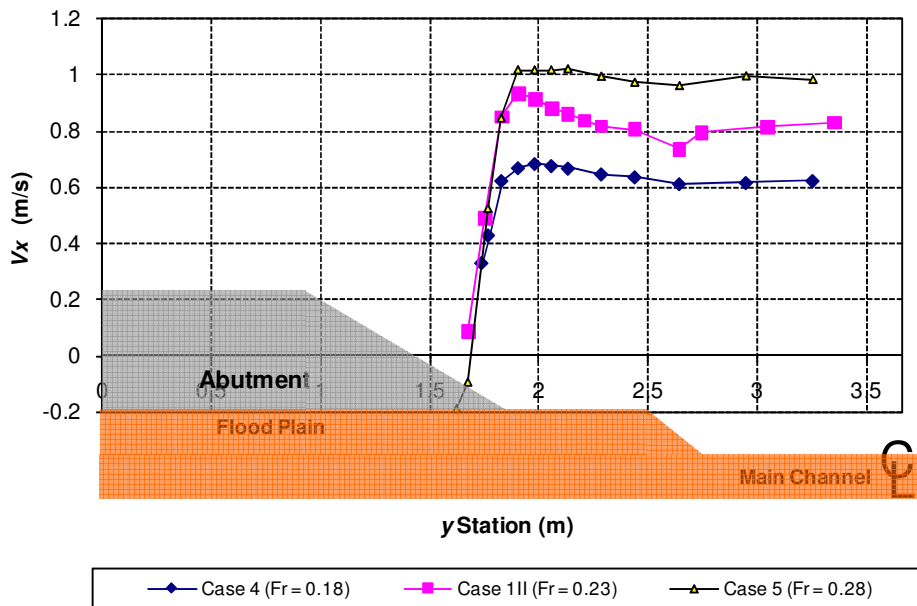
(b) Effect of velocity with the same approach water depth and abutment length

Figure 4.5. Streamwise velocity distribution in the contracted section along the
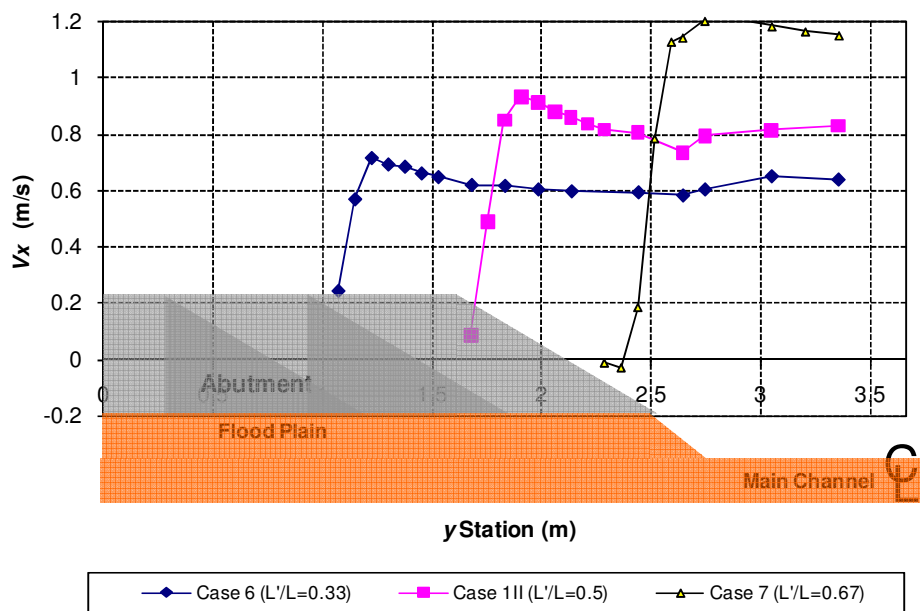
abutment centerline

(c) Effect of abutment length with the same flow condition
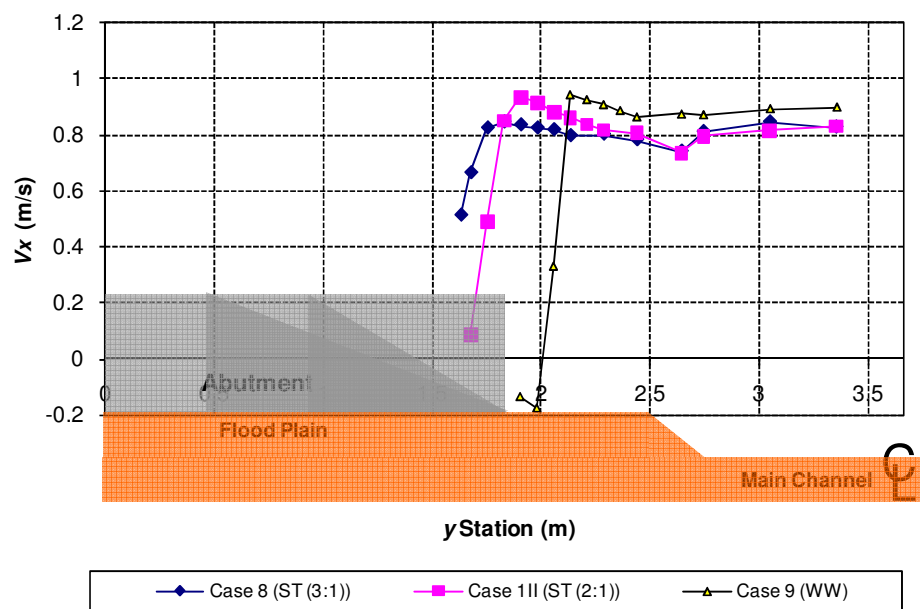
(d) Effect of abutment shape with the same abutment length and flow condition

Figure 4.5. (continued)
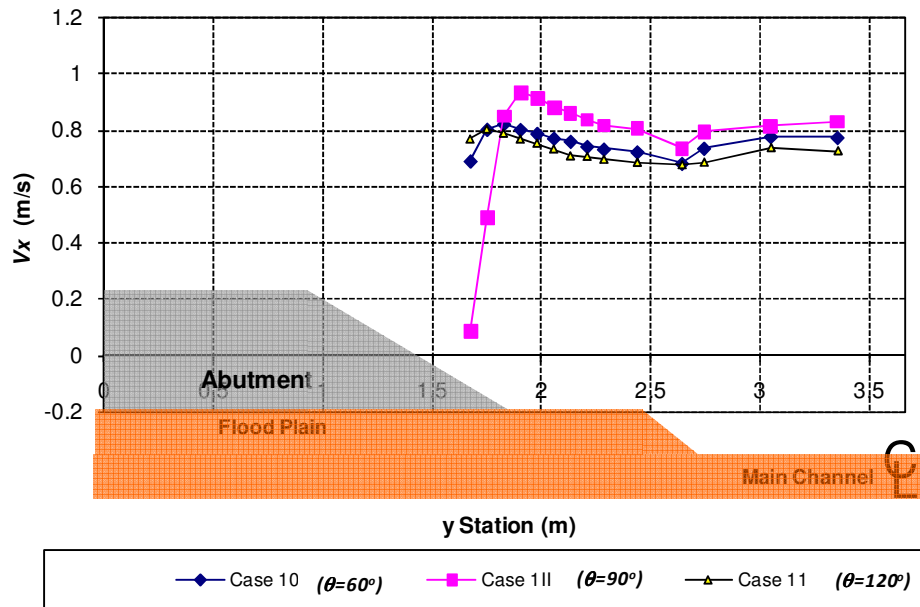
(e) Effect of abutment alignment with the same flow condition and abutment length

Figure 4.5. (continued)
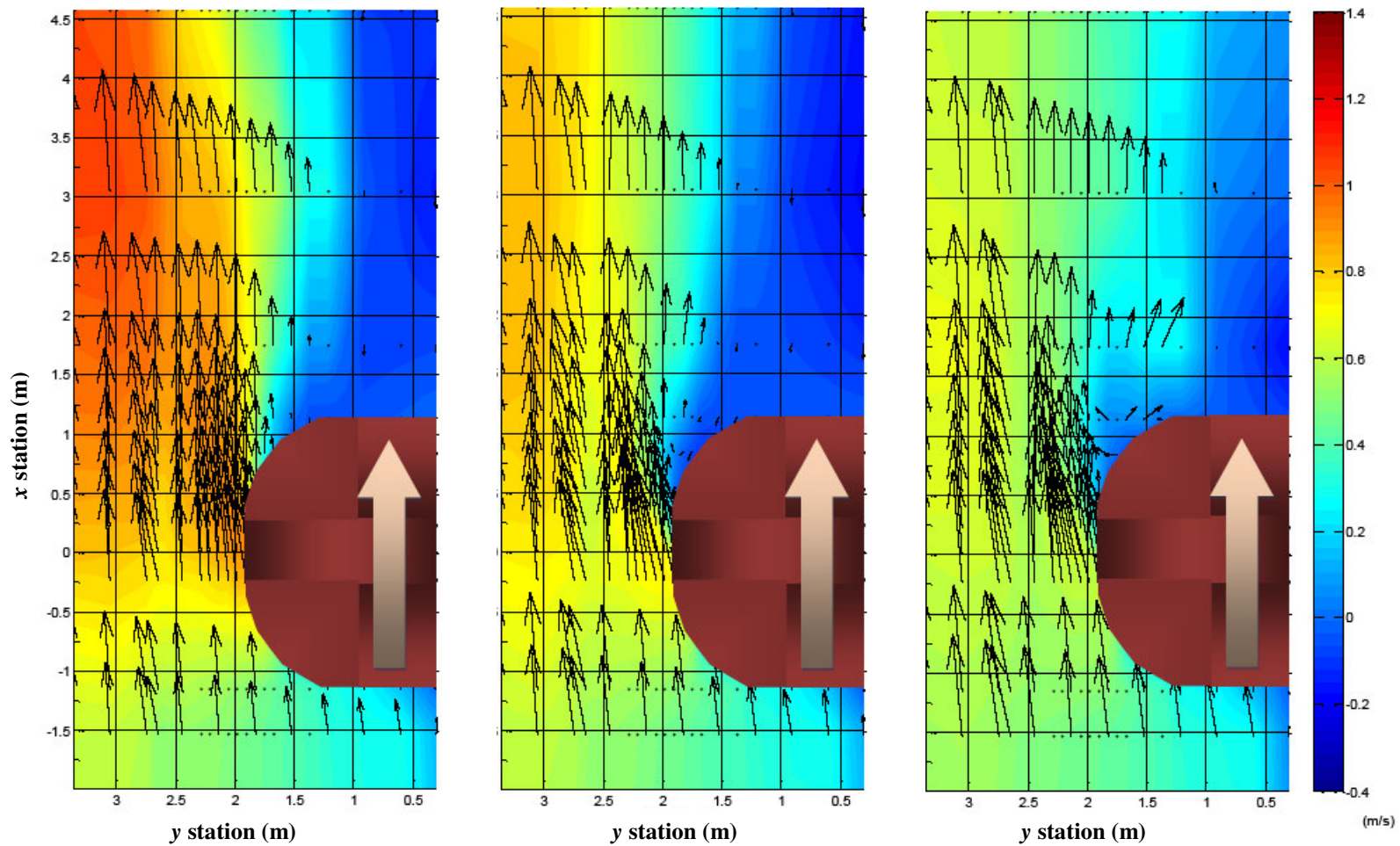
(a) Beginning of experiment (b) After 124 hours (c) After 296 hours

Figure 4.6. Pattern of velocity distribution (case 1II)

(a) Beginning of experiment   (b) After 124 hours   (c) After 296 hours
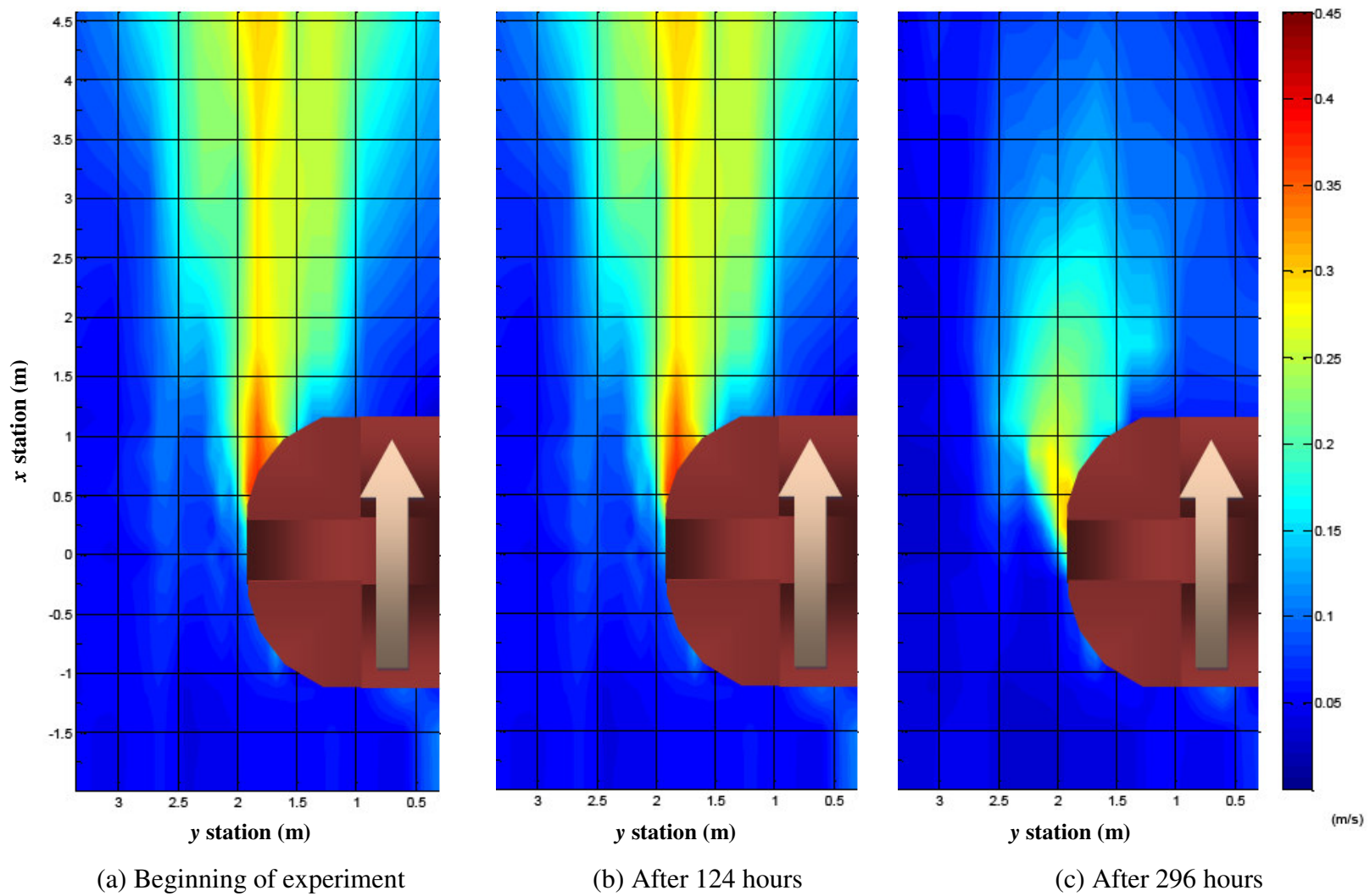
Figure 4.7. Pattern of turbulence intensity distribution (case 1II)

4.1.4 Scour development

The erosion rate of cohesive soil is much lower than that of cohesionless soil, and the water was very muddy so it is impossible to see the eroded channel bottom during flume tests. The bed profiler and point gauge (mentioned in Chapter III) were used to scan the channel bottom and locate the deepest scour hole. Each test usually took more than 10 days. The interval of measurement in the first 5 days was every 20 hours and then approximately every 44 hours after that. This was done because the scour rate decreases with an increase in scour hole development. Figure 4.8, Figure 4.9 and Figure 4.10 show the channel bottom topography changes for case 1II ($L'/L_f = 0.75$), case 6 ($L'/L_f = 0.5$), and case 7 ($L'/L_f = 1.0$), respectively. case 7 was stopped after 257 hours of test run while the other cases were stopped after 320 hours because the abutment scour depth of case 7 at 257 hour test run was almost close to the thickness of the clay layer. Detailed results for all the tests are presented in Appendix B. Figure 4.11, Figure 4.12 and Figure 4.13 show the views of test area before and after the test for case 1II, case 6 and case 7, respectively. The pictures for all the tests are presented in Appendix C.
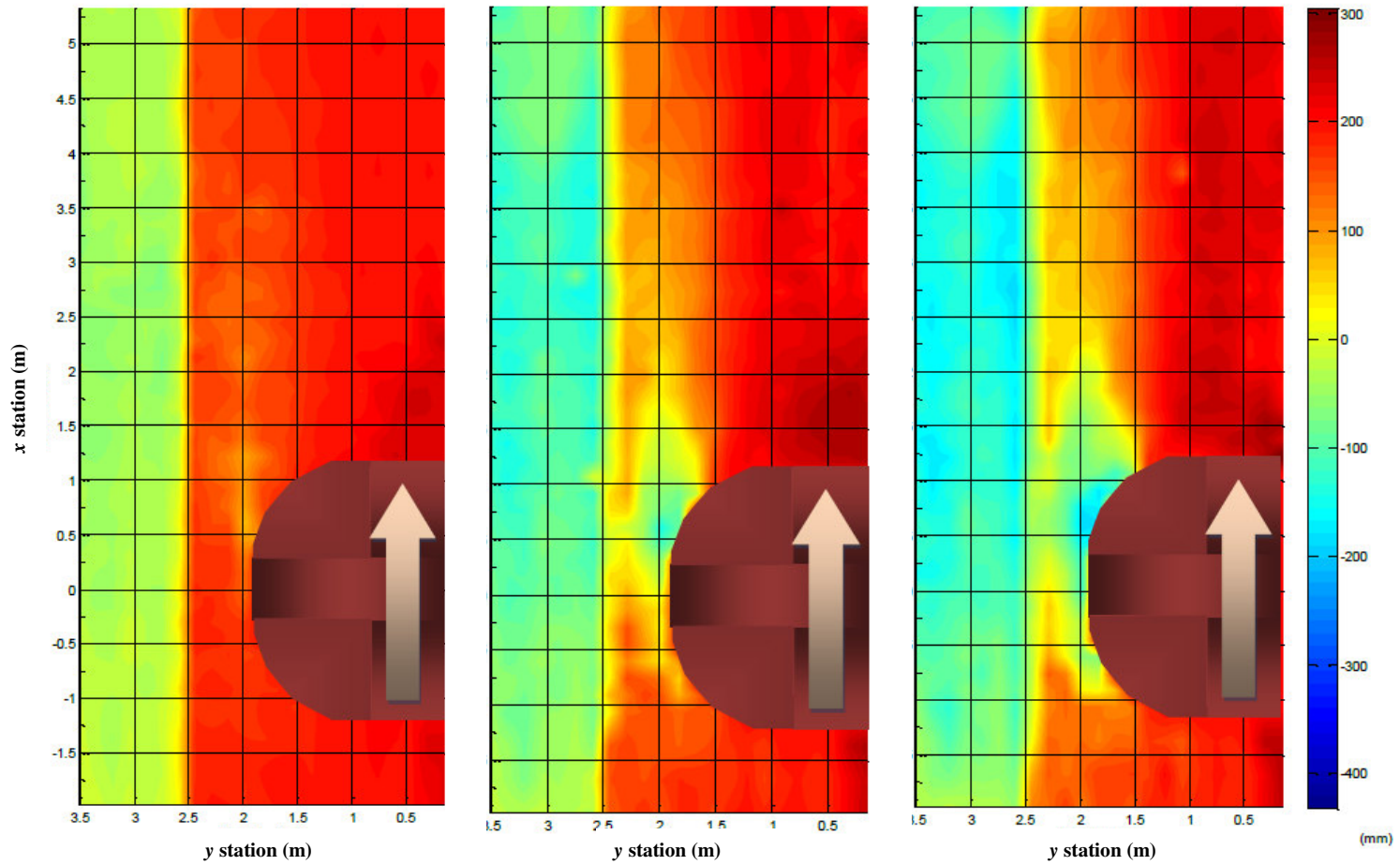
(a) After 60 hours   (b) After 189 hours   (c) After 320 hours

Figure 4.8. Evolution of channel bottom topography (case 1II)
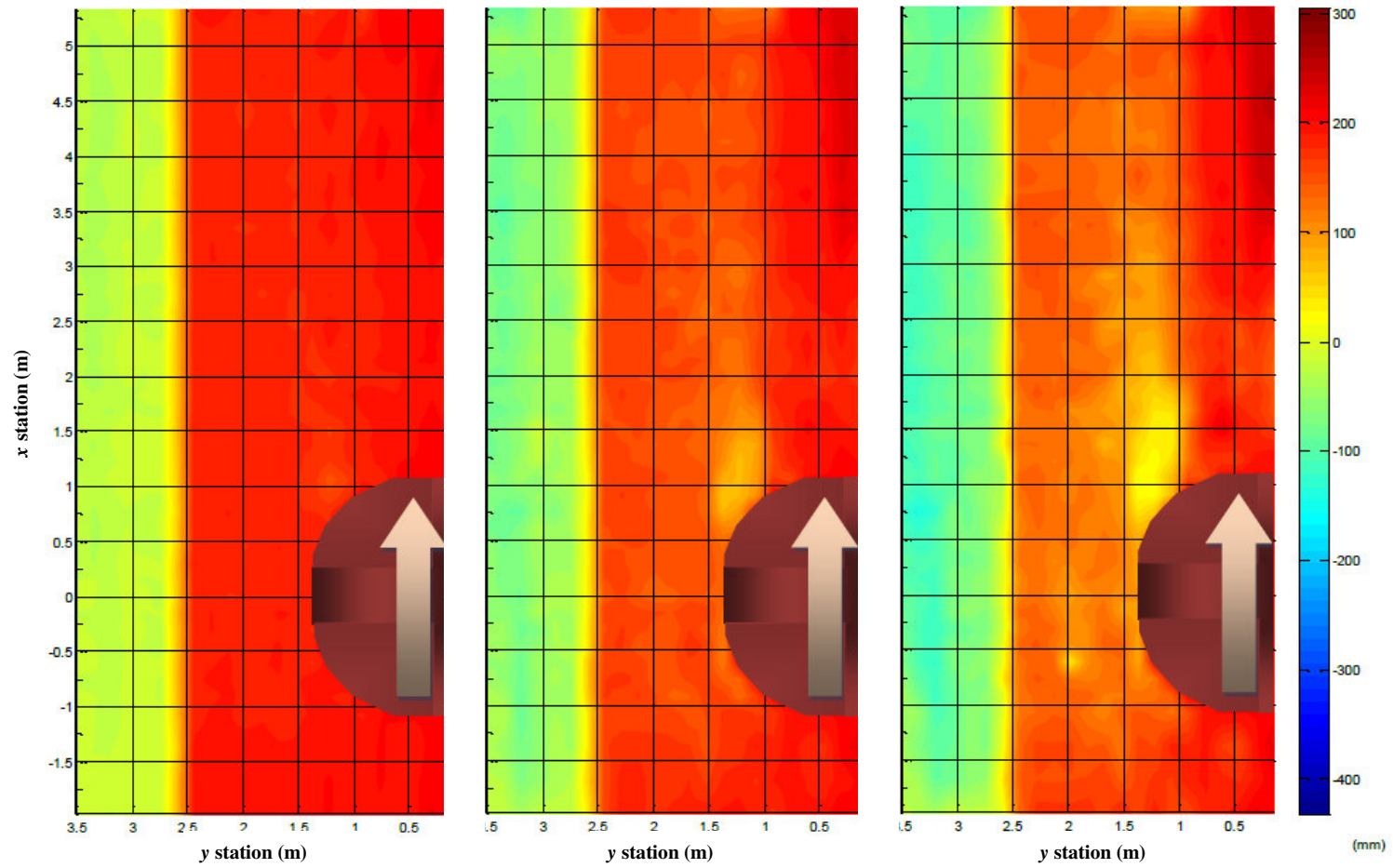
(a) After 60 hours   (b) After 188 hours   (c) After 320 hours

Figure 4.9. Evolution of channel bottom topography (case 6)
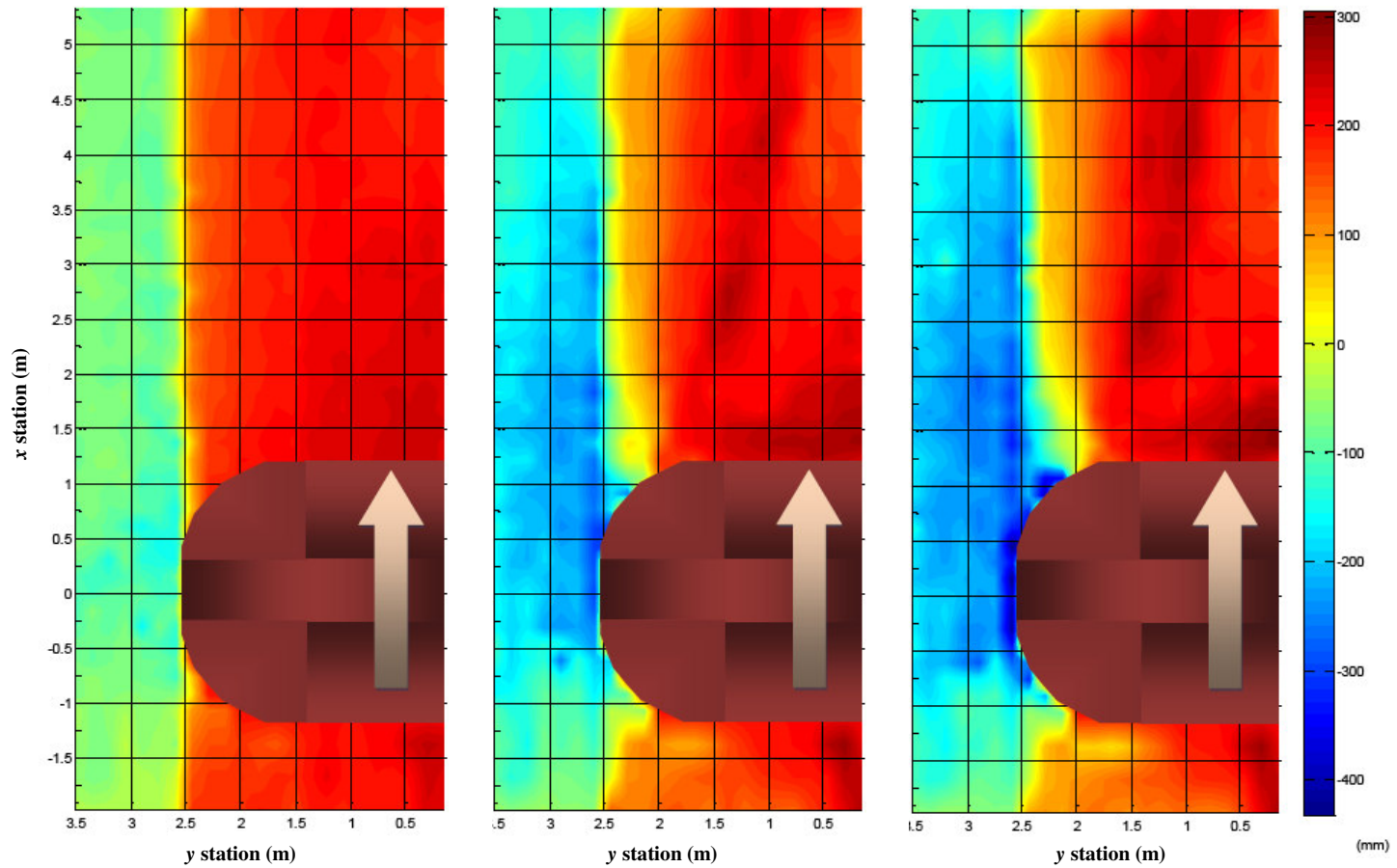
(a) After 60 hours   (b) After 188 hours   (c) After 257 hours

Figure 4.10. Evolution of channel bottom topography (case 7)

(a) Before experiment

(b) After experiment (320 hours)

Figure 4.11. View of test section (case 1II, $L'/L_f = 0.75$)

(a) Before experiment

(b) After experiment (320 hours)

Figure 4.12. View of test section (case 6, $L'/L_f = 0.5$)

(a) Before experiment

(b) After experiment (257 hours)

Figure 4.13. View of test section (case 7, $L'/L_f = 1.0$)

The deepest abutment scour hole is usually located around the toe of the abutment but slightly downstream. The deepest contraction scour hole is usually located close to the wall away from the abutment and downstream of the abutment. This means that the deepest contraction scour hole occurred along the centerline of the river. This is consistent with the finding in Briaud et al. (2003) that the maximum contraction scour occurred at the centerline of the main channel if the channel is symmetrical.

Interestingly, the abutment scour pattern is similar to the pattern of *TI* (Turbulence Intensity) and the contraction scour pattern is similar to the time averaged velocity pattern as shown in Figure 4.14. The marked ellipses with dashed lines in that figure indicate the location where the maximum values were measured.

It is known that a different geometry of abutment will result in a different flow pattern and abutment scour pattern. In the present study, 3 types of abutment, spill-through with a 3(H):1(V) slope, spill-through with a 2(H):1(V) slope, and wing-wall shape, were used to examine the abutment shape effect on the flow pattern and the abutment scour pattern. In addition, 3 types of different abutment alignments, $\theta=60^{o}$, $\theta=90^{o}$ and $\theta=120^{o}$, were used with the same discharge and embankment length ($L'/L_f=0.75$) for a spill-through abutment with a 2(H):1(V) slope.
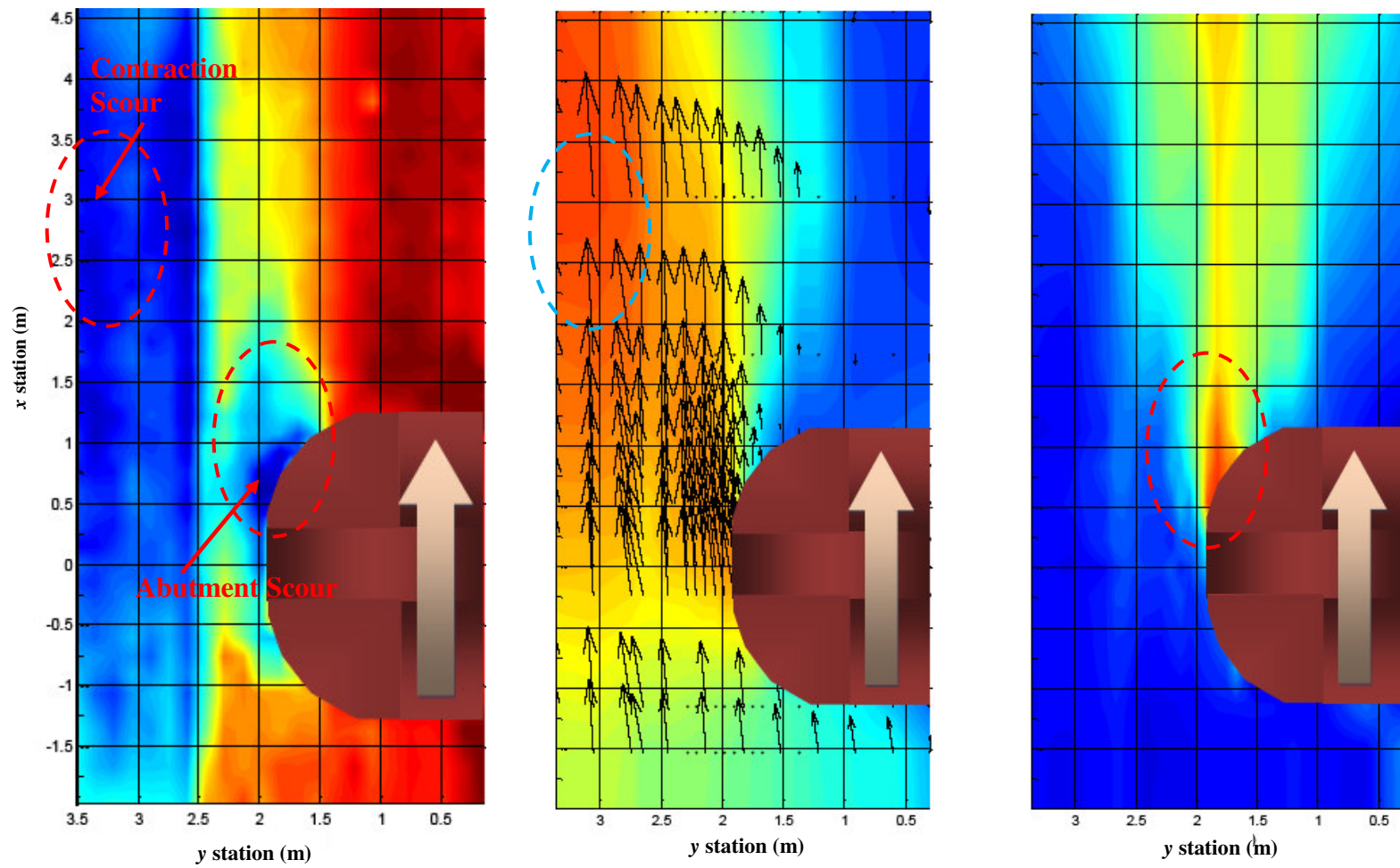
(a) Scour pattern after 320 hours   (b) Initial time averaged velocity   (c) Initial turbulence intensity

Figure 4.14. Comparisons of scour pattern and velocity pattern (case 1II)

The flow passing through the bridge section concentrates on the main channel. A steeper slope with a same embankment length induces a more concentration of flow to the main channel. The pattern of turbulence intensity shown in Figure 4.15 indicates that the high turbulence occurred on the floodplain for the spill-through abutment but on the main channel slope for the wing-wall abutment. Accordingly, a longer local scour pattern on the floodplain was observed for the spill-through abutment while a shorter local scour on the floodplain for the wing-wall abutment for the condition of L'/L_f=0.75. Figure 4.15 shows the initial turbulence intensity and Figure 4.16 shows the channel bottom bathymetry of 3 types of abutments. Note that the red dot lines are the slope of main channel. The test running time was 320 hours, 308 hours and 271 hours for case 8, case 1II and case 9, respectively.

The skewed spill-through abutment induced a smoother flow than the abutment normally aligned to the flow. The finding consistent with previous research results for the abutment skewed toward downstream (θ=60$^\text{o}$), however for the abutment skewed toward upstream (θ=120$^\text{o}$) the result contradicts to that in previous studies. The opposite result for the abutment skewed toward upstream may come from the shape of abutment because vertical wall abutments were used in previous studies while a spill-through abutment is used in the present study. As shown in Figure 4.17, the spill-through abutment skewed toward upstream induced a relatively smooth flow than the abutment perpendicularly aligned to the flow. The test running time for each case was 320 hours.
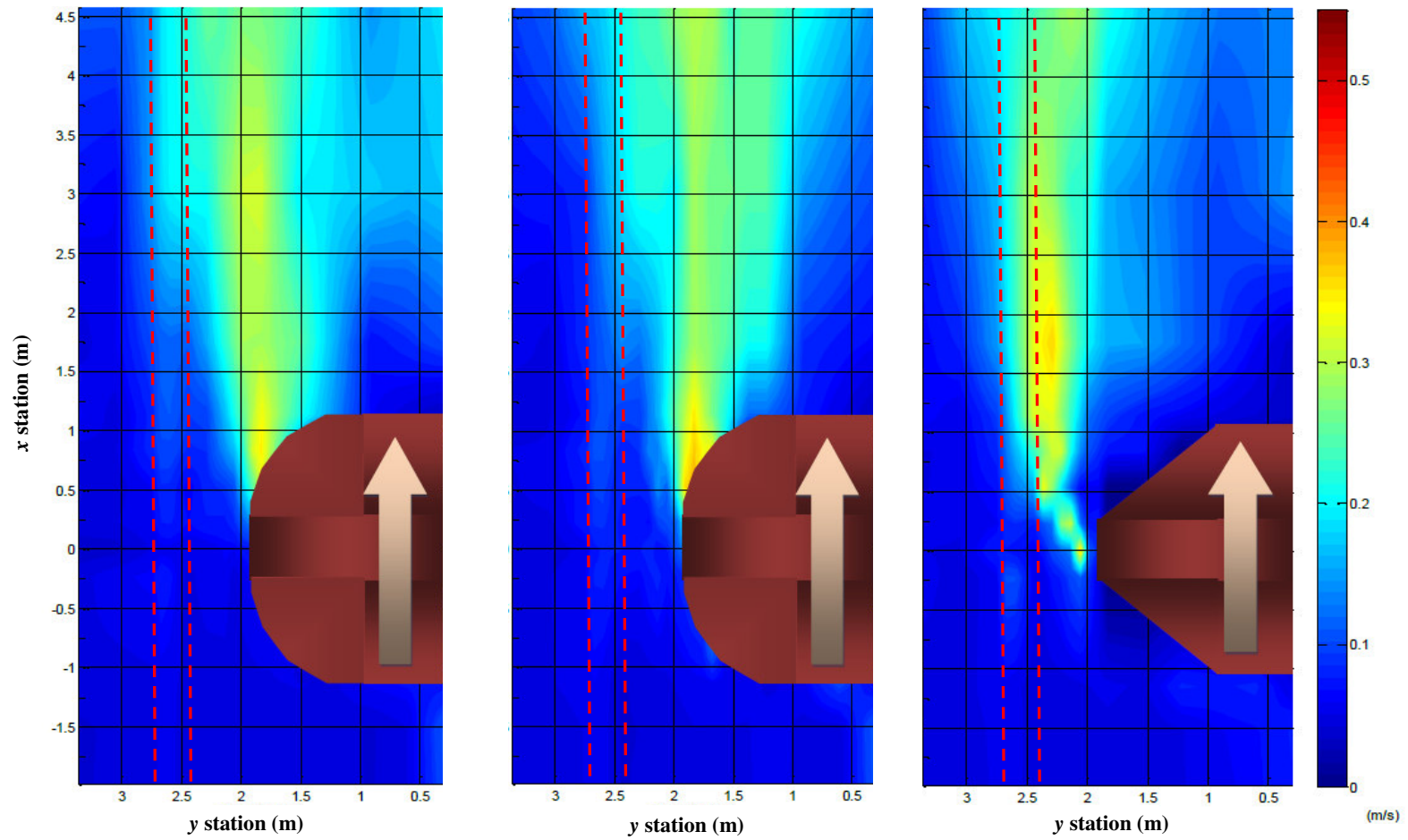
(a) Case 8 - ST (3(H):1(V))   (b) Case 1II - ST (2(H):1(V))   (c) Case 9 - WW

Figure 4.15. Turbulence intensity for different abutment shape
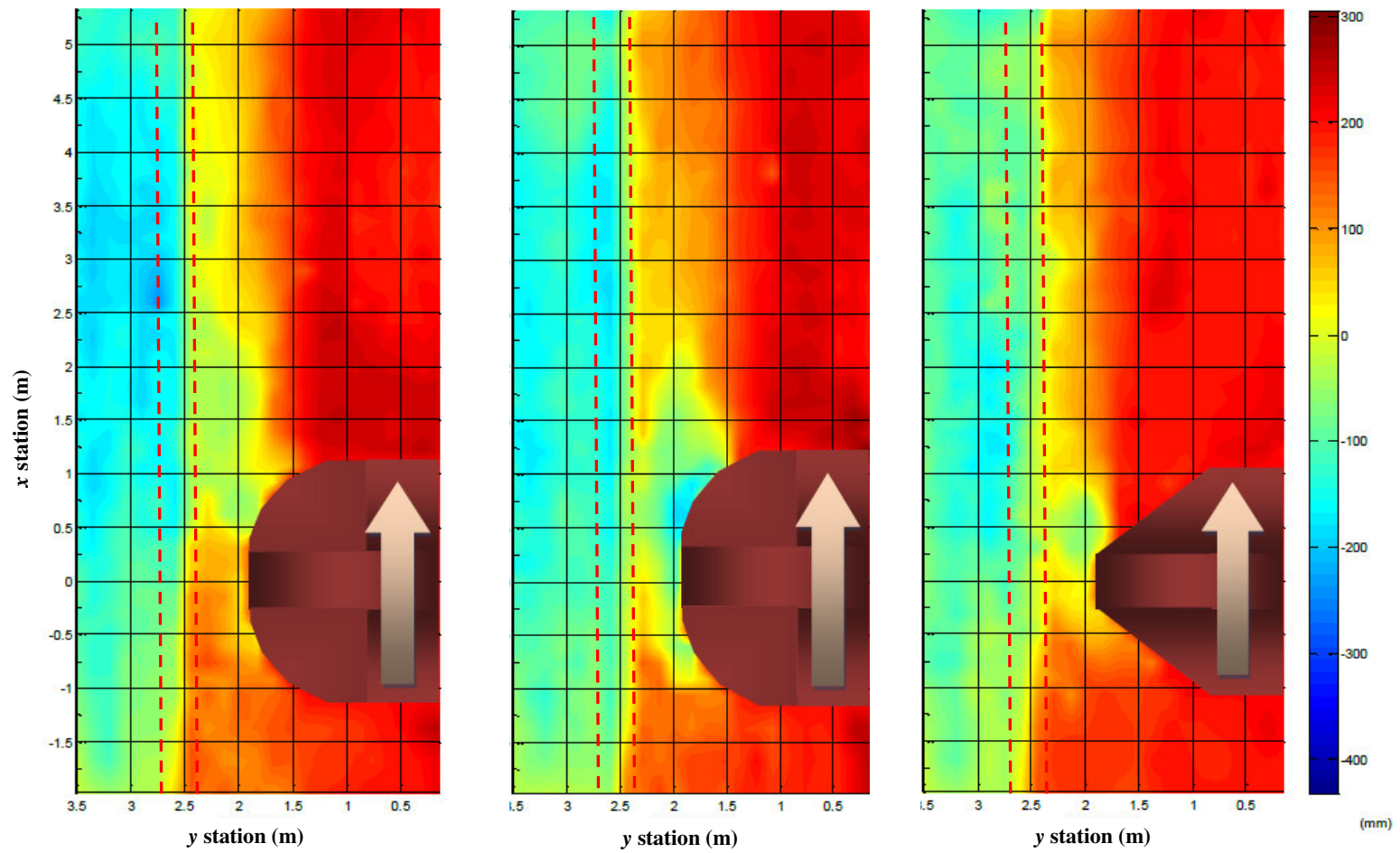
(a) Case 8 - ST (3(H):1(V))　　　　(b)Case 1II - ST (2(H):1(V))　　　　(c) Case 9 - WW

Figure 4.16.　Channel bottom bathymetry for different abutment shape

(a) Case 10 - θ=60° (b) Case 1II - θ=90° (c) Case 11 - θ=120°
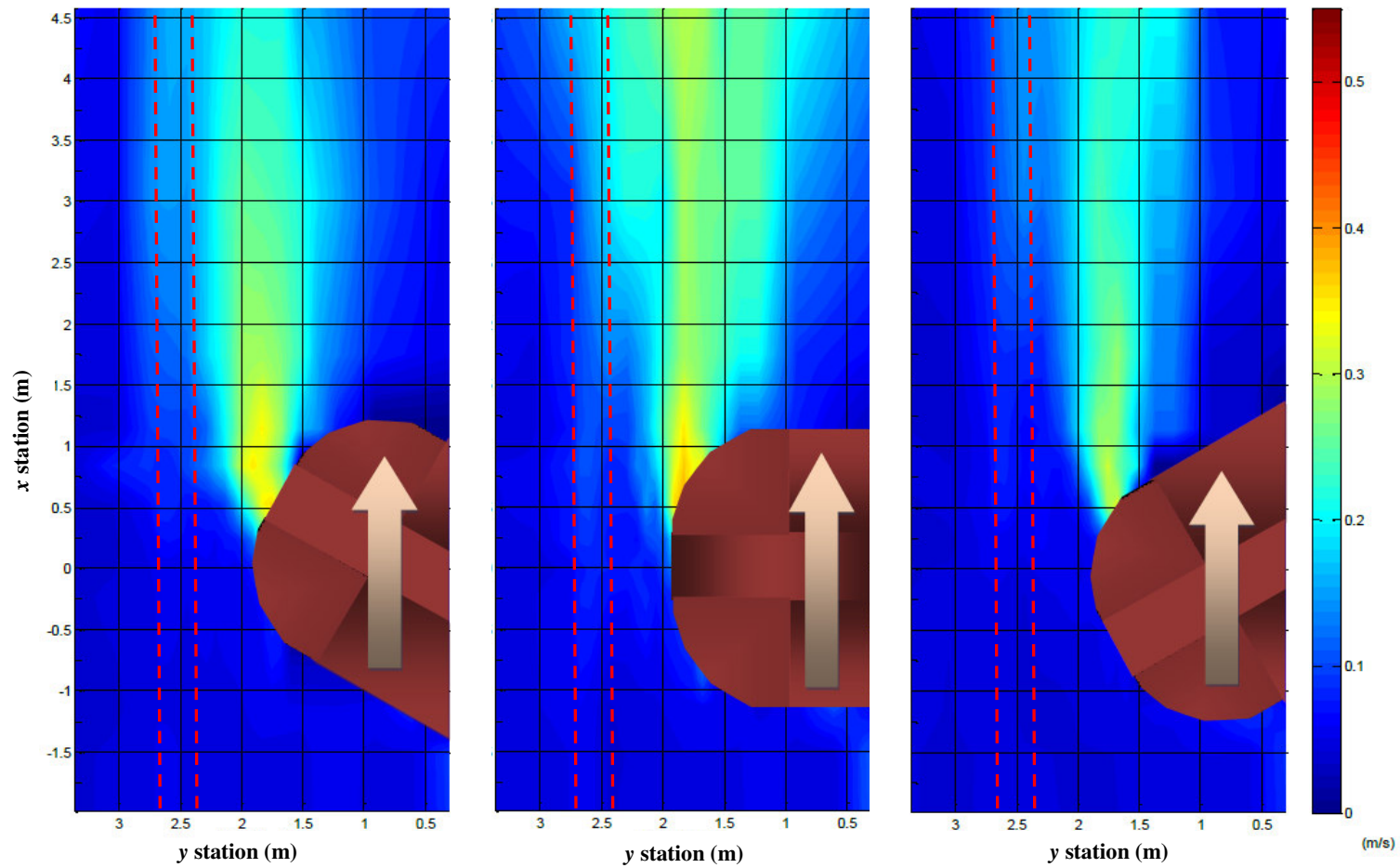
Figure 4.17. Turbulence intensity for different abutment alignment for spill-through abutment (2(H):1(V))
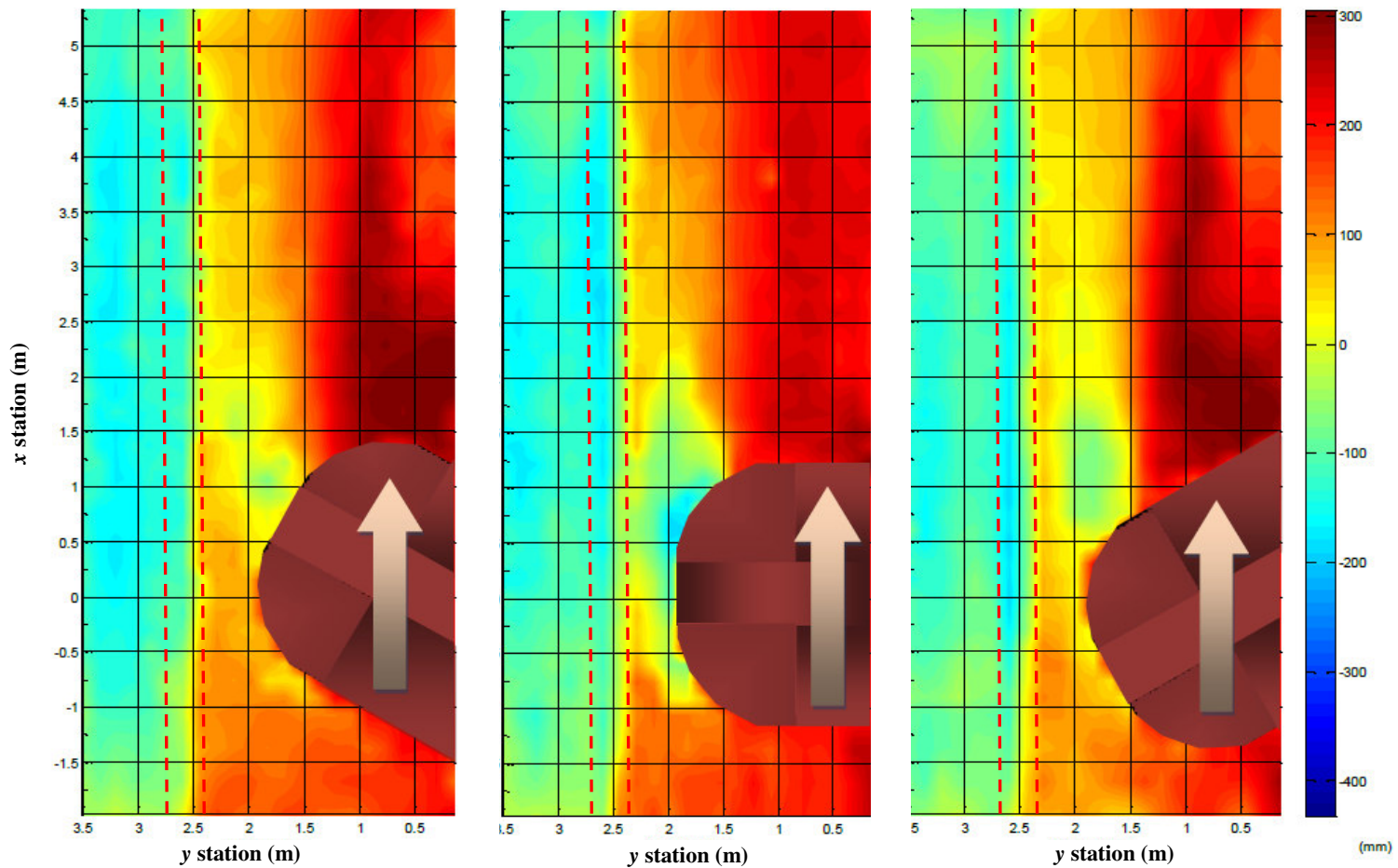
(a) Case 10 - θ=60°　　　　　(b) Case 1II - θ=90°　　　　　(c) Case 11 - θ=120°

Figure 4.18. Channel bottom bathymetry for different abutment alignment for spill-through abutment (2(H):1(V))

4.2   Maximum scour depth

The depth of the deepest abutment scour hole and contraction scour hole were obtained from the measurements at every time step. Figure 4.19 shows the abutment scour depth developments for different abutment length and abutment alignment condition in the compound channel. The contraction scour depth developments for those two conditions show similar trends but not the same magnitude.

Although the duration for all the flume tests lasted more than 240 hours (10 days), the scour depth was still increasing at the end of each flume test. In the present study, the maximum scour depth was not directly measured but estimated by applying a hyperbolic model. This is due to the fact that the scour and erosion rates of cohesive soils are very low and much lower than that of cohesionless soils. The erosion rate of soils has been studied by Briaud et al. (1999(b), 2003). They found that the scour rate of cohesive soils can be 1000 times slower than that of cohesionless soils and a 10-day test may generate only a percentage of the maximum scour depth.

Using the measurement results in Figure 4.19, a hyperbolic model was applied to obtain the maximum scour depth for abutment scour and contraction scour. The form of the models used in the scour predictions for the abutment scour and contraction scour are

$$y_{s(Abut)} = \frac{t}{a_1 \cdot t + b_1}$$

(4.2)

$$y_{s(Cont)} = \frac{t}{a_2 \cdot t + b_2}$$

(4.3)

where $y_{s(Abut)}$ is the abutment scour depth, $y_{s(Cont)}$ is the contraction scour depth, t is time,

a is the inverse of the asymptotive scour depth , and b is the inverse of the initial tangent to the scour depth versus time curve. The equations can be rewritten to the form of $(t/y) = at + b$ and fitted with a straight line.
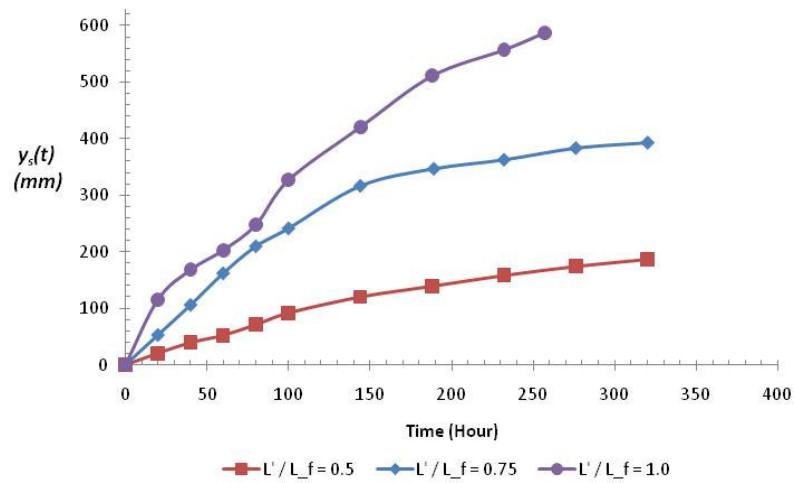
(a) Effect of abutment length (case 6, case 1II, case 7)
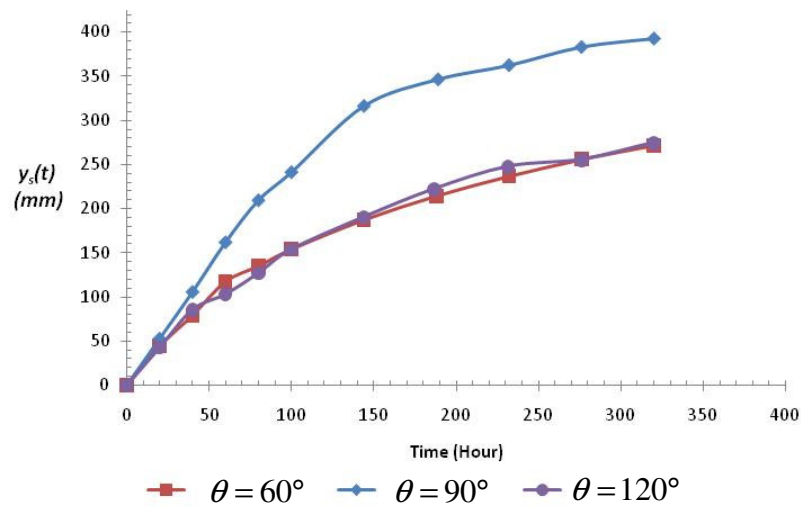
(b) Effect of abutment alignment (case 10, case 1II, case 11)

Figure 4.19. Development of abutment scour depth

Figure 4.20 shows the fitting of the hyperbolic model for both the abutment scour and contraction scour data for case 17. The values of *a* and *b* for abutment scour are less than the *a* and *b* values for contraction scour in the test. This means that the initial scour rate and the maximum scour depth of abutment scour are higher and deeper than that of contraction scour. Figure 4.21 shows the comparison between the measurement and the hyperbolic model obtained by data fitting in Figure 4.20. The hyperbolic model seems to be in good agreement with the measurements. The maximum scour depths may be calculated as time reaches infinite ($t \rightarrow \infty$). These values are equal to $1/a_1$ and $1/a_2$ for abutment scour and contraction scour, respectively. Based on this approach, the values of *a* and *b* were calculated and presented in Table 4.3 for all the flume tests along with the calculated maximum scour depths.
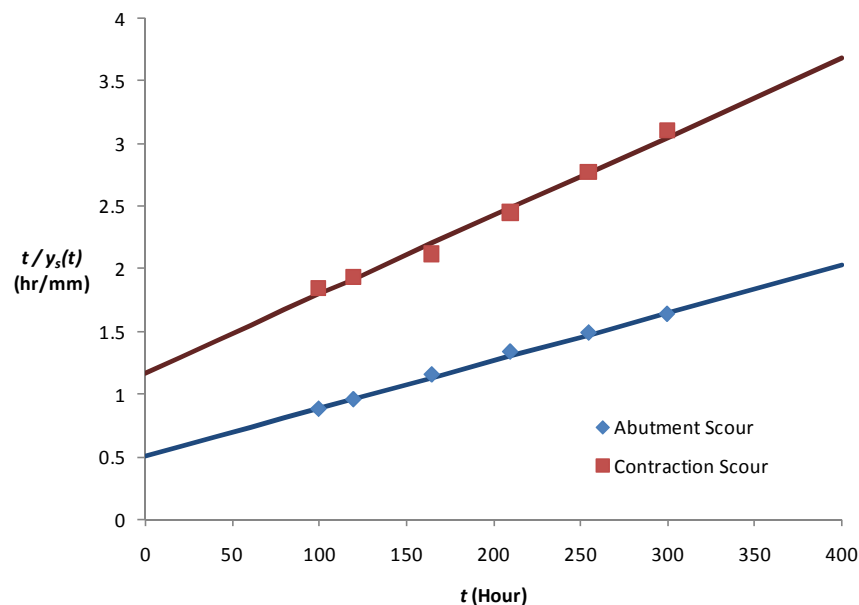
Figure 4.20. Data fitting of hyperbolic model (case 17)
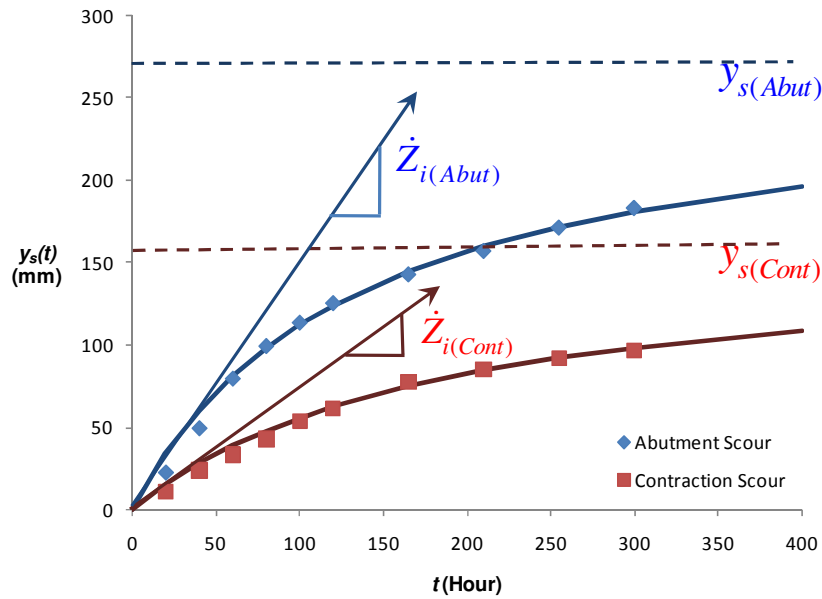
Figure 4.21. Comparison between measurement and hyperbolic model (case 17)

Table 4.3. Summary of hyperbolic model and maximum scour depth.

	Abutment Scour			Contraction Scour		
	a_1 (mm^{-1})	b_1 (hour/mm)	$y_{s(Abut)}$ (mm)	a_2 (mm^{-1})	b_2 (hour/mm)	$y_{s(Cont)}$ (mm)
Case1	0.0023	0.1861	439	0.0048	0.7668	206
Case1II	0.0020	0.1623	490	0.0045	0.4049	224
Case2	0.0035	1.3509	282	0.0077	1.3868	130
Case3	0.0017	0.9482	589	0.0035	1.0177	282
Case4	0.0033	0.8745	300	0.0130	1.8744	77
Case5	0.0012	0.6025	808	0.0036	0.7867	277
Case6	0.0028	0.7976	351	0.0052	0.9581	191
Case7	0.0008	0.2198	1195	0.0029	0.2576	343
Case8	0.0024	0.4541	413	0.0040	0.3149	251
Case9	0.0015	0.5542	670	0.0038	0.7270	266
Case10	0.0024	0.4201	418	0.0045	0.4505	225
Case11	0.0023	0.4269	436	0.0042	0.6254	237
Case12B	0.0007	0.6804	1429	0.0040	0.6641	253
Case13	0.0151	2.3458	66	0.0214	4.3641	47
Case14	0.0033	0.4165	305	0.0069	0.5733	144
Case15	0.0030	0.5693	334	0.0045	0.3877	222
Case16	0.0022	0.3112	448	-	-	-
Case17	0.0038	0.5103	262	0.0063	1.1671	159

CHAPTER V

COMPARISON WITH ONE DIMENSIONAL SIMULATIONS

5.1 Introduction

HEC-RAS (Hydrologic Engineering Center River Analysis System) is well known one dimensional simulation program. HEC-RAS uses the energy equation to calculate the water surface profiles from one cross section to the next section for the steady flow. On the contrary, the momentum equation is used whenever the water surface passes through critical depth in HEC-RAS.

Although the results of one dimensional simulation, compared to 2 dimensional and 3 dimensional analysis, are not accurate to predict the local velocity and water depth around the bridge structure, more than 95 percentages of engineers in the US use one dimensional simulation for the design of bridge. In this chapter, the results of one dimensional simulations using HEC-RAS are compared with measurement results.

5.2 Selection of Manning's *n* value

If the channel geometry data and hydraulic data which are identical to the flume test conditions are input, Manning's *n* value is an important parameter to control the prediction for the steady flow.

Manning's *n* value is an important parameter in open channel flow, and many researchers have proposed different methods to find Manning's *n* value using soil particle size and water depth in cohesionless soil. However, those methods are inappropriate for cohesive soils due to its very small particle. For example, the mean

diameter of Porcelain clay is 0.035×10^{-3} m and Strikler approximation $\left(n = 0.041 D_{50}^{1/6}\right)$ (after Richardson and Davis, 1995) results in $n = 0.0074$. This n value is much lower than the minimum value of HEC-RAS recommendation, which is 0.011.

To compare with HEC-RAS results, the Manning's n value was determined by matching the calculation with the flume test results after several trials. In order to find the best Manning's n value, the water depth was used for the comparison because the HEC-RAS velocity does not agree well with the measurement in the compound channel. The followings are the steps to find the most appropriate Manning's n value.

(a) Input the geometry data identical to the flume test setup.

(b) Input an arbitrary Manning's n value.

(c) Input the flow data obtained from flume tests.

(d) Run HEC-RAS.

(e) Compare water depth results between the computation and the measurement for the approach section. There is no sudden change of water depth due to the bridge contraction. $x = -5$ m according to the flume tests.

(f) Change the Manning's n value but make sure it is in the reasonable range (referring HEC-RAS manual) and repeat steps (d) and (e).

(g) Repeat step (f) until the computed result matches the measurement.

The best Manning's n value is 0.011 after performing the steps above. This value is the minimum value recommended in the HEC-RAS manual for the trowel finished concrete channel. Figure 5.1 is a view of the flume after the setup of case 7. Figure 5.2 is the channel geometry used in HEC-RAS calculation for case 7. Figure 5.3 shows an

example of the water depth change comparison between the measurement and the HEC-

RAS calculation with different Manning's *n* values.
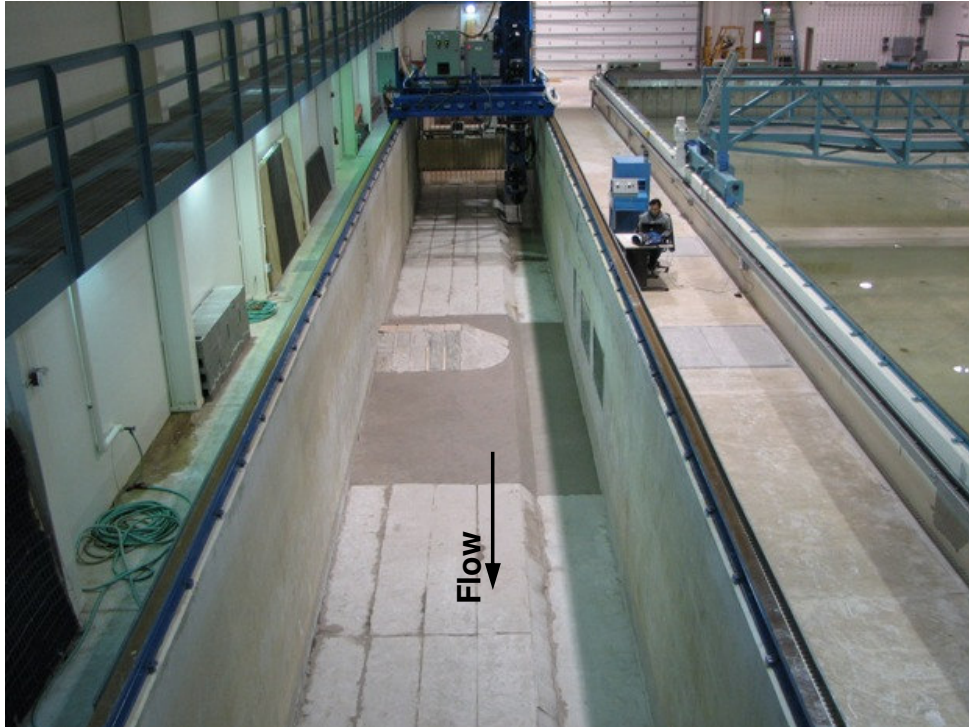
Figure 5.1. View of flume after setup (case 7)
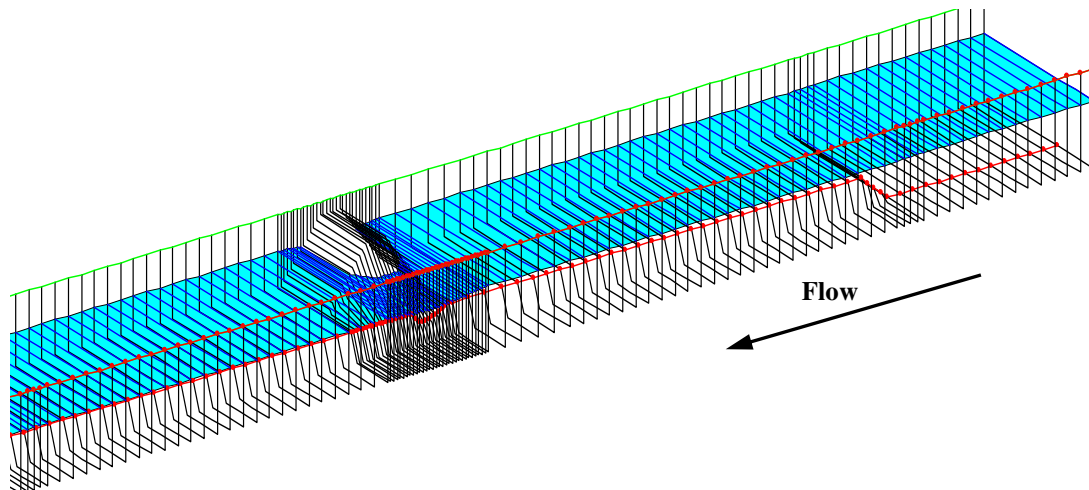
Figure 5.2. Channel geometry for HEC-RAS calculation (case 7)
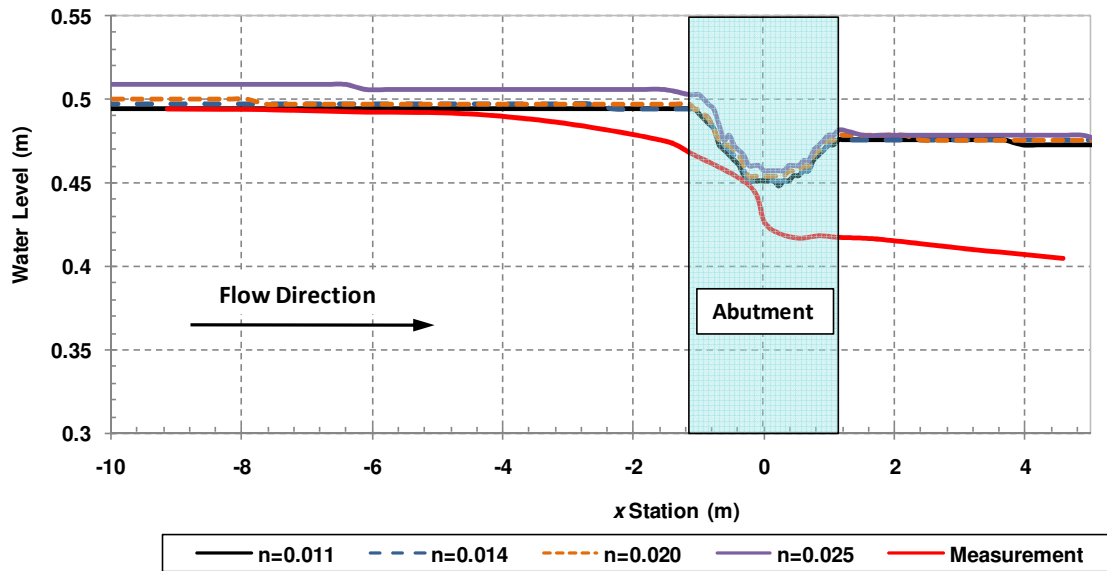
Figure 5.3. HEC-RAS water level comparison to measurement with different Manning's

n values (case 7)

5.3 Comparison between HEC-RAS simulation and measurements

The water surface profiles and velocity distributions calculated by HEC-RAS are compared with the laboratory test results. The calculated water surface profiles are compared with the measurement results for the same experimental conditions as shown in Figure 5.4. The profiles at the approach section (up to x = -1.43 m) calculated by HEC-RAS are almost constant in all test conditions, while smoothly decreasing water surface profiles were measured. The differences between the measurements and calculations increase with an increase in velocity and abutment (embankment) length. The maximum difference of water surface elevation between the HEC-RAS calculation and the measurement for all the test cases at x = -1.43 m (the section right before bridge contraction) is around 6%. The computed water surface decreases suddenly at the bridge

section and then returns back to a level close to the approach water surface at the downstream side. On the contrary, the measured water level decrease does not recover after the bridge section.
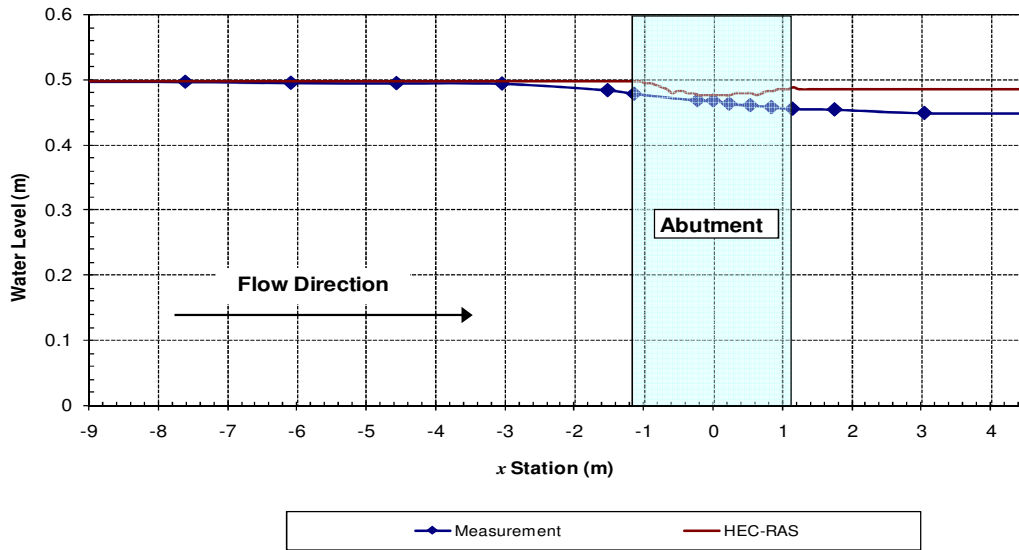
(a) Case 1II (ST abutment, $L'/L_f = 0.75$, $V_1 = 0.44$ m/s)
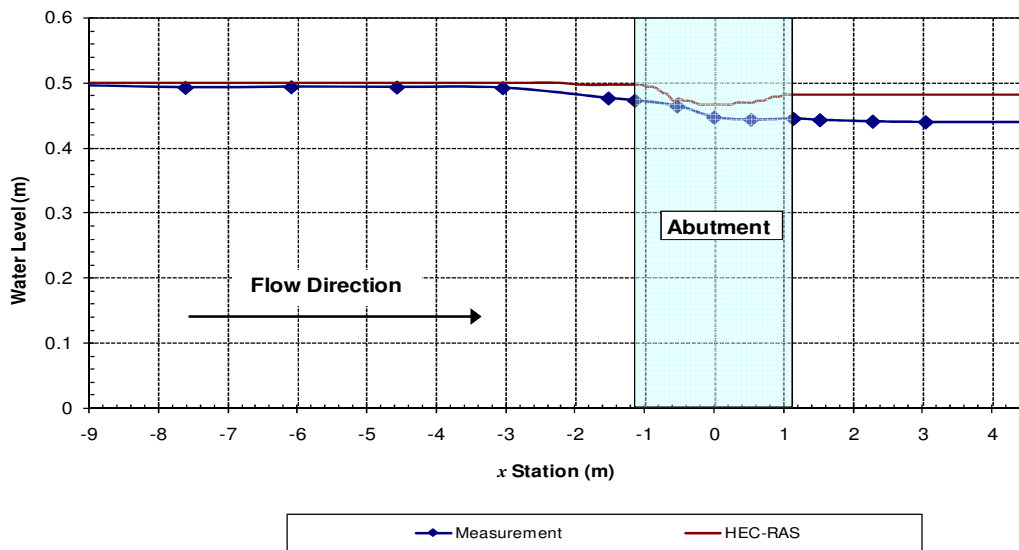
(b) Case 5 (ST abutment, $L'/L_f = 0.75$, $V_1 = 0.51$ m/s)

Figure 5.4. Measured and HEC-RAS calculated water surface profiles. "ST" indicates spill-through abutment
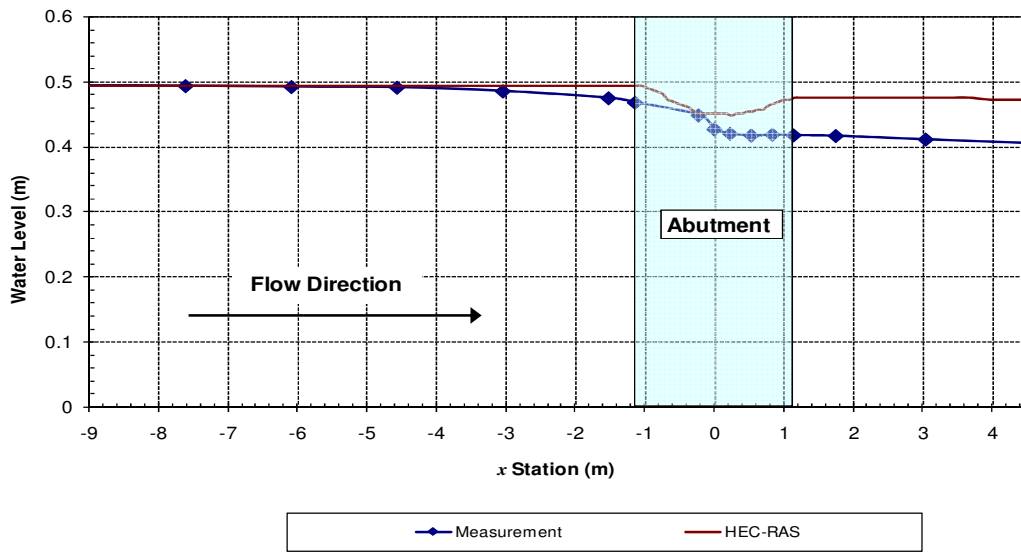
(c) Case 7 (ST abutment, L'/L_f=1.0, V_1=0.44m/s)

Figure 5.4. (continued)

The calculated and measured streamwise velocity distributions at the approach section (x = -9.1 m), at the middle of the bridge section, and at the downstream section are also compared and shown in Figure 5.5, Figure 5.6 and Figure 5.7, respectively. The calculated velocity distribution at the approach section in the floodplain matches the measurement well but the agreement does not occur in the main channel. The calculated velocity in the main channel is consistently 20% to 25% higher than the calculated velocity on the floodplain. This differs from the fact that the measured velocity in the main channel is no more than 10% higher than that in the floodplain as shown in Figure 5.5. The averaged values of streamwise velocities at the approach section on the floodplain obtained by measurements and HEC-RAS calculation were compared and shown in Figure 5.8. Again, the HEC-RAS calculation under predicts the velocity on the floodplain and over predicts the velocity in the main channel at the approach section.

In Figure 5.6, the calculated velocity using HEC-RAS at the bridge section agrees reasonably well with the measurement taken in the main channel. However, the calculated velocity on the floodplain where the maximum value was measured under predicts the measurements. The HEC-RAS velocity calculation in the main channel at the bridge section is consistently higher than that on the floodplain. The reverse is true for measurements.

In Figure 5.7, the calculated velocity at downstream shows almost same trend and magnitude with the pattern of the approach velocity, while the measurement shows recirculation on the floodplain and much higher velocity than HEC-RAS calculation on the main channel. This is the limitation of one dimensional analysis.

From the comparison with measurement results, HEC-RAS makes reasonable predictions at approach section as shown in Figure 5.8, but is not able to predict the velocity and water from starting section of bridge to downstream because the flow in the vicinity of the abutment becomes the accelerating nonuniform flow. Although HEC-RAS uses the momentum equation to the section where the significant channel change exists such as bridge constriction, weirs, stream junctions and etc, and the energy equation for the downstream, the prediction at downstream does not make agreement with measurement at all.
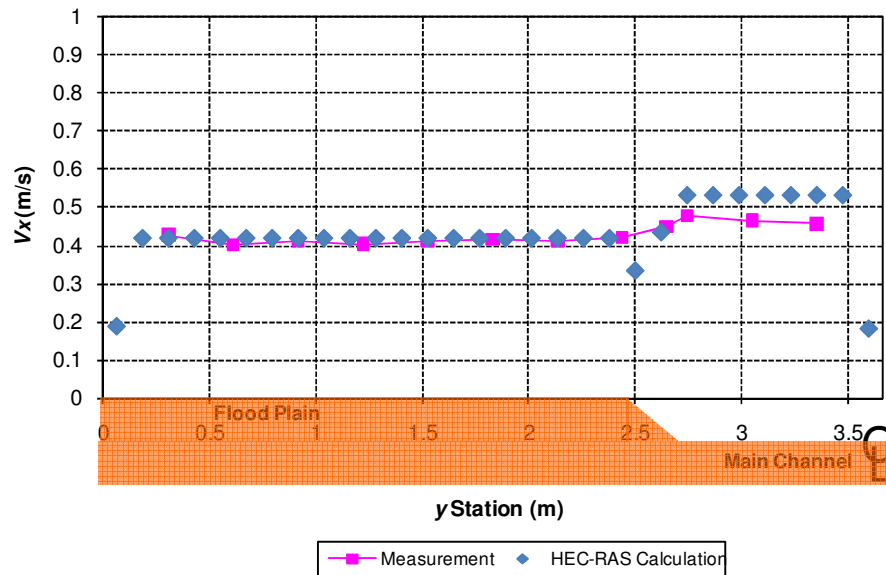
(a) Case 1II (ST abutment, L'/L_f=0.75, V_1=0.44m/s)
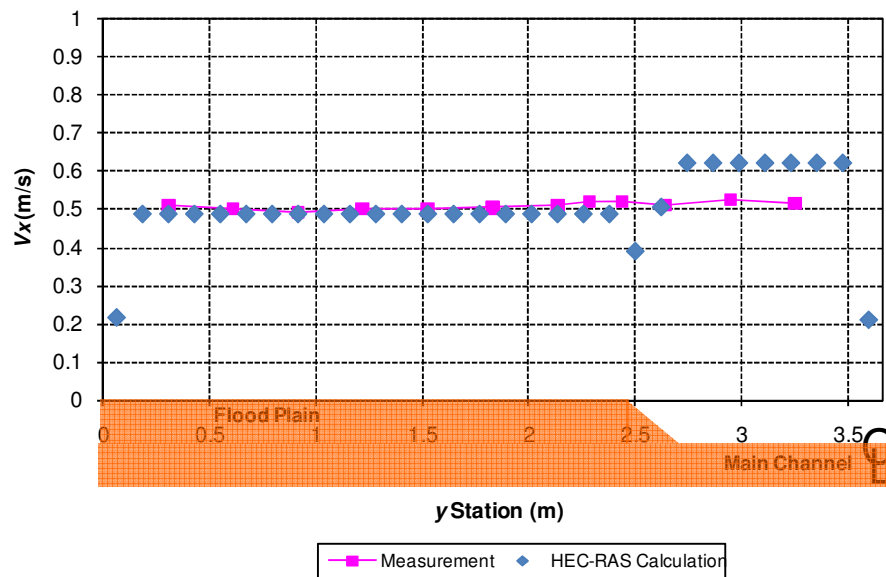
(b) Case5 (ST abutment, L'/L_f=0.75, V_1=0.51m/s)

Figure 5.5. Comparison of velocity distribution at approach section (x = -9.1 m)

between measurement and HEC-RAS calculation
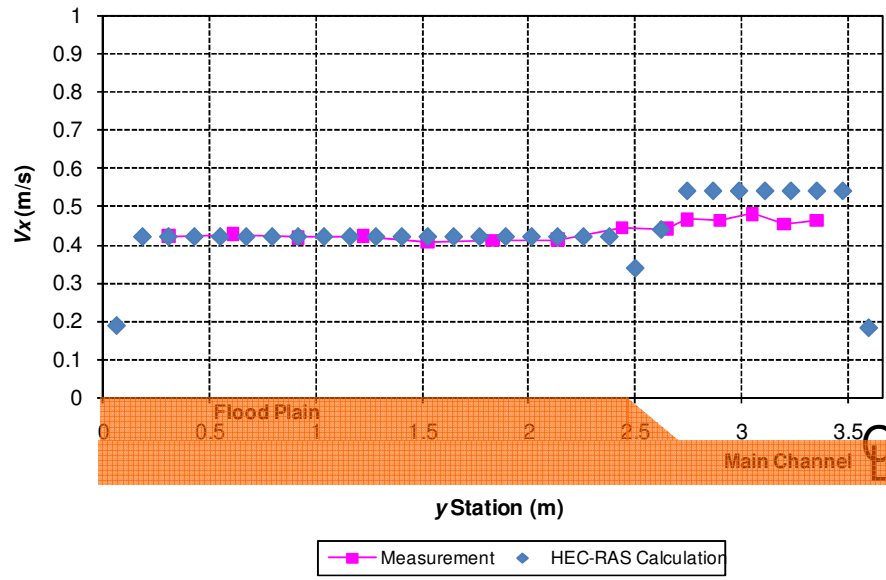
(c) Case7 (ST abutment, L'/L_f=1.0, V_1=0.44m/s)

Figure 5.5. (continued)
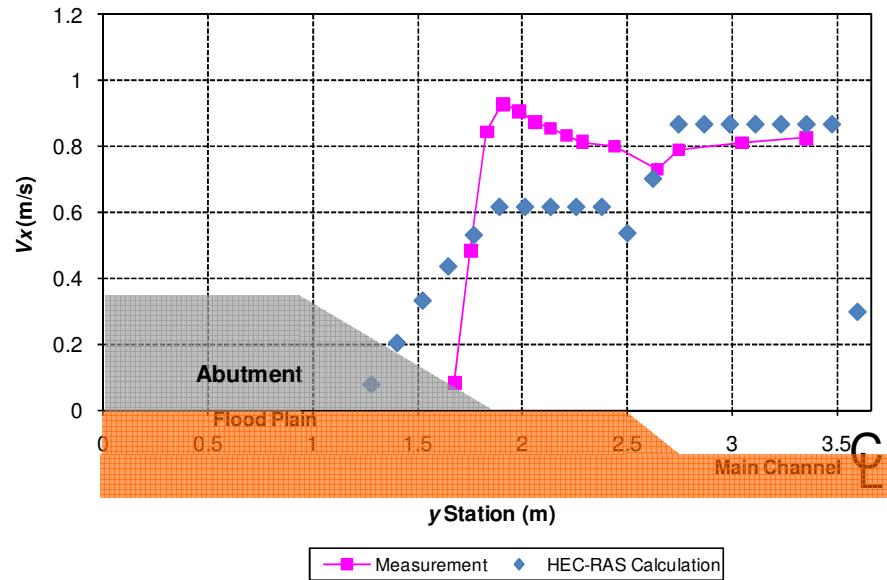
(a) Case1II (ST abutment, L'/L_f=0.75, V_1=0.44m/s)

Figure 5.6. Comparison of velocity distribution at bridge section between measurement

and HEC-RAS calculation
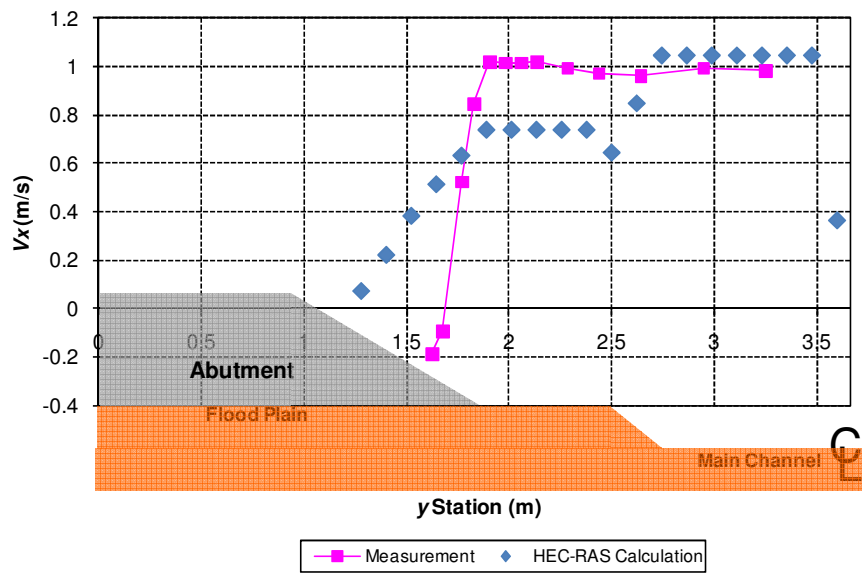
(b) Case5 (ST abutment, L'/L_f=0.75, V_1=0.51m/s)
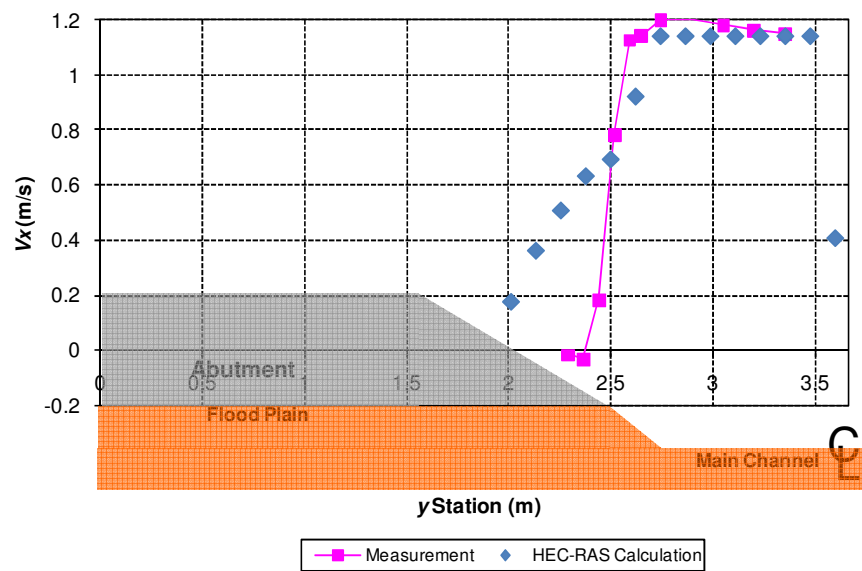
(c) Case7 (ST abutment, L'/L_f=1.0, V_1=0.44m/s)

Figure 5.6. (continued)
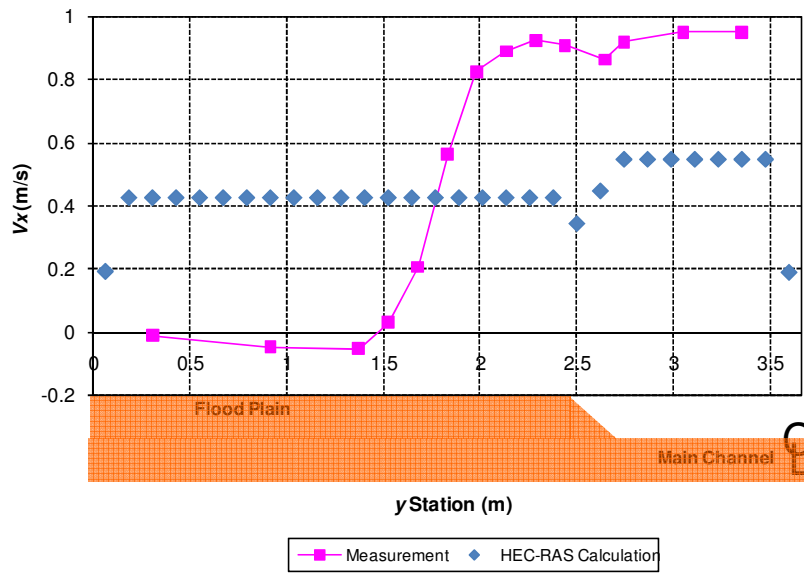
(a) Case1II (ST abutment, L'/L_f=0.75, V_1=0.44m/s)
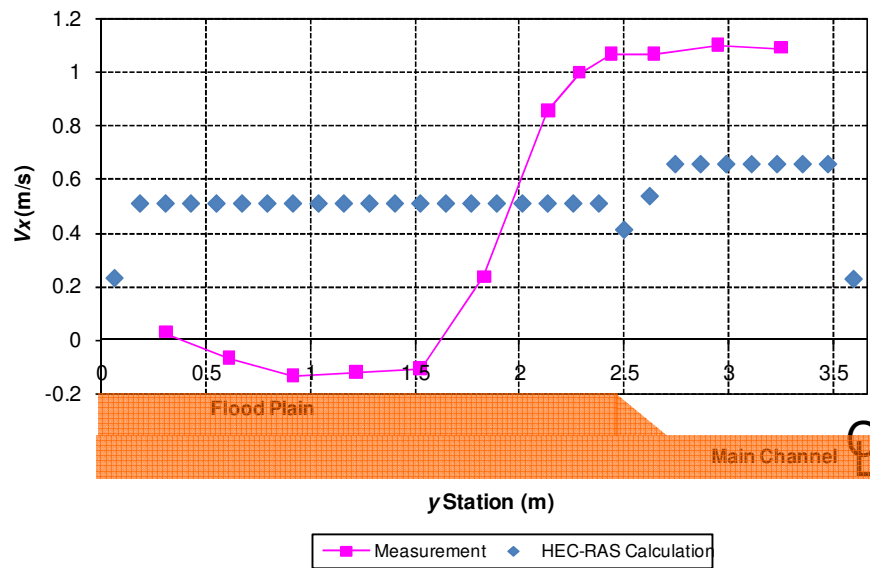
(b) Case5 (ST abutment, L'/L_f=0.75, V_1=0.51m/s)

Figure 5.7. Comparison of streamwise velocity at downstream (x = 1.14 m) between

measurement and HEC-RAS calculation
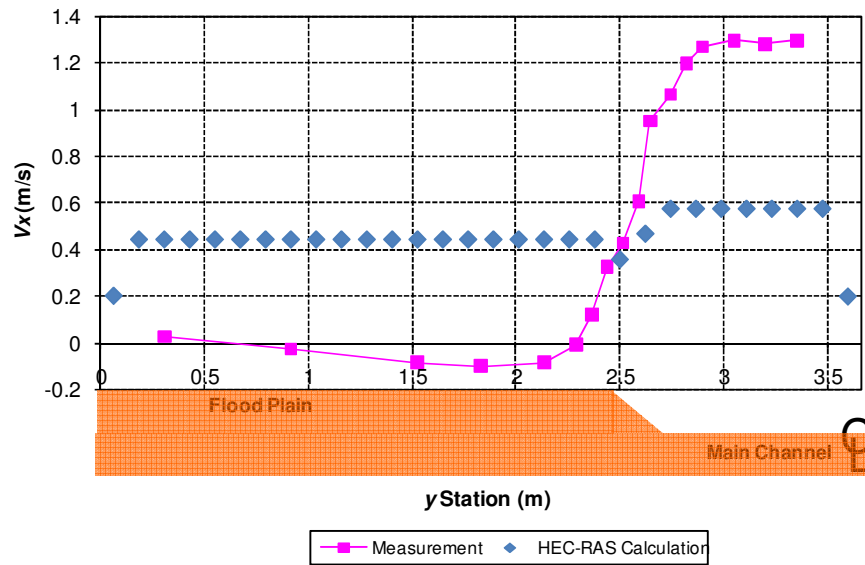
(c) Case7 (ST abutment, L'/L_f=1.0, V_1=0.44m/s)

Figure 5.7. (continued)
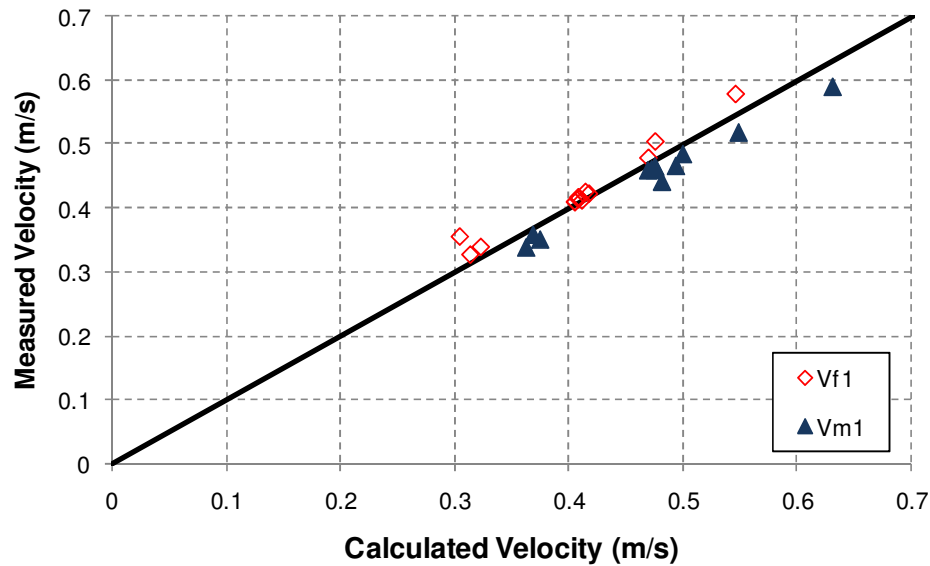
Figure 5.8. Comparison of average streamwise velocity at approach section (at y = -9.1m) on the floodplain and in the main channel between measurement and HEC-RAS calculation (V_{f1} is the velocity on the floodplain and V_{m1} is the velocity in the main channel)

CHAPTER VI

PIER SCOUR IN COHESIVE SOIL

6.1 Introduction

Gudavalli (1997) conducted experimental research on pier scour using circular piers in deep water condition. He used 2 types of sand and 3 types of clay, and proposed a formulation to predict the maximum pier scour. Li (2002) conducted experimental research on complex pier scour using Porcelain clay as channel bottom. The shallow water effect, abutment shape effect, attack angle effect and group pier effect were studied and several correction factors were presented. It was recommended to multiply all correction factors proposed by Li (2002) to the formulation suggested by Gudavalli (1997).

Although 5 types of soil were used in Gudavalli (1997), the soil property was not included in his formulation. In this chapter, his data is reanalyzed and new methodology is proposed. In addition, experiment results of Li (2002) are also reanalyzed and correction factors are proposed to be applicable to the equation considering the property of channel bed soils.

6.2 Flume test results

Gudavalli (1997) conducted 43 flume tests with 2 types of sand (D_{50} = 0.6 mm, 0.14 mm) and 3 types of clay (Porcelain, Armstone and Bentonite clay) in deep water condition $\left(y_1 \geq 1.43 \right)$. A variable slope flume with 0.45 m width was used for experiments with 25 mm and 75 mm diameter piers, and a concrete flume with 1.5 m

width was used for experiments with 25 mm, 75 mm, 150 mm and 210 mm diameter piers. The properties of soil used in his tests are summarized in the Table 6.1.

Li (2002) conducted two series of flume tests with Porcelain clay as channel bed material. One series of flume tests are for complex pier scour, and the other series of tests are for contraction scour in the rectangular channel. The flume test results for complex pier scour are used in this chapter, and the contraction scour results are dealt in other chapter for contraction scour in cohesive soil. The concrete flume, which is 1.5 m wide, 30.48 m long and 3.48 m deep, is used to conduct the complex pier scour tests. The properties of soil used in Li (2002) are summarized in the Table 6.2.

Table 6.1. Geotechnical properties of soils used by Gudavalli (1997)

	Sand A	Sand B	Porcelain clay	Armstone clay	Bentonite clay
D_{50} (mm)	0.6	0.14	-	-	-
Plasticity Index (%)	-	-	14.15	25.81	39.78
Clay content (%)	0	0	100	75	0
Water content (%)	-	-	28.51	26.18	39.28
τ_c (Pa)	0.456	0.107	0.515	0.761	0.7

Table 6.2. Geotechnical properties of Porcelain clay used by Li (2002)

Property	Test 1	Test 2
Liquid Limit (LL) (%)	40.23	37.7
Plastic Limit (PL) (%)	19.17	14.4
Plasticity Index (PI) (%)	21.06	23.3
Water Content (%)	27.35	30.5
Bulk Unit Weight (kN/m^3)	19.65	24.99
Undrained Shear Stress (kPa)	10.7	18.1

6.3 Dimensional analysis

The clear water pier scour occurs if the shear stress (τ) acting around pier is bigger than critical shear stress (τ_c). The shear stress decreases with scour development and it continues until the shear stress becomes critical shear stress ($\tau = \tau_c$). The parameters influencing on pier scour can be listed as following:

$$y_{s(Pier)} = f(a, L, y_1, \theta, g, \tau, \tau_c, S, sh) \tag{6.1}$$

where $y_{s(Pier)}$ is maximum pier scour depth, a is width of pier, L is length of pier, y_1 is approach water depth, θ is attack angle, g is gravitational acceleration, τ is shear stress around pier, τ_c is critical shear stress, S is spacing between adjacent two piers (measured center to center) and sh is shape of pier nose. The shear stress applying on between channel bottom and flow in the open channel is governed by flow velocity, roughness of channel bottom and water depth. Richardson and Davis (1995) built the relationship between shear stress and water depth, velocity and roughness of channel. The relationship is written in equation (6.2):

$$\tau = \rho g n^2 V^2 \Big/ y^{1/3} \tag{6.2}$$

The critical shear stress of the cohesive and cohesionless soil can be decided by using EFA test if EFA test is available. However, mostly the critical shear stress for cohesionless soil is decided by D_{50} using Shields diagram. Obtaining the critical shear stress using EFA test or Shields diagram, the critical velocity can be calculated using equation (6.2) as:

$$V_c = \sqrt{\frac{\tau_c \cdot y^{1/3}}{\rho \cdot g \cdot n^2}} \tag{6.3}$$

The shear stress terms in equation (6.1) can be rearranged using equation (6.3), and it is:

$$y_{s(Pier)} = f(a, L, y_1, \theta, g, V_1, V_c, S, sh) \tag{6.4}$$

Buckingham Π theorem is applied to perform the dimensional analysis with the repeating variable a and g. The width of pier (a) is used by referring Melville's study (1997). In his studies he found that the pier scour depth in deep water condition $(y \geq 1.43 \cdot a)$ is independent on the water depth as shown in Figure 2.2. Thus selecting pier width as repeating variable is more reasonable instead of using water depth.

Dimensional analysis yields the following dimensionless parameters:

$$\frac{y_{s(Pier)}}{a} = f\left(\frac{L}{a}, \frac{y_1}{a}, \theta, Fr_{(pier)}, Fr_{c(pier)}, \frac{S}{a}, sh\right) \tag{6.5}$$

where $Fr_{(pier)}$ is Froude number based on approach velocity and pier width $\left(Fr_{(pier)} = \frac{V_1}{\sqrt{g \cdot a}}\right)$, and $Fr_{c(pier)}$ is the critical Froude number based on critical velocity and pier width $\left(Fr_{c(pier)} = \frac{V_c}{\sqrt{g \cdot a}}\right)$

Since the pier scour develops until the shear stress acting around pier equals to the critical shear stress, the maximum pier scour equation can be expressed as:

$$\frac{y_{s(Pier)}}{a} = K_1 \cdot K_2 \cdot K_L \cdot K_w \cdot K_{sp} \cdot \alpha_1 \left(\beta_1 \cdot Fr_{(pier)} - Fr_{c(pier)}\right)^{\chi_1} \tag{6.6}$$

where K_1 is the correction factor for pier nose shape, K_2 is the correction factor for attack angle, K_L is the correction factor for aspect ratio of rectangular pier, K_w is the correction factor for water depth effect, K_{sp} is the correction factor for spacing between center of two piers, α_1, β_1 and χ_1 are constant. Note that the amplification factor β_1 considering the turbulence around pier is required, and β_1 should be always bigger than 1.0

6.3.1 Prediction equation

Although Gudavalli proposed maximum pier scour equation, the property of channel bottom soil was not included in his scour prediction. In this chapter, another study including soil characteristic especially the critical shear stress was conducted using Gudavalli's flume test results and Li's flume test results in deep water condition $(y \geq 1.43 \cdot a)$. Circular cylinder piers with 5 different diameters were used in Gudavalli's flume tests, and 2 different diameters were used in Li's flume tests in deep water condition. The tests results in dimensional form and dimensionless form are summarized in Table 6.3 and Table 6.4, respectively.

Since all test results in Table 6.3 and Table 6.4 are for singular circular pier in deep water condition, the equation (6.6) can be simplified as:

$$\frac{y_{s(Pier)}}{a} = \alpha_1 \left(\beta_1 \cdot Fr_{(pier)} - Fr_{c(pier)} \right)^{\chi_1} \tag{6.7}$$

The constants α_1, β_1 and χ_1 are determined experimentally by curve fitting on Figure 6.1. The proposed maximum pier scour equation of circular cylinder pier is:

$$\frac{y_{s(Pier)}}{a} = 2.2\left(2.6 \cdot Fr_{(pier)} - Fr_{c(pier)}\right)^{0.7} \tag{6.8}$$

The correction coefficient R^2 in the relation between equation (6.8) and flume test results is 0.803. The equations representing upper and lower boundary envelop are:

Lower boundary

$$\frac{y_{s(Pier)}}{a} = 0.5 \cdot 2.2\left(2.6 \cdot Fr_{(pier)} - Fr_{c(pier)}\right)^{0.7} \tag{6.9}$$

Upper boundary

$$\frac{y_{s(Pier)}}{a} = 1.5 \cdot 2.2\left(2.6 \cdot Fr_{(pier)} - Fr_{c(pier)}\right)^{0.7} \tag{6.10}$$

A factor of safety provides a margin of error that allows for a considerable variation from an expected pier scour depth. Figure 6.2 shows the comparison between flume test results and prediction by equations from (6.8) to (6.10). The equation (6.10) with factor of safety 1.5 satisfies all experiment results.

Table 6.3. Summary of singular circular pier in deep water by Gudavalli (1997) and Li (2002) in dimensional form

Expt No.	y_1 (m)	a (mm)	Soil Type	Pier Shape	τ_c (Pa)	V_1 (m/s)	V_c (m/s)	$y_{s(Pier)}$ (mm)
1	0.4	25	Porcelain	Circular	0.515	0.47	0.44	95.9
2	0.4	25	Porcelain	Circular	0.515	0.4	0.44	71.8
3	0.4	25	Porcelain	Circular	0.515	0.61	0.44	123.4
4	0.4	25	Porcelain	Circular	0.515	0.32	0.44	55.8
5	0.4	25	Porcelain	Circular	0.515	0.2	0.44	21.7
6	0.4	25	Porcelain	Circular	0.515	0.4	0.44	66.6
7	0.4	25	Porcelain	Circular	0.515	0.83	0.44	114.8
8	0.4	75	Porcelain	Circular	0.515	0.61	0.44	158
9	0.4	75	Porcelain	Circular	0.515	0.32	0.44	77.9
10	0.4	75	Porcelain	Circular	0.515	0.2	0.44	23.2
11	0.4	75	Porcelain	Circular	0.515	0.4	0.44	115.7
12	0.4	75	Porcelain	Circular	0.515	0.48	0.44	137.4
13	0.4	75	Porcelain	Circular	0.515	0.39	0.44	160.9
14	0.4	75	Porcelain	Circular	0.515	0.32	0.44	55.1
15	0.4	75	Porcelain	Circular	0.515	0.48	0.44	178.2
16	0.4	75	Porcelain	Circular	0.515	0.83	0.44	190.9
17	0.16	25	Porcelain	Circular	0.515	0.27	0.38	48.8
18	0.16	75	Porcelain	Circular	0.515	0.27	0.38	75.9
19	0.16	25	Porcelain	Circular	0.515	0.35	0.38	64.9
20	0.16	75	Porcelain	Circular	0.515	0.35	0.38	100.9
21	0.4	25	Armstone	Circular	0.761	0.47	0.54	60
22	0.4	25	Armstone	Circular	0.761	0.32	0.54	43.9
23	0.4	25	Armstone	Circular	0.761	0.41	0.54	83.8
24	0.4	25	Armstone	Circular	0.761	0.41	0.54	58.82
25	0.4	25	Bentonite	Circular	0.7	0.32	0.52	62.4
26	0.4	25	Bentonite	Circular	0.7	0.39	0.52	58.8
27	0.17	50	Sand A	Circular	0.456	0.24	0.36	67
28	0.17	50	Sand A	Circular	0.456	0.25	0.36	48
29	0.32	50	Sand A	Circular	0.456	0.35	0.40	85
30	0.33	50	Sand A	Circular	0.456	0.45	0.41	115
31	0.4	25	Sand B	Circular	0.107	0.24	0.20	35
32	0.4	25	Sand B	Circular	0.107	0.28	0.20	41
33	0.4	75	Sand B	Circular	0.107	0.21	0.20	70
34	0.4	25	Porcelain	Circular	0.515	0.3	0.44	28.6
35	0.4	75	Porcelain	Circular	0.515	0.3	0.44	106.5
36	0.4	25	Porcelain	Circular	0.515	0.4	0.44	73.1
37	0.4	75	Porcelain	Circular	0.515	0.4	0.44	112.3
38	0.4	75	Porcelain	Circular	0.515	0.37	0.44	141.5
39	0.3	150	Porcelain	Circular	0.515	0.39	0.42	227.1
40	0.25	150	Porcelain	Circular	0.515	0.3	0.41	171.6
41	0.3	210	Porcelain	Circular	0.515	0.32	0.42	208.6
42	0.3	210	Porcelain	Circular	0.515	0.4	0.42	222.1
43	0.3	210	Porcelain	Circular	0.515	0.32	0.42	165.8
Sw-1	0.683	273	Porcelain	Circular	0.674	0.3	0.56	112.94
Sw-2	0.546	273	Porcelain	Circular	0.674	0.3	0.54	129.62
Sw-8	0.4	160	Porcelain	Circular	0.674	0.4	0.51	76.92
Sw-9	0.32	160	Porcelain	Circular	0.674	0.4	0.49	109.67

Table 6.4. Summary of singular pier in deep water by Gudavalli (1997) and Li (2002) in dimensionless form

Expt No.	y_1/a	$y_{s(Pier)}/a$	$Fr_{(Pier)}$	$Fr_{c(Pier)}$	Expt No.	y_1/a	$y_{s(Pier)}/a$	$Fr_{(Pier)}$	$Fr_{c(Pier)}$
1	16.00	3.84	0.95	0.90	25	16.00	2.50	0.65	1.05
2	16.00	2.87	0.81	0.90	26	16.00	2.35	0.79	1.05
3	16.00	4.94	1.23	0.90	27	3.40	1.34	0.34	0.52
4	16.00	2.23	0.65	0.90	28	3.40	0.96	0.36	0.52
5	16.00	0.87	0.40	0.90	29	6.40	1.70	0.50	0.58
6	16.00	2.66	0.81	0.90	30	6.60	2.30	0.64	0.58
7	16.00	4.59	1.68	0.90	31	16.00	1.40	0.48	0.41
8	5.33	2.11	0.71	0.52	32	16.00	1.64	0.57	0.41
9	5.33	1.04	0.37	0.52	33	5.33	0.93	0.24	0.24
10	5.33	0.31	0.23	0.52	34	16.00	1.14	0.61	0.90
11	5.33	1.54	0.47	0.52	35	5.33	1.42	0.35	0.52
12	5.33	1.83	0.56	0.52	36	16.00	2.92	0.81	0.90
13	5.33	2.15	0.45	0.52	37	5.33	1.50	0.47	0.52
14	5.33	0.73	0.37	0.52	38	5.33	1.89	0.43	0.52
15	5.33	2.38	0.56	0.52	39	2.00	1.51	0.32	0.35
16	5.33	2.55	0.97	0.52	40	1.67	1.14	0.25	0.34
17	6.40	1.95	0.55	0.77	41	1.43	0.99	0.22	0.30
18	2.13	1.01	0.31	0.45	42	1.43	1.06	0.28	0.30
19	6.40	2.60	0.71	0.77	43	1.43	0.79	0.22	0.30
20	2.13	1.35	0.41	0.45	Sw-1	2.50	0.41	0.18	0.34
21	16.00	2.40	0.95	1.09	Sw-2	2.00	0.47	0.18	0.33
22	16.00	1.76	0.65	1.09	Sw-8	2.50	0.48	0.32	0.41
23	16.00	3.35	0.83	1.09	Sw-9	2.00	0.69	0.32	0.39
24	16.00	2.35	0.83	1.09					

where y_1 is approach water depth, a is pier width, S is spacing between adjacent two piers (measured center to center), L is length of pier of rectangular pier, a' is projected pier width, τ_c is critical shear stress of channel bottom soil, V_1 is approach velocity, V_c is critical velocity of channel bottom soil, $y_{s(Pier)}$ is maximum pier scour depth, $Fr_{(pier)}$ is Froude number based on approach velocity and pier width, and $Fr_{c(pier)}$ is the critical Froude number based on critical velocity and pier width.
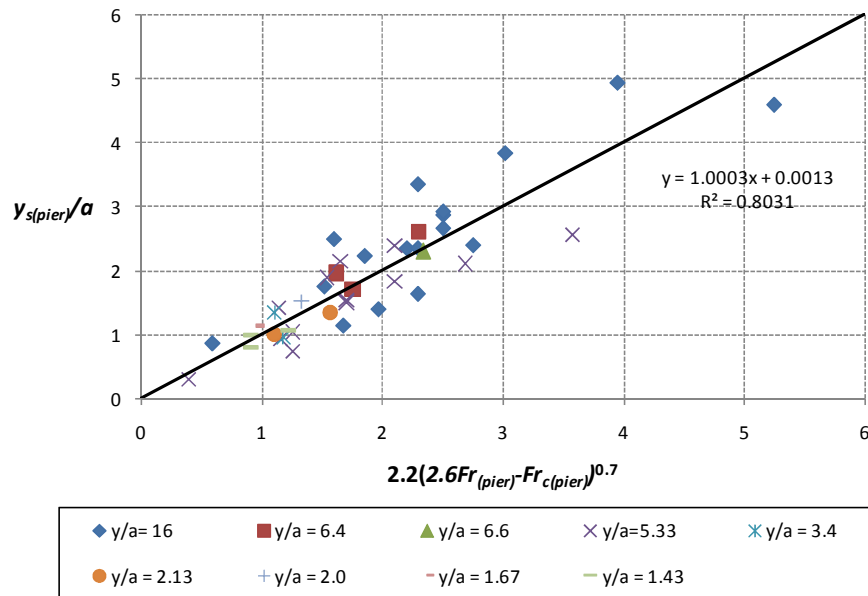
Figure 6.1. Normalized maximum pier scour depth based on equation (6.8)
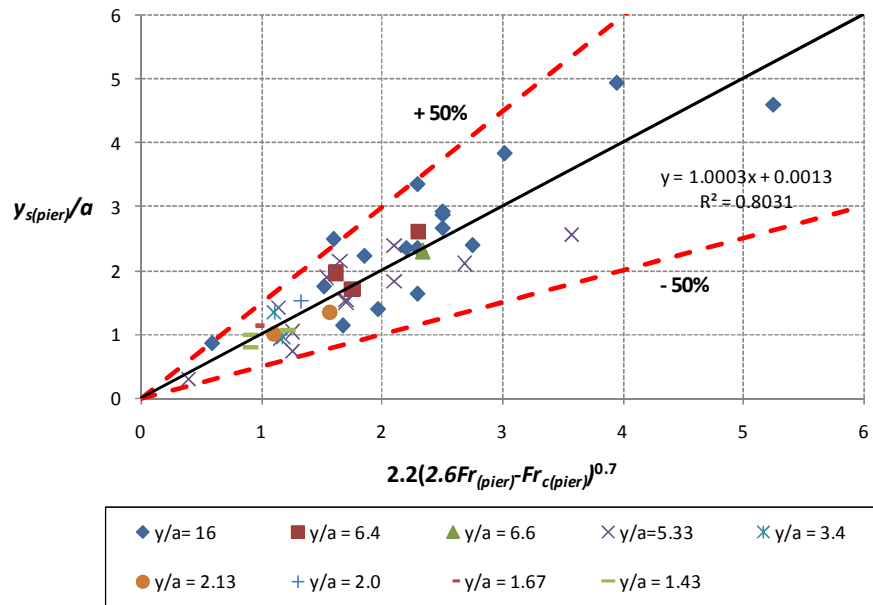
Figure 6.2. Pier scour prediction including safety factor and measurement results for

circular pier in deep water condition

6.3.2 Correction factors for complex pier scour

Equation (6.8) is developed with data for single circular pier in deep water condition. Li (2002) performed flume tests to find the effect of pier nose shape, attack angle, water depth and pier spacing. Parameters are schematically explained in Figure 6.3. Flume test results by Li are summarized in Table 6.5.

(a) Water depth effect

(b) Pier spacing effect

(c) Pier shape effect

(d) Attack angle effect
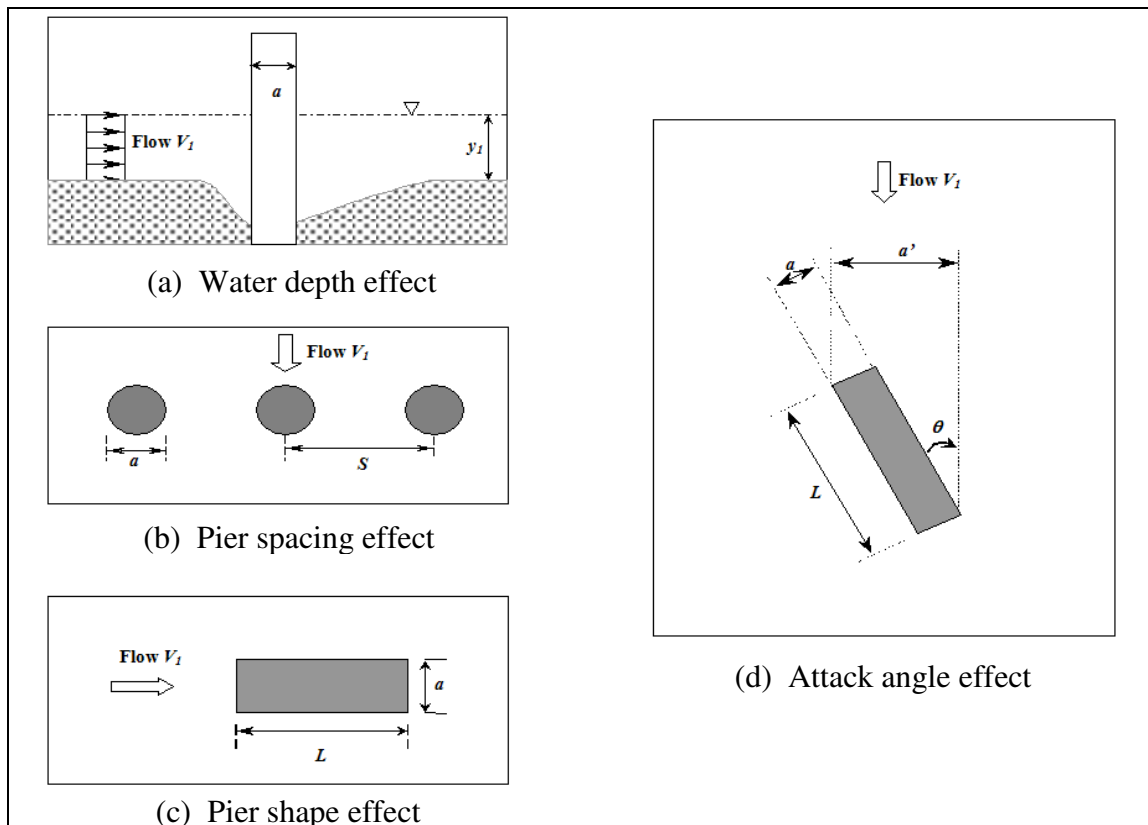
Figure 6.3. Schematic definition of parameters

Table 6.5. Flume test results conducted by Lin (2002) in dimensional form

Expt. No.	Pier Nose Shape	y_1 (mm)	a (mm)	S (mm)	L (mm)	θ (°)	a' (mm)	τ_c (Pa)	V_1 (m/s)	V_c (m/s)	$y_{s(pier)}$ (mm)
SW-1	Circ.	683	273	Single	273	0	273.00	0.674	0.3	0.556	112.94
SW-2	Circ.	546	273	Single	273	0	273.00	0.674	0.3	0.536	129.62
SW-3	Circ.	258	273	Single	273	0	273.00	0.674	0.3	0.473	79.37
SW-4	Circ.	137	273	Single	273	0	273.00	0.674	0.3	0.427	57.8
SW-5	Circ.	60	273	Single	273	0	273.00	0.674	0.3	0.372	81.3
SW-6	Circ.	60	273	Single	273	0	273.00	0.674	0.3	0.372	61.35
SW-7	Circ.	25.8	273	Single	273	0	273.00	0.674	0.3	0.324	35.59
SW-8	Circ.	400	160	Single	160	0	160.00	0.674	0.4	0.509	76.92
SW-9	Circ.	320	160	Single	160	0	160.00	0.674	0.4	0.491	109.67
SW-10	Circ.	170	160	Single	160	0	160.00	0.674	0.4	0.442	77.73
SW-11	Circ.	85	160	Single	160	0	160.00	0.674	0.4	0.394	53.48
GR-1	Circ.	380	160	750	160	0	160.00	0.583	0.33	0.469	165.56
GR-2	Circ.	380	160	500	160	0	160.00	0.583	0.33	0.469	157.44
GR-3	Circ.	380	160	375	160	0	160.00	0.583	0.33	0.469	208.08
GR-4	Circ.	380	160	300	160	0	160.00	0.583	0.33	0.469	250
SP-1	Circ.	380	61	Single	61	0	61.00	0.583	0.33	0.469	68.03
SP-2	Rect.	380	61	Single	61	0	61.00	0.583	0.33	0.469	73.53
SP-3	Rect.	380	61	Single	244	0	61.00	0.583	0.33	0.469	72.99
SP-4	Rect.	380	61	Single	488	0	61.00	0.583	0.33	0.469	74.63
SP-5	Rect.	380	61	Single	732	0	61.00	0.583	0.33	0.469	75.19
AT-1	Rect.	375	61	Single	244	15	122.07	0.583	0.33	0.468	72.99
AT-2	Rect.	375	61	Single	244	30	174.83	0.583	0.33	0.468	103.09
AT-3	Rect.	375	61	Single	244	45	215.67	0.583	0.33	0.468	151.5
AT-4	Rect.	375	61	Single	244	60	241.81	0.583	0.33	0.468	196.08
AT-5	Rect.	375	61	Single	244	90	244.00	0.583	0.33	0.468	208.77
AT-6	Rect.	375	61	Single	61	45	86.27	0.583	0.33	0.468	147.06
AT-7	Rect.	375	61	Single	122	45	129.40	0.583	0.33	0.468	161.29
AT-8	Rect.	375	61	Single	366	45	301.93	0.583	0.33	0.468	185.19
CP-2	Rect.	375	61	500	244	45	215.67	0.583	0.33	0.468	285.7
CP-1	Rect.	375	61	500	244	15	122.07	0.583	0.33	0.468	175.4

where y_1 is approach water depth, a is pier width, S is spacing between adjacent two piers (measured center to center), L is length of pier of rectangular pier, θ is attack angel, a' is projected pier width, τ_c is critical shear stress of channel bottom soil, V_1 is approach velocity, V_c is critical velocity of channel bottom soil, and $y_{s(Pier)}$ is maximum pier scour depth.

He developed a pier scour equation using Gudavalli's equation mentioned in equation (2.26), while another approach with the differential of Froude number used in equation (6.8) is conducted in this study.

6.3.2.1 Water depth effect (K_w)

The equation (6.8) is developed in the condition of deep water. In the shallow water condition, the correction factor for water depth effect should be considered to apply equation (6.8) to shallow water condition. The correction factor for water depth, K_w, is the ratio of the maximum scour depth in shallow water to the maximum scour depth in deep water condition. In Table 6.6, Test SW-1 and SW-8 were conducted in deep water condition ($y \geq 1.43 \cdot a$), and test SW-1 has identical test condition with tests from SW-2 to SW-7, and test SW-8 is identical to tests from SW-10 to SW-11 except water depth. Figure 6.4 shows the ratio of the maximum scour depth in shallow water to the maximum scour depth in deep water condition (K_w).

The correction factor for water depth effect K_w is:

$$K_w = \begin{cases} 0.89\left(\dfrac{y_1}{a}\right)^{0.33} & , \text{for } \dfrac{y_1}{a} < 1.43 \\ 1.0 & , \text{otherwise} \end{cases}$$

(6.11)

Table 6.6. Test results for shallow water effect by Li (2002)

Expt. No.	y_1 (mm)	a (mm)	y_1/a	$y_{s(Pier)}/a$	V_1 (m/s)	Ratio	K_w
SW-1	683	273	2.50	0.41	0.67	Reference	1.00
SW-2	546	273	2.00	0.47	0.67	1.15	1.00
SW-3	258	273	0.95	0.29	0.67	0.70	0.87
SW-4	137	273	0.50	0.21	0.67	0.51	0.71
SW-5	60	273	0.22	0.30	0.67	0.72	0.54
SW-6	60	273	0.22	0.22	0.67	0.54	0.54
SW-7	25.8	273	0.09	0.13	0.67	0.32	0.41
SW-8	400	160	2.50	0.48	0.67	Reference	1.00
SW-10	170	160	1.06	0.49	0.67	1.01	0.91
SW-11	85	160	0.53	0.33	0.67	0.70	0.72
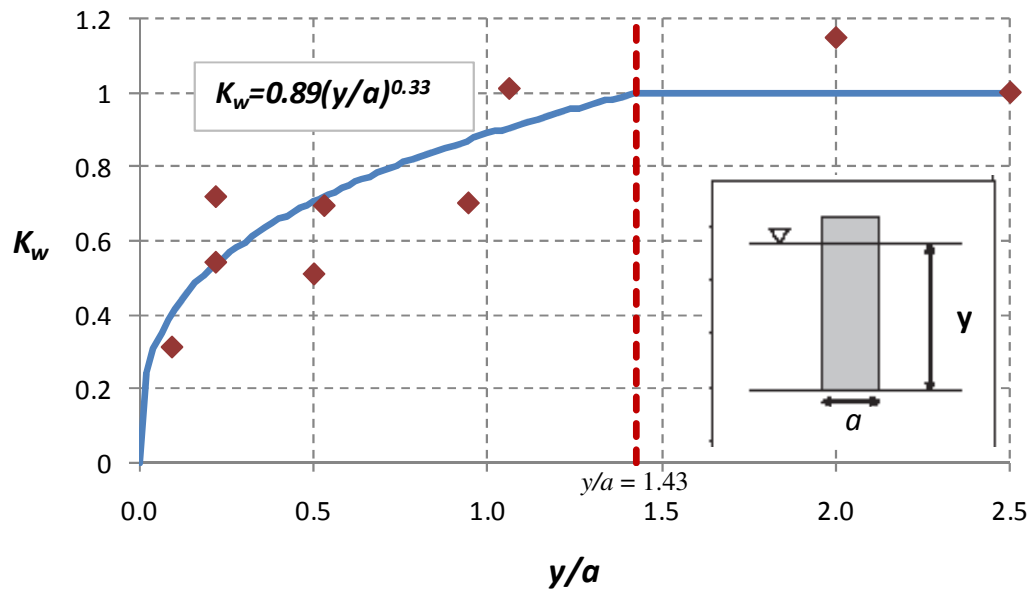
Figure 6.4. Correction factor for water depth effect on maximum pier scour depth

6.3.2.2 Pier spacing effect (K_{sp})

The flow around group pier is more turbulent than that around single pier. The narrower gap makes the more turbulent flow, and this turbulent flow induces deeper

scour hole around pier. The parameters and results of four tests for the effect of pier spacing, which are conducted by Li (2002), are summarized in Table 6.7. In order to apply equation (6.8) developed for singular circular pier to group pier, the correction factor for group pier is required if the flow is influenced by adjacent piers. Tests from GR-1 to GR-4 in Table 6.7 were elaborated to find the effect of pier spacing between two piers. In those four tests, all test conditions were maintained constant except pier spacing, S, by Li (2002). The pier spacing effect was examined by varying the gap between two piers. The correction factor for pier spacing K_{sp} is the ratio of the measured maximum pier scour depth to the predicted maximum pier scour depth by equation (6.8). The relationship between K_{sp} and the normalized distance between two piers by pier diameter is shown in Figure 6.5. The correction factor for pier spacing effect K_{sp} is:

$$K_{sp} = \begin{cases} 2.9\left(\dfrac{S}{a}\right)^{-0.91} & \text{, for } \dfrac{S}{a} < 3.2 \\ 1.0 & \text{, else} \end{cases}$$

(6.12)

Table 6.7. Test results for pier spacing effect by Li (2002)

Expt. No.	y_1/a'	$y_{s(Pier)}/a'$	L/a'	S/a'	V_1 (m/s)	Ratio	K_{sp}
GR-1	2.38	1.03	1	4.69	0.33	1.07	1.00
GR-2	2.38	0.98	1	3.13	0.33	1.01	1.03
GR-3	2.38	1.30	1	2.34	0.33	1.34	1.34
GR-4	2.38	1.56	1	1.88	0.33	1.61	1.64
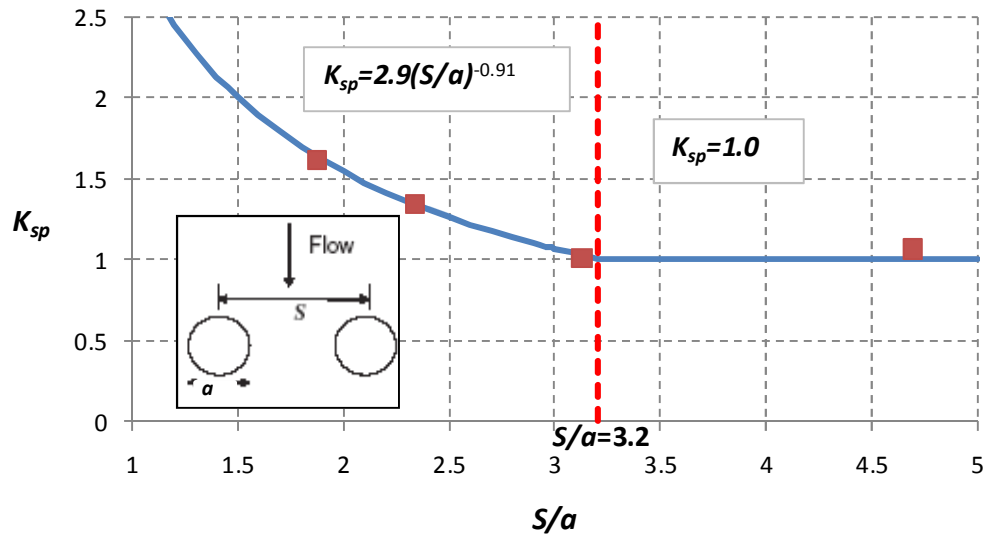
Figure 6.5. Correction factor for pier spacing

6.3.2.3 Pier shape effect (K_1) and aspect ratio (K_L)

Pier nose shape is another important variable to affect velocity pattern around piers. In the design of new bridge, most piers have round or circular pier nose to produce smooth transition of flow around the nose of pier. However, Li (2002) used rectangular piers with variation of aspect ratio (*L/B*) for the comparison with previous studies. The parameters and results of four tests for the effect of pier shape and aspect ratio, which are conducted by Li (2002), are summarized in Table 6.8. In the Table 6.8, the test SP-1 which is the test in deep water condition with circular cylinder pier was conducted, and the maximum scour depth ratio of rectangular pier to circular cylinder pier was compared. The flow condition and pier width were kept constant in his study. The comparison result is shown in Figure 6.6. It is found that the aspect ratio is irrelevant to scour depth and only pier nose shape effect on scour depth. The correction factor K_1 for

rectangular pier is 1.1 and it matches up to previous studies such as Laursen and Toch (1956) and Richardson and et al.'s equation (2001). Note that Laursen and Toch (1956)'s the pier nose correction factor for rectangular pier and for circular cylinder pier is 1.0 and 0.9, respectively. Their correction factor ratio of rectangular pier nose shape to circular cylinder pier is 1.1.

The correction factor for rectangular pier nose perfectly agrees with two studies mentioned in previous sentence. Thus it may be reasonable to adopt the correction factor for other pier nose shape from the results of Richardson et al. (2001).

The correction factor for aspect ratio in rectangular pier is:

$$K_L = 1.0, \quad \text{for whole range of } L/a \tag{6.13}$$

Table 6.8. Test results for pier shape and aspect ratio by Li (2002)

Expt. No.	Pier Nose Shape	a' (mm)	y_1/a'	$y_{s(Pier)}/a'$	L/a'	Ratio	$K_1 K_L$
SP-1	Circ.	61.00	6.23	1.12	1	Reference	1.00
SP-2	Rect.	61.00	6.23	1.21	1	1.08	1.10
SP-3	Rect.	61.00	6.23	1.20	4	1.07	1.10
SP-4	Rect.	61.00	6.23	1.22	8	1.10	1.10
SP-5	Rect.	61.00	6.23	1.23	12	1.11	1.10
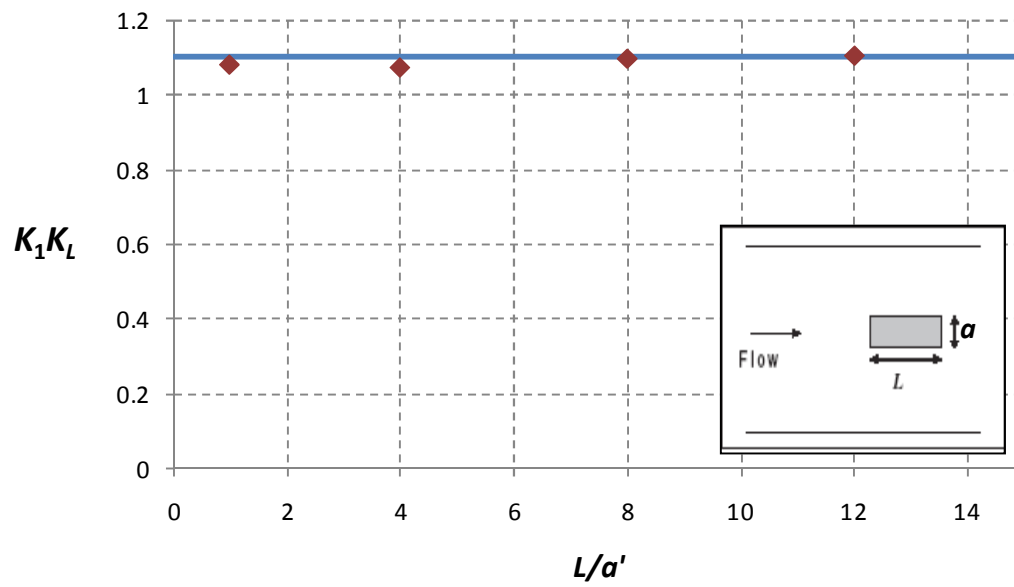
Figure 6.6. Correction factor for pier nose shape

The correction factor for pier nose shape is listed in Table 6.9:

Table 6.9. Correction factor for pier nose shape (K_1)

Shape of pier nose	K_1	Shape of pier nose	K_1
Square nose	1.1	Circular cylinder	1.0
Round nose	1.0	Sharp nose	0.9

6.3.2.4 Attack angle effect

The attack angle θ is the angle between the direction of flow and of pier. The attack angle leads to the change of the shape pier nose shape and the pier width. For rectangular pier, the shape of pier nose becomes sharp nose and the projected pier width changes with increase of attack angle θ or of aspect ratio L/B as shown in Figure 6.7. Richardson et al. (2001) recommended to ignore the effect of pier nose shape if $\theta \geq 5°$, and to use the correction factor for attack angle $\left(K_2 = \left(\cos\theta + L/a \cdot \sin\theta \right)^{0.65} \right)$ mentioned in equation (2.14).

The correction factor for attack angle K_2 is the ratio of maximum scour depth for piers with attack angle $\left(\theta > 0° \right)$ to the pier parallel with flow $\left(\theta = 0° \right)$ in same flow condition and pier dimension. The ratio of the measured scour depths for attack angle effect (experiments from AT-1 to AT-5) to SP-2 is compared in Figure 6.8. Although the water depth for SP-2 is 5 mm deeper than other 5 cases, it is reasonable because the difference is ignorable and water depth is irrelevant in deep water condition as mentioned in the correction factor for water depth. The trend of the correction factor for attack angle is compared with Laursen and Toch (1956) and Richardson et al. (2001). The relation proposed by Richardson et al. (2001) is compared to other measurements in different aspect ratio (L/a = 1.0, 2.0, 4.0 and 6.0, which are experiments AT-6, 7, 3 and 8, respectively) for $\theta = 45°$ in Figure 6.9 as well. Figure 6.8, the effect of attack angle is not significant if $\theta \leq 30°$ while reasonable agreement is made if $\theta > 30°$. Both Figure

6.8 and Figure 6.9 show that the correction factor for attack angle presented by Richardson et al. (2001) is reasonable.

The projected pier width of rectangular pier is shown in Figure 6.10 and it is:

$$a' = a\left(\cos\theta + \frac{L}{a} \cdot \sin\theta\right) \tag{6.14}$$

If the correction factor for attack angle, K_2, in equation (2.13) is substituted by equation (6.14) , equation (2.13) proposed by Richardson et al. (2001) can be rewritten as:

$$y_{s(pier)} = 2.0 K_1 \cdot K_3 \cdot K_4 \cdot a'^{0.65} \cdot y_1^{0.35} Fr_1^{0.43} \tag{6.15}$$

Substituting a (pier width) in equation (6.8) with a' (projected pier width), the pier scour depth equation for single rectangular pier in deep water condition is:

$$\frac{y_{s(Pier)}}{a'} = 2.2 \cdot \left(2.6 \cdot Fr_{(pier)} - Fr_{c(pier)}\right)^{0.7}$$
$$= 2.2 \cdot \left(2.6 \cdot \frac{V_1}{\sqrt{g \cdot a'}} - \frac{V_c}{\sqrt{g \cdot a'}}\right)^{0.7} \tag{6.16}$$

$$y_{s(Pier)} = 2.2 \cdot a' \cdot \left(2.6 \cdot \frac{V_1}{\sqrt{g \cdot a'}} - \frac{V_c}{\sqrt{g \cdot a'}}\right)^{0.7}$$
$$= 2.2 \cdot a'^{0.65} \left(2.6 \cdot \frac{V_1}{\sqrt{g}} - \frac{V_c}{\sqrt{g}}\right)^{0.7} \tag{6.17}$$

where K_1 is correction factor for pier shape ($K_1 = 1.0$, for $\theta > 30°$, other case K_1 is the value in Table 6.9. The scour depth predicted by equation (6.17) is proportional to $a'^{0.65}$ and it is consistent to equation (6.15).
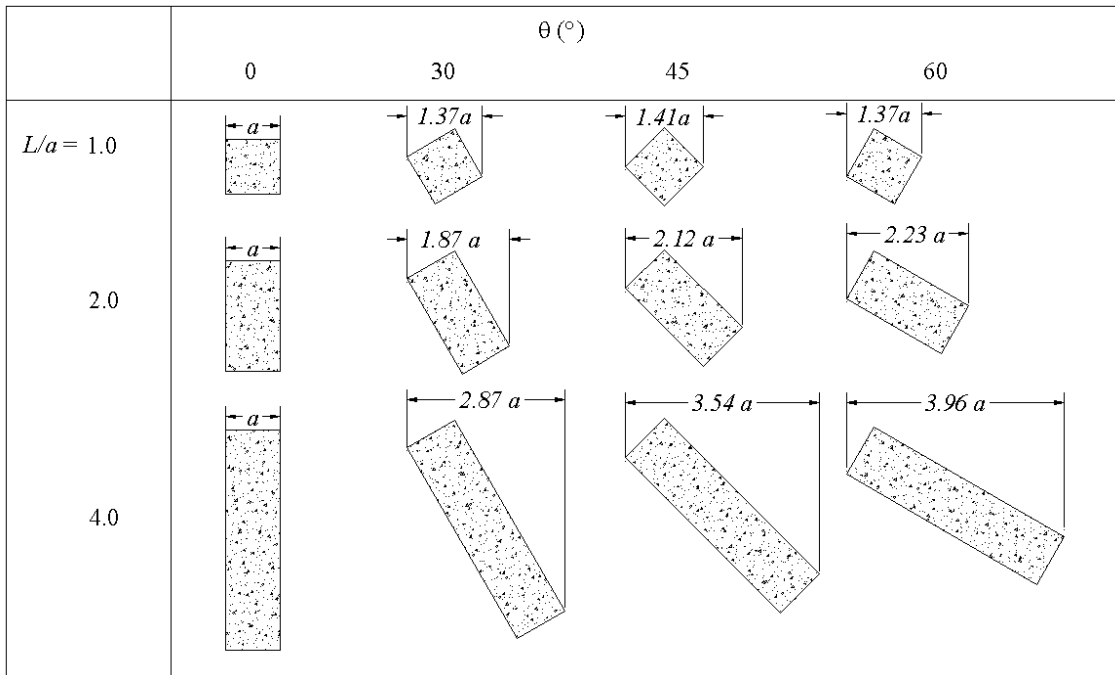
Figure 6.7. Variation of projected width (*a'*) with change of attack angle and aspect
ratio
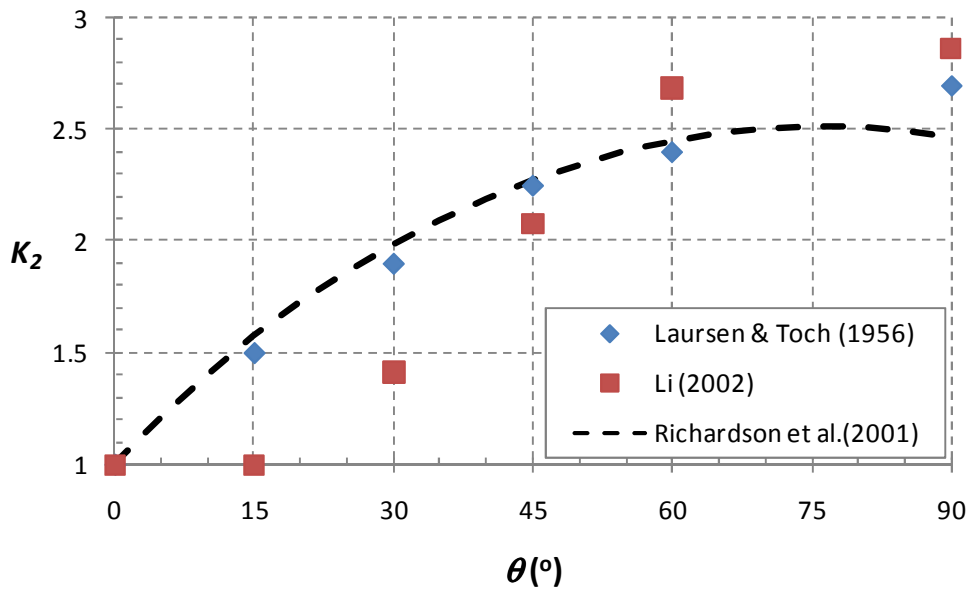
Figure 6.8. Correction factor for attack angle (*L/a* = 4.0)
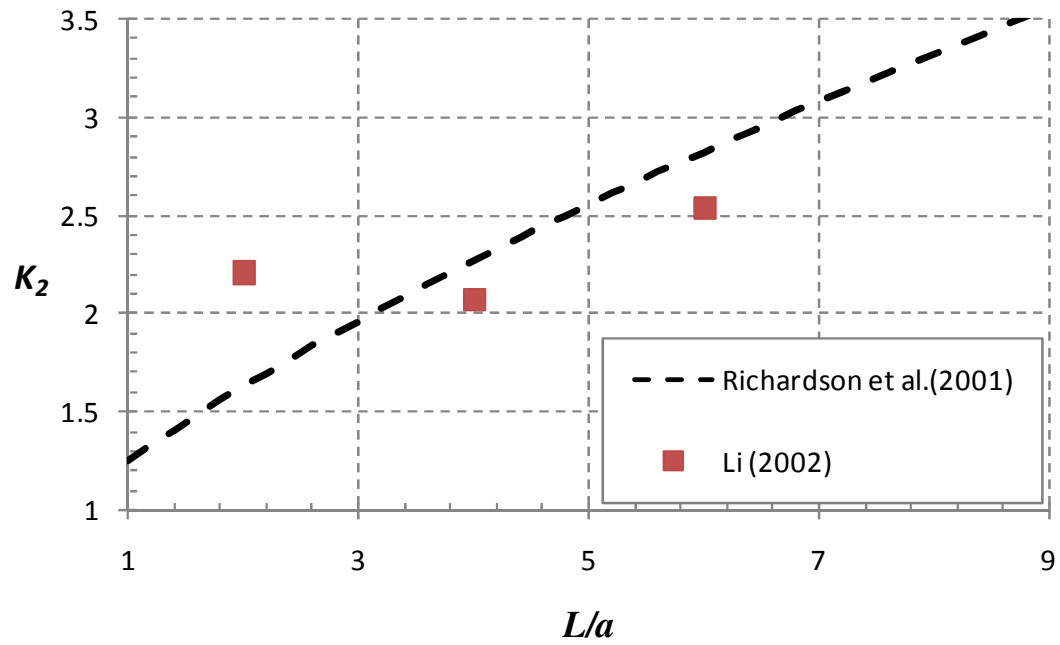
Figure 6.9. Correction factor for attack angle in different aspect ratio (θ=45$^{\text{o}}$)
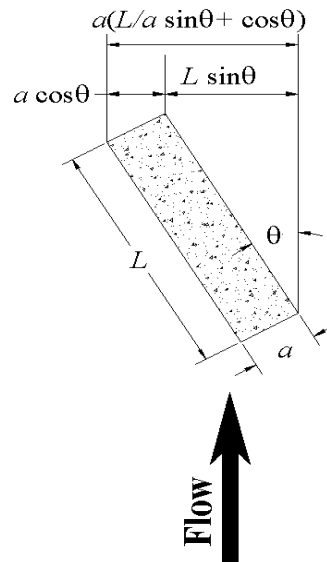
Figure 6.10. Definition of projected pier width

6.3.2.5 Maximum pier scour depth in complex pier

Individual effects on the maximum pier scour depth are studied in previous section, and the pier scour equation considering all conditions is:

$$\frac{y_{s(Pier)}}{a'} = 2.2 \cdot K_w \cdot K_1 \cdot K_L \cdot K_{sp} \cdot \left(2.6 \cdot Fr_{(pier)} - Fr_{c(pier)}\right)^{0.7} \qquad (6.18)$$

where K_w is the correction factor for water depth effect, K_1 is correction factor for pier shape, K_L is he correction factor for aspect ratio in rectangular pier, K_{sp} is correction factor for pier spacing, a' is projected pier width, $Fr_{(pier)}$ is Froude number based on approach velocity and a', and $Fr_{c(pier)}$ is Froude number based on critical velocity and a'.

$$K_w = \begin{cases} 0.89\left(\dfrac{y_1}{a'}\right)^{0.33} & , \text{for } \dfrac{y_1}{a'} < 1.43 \\ 1.0 & , \text{else} \end{cases}$$

$$K_1 = 1.0, \text{for } \theta > 30°,$$

for other case K_1 is the value in Table 6.9

$$K_L = 1.0, \quad \text{for whole range of } L/a$$

$$K_{sp} = \begin{cases} 2.9\left(\dfrac{S}{a'}\right)^{-0.91} & , \text{for } \dfrac{S}{a'} < 3.42 \\ 1.0 & , \text{else} \end{cases}$$

$$Fr_{(pier)} = \frac{V_1}{\sqrt{g \cdot a'}}, \quad Fr_{c(pier)} = \frac{V_c}{\sqrt{g \cdot a'}}, \quad a' = a\left(\cos\theta + \frac{L}{a} \cdot \sin\theta\right)$$

Two flume tests in complex pier condition were conducted by Li (2002), and the configuration is shown in Figure 6.11. The main parameters and results are summarized

in Table 6.10. In Table 6.10, the maximum pier scour depths predicted by equation (6.18) make reasonable agreement to measured scour depths with 15% error.
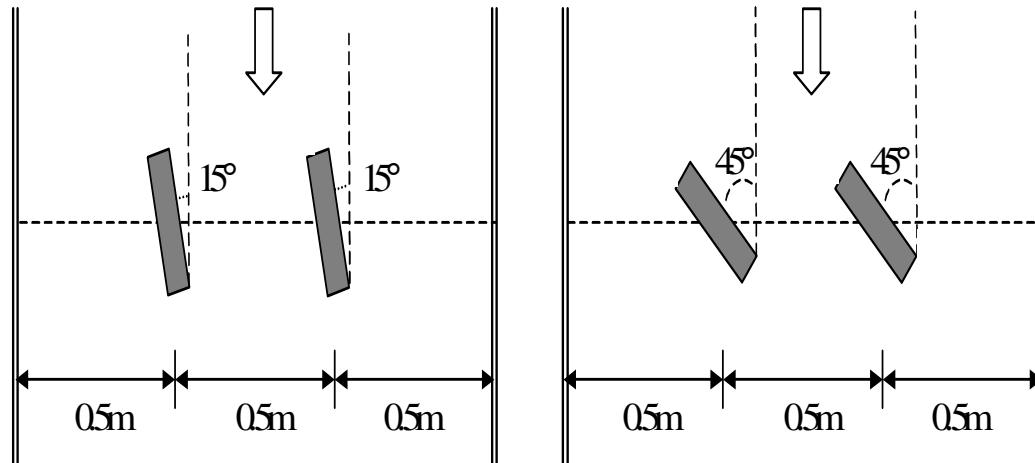
Figure 6.11. Configuration of flume tests for the complex pier condition

Table 6.10. Flume test parameters and maximum pier scour depths obtained by measurement and prediction using equation (6.18)

Expt. No.	Pier Nose Shaep	y_1 (mm)	a (mm)	S (mm)	L (mm)	θ (°)	V_1 (m/s)	V_c (m/s)	Meas. (mm)	Prediction (mm)	Error (%)
CP-2	Rectangular	375	61	500	244	45	0.33	0.468	285.7	242	-15
CP-1	Rectangular	375	61	500	244	15	0.33	0.468	175.4	149	-15

In Figure 6.12, the scour depth predicted by equation (6.18) is applied to all experiment results obtained from Gudavalli (1997) and Li (2002) in order to check the compatibility of correction factors. Since all correction factors are developed under independent condition on other parameters, equation (6.18) shows good agreement to both Gudavalli and Li's test results.
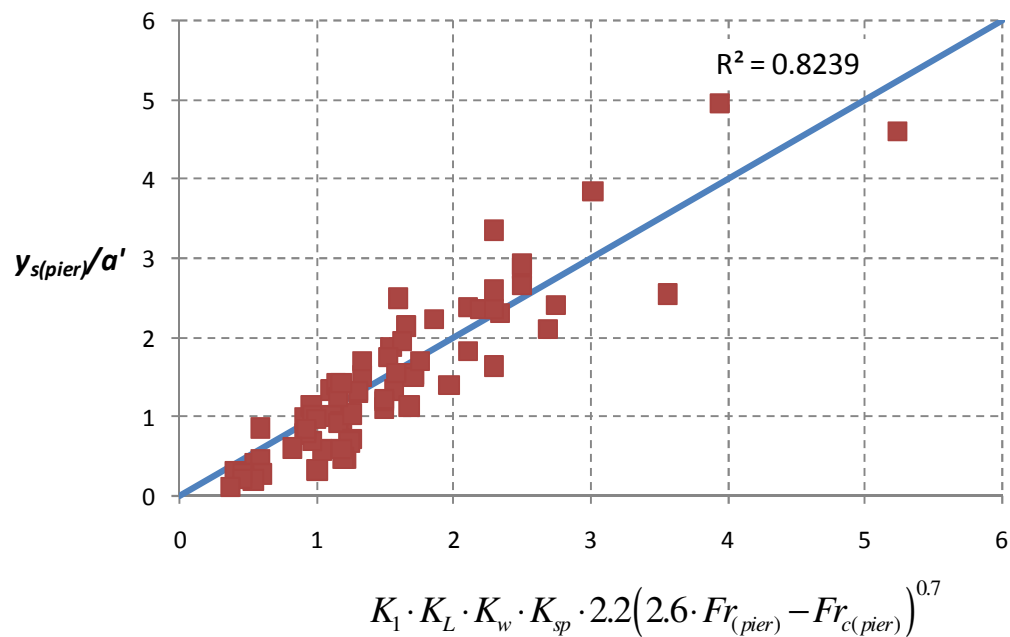
Figure 6.12. Compatibility of correction factors

6.4 Verification of equation

The equation (6.18) is elaborated on the basis of flume test using both cohesive and cohesionless materials. The critical shear stresses of soil material were obtained from EFA tests. In this chapter, the equation (6.18) is applied to full scale case histories for the verification. For the scour depth calculation, the database should satisfy following requirements:

1. Flow data – water depth, flow velocity, and attack angle to pier

2. Pier data – pier width, pier length, pier nose shape

3. Soil data – critical shear stress

Database from Froehlich (1988) and Muller and Landers (1996) were obtained from the study of case histories. These two databases have good information about flow

and pier data, but critical shear stresses and roughness of soil are not listed. To use the databases, critical shear stresses of channel bed materials are calculated using Shields diagram, and the Manning's roughness coefficient are calculated using Strikler approximation. In addition, single pier is assumed to calculate maximum pier scour depth because there is no information about pier spacing.

6.4.1 Froehlich (1988) database

The Froehlich database was acquired from ASCE conference proceeding paper "Analysis of onsite measurement of scour at piers". Three types of pier – square, round and sharp pier nose shape - are found in his database. The median size of soil (D_{50}) is in the range of between 0.008 mm and 20 mm. The details of data are listed in Table 6.11. The comparison of prediction by equation (6.18) and Froehlich's database is shown in Figure 6.13. The maximum pier scour depths predicted by equation (6.18) are conservative. Li (2004) calculated maximum pier scour depth using HEC-18 method and compared those to same database. Figure 6.14 shows that HEC-18 method is also conservative. The scour depths calculated by equation (6.18) are compared to the scour depths obtained by HEC-18 method with Froehlich database in Figure 6.15. It appears that HEC-18 method yields more conservative maximum pier scour depth than equation (6.18).

Figure 6.13. Prediction by equation (6.18) versus Froehlich (1988) data base

Figure 6.14. HEC-18 Predictions versus Froehlich (1988) data base (cited from Li (2002))
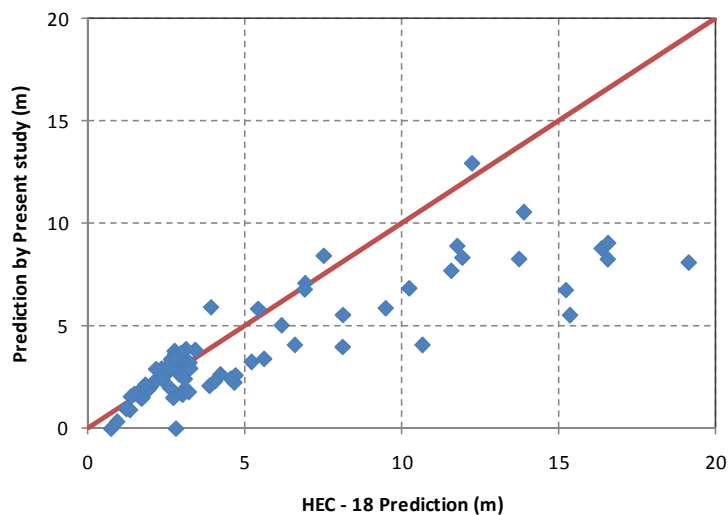
Figure 6.15. Prediction by equation (6.18) versus HEC-18 prediction using Froehlich (1988) database

Table 6.11. Froehlich (1988) database

Test No.	Shape of Pier Nose	a (m)	L (m)	y_1 (m)	V_1 (m/s)	θ (°)	D_{50} (mm)	Measured Scour Depth (m)	τ_c (Pa)	V_c (m/s)	a' (m)	K_1	K_w	Predicted Scour Depth (m)
1	Round	4.5	14	18.8	1.84	0	0.25	**4.3**	0.19	0.64	4.50	1.0	1.00	**7.11**
2	Round	4.5	14	17.4	2.28	0	0.25	**3**	0.19	0.64	4.50	1.0	1.00	**8.44**
3	Round	1.92	17.37	5.39	1.8	5	0.5	**1.74**	0.28	0.61	3.43	1.0	1.00	**5.88**
4	Round	8.5	8.5	9	0.65	12	0.67	**7.8**	0.35	0.70	10.08	1.0	0.91	**3.99**
5	Square	2.4	8.85	3.45	0.96	10	0.78	**2.75**	0.39	0.62	3.90	1.1	1.00	**4.09**
6	Sharp	1.52	6.1	5.8	1.98	0	70	**0.76**	52.77	3.73	1.52	0.9	1.00	**1.50**
7	Sharp	1.52	6.1	4.1	2.59	0	70	**0.76**	52.77	3.52	1.52	0.9	1.00	**2.65**
8	Sharp	1.52	6.1	3.4	2.13	0	70	**0.61**	52.77	3.41	1.52	0.9	1.00	**1.98**
9	Sharp	1.52	6.1	5.3	3.05	0	70	**0.61**	52.77	3.67	1.52	0.9	1.00	**3.22**
10	Sharp	1.52	6.1	6.6	2.9	0	70	**0.61**	52.77	3.81	1.52	0.9	1.00	**2.94**
11	Sharp	1.52	6.1	5.2	3.51	0	70	**0.61**	52.77	3.66	1.52	0.9	1.00	**3.84**
12	Sharp	1.8	9.6	5.5	3.67	0	1.5	**0.82**	0.77	0.84	1.80	0.9	1.00	**5.93**
13	Round	1.52	11.58	1.2	0.49	0	0.5	**0.3**	0.28	0.48	1.52	1.0	0.82	**0.91**
14	Round	1.52	11.58	1.5	0.76	0	0.5	**0.3**	0.28	0.49	1.52	1.0	0.89	**1.52**
15	Round	1.52	11.58	1.2	0.88	0	0.5	**0.3**	0.28	0.48	1.52	1.0	0.82	**1.62**
16	Round	1.52	11.58	0.5	0.27	0	0.5	**0.76**	0.28	0.41	1.52	1.0	0.62	**0.34**
17	Round	1.52	11.58	0.6	0.15	0	0.5	**1.22**	0.28	0.42	1.52	1.0	0.65	**0.00**
18	Round	1.52	11.58	2.1	1.52	0	1.6	**0.61**	0.82	0.74	1.52	1.0	0.99	**2.91**
19	Round	1.52	11.58	2	1.55	0	1.6	**0.61**	0.82	0.73	1.52	1.0	0.97	**2.92**
20	Round	1.52	11.58	3	1.58	0	1.6	**0.91**	0.82	0.78	1.52	1.0	1.00	**3.01**
21	Round	1.52	11.58	3.2	1.98	0	1.6	**1.22**	0.82	0.79	1.52	1.0	1.00	**3.64**
22	Round	1.52	11.58	3	1.8	0	1.6	**1.37**	0.82	0.78	1.52	1.0	1.00	**3.37**
23	Round	1.52	11.58	2.6	2.07	0	1.6	**1.07**	0.82	0.76	1.52	1.0	1.00	**3.79**
24	Round	1.52	11.58	3	1.83	0	1.6	**1.83**	0.82	0.78	1.52	1.0	1.00	**3.41**
25	Round	1.52	11.58	0.9	0.94	0	1.6	**0.46**	0.82	0.64	1.52	1.0	0.75	**1.47**

Table 6.11. (continued)

Test No.	Shape of Pier Nose	a (m)	L (m)	y₁ (m)	V₁ (m/s)	θ (°)	D₅₀ (mm)	Measured Scour Depth (m)	τ_c (Pa)	V_c (m/s)	a' (m)	K₁	K_w	Predicted Scour Depth (m)
26	Round	1.52	11.58	0.9	0.98	0	1.6	**0.61**	0.82	0.64	1. 52	1.0	0.75	**1.53**
27	Round	1.52	11.58	1.8	1.1	0	1.6	**0.46**	0.82	0.72	1. 52	1.0	0.94	**2.08**
28	Round	1.52	11.58	2.4	1.16	0	1.6	**0.61**	0.82	0.75	1. 52	1.0	1.00	**2.30**
29	Round	1.52	11.58	2.3	1.13	0	1.6	**0.76**	0.82	0.75	1. 52	1.0	1.00	**2.25**
30	Round	1.52	11.58	1.5	1.13	0	1.6	**0.46**	0.82	0.70	1. 52	1.0	0.89	**2.02**
31	Round	1.52	11.58	2	0.98	0	1.6	**0.76**	0.82	0.73	1. 52	1.0	0.97	**1.92**
33	Sharp	4.6	4.6	3.7	2.9	0	90	**1.5**	67.87	3.76	4. 60	0.9	0.83	**5.05**
34	Sharp	4.6	4.6	4.6	3.51	0	90	**1.7**	67.87	3.90	4. 60	0.9	0.89	**6.80**
35	Sharp	4.6	4.6	1.5	0.61	0	90	**0.9**	67.87	3.23	4. 60	0.9	0.61	**0.00**
36	Round	1.52	10.36	3.7	2.16	35	14	**1.8**	10.09	1.98	7. 19	1.0	1.00	**8.81**
37	Round	1.52	10.36	3.7	2.22	35	14	**2.1**	10.09	1.98	7. 19	1.0	1.00	**9.07**
38	Round	1.52	10.36	4.6	2.07	35	14	**1.8**	10.09	2.05	7. 19	1.0	1.00	**8.28**
39	Round	1.52	10.36	4.3	1.74	35	14	**2.4**	10.09	2.03	7. 19	1.0	1.00	**6.77**
40	Round	3.05	17.6	6.7	2.59	0	15	**1.8**	10.86	2.24	3. 05	1.0	1.00	**5.85**
41	Round	0.98	0.98	1.7	1.61	0	8	**0.9**	5.48	1.40	0. 98	1.0	1.00	**2.00**
44	Round	8.2	8.2	4.9	0.46	0	0.06	**3.7**	0.08	0.35	8. 20	1.0	0.75	**2.60**
45	Round	8.2	8.2	4.3	0.61	0	0.06	**4.3**	0.08	0.34	8. 20	1.0	0.72	**3.26**
46	Round	13	38	4.1	0.55	5	0.027	**7.3**	0.05	0.27	16. 26	1.0	0.61	**4.09**
47	Round	13	38	3.4	0.66	15	0.027	**6.8**	0.05	0.26	22. 39	1.0	0.57	**5.54**
48	Round	13	13	5.4	1.16	20	0.027	**8.5**	0.05	0.28	16. 66	1.0	0.67	**8.29**
49	Sharp	9.8	12.5	11	0.73	5	0.008	**4.3**	0.03	0.23	10. 85	0.9	0.92	**5.55**
50	Sharp	9.8	12.5	12.8	0.81	30	0.008	**8.2**	0.03	0.23	14. 74	0.9	0.97	**7.71**
51	Sharp	9.8	12.5	13.6	1.08	15	0.008	**4.6**	0.03	0.24	12. 70	0.9	0.99	**8.92**
52	Sharp	9.8	12.5	16.3	1.22	25	0.008	**7.9**	0.03	0.24	14. 16	0.9	1.00	**10.58**
53	Sharp	9.8	12.5	11.6	0.82	15	0.008	**4**	0.03	0.23	12. 70	0.9	0.94	**6.85**
54	Sharp	9.8	12.5	13.4	0.91	25	0.008	**7.6**	0.03	0.24	14. 16	0.9	0.99	**8.35**
55	Square	9.4	19.5	19.5	1.8	0	0.036	**6.1**	0.06	0.38	9. 40	1.1	1.00	**12.96**
56	Round	19.5	38	11.3	0.66	15	0.036	**10.4**	0.06	0.35	28. 67	1.0	0.74	**8.11**
57	Round	3.66	17.3	3.6	0.64	0	0.1	**2.8**	0.11	0.38	3. 66	1.0	0.89	**2.42**
58	Round	1.5	1.5	3.1	2.38	0	20	**1.3**	14.71	2.18	1. 50	1.0	1.00	**3.40**
59	Round	1.5	1.5	3	2.69	0	20	**1.3**	14.71	2.17	1. 50	1.0	1.00	**3.87**
60	Round	1.5	1.5	2.5	2.54	0	20	**0.8**	14.71	2.11	1. 50	1.0	1.00	**3.69**
61	Round	1.5	1.5	1.4	2.65	0	20	**0.9**	14.71	1.91	1. 50	1.0	0.87	**3.45**
62	Round	1.5	1.5	1.3	2.43	0	20	**0.9**	14.71	1.89	1. 50	1.0	0.85	**3.10**
63	Round	1.5	1.5	1.3	2.68	0	20	**0.4**	14.71	1.89	1. 50	1.0	0.85	**3.41**
64	Round	1.5	1.5	1	2.39	0	20	**0.4**	14.71	1.81	1. 50	1.0	0.78	**2.83**
65	Round	1.5	1.5	0.9	2.33	0	20	**0.5**	14.71	1.78	1. 50	1.0	0.75	**2.68**
66	Round	1.5	1.5	0.9	2.56	0	20	**0.4**	14.71	1.78	1. 50	1.0	0.75	**2.94**
67	Round	1.5	1.5	0.7	2.24	0	20	**0.4**	14.71	1.70	1. 50	1.0	0.69	**2.40**
69	Square	0.29	3.66	0.76	1.04	15	1.5	**0.61**	0.77	0.61	1. 23	1.1	1.00	**2.09**
70	Square	0.29	3.66	0.61	1.36	15	1.5	**0.61**	0.77	0.58	1. 23	1.1	1.00	**2.65**
71	Square	0.29	3.66	0.73	1.17	15	1.5	**0.52**	0.77	0.60	1. 23	1.1	1.00	**2.32**
72	Square	0.29	3.66	0.43	1.13	10	2.3	**0.58**	1.27	0.66	0. 92	1.1	1.00	**1.83**
73	Square	0.29	3.66	0.58	1.02	10	2.3	**0.46**	1.27	0.70	0. 92	1.1	1.00	**1.65**
74	Square	0.29	3.66	0.7	1.12	10	2.3	**0.49**	1.27	0.72	0. 92	1.1	1.00	**1.79**
75	Square	0.29	3.66	1.81	1.22	15	2.3	**0.66**	1.27	0.84	1. 23	1.1	1.00	**2.25**
76	Round	1.22	6.4	2.13	1.17	0	0.6	**0.64**	0.32	0.54	1. 22	1.0	1.00	**2.14**
77	Round	1.22	6.4	0.55	0.69	0	0.6	**0.4**	0.32	0.43	1. 22	1.0	0.68	**0.96**
78	Round	1.22	6.4	2.32	1.7	0	0.6	**1.22**	0.32	0.55	1. 22	1.0	1.00	**2.90**
79	Round	1.22	6.4	0.7	0.66	0	0.6	**0.61**	0.32	0.45	1. 22	1.0	0.74	**0.98**
80	Sharp	0.94	27.43	1.4	1.54	0	7.9	**0.37**	5.41	1.35	0. 94	0.9	1.00	**1.69**
81	Sharp	0.94	27.43	1.22	1.35	0	4.3	**0.15**	2.69	1.03	0. 94	0.9	0.97	**1.57**
82	Sharp	0.52	8.29	3.21	1.68	10	1.2	**0.98**	0.60	0.71	1. 95	0.9	1.00	**3.41**
83	Sharp	0.52	8.29	2.14	1.17	10	1.8	**0.65**	0.95	0.78	1. 95	0.9	1.00	**2.44**

6.4.2 Muller and Landers (1996) database

Mueller and Landers (1996) collected more than 380 pier scour measurements at 56 bridge sites in Alaska, Arkansas, Colorado, Delaware, Georgia, Illinois, Indiana, Louisiana, Maryland, Mississippi, Montana, New York, Ohio, and Virginia. The database was acquired from the report FHWA-RD-95-184 entitled "Channel Scour at Bridges in the United States". The details of data and maximum pier scour depth using equation (6.18) are listed in Table 6.12. Figure 6.16 shows the comparison between the pier scour depth calculated by equation (6.18) and the measurements in the database. Figure 6.17 shows the comparison between the pier scour depths calculated using HEC-18 equation and the same database. Both equation (6.18) and HEC-18 equation are conservative. The scour depths calculated by equation (6.18) are compared to the scour depths obtained by HEC-18 method with Muller and Landers' database in Figure 6.18. It appears that HEC-18 method yields more conservative maximum pier scour depth than equation (6.18).

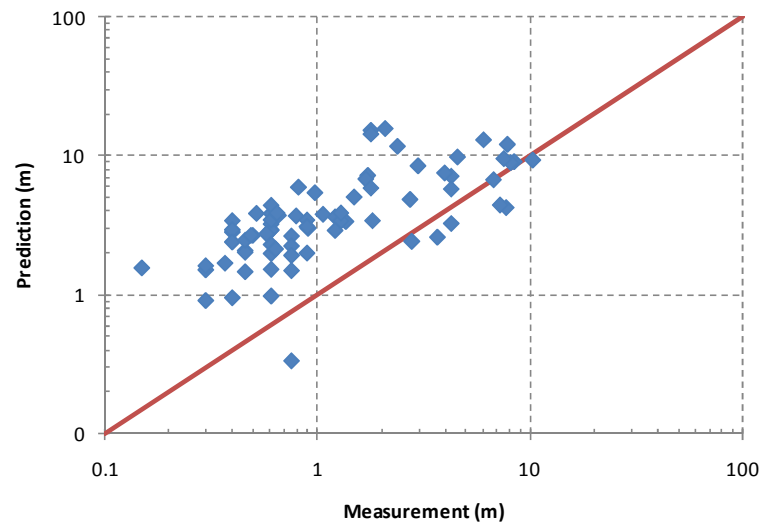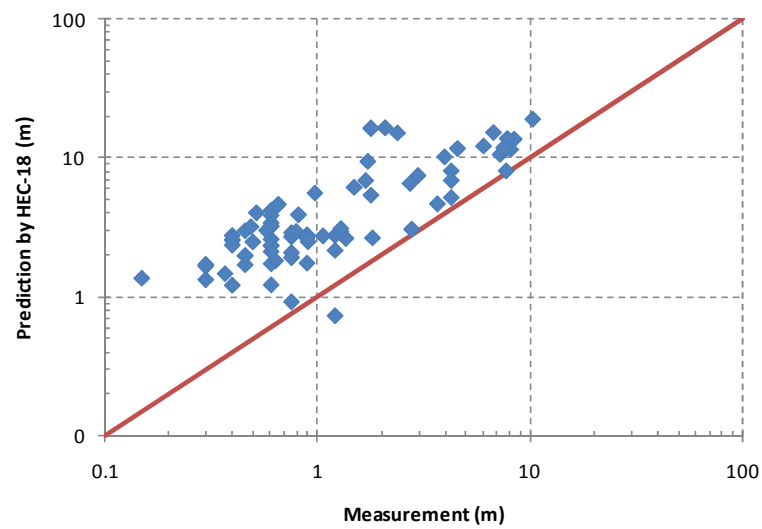Figure 6.16. Prediction by equation (6.18) versus Muller and Landers' (1996) database

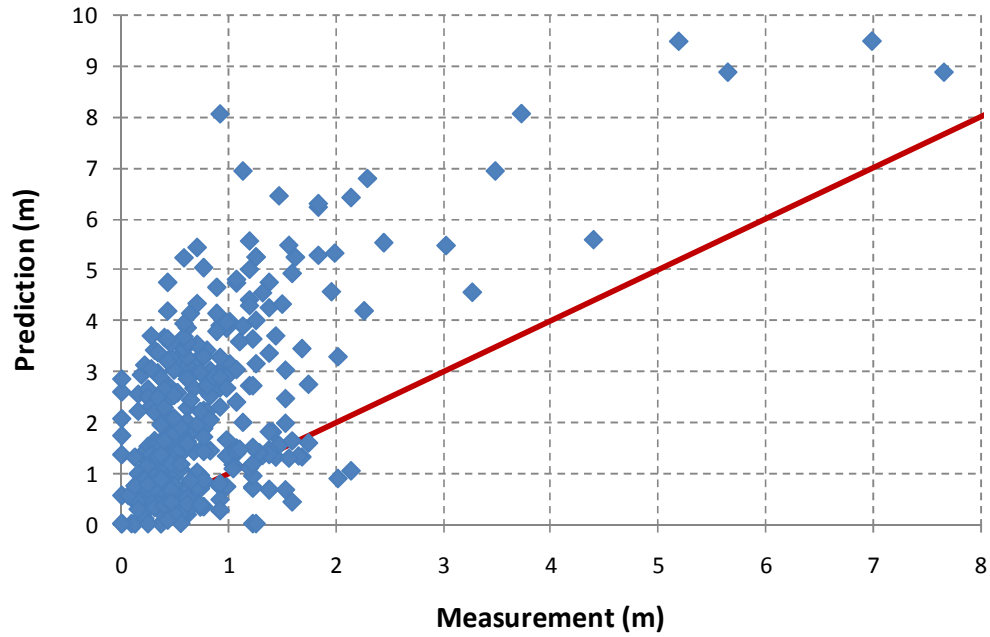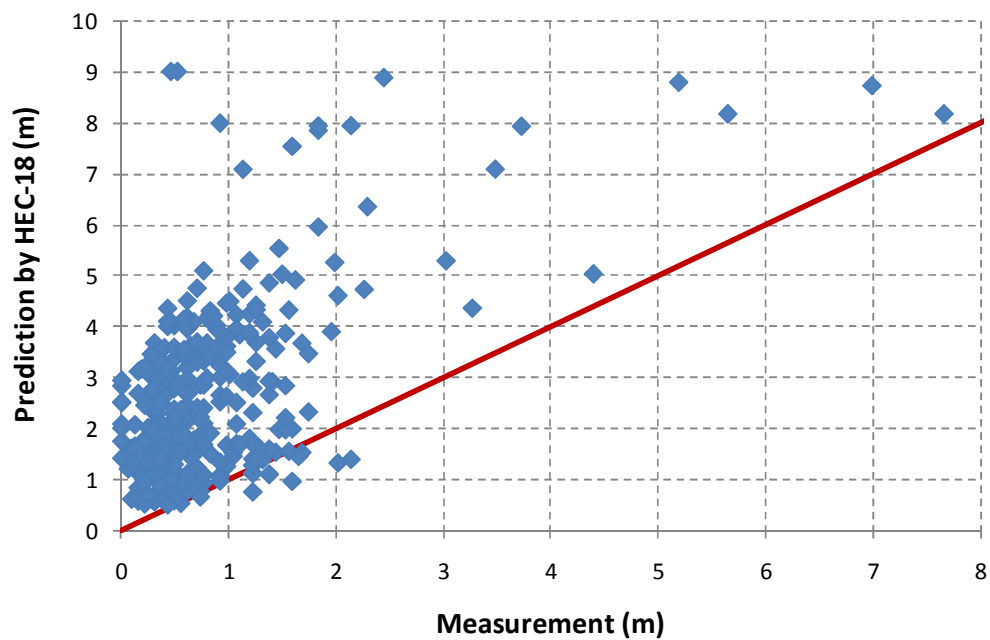Figure 6.17. HEC-18 predictions versus Muller and Landers' (1996) database
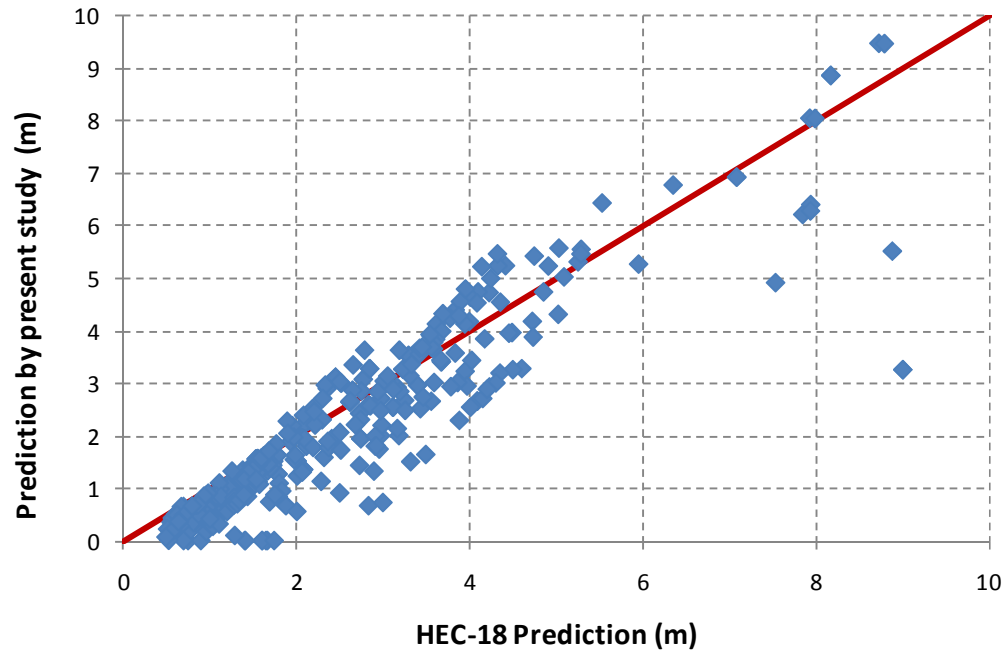
Figure 6.18. Prediction by equation (6.18) versus HEC-18 prediction using Muller and Landers' (1996) database

Table 6.12. Muller and Landers' (1996) database

No.	Pier Shape	a (m)	L (m)	θ (°)	a' (m)	V_1 (m/s)	y_1 (m)	D_{50} (mm)	Measured $y_{s(pier)}$ (m)	τ_c (Pa)	Vc (m/s)	K_1	K_w	Predicted Scour Depth (m)
1	Sharp	1.52	6.10	0	1.52	1.98	5.79	70.00	0.76	52.77	3.72	0.9	1.00	1.50
2	Sharp	1.52	6.10	0	1.52	3.05	5.33	70.00	0.61	52.77	3.67	0.9	1.00	3.22
3	Sharp	1.52	6.10	0	1.52	2.59	4.11	70.00	0.76	52.77	3.52	0.9	1.00	2.65
4	Sharp	1.52	6.10	0	1.52	2.90	6.55	70.00	0.61	52.77	3.80	0.9	1.00	2.94
5	Sharp	1.52	6.10	0	1.52	2.13	3.35	70.00	0.61	52.77	3.40	0.9	1.00	2.00
6	Sharp	1.52	6.10	0	1.52	3.51	5.18	70.00	0.61	52.77	3.66	0.9	1.00	3.84
7	Sharp	1.52	6.10	0	1.52	1.52	4.11	70.00	1.52	52.77	3.52	0.9	1.00	0.66
8	Sharp	1.52	6.10	0	1.52	2.90	5.33	70.00	1.52	52.77	3.67	0.9	1.00	3.01
9	Round	1.52	11.25	0	1.52	1.52	2.13	1.80	0.61	0.95	0.78	1	0.99	2.91
10	Round	1.52	11.25	0	1.52	0.94	0.91	1.80	0.46	0.95	0.67	1	0.75	1.47
11	Round	1.52	11.25	0	1.52	1.55	1.98	1.80	0.61	0.95	0.77	1	0.97	2.90
12	Round	1.52	11.25	0	1.52	0.98	0.91	1.80	0.61	0.95	0.67	1	0.75	1.51
13	Round	1.52	11.25	0	1.52	0.49	1.22	0.58	0.30	0.31	0.49	1	0.83	0.90
14	Round	1.52	11.25	0	1.52	1.58	3.05	1.80	0.91	0.95	0.82	1	1.00	3.00
15	Round	1.52	11.25	0	1.52	1.10	1.83	1.80	0.46	0.95	0.76	1	0.95	2.06
16	Round	1.52	11.25	0	1.52	0.76	1.52	0.58	0.30	0.31	0.51	1	0.89	1.52
17	Round	1.52	11.25	0	1.52	1.98	3.20	1.80	1.22	0.95	0.83	1	1.00	3.62
18	Round	1.52	11.25	0	1.52	1.16	2.44	1.80	0.61	0.95	0.79	1	1.00	2.27
19	Round	1.52	11.25	0	1.52	0.88	1.22	0.58	0.30	0.31	0.49	1	0.83	1.63
20	Round	1.52	11.25	0	1.52	1.80	3.05	1.80	1.37	0.95	0.82	1	1.00	3.34
21	Round	1.52	11.25	0	1.52	1.13	2.29	1.80	0.76	0.95	0.79	1	1.00	2.22
22	Round	1.52	11.25	0	1.52	0.27	0.46	0.58	0.76	0.31	0.42	1	0.60	0.33
23	Round	1.52	11.25	0	1.52	1.13	1.52	1.80	0.46	0.95	0.73	1	0.89	2.01
24	Round	1.52	11.25	0	1.52	0.15	0.61	0.58	1.22	0.31	0.44	1	0.66	0.00
25	Round	1.52	11.25	0	1.52	0.98	1.98	1.80	0.76	0.95	0.77	1	0.97	1.88
26	Round	1.52	9.45	37	6.90	2.16	3.66	14.00	1.83	10.09	1.97	1	0.72	6.21
27	Round	1.52	9.45	37	6.90	2.23	3.66	14.00	2.13	10.09	1.97	1	0.72	6.40
28	Round	1.52	9.45	37	6.90	2.07	4.57	14.00	1.83	10.09	2.05	1	0.78	6.28
29	Round	1.52	13.53	37	9.36	1.74	4.27	14.00	2.44	10.09	2.02	1	0.69	5.51
30	Sharp	3.05	14.63	0	3.05	2.59	6.71	15.00	1.83	10.86	2.24	0.9	1.00	5.26
31	Round	2.99	10.91	0	2.99	1.89	11.73	0.32	4.39	0.21	0.64	1	1.00	5.57
32	Round	2.99	10.91	0	2.99	1.46	9.11	0.32	3.26	0.21	0.61	1	1.00	4.54
33	Sharp	0.53	7.09	20	2.92	1.40	1.83	1.10	0.34	0.55	0.62	0.9	0.76	2.96
34	Sharp	0.53	7.09	20	2.92	1.40	1.83	1.10	0.67	0.55	0.62	0.9	0.76	2.96
35	Sharp	0.53	7.09	20	2.92	1.77	1.55	1.10	0.30	0.55	0.61	0.9	0.72	3.40
36	Sharp	0.53	7.09	20	2.92	1.77	1.55	1.10	0.79	0.55	0.61	0.9	0.72	3.40
37	Sharp	0.53	7.09	43	5.22	0.98	1.40	1.10	0.46	0.55	0.60	1	0.58	2.66
38	Sharp	0.53	7.09	43	5.22	0.98	1.40	1.10	0.67	0.55	0.60	1	0.58	2.66
39	Sharp	0.53	7.09	20	2.92	1.40	1.31	1.10	0.91	0.55	0.59	0.9	0.68	2.67
40	Sharp	0.53	7.09	43	5.22	1.04	1.01	1.10	0.49	0.55	0.57	1	0.52	2.54
41	Square	0.29	7.32	26	3.47	0.79	1.01	0.94	0.61	0.47	0.54	1.1	0.59	1.94
42	Square	0.29	7.32	26	3.47	0.79	1.01	0.94	0.58	0.47	0.54	1.1	0.59	1.94
43	Square	0.29	7.32	15	2.17	0.70	0.58	0.94	0.21	0.47	0.49	1.1	0.58	1.27
44	Square	0.29	7.32	15	2.17	0.70	0.58	0.94	0.43	0.47	0.49	1.1	0.58	1.27
45	Square	0.29	7.32	26	3.47	1.07	1.01	0.94	0.15	0.47	0.54	1.1	0.59	2.54
46	Square	0.29	7.32	26	3.47	1.07	1.01	0.94	0.46	0.47	0.54	1.1	0.59	2.54
47	Square	0.29	7.32	14	2.05	1.16	1.01	0.94	0.30	0.47	0.54	1.1	0.70	2.30
48	Square	0.29	7.32	14	2.05	1.16	1.01	0.94	0.34	0.47	0.54	1.1	0.70	2.30
49	Square	0.29	7.32	20	2.77	0.82	0.34	0.94	0.30	0.47	0.45	1.1	0.44	1.35
50	Square	0.29	7.32	20	2.77	0.82	0.34	0.94	0.00	0.47	0.45	1.1	0.44	1.35
51	Square	0.29	7.32	23	3.12	1.19	1.31	0.94	0.18	0.47	0.56	1.1	0.67	2.92
52	Square	0.29	7.32	23	3.12	1.19	1.31	0.94	0.34	0.47	0.56	1.1	0.67	2.92
53	Square	0.29	7.32	16	2.29	1.01	0.34	0.94	0.37	0.47	0.45	1.1	0.47	1.51
54	Square	0.29	7.32	16	2.29	1.01	0.34	0.94	0.24	0.47	0.45	1.1	0.47	1.51
55	Square	0.29	7.32	16	2.29	1.25	1.86	0.94	0.64	0.47	0.59	1.1	0.83	3.07
56	Square	0.29	7.32	16	2.29	1.25	1.86	0.94	0.49	0.47	0.59	1.1	0.83	3.07
57	Square	0.29	7.32	11	1.68	1.13	0.43	0.94	0.55	0.47	0.46	1.1	0.57	1.62
58	Square	0.29	7.32	11	1.68	1.13	0.43	0.94	0.40	0.47	0.46	1.1	0.57	1.62
59	Square	0.29	7.32	16	2.29	1.19	2.65	0.94	0.73	0.47	0.63	1.1	0.93	3.27
60	Square	0.29	7.32	16	2.29	1.19	2.65	0.94	0.76	0.47	0.63	1.1	0.93	3.27

Table 6.12. (continued)

No.	Pier Shape	a (m)	L (m)	θ (°)	a' (m)	V_1 (m/s)	y_1 (m)	D_{50} (mm)	Measured $y_{s(pier)}$ (m)	τ_c (Pa)	Vc (m/s)	K_1	K_w	Predicted Scour Depth (m)
61	Square	0.29	7.32	8	1.30	1.10	0.52	0.94	0.52	0.47	0.48	1.1	0.66	1.55
62	Square	0.29	7.32	8	1.30	1.10	0.52	0.94	0.40	0.47	0.48	1.1	0.66	1.55
63	Square	0.29	7.32	13	1.93	1.13	0.67	0.94	0.52	0.47	0.50	1.1	0.63	1.95
64	Square	0.29	7.32	13	1.93	1.13	0.67	0.94	0.37	0.47	0.50	1.1	0.63	1.95
65	Square	0.29	7.32	11	1.68	1.31	2.87	0.94	0.21	0.47	0.64	1.1	0.63	3.11
66	Square	0.29	7.32	11	1.68	1.31	2.87	0.94	0.61	0.47	0.64	1.1	1.00	3.11
67	Round	1.22	6.40	12	2.52	1.01	2.10	1.19	0.64	0.59	0.66	1	0.84	2.42
68	Round	1.22	6.40	12	2.52	1.01	2.10	1.19	0.43	0.59	0.66	1	0.84	2.42
69	Round	1.22	6.40	0	1.22	0.67	0.64	1.19	0.30	0.59	0.54	1	0.72	0.92
70	Round	1.22	6.40	0	1.22	0.67	0.64	1.19	0.30	0.59	0.54	1	0.72	0.92
71	Round	1.22	6.40	0	1.22	1.01	1.04	1.19	0.30	0.59	0.58	1	0.84	1.56
72	Round	1.22	6.40	0	1.22	1.01	1.04	1.19	0.34	0.59	0.58	1	0.84	1.56
73	Sharp	0.91	27.43	26	12.85	1.65	1.22	29.80	0.52	22.22	2.15	0.9	0.41	3.25
74	Sharp	0.91	27.43	26	12.85	1.65	1.22	29.80	0.46	22.22	2.15	0.9	0.41	3.25
75	Square	0.38	8.23	0	0.38	0.55	4.69	0.40	0.15	0.24	0.58	1.1	1.00	0.53
76	Square	0.38	8.23	0	0.38	0.68	5.27	0.40	0.24	0.24	0.59	1.1	1.00	0.65
77	Square	0.38	8.23	0	0.38	0.41	4.79	0.40	0.30	0.24	0.58	1.1	1.00	0.35
78	Square	0.38	8.23	0	0.38	0.66	4.24	0.40	0.24	0.24	0.57	1.1	1.00	0.64
79	Square	0.38	8.23	0	0.38	0.43	4.72	0.40	0.30	0.24	0.58	1.1	1.00	0.38
80	Square	0.38	8.23	0	0.38	0.49	4.63	0.40	0.15	0.24	0.58	1.1	1.00	0.45
81	Square	0.38	8.23	0	0.38	0.50	4.57	0.40	0.18	0.24	0.57	1.1	1.00	0.47
82	Square	0.38	8.23	0	0.38	0.49	4.24	0.40	0.21	0.24	0.57	1.1	1.00	0.46
83	Square	0.38	8.23	0	0.38	0.46	3.75	0.40	0.15	0.24	0.56	1.1	1.00	0.43
84	Square	0.38	8.23	0	0.38	0.53	4.02	0.40	0.09	0.24	0.56	1.1	1.00	0.50
85	Square	0.38	8.23	0	0.38	0.52	4.94	0.40	0.27	0.24	0.58	1.1	1.00	0.49
86	Cylind	0.76	13.11	0	0.76	0.27	3.17	0.18	0.73	0.15	0.44	1	1.00	0.32
87	Cylind	0.76	13.11	0	0.76	0.33	3.08	0.18	0.52	0.15	0.44	1	1.00	0.45
88	Cylind	0.76	13.11	0	0.76	0.26	3.11	0.18	0.34	0.15	0.44	1	1.00	0.30
89	Cylind	0.76	13.11	0	0.76	0.34	7.99	0.18	1.58	0.15	0.51	1	1.00	0.43
90	Cylind	0.76	13.11	0	0.76	0.47	7.77	0.18	1.37	0.15	0.51	1	1.00	0.66
91	Cylind	0.76	13.11	0	0.76	0.48	7.77	0.18	1.37	0.15	0.51	1	1.00	0.67
92	Cylind	0.76	13.11	0	0.76	0.43	7.13	0.18	0.46	0.15	0.50	1	1.00	0.60
93	Cylind	0.76	13.11	0	0.76	0.51	7.62	0.18	1.22	0.15	0.51	1	1.00	0.72
94	Cylind	0.76	13.11	0	0.76	0.49	7.56	0.18	1.22	0.15	0.51	1	1.00	0.70
95	Cylind	0.76	13.11	0	0.76	0.28	3.84	0.18	0.43	0.15	0.45	1	1.00	0.34
96	Cylind	0.76	13.11	0	0.76	0.32	3.72	0.18	0.15	0.15	0.45	1	1.00	0.42
97	Cylind	0.76	13.11	0	0.76	0.24	1.49	0.18	0.46	0.15	0.39	1	1.00	0.31
98	Cylind	0.76	13.11	0	0.76	0.18	1.46	0.18	0.46	0.15	0.38	1	1.00	0.15
99	Cylind	0.76	13.11	0	0.76	0.22	0.30	0.18	0.21	0.15	0.30	1	0.66	0.22
100	Square	1.22	9.91	0	1.22	0.58	5.70	1.00	2.13	0.50	0.73	1.1	1.00	1.04
101	Square	1.22	9.91	0	1.22	0.52	5.52	1.00	2.01	0.50	0.73	1.1	1.00	0.89
102	Square	1.22	10.82	0	1.22	0.55	7.07	1.00	1.22	0.50	0.76	1.1	1.00	0.93
103	Square	1.22	10.82	0	1.22	0.70	6.37	1.00	1.43	0.50	0.74	1.1	1.00	1.31
104	Square	1.22	10.82	0	1.22	0.70	6.16	1.00	1.68	0.50	0.74	1.1	1.00	1.31
105	Square	1.83	10.82	0	1.83	0.52	8.05	1.00	1.19	0.50	0.77	1.1	1.00	1.09
106	Square	1.83	10.82	0	1.83	0.66	7.56	1.00	1.46	0.50	0.77	1.1	1.00	1.54
107	Square	1.83	10.82	0	1.83	0.68	7.04	1.00	1.58	0.50	0.76	1.1	1.00	1.62
108	Round	0.91	10.21	0	0.91	0.31	5.12	0.50	0.43	0.28	0.61	1	1.00	0.30
109	Round	0.91	10.21	0	0.91	0.76	5.94	0.50	1.04	0.28	0.62	1	1.00	1.16
110	Round	0.91	10.52	5	1.83	1.58	9.42	0.34	0.70	0.22	0.63	1	1.00	3.51
111	Round	0.91	10.52	5	1.83	1.58	9.42	0.30	0.46	0.21	0.60	1	1.00	3.53
112	Round	0.91	14.48	5	2.17	1.10	3.44	0.90	0.37	0.45	0.65	1	1.00	2.85
113	Round	0.91	14.48	5	2.17	1.01	3.17	0.90	0.40	0.45	0.64	1	1.00	2.64
114	Round	0.91	14.48	5	2.17	1.01	3.17	0.90	0.24	0.45	0.64	1	1.00	2.64
115	Round	0.91	13.11	0	0.91	1.28	5.09	0.90	0.67	0.45	0.69	1	1.00	1.84
116	Round	0.61	12.80	10	2.82	1.65	6.55	0.90	1.07	0.45	0.72	1	1.00	4.72
117	Round	0.61	12.80	10	2.82	1.86	6.16	0.90	1.25	0.45	0.72	1	1.00	5.23
118	Sharp	4.27	16.46	0	4.27	2.56	11.58	0.30	3.72	0.21	0.63	0.9	1.00	8.04
119	Sharp	4.27	16.46	0	4.27	2.56	12.25	0.30	0.91	0.21	0.63	0.9	1.00	8.04
120	Sharp	4.27	16.46	0	4.27	2.10	9.42	0.30	3.47	0.21	0.60	0.9	1.00	6.92

Table 6.12. (continued)

No.	Pier Shape	a (m)	L (m)	θ (°)	a' (m)	V₁ (m/s)	y₁ (m)	D₅₀ (mm)	Measured y_s(pier) (m)	τ_c (Pa)	Vc (m/s)	K₁	K_w	Predicted Scour Depth (m)
121	Sharp	4.27	16.46	0	4.27	2.10	9.39	0.30	1.13	0.21	0.60	0.9	1.00	6.92
122	Sharp	4.27	16.46	0	4.27	3.17	11.95	0.30	6.98	0.21	0.63	0.9	1.00	9.47
123	Sharp	4.27	16.46	0	4.27	3.17	12.62	0.30	5.18	0.21	0.63	0.9	1.00	9.46
124	Sharp	4.27	16.46	0	4.27	2.90	9.78	0.30	7.65	0.21	0.61	0.9	1.00	8.86
125	Sharp	4.27	16.46	0	4.27	2.90	9.78	0.30	5.64	0.21	0.61	0.9	1.00	8.86
126	Sharp	1.52	12.71	0	1.52	2.33	2.41	108.00	0.34	81.42	3.72	0.9	1.00	2.13
127	Sharp	1.52	12.71	0	1.52	2.09	2.07	108.00	0.43	81.42	3.63	0.9	0.99	1.74
128	Sharp	1.52	12.71	0	1.52	2.63	3.02	108.00	0.82	81.42	3.86	0.9	1.00	2.51
129	Sharp	1.52	12.71	0	1.52	1.89	2.44	108.00	0.52	81.42	3.73	0.9	1.00	1.32
130	Round	1.22	9.75	0	1.22	0.80	3.54	22.00	0.37	16.24	2.31	1	1.00	0.00
131	Round	1.22	9.75	0	1.22	1.30	3.11	22.00	0.43	16.24	2.26	1	1.00	1.23
132	Round	1.22	9.75	0	1.22	1.13	2.44	22.00	0.73	16.24	2.17	1	1.00	0.94
133	Round	1.22	9.75	0	1.22	1.58	2.44	22.00	0.55	16.24	2.17	1	1.00	1.80
134	Round	1.22	9.75	0	1.22	1.01	1.92	22.00	0.30	16.24	2.08	1	1.00	0.74
135	Round	1.22	9.75	0	1.22	1.64	2.01	22.00	0.37	16.24	2.10	1	1.00	1.94
136	Round	1.22	9.75	0	1.22	1.60	3.08	22.00	0.52	16.24	2.26	1	1.00	1.77
137	Unkn	1.22	10.67	0	1.22	0.66	1.89	0.38	1.22	0.24	0.49	0.9	1.00	1.17
138	Unkn	1.22	10.67	0	1.22	0.77	3.08	0.38	1.65	0.24	0.53	0.9	1.00	1.33
139	Unkn	1.22	10.67	0	1.22	0.77	2.23	0.38	1.31	0.24	0.51	0.9	1.00	1.34
140	Unkn	1.22	10.67	0	1.22	0.41	2.16	0.38	0.73	0.24	0.50	0.9	1.00	0.69
141	Unkn	1.22	10.67	0	1.22	0.22	1.49	0.38	0.61	0.24	0.47	0.9	0.95	0.18
142	Unkn	1.22	10.67	0	1.22	0.27	1.13	0.38	0.49	0.24	0.45	0.9	0.87	0.34
143	Unkn	1.22	10.67	0	1.22	0.58	2.13	0.38	0.70	0.24	0.50	0.9	1.00	1.01
144	Unkn	1.22	10.67	0	1.22	0.32	1.46	0.38	0.67	0.24	0.47	0.9	0.95	0.46
145	Square	0.41	8.02	16	2.60	1.15	8.90	0.54	0.40	0.30	0.67	1.1	1.00	3.65
146	Square	0.41	8.02	14	2.33	1.34	8.84	0.54	0.91	0.30	0.67	1.1	1.00	3.89
147	Square	0.81	8.02	16	2.99	1.21	8.84	0.54	0.43	0.30	0.67	1.1	1.00	4.17
148	Square	0.81	8.02	8	1.92	1.43	8.20	0.54	0.43	0.30	0.66	1.1	1.00	3.62
149	Cylind	1.77	6.25	11	2.93	0.87	5.33	0.39	0.61	0.24	0.59	1	1.00	2.84
150	Cylind	1.65	6.25	16	3.30	1.03	6.71	0.39	1.10	0.24	0.61	1	1.00	3.57
151	Cylind	1.43	6.25	11	2.60	1.06	6.52	0.39	1.25	0.24	0.61	1	1.00	3.14
152	Cylind	1.77	6.25	11	2.93	0.40	5.30	0.39	0.49	0.24	0.59	1	1.00	1.12
153	Cylind	1.62	6.25	16	3.28	0.58	6.43	0.39	0.61	0.24	0.61	1	1.00	2.00
154	Cylind	1.49	6.25	14	2.96	0.67	6.80	0.39	0.79	0.24	0.61	1	1.00	2.20
155	Square	0.41	8.02	16	2.60	1.55	9.33	0.54	0.43	0.30	0.68	1.1	1.00	4.73
156	Square	0.81	8.02	16	2.99	1.19	8.38	0.54	0.88	0.30	0.67	1.1	1.00	4.12
157	Square	0.81	8.02	11	2.33	1.43	8.11	0.54	0.64	0.30	0.66	1.1	1.00	4.13
158	Cylind	1.68	6.25	16	3.33	0.85	7.10	0.39	0.49	0.24	0.62	1	1.00	3.01
159	Cylind	1.46	6.25	8	2.32	0.98	6.61	0.39	1.19	0.24	0.61	1	1.00	2.70
160	Cylind	1.55	6.25	20	3.60	0.73	6.16	0.39	1.74	0.24	0.60	1	1.00	2.73
161	Cylind	1.55	6.25	14	3.02	0.61	7.01	0.39	1.13	0.24	0.62	1	1.00	1.99
162	Cylind	2.44	2.44	0	2.44	1.89	3.05	7.51	1.25	5.11	1.51	1	0.96	3.99
163	Cylind	2.44	2.44	0	2.44	1.90	2.59	7.51	0.98	5.11	1.47	1	0.91	3.83
164	Cylind	2.44	2.44	0	2.44	2.13	3.93	7.51	0.88	5.11	1.58	1	1.00	4.64
165	Cylind	2.44	2.44	0	2.44	1.86	2.65	7.51	0.88	5.11	1.48	1	0.91	3.77
166	Cylind	2.44	2.44	0	2.44	2.12	2.90	7.51	1.19	5.11	1.50	1	0.94	4.39
167	Cylind	2.44	2.44	0	2.44	2.26	2.65	7.51	1.95	5.11	1.48	1	0.91	4.55
168	Cylind	2.44	2.44	0	2.44	1.75	3.05	7.51	1.43	5.11	1.51	1	0.96	3.68
169	Cylind	2.44	2.44	0	2.44	2.00	3.11	7.51	1.37	5.11	1.52	1	0.96	4.24
170	Square	1.65	8.17	14	3.57	2.13	6.80	6.90	1.46	4.64	1.67	1.1	1.00	6.43
171	Square	1.65	8.17	8	2.77	2.13	7.50	6.90	0.70	4.64	1.70	1.1	1.00	5.42
172	Square	1.86	8.17	8	2.98	1.98	8.56	6.90	1.62	4.64	1.74	1.1	1.00	5.23
173	Square	1.83	8.17	11	3.35	1.95	8.81	6.90	1.19	4.64	1.74	1.1	1.00	5.55
174	Square	1.68	8.08	0	1.68	1.07	8.05	6.90	1.74	4.64	1.72	1.1	1.00	1.58
175	Square	1.74	8.08	11	3.25	1.55	9.17	6.90	2.26	4.64	1.76	1.1	1.00	4.17
176	Square	1.19	7.01	0	1.19	0.58	7.01	6.90	1.25	4.64	1.68	1.1	1.00	0.00
177	Square	1.25	7.01	0	1.25	0.88	8.81	6.90	0.76	4.64	1.74	1.1	1.00	0.83
178	Cylind	1.68	6.40	16	3.38	1.69	9.17	6.90	1.49	4.64	1.76	1	1.00	4.31
179	Cylind	1.68	6.40	14	3.18	2.12	8.44	6.90	1.98	4.64	1.73	1	1.00	5.31
180	Cylind	1.77	6.40	18	3.66	1.29	7.65	6.90	2.01	4.64	1.70	1	1.00	3.27

Table 6.12. (continued)

No.	Pier Shape	a (m)	L (m)	θ (°)	a' (m)	V_1 (m/s)	y_1 (m)	D_{50} (mm)	Measured $y_{s(pier)}$ (m)	τ_c (Pa)	Vc (m/s)	K_1	K_w	Predicted Scour Depth (m)
181	Cylind	1.65	6.40	14	3.15	2.19	8.32	6.90	3.02	4.64	1.73	1	1.00	5.46
182	Cylind	1.68	6.40	22	3.95	2.34	8.66	6.90	2.29	4.64	1.74	1	1.00	6.77
183	Cylind	1.95	6.40	8	2.82	1.73	8.72	6.90	1.01	4.64	1.74	1	1.00	3.96
184	Cylind	1.77	6.40	16	3.46	1.32	7.83	6.90	0.61	4.64	1.71	1	1.00	3.26
185	Cylind	1.68	6.40	11	2.87	2.02	8.81	6.90	1.37	4.64	1.74	1	1.00	4.73
186	Cylind	1.65	6.40	8	2.52	1.62	8.20	6.90	0.58	4.64	1.72	1	1.00	3.43
187	Cylind	1.68	6.40	8	2.55	1.41	7.62	6.90	0.98	4.64	1.70	1	1.00	2.93
188	Cvlind	1.68	6.40	11	2.87	1.57	8.87	6.90	0.43	4.64	1.75	0.9	1.00	3.19
189	Sharp	1.31	15.24	5	2.63	2.55	2.62	39.00	1.13	29.24	2.68	0.9	0.89	3.88
190	Sharp	1.31	15.24	5	2.63	2.15	1.95	39.00	0.82	29.24	2.55	0.9	0.81	2.93
191	Sharp	1.31	15.24	5	2.63	2.13	2.29	39.00	0.82	29.24	2.62	0.9	0.85	3.00
192	Sharp	1.31	15.24	5	2.63	1.52	1.40	39.00	0.98	29.24	2.41	0.9	0.72	1.64
193	Sharp	1.31	15.24	5	2.63	1.99	2.16	39.00	0.79	29.24	2.59	0.9	0.83	2.71
194	Sharp	1.31	15.24	5	2.63	1.83	1.71	39.00	0.91	29.24	2.49	0.9	0.77	2.29
195	Sharp	1.31	15.24	5	2.63	2.13	1.92	39.00	0.85	29.24	2.54	0.9	0.80	2.88
196	Sharp	1.31	15.24	5	2.63	1.11	1.25	39.00	0.91	29.24	2.37	0.9	0.70	0.73
197	Sharp	1.04	11.98	3	1.66	2.56	1.46	95.00	0.24	71.63	3.28	0.9	0.85	2.48
198	Sharp	1.04	11.98	3	1.66	1.55	1.01	95.00	0.37	71.63	3.08	0.9	0.75	0.91
199	Sharp	1.04	11.98	3	1.66	1.89	1.04	95.00	0.58	71.63	3.10	0.9	0.76	1.43
200	Sharp	1.04	12.04	3	1.67	3.23	1.68	95.00	1.68	71.63	3.35	0.9	0.89	3.44
201	Sharp	1.04	12.04	3	1.67	2.13	1.13	95.00	1.40	71.63	3.14	0.9	0.78	1.80
202	Sharp	1.04	12.04	3	1.67	2.13	1.16	95.00	1.37	71.63	3.15	0.9	0.79	1.80
203	Sharp	0.94	10.36	0	0.94	2.44	2.65	73.00	0.76	55.04	3.32	0.9	1.00	1.86
204	Sharp	0.94	10.36	0	0.94	2.50	2.53	73.00	0.70	55.04	3.29	0.9	1.00	1.94
205	Sharp	0.94	10.36	0	0.94	1.49	2.01	73.00	0.58	55.04	3.17	0.9	1.00	0.68
206	Sharp	0.98	10.36	0	0.98	2.32	2.50	73.00	0.49	55.04	3.28	0.9	1.00	1.77
207	Sharp	0.94	10.36	0	0.94	2.44	2.38	73.00	0.55	55.04	3.26	0.9	1.00	1.89
208	Sharp	0.98	10.36	0	0.98	1.46	1.89	73.00	0.34	55.04	3.13	0.9	1.00	0.66
209	Sharp	0.94	10.36	0	0.94	1.01	2.26	73.00	0.09	55.04	3.23	0.9	1.00	0.00
210	Sharp	0.94	10.36	0	0.94	1.10	2.07	73.00	0.12	55.04	3.18	0.9	1.00	0.00
211	Sharp	0.94	10.36	0	0.94	1.07	1.83	73.00	0.12	55.04	3.12	0.9	1.00	0.00
212	Sharp	1.04	10.97	0	1.04	1.65	0.52	8.00	0.37	5.48	1.15	0.9	0.71	1.43
213	Sharp	1.04	10.97	0	1.04	1.34	0.46	8.00	0.52	5.48	1.13	0.9	0.68	1.13
214	Sharp	1.04	10.97	0	1.04	1.28	0.40	8.00	0.46	5.48	1.10	0.9	0.65	1.03
215	Sharp	1.04	10.97	0	1.04	1.65	0.40	8.00	0.98	5.48	1.10	0.9	0.65	1.33
216	Sharp	1.04	10.97	0	1.04	1.43	0.30	8.00	1.04	5.48	1.06	0.9	0.59	1.08
217	Sharp	1.04	10.97	0	1.04	1.65	0.46	8.00	1.07	5.48	1.13	0.9	0.68	1.38
218	Sharp	1.04	10.97	0	1.04	1.25	0.27	8.00	0.49	5.48	1.04	0.9	0.57	0.91
219	Sharp	1.04	10.97	0	1.04	0.76	0.12	8.00	0.30	5.48	0.91	0.9	0.44	0.42
220	Sharp	1.04	10.97	0	1.04	0.64	0.15	8.00	0.37	5.48	0.94	0.9	0.47	0.34
221	Round	0.91	12.19	30	6.89	2.07	3.14	32.00	1.58	23.90	2.58	1	0.69	4.91
222	Round	1.52	14.63	0	1.52	0.49	1.74	27.00	0.00	20.08	2.20	1	0.93	0.00
223	Round	1.52	14.63	0	1.52	2.65	5.79	27.00	0.61	20.08	2.69	1	1.00	3.55
224	Round	1.52	14.63	0	1.52	2.26	3.78	27.00	0.27	20.08	2.51	1	1.00	3.04
225	Round	1.52	14.63	0	1.52	1.65	2.59	27.00	0.00	20.08	2.35	1	1.00	2.06
226	Round	1.52	14.63	0	1.52	0.76	2.04	27.00	0.00	20.08	2.26	1	0.98	0.00
227	Round	1.52	14.63	0	1.52	3.20	8.08	27.00	1.19	20.08	2.85	1	1.00	4.28
228	Round	1.52	14.63	0	1.52	2.71	5.43	27.00	0.58	20.08	2.66	1	1.00	3.66
229	Round	1.52	14.63	0	1.52	1.98	3.60	27.00	0.00	20.08	2.49	1	1.00	2.58
230	Round	1.52	14.63	0	1.52	1.01	2.38	27.00	0.00	20.08	2.32	1	1.00	0.55
231	Round	1.52	14.63	0	1.52	3.41	9.72	27.00	1.31	20.08	2.94	1	1.00	4.53
232	Round	1.52	14.63	0	1.52	2.90	5.70	27.00	0.58	20.08	2.69	1	1.00	3.93
233	Round	1.52	14.63	0	1.52	2.13	3.75	27.00	0.00	20.08	2.50	1	1.00	2.84
234	Round	1.52	14.63	0	1.52	1.52	3.41	27.00	0.00	20.08	2.47	1	1.00	1.73
235	Round	1.52	14.63	0	1.52	3.75	9.57	27.00	1.19	20.08	2.93	1	1.00	4.99
236	Round	1.52	14.63	0	1.52	3.17	5.79	27.00	0.70	20.08	2.69	1	1.00	4.32
237	Round	1.52	14.63	0	1.52	2.32	3.84	27.00	1.01	20.08	2.51	1	1.00	3.13
238	Round	1.52	14.63	0	1.52	1.83	3.66	27.00	0.27	20.08	2.49	1	1.00	2.30
239	Round	1.52	14.63	0	1.52	3.93	9.48	27.00	1.25	20.08	2.92	1	1.00	5.23
240	Round	1.52	14.63	0	1.52	2.44	4.94	27.00	0.91	20.08	2.62	1	1.00	3.26

Table 6.12. (continued)

No.	Pier Shape	a (m)	L (m)	θ (°)	a' (m)	V₁ (m/s)	y₁ (m)	D₅₀ (mm)	Measured y_{s(pier)} (m)	τ_c (Pa)	Vc (m/s)	K₁	K_w	Predicted Scour Depth (m)
241	Round	1.52	14.63	0	1.52	1.98	3.81	27.00	0.52	20.08	2.51	1	1.00	2.57
242	Round	1.52	14.63	0	1.52	4.08	8.32	27.00	1.55	20.08	2.86	1	1.00	5.46
243	Round	1.68	13.11	0	1.68	3.35	5.09	33.00	1.07	24.67	2.82	1	1.00	4.79
244	Round	1.68	13.11	0	1.68	3.66	5.46	33.00	0.58	24.67	2.86	1	1.00	5.22
245	Round	1.52	12.19	0	1.52	2.53	5.52	28.00	0.34	20.84	2.70	1	1.00	3.36
246	Round	1.52	12.19	0	1.52	2.74	5.58	28.00	0.27	20.84	2.71	1	1.00	3.68
247	Round	1.52	12.19	0	1.52	2.23	5.12	28.00	0.98	20.84	2.67	1	1.00	2.88
248	Sharp	1.83	6.71	0	1.83	2.90	6.40	27.00	0.98	20.08	2.74	0.9	1.00	3.95
249	Round	1.07	24.93	0	1.07	1.37	3.87	1.82	0.49	0.96	0.86	1	1.00	2.07
250	Round	1.07	24.93	0	1.07	1.37	4.08	0.78	0.30	0.39	0.64	1	1.00	2.19
251	Round	0.76	9.14	22	4.13	1.52	5.33	2.85	0.76	1.64	1.11	1	0.97	5.02
252	Round	0.76	9.14	16	3.25	0.67	4.24	0.17	0.34	0.15	0.45	1	0.97	2.47
253	Round	0.98	10.85	0	0.98	1.19	1.95	18.00	0.55	13.17	1.95	1	1.00	1.07
254	Round	0.76	7.41	0	0.76	1.40	2.56	10.20	0.18	7.17	1.65	1	1.00	1.34
255	Round	0.76	7.41	0	0.76	1.46	2.32	10.20	0.82	7.17	1.62	1	1.00	1.43
256	Round	0.76	7.41	0	0.76	1.13	1.71	60.00	0.21	45.20	2.88	1	1.00	0.10
257	Round	0.76	11.37	0	0.76	0.76	1.65	4.00	0.76	2.47	1.05	1	1.00	0.79
258	Round	0.76	11.37	0	0.76	1.28	3.17	4.00	0.67	2.47	1.17	1	1.00	1.42
259	Round	0.76	11.37	0	0.76	0.24	1.49	0.25	0.15	0.18	0.42	1	1.00	0.28
260	Round	0.76	11.37	0	0.76	0.67	3.11	0.25	0.15	0.18	0.47	1	1.00	0.98
261	Sharp	1.14	10.18	8	2.55	0.37	1.83	0.17	0.21	0.15	0.39	0.9	0.80	0.87
262	Sharp	1.14	10.18	8	2.55	0.49	2.53	0.17	0.12	0.15	0.41	0.9	0.89	1.30
263	Sharp	1.14	10.18	8	2.55	0.76	4.24	0.17	0.15	0.15	0.45	0.9	1.00	2.21
264	Round	1.13	11.89	0	1.13	1.58	1.55	5.00	0.40	3.21	1.15	1	0.99	2.27
265	Round	1.13	11.89	0	1.13	2.13	2.87	5.00	0.73	3.21	1.27	1	1.00	2.96
266	Round	1.13	11.89	0	1.13	1.80	3.08	5.00	0.49	3.21	1.28	1	1.00	2.52
267	Round	1.31	11.89	0	1.31	1.68	2.04	17.00	0.73	12.40	1.92	1	1.00	2.20
268	Round	1.34	11.89	0	1.34	2.13	3.20	17.00	0.91	12.40	2.07	1	1.00	2.86
269	Round	1.37	11.89	0	1.37	1.98	3.38	17.00	0.98	12.40	2.09	1	1.00	2.66
270	Round	0.76	9.60	0	0.76	0.73	2.23	0.19	0.40	0.16	0.42	1	1.00	1.09
271	Round	0.76	9.60	0	0.76	0.91	2.77	0.19	0.43	0.16	0.43	1	1.00	1.32
272	Round	0.91	10.67	0	0.91	0.53	6.46	0.70	0.98	0.36	0.67	1	1.00	0.73
273	Round	0.91	10.67	0	0.91	0.31	5.00	0.70	0.91	0.36	0.65	1	1.00	0.25
274	Round	0.91	10.67	0	0.91	0.37	5.03	0.70	0.49	0.36	0.65	1	1.00	0.41
275	Round	0.91	10.67	0	0.91	0.40	5.33	0.70	0.91	0.36	0.65	1	1.00	0.47
276	Round	0.91	10.67	0	0.91	0.31	5.15	0.70	0.61	0.36	0.65	1	1.00	0.26
277	Round	0.91	10.67	0	0.91	0.29	4.75	0.70	0.55	0.36	0.64	1	1.00	0.20
278	Round	0.91	10.67	0	0.91	0.48	5.52	0.70	0.49	0.36	0.66	1	1.00	0.64
279	Round	0.91	10.67	0	0.91	0.41	5.61	0.70	0.61	0.36	0.66	1	1.00	0.50
280	Round	0.91	10.67	0	0.91	0.52	5.76	0.70	0.70	0.36	0.66	1	1.00	0.72
281	Round	0.91	10.67	0	0.91	1.39	8.75	0.70	1.52	0.36	0.71	1	1.00	1.97
282	Round	0.91	10.67	0	0.91	0.96	7.32	0.70	0.76	0.36	0.69	1	1.00	1.42
283	Round	0.91	10.67	0	0.91	0.97	4.94	0.70	1.37	0.36	0.64	1	1.00	1.45
284	Round	0.91	10.67	0	0.91	1.01	6.95	0.70	1.07	0.36	0.68	1	1.00	1.48
285	Round	0.91	10.67	0	0.91	0.92	6.71	0.70	1.37	0.36	0.68	1	1.00	1.36
286	Round	0.91	10.67	0	0.91	0.87	6.49	0.70	1.55	0.36	0.67	1	1.00	1.28
287	Round	0.91	10.67	0	0.91	0.94	6.61	0.70	1.28	0.36	0.68	1	1.00	1.39
288	Round	0.91	10.67	0	0.91	1.02	7.50	0.70	1.22	0.36	0.69	1	1.00	1.49
289	Round	0.91	10.67	0	0.91	0.98	7.44	0.70	1.07	0.36	0.69	1	1.00	1.44
290	Round	0.91	10.67	0	0.91	0.99	7.56	0.70	1.10	0.36	0.69	1	1.00	1.46
291	Round	0.91	10.67	0	0.91	0.57	8.02	0.70	0.91	0.36	0.70	1	1.00	0.79
292	Round	0.91	10.67	0	0.91	0.38	5.94	0.70	0.46	0.36	0.66	1	1.00	0.43
293	Round	0.91	10.67	0	0.91	0.37	6.10	0.70	0.61	0.36	0.67	1	1.00	0.39
294	Round	0.91	10.67	0	0.91	0.25	5.73	0.70	0.37	0.36	0.66	1	1.00	0.00
295	Round	0.91	10.67	0	0.91	0.33	5.64	0.70	0.46	0.36	0.66	1	1.00	0.29
296	Round	0.91	10.67	0	0.91	0.29	5.88	0.70	0.40	0.36	0.66	1	1.00	0.17
297	Round	0.91	10.67	0	0.91	0.35	6.34	0.70	0.46	0.36	0.67	1	1.00	0.35
298	Round	0.91	10.67	0	0.91	0.33	6.40	0.70	0.46	0.36	0.67	1	1.00	0.28
299	Round	0.91	10.67	0	0.91	0.33	7.13	0.70	0.91	0.36	0.69	1	1.00	0.27
300	Round	0.88	9.75	0	0.88	0.85	4.27	0.74	0.27	0.38	0.64	1	1.00	1.26

Table 6.12. (continued)

No.	Pier Shape	a (m)	L (m)	θ (°)	a' (m)	V_1 (m/s)	y_1 (m)	D_{50} (mm)	Measured $y_{s(pier)}$ (m)	τ_c (Pa)	Vc (m/s)	K_1	K_w	Predicted Scour Depth (m)
301	Round	0.88	9.75	0	0.88	0.78	4.39	0.74	0.24	0.38	0.64	1	1.00	1.15
302	Round	0.88	9.75	0	0.88	0.92	4.51	0.74	0.27	0.38	0.64	1	1.00	1.36
303	Round	0.88	9.75	0	0.88	0.86	4.27	0.74	0.34	0.38	0.64	1	1.00	1.26
304	Round	0.88	9.75	0	0.88	0.86	4.39	0.74	0.49	0.38	0.64	1	1.00	1.27
305	Round	0.88	9.75	0	0.88	1.01	4.63	0.74	0.43	0.38	0.65	1	1.00	1.48
306	Round	0.88	9.75	0	0.88	0.96	4.36	0.74	0.43	0.38	0.64	1	1.00	1.40
307	Round	0.88	9.75	0	0.88	1.02	4.63	0.74	0.55	0.38	0.65	1	1.00	1.49
308	Round	0.88	9.75	0	0.88	0.95	4.63	0.74	0.46	0.38	0.65	1	1.00	1.40
309	Round	0.88	9.75	0	0.88	0.99	4.69	0.74	0.40	0.38	0.65	1	1.00	1.44
310	Round	0.88	9.75	0	0.88	0.91	4.72	0.74	0.34	0.38	0.65	1	1.00	1.33
311	Round	0.88	9.75	0	0.88	0.80	4.88	0.74	0.46	0.38	0.65	1	1.00	1.17
312	Round	0.88	9.75	0	0.88	0.99	5.03	0.74	0.37	0.38	0.66	1	1.00	1.45
313	Round	0.88	9.75	0	0.88	1.04	4.79	0.74	0.37	0.38	0.65	1	1.00	1.51
314	Round	0.88	9.75	0	0.88	0.92	4.48	0.74	0.37	0.38	0.64	1	1.00	1.36
315	Round	0.88	9.75	0	0.88	1.12	5.03	0.74	0.40	0.38	0.66	1	1.00	1.62
316	Round	0.88	9.75	0	0.88	1.00	5.09	0.74	0.55	0.38	0.66	1	1.00	1.45
317	Round	0.88	9.75	0	0.88	1.12	4.85	0.74	0.61	0.38	0.65	1	1.00	1.61
318	Round	0.88	9.75	0	0.88	1.05	5.15	0.74	0.61	0.38	0.66	1	1.00	1.52
319	Round	0.88	9.75	0	0.88	1.09	4.69	0.74	0.61	0.38	0.65	1	1.00	1.57
320	Round	0.76	13.11	0	0.76	0.64	2.71	0.92	0.76	0.46	0.63	1	1.00	0.85
321	Round	0.98	25.30	0	0.98	1.60	6.25	0.28	1.07	0.20	0.55	1	1.00	2.39
322	Round	0.98	25.30	0	0.98	1.88	7.92	0.28	1.22	0.20	0.58	1	1.00	2.70
323	Round	0.98	25.30	0	0.98	1.32	5.82	0.28	0.82	0.20	0.55	1	1.00	2.04
324	Round	0.98	25.30	0	0.98	2.17	9.30	0.28	1.07	0.20	0.59	1	1.00	3.02
325	Round	0.98	25.30	0	0.98	1.66	8.38	0.28	1.52	0.20	0.58	1	1.00	2.45
326	Round	0.61	12.50	0	0.61	0.56	0.46	72.00	0.24	54.28	2.46	1	0.81	0.00
327	Round	0.61	12.50	0	0.61	1.55	0.67	72.00	0.18	54.28	2.62	1	0.92	0.84
328	Round	0.61	12.50	0	0.61	1.59	1.68	72.00	0.49	54.28	3.06	1	1.00	0.76
329	Round	0.61	12.50	0	0.61	1.23	1.22	72.00	0.30	54.28	2.90	1	1.00	0.32
330	Round	0.61	12.50	0	0.61	1.62	1.52	72.00	0.37	54.28	3.01	1	1.00	0.81
331	Round	0.61	12.50	0	0.61	2.59	2.62	72.00	0.76	54.28	3.29	1	1.00	1.70
332	Round	0.69	8.53	0	0.69	0.66	1.71	0.69	0.40	0.35	0.54	1	1.00	0.86
333	Round	0.69	8.53	0	0.69	0.69	1.80	0.69	0.37	0.35	0.54	1	1.00	0.90
334	Round	0.69	8.53	0	0.69	0.64	1.55	0.69	0.21	0.35	0.53	1	1.00	0.85
335	Round	0.69	8.53	0	0.69	0.38	0.88	0.69	0.40	0.35	0.48	1	0.97	0.47
336	Round	0.69	8.53	0	0.69	0.52	1.40	0.69	0.43	0.35	0.52	1	1.00	0.68
337	Round	0.69	8.53	0	0.69	0.52	1.62	0.69	0.37	0.35	0.53	1	1.00	0.68
338	Round	0.69	8.53	0	0.69	0.19	0.98	0.69	0.55	0.35	0.49	1	1.00	0.01
339	Round	0.69	8.53	0	0.69	0.32	0.88	0.69	0.73	0.35	0.48	1	0.97	0.36
340	Round	0.69	8.53	0	0.69	0.24	0.88	0.69	0.49	0.35	0.48	1	0.97	0.19
341	Round	0.69	8.53	0	0.69	0.32	0.79	0.69	0.40	0.35	0.47	1	0.93	0.36
342	Round	0.69	8.53	0	0.69	0.19	0.61	0.69	0.43	0.35	0.45	1	0.86	0.07
343	Round	0.69	8.53	0	0.69	0.50	1.07	0.69	0.46	0.35	0.50	1	1.00	0.66
344	Round	0.61	9.14	0	0.61	1.13	0.76	55.00	0.46	41.41	2.45	1	0.96	0.41
345	Round	0.61	9.14	0	0.61	1.68	3.20	55.00	0.64	41.41	3.11	1	1.00	0.84
346	Round	0.61	9.14	0	0.61	1.97	3.20	55.00	0.55	41.41	3.11	1	1.00	1.17
347	Round	0.61	8.99	0	0.61	1.24	2.16	37.00	0.06	27.72	2.55	1	1.00	0.55
348	Round	0.61	8.99	0	0.61	1.40	2.41	37.00	0.12	27.72	2.59	1	1.00	0.74
349	Round	0.61	8.99	0	0.61	1.36	2.59	37.00	0.24	27.72	2.63	1	1.00	0.68
350	Round	0.61	8.99	0	0.61	1.40	2.96	37.00	0.30	27.72	2.68	1	1.00	0.70
351	Round	0.61	8.99	0	0.61	1.46	3.02	37.00	0.24	27.72	2.69	1	1.00	0.77
352	Round	0.61	8.99	0	0.61	1.55	3.26	37.00	0.37	27.72	2.73	1	1.00	0.87

6.4.3 Remarks

The predicted maximum scour depths using equation (6.18) are conservative, but less conservative than HEC-18 prediction. However, the data are still scattered in Figure 6.13 and Figure 6.16. These scatters may come from the uncertainties of data, and the following two are the possible uncertainties. It is believed that if the following two uncertainties are taken out, the magnitude scatter will be decreased tremendously.

1. The critical shear stress of channel bed soil: it is assumed that the channel beds are consisted with cohesionless soil, and the critical shear stresses are calculated using only D_{50}, which does not include the distribution of soil particles. The calculated critical shear stresses are usually different from the real critical shear stresses. Since the well distributed soil particles are less erodible than poorly distributed soil by the reason of armoring effect.

2. Time effect: the equation (6.18) is for the maximum scour depth, and it is assumed that the duration of flood is long enough to yield the maximum scour depth in order to apply the equation. However, if the real erosion rate of channel bed soil is very slow and the duration of the biggest flood is just several days, the measured scour depth will be shallower than the maximum scour depth.

CHAPTER VII

CONTRACTION SCOUR IN COHESIVE SOIL

7.1 Introduction

Many methods to predict the contraction scour depth in the condition of long contraction have been derived after Straub's (1934) research. Generally long contraction is called when the contraction length (W_a) is more than 2 times longer than the approach channel width (L_1) as shown in Figure 7.1. In long contraction condition, both the uniform flow and uniform scour are assumed at contracted section. In addition, if the increased velocity by the channel narrowing is higher than the critical velocity of channel bottom soil, the contraction scour will occur and continue until the shear stress acting on the channel bottom reaches to the critical shear stress in uniform discharge.
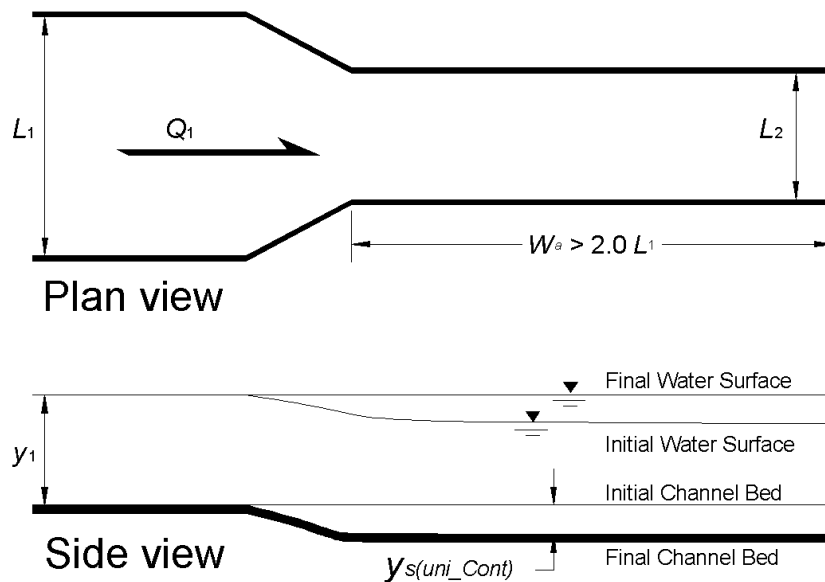
Figure 7.1. Uniform flow and uniform contraction scour through a long contraction in rectangular channel

However those methods are for the ideal cases where only laboratory test conditions can be satisfied. Li (2002) had several questions about the difference between test condition and the reality. The main differences are summarized in followings.

1. Soil bed: The previous contraction scour equations were typically developed using uniform sand, but in the reality the channel bottom may consist with cohesive soil.

2. Research content: All available equations are limited to predict the uniform contraction scour depth in a long contraction channel. But the knowledge on how the contraction scour distributes, where and how big the maximum contraction scour is, are more critical in bridge scour evaluations (Figure 7.2).

3. Contraction shape: Bridges typically impose short, abrupt contractions. The applicability of the long rectangular contraction solution is uncertain for this case (Melville and Coleman, 2000). Further study on the influence of contraction length (W_a) and transition angle (α) is necessary for a comprehensive understanding of the bridge contraction scour.

4. Flow condition: Uniform flow in both approach and contracted section is assumed to derive the long contraction scour equations. However, the flow un-uniformity, which could attribute additional erosion especially at the inlet of the contraction, would possibly lead to an underestimated contraction scour.
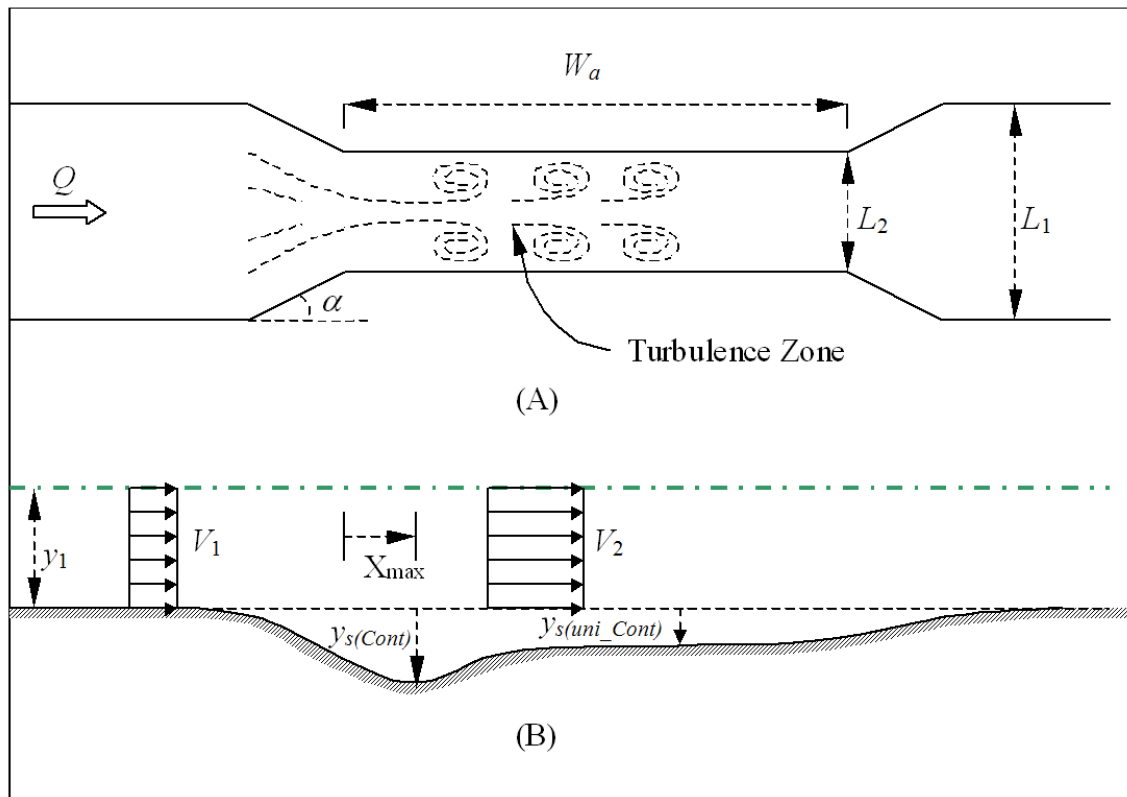
Figure 7.2. Definition of contraction scour

In order to solve these questions Li (2002) studied contraction scour in rectangular channels using Porcelain clay as the channel bed material. The four types of transition angle and three short contractions were considered in his study.

The scour depth along the centerline of the channel in a symmetrical contraction was used to determine the maximum contraction scour and uniform scour depths. He found that the maximum contraction scour depth is dependent not on the contraction shape but on discharge and contraction ratio, while the location of maximum contraction is related with contraction shape and contraction ratio. He also found that the maximum contraction scour is approximately 35 % deeper than the uniform contraction scour depth.

The total of 12 experiments in compound channels and 4 experiments in rectangular channels were performed in the present study. The more realistic abutments, which are wing-wall and spill-through type, were used in the half of the channel to maximize the channel scale. The maximum contraction scour depth close to the wall but not at the wall on the other side of the abutment was measured for the determinations of the maximum contraction scour depth. This is to avoid the effect of the side wall. The channel configuration in large flume test is shown in Figure 7.3.

The experimental results by Li (2002) summarized in Table 7.1 and large flume test results summarized in Table 7.2 are used for the formulization of the maximum contraction scour depth in cohesive soil.

Table 7.1. Variables and results of contraction scour in Li (2002)

Test No.	Contraction Shape	Channel Type	$0.5L_1$ (m)	θ (^{o})	y_{m1} (m)	L' (m)	W_a (m)	V_1 (m/s)	Q (m^3/s)	Q_{block} (m^3/s)	C_R	$y_{s(cont)}$ (mm)
Ya-Ll 1	VW (90^0)	Rect.	0.225	90	0.165	0.169	1.319	0.341	0.0253	0.019	0.250	357
Ya-Ll 2	VW (90^0)	Rect.	0.225	90	0.162	0.113	1.741	0.310	0.023	0.011	0.500	116
Ya-Ll 3	VW (90^0)	Rect.	0.225	90	0.106	0.056	1.521	0.459	0.022	0.005	0.750	73
Ya-Ll 4	VW (90^0)	Rect.	0.225	90	0.108	0.113	1.521	0.205	0.010	0.005	0.500	29
Ya-Ll 5	VW (90^0)	Rect.	0.225	90	0.251	0.113	1.521	0.207	0.023	0.012	0.500	38
Ya-Ll 6	VW (90^0)	Rect.	0.225	90	0.172	0.113	1.521	0.205	0.016	0.008	0.500	36
Ya-Ll 7	VW (90^0)	Rect.	0.225	90	0.174	0.113	1.521	0.390	0.031	0.015	0.500	143
Ya-Ll 9	VW (15^0)	Rect.	0.225	90	0.160	0.113	1.741	0.302	0.022	0.011	0.500	91
Ya-Ll 10	VW (45^0)	Rect.	0.225	90	0.152	0.113	1.521	0.302	0.021	0.010	0.500	128
Ya-Ll 11	VW (60^0)	Rect.	0.225	90	0.163	0.113	1.521	0.293	0.022	0.011	0.500	80
Ya-Ll 12	VW (90^0)	Rect.	0.225	90	0.161	0.113	0.380	0.330	0.024	0.012	0.500	111
Ya-Ll 13	VW (90^0)	Rect.	0.225	90	0.162	0.113	0.113	0.330	0.024	0.012	0.500	128
Ya-Ll 14	VW (90^0)	Rect.	0.225	90	0.165	0.113	0.056	0.341	0.025	0.013	0.500	208

Table 7.2. Variables and results of contraction scour in large flume test

Test No.	Contraction Shape	Channel Type	$0.5L_1$ (m)	θ (^{o})	y_{m1} (m)	L' (m)	W_a (m)	V_1 (m/s)	$0.5Q$ (m^3/s)	V_2 (m/s)	C_R	$y_{s(cont)}$ (mm)
Case 1	ST (2:1)	Comp.	3.658	90	0.496	1.829	0.457	0.441	0.573	0.675	0.653	206
Case 1II	ST (2:1)	Comp.	3.658	90	0.497	1.829	0.457	0.432	0.562	0.644	0.671	224
Case 2	ST (2:1)	Comp.	3.658	90	0.386	1.829	0.457	0.357	0.320	0.537	0.665	130
Case 3	ST (2:1)	Comp.	3.658	90	0.603	1.829	0.457	0.480	0.812	0.721	0.666	282
Case 4	ST (2:1)	Comp.	3.658	90	0.494	1.829	0.457	0.342	0.442	0.522	0.656	77
Case 5	ST (2:1)	Comp.	3.658	90	0.499	1.829	0.457	0.506	0.662	0.773	0.655	277
Case 6	ST (2:1)	Comp.	3.658	90	0.496	1.219	0.457	0.432	0.561	0.539	0.802	191
Case 7	ST (2:1)	Comp.	3.658	90	0.494	2.438	0.457	0.437	0.564	0.812	0.538	342
Case 8	ST (3:1)	Comp.	3.658	90	0.493	1.829	0.457	0.442	0.570	0.631	0.700	251
Case 9	WW	Comp.	3.658	90	0.497	1.829	0.457	0.436	0.568	0.714	0.610	226
Case 10	ST (2:1)	Comp.	3.658	60	0.496	1.829	0.457	0.436	0.565	0.656	0.664	225
Case 11	ST (2:1)	Comp.	3.658	120	0.495	1.829	0.457	0.436	0.564	0.651	0.669	237
Case 12B	WW	Comp.	3.658	90	0.497	1.829	0.457	0.582	0.759	0.987	0.590	256
Case 13	WW	Rect.	3.658	90	0.366	1.015	0.457	0.328	0.439	0.454	0.722	48
Case 14	WW	Rect.	3.658	90	0.371	1.625	0.457	0.326	0.442	0.587	0.556	144
Case 15	WW	Rect.	3.658	90	0.384	2.234	0.457	0.310	0.435	0.828	0.374	222
Case 17	WW	Rect.	3.658	90	0.364	1.320	0.457	0.364	0.485	0.573	0.635	159

In the tables, VW is a vertical wall abutment, ST is a spill-through abutment, WW is a wing-wall abutment, Rect. is a rectangular channel, L_1 is the width of channel at the approach section, W_a is the length of contraction channel, Q is total discharge, C_R is contraction ratio $C_R = (Q - Q_{block})/Q$, V_1 is the average approach velocity, V_2 is the average velocity at the contracted section, y_{m1} is water depth in the main channel immediately upstream of the bridge contraction, y_{f1} is the water depth at the toe of the abutment estimated as the water depth immediately upstream of the toe of the abutment, and $y_{s(Cont)}$ is the maximum contraction scour depth in the middle of channel

(a) Rectangular Channel

(b) Compound Channel
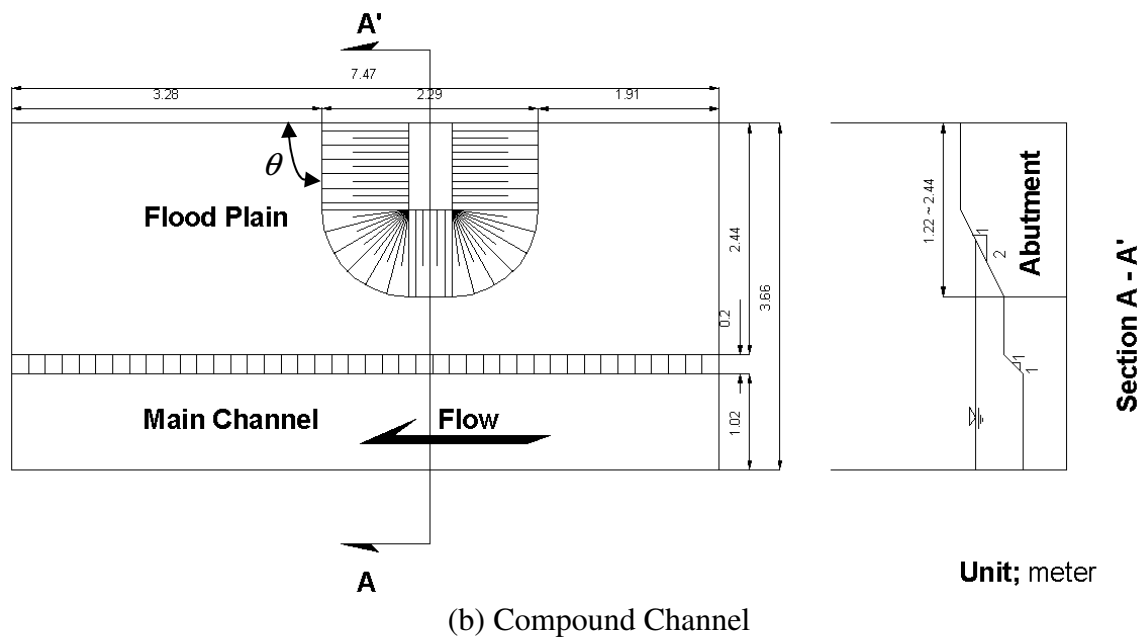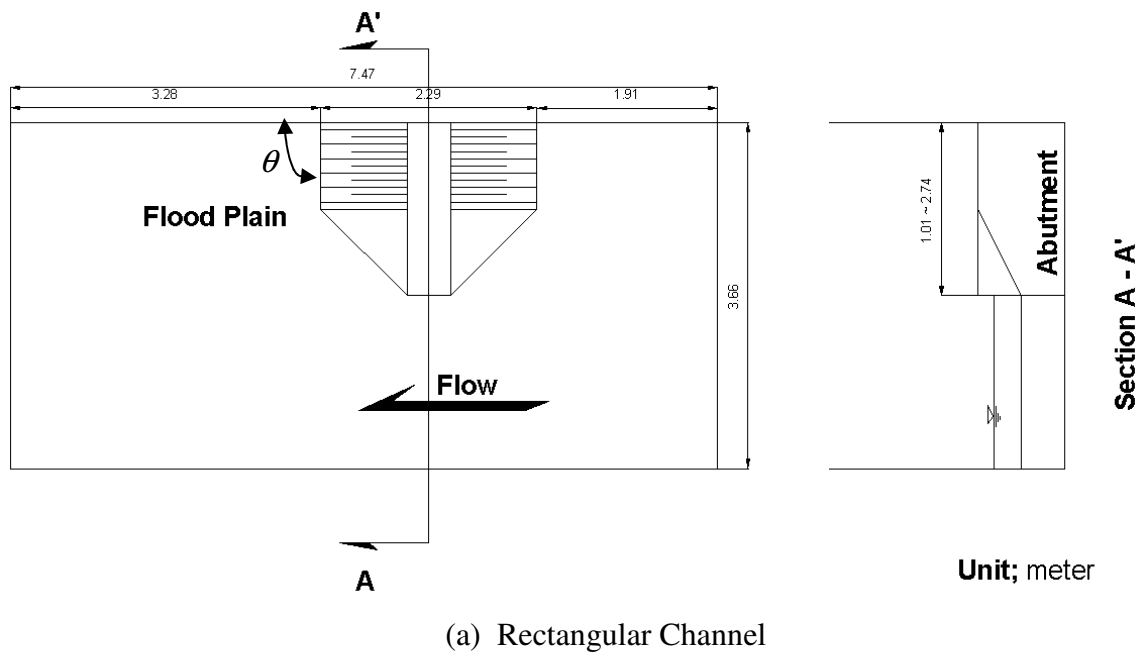
Figure 7.3. Channel configuration in large flume test

7.2 Dimensional analysis

The variables affecting the maximum contraction scour can be listed as following

$$y_{s(Cont)} = f(y_{m1}, g, V_1, C_R, \rho_s, \rho, \mu, V_{mc}, sh, W_a, L_1) \tag{7.1}$$

Dimensional analysis yields the following dimensionless parameters:

$$\frac{y_{s(Cont)}}{y_{m1}} = f\left(\frac{\rho_s}{\rho}, Fr_{m1}, C_R, Fr_{mc}, \text{Re}, sh, \frac{W_a}{L_1}\right) \tag{7.2}$$

$$Fr_{m1} = \frac{V_1}{\sqrt{gy_{m1}}} \; ; \; \text{Re} = \frac{\rho y_{m1} V_1}{\mu} \; ; \; Fr_{mc} = \frac{V_{mc}}{\sqrt{gy_{m1}}} = \frac{\sqrt{\tau_c / \rho}}{gny_{m1}^{1/3}}$$

where $y_{s(Cont)}$ is the maximum contraction scour depth, y_{m1} is the main channel depth at the approach section, Fr_{m1} is the Froude number of the main-channel at the approach section, Fr_{mc} is the critical Froude number for the main-channel, C_R is contraction ratio $C_R = (Q - Q_{block})/Q$, V_1 is the average velocity at the approach section, g is the gravitational acceleration, τ_c is the critical shear stress, n is Manning's roughness coefficient, ρ_s is the soil density, ρ is the water density, μ is the viscosity of water, sh is the shape of contraction, and V_{mc} is the critical velocity in the main channel. The bed material used in the present study is a Porcelain clay so the value of ρ_s / ρ is fixed. Reynolds number in the experiments is very large (of the order of 10^5) so it may be reasonable to neglect the viscous effect. As mentioned in Section 4.1.2, the water depth at immediately upstream of the contraction section is used for dimensional analysis. Because the water surface at the approach section was almost constant while scour was progressing, but there were significant changes in the surface elevation after the

approach section. The water level after the approach section increased as scour progressed. It finally reached the same level as that of the approach section and reached an equilibrium condition. However, the approach water depth in a real channel is not constant through the flow direction while it is nearly constant in the flume test. Thus the water depth immediately upstream of the abutment is used to evaluate the clear water scour depth for not only the laboratory tests but also in the real channel.

As a result, the relation is reduced to

$$\frac{y_{s(Cont)}}{y_{m1}} = f\left(Fr_{m1}, C_R, Fr_{mc}, sh, \frac{W_a}{L_1}\right)$$
(7.3)

If the flow at the contracted section is uniform, the velocity at the contracted section will be $V_2 = V_1 / C_R$ and the equation (7.3) may be reduced to

$$\frac{y_{s(Cont)}}{y_{m1}} = f\left(Fr_{m2}, Fr_{mc}, sh, \frac{W_a}{L_1}\right)$$
(7.4)

7.3 Prediction of contraction scour

Although the uniform flow at the contracted section is assumed, the flow passing through the contracted section becomes non-uniform and the amplification factor describing the non-uniform flow is required. The scour continues until the velocity at the contracted section equals to the critical velocity of channel bed soil. Thus the maximum contraction scour equation for a given abutment shape may be expressed as

$$\frac{y_{s(Cont)}}{y_{m1}} = K_{sh} \cdot K_{CL} \cdot \alpha_1 \left(\beta_1 Fr_{m2} - Fr_{mc}\right)^{\gamma_1}$$
(7.5)

where α_1, β_1 and γ_1 are correction factors to be determined experimentally, $Fr_{m2} = \dfrac{V_2}{\sqrt{gy_{m1}}}$,

and $Fr_{mc} = \dfrac{V_{mc}}{\sqrt{gy_{m1}}} = \dfrac{\sqrt{\tau_c/\rho}}{gny_{m1}^{1/3}}$.

The values of τ_c and n were 0.7 Pa and 0.014 in Li's (2002) study. Nevertheless $\tau_c = 0.8$ Pa and $n = 0.011$ are used in the present study. Manning's n value in the large scale tests is decided from HEC-RAS results, using $n = 0.011$ agrees well with the measurements at the approach section as mentioned in Section 5.2. Data regression was performed using Li's data with $\tau_c = 0.7$ Pa and $n = 0.014$ and using data in the 4 test cases in the large scale tests for rectangular channel (cases 13 to 15 and 17) with $\tau_c = 0.8$ Pa and $n = 0.011$. Although the test condition in large scale tests is short contraction with transition, it is reasonable to apply the flume test results of large scale tests to the Li's data since it was found that the maximum scour depth is independent on the contraction length and transition by Li (2002).

The resulting prediction equation for contraction scour, as shown in Figure 7.4, is

$$\frac{y_{s(Cont)}}{y_{m1}} = 1.27\left(1.83Fr_{m2} - Fr_{mc}\right) \tag{7.6}$$

where $y_{s(Cont)}$ is the maximum contraction scour depth, y_{m1} is the main channel depth at the approach section, $Fr_{m2}\left(=\dfrac{V_2}{\sqrt{gy_{m1}}}\right)$ is the Froude number of the main-channel at the bridge section, $Fr_{mc}\left(=\dfrac{V_{mc}}{\sqrt{gy_{m1}}} = \dfrac{\sqrt{\tau_c/\rho}}{gny_{m1}^{1/3}}\right)$ is the critical Froude number of the main-

channel, V_2 is the average velocity at the contracted section defined as $V_2 = V_1 / C_R$, V_{mc} is the critical velocity in the main channel, τ_c is the critical shear stress, n is Manning's roughness coefficient, and ρ is the water density.
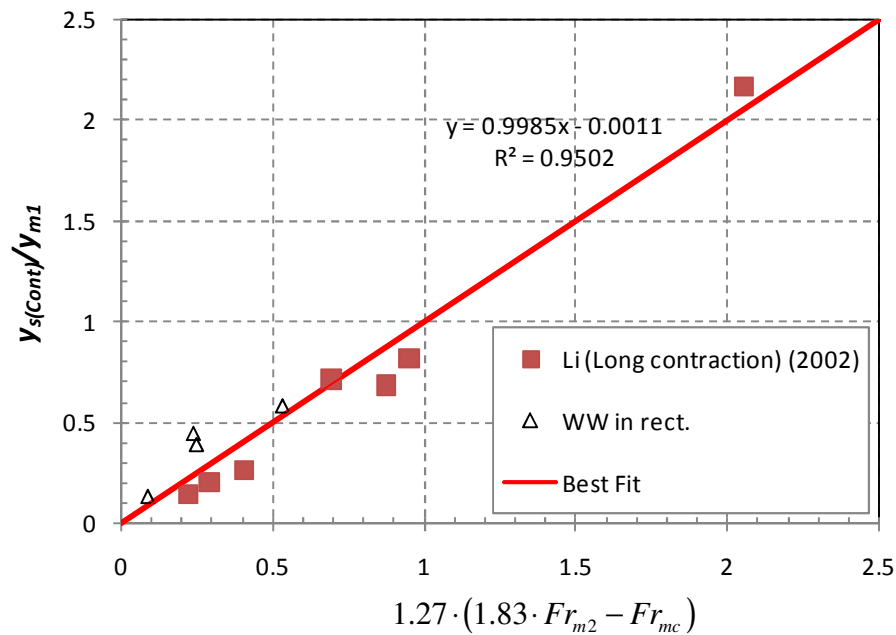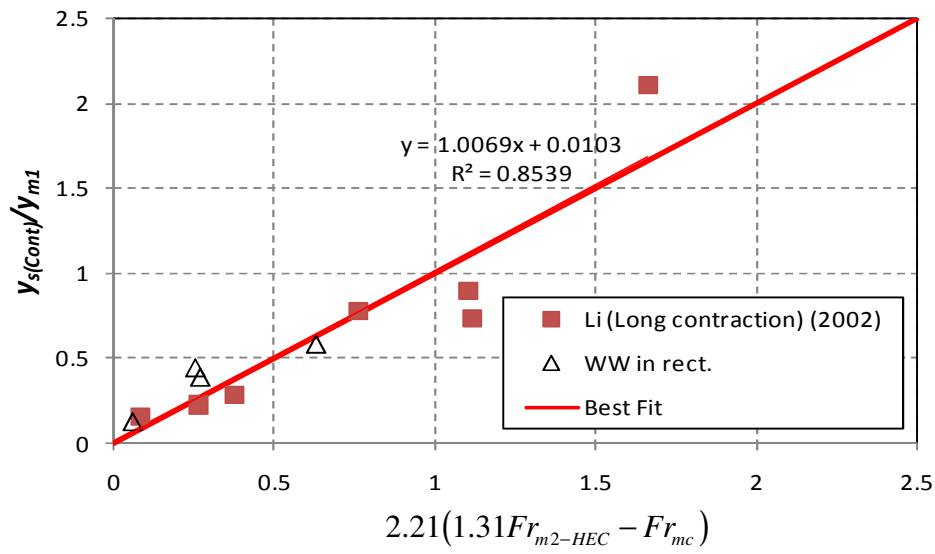

Figure 7.4. Maximum contraction scour in rectangular channel: measurement versus prediction

7.4 Maximum contraction scour depth for spill-through abutment and compound channel

The prediction equation for contraction scour in equation (7.6) is based on experimental data using rectangular channels. The prediction equation (7.6) is applied to the Li's other data in the rectangular channel and the wing-wall abutment in the compound channel, and compared in Figure 7.5. Figure 7.5 shows that the equation (7.6) agrees well with the experiment results regardless the shape of channel. Interestingly, the

equation predicts contraction scour well when applied to the spill-through abutment in compound channels, as shown in Figure 7.6.

For the maximum contraction scour depth, the channel geometry and contraction shape seem to have no effect on the maximum contraction scour depth. Thus the maximum contraction scour depth can be explained as equation (7.6).
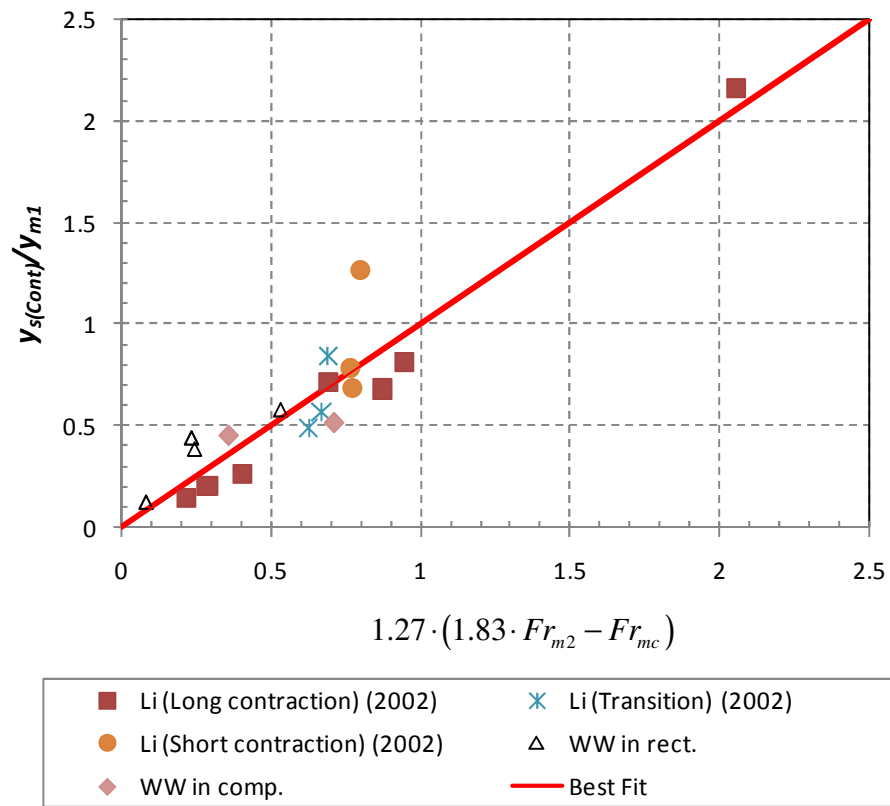
Figure 7.5. Maximum contraction scour in rectangular channel and compound channel: measurement versus prediction
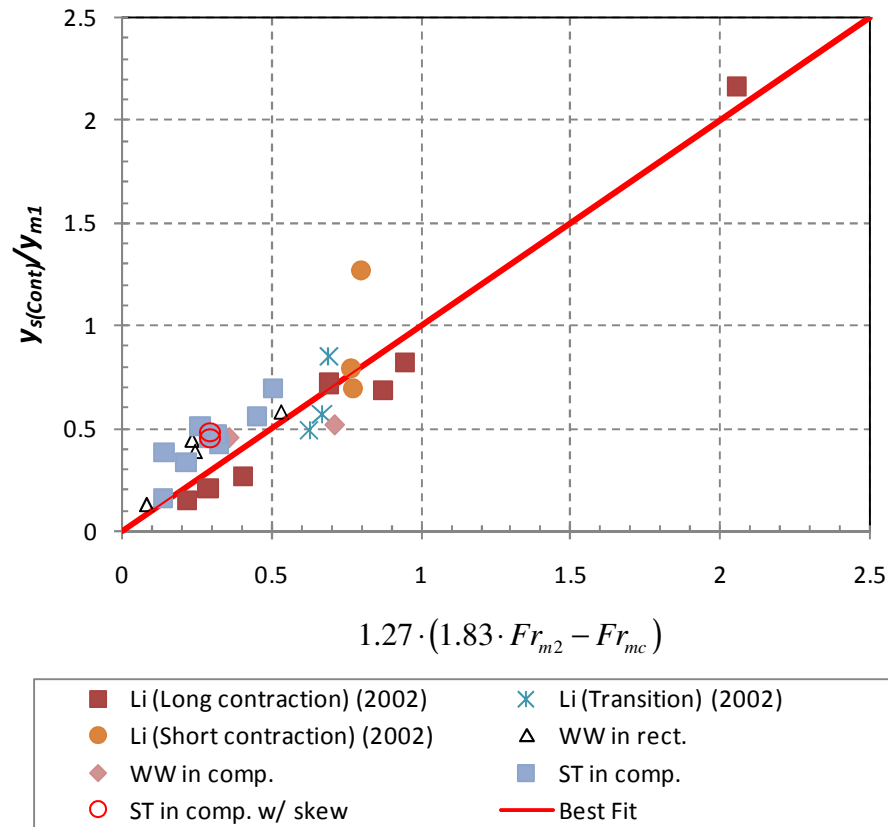
Figure 7.6. Maximum contraction scour in rectangular channel and compound channel for different contraction shape: measurement versus prediction

The equation (7.6) is elaborated to find the maximum contraction scour depth on the basis of flume test using cohesive materials. The critical shear stress of the Porcelain clay was obtained from EFA tests. Li (2002) found that the uniform contraction scour depth is approximately 74 % of the maximum contraction scour depth. Thus the equation (7.6) for the maximum contraction scour depth is converted to:

$$\frac{y_{s(uni\_Cont)}}{y_{m1}} = 0.94\left(1.83 Fr_{m2} - Fr_{mc}\right) \tag{7.7}$$

where $y_{s(uni\_Cont)}$ is the uniform contraction scour depth, y_{m1} is the main channel depth at

the approach section, $Fr_{m2}\left(=\dfrac{V_2}{\sqrt{gy_{m1}}}\right)$ is the Froude number of the main-channel at the

bridge section, $Fr_{mc}\left(=\dfrac{V_{mc}}{\sqrt{gy_{m1}}}=\dfrac{\sqrt{\tau_c/\rho}}{gny_{m1}^{1/3}}\right)$ is the critical Froude number of the main-

channel, V_2 is the average velocity at the contracted section defined as $V_2 = V_1/C_R$, V_{mc}

is the critical velocity in the main channel, τ_c is the critical shear stress, n is Manning's

roughness coefficient, and ρ is the water density.

7.5   Verification of maximum contraction scour equation

Experimental data in Gill (1981) were used for comparison of contraction scour

depth. Gill conducted a series of contraction scour tests in the laboratory. The

experiments were conducted in a rectangular channel which is 11.4 m long, 0.76 m wide

and 0.46 m deep. Two contracted sections were used in the channel. In the first series of

experiments, the effective length of the contraction is 1.83 m, excluding the 0.46 m long

upstream (inlet) and 0.46 m long downstream (outlet) transitions. In the second series of

experiments, the effective length of the contraction is 2.44 m with the transitions. The

width of the contracted section is 0.5 m. Two types of nearly uniform sand were used in

the experiments. The average size of the coarse sand, D_{50}, is 1.53 mm while D_{50} of the

fine sand is 0.92 mm. The angle of transition at the contraction is approximately 15°. He

measured the uniform contraction scour depths in the flume tests. Thus the equation

(7.7) is applied for the verification.

Although the equation (7.7) is developed to calculate the uniform contraction

scour in cohesive soil, this equation also can be easily extended to the contraction scour

in cohesionless soil because the soil properties are represented by the critical shear stress.

The Shields diagram is used to find the critical shear stress of cohesionless soil, and

Manning's *n* value is obtained by Strikler approximation $\left(n = 0.013D_{50}^{1/6}\right)$ (after

Richardson and Davis, 1995).

The basic parameters for Gill's flume tests are summarized in Table 7.3. The

comparison between predictions based on the equation (7.7) and that in Gill's test results

is shown in Figure 7.7. The comparison between predictions using the HEC-18 method

and that in Gill's test results (conducted in NCHRP 24-15) is shown in Figure 7.8.

According to the figures, the predictions based on the present study are in reasonable

agreement with the database while the HEC-18 method (Laursen's equation) severely

under predicts the scour depths.

Table 7.3. Gill's test parameters and scour depth results of both measurement and
prediction by equation (7.7)

Test No.	y_1 (mm)	Q (m³/s)	y_2 (mm)	D_{50} (mm)	$1/C_R$	V_1 (m/s)	n value	τ_c (Pa)	V_c (m/s)	ScourDepth (mm) Measured.	ScourDepth (mm) Predicted.
1	67.1	0.01504	91.4	1.53	1.52	0.29	0.014	1.12	0.49	24.3	30.6
2	72.5	0.01646	100.6	1.53	1.52	0.3	0.014	1.12	0.49	28.1	33.7
3	80.5	0.0199	115.8	1.53	1.52	0.32	0.014	1.12	0.50	35.3	39.6
4	80.8	0.0224	131.1	1.53	1.52	0.36	0.014	1.12	0.50	50.3	49.3
5	36.3	0.0091	48.8	1.53	1.52	0.33	0.014	1.12	0.44	12.5	31.3
6	47.6	0.0133	91.4	1.53	1.52	0.37	0.014	1.12	0.46	43.8	42.1
7	63.4	0.015	85.3	1.53	1.52	0.31	0.014	1.12	0.48	21.9	34.3
8	68.3	0.0165	97.5	1.53	1.52	0.32	0.014	1.12	0.49	29.2	37.4
9	74.1	0.0196	106.7	1.53	1.52	0.35	0.014	1.12	0.50	32.6	45.4
10	83.5	0.021	118.9	1.53	1.52	0.33	0.014	1.12	0.51	35.4	42.6
11	40.8	0.0122	88.4	1.53	1.52	0.39	0.014	1.12	0.45	47.6	43.0
12	65.5	0.0122	82.3	0.92	1.52	0.25	0.013	0.67	0.41	16.8	27.2
13	68.6	0.0165	100.6	0.92	1.52	0.32	0.013	0.67	0.41	32	43.1
14	38.7	0.0071	48.8	0.92	1.52	0.24	0.013	0.67	0.38	10.1	21.0
15	43.6	0.0094	67.1	0.92	1.52	0.28	0.013	0.67	0.38	23.5	28.9
16	53.3	0.0122	82.3	0.92	1.52	0.3	0.013	0.67	0.40	29	35.1
17	54.3	0.0133	88.4	0.92	1.52	0.32	0.013	0.67	0.40	34.1	39.3
18	27.4	0.0051	39.6	0.92	1.52	0.25	0.013	0.67	0.35	12.2	19.9
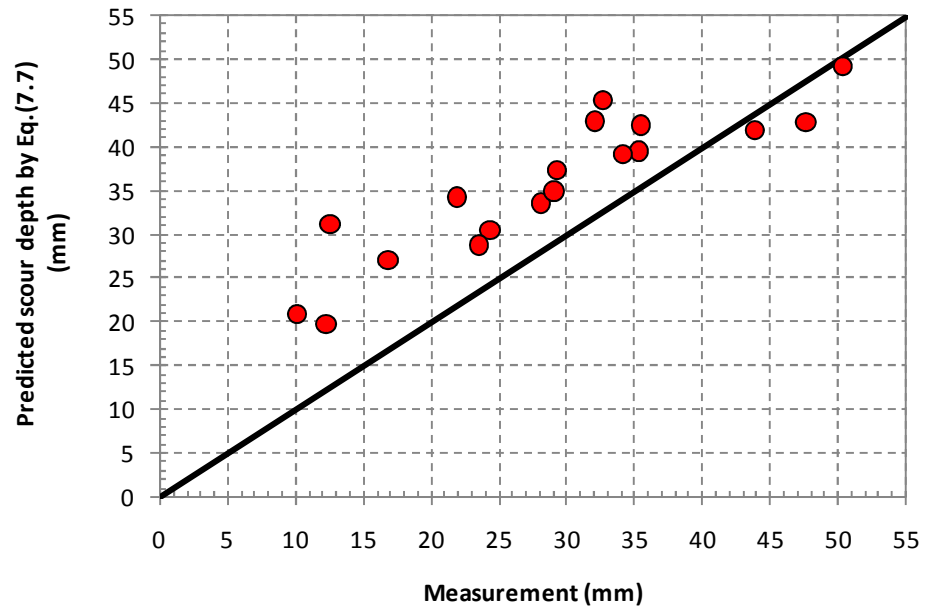
Figure 7.7. Prediction by equation (7.7) versus Gill's measurement (1981)
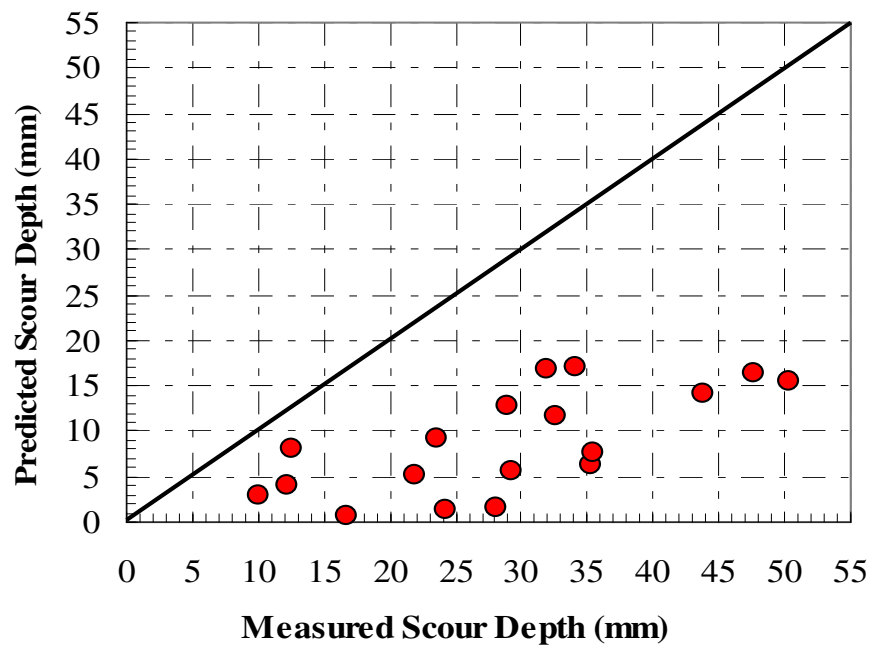
Figure 7.8. HEC-18 method versus Gill (1981) database (cited from Briaud et al.

(2003))

7.6 Methodology using HEC-RAS results

Although HEC-RAS results are not accurate to predict the local, more than 90 % of engineers in the United States use it for the bridge design. A new method using the velocity calculated by HEC-RAS at the contracted section is suggested for the HEC-RAS users.

The maximum contraction scour equation for a given abutment shape may be expressed as

$$\frac{y_{s(Cont)}}{y_{m1}} = \alpha_1 \left(\beta_1 Fr_{m2\_HEC} - Fr_{mc} \right) \tag{7.8}$$

where α_1 and β_1 are correction factors to be determined experimentally,

$$Fr_{m2\_HEC} = \frac{V_{2\_HEC}}{\sqrt{g y_{m1}}}, \text{ and } Fr_{mc} = \frac{V_{mc}}{\sqrt{g y_{m1}}} = \frac{\sqrt{\tau_c / \rho}}{g n y_{m1}^{1/3}}.$$

Data regression was performed using Li's data and using data in the 4 test cases in the present study for rectangular channel (cases 13 to 15 and 17). The resulting prediction equation for contraction scour, as shown in Figure 7.9, is

$$\frac{y_{s(Cont)}}{y_{m1}} = 2.21 \left(1.31 Fr_{m2\_HEC} - Fr_{mc} \right) \tag{7.9}$$

The prediction equation for contraction scour in equation (7.9) was based on experimental data using rectangular channels. Interestingly, the equation predicts contraction scour well when applied to compound channels, as shown in Figure 7.10. Thus it may be concluded that the shape of abutment and the channel geometry have no effect on the depth of maximum contraction scour.

Figure 7.9. Maximum contraction scour in rectangular channel: measurement versus prediction using HEC-RAS velocity
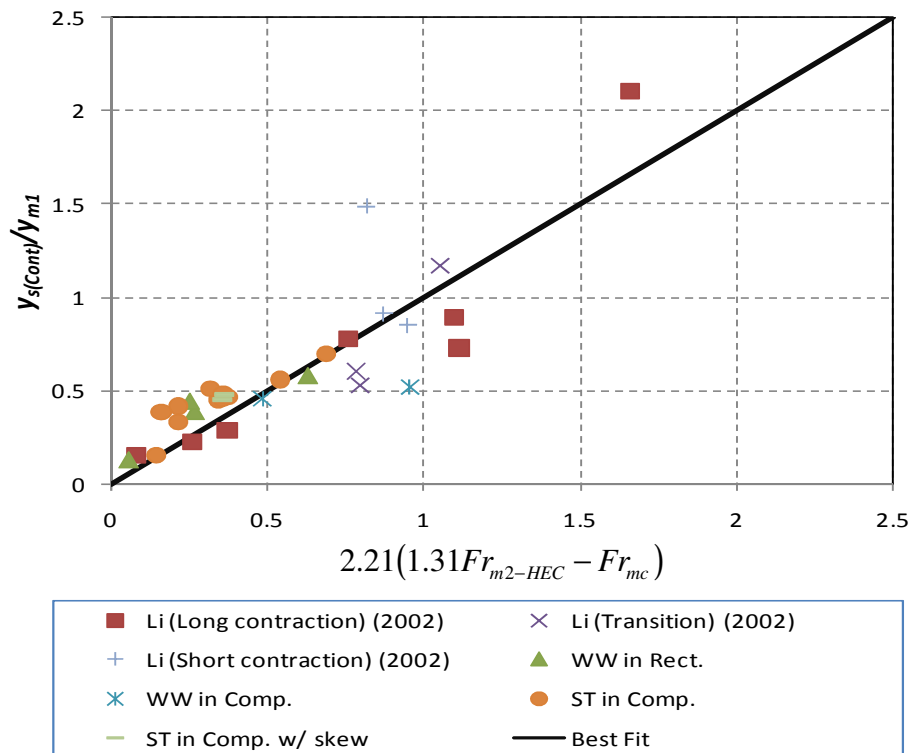
Figure 7.10. Maximum contraction scour in rectangular channel and compound channel: measurement versus prediction using HEC-RAS velocity

Li (2002) found that the uniform contraction scour depth is approximately 74 % of the maximum contraction scour depth. Thus the equation (7.9) for the maximum contraction scour depth is converted to:

$$\frac{y_{s(uni\_Cont)}}{y_{m1}} = 1.66\left(1.31 Fr_{m2\_HEC} - Fr_{mc}\right) \tag{7.10}$$

where $y_{s(uni\_Cont)}$ is the uniform contraction scour depth, y_{m1} is the main channel depth at

the approach section, $Fr_{m2\_Hec}\left(=\dfrac{V_{2\_HEC}}{\sqrt{gy_{m1}}}\right)$ is the Froude number of the main-channel at

the bridge section, $Fr_{mc}\left(=\dfrac{V_{mc}}{\sqrt{gy_{m1}}}=\dfrac{\sqrt{\tau_c/\rho}}{gny_{m1}^{1/3}}\right)$ is the critical Froude number of the main-

channel.

The amplification factor β_1 in the equations in Section 7.4 is 1.83, but decreased to 1.31 in Section 7.6. This difference comes from the use of different velocities. Note that the velocities at the bridge section in Section 7.6 are from 1D simulation results, which include the water depth changes at the bridge section. On the contrary, the water depth change is not considered in Section 7.4 because the amplification factor β_1 is obtained by assuming that the water depth change between the approach section and the bridge section is ignorable.

7.7 Conclusions

The maximum contraction scour equation is proposed on the basis of Li's flume test results (2002) and a series of new flume test for the present study using Porcelain clay as channel bed material. In addition, the uniform contraction scour equation is proposed using the relationship between the maximum contraction scour and the uniform contraction scour proposed by Li (2002). The property of soil, especially the critical shear stress, is included in the equation. The transition angle effect and the contraction length effect are negligible to the scour depth, but the flow velocity at the contracted section, which is suggested by the approach velocity and contraction ratio, is the crucial parameter to predict the contraction scour depth.

The uniform contraction scour equation is applied to flume test results conducted by Gill (1981) in order to check the validity of the equation. The tests are conducted in the rectangular flume with cohesionless soil bed. The critical shear stresses are obtained by Shields diagram and Manning's *n* value is obtained by Strikler approximation. Although the equation is developed under flume test results in cohesive soil, the satisfactory results are made from the comparison between the measurement and prediction.

New equations are developed for the HEC-RAS users. A linear relationship is built between the measurement and HEC-RAS calculated velocity at the contracted section; the proposed approach can be applied into contraction scour developed in channels with complex cross sections.

CHAPTER VIII

ABUTMENT SCOUR IN COHESIVE SOIL

8.1 Variables and experimental results of abutment scour

The variables influencing local scour around an abutment are the soil properties, the geometry of channel, the length of abutment, the shape of abutment, the approach velocity, and the alignment of the abutment. They are discussed below with the variables and test results being summarized in Table 8.1.

Soil properties. Porcelain clay was used as the channel bed material. The relation between the shear stress and erosion rate for the Porcelain clay was obtained from 11 EFA (Erosion Function Apparatus) tests (Figure 3.7). The critical shear stress was defined as the shear stress when the initiation of soil erosion occurs. In the tests, a 0.1 mm/hour erosion rate was used as the initiation of erosion and the corresponding value of shear stress was 0.8 Pa.

1. Geometry of the channel: The flume used for the tests is 45.7 m (150 ft) long, 3.05 m (10 ft) deep, and 3.66 m (12ft) wide. For compound channels, the width of the floodplain was 2.44 m and the half width of main channel was 1.22 m, as shown in Figure 8.1.

2. Shape of abutment: 3 types of abutment were tested in this study: The first one is of wing-wall shape, the second one is of spill-through with a 2(H):1(V) slope, and the third one is of spill-through with a 3(H):1(V) slope as depicted in Figure 8.2.

3. Water depth and approach velocity: 3 tests with different velocities in the same water depth and 3 tests with different water depths but a constant Froude number

were conducted to examine the effect of these two variables.

4. Alignment of abutment: 3 tests with different alignment angles with the spill-through abutment have been conducted. They are 60°, 120°, and 90°, as shown in Figure 8.3. Note that the 90° angle alignment indicates the abutment is normal to the flow direction, while for 60° and 120° the abutment is skewed towards downstream and upstream, respectively.

Rectangular Channel   Compound Channel
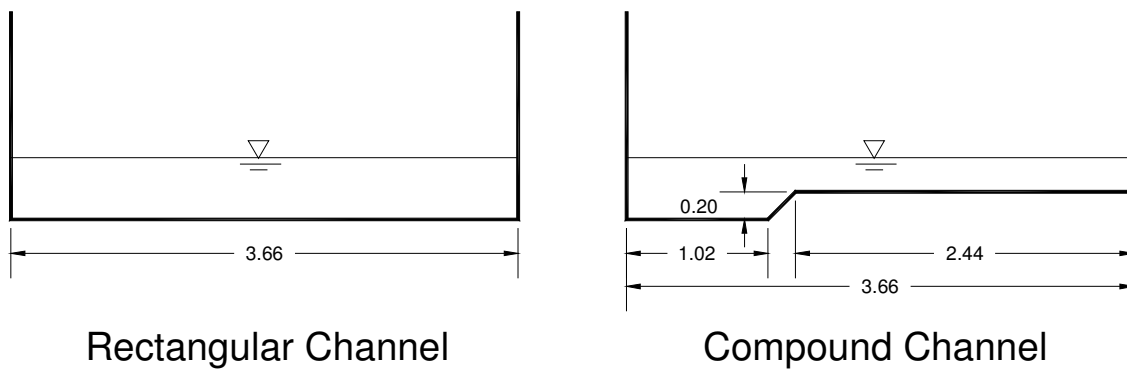
Figure 8.1. Channel configurations (all dimensions are in meters)

Wing Wall   Spill-Through   Spill-Through
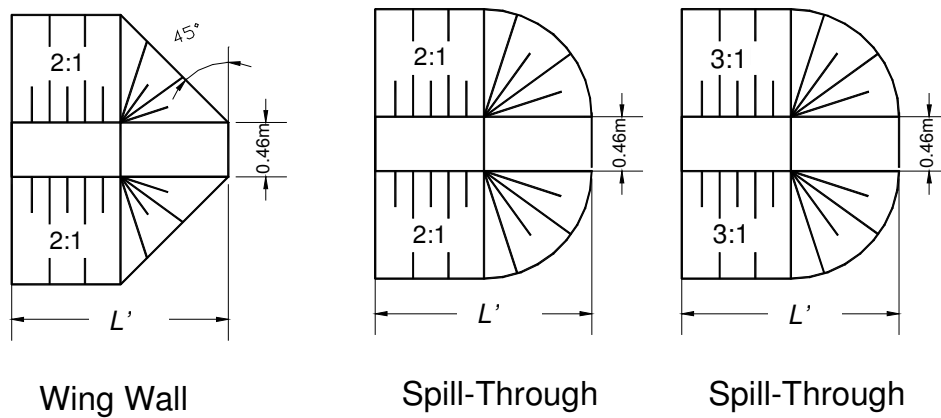
Figure 8.2. Abutment shapes
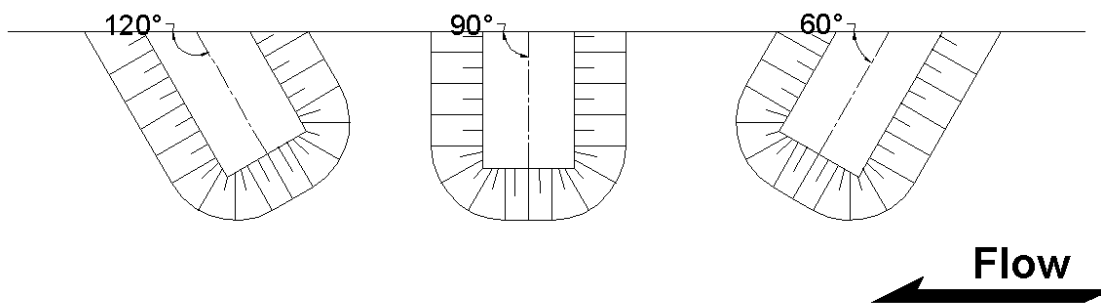
Figure 8.3. Abutment alignment

Table 8.1. Variables and test results

Test No.	Abutment Shape	Channel Type	V_{f1} (m/s)	V_1 (m/s)	y_{f1} (m)	y_{m1} (m)	L_f (m)	L' (m)	θ (°)	$0.5Q_{total}$ (m³/s)	Q_{block} (m³/s)	C_R	$y_{s(abut)}$ (mm)
Case1	ST (2:1)	Comp.	0.442	0.441	0.293	0.496	2.438	1.829	90	0.573	0.199	0.653	439
Case 1II	ST (2:1)	Comp.	0.410	0.432	0.293	0.497	2.438	1.829	90	0.562	0.185	0.671	490
Case2	ST (2:1)	Comp.	0.356	0.357	0.183	0.386	2.438	1.829	90	0.320	0.107	0.665	282
Case3	ST (2:1)	Comp.	0.475	0.481	0.400	0.603	2.438	1.829	90	0.813	0.272	0.666	589
Case4	ST (2:1)	Comp.	0.340	0.342	0.291	0.494	2.438	1.829	90	0.442	0.152	0.656	300
Case5	ST (2:1)	Comp.	0.504	0.506	0.295	0.499	2.438	1.829	90	0.662	0.228	0.655	808
Case6	ST (2:1)	Comp.	0.409	0.432	0.293	0.496	2.438	1.219	90	0.561	0.111	0.802	351
Case7	ST (2:1)	Comp.	0.417	0.437	0.291	0.494	2.438	2.438	90	0.564	0.261	0.538	1190
Case8	ST (3:1)	Comp.	0.422	0.442	0.290	0.493	2.438	1.829	90	0.570	0.171	0.700	413
Case9	WW	Comp.	0.412	0.436	0.294	0.497	2.438	1.829	90	0.568	0.222	0.610	667
Case10	ST (2:1)	Comp.	0.414	0.427	0.292	0.496	2.438	1.829	60	0.554	0.186	0.664	418
Case11	ST (2:1)	Comp.	0.417	0.436	0.292	0.495	2.438	1.829	120	0.565	0.187	0.669	436
Case12	WW	Comp.	0.327	0.333	0.293	0.497	2.438	1.829	90	0.433	0.175	0.595	155
Case12B	WW	Comp.	0.578	0.582	0.294	0.497	2.438	1.829	90	0.759	0.311	0.590	1429
Case13	WW	Rect.	0.322	0.322	0.366	0.366	3.658	1.015	90	0.431	0.120	0.723	66
Case14	WW	Rect.	0.320	0.320	0.371	0.371	3.658	1.625	90	0.433	0.193	0.556	304
Case15	WW	Rect.	0.302	0.302	0.384	0.384	3.658	2.234	90	0.424	0.259	0.389	334
Case16	WW	Rect.	0.208	0.208	0.373	0.373	3.658	2.743	90	0.284	0.213	0.250	448
Case17	WW	Rect.	0.364	0.364	0.364	0.364	3.658	1.320	90	0.484	0.175	0.639	262

In Table 8.1, ST is the spill-through abutment, WW is the wing-wall abutment, Comp. is the compound channel, Rect. is the rectangular channel, V_1 is the average velocity at the approach section, y_{m1} is the water depth of main-channel at the approach section, y_{f1} is the water depth of floodplain at the approach section, L_f is the width of floodplain, L' is the projected length of abutment normal to the flow, θ is the alignment angle of abutment ($\theta = 90°$ for normal to flow, $\theta > 90°$ for skewed upstream, $\theta < 90°$ for skewed

to downstream), Q_{Total} is the total discharge, Q_{block} is the discharge blocked by approach

embankment, C_R is contraction ratio $C_R = (Q - Q_{block})/Q$, $y_{s(Abut)}$ is the maximum

abutment scour depth, and $y_{s(Abut)}$ is the maximum abutment scour depth.

8.2 Dimensional analysis

In addition to the variables mentioned above, there are several more variables

affecting abutment scour. The influential variables are listed as following

$$y_{s(Abut)} = f(y_{m1}, y_{f1}, L_m, L_f, L', \beta_m, \beta_a, \theta, g, V_{f2}, \rho_s, \rho, \mu, V_{fc}) \qquad (8.1)$$

Dimensional analysis yields the following dimensionless parameters:

$$\frac{y_{s(Abut)}}{y_{f1}} = f\left(\frac{y_{f1}}{y_{m1}}, \frac{L_m}{y_{m1}}, \frac{L_f}{L_m}, \frac{L'}{L_f}, \frac{\rho_s}{\rho} \beta_m, \beta_a, \theta, Fr_{f2}, Fr_{fc}, \mathrm{Re}\right) \qquad (8.2)$$

where L_m is the half-width of main channel, L_f is the width of floodplain, L' is the length

of abutment, β_m is the slope of the main channel bank, β_a is the abutment slope, θ is the

alignment angle of abutment, g is the gravitational acceleration, V_{f2} is the velocity

around the toe of the abutment, ρ_s is the soil density, ρ is the water density, μ is the

viscosity of water, and V_{fc} is the critical velocity in the floodplain, y_{f1} is the water depth

of floodplain at the approach section, $y_{s(Abut)}$ is the maximum abutment scour depth,

$Fr_{f2} = \dfrac{V_{f2}}{\sqrt{gy_{f1}}}$, $\mathrm{Re} = \dfrac{\rho y_f V_1}{\mu}$, and $Fr_{fc} = \dfrac{V_{fc}}{\sqrt{gy_{f1}}} = \dfrac{\sqrt{\tau_c/\rho}}{gny_{f1}^{1/3}}$ Note that the value of ρ_s/ρ is

fixed due to the fixed soil type and Re is large enough to neglect the viscous effect.

The contraction ratio C_R is a good parameter to calculate the velocity at the

contracted section and it was verified in Chapter VII. However it cannot be used for the

all conditions. For example, if the toe of abutment locates far away from the end of main

channel, the flow on the floodplain is not mixed with main-channel flow. In order to consider all flow conditions, the approach used in Maryland SHA Bridge Scour Program (ABSCOUR) (2003) is adopted to calculate the local velocity around the abutment. Figure 8.4 shows the definition of degree of setback used in ABSCOUR method, and the method for converting the flow discharge to the local velocity is as follows.
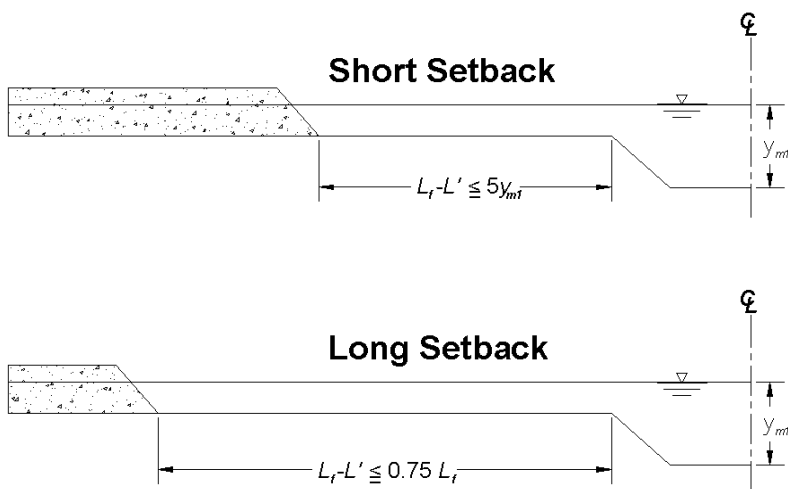
Figure 8.4. Definition of degree of setback

$$
V_{f2} = \begin{cases}
\dfrac{Q_{total}}{A_2}, \text{ for short setback } \left((L_f - L') \leq 5y_{m1}\right) \\[2ex]
\dfrac{Q_{fp1}}{A_{f2}}, \text{ for long setback } \left(L' \leq 0.25L_f\right) \\[2ex]
\text{otherwise use a linearly interpolated velocity between} \\[1ex]
\dfrac{Q_{total}}{A_2} \text{ for } (L_f - L') = 5y_{m1} \text{ and } \dfrac{Q_{fp1}}{A_{f2}} \text{ for } L' = 0.25L_f
\end{cases}
\tag{8.3}
$$

where Q_{total} is the total discharge, Q_{fp1} is the discharge on the floodplain at the approach section immediately upstream of the abutment, A_2 is total flow area at the contracted section, A_{f2} is the flow area on the floodplain at the contracted section, and $L_f - L'$ is

the width of floodplain at the contracted section. As a result, the relation is reduced to

$$\frac{y_{s(Abut)}}{y_{f1}} = f\left(\frac{L_f - L'}{y_{f1}}, \beta_a, \theta, Fr_{f2}, Fr_{fc}\right)$$

(8.4)

where L_f is the width of floodplain, L' is the length of abutment, β_a is the abutment slope,

θ is the alignment angle of abutment, $Fr_{f2} = \dfrac{V_{f2}}{\sqrt{gy_{f1}}}$, $Fr_{fc} = \dfrac{V_{fc}}{\sqrt{gy_{f1}}} = \dfrac{\sqrt{\tau_c/\rho}}{gny_{f1}^{1/3}}$, V_{f2} is the

velocity around the toe of the abutment using equation (8.3), g is the gravitational acceleration, ρ_s is the soil density, ρ is the water density, μ is the viscosity of water, and V_{fc} is the critical velocity in the floodplain.

8.2.1 Prediction equation

The flow around an abutment may be very similar to that around a wide pier, as shown in Figure 8.5. The abutment may be regarded as one half of the wide pier.

(a) Around wide pier
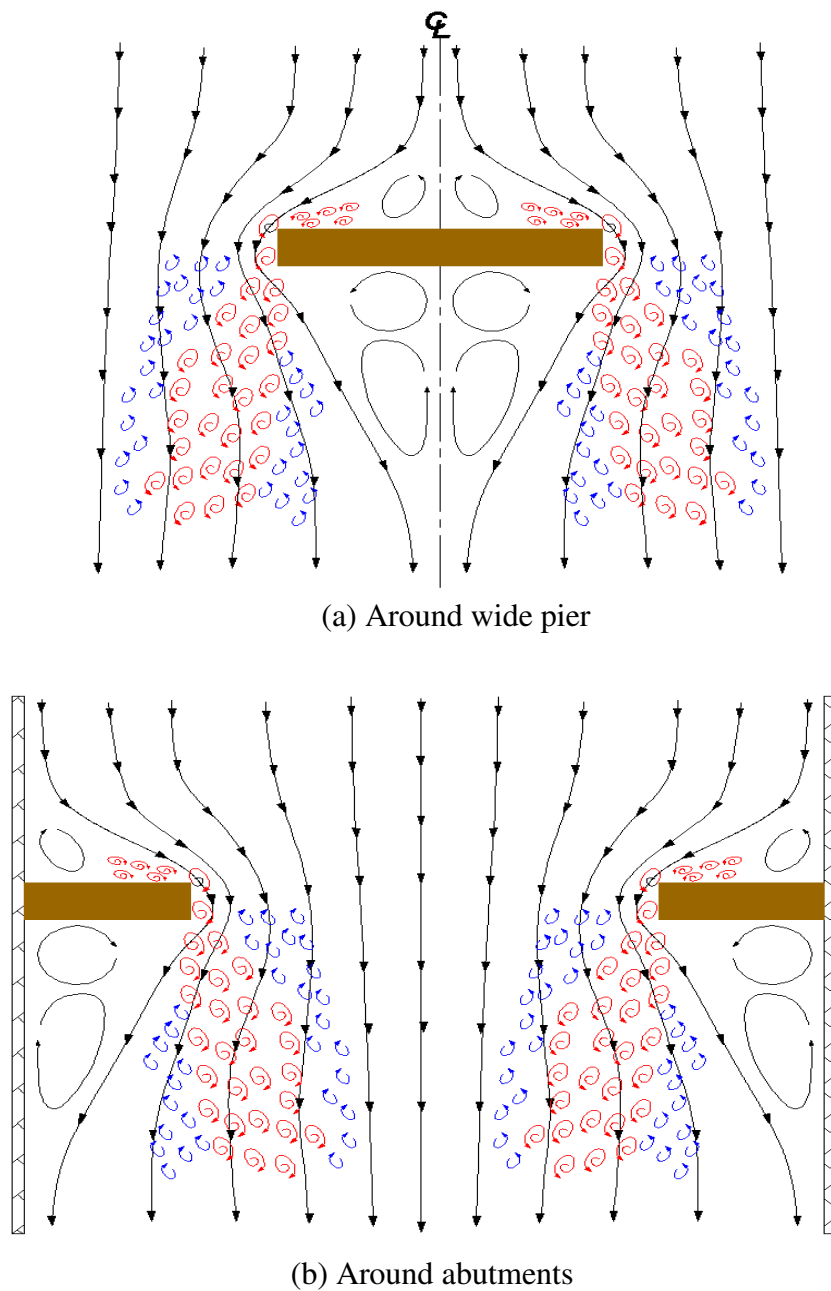
(b) Around abutments

Figure 8.5. Flow around bridge structure

If the abutment is assumed as one half of the wide pier, the dimensionless form of

the abutment scour depth may be expressed as:

$$\frac{y_{s(Abut)}}{y_{f1}} = \alpha \left(\beta Fr_{f2} - Fr_{fc} \right)^{0.7} \tag{8.5}$$

where the constant β is the amplification factor describing the higher flow around abutments, and the constant α and β are obtained by curve fitting using the flume test data, $y_{s(Abut)}$ is the maximum abutment scour depth, y_{f1} is the water depth at the toe of the abutment estimated as the water depth immediately upstream of the toe of the abutment,

$$Fr_{f2} = \frac{V_{f2}}{\sqrt{gy_{f1}}} \text{, and } Fr_{fc} = \frac{V_{fc}}{\sqrt{gy_{f1}}} = \frac{\sqrt{\tau_c / \rho}}{gny_{f1}^{1/3}}$$

The constant α and β were obtained by curve fitting using the data for wing-wall abutment as shown in Figure 8.6. Accordingly, the proposed equation for wing-wall abutment becomes

$$\frac{y_{s(Abut)}}{y_{f1}} = 6.67 \cdot \left(1.57 \cdot Fr_{f2} - Fr_{fc} \right)^{0.7} \tag{8.6}$$
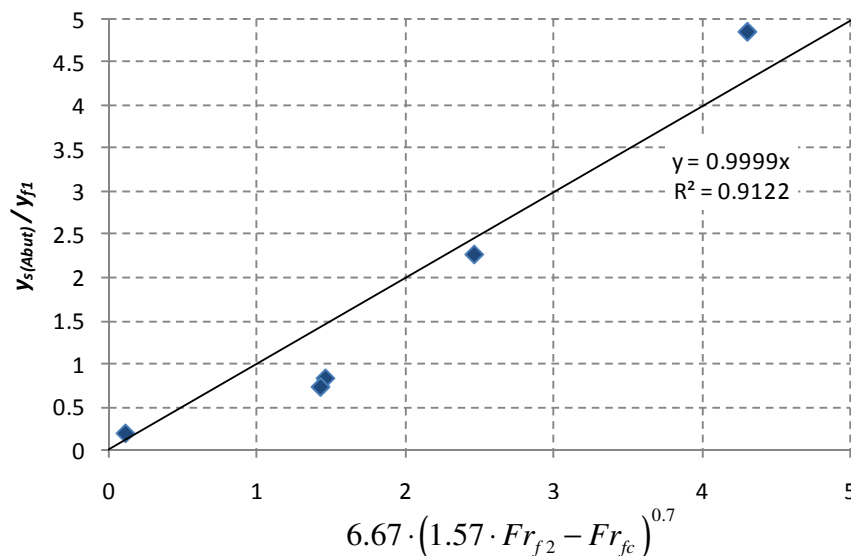
Figure 8.6. Normalized maximum abutment scour depth based on equation (8.6)

8.2.2 Correction factor for abutment scour

8.2.2.1 Abutment shape effect (K_1)

Three types of abutments were used in the compound channel. They are wing-wall abutment with a 2:1 slope at the upstream and downstream, spill-through abutment with a 2:1 slope, and spill-through abutment with a 3:1 slope. Equation (8.6) which is based on the wing-wall abutment was applied to the spill-through abutment to find the shape correction factor. The correction factor for abutment shape was calculated based on the slope shown in Figure 8.7 with values as follows:

$$K_1 = \begin{cases} 1.0 & \text{for Wing-wall abutment} \\ 0.78 & \text{for Spill-through abutment with 2:1 Slope} \\ 0.68 & \text{for Spill-through abutment with 3:1 Slope} \end{cases} \quad (8.7)$$
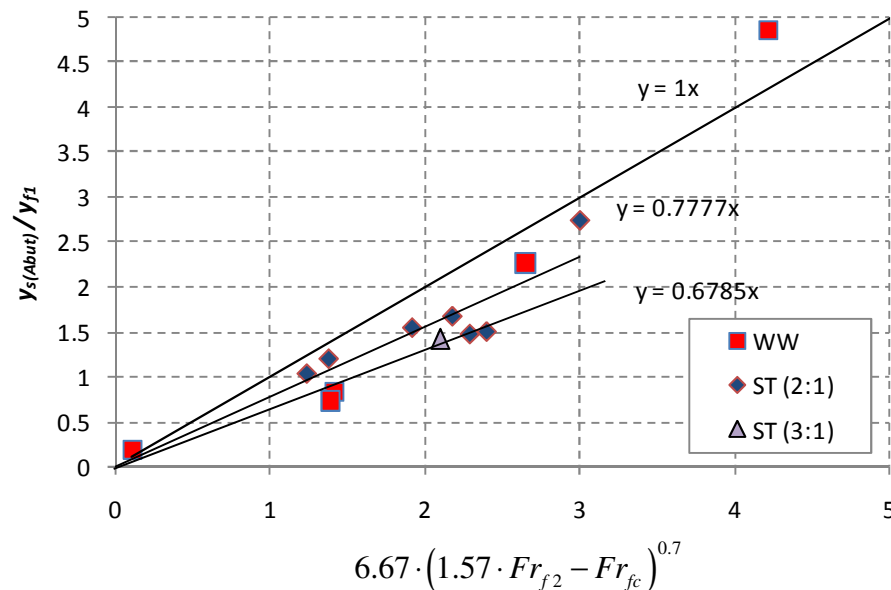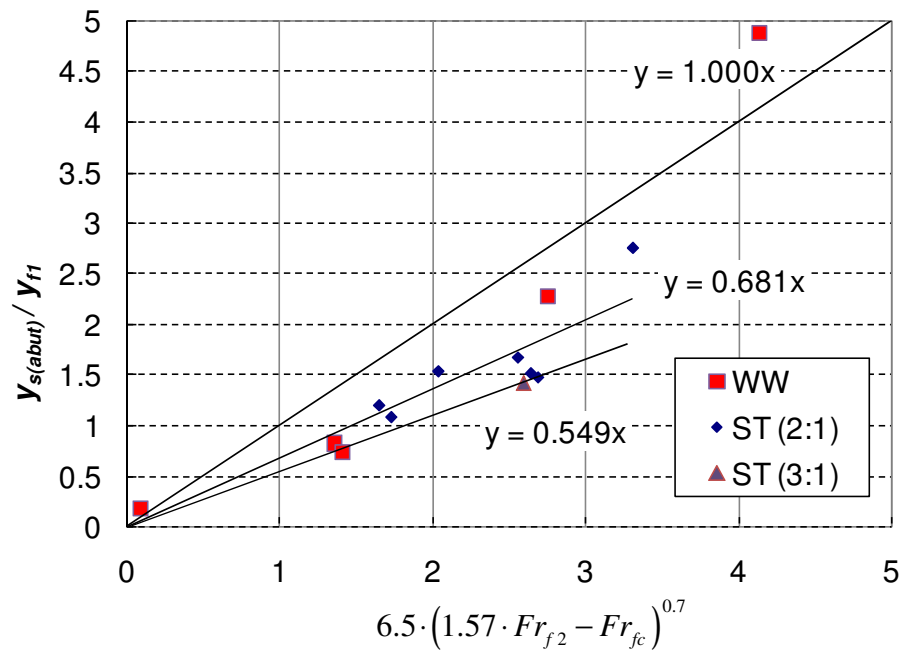

Figure 8.7. Normalized maximum abutment scour depth with different abutment shape

8.2.2.2 Abutment alignment effect (K_2) and abutment location effect (K_L)

Two tests were conducted to examine the effect of abutment alignment using the spill through abutment with a 2:1 slope. One has a 30° skewed angle ($\theta = 120^o$) toward the upstream flow while the other has a 30° skewed angle ($\theta = 60^o$) toward the downstream flow. The maximum abutment scour depth for skewed abutment was compared with the prediction equation with the effect of abutment shape accounted. The comparison is shown in Figure 8.8. The maximum abutment scour depths for 30° skewed abutment toward both the upstream and the downstream flow are 15 % less than the predicted abutment scour depths. As expected the correction factor for $\theta = 60^o$ is less than 1.0. However the value for $\theta = 120^o$ is also less than 1.0 which is in contrary to previous research results. Since the abutment used in this study is a spill-through abutment, the abutment induced a relatively smooth flow during the transition even though the abutment is aligned toward upstream. This may be the reason for the lower correction factor. The turbulence level around the abutment is compared and shown in Figure 8.9.

In real channels, the skewed angle of bridge embankment may be between $60° \leq \theta \leq 120°$. If a linear relationship is assumed in the range, the correction factor for abutment alignment can be expressed as follows:

$$K_2 = \begin{cases} 1.0 - 0.005|\theta - 90°| & \textit{for } 60° \leq \theta \leq 120° \\ 0.85 & \textit{otherwise} \end{cases} \tag{8.8}$$

The maximum scour depth increased suddenly when the toe of abutment was at the end of floodplain (i.e., $L'/L_f = 1.0$), as shown in Figure 8.8. If a linear increase of the abutment scour depth with the decrease of distance between the toe of abutment and the end of floodplain is assumed, the correction factor for abutment location can be expressed as follows:

$$K_L = \begin{cases} -0.37\dfrac{L_f - L'}{y_{f1}} + 1.55 & \text{for } \dfrac{L_f - L'}{y_{f1}} < 1.5 \\ 1.0 & \text{otherwise} \end{cases} \qquad (8.9)$$
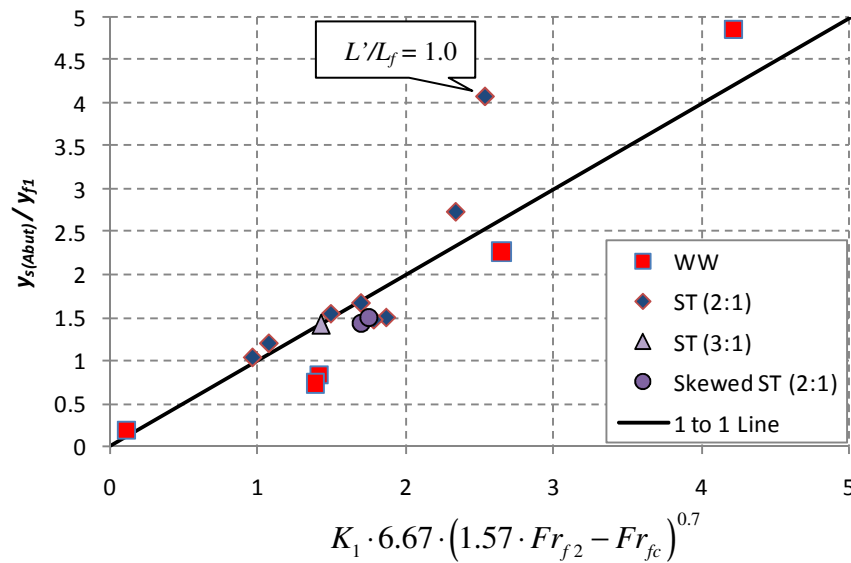
Figure 8.8. Normalized maximum abutment scour depth versus prediction with abutment shape being accounted for

(a) $\theta = 60°$ (b) $\theta = 90°$ (c) $\theta = 120°$
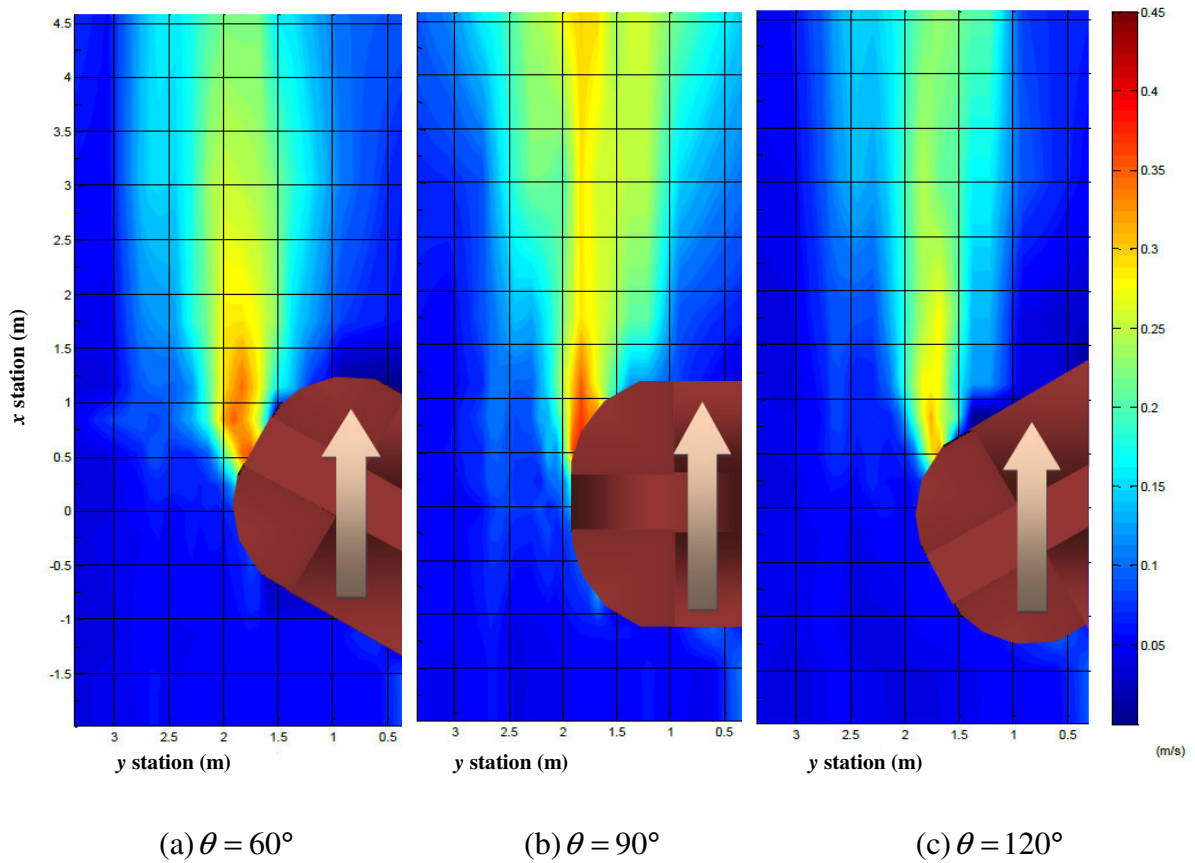
Figure 8.9. Variation of turbulence intensity with different attack angles at the initial test condition

8.2.2.3 Maximum abutment scour depth in compound channel

The prediction equation for the maximum abutment scour depth has thus been developed. There are three correction factors to account for the shape of abutment, the attack angle of the flow, and the abutment location. The final abutment scour prediction equation is

$$\frac{y_{s(Abut)}}{y_{f1}} = K_1 \cdot K_2 \cdot K_L \cdot 6.67 \cdot \left(1.57 \cdot Fr_{f2} - Fr_{fc}\right)^{0.7} \tag{8.10}$$

In equation (8.10), $y_{s(Abut)}$ is the maximum abutment scour depth, y_{f1} is the water depth at

the toe of the abutment estimated as the water depth immediately upstream of the toe of

the abutment, $Fr_{f2} = \dfrac{V_{f2}}{\sqrt{gy_{f1}}}$, $Fr_{fc} = \dfrac{V_{fc}}{\sqrt{gy_{f1}}} = \dfrac{\sqrt{\tau_c/\rho}}{gny_{f1}^{1/3}}$, K_1 is the correction factor for the

abutment shape, K_2 is the correction factor for the abutment skew angle, K_L is the

correction factor for the abutment location. Their values and formulas are as follows:

$$K_1 = \begin{cases} 1.0 & \text{for Wing-wall abutment} \\ 0.78 & \text{for Spill-through abutment with 2:1 Slope} \\ 0.68 & \text{for Spill-through abutment with 3:1 Slope} \end{cases}$$

$$K_2 = \begin{cases} 1.0 - 0.005|\theta - 90°| & \text{for } 60° \leq \theta \leq 120° \\ 0.85 & \text{otherwise} \end{cases}$$

$$K_L = \begin{cases} -0.37\dfrac{L_f - L'}{y_{f1}} + 1.55 & \text{for } \dfrac{L_f - L'}{y_{f1}} < 1.5 \\ 1.0 & \text{otherwise} \end{cases}$$

Figure 8.10 shows prediction using the prediction equation versus the measurements for the flume test cases.
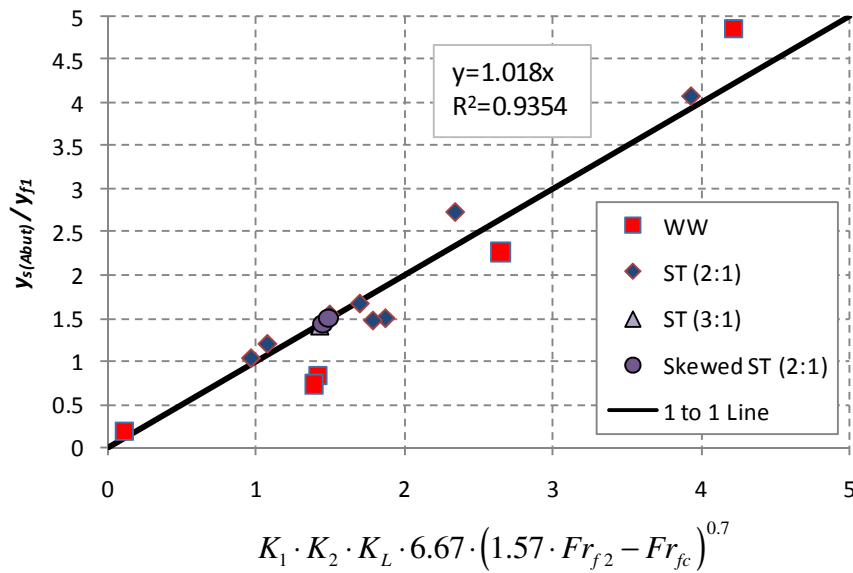
Figure 8.10. Normalized maximum abutment scour depth: test results versus prediction

8.3 Methodology using HEC-RAS results

The water level around bridge section decreases, and increases with scour development and then finally will become the same water level with approach section, as shown in Figure 8.11. Note that although the duration for all the flume tests lasted more than 240 hours (10 days), the scour depth was still increasing at the end of each flume test. The water depth as an important parameter for dimensional analysis for flume test results is selected where no influence of water depth change occurred. The flume tests were conducted in the ideal conditions in which the channel bottom is flat, and the channel width is constant through entire channel; on the contrary, the slope and shape of real channel are irregular, as shown in Figure 8.12. Since the water depth of channel is not constant in reality, the predicted scour depth by equation (8.10) varies with the water depths selected from different locations.
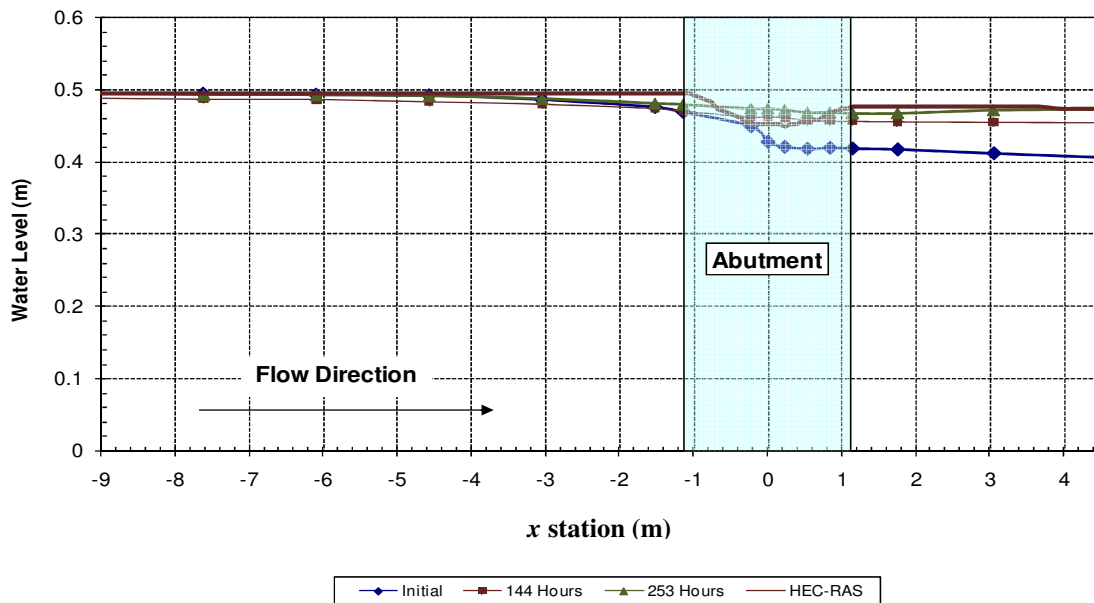
Figure 8.11. Water depth change and HEC-RAS
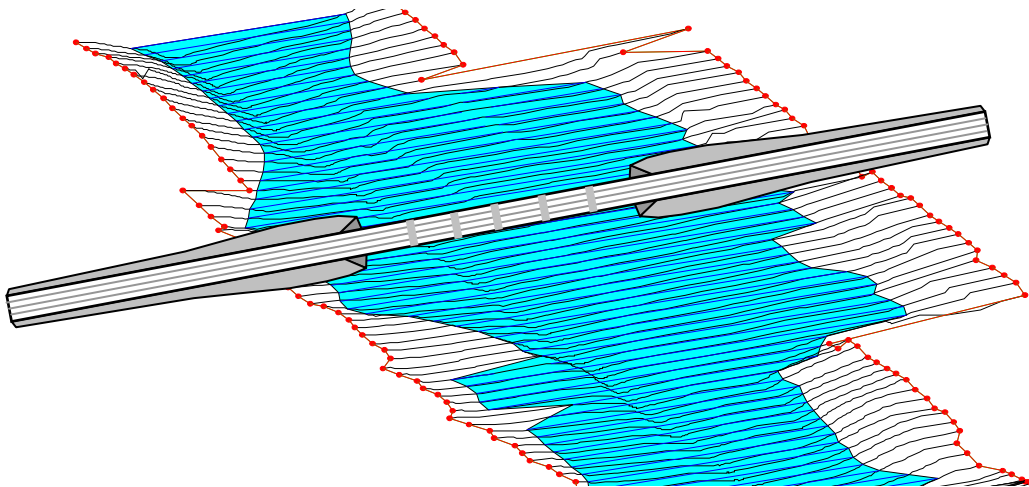
Figure 8.12. Typical channel and bridge (cited from Briaud et al. (2003))

HEC-RAS results may be very helpful to find the water depth. In Figure 8.11, the water depth from HEC-RAS result at approach section is almost constant before the bridge section (x = -1.41 m). Since there is no particle feed from upstream in the clear water scour condition, the water depth just before the bridge section is most reasonable

parameter to evaluate the scour depth. The variables and HEC-RAS results are summarized in Table 8.2.

Using the HEC-RAS results, another dimensional analysis is conducted with same procedure which is performed in Section 8.2. The prediction equation for the wing-wall abutment is obtained by data fitting using HEC-RAS results and scour depths acquired from flume test result, as shown in Figure 8.13. Accordingly, the proposed equation for wing-wall abutment becomes

$$\frac{y_{s(Abut)}}{y_{f1}} = 6.5 \cdot \left(1.57 \cdot Fr_{f2} - Fr_{fc}\right)^{0.7} \tag{8.11}$$

Table 8.2. Variables and HEC-RAS results

Test No.	Abutment Shape	Channel Type	V_1 (m/s)	y_{f1} (m)	y_{m1} (m)	L (m)	L_f (m)	L' (m)	θ (°)	V_2 (m/s)	Fr_{f2}	Fr_{fc}	$y_{s(Abut)}$ (mm)
Case1	ST (2:1)	Comp.	0.464	0.291	0.494	3.658	2.438	1.829	90	0.722	0.428	0.396	439
Case 1ll	ST (2:1)	Comp.	0.456	0.294	0.497	3.658	2.438	1.829	90	0.711	0.419	0.394	490
Case2	ST (2:1)	Comp.	0.377	0.184	0.387	3.658	2.438	1.829	90	0.557	0.415	0.461	282
Case3	ST (2:1)	Comp.	0.496	0.400	0.604	3.658	2.438	1.829	90	0.806	0.407	0.356	589
Case4	ST (2:1)	Comp.	0.358	0.278	0.482	3.658	2.438	1.829	90	0.582	0.352	0.401	300
Case5	ST (2:1)	Comp.	0.546	0.294	0.497	3.658	2.438	1.829	90	0.837	0.493	0.394	808
Case6	ST (2:1)	Comp.	0.432	0.294	0.497	3.658	2.438	1.219	90	0.579	0.341	0.394	351
Case7	ST (2:1)	Comp.	0.472	0.291	0.494	3.658	2.438	2.438	90	0.930	0.551	0.396	1190
Case8	ST (3:1)	Comp.	0.456	0.291	0.494	3.658	2.438	1.829	90	0.715	0.423	0.396	413
Case9	WW	Comp.	0.453	0.294	0.497	3.658	2.438	1.829	90	0.743	0.438	0.394	667
Case10	ST (2:1)	Comp.	0.458	0.291	0.494	3.658	2.438	1.829	60	0.706	0.418	0.396	418
Case11	ST (2:1)	Comp.	0.457	0.291	0.494	3.658	2.438	1.829	120	0.720	0.426	0.396	436
Case12B	WW	Comp.	0.635	0.294	0.497	3.658	2.438	1.829	90	0.993	0.585	0.394	1429
Case13	WW	Rect.	0.328	0.366	0.366	3.658	3.658	1.015	90	0.445	0.235	0.367	66
Case14	WW	Rect.	0.326	0.372	0.372	3.658	3.658	1.625	90	0.573	0.300	0.364	304
Case15	WW	Rect.	0.310	0.384	0.384	3.658	3.658	2.234	90	0.761	0.392	0.361	334
Case16	WW	Rect.	0.233	0.347	0.347	3.658	3.658	2.743	90	0.896	0.485	0.373	448
Case17	WW	Rect.	0.364	0.360	0.360	3.658	3.658	1.320	90	0.576	0.307	0.369	262
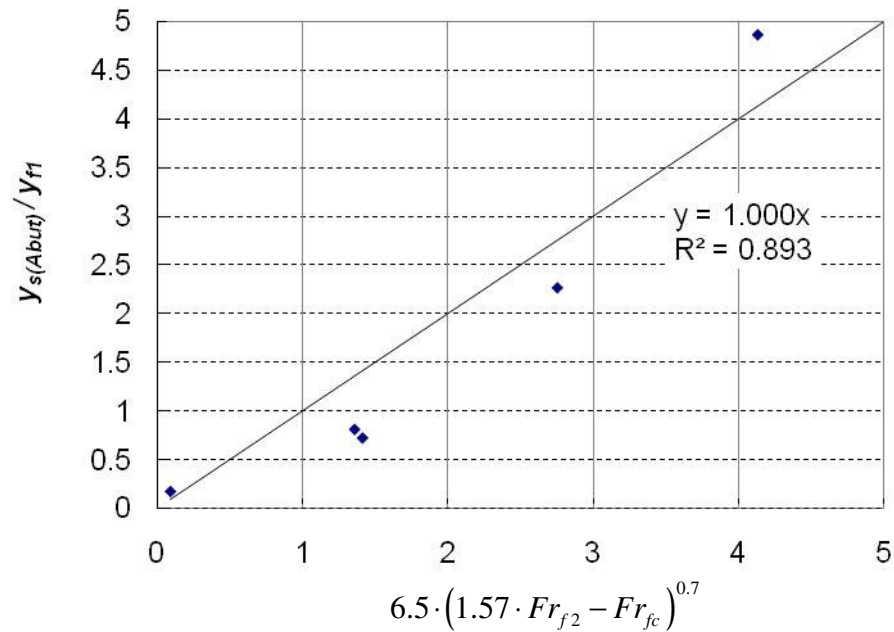
Figure 8.13. Normalized maximum abutment scour depth based on equation

Three types of abutments – wing-wall abutment, spill-through abutment with 2:1 slope, and spill-through abutment with 3:1 slope - were used in the compound channel. The equation (8.11) which was based on the wing-wall abutment was applied to the spill-through abutments to find the abutment shape correction factor. The correction factor for abutment shape was calculated based on the slope shown in Figure 8.14.

$$K_1 = \begin{cases} 1.0 & \text{for Wing-wall abutment} \\ 0.68 & \text{for Spill-through abutment with 2:1 Slope} \\ 0.55 & \text{for Spill-through abutment with 3:1 Slope} \end{cases} \tag{8.12}$$

Figure 8.14. Normalized maximum abutment scour depth with different abutment shape.

Two tests were conducted to examine the effect of abutment alignment using the spill through abutment with a 2:1 slope. One has a 30° skewed angle ($\theta = 120^{\circ}$) toward the upstream flow while the other has a 30° skewed angle ($\theta = 60^{\circ}$) toward the downstream flow. The maximum abutment scour depth for skewed abutment was compared with the prediction equation with the effect of abutment shape accounted. The comparison is shown in Figure 8.15, and the correction faction is obtained as:

$$K_2 = \begin{cases} 1.0 - 0.005|\theta - 90^{\circ}| & for\ 60^{\circ} \leq \theta \leq 120^{\circ} \\ 0.85 & otherwise \end{cases} \tag{8.13}$$

The maximum scour depth increased suddenly when the toe of abutment was at the end of floodplain (i.e., $L'/L_f = 1.0$), as shown in Figure 8.15. If a linear increase of the abutment scour depth with the decrease of distance between the toe of abutment and

the end of floodplain is assumed, the correction factor for abutment location can be expressed as follows:

$$K_L = \begin{cases} -0.37\dfrac{L_f - L'}{y_{f1}} + 1.55 & \text{for } \dfrac{L_f - L'}{y_{f1}} < 1.5 \\ 1.0 & \text{otherwise} \end{cases} \tag{8.14}$$

The prediction equation for the maximum abutment scour depth has been developed. There are three correction factors to account for the shape of abutment, the attack angle of the flow, and the abutment location. The final abutment scour prediction equation is

$$\frac{y_{s(Abut)}}{y_{f1}} = K_1 \cdot K_2 \cdot K_L \cdot 6.5 \cdot \left(1.57 \cdot Fr_{f2} - Fr_{fc}\right)^{0.7} \tag{8.15}$$

In equation (8.15), $y_{s(Abut)}$ is the maximum abutment scour depth, y_{f1} is the water depth at the toe of the abutment estimated as the water depth immediately upstream of the toe of

the abutment, $Fr_{f2} = \dfrac{V_{f2}}{\sqrt{gy_{f1}}}$, $Fr_{fc} = \dfrac{V_{fc}}{\sqrt{gy_{f1}}} = \dfrac{\sqrt{\tau_c/\rho}}{gny_{f1}^{1/3}}$, K_1 is the correction factor for the

abutment shape, K_2 is the correction factor for the abutment skew angle, K_L is the correction factor for the abutment location. Their values and formulas are as follows:

$$K_1 = \begin{cases} 1.22 & \text{for Vertical-wall abutment} \\ 1.0 & \text{for Wing-wall abutment} \\ 0.68 & \text{for Spill-through abutment with 2:1 Slope} \\ 0.55 & \text{for Spill-through abutment with 3:1 Slope} \end{cases}$$

$$K_2 = \begin{cases} 0.85 & \text{for } \theta = 60° \\ 1.0 & \text{for } \theta = 90° \\ 0.85 & \text{for } \theta = 120° \end{cases}$$

$$K_L = \begin{cases} -0.37 \dfrac{L_f - L'}{y_{f1}} + 1.55 & \text{for } \dfrac{L_f - L'}{y_{f1}} < 1.5 \\ 1.0 & \text{otherwise} \end{cases}$$

Figure 8.16 shows prediction using the prediction equation versus the measurements for the flume test cases.

$$K_1 \cdot K_2 \cdot 6.5 \cdot \left(1.57 \cdot Fr_{f2} - Fr_{fc}\right)^{0.7}$$
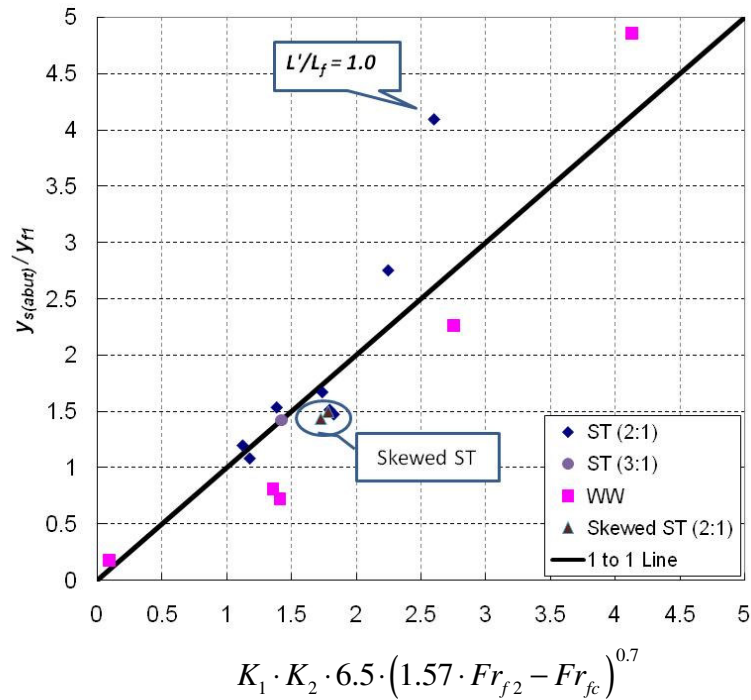
Figure 8.15. Normalized maximum abutment scour depth versus prediction with abutment shape being accounted for
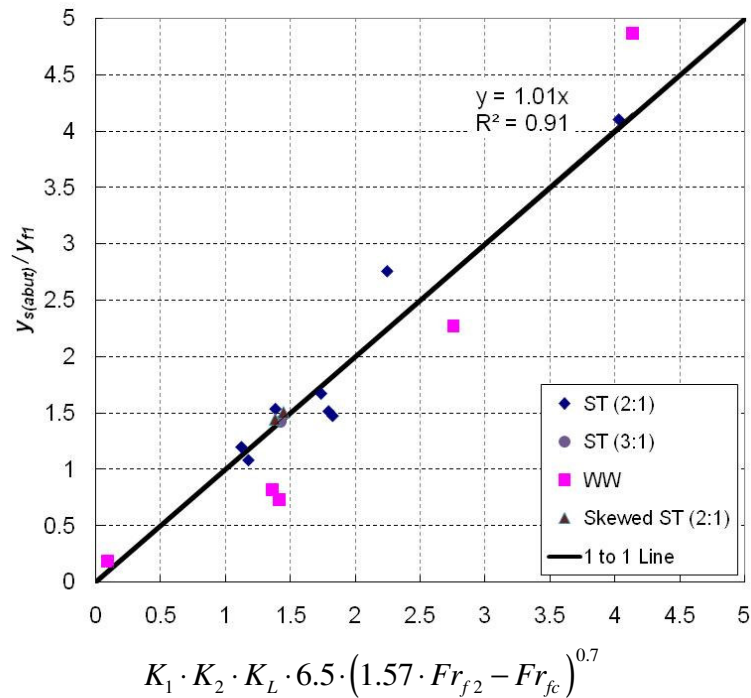
Figure 8.16. Normalized maximum abutment scour depth: test results versus prediction

8.4   Verification of maximum abutment scour equation

8.4.1   Comparison with laboratory test results

The abutment scour prediction equation developed in the present study has also

been applied to non-cohesive soil. Data from Sturm (2004) taken in compound channels

and data from Froehlich (1989) (which was cited in Palaviccini's Ph.D. dissertation in

1993) taken in rectangular channels were used for the comparisons. Comparisons with

the study of NCHRP 24-20 (2008) was also performed for the scour condition B (the

long set back condition in NCHRP 24-20).

In Sturm (2004) and Froehlich (1989), vertical wall abutments were used as the

reference in the development of the correction factor for abutment shape. However,

vertical wall abutments were not used in the present study. The correction factor for

abutment shape for vertical wall abutment was obtained using the ratio between the correction factor for abutment shapes in Froehlich's equation and that in the present study. The correction factor in Froehlich's study is 1.0, 0.82, and 0.55 for vertical wall, wing wall and spill-through abutments, respectively. While the correction factor for abutment shape in the present study is 1.0 and 0.68 for wing-wall and spill-through abutment, respectively. Thus the value of 1.22 ($1.0{:}0.82 = K_1{:}1.0$) is used for vertical-wall abutments in Sturm (2004) and Froehlich (1989) so it is consistent with the present study.

8.4.1.1 Data in Sturm (2004)

Sturm (2004) used three types of abutments: vertical-wall, spill-through, and wing-wall. The length of abutments was varied and 3 different types of sands were used in a compound channel. The experiments were conducted in a 4.2 m wide and 24.4 m long flume. The ratio of the abutment length to the floodplain width (L'/L_f) was varied from 0.22 to 1.0. The median sizes of the 3 types of sand are 3.3 mm, 2.7 mm, and 1.1 mm.

Figure 8.17 shows the comparison between Sturm's data and predictions using the prediction equation in the present study. Based on the figure, equation (8.15) mostly under predicts the scour depth. Note that in

Figure 8.17 "VW" represents vertical wall abutments, "ST" represents spill-through abutments, "WW" represents wing-wall abutments, "Long" indicates long setback $\left(L_f - L' > 5 y_m \right)$, "Short" indicates short setback $\left(L' \le 0.25 L_f \right)$, and "Inter" indicates intermediate setback.
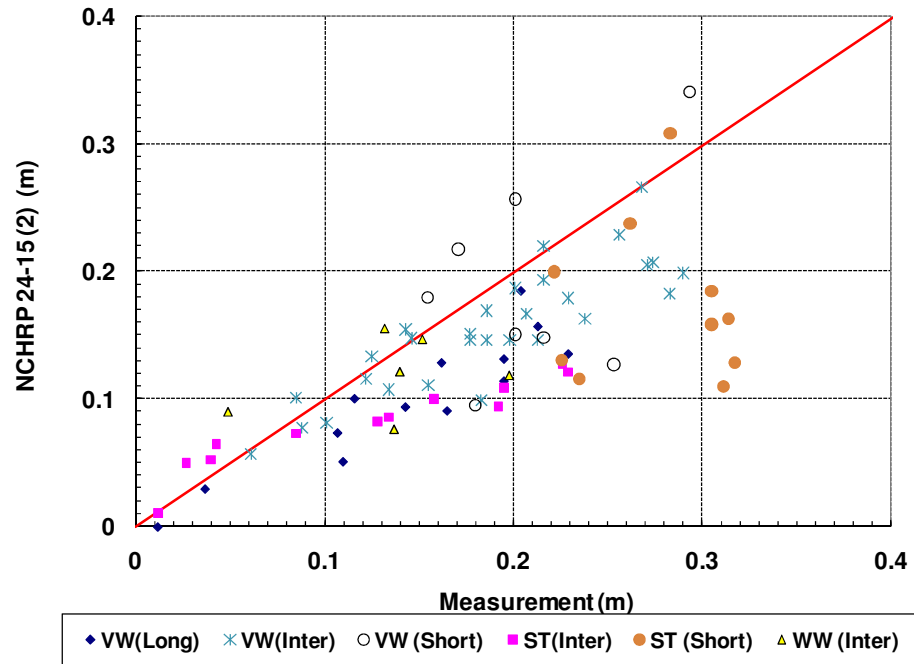
Figure 8.17. Comparison with Sturm's (2004) data

8.4.1.2 Froehlich's database (1989)

Froehlich analyzed 170 live-bed scour and 230 clear-water scour measurements taken by other researchers in rectangular channels in different laboratory flumes. Many types of abutments, such as vertical board, vertical wall, semicircular, triangular, wing-wall, and spill-through abutments were covered in the analysis. A total of 195 clear-water scour measurements (101 for vertical-wall, 45 for spill-through, and 45 for wing-wall) were selected from Froehlich's 230 clear-water scour cases for comparison. Figure 8.18 shows the comparison between Froehlich's database and the predictions based on the present study. Equation (8.15) mostly over predicts Froehlich's (1989) database.
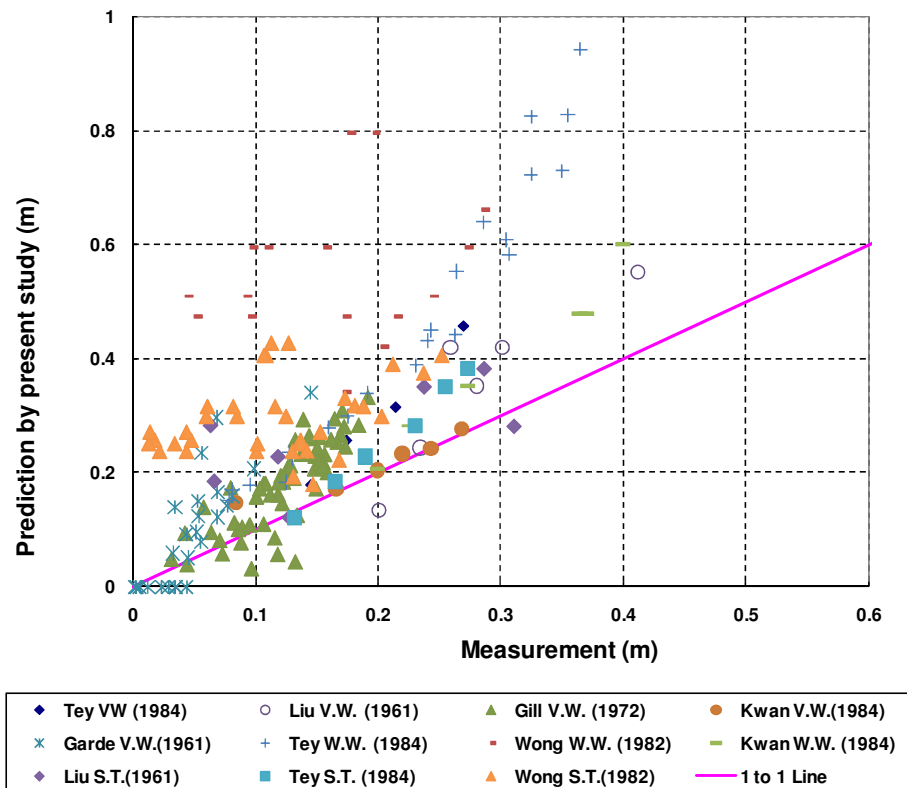
Figure 8.18. Comparison with Froehlich's (1989) data

8.4.1.3 Comparison with Ettema et al. (2008)

Using the maximum contraction scour equation (equation (7.9)) and the abutment scour equation (equation (8.15)) in the present study, the predicted scour depth to flow depth ratio is compared with that in Ettema et al. (2008). The simple rectangular channel condition (Condition B) was assumed and 3 velocity ratios (V_1/V_c = 1.0, 0.95, 0.75) were used in the comparison. Figure 8.19 shows the comparison. The scour depth ratio, in Ettema et al. (2008), increases rapidly for a small unit discharge ratio q_2/q_1 ($q_2/q_1 \leq 1.2$ for wing-wall abutments and $q_2/q_1 \leq 1.5$ for spill-through abutments) and then it decreases gradually. The predicted trend for the spill-through abutment agrees

well with that in their study for a small unit discharge ratio of $q_2/q_1 < 2.0$. The comparison then deviates with the increase of the unit discharge ratio. The predicted trend curve for the wing-wall abutment is about 20% greater at the peak and then diverges more from the result in Etteam et al. (2008). Note that in Figure 8.19 y_{max} is the abutment scour flow depth ($y_{max} = y_{s(Abut)} + y_{f1}$), y_c is the contraction scour flow depth ($y_c = y_{s(Cont)} + y_{f1}$), q_1 is the unit discharge at the approach section, and q_2 is the unit discharge at the bridge section.
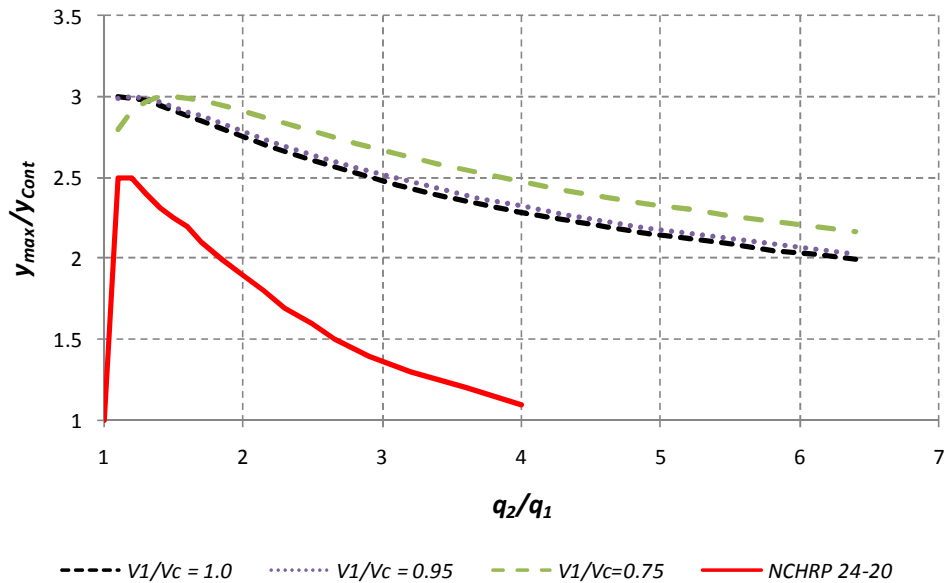
(a) Wing-Wall shape abutment

Figure 8.19. Comparison with Ettema et al. (2008)
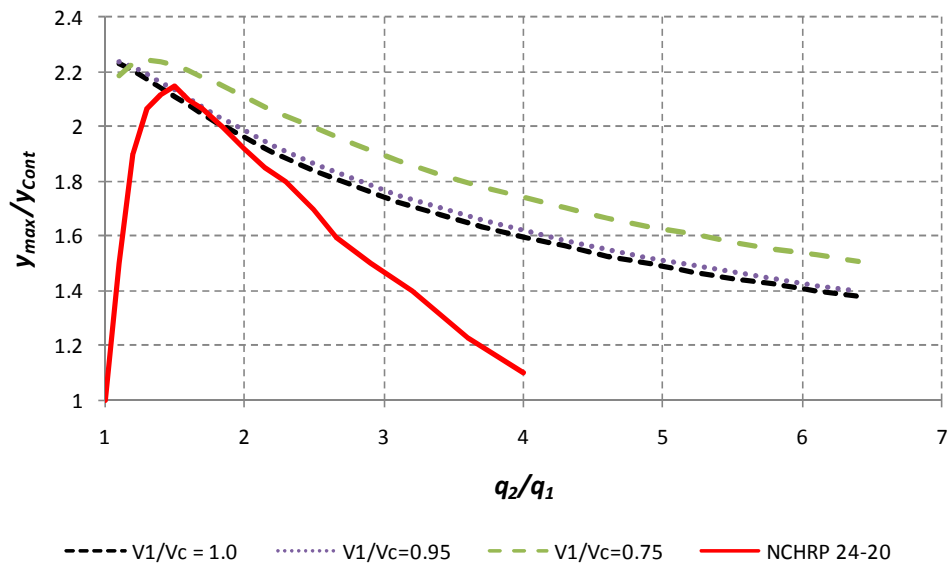
(b) Spill-Through abutment

Figure 8.19. (continued)

8.4.2 Comparison with full scale measurement

Benedict et al. (2006) conducted field survey at 144 bridges in South Carolina for abutment scour depth. Their database is available for download at the USGS web site at http://pubs.usgs.gov/of/2003/ofr03-295/index.html (as of March 2009). The data for Q100 and historic data in the Piemont area were compared with the predictions based on the present study. All the soil materials were assumed as cohesionless in the calculation of critical shear stress and critical velocity. Figure 8.20 shows the comparison. Based on the comparison, equation (8.15) mostly over predicts the field data.
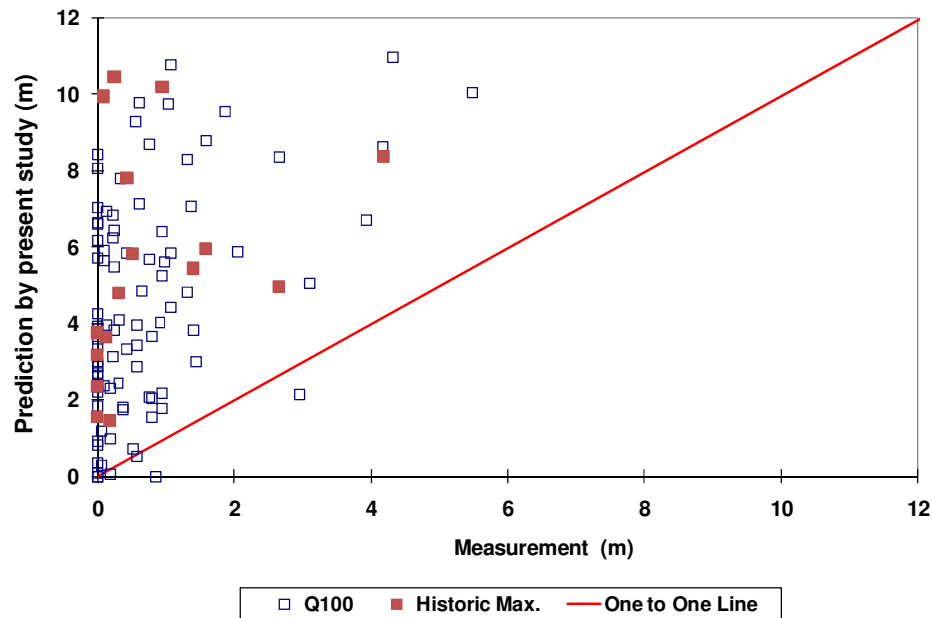
Figure 8.20. Comparison with Benedict and et al.'s (2006) data

8.4.3   Comparison with previous equations for abutment scour depth using imaginary condition

Due to the scarce of field data and the unknown property of the soil, imaginary bridge conditions were made up to calculate the scour depth for full scale bridges. The proposed maximum abutment scour depth equation in the present study and equations in other reports were used for the prediction. The full scale imaginary bridge properties are summarized in Table 8.3 and Table 8.4 in dimensionless form and dimensional form, respectively. Three types of sand (D_{50} = 0.4 mm, 2.0 mm and 10 mm) were considered. The half width of the main channel was fixed as 77.1 m and the slope of main channel was assumed as 3(H):1(V). The spill-through abutment with a 2(H):1(V) abutment slope

was assumed. The schematic diagram of the imaginary full scale channel is shown in Figure 8.21.

A series of HEC-RAS runs were performed to obtain the velocities and water depths. The back water effect was neglected in the predictions. The water depths and velocities at the approach section in Sturm's (2004) study were calculated with the presence of embankment in the HEC-RAS runs. The comparisons are presented in Figure 8.22.

According to Figure 8.22, the abutment scour depths predicted based on Sturm's (2004) and Melville's (1992) studies are greater while the depths predicted based on Chang and Davis' (1999) study are shallower when compared with the predictions based on the present study. The abutment scour depths calculated based on the HEC-18 recommendation and based on Gill's (1972) formula agree well with that predicted based on equation (8.15). Note that the HEC-18 method is based on the HIRE (Richardson et al. (2001)) equation for $L'/y_{f1} > 25$ and Froehlich's (1989) live bed scour equation for $L'/y_{f1} \le 25$.
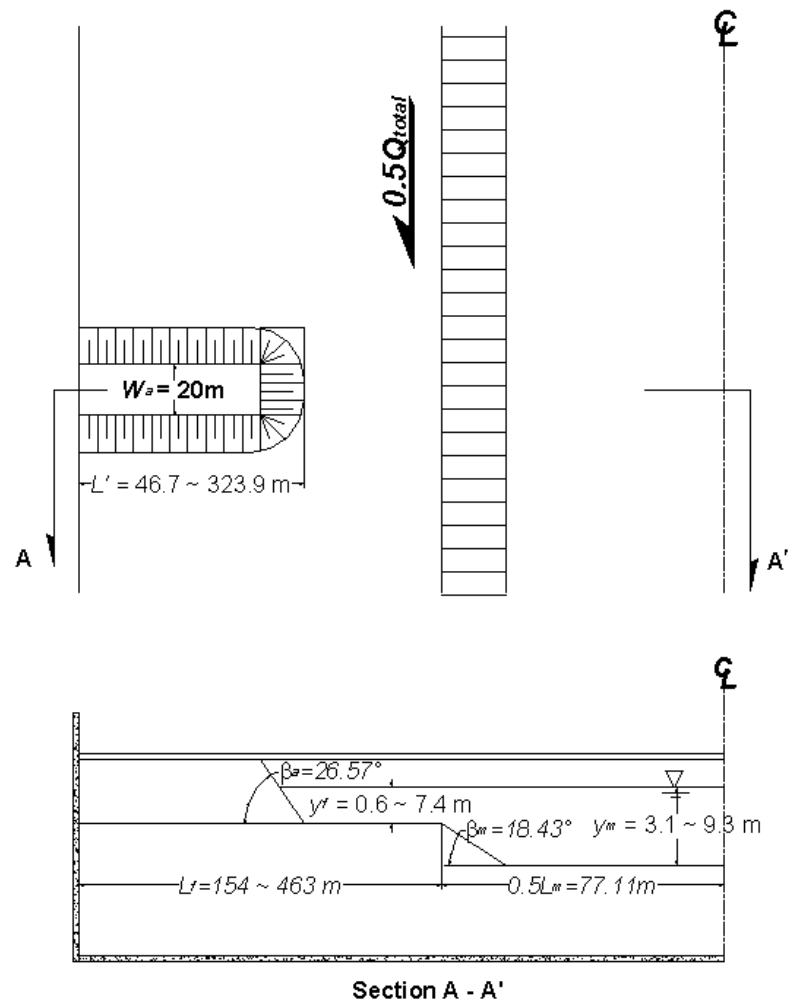
Figure 8.21. Schematic diagram of imaginary full scale channel

Table 8.3. Summary of the imaginary test conditions in dimensionless form for comparisons with different prediction equations

Case No.	$L_{f1}/0.5L_{m1}$	L'/L_{f1}	$y_{m1}/0.5L_{m1}$	y_{f1}/y_{m1}	L_{m1} (m)	β_m (°)	β_a (°)	D_{50} (mm)	$0.5Q$ (m³/s)
1	2	0.4	0.04	0.2	77.11	18.43	26.57	0.4	122.29
2	2	0.4	0.04	0.2	77.11	18.43	26.57	2	155.51
3	2	0.4	0.04	0.2	77.11	18.43	26.57	10	294.42
4	2	0.4	0.12	0.2	77.11	18.43	26.57	0.4	415.74
5	2	0.4	0.12	0.2	77.11	18.43	26.57	2	528.67
6	2	0.4	0.12	0.2	77.11	18.43	26.57	10	1000.92
7	2	0.4	0.20	0.2	77.11	18.43	26.57	0.4	709.37
8	2	0.4	0.20	0.2	77.11	18.43	26.57	2	902.06
9	2	0.4	0.20	0.2	77.11	18.43	26.57	10	1707.86
10	2	0.7	0.04	0.2	77.11	18.43	26.57	0.4	122.29
11	2	0.7	0.04	0.2	77.11	18.43	26.57	2	155.51
12	2	0.7	0.04	0.2	77.11	18.43	26.57	10	294.42
13	2	0.7	0.12	0.2	77.11	18.43	26.57	0.4	415.74
14	2	0.7	0.12	0.2	77.11	18.43	26.57	2	528.67
15	2	0.7	0.12	0.2	77.11	18.43	26.57	10	1000.92
16	2	0.7	0.20	0.2	77.11	18.43	26.57	0.4	709.37
17	2	0.7	0.20	0.2	77.11	18.43	26.57	2	902.06
18	2	0.7	0.20	0.2	77.11	18.43	26.57	10	1707.86
19	2	1.0	0.12	0.2	77.11	18.43	26.57	0.4	415.74
20	2	1.0	0.12	0.2	77.11	18.43	26.57	2	528.67
21	2	1.0	0.12	0.2	77.11	18.43	26.57	10	1000.92
22	2	1.0	0.12	0.4	77.11	18.43	26.57	0.4	630.24
23	2	1.0	0.12	0.4	77.11	18.43	26.57	2	801.43
24	2	1.0	0.12	0.4	77.11	18.43	26.57	10	1517.34
25	2	1.0	0.12	0.8	77.11	18.43	26.57	0.4	1057.05
26	2	1.0	0.12	0.8	77.11	18.43	26.57	2	1344.18
27	2	1.0	0.12	0.8	77.11	18.43	26.57	10	2544.92
28	4	0.7	0.08	0.8	77.11	18.43	26.57	0.4	1065.71
29	4	0.7	0.08	0.8	77.11	18.43	26.57	2	1355.20
30	4	0.7	0.08	0.8	77.11	18.43	26.57	10	2565.77
31	6	0.7	0.12	0.8	77.11	18.43	26.57	0.4	2361.65
32	6	0.7	0.12	0.8	77.11	18.43	26.57	2	3003.16
33	6	0.7	0.12	0.8	77.11	18.43	26.57	10	5685.83

Table 8.4. Summary of the imaginary test conditions in dimensional form for comparisons with different prediction equations

Case No.	L' (m)	V_1 (m/s)	y_{f1} (m)	y_{m1} (m)	V_{f1} (m/s)	V_{m1} (m/s)	τ_c (Pa)	V_{fc} (m/s)
1	46.69	0.378	0.652	3.120	0.170	0.460	0.364	0.508
2	46.69	0.480	0.652	3.120	0.210	0.580	1.006	0.646
3	46.69	0.909	0.652	3.120	0.410	1.100	6.164	1.223
4	46.69	0.453	1.847	9.250	0.230	0.560	0.364	0.604
5	46.69	0.577	1.847	9.250	0.290	0.710	1.006	0.769
6	46.69	1.092	1.827	9.230	0.540	1.350	6.164	1.452
7	46.69	0.494	3.112	15.450	0.270	0.600	0.364	0.659
8	46.69	0.628	3.092	15.430	0.340	0.770	1.006	0.837
9	46.69	1.189	3.062	15.400	0.650	1.460	6.164	1.583
10	107.96	0.378	0.612	3.080	0.170	0.470	0.364	0.503
11	107.96	0.480	0.642	3.110	0.210	0.580	1.006	0.645
12	107.96	0.909	0.602	3.070	0.400	1.130	6.164	1.207
13	107.96	0.453	1.847	9.250	0.230	0.560	0.364	0.604
14	107.96	0.577	1.847	9.250	0.290	0.710	1.006	0.769
15	107.96	1.092	1.837	9.240	0.540	1.350	6.164	1.454
16	107.96	0.494	3.082	15.420	0.270	0.610	0.364	0.658
17	107.96	0.628	3.082	15.420	0.340	0.770	1.006	0.837
18	107.96	1.189	3.072	15.410	0.650	1.460	6.164	1.584
19	154.23	0.453	1.847	9.250	0.230	0.560	0.364	0.604
20	154.23	0.577	1.847	9.250	0.290	0.710	1.006	0.769
21	154.23	1.092	1.847	9.250	0.540	1.350	6.164	1.455
22	154.23	0.509	3.698	9.250	0.380	0.620	0.364	0.679
23	154.23	0.647	3.698	9.250	0.480	0.790	1.006	0.863
24	154.23	1.225	3.698	9.250	0.910	1.500	6.164	1.634
25	154.23	0.571	7.399	9.250	0.550	0.610	0.364	0.762
26	154.23	0.727	7.399	9.250	0.700	0.770	1.006	0.969
27	154.23	1.375	7.399	9.250	1.320	1.460	6.164	1.834
28	215.92	0.534	4.936	6.170	0.520	0.580	0.364	0.712
29	215.92	0.679	4.936	6.170	0.660	0.740	1.006	0.905
30	215.92	1.286	4.936	6.170	1.260	1.390	6.164	1.714
31	323.88	0.571	7.399	9.250	0.560	0.610	0.364	0.762
32	323.88	0.727	7.399	9.250	0.720	0.770	1.006	0.969
33	323.88	1.375	7.399	9.250	1.360	1.460	6.164	1.834
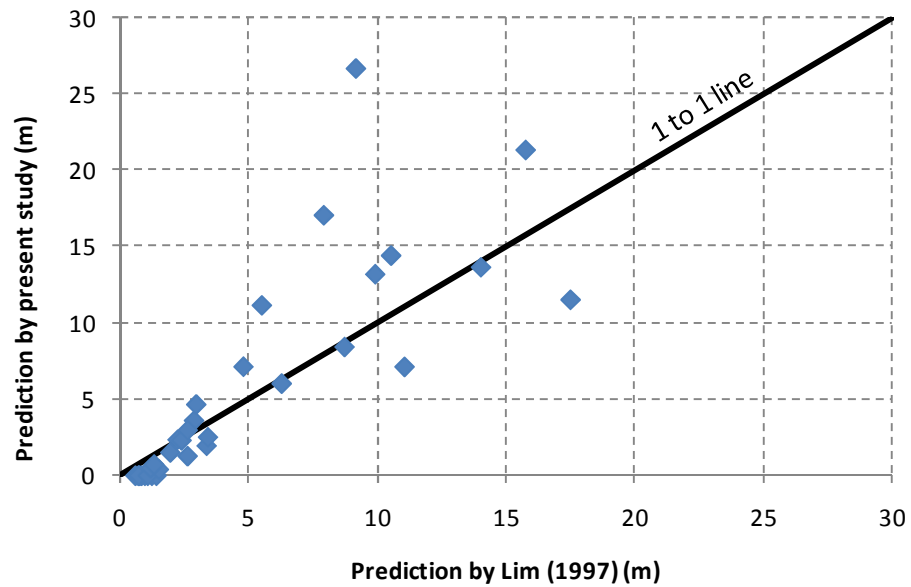
(a) Comparison with Lim's (1997) equation
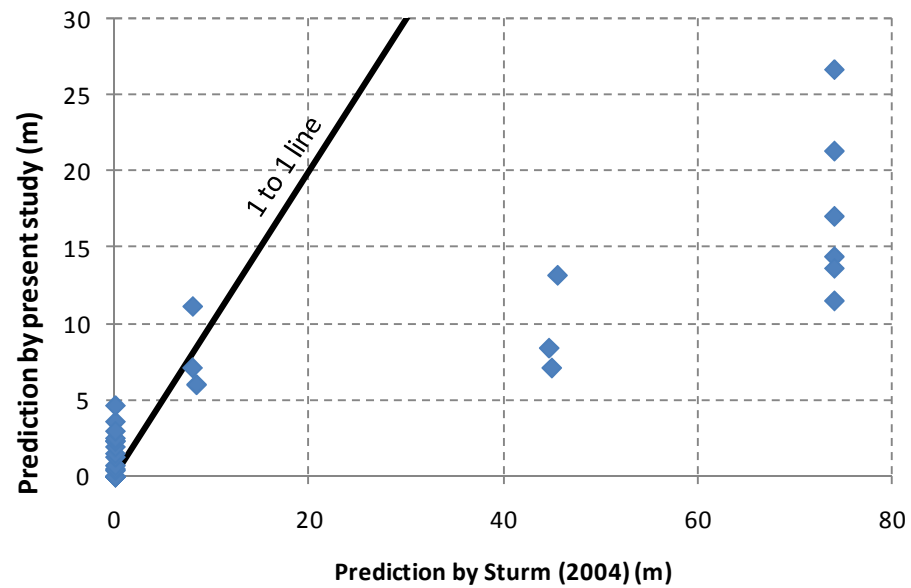
(b) Comparison with Sturm's (2004) equation

Figure 8.22. Comparisons with other prediction equations for full scale bridge
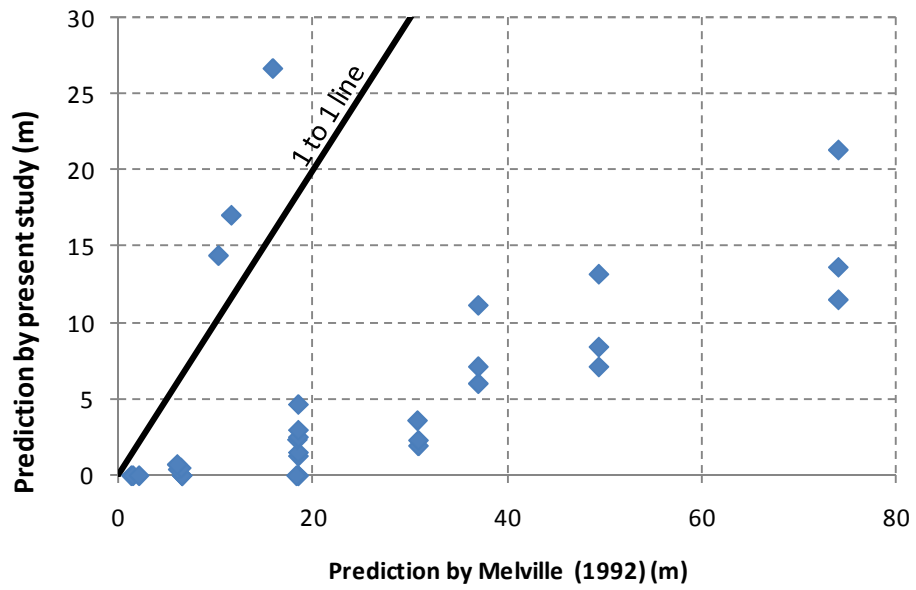
(c) Comparison with Melville's (1992) equation
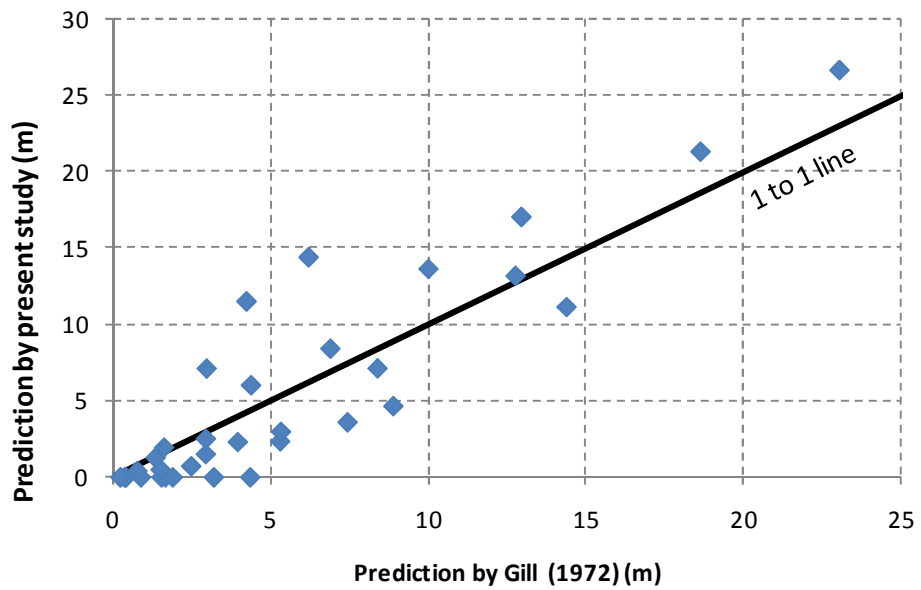
(d) Comparison with Gill's (1972) equation

Figure 8.22. (Continued)
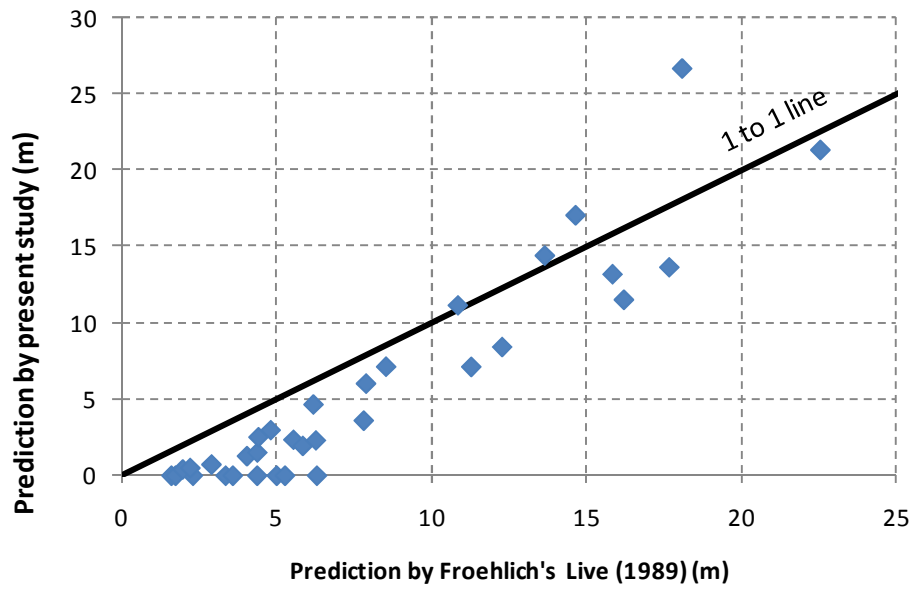
(e) Comparison with Froehlich's (1989) equation
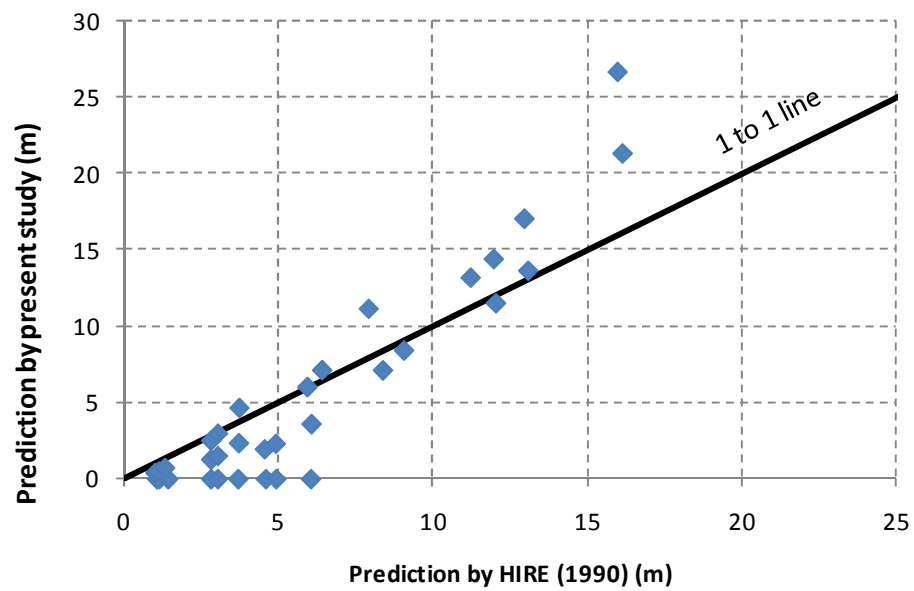
(f) Comparison with HIRE (1990) equation

Figure 8.22. (Continued)
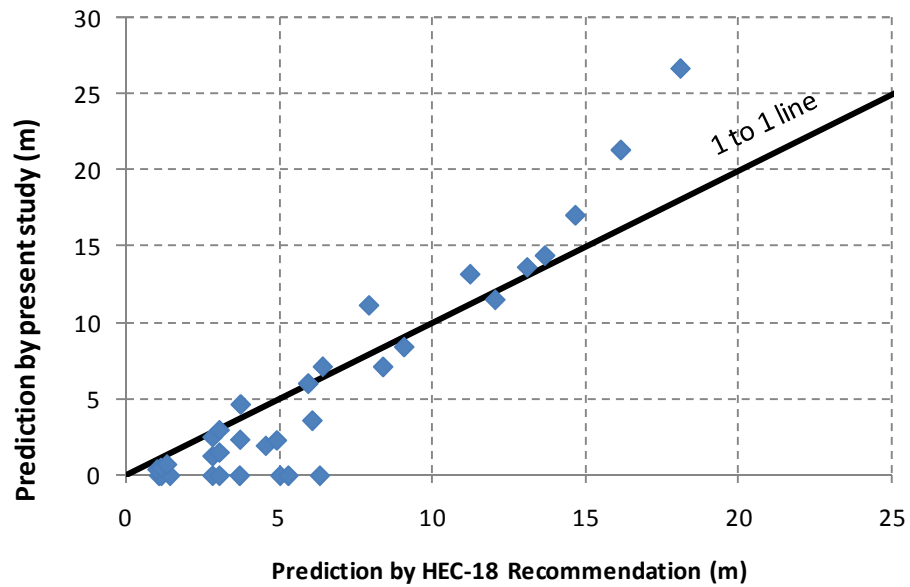
(g) Comparison with HEC-18 recommendation
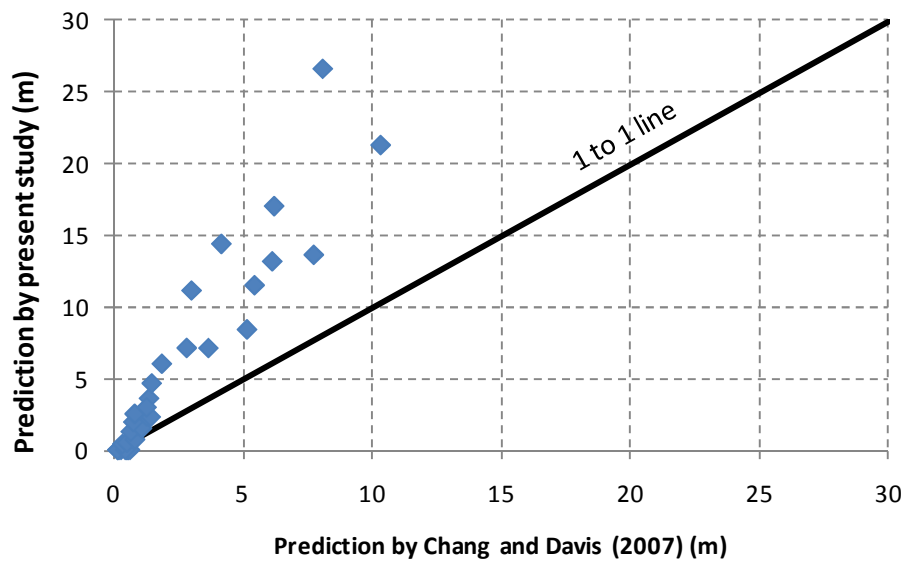
(h) Comparison with Chang and Davis' (2007) equation

Figure 8.22. (Continued)

8.5 Conclusions

The maximum abutment scour equation is proposed on the basis of a series of large flume test with Porcelain clay as channel bed material. The abutment is regarded as the half of wide pier, and the prediction equation form of abutment scour is same to that of pier scour. The property of soil, especially the critical shear stress, is included in the equation.

The experimental results can be summarized as followings:

1. The wing-wall shape abutment induces deeper scour than the spill-through abutment.

2. The effect of abutment alignment was checked with two experiments which are aligned 30° upstream and downstream, respectively. The measured abutment scour depth for the abutment aligned downstream shows same trend with previous studies for the abutment scour, but for the abutment aligned upstream shows opposite trend. Since the abutment used in this study is a spill-through abutment, the abutment induced a relatively smooth flow during the transition even though the abutment is aligned toward upstream.

3. If the toe of abutment locates close to the end of floodplain, the abutment scour depth is much deeper than the prediction, and new correction factor for this condition is required.

The abutment scour prediction equation developed in the present study has also been applied to non-cohesive soil. Data from Sturm (2004) taken in compound channels and data from Froehlich (1989) (which was cited in Palaviccini's Ph.D. dissertation in

1993) taken in rectangular channels were used for the comparisons. The critical shear stresses are obtained by Shields diagram and Manning's *n* value is obtained by Strikler approximation. Based on the figures, equation (8.15) mostly under predicts the scour depth, and mostly over predicts Froehlich's (1989) database.

Due to the scarce of field data and the unknown property of the soil, imaginary bridge conditions were built up to calculate the scour depth for full scale bridges. The predicted abutment scour depths based on Sturm's (2004) and Melville's (1992) studies were deeper while the depths based on Chang and Davis' (2007) study were shallower when those were compared with the predicted abutment scour depths based on the present study. The abutment scour depths calculated based on the HEC-18 recommendation and based on Gill's (1972) formula agreed well with that predicted based on the present study.

CHAPTER IX

NEW SRICOS-EFA METHOD

9.1   Background

The new SRICOS-EFA method is developed to predict complex pier scour, contraction scour, and abutment with consideration of time effect. It can handle each scour alone, and combined case of pier scour, contraction scour and abutment scour simultaneously. The conventional method which is used in HEC-18 calculates the individual scour depths independently and simply adds them up. This method results in too conservative scour depth. The new SRICOS-EFA method is not just adding the individual scour depths. The method considers the time factor, soil properties and three types of scour – abutment scour, contraction scour and pier scour. The new method is capable of handling different scour types individually or of considering the interaction between the contraction scour and the pier scour.

9.2   Input for the SRICOS-EFA program

The input includes parameters of the soil, flow, and channel geometry problem.

9.2.1   Soil properties

Different with cohesionless soil, the scour rate is very important parameter because the scour rate is much slower than that of cohesionless soil, and the flood in several days may generate small portion of the maximum scour depth. The soil erosion function is the relationship between the erosion rate $\dot{z}$ of the soil and the hydraulic shear stress τ acting on channel bottom. It is obtained by conducting an EFA test (Briaud et

al., 2001(a), 2001(b)) on the soil sample obtained around the bridge structure. The erosion function (Figure 9.1) is required for each layer in the range of the potential scour depth at bridge site. Briaud (2008) proposed the categories of the erosion function based on 15 years of erosion testing experience (Figure 9.2). The engineer can use either the EFA to get the erodibility curves (preferred to get more accurate result) or the proposed the categories.
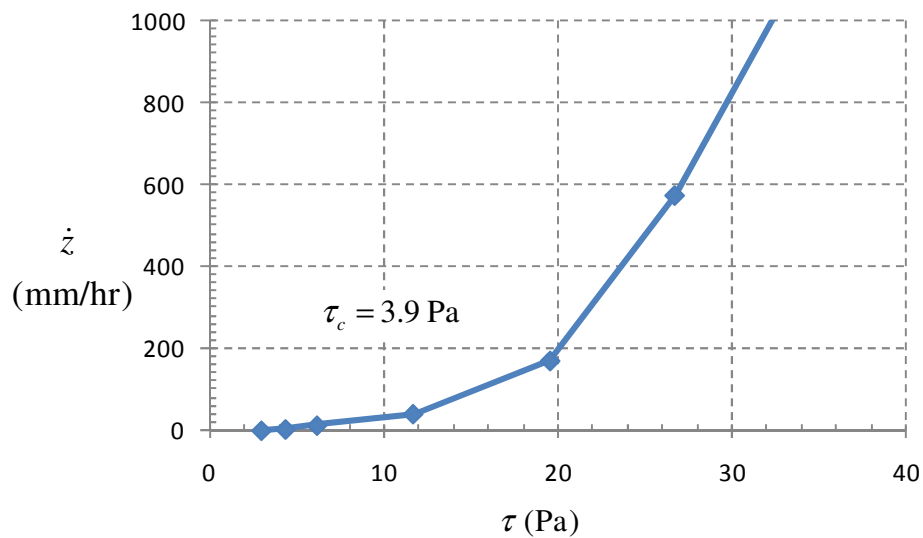
Figure 9.1. Typical EFA test result
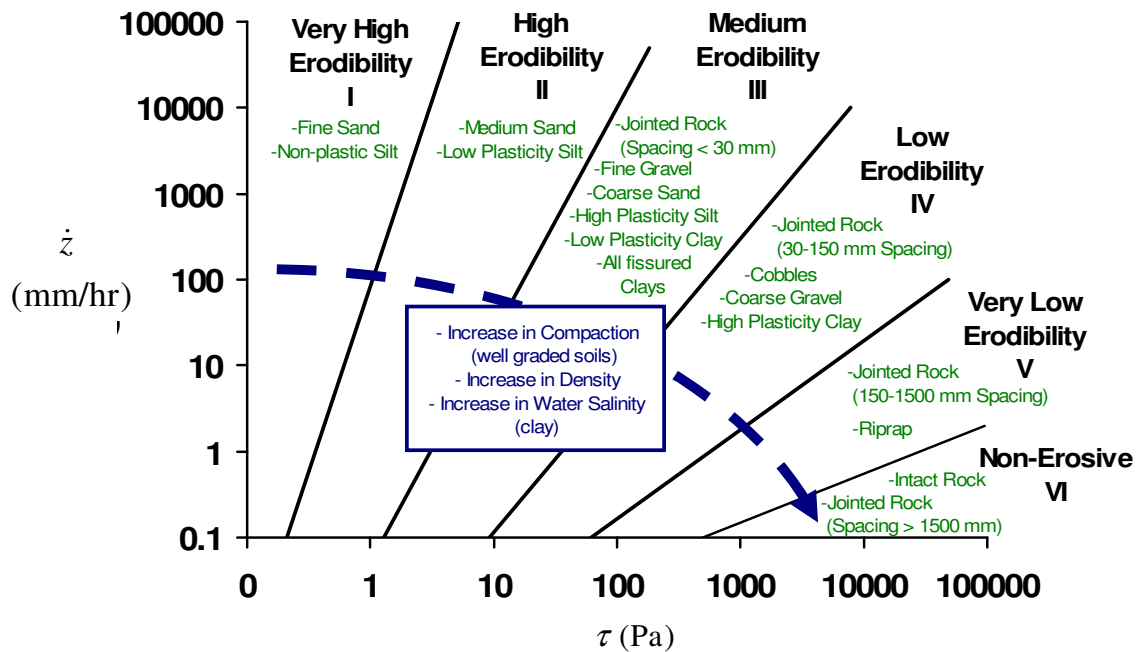
Figure 9.2. Proposed erosion categories for soils and rocks (Briaud, 2008)

9.2.2 Geometry

The geometry input includes the channel information for both approach section and bridge section. The previous version required channel width to calculate the contraction ratio because the simple channel was assumed. On the contrary, the new version requires channel slope, floodplain width at both side, main channel width, and abutment length and slope at both sides, because the compound channel is assumed. The pier dimension, shape, spacing, and attack angle are required for pier scour calculations. The information for bridge deck is also required to calculate abutment scour depths. Figure 9.3 shows the typical channel geometry at both approach section and bridge section.
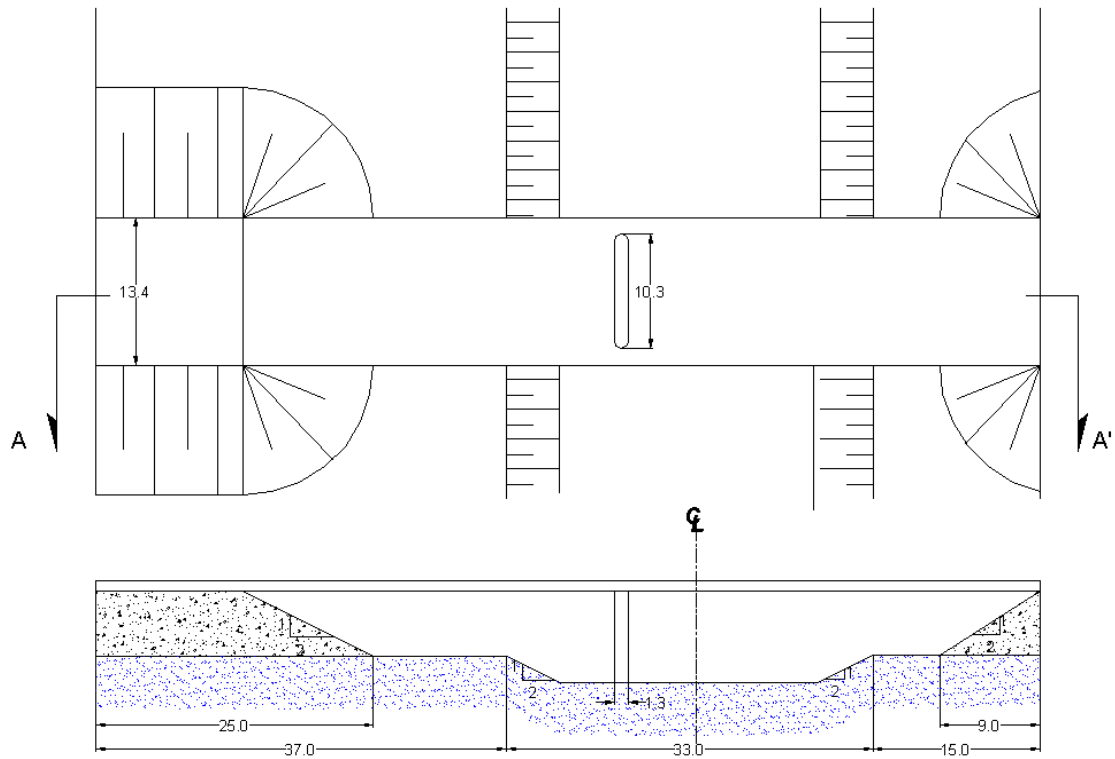
Figure 9.3. Typical channel geometry at both approach section and bridge section

9.2.3   Flow data

The hydrograph can be obtained from a nearby gauge station. The hydrograph should last as long as the required period of prediction. Furthermore, if the hydrograph obtained from the gauge station does not contain a 100-year flood, it can be spiked artificially to include such a large event if required by design. The hydrograph is typically in the form of discharge as a function of time. It should be converted to the form of velocity as a function of time, and the form of water depth as a function of time, because the input for scour calculations is the velocity and water depth. This can be done by using a program such as HEC-RAS (Hydrologic Center's River Analysis System,

HEC-RAS, 1997), which was developed by US Army Corps of Engineers. In order to run HEC-RAS, several geographical features are necessary such as: the average slope of channel bed, the channel cross-section, and the roughness coefficient of the riverbed. Figure 9.4 shows the discharge hydrograph, Figure 9.5 shows the discharge versus velocity curve and the discharge versus discharge obtained from HEC-RAS runs, the water depth versus time is shown in Figure 9.6, and the velocity versus time is shown in Figure 9.7.
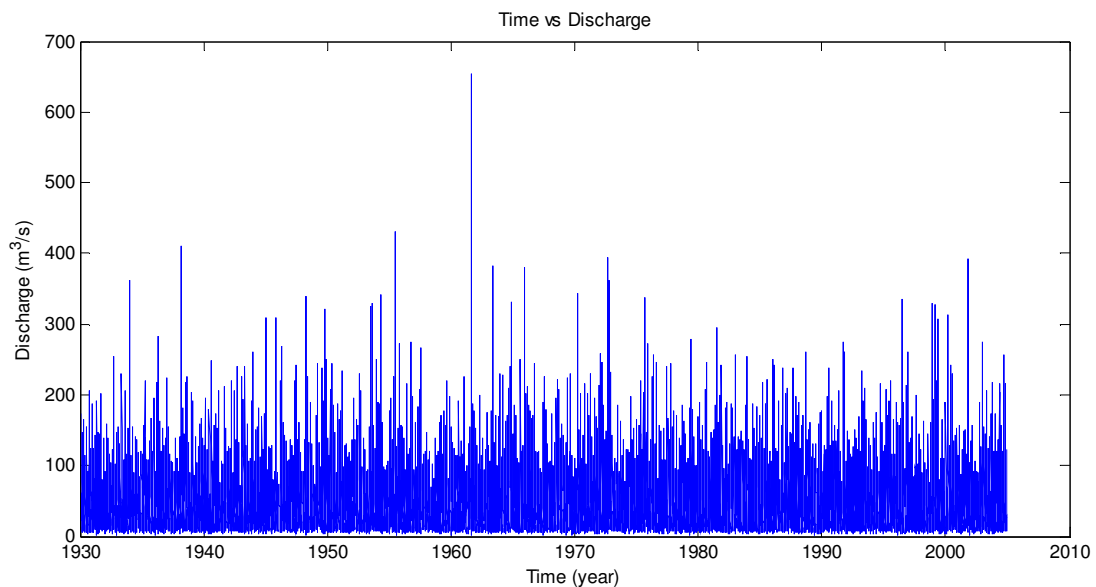
Figure 9.4. Discharge as function of time
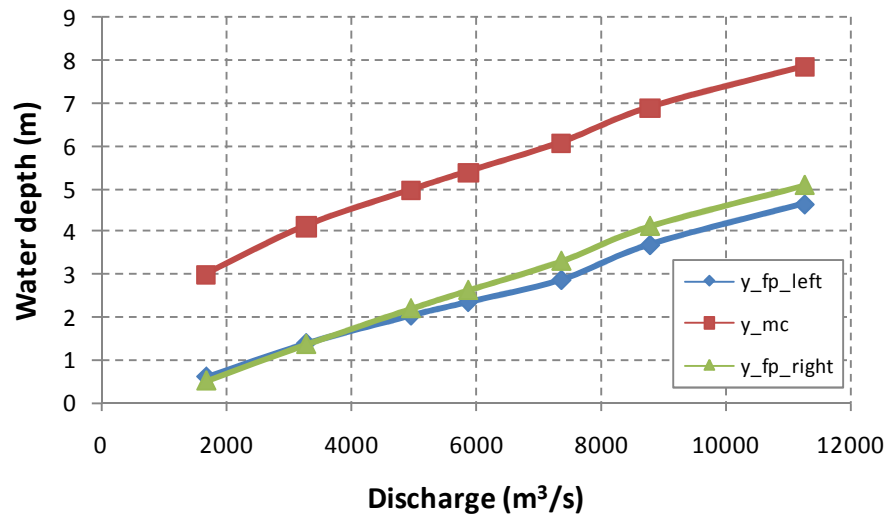
(a) Water depth versus discharge
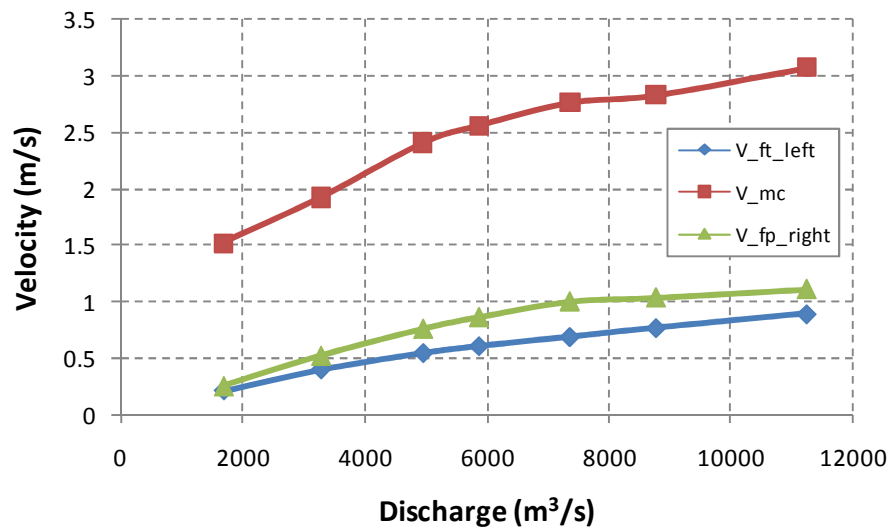
(b) Velocity versus discharge

Figure 9.5. HEC-RAS results
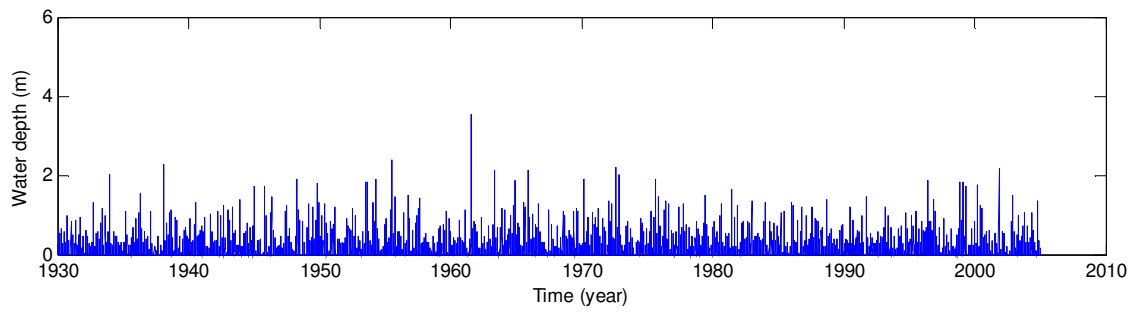
(a) Left floodplain
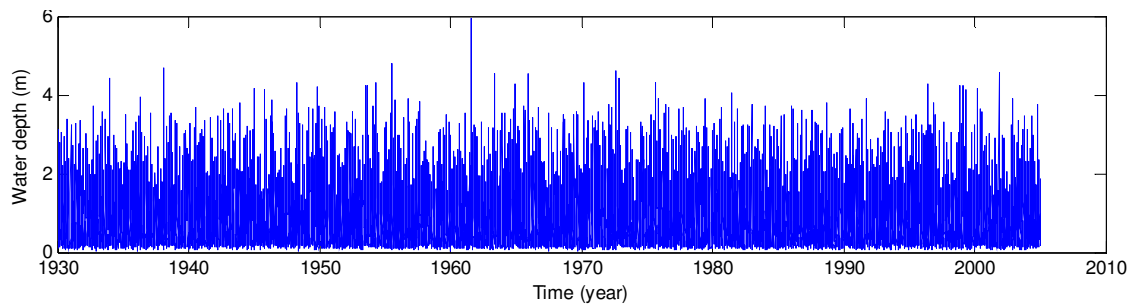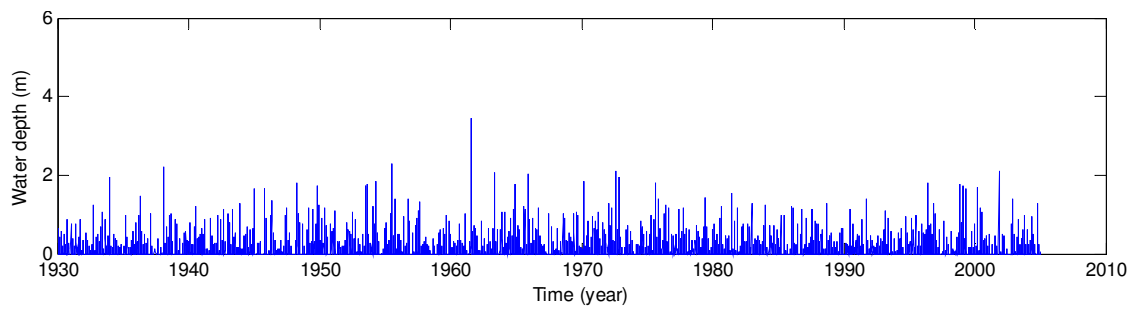
(b) Main channel

(c) Right floodplain

Figure 9.6. Water depth versus time
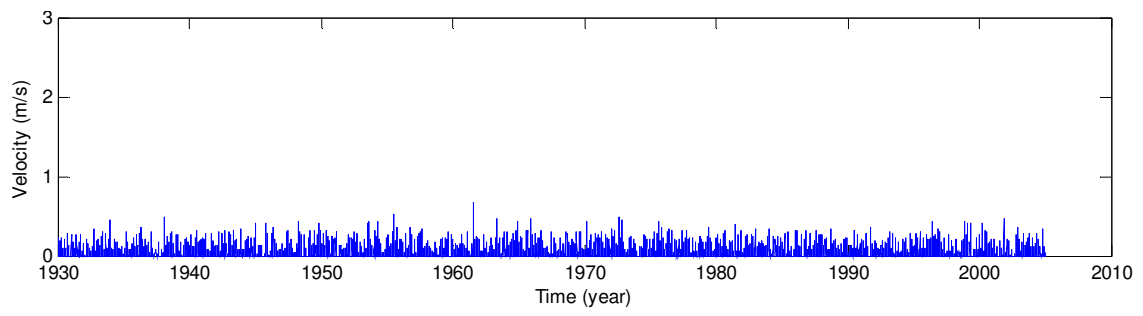
(a) Left floodplain
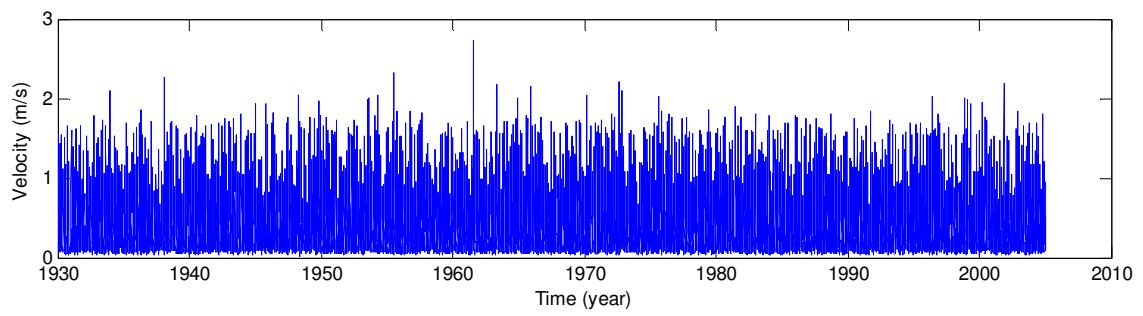
(b) Main channel
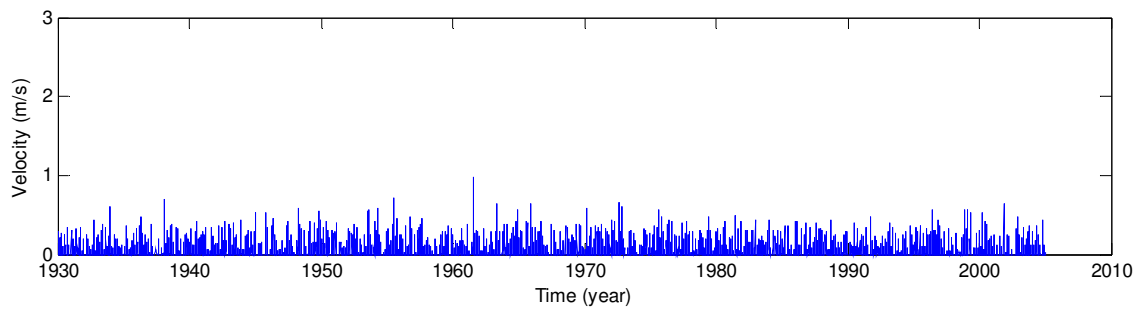
(c) Right floodplain

Figure 9.7. Velocity versus time

9.3 Principle of SRICOS-EFA method

The EFA (Erosion Function Apparatus) is a device to get the erosion properties of soil. SRICOS-EFA (Scour Rate In COhesive Soil-Erosion Function Apparatus) is a method to predict the scour depth with the function of time considering the erosion properties of soil. The procedure of SRICOS-EFA (after Briaud et al., 1999(a)) for uniform flow and uniform soil is summarized as following. Note that the following procedure is for the calculation assuming that scour happens independently to another type of scour;

1. Perform EFA (Erosion Function Apparatus) tests on the samples and obtain the relation of the erosion rate $\dot{z}$ to the hydraulic shear stress τ.

2. Determine the initial maximum bed shear stress τ_{max} around the hydraulic structure before the scour process using the equation obtained from numerical simulations.

3. Obtain the initial scour rate $\dot{z}_i$ corresponding to τ_{max} on the $\dot{z}$-τ curve.

4. Calculate the maximum scour depth y_s.

5. Develop the complete scour depth y_s versus time t curve.

$$y_s(t) = \frac{t}{\dfrac{1}{\dot{z}_i} + \dfrac{t}{y_s}} \tag{9.1}$$

6. Predict the scour depth at the time corresponding to the duration of the flood by reading $y_s(t)$.

9.3.1 Maximum hydraulic shear stress

After Briaud et al. (1999(a)) proposed the maximum hydraulic shear stress τ_{max} acting on the channel bottom around a cylindrical circular pier in deep water condition, τ_{max} for the complex pier, τ_{max} for the contraction scour, and τ_{max} for the abutment scour have been proposed. Each equation is listed in the following.

9.3.1.1 Maximum shear stress for complex pier

Nurtjahyo (2003) further extended Wei's equation to the complex pier conditions, including the effect of water depth k_w, the effect of pier spacing k_{sp}, the effect of shape k_{sh}, and the effect of attack angle k_θ.

$$\tau_{max(pier)} = k_w k_{sh} k_{sp} k_\theta \cdot 0.094 \rho V_1^2 \left[\frac{1}{\log \text{Re}} - \frac{1}{10} \right] \tag{9.2}$$

where ρ is the density of water (kg/m^3), V_1 is the approach velocity (m/sec), θ is the attack angle (in degree), S is spacing between adjacent two piers (measured center to center), a is width of pier, L is length of pier, y_1 is approach water depth, $\text{Re}\left(= V_1 a / v\right)$ is the Reynolds number, k_w the correction factor for the water depth effect, k_{sh} is the correction factor for the pier shape, k_θ is the correction factor for the attack angle effect, and k_{sp} is the correction factor for the pier spacing

$$k_w = 1 + 16 \exp\left(-4y/a\right) \qquad\qquad k_{sh} = 1.15 + 7 \exp\left(-4L/a\right)$$

$$k_\theta = 1 + 1.5 \left(\theta/90\right)^{0.57} \qquad\qquad k_{sp} = 1 + 5 \exp\left(-1.1S/a\right),$$

9.3.1.2 Maximum shear stress for contraction scour

Nurtjahyo (2003) numerically studied the maximum bed shear stress at the center of the channel under long contraction. The equation is generated by correcting the open channel flow equation including several correction factors for channel geometry and water depth effect.

$$\tau_{max(Cont)} = k_R k_{Wa} k_\alpha k_w \rho g n^2 V_1^2 R_h^{-\frac{1}{3}} \tag{9.3}$$

where ρ is the density of water (kg/m^3), V_1 is the approach velocity (m/sec), g is the gravitational acceleration, n is Manning's coefficient, R_h is the hydraulic radius, α is the transition angle (in degree), W_a is the top width of the abutment, A_1 is the channel area at approach section, A_2 is the channel area at bridge section, L'_{left} is the length of left bridge embankment, L'_{right} is the length of right bridge embankment, k_R is the correction factor for the contraction ratio, k_α is the correction factor for the transition angle, k_{wa} is the correction factor for the contraction length, and k_w is the correction factor for the water depth and it is 1.0 for all conditions

$$k_R = 0.62 + 0.38 \left(\frac{A_1}{A_2} \right)^{1.75},$$

$$k_\alpha = 1.0 + 0.9 \left(\frac{\alpha}{90} \right)^{1.5},$$

$$k_{wa} = \begin{bmatrix} 0.77 + 1.36 \left(\dfrac{W_a}{L'_{left} + L'_{right}} \right) - 1.98 \left(\dfrac{W_a}{L'_{left} + L'_{right}} \right)^2, & \text{for } \dfrac{W_a}{L'_{left} + L'_{right}} \leq 0.35 \\ 1.0 & , \quad \text{for} \quad \text{otherwise} \end{bmatrix}$$

9.3.1.3 Maximum shear stress for abutment scour

Chen (2008) numerically studied the maximum bed shear stress around the toe of abutment considering Froude number effect, aspect ratio effect, abutment shape effect, abutment alignment effect, and overtopping flow effect. The maximum shear stress equation around abutment is:

$$\tau_{\max(Abut)} = 12.45 k_{Cr} k_{sh} k_{Fr} k_s k_{sk} k_L k_o \rho V_1^2 \, \text{Re}^{-0.45} \tag{9.4}$$

where ρ is the density of water (kg/m^3), V_1 is the approach velocity (m/sec), $\text{Re}(= V_1 W_a / \nu)$ is the Reynolds number defined with top width of the abutment, q_1 is the unit discharge at approach section, q_2 is the unit discharge at bridge section, d_1 is the distance from the water surface to the low chord of the bridge at upstream face of the bridge, d_{deck} is the thickness of the bridge deck, k_{sh} is the correction factor for the aspect ratio of the approach embankment, k_{Fr} is the correction factor for Froude number, k_s is the correction factor for abutment shape, k_{sk} is the correction factor for abutment alignment, k_o is the correction factor for overtopping

$$k_c = 3.65 \frac{q_2}{q_1} - 2.91$$

$$k_{Fr} = \begin{cases} 2.07 Fr + 0.8 & Fr > 0.1 \\ 1.0 & Fr \le 0.1 \end{cases}$$

$$k_{sk} = 1.0$$

$$k_{sh} = 0.85 \times \left(\frac{L'}{W_a} \right)^{-0.24}$$

$$k_s = \begin{cases} 1.0 & \text{vertical-wall abutment} \\ 0.65 & \text{wing-wall abutment} \\ 0.58 & \text{spill-through abutment} \end{cases}$$

$$k_L = \begin{cases} 1.0 & \text{for } \left(L_f - L'\right)/y_f \le -2 \\ 0.6(L_f - L')/y_f + 1.2 & \text{for } -2 < (L_f - L')/y_f \le 0 \\ -1.2(L_f - L')/y_f + 1.2 & \text{for } 0 < (L_f - L')/y_f \le 1 \\ 1.0 & \text{for } 1 \le (L_f - L')/y_f \end{cases}$$

$$k_o = \begin{cases} 0.92 \cdot \left(d_1/d_{deck}\right) + 1.0 & \text{for } d_1/d_{deck} < 1.0 \\ 0.21\left(d_1/d_{deck}\right)^2 - 1.27\left(d_1/d_{deck}\right) + 2.97 & \text{for } 1.0 \le d_1/d_{deck} \le 3.0 \\ 1.0 & \text{for } 3.0 < d_1/d_{deck} \end{cases}$$

9.3.2   Maximum scour depth

A lot of flume tests for scour have been conducted in Texas A&M university since 1999. The flume tests can be categorized into three types – pier scour, contraction scour, and abutment scour. Three scour equations are listed in the following.

9.3.2.1 Maximum scour depth for the complex pier

The pier scour equation proposed by Gudavalli (1997) and Li (2002) was changed in this study after reanalysis of their flume test results, since the soil property is not considered. The new equation considering soil property is developed with flume test results in the deep water condition for single circular pier. The correction factors for the shallow water effect, pier shape, attack angle, aspect ratio, and pier spacing are newly obtained. The pier scour equation considering all conditions is:

$$\frac{y_{s(Pier)}}{a'} = 2.2 \cdot K_w \cdot K_1 \cdot K_L \cdot K_{sp} \cdot \left(2.6 \cdot Fr_{(pier)} - Fr_{c(pier)}\right)^{0.7} \tag{9.5}$$

where K_w is the correction factor for water depth effect, K_1 is correction factor for pier shape, K_L is he correction factor for aspect ratio in rectangular pier, K_{sp} is correction

factor for pier spacing, a' is projected pier width, $Fr_{(pier)}$ is Froude number based on approach velocity and a', and $Fr_{c(pier)}$ is Froude number based on critical velocity and a'.

$$K_w = \begin{cases} 0.89 \left(\dfrac{y_1}{a'} \right)^{0.33} & , \text{for } \dfrac{y_1}{a'} < 1.43 \\ 1.0 & , \text{else} \end{cases}$$

$K_1 = 1.0$, for $\theta > 30°$, other case K_1 is the value in Table 6.9

$K_L = 1.0$, for whole range of L/a

$$K_{sp} = \begin{cases} 2.9 \left(\dfrac{S}{a'} \right)^{-0.91} & , \text{for } \dfrac{S}{a'} < 3.42 \\ 1.0 & , \text{else} \end{cases}$$

$$Fr_{(pier)} = \frac{V_1}{\sqrt{g \cdot a'}}, \quad Fr_{c(pier)} = \frac{V_c}{\sqrt{g \cdot a'}}, \quad a' = a \left(\cos\theta + \frac{L}{a} \cdot \sin\theta \right)$$

9.3.2.2 Maximum and uniform contraction scour depth

The contraction scour equation is developed on the basis of flume test results in both rectangular channels and compound channels. Instead of using channel width, the contraction ratio is used to get the average velocity at the contracted section. The maximum contraction scour equation, and the uniform contraction scour equation are:

$$\frac{y_{s(Cont)}}{y_{m1}} = 2.21 \left(1.31 Fr_{m2} - Fr_{mc} \right) \tag{9.6}$$

$$\frac{y_{s(uni\_Cont)}}{y_{m1}} = 1.66 \left(1.31 Fr_{m2} - Fr_{mc} \right) \tag{9.7}$$

where $y_{s(Cont)}$ is the maximum contraction scour depth, $y_{s(uni\_Cont)}$ is the uniform contraction scour depth, y_{m1} is the main channel depth at the approach section,

$$Fr_{m2}\left(=\frac{V_2}{\sqrt{gy_{m1}}}\right) \text{ is the Froude number of the main-channel at the bridge section,}$$

$$Fr_{mc}\left(=\frac{V_{mc}}{\sqrt{gy_{m1}}}=\frac{\sqrt{\tau_c/\rho}}{gny_{m1}^{1/3}}\right) \text{ is the critical Froude number of the main-channel, } V_2 \text{ is the}$$

average velocity at the contracted section defined, V_{mc} is the critical velocity in the main

channel, τ_c is the critical shear stress, n is Manning's roughness coefficient, and ρ is the

water density.

9.3.2.3 Maximum abutment scour depth

The equation predicting the maximum abutment scour depth is developed on the

basis of flume test results and the results of 3D numerical analysis by Chen (2008).

$$\frac{y_{s(Abut)}}{y_{f1}}=K_1\cdot K_2\cdot K_L\cdot K_p\cdot 6.5\cdot\left(1.57\cdot Fr_{f2}-Fr_{fc}\right)^{0.7} \tag{9.8}$$

Note that y_{f1} should be replaced by h under the pressure flow condition (i.e., $y_{f1} > h$).

In equation (9.7), $y_{s(Abut)}$ is the maximum abutment scour depth, y_{f1} is the water depth at

the toe of the abutment estimated as the water depth immediately upstream of the toe of

the abutment, h is the distance from the low chord of the bridge to the river bottom

before scour starts, $Fr_{f2}=\dfrac{V_{f2}}{\sqrt{gy_{f1}}}$, $Fr_{fc}=\dfrac{V_{fc}}{\sqrt{gy_{f1}}}=\dfrac{\sqrt{\tau_c/\rho}}{gny_{f1}^{1/3}}$, K_1 is the correction factor for

the abutment shape, K_2 is the correction factor for the abutment skew angle, K_L is the

correction factor for the abutment location, K_p is the correction factor for the pressure

flow. Their values and formulas are as follows:

$$V_{f2} = \begin{cases} \dfrac{Q_{total}}{A_2}, \text{for short setback } \left((L_f - L') \le 5y_{m1}\right) \\[2ex] \dfrac{Q_{fp1}}{A_{f2}}, \text{for long setback } \left(L' \le 0.25L_f\right) \\[2ex] \text{otherwise use a linearly interpolated velocity between} \\[1ex] \dfrac{Q_{total}}{A_2} \text{ for } (L_f - L') = 5y_{m1} \text{ and } \dfrac{Q_{fp1}}{A_{f2}} \text{ for } L' = 0.25L_f \end{cases}$$

$$K_1 = \begin{cases} 1.22 & \text{for Vertical-wall abutment} \\ 1.0 & \text{for Wing-wall abutment} \\ 0.68 & \text{for Spill-through abutment with 2:1 Slope} \\ 0.55 & \text{for Spill-through abutment with 3:1 Slope} \end{cases}$$

$$K_2 = \begin{cases} 1.0 - 0.005|\theta - 90°| & for\ 60° \le \theta \le 120° \\ 0.85 & otherwise \end{cases}$$

$$K_L = \begin{cases} -0.37\dfrac{L_f - L'}{y_{f1}} + 1.55 & \text{for } \dfrac{L_f - L'}{y_{f1}} < 1.5 \\ 1.0 & \text{otherwise} \end{cases}$$

$$K_p = \begin{cases} 0.92 \cdot (d_1 / d_{deck}) + 1.0 & \text{for } d_1 / d_{deck} < 1.0 \\ 0.21(d_1 / d_{deck})^2 - 1.27(d_1 / d_{deck}) + 2.97 & \text{for } 1.0 \le d_1 / d_{deck} \le 3.0 \\ 1.0 & \text{for } 3.0 < d_1 / d_{deck} \end{cases}$$

9.4   Principle of the integrated SRICOS-EFA method

If bridge piers exist at the contracted section, both contraction scour and pier scour happen at same time. In order to simplify this condition, it is assumed that the contraction scour happens first, and then the pier scour happens. The contraction scour continues until the average velocity at the bridge section becomes to the critical velocity. Thus the pier scour calculations are made using the critical velocity, not the actual

velocity, because when contraction scour has stopped ($y_{s(Cont)}$ and $y_{s(uni\_Cont)}$ are reached), the velocity in the contracted section is the critical velocity V_c. The water depth for the pier scour calculations is the water depth in the contracted section after the contraction scour has occurred. The bottom profile of the river after scour has occurred is obtained by adding the contraction scour and the pier scour.

The location of maximum contraction scour depth varies with the blockage ratio. The larger blockage ratio (L_2/L_1) places the location of the maximum contraction scour depth to the out of bridge section, and the location becomes closer to the bridge section if the blockage ratio becomes smaller. Thus it is more reasonable to select the type of contraction scour with blockage ratio. In SRICOS-EFA, the uniform contraction scour is selected if the blockage ratio is bigger than 50 %, and the maximum contraction scour is selected for other cases.

This approach is valid for the maximum scour depth calculations. For the time stepping process, the maximum scour depth is not reached at each step but the maximum scour depth is calculated as part of each step and used to calculate the partial scour depth. Therefore the above technique is included in each time step. The other parameter calculated at each time step is the initial maximum shear stress; this shear stress is used to read the initial scour rate on the erosion function obtained from the EFA tests. Both parameters, y_s and $\dot{z}_i$, are used to generate the scour depth versus time curve and the actual scour depth is read on that curve at the value equal to the time step. The details of that procedure are presented in following.

1. **Calculation of maximum shear stress**

   - Complex pier scour:

$$\tau_{\max(Pier)} = k_w k_{sh} k_{sp} k_\theta \cdot 0.094 \rho V_2^2 \left[\frac{1}{\log \mathrm{Re}} - \frac{1}{10} \right]$$

   - Contraction scour:

$$\tau_{\max(Cont)} = k_R k_{Wa} k_\alpha k_w \rho g n^2 V_1^2 R_h^{-\frac{1}{3}}$$

   - Abutment scour:

$$\tau_{\max(Abut)} = 12.45 k_{Cr} k_{sh} k_{Fr} k_s k_{sk} k_L k_o \rho V_1^2 \, \mathrm{Re}^{-0.45}$$

2. **Calculation of maximum scour depth**

   - Complex pier scour:

$$y_{s(Pier)} = 2.2 \cdot K_w \cdot K_1 \cdot K_L \cdot K_{sp} \cdot \left(2.6 \cdot \frac{V_2}{\sqrt{g \cdot a'}} - \frac{V_c}{\sqrt{g \cdot a'}} \right)^{0.7} \cdot a' \geq 0 \quad \text{for } V_2 < V_c$$

$$y_{s(Pier)} = 2.2 \cdot K_w \cdot K_1 \cdot K_L \cdot K_{sp} \cdot \left(1.6 \cdot \frac{V_c}{\sqrt{g \cdot a'}} \right)^{0.7} \cdot a' \geq 0 \qquad \text{for } V_2 \geq V_c$$

   - Contraction scour:

$$y_{s(Cont)} = 1.27 \left(1.83 Fr_{m2} - Fr_{mc} \right) \cdot y_{m1} \geq 0 \qquad \text{for } L_2 \big/ L_1 < 0.5$$

$$y_{s(Cont)} = 0.94 \left(1.83 Fr_{m2} - Fr_{mc} \right) \cdot y_{m1} \geq 0 \qquad \text{for } L_2 \big/ L_1 \geq 0.5$$

   - Total pier scour

     Thus the total pier scour depth is:

$$y_{s(Pier\_total)} = y_{s(Cont)} + y_{s(Pier)} \tag{9.9}$$

- Abutment scour:

$$y_{s(Abut)} = K_1 \cdot K_2 \cdot K_L \cdot K_p \cdot 6.5 \cdot \left(1.57 \cdot Fr_{f2} - Fr_{fc}\right)^{0.7} \cdot y_{f1} \geq 0$$

3. Time history of the bridge scour (cited from Kwak, 2000)

The maximum shear stress τ_{max} around the bridge structures and the corresponding initial erosion rate $\dot{z}_i$ is obtained from the erosion function (measured in the EFA), the maximum scour depth due to contraction scour and pier scour is calculated from equation (9.9), and the maximum abutment scour is calculated from equation (9.8). With these $\dot{z}_i$ and y_s defining the tangent to the origin and the asymptotic value of the scour depth versus time curve, a hyperbola is defined to describe the entire curve.

$$y_s(t) = \frac{t}{\frac{1}{\dot{z}_i} + \frac{t}{y_s}} \tag{9.10}$$

where $y_s(t)$ is the scour depth due to a flood, t is the flood duration, $\dot{z}_i$ is the initial erosion rate, y_s is the maximum scour depth due to the flood (equation (9.8) or equation (9.9)). In the case of a complete hydrograph and of a multi-layer soil system, the accumulation algorithms are as follows.

(1) Multi-flood system (cited from Kwak, 2000)

The hydrograph of a river indicates how the velocity varies with time. The fundamental basis of the accumulation algorithms is that the velocity histogram is a step function with a constant velocity value for each time step. When this time step is taken as one day, the gauge station value is constant for that day because only daily records are

kept. The case of a sequence of two different constant velocity floods scouring a uniform soil is considered (Figure 9.8). Flood 1 has velocity V_1 and lasts a time t_1 while flood 2 has a velocity V_2 and lasts a time t_2. After flood 1, a scour depth $y_{s1}(t)$ is reached at time t_1 (Point A on Figure 9.8 (b)) and can be calculated as follows:

$$y_{s1}(t) = \frac{t_1}{\dfrac{1}{\dot{z}_{i1}} + \dfrac{t_1}{y_{s1}}} \tag{9.11}$$

For flood 2, the scour depth will be:

$$y_{s2}(t) = \frac{t_2}{\dfrac{1}{\dot{z}_{i2}} + \dfrac{t_2}{y_{s2}}} \tag{9.12}$$

The scour depth $y_{s1}(t)$ also could have been created by flood 2 in a time t_e (Point B on Figure 9.8 (c)). The time t_e is called the equivalent time. The time t_e can be obtained by using Equations (9.11) and (9.12) with $y_{s2}(t) = y_{s1}(t)$ and $t_2 = t_e$.

$$t_e = \frac{t_1}{\dfrac{\dot{z}_{i2}}{\dot{z}_{i1}} + t_1 \dot{z}_{i2} \left(\dfrac{1}{y_{s1}} - \dfrac{1}{y_{s2}} \right)} \tag{9.13}$$

When flood 2 starts, even though the scour depth $y_{s1}(t)$ was due to flood 1 over a time t_1, the situation is equivalent to having had flood 2 for a time t_e. Therefore when flood 2 starts, the scour depth versus time curve proceeds from point B on Figure 9.8 (c) until point C after a time t_2. The y_s versus t curve for the sequence of flood 1 and 2 follows the path OA on the curve for flood 1 then switches to BC on the curve for flood 2. This is shown as the curve OAC on Figure 9.8 (d).

The procedure described above is for the case of a velocity V_1 followed by a velocity V_2 higher than V_1. In the opposite case, where V_2 is less than V_1, flood 1 creates a scour depth $y_{s1}(t)$. This depth is compared with y_{s2} due to flood 2. If $y_{s1}(t)$ is larger than y_{s2}, it means that when flood 2 starts the scour hole is already larger than the whole the maximum scour depth that flood 2 can be create. Hence, flood 2 cannot create any additional scour and the scour depth versus time curve remains flat during flood 2. If $y_{s1}(t)$ is less than y_{s2}, the procedure of Figure 9.8 (d) should be followed.

In the general case, the complete velocity hydrograph is divided into a series of partial flood events, each lasting Δt. The scour depth due to floods 1 and 2 in the hydrograph will be handled by following the procedure of Figure 9.8 (d). At this point the situation is reduced to a single flood 2 which lasts t_{e2}. Then the process will consider flood 3 as a new "flood 2" and will repeat the procedure of Figure 9.8 (d) applied to flood 2 lasting t_{e2} and flood 3. Therefore the process advances with only two floods to be considered: the previous flood with its equivalent time and the new "flood 2". The time step Δt is typically one day and the velocity hydrograph can be 70 years long.
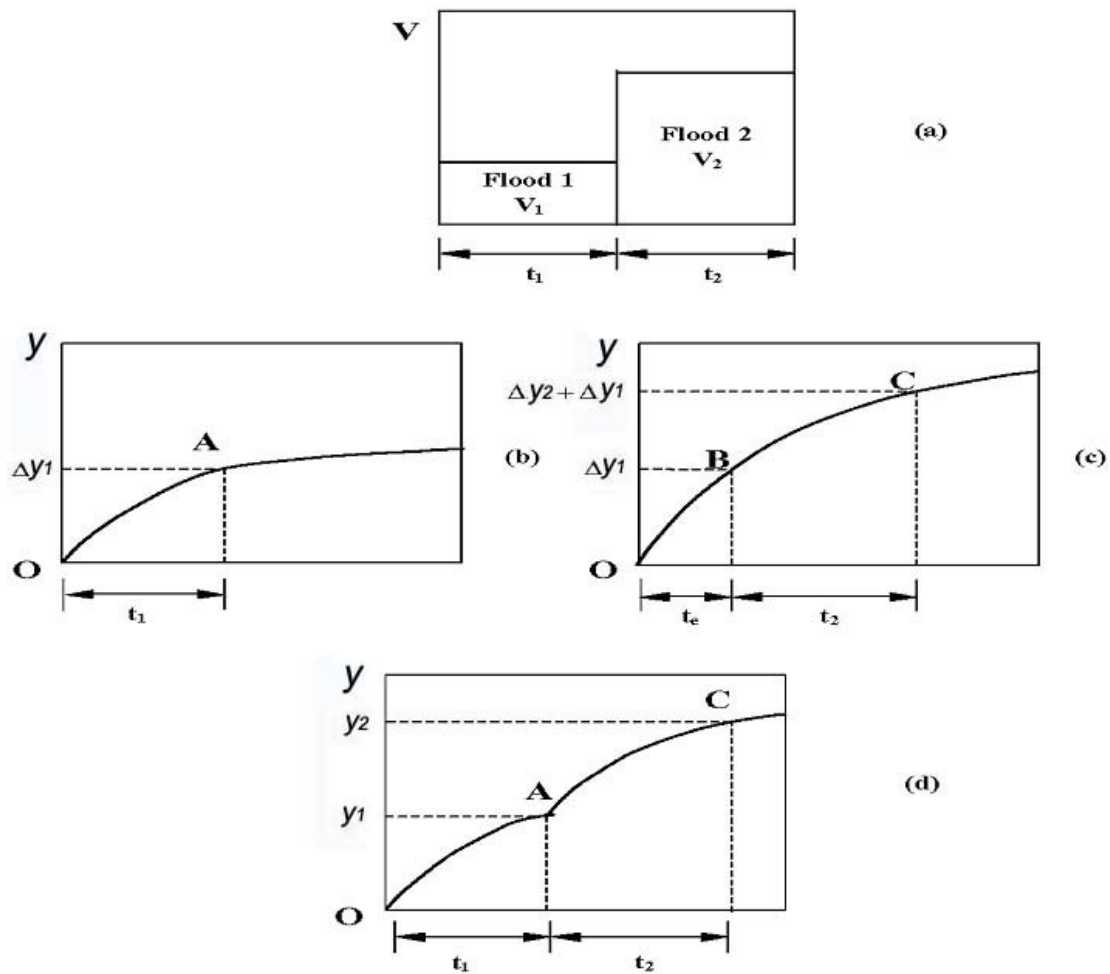
Figure 9.8. Scour due to a sequence of two flood events.

(2) Multi-layer system (cited from Kwak, 2000)

In the multi-flood system analysis, the soil is assumed to be uniform. In reality, the soil involves different layers and the layer characteristics can vary significantly with depth. It is necessary to have an accumulation process which can handle the case of a multi-layer system. Consider the case of a first layer with a thickness equal to Δy_1 and a second layer with a thickness equal to Δy_2. The river bed is subjected to a constant

velocity V (Figure 9.9 (a)). The scour depth $y_s(t)$ versus time t curves for layer 1 and layer 2 are given by equations (9.11) and (9.12) (Figure 9.9 (b), Figure 9.9 (c)). If the thickness of Layer 1 Δy_1 is larger than the maximum scour depth y_{s1}, given by equation (9.8) or (9.9), then the scour process only involves Layer 1. This case is the case of a uniform soil. On the other hand, if the maximum scour depth y_{s1} exceeds the thickness Δy_1, then layer 2 will also be involved in the scour process. In this case, the scour depth Δy_1 (point A on Figure 9.9 (b)) in layer 1 is reached after a time t_1; at that time, the situation is equivalent to having had layer 2 scoured over an equivalent time t_e (point B on Figure 9.9 (c)). Therefore when layer 2 starts to be eroded, the scour depth versus time curve proceeds from point B to point C on Figure 9.9 (c). The combined scour process for the two-layer system corresponds to the path OAC on Figure 9.9 (d).

In reality, there may be a series of soil layers with different erosion functions. The computations proceed by stepping forward in time. The time steps are Δt long, the velocity is the one for the corresponding flood event, and the erosion function ($\dot{z}$ vs τ) is the one for the soil layer corresponding to the current scour depth (bottom of the scour hole). When Δt is such that the scour depth enters a new soil layer, the computations follow the process described in Figure 9.9 (d).
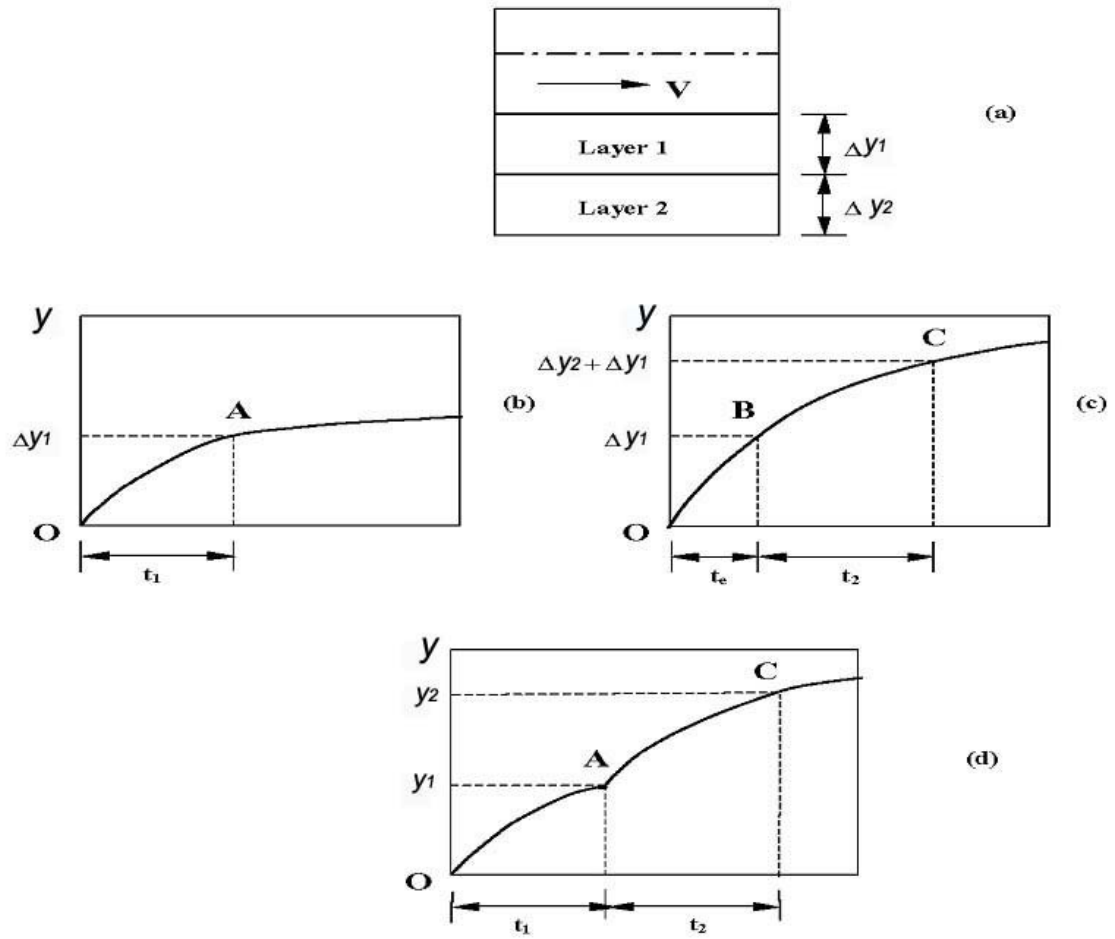
Figure 9.9. Scour of a two-layer soil system

9.5   Output of the SRICOS-EFA program

Once the SRICOS-EFA program finishes all calculations successfully, the output file is automatically created. The output file includes the following columns: time, flow velocity, water depth, shear stress, maximum scour depth (abutment, pier, contraction, or total pier), and instantaneous scour depth (abutment, pier, contraction, or total pier). The format of the output file is a text file, and the output can be plot as Figure 9.10.
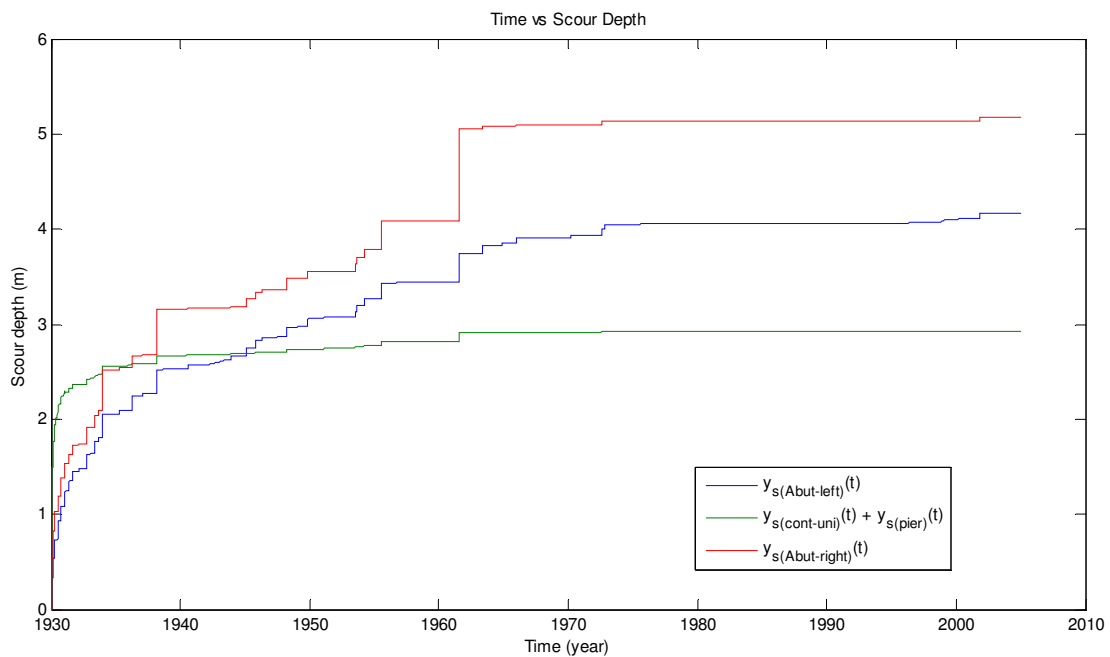
Figure 9.10. Example of plots generated from SRICOS-EFA program output

CHAPTER X

CONCLUSIONS AND RECOMMENDATIONS

10.1 Conclusions

Bridge scour is the main cause of bridge failures in United States. Many methods to predict scour depths have been developed, but those methods are developed for cohesionless soils. Those equations yield very conservative scour depths when applied to cohesive soils. In order to make the reasonable prediction for cohesive soil, the extensive studies have been done in Texas A&M University since 1997.

Flume test results for pier scour, contraction scour, and abutment scour have been conducted in Texas A&M University since 1997 are analyzed in this study. The followings are the main conclusions obtained from present study.

1. By comparing the pattern of the flow and the scour hole, the maximum local scour developed where the maximum turbulence was measured; while the maximum contraction scour happened where the maximum streamwise velocity was measured.

2. The complex pier scour equation is developed using the difference between the approach Froude number and critical Froude number, and those numbers are based on the pier width.

3. If the water depth is deeper than 1.43 times of pier width, the scour depth is independent on the water depth. On the contrary, if the water depth is shallower than 1.43 times of pier width, the water depth effect is found.

4. The narrower gap between adjacent piers makes the deeper scour hole around the pier, and this effect becomes negligible when the gap is larger than 3.2 times of pier width.

5. The scour hole around a rectangular pier is 10 % deeper than the hole around a circular pier when the rectangular pier is aligned parallel to flow, and there is no effect of the aspect ratio of pier at this flow condition.

6. If the rectangular pier is skewed to the flow, the pier nose shape and the pier width vary with skew angle. The skewed rectangular pier makes the smoother transition, and the effect of pier shape becomes negligible. However, the projected pier width varies with the skew angle and the aspect ratio. Replacing the pier width with the projected width, the normalized scour depth makes good agreement with the prediction for the circular pier.

7. The equation for the complex pier scour is made by superposing the correction factors, and agrees well to the flume test results of the complexly installed pier. The prediction is conservative when it is applied to Froehlich's database (1988), and Muller and Landers' database (1996), but it yields less conservative scour depths than the HEC-18 method.

8. Both the maximum contraction scour equation and the uniform contraction scour equation applicable to compound channel are developed on the basis on the flume tests. The contraction ratio defined with discharge ratio is used to get the average velocity at the contracted section. The contraction scour depth is the function of the difference between the Froude number at the contracted section and the critical

Froude number. The uniform contraction scour is 26 % shallower than the maximum contraction scour.

9. It is found that the effects of the contraction length, the transition angle, and the shape of abutment are not clear and negligible to both the maximum contraction scour and the uniform contraction scour.

10. Although the equations to predict the maximum contraction scour and the uniform scour are developed for the cohesive soils, these equations can be used to the cohesionless soils because the equations are function of the critical shear stress. The scour depths predicted by the uniform contraction scour equation agree well with Gill's flume test results (1981).

11. The abutment is assumed as a half of wide pier, and the equation to predict the abutment scour depth is developed. The scour depth is the function of the difference between the Froude number and the critical Froude number, and the form of equation of abutment scour is very similar to that of pier scour.

12. The spill-through abutment with smooth transition makes less turbulent flow than the wing-wall abutment, and the maximum local scour depth of the spill-through abutment is 22 % shallower than that of the wing-wall abutment.

13. The skewed spill-through abutment decreases the turbulence level with smoother transition. The abutment skewed to downstream makes the same trend with previous studies, while the abutment skewed to upstream makes the opposite trend with previous researches. The opposite trend may result from use of a different type of abutment. The vertical walls were used in previous research to find the effect of

abutment alignment, while the smooth spill-thorough abutment is used in present study.

14. When the abutment is very close to the main channel slope, the measured scour depth is much deeper than that of other conditions.

15. Compared to other flume test results of the abutment scour, the equation yields shallower scour than Sturm's, and deeper scour than Froehlich's. Comparisons with previous equations are performed to evaluate the abutment scour equation developed in this study with the imaginary test conditions. Melville's (1992) and Sturm's (2004) equations make more conservative results than present study. The present study makes more conservative results than Chang and Davis's (2007) equation. In addition, the present equation makes reasonable match with HEC-18 method and Gill's (1972) method.

10.2 Recommendations for future research

Much of this study is composed of the analysis of flume test results obtained from many flume tests at Texas A&M University since 1997. All flume tests were performed in the simplified test conditions, but engineers will meet more complicate conditions when new methods are applied to the real channels. The followings are recommended for the universal application.

1. Flume tests for pier scour should be conducted with more complicated channel geometries, because the tests were conducted in rectangular channels.

2. For abutment scour, field measurements of local velocity and scour depth for long setback condition should be conducted. Although the rectangular channel in flume

tests is regarded as the long setback, the effect of contraction is not ignorable in lab scale tests.

3. More comparisons with flume the velocity measurements and HEC-RAS results should be preformed to find a method to match HEC-RAS results and measurement results. Because the number of comparison between HEC-RAS results and measurement is not enough to explain all conditions engineers may meet.

4. The method to predict the maximum abutment scour depth should be developed more, because the prediction yields very conservative scour depth when the method is applied to field data.

REFERENCES

Abdou, M. I. (1993). "Effect of sediment gradation and coarse material fraction on clear water scour round bridge piers." Ph. D. dissertation, Colorado State University, Fort Collins, CO.

Annandale, G. W. (1995). "Erodibility." *J. Hydr. Res.*, 33(4), 471-494.

Benedict et al. (2006). "Trends of abutment-scour prediction equations applied to 144 fields sites in south Carolina" *Open-File Rep. 2003-295*, U.S. Geology Survey, Washington, DC.

Briaud, J.-L., Ting, F., Chen, H.C., Gudavalli, S.R., Perugu, S., and Wei, G. (1999 (b)). "SRICOS: Prediction of scour rate in cohesive soils at bridge piers." *J. Geotech. Eng.*, ASCE, 125, 237-246.

Briaud, J.-L., Ting, F., Chen, H.C., Cao, Y., Han, S.-W., Kwak, K. (2001 (a)). "Erosion function apparatus for scour rate predictions." *J. Geotech. Geoenviron. Eng.*, ASCE, 127(2), 105-113.

Briaud, J. L., Chen, H. C., Kwak K., Han S-W., Ting F. (2001 (b)). "Multiflood and multilayer method for scour rate prediction at bridge piers." *J. Geotech. Geoenviron. Eng.*, ASCE, 127(2), 105-113.

Briaud, J.-L., Chen, H.-C., Li, Y., Nurtjahyo, P., Wang, J. (2003). "Complex pier scour and contraction scour in cohesive soils." *NCHRP Rep. No. 24-15*, Trans. Res. Board Nat. Res. Council, Washington, DC.

Briaud, J.-L. (2008). "Case histories in soil and rock erosion - Woodrow Wilson Bridge,

Brazos River meander, Normandy cliffs, and New Orleans levees." *The 9th Ralph B. Peck Lecture*, Denver, CO.

Briaud, J.-L., Ting, F., Chen, H.-C., Gudavalli, R., Kwak, K., Philogene, B., Han, S.-W., Perugu, S., Wei, G. S., Nurtjahyo, P., Cao, Y. W., and Li, Y. (1999 (a)). "SRICOS: Prediction of scour rate at bridge piers." *TTI Rep. No. 2937-1*, Texas A&M University, College Station, TX.

Chabert, J., and Engeldinger, P. (1956). "Etude des affouillements autour des piles des ponts." *Laboratoire d` Hydraulique*, Chatou, France.

Chang, F., and Davis, S. (1999 (a)). "Maryland SHA procedure for estimating scour at bridge abutments, part 1 - live bed scour.", *Stream stability and scour at highway bridges, Compend. papers ASCE water resources eng. conf. 1991 to 1998*, E.V. Richardson and P.F. Lagasse, eds., ASCE, Reston, VA, 401-411.

Chang, F., and Davis, S. (1999 (b)). "Maryland SHA procedure for estimating scour at bridge abutments, part 2 - clear water scour." *Stream stability and scour at highway bridges, Compend. papers ASCE water resources eng. conf. 1991 to 1998*, E.V. Richardson and P.F. Lagasse, eds., ASCE, Reston, VA, 412-416.

Chang, F., and Davis, S. (2007). "Maryland state highway administration office of bridge development." *ABSCOUR program*, <http://www.gishydro.umd.edu/ sha_soft.htm> (Jun. 18, 2008).

Chee, R. K. W. (1982). "Live-bed scour at bridge piers." *Rep. No. 290*, University of Auckland, School of Eng., Auckland, New Zealand.

Chen, X. (2008). "Numerical study of abutment scour in cohesive soils," Ph.D.

Dissertation, Texas A&M University, College Station, TX.

Chiew, Y. M. (1984). "Local scour at bridge piers." *Rep. No. 355*, University of Auckland, School of Eng., Auckland, New Zealand.

Davoren, A. (1985). "Local scour around a cylindrical pier." *Publication, No. 3,* Hydrology Centre, Christchurch, New Zealand.

Dongol, D. M. S. (1994). "Local scour at bridge Abutments." *Rep. No. 544*, School of Eng., University of Auckland, Auckland, New Zealand.

Ettema, R. (1980). "Scour at bridge piers." *Rep. No. 216*, Dep. of Civil Eng., University of Auckland, Auckland, New Zealand.

Ettema, R., Nakato, T., and Muste, M. (2008). "Estimation of scour depth at bridge abutment." *NCHRP Rep. No. 24-20*, Trans. Res. Board, Washington, DC.

Flaxman, E. M. (1963). "Channel stability in undisturbed cohesive soils." *J. Hydr. Div.*, ASCE 89 (HY2), 89-96.

Froehlich, D. C. (1988). "Analysis of onsite measurement of scour at piers." *Proc. of ASCE Nat. Hydraulic Eng. Conf.,* Colorado Springs, CO.

Froehlich, D. C. (1989). "Local scour at bridge Abutment." *Proc. of Nat. Conf. on Hydraulic Eng.*, New York, 13-18.

Garde, R. J., Subramanya, K., and Nambudripad, K. D. (1961). "Study of scour around spur-dikes." *J. Hydr. Div.*, 87(HY 6), 23-37.

Gill, M. A. (1972). "Erosion of sand beds around spur dikes." *J. Hydr. Div.*, 98(HY9), 1587 - 1602.

Gill, M. A. (1981). "Bed erosion in rectangular long contraction." *J. Hydr. Div.*,

107(HY3), 273 - 284.

Gudavalli, S. R. (1997). "Prediction model for scour rate around bridge piers in cohesive soils on the basis of flume tests," Ph.D. Dissertation, Texas A&M Uninversity, College Station, TX.

Hosny, H. M. (1995). "Experimental study of local scour around circular bridge piers in cohesive soils," Ph.D. Dissertation, Colorado State University, Fort Collins, CO.

Ivarson, W. R. (1999). "Scour and erosion in clay soils." *Stream stability and scour at highway bridges, Compend. papers ASCE water resources eng. conf. 1991 to 1998*, E.V. Richardson and P.F. Lagasse, eds., ASCE, Reston, VA, 104 -119.

Jain, S. C., and Fischer, E. E. (1980). "Scour around bridge piers at high flow velocities." *J. Hydr. Div.*, 106(11), 1827-1842.

Kirsten, H. A. D. (1982). "A classification system for excavation in natural materials." *Civil Engineer in South Africa*, 24, 293-308.

Komura, S. (1966). "Equilibrium depth of scour in long constrictions." *J. Hydr. Div.*, 92(HY5), 17-38.

Kouchakzadeh, S., and Townsend, R. D. (1997). "Maximum scour depth at bridge abutment terminating in the floodplain zones." *Canadian J. Civil Eng.*, 24(6), 996-1006.

Kwak, K. (2000). "Prediction of scour depth versus time for bridge piers in cohesive soils in the case of multi-flood and layered soil systems," Ph.D. Dissertation, Texas A&M University, College Station, TX.

Larras, J. (1963). "Profondeures maximales d'erosion des fonds mobiles autour des piles

de ponts." *Proc., 14th LAHR Congress*, Paris, France, 299-313.

Laursen, E. M. (1958). "The total sediment load of streams." *J. Hydr. Div.*, 84(1530), 1-36.

Laursen, E. M. (1960). "Scour at bridge crossings." *J. Hydr. Div.*, 86(HY 2), 39-54.

Laursen, E. M. (1963). "An analysis of relief bridge scour." *J. Hydr. Div.*, 89(HY3), 93-118.

Laursen, E. M., and Toch, A. (1956). "Scour around bridge piers and abutments." *Bulletin No. 4*, Iowa Highway Res. Board, Ames, IA.

Li, Y. (2002). "Bridge pier scour and contraction scour in cohesive soils on the basis of flume tests." Ph. D. Dissertation, Texas A&M University, College Station, TX.

Lim, S.-Y. (1997). "Equilibrium clear-water scour around an abutment." *J. Hydr. Eng.*, 123(3), 237-243.

Lim, S.-Y., and Cheng, N.-S. (1998 (a)). "Scouring in long contractions." *J. Irrig. Drain. Eng.*, 124(5), 258-261.

Lim, S. Y., and Cheng, N. S. (1998 (b)). "Prediction of live-bed scour at bridge abutments." *J. Hydr. Eng.*, 124(6), 635-638.

Melville, B. W. (1975). "Local scour at bridge site." *Rep. No. 117*, School of Eng., The University of Auckland, Auckland, New Zealand.

Melville, B. W. (1992). "Local scour at bridge abutment." *J. Hydr. Eng.*, 118(4), 615-631.

Melville, B. W. (1995). "Bridge abutment scour in compound channels." *J. Hydr. Eng.*, 121(12), 863-868.

Melville, B. W. (1997). "Pier and abutment scour: Integrated approach." *J. Hydr. Div.*, 123(2), 125-136.

Melville, B. W., and Coleman, S. E. (2000). "Bridge scour." *Water Resources Publications*, LLC, Highlands Ranch, CO.

Melville, B. W., and Sutherland, A. J. (1988). "Design method for local scour at bridge piers." *J. Hydr. Eng.*, 114(10), 1210-1226.

Molinas, A., Jones, S., and Hosny, M. (1999). "Effect of cohesive material properties on local scour around piers." *Trans. Res. Board*, 78th Annual Meeting, Washington, DC, 164-174.

Muller, D. S., and Landers, M. (1996). "Channel scour at bridges in the United States." *Fed. Highway Admin.*, McLean, VA.

Neill, C. R. (1973). "Guide to bridge hydraulics." *Roads and Trans. Assoc. of Canada by University of Toronto Press*, Toronto and Buffalo, Canada.

Nurtjahyo. (2003). "Chimera RNAS simulations of pier scour and contraction scour in cohesive soils." Ph.D. Dissertation, Texas A&M University, College Station, TX.

Palaviccini, M. (1993). "Scour Predictor Model at Bridge Abutments." Ph.D. Dissertation, Catholic University of America, Washington, DC.

Rajaratnam, M., and Nwachukwu, B. A. (1983). "Flow near groin-like structure." *J. Hydr. Div.*, 109(3), 463-480.

Rana, M. Y. (1986). "Flume experiments on sediment bed in steady non-uniform flow," M.E. Thesis, Asian Institute of Technology, Bangkok, Thailand.

Richardson, E. V., Davis, S. M. (1995). "Evaluating scour at bridges." *No. FWHA-IP-*

90-017, HEC No.18, U.S. Dep. of Trans., Washington, DC.

Richardson, E. V., Simons, D. B., and Lagasse, P. F. (2001). "River engineering for highway encroachments - highways in the river environment." *FHWA NHI 01-004*, Federal Highway Administration, Hydraulic series No. 6, Washington, DC.

Shen, H. W., Schneider, V. R., and Karaki, S. S. (1966). "Mechanics of local scour." *Rep. No. CER66-67HWS27*, Data Supplement, Prepared for Bureau of Public Roads, Office of Research and Development, Civil Eng. Dep., Colorado State University, Fort Collins, CO.

Shirole, A.M., and Holt, R.C. (1991). "Planning for a comprehensive bridge safety assurance program." *Trans. Res. Record 1290*, Trans. Res. Board of the Nat. Academies, Washington, DC, 39-50.

Straub, L. G. (1934). "Effect of channel contraction works upon regime of movable bed streams." *American Geophysical Union*, Transactions of the 15th annual meeting, Part II, Washington, DC, 454-463.

Straub, L. G. (1940). "Approaches to the study of the mechanics of bed movement." *Proc., 1st Hydraulics Conf. of Iowa Studies in Eng.*, Iowa City, IA.

Sturm, T. W. (2004). "Enhanced abutment scour studies for compound channels." *Rep. No. FHWA-RD-99-156*, Georgia Institute of Technology, School of Civil and Environmental Engineering, Atlanta, GA.

Sturm, T. W., and Janjua, N. S. (1994). "Clear-water scour around abutments in floodplains." *J. Hydr. Eng.*, 120(8), 956-972.

Sturm, T. W. (1999). "Abutment scour in compound channels." *Stream stability and*

scour at highway bridges, Compend. papers ASCE water resources eng. conf. 1991 to 1998, E.V. Richardson and P.F. Lagasse, eds., ASCE, Reston, VA, 443-456.

Tison, L. J. (1940). "Erosion autour des piles de ponts en riviere." *Annales des Travaux publics de Belgique*, 41(6), 813-817.

Tison, L. J. (1961). "Local scour in rivers." *J. Geoph. Res.*, 66(12), 4227 - 4232.

Venkatadri, G., Rao, G. M., Hussain, S. T., and Asthana, K. C. (1965). "Scour around bridge piers and abutments." *Irrigation Power*, 22(1), 35-42.

Wei, G., Chen, H. C., Ting, F., Briaud, J.-L., Gudavalli, S. R., and Perugu, S. (1997). "Numerical simulation to study scour rate in cohesive soils." *Res. Rep. to the Texas Dep. of Trans.*, Dep. of Civil Engineering, Texas A&M University, College Station, TX.

Yakoub, N. G. R. (1995). "Effect of cohesion on bridge abutment scour," Ph. D. Dissertation, Colorado State University, Fort Collins, CO.

APPENDIX A

DISTRIBUTION OF VELOCITY AND TURBULENCE INTENSITY
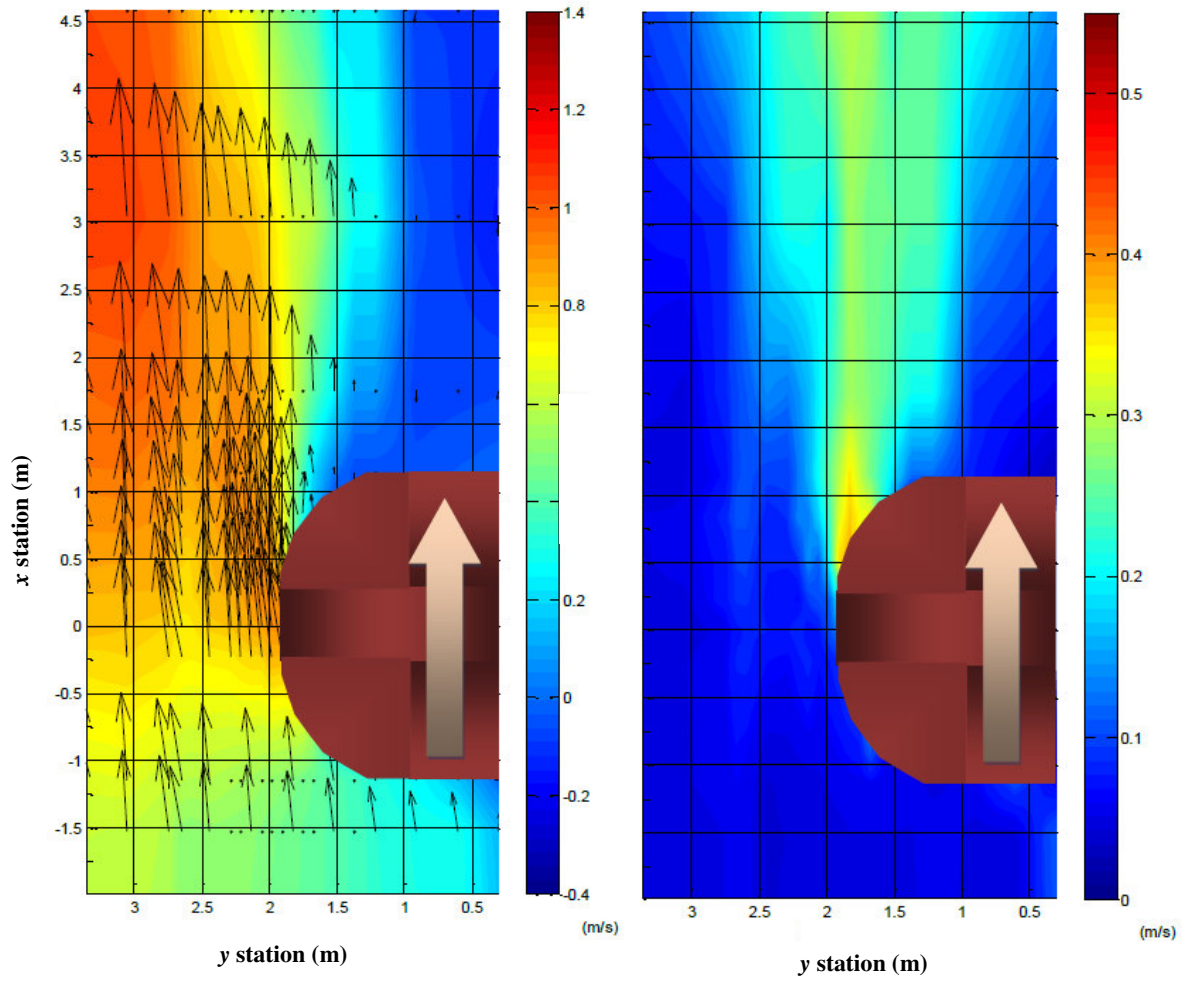
(a) Time average velocity (initial)   (b) Turbulence intensity (initial)

Figure A.1. Case 1II

(c) Time average velocity
(after 124hour run)

(d) Turbulence intensity
(after 124hour run)

Figure A.1. (continued)

(e) Time average velocity
(after 296hour run)

(f) Turbulence intensity
(after 296hour run)
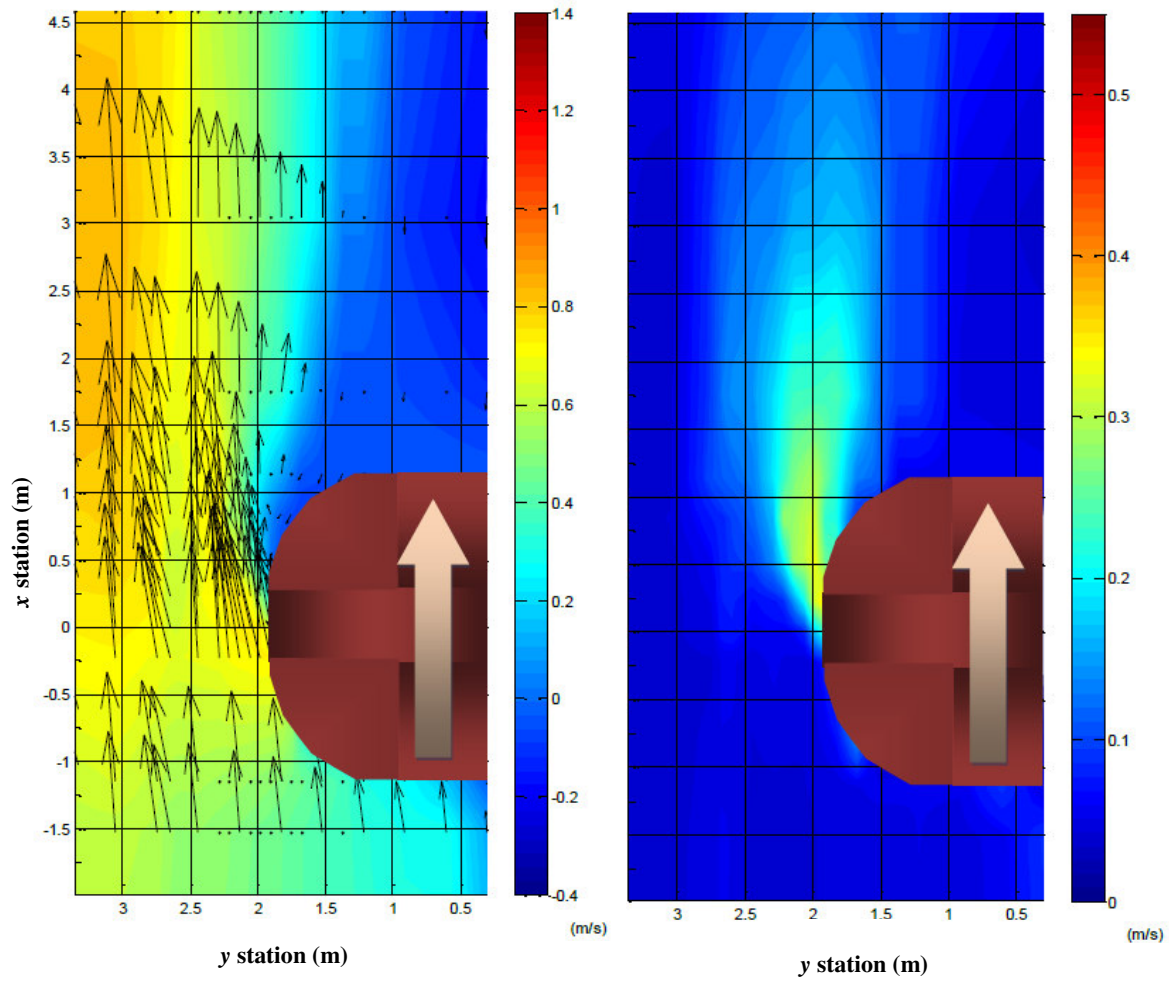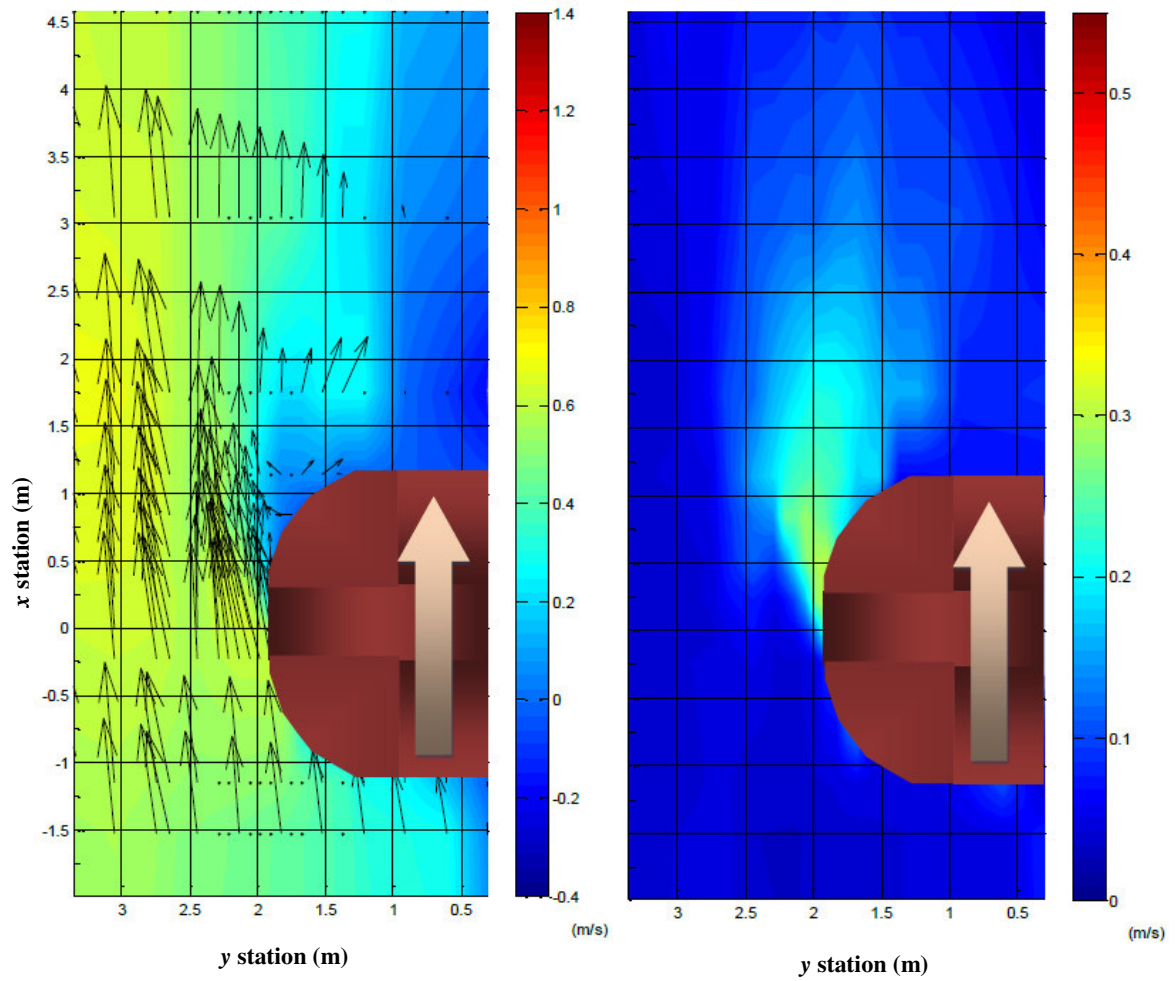
Figure A.1. (continued)
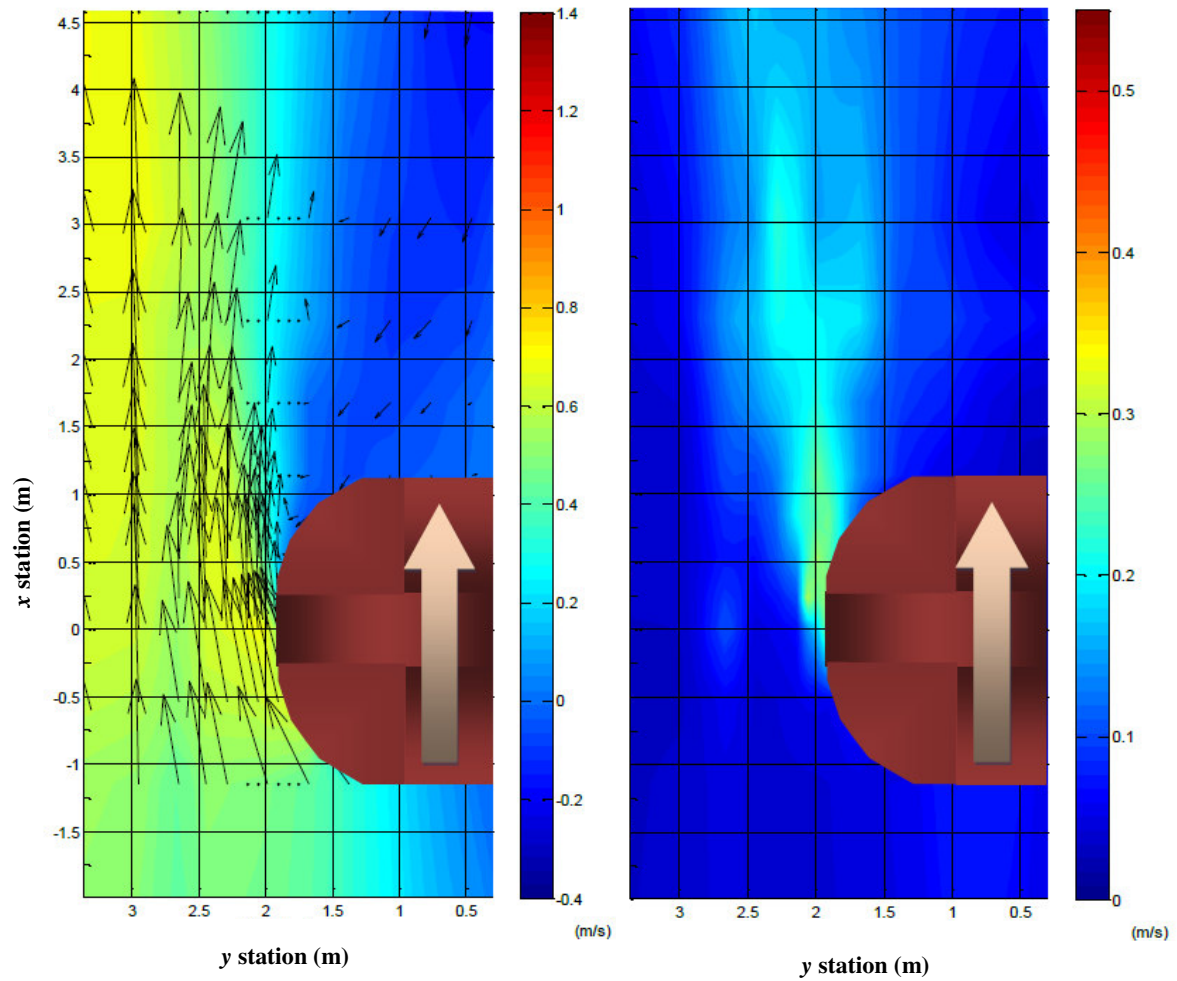
(a) Time average velocity
(initial)

(b) Turbulence intensity
(initial)

Figure A.2. Case 2
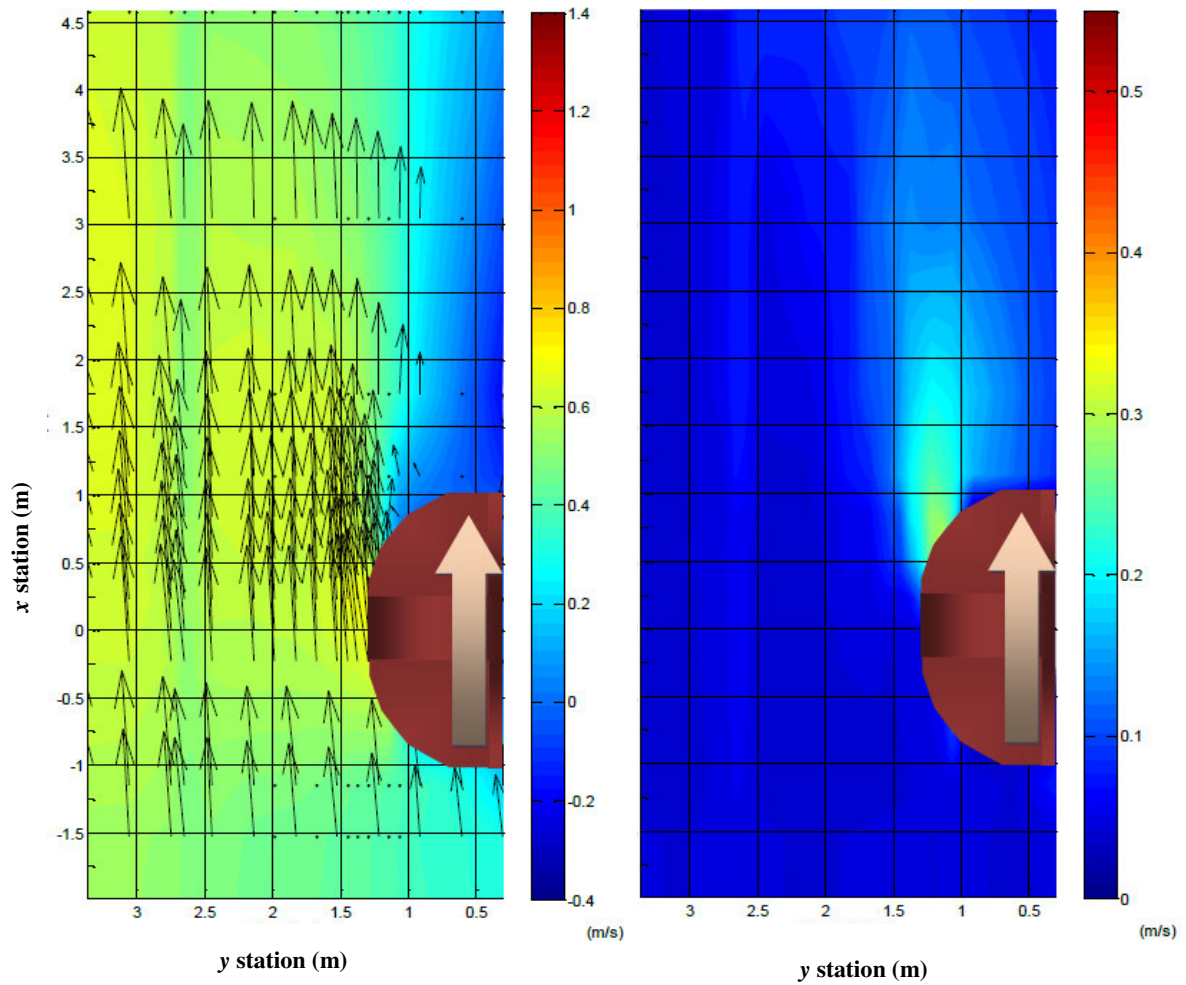
(a) Time average velocity
(initial)

(b) Turbulence intensity
(initial)

Figure A.3. Case 6

(c) Time average velocity
(after 120 hour run)

(d) Turbulence intensity
(after 120 hour run)

Figure A.3. (continued)
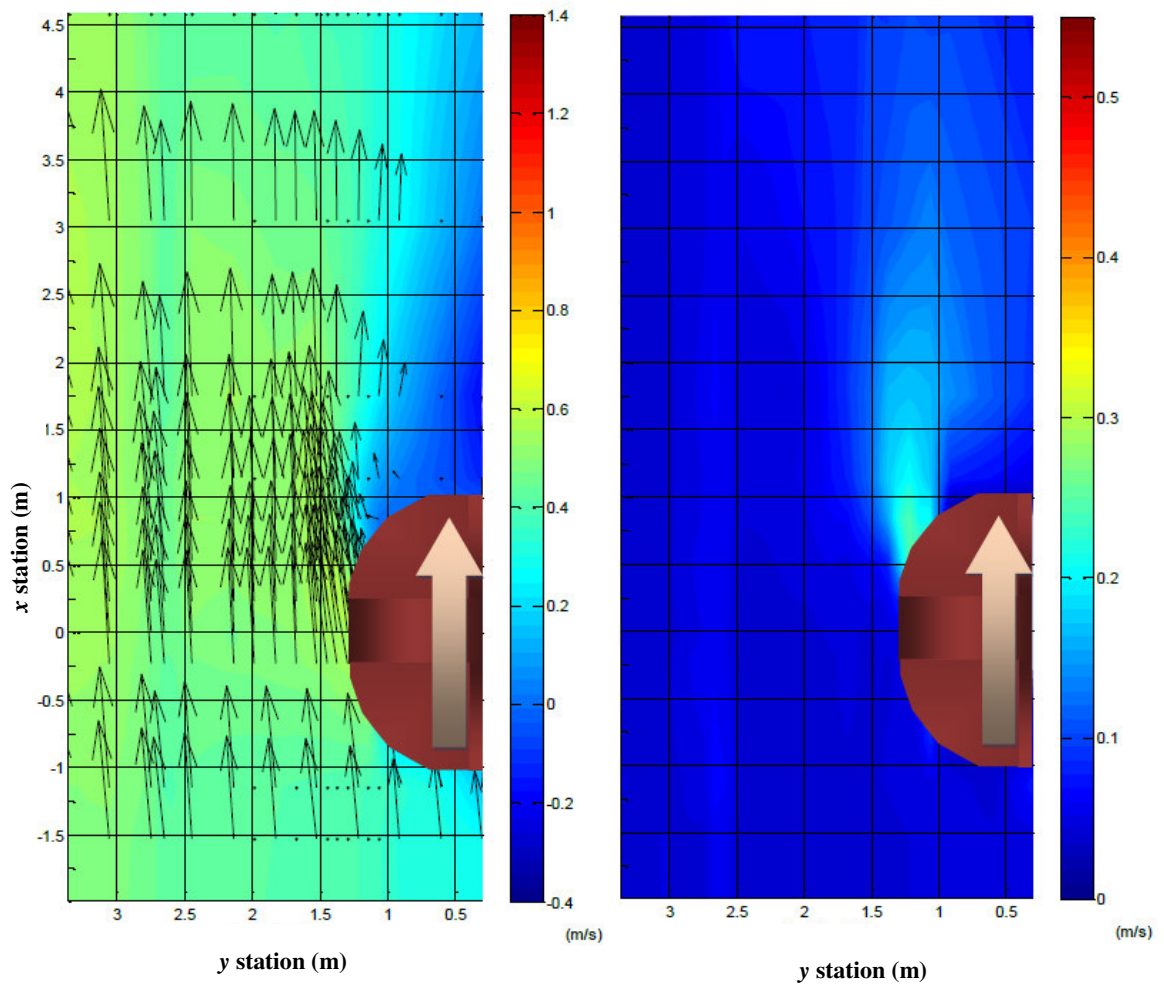
(e) Time average velocity
(after 297 hour run)

(f) Turbulence intensity
(after 297 hour run)

Figure A.3. (continued)
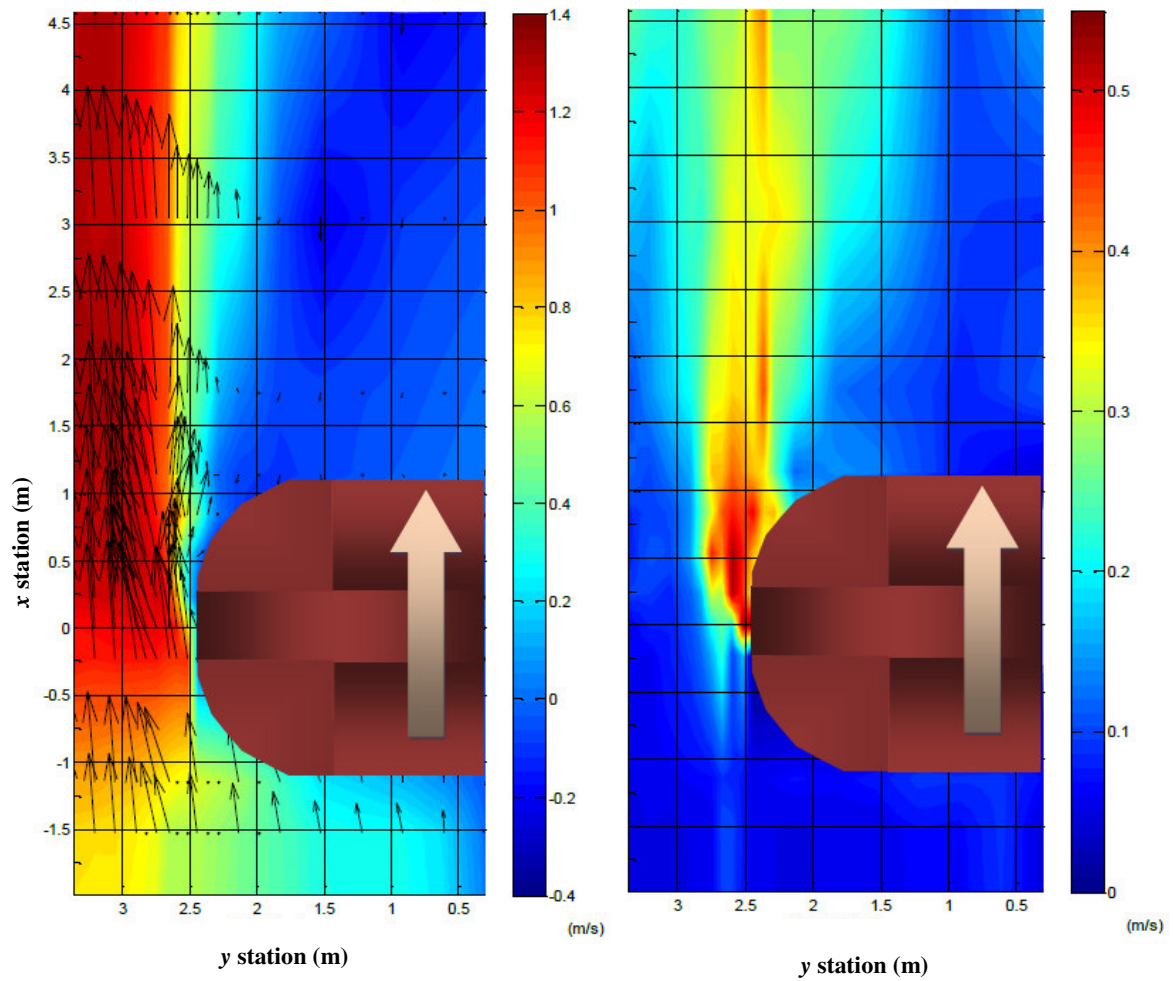
(a) Time average velocity
(initial)

(b) Turbulence intensity
(initial)

Figure A.4. Case 7
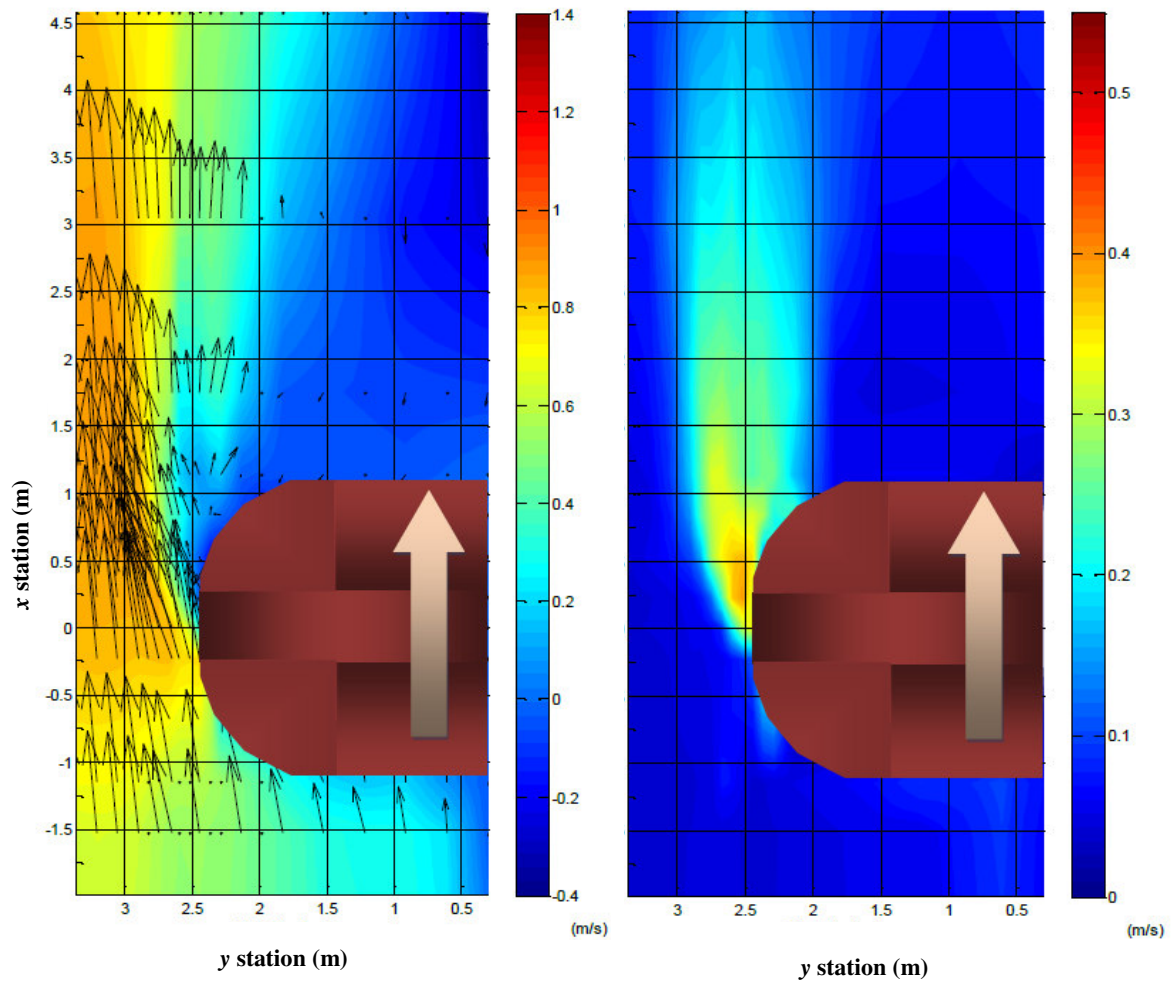
(c) Time average velocity
(after 120 hour run)

(d) Turbulence intensity
(after 120 hour run)

Figure A.4. (continued)

(e) Time average velocity
(After 253 hour run)

(f) Turbulence intensity
(After 253 hour run)

Figure A.4. (continued)

(a) Time average velocity
(initial)
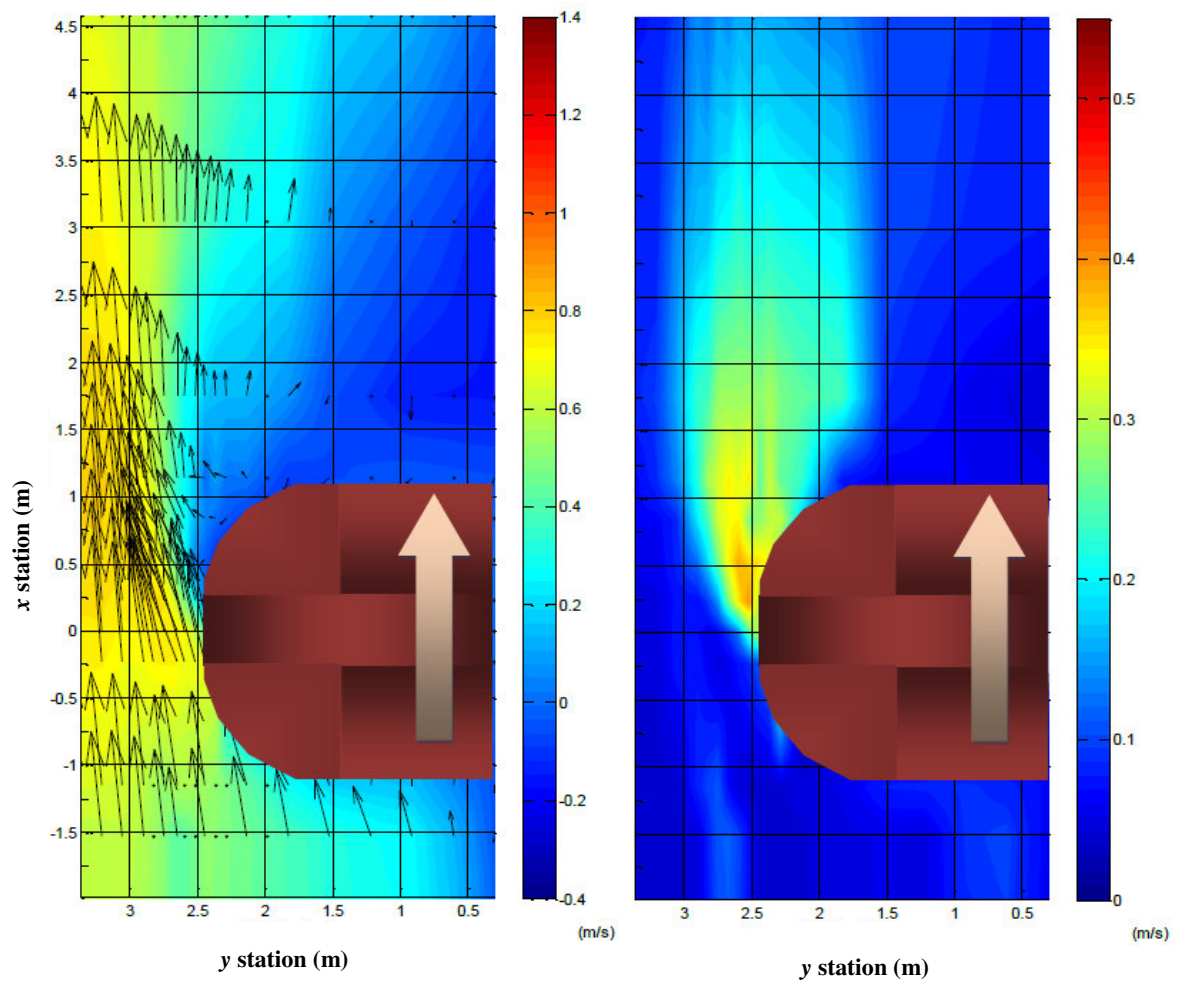
(b) Turbulence intensity
(initial)
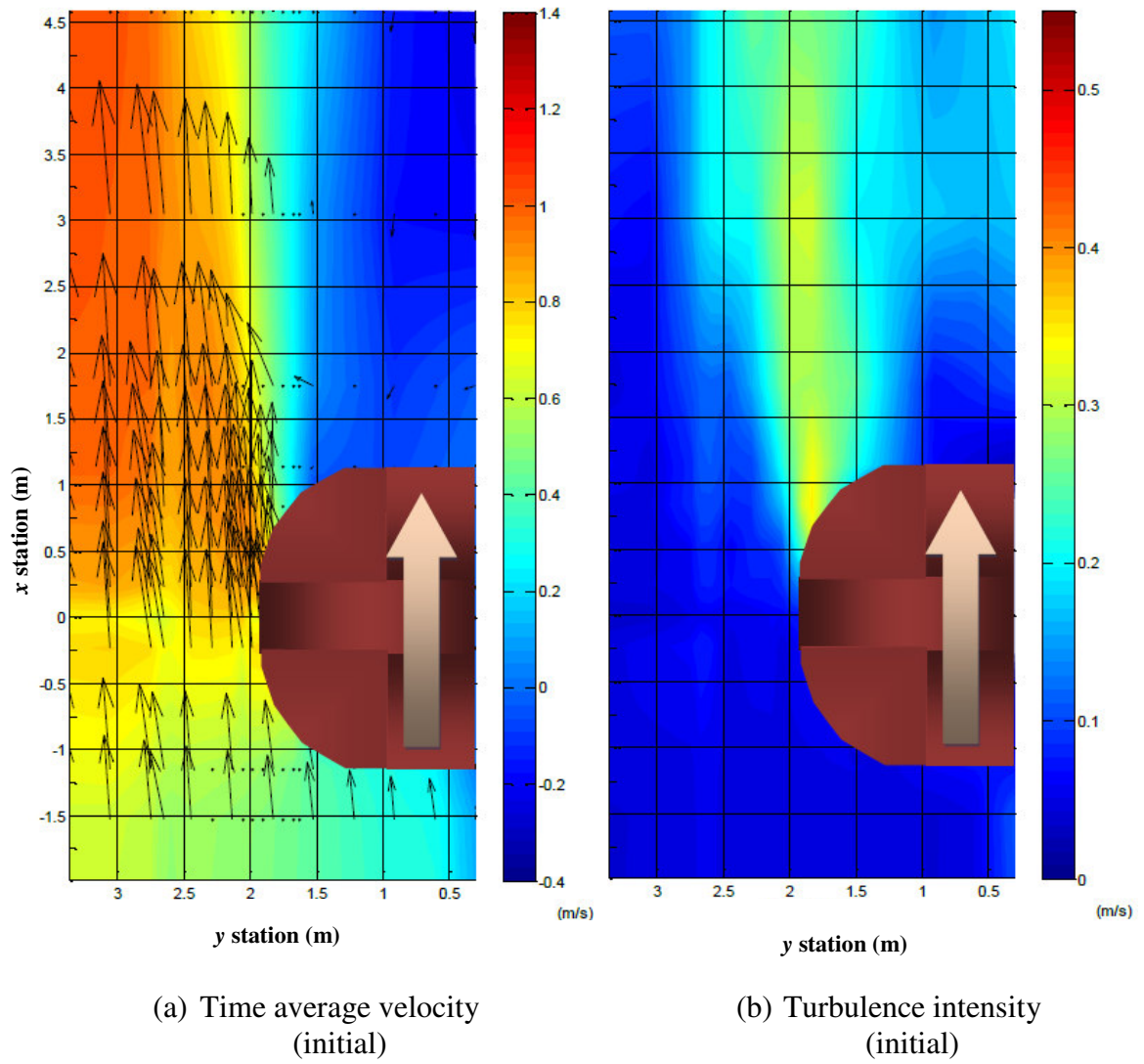
Figure A.5. Case 8

(c) Time average velocity
(after 123 hour run)

(d) Turbulence intensity
(after 123 hour run)

Figure A.5. (continued)
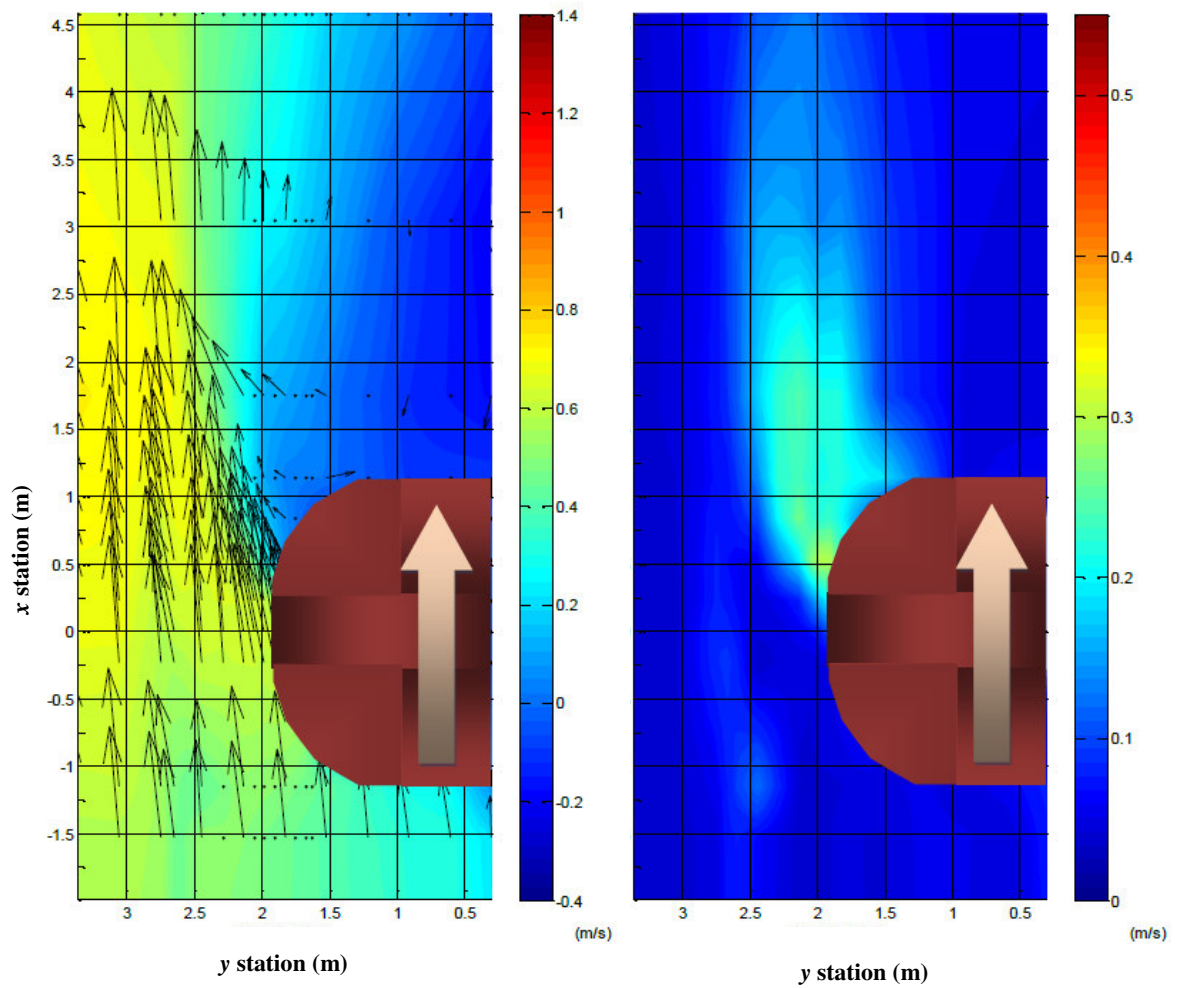
(e) Time average velocity
(after 275 hour run)

(f) Turbulence intensity
(after 275 hour run)

Figure A.5. (continued)
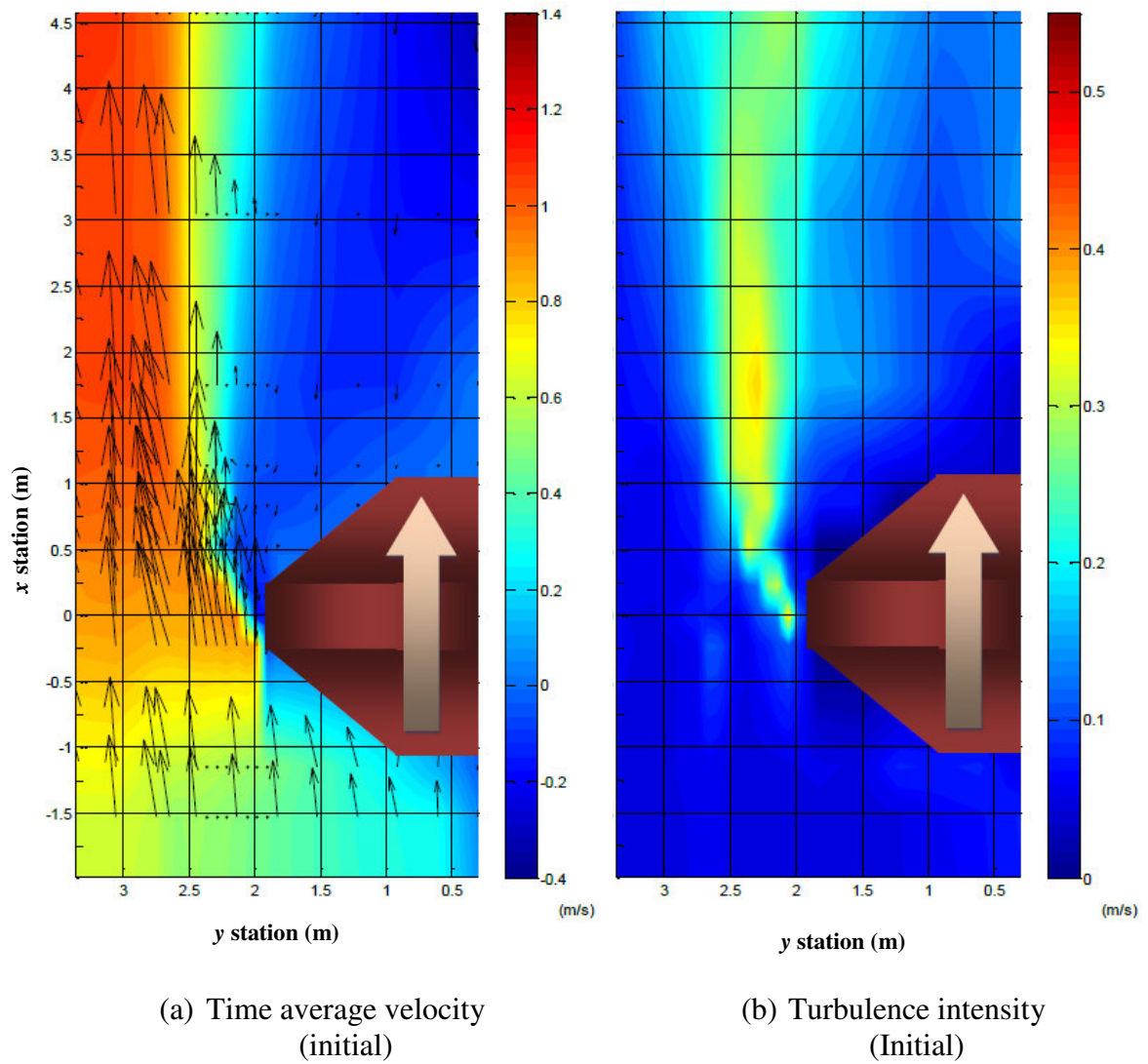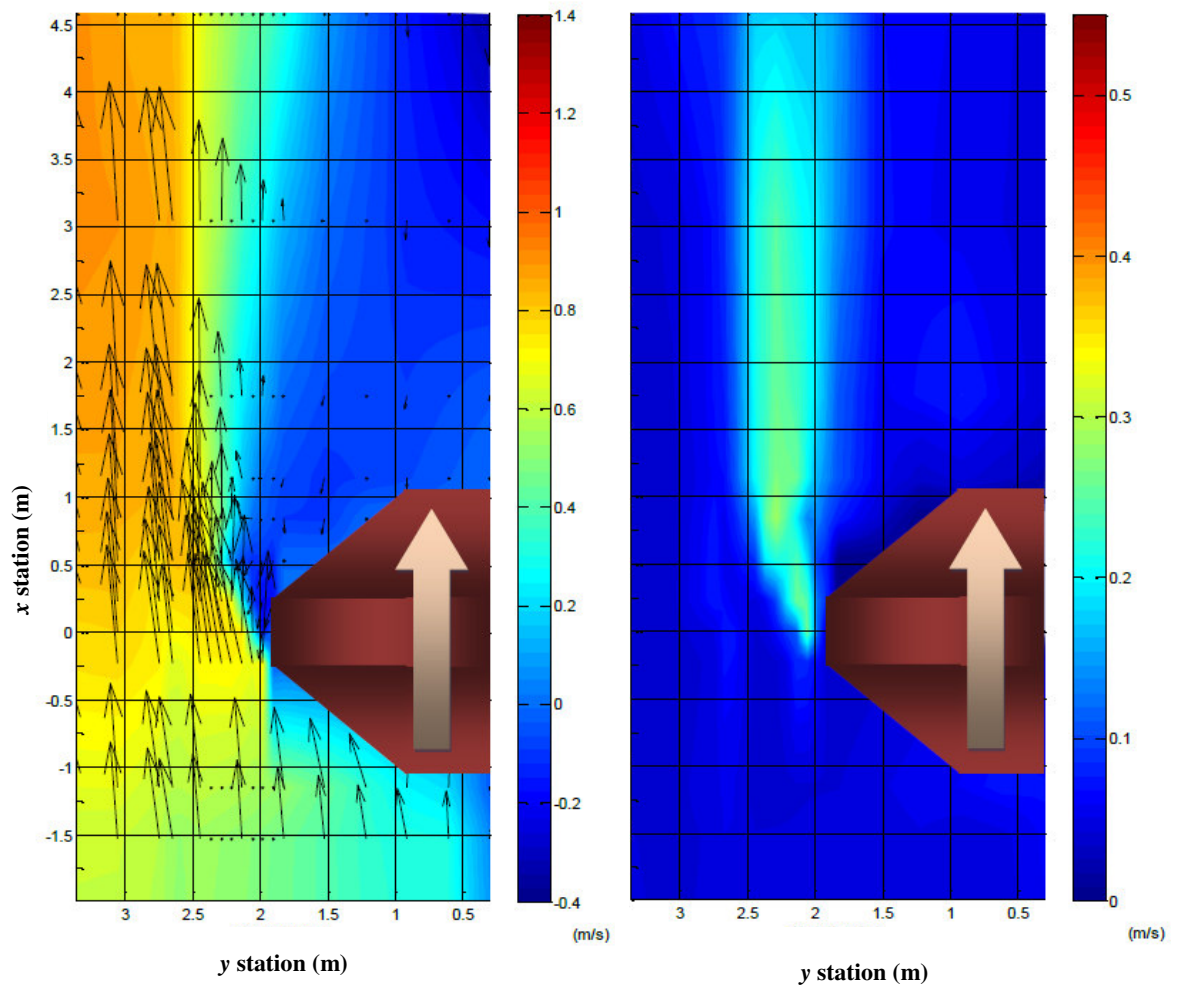
(a) Time average velocity
(initial)

(b) Turbulence intensity
(Initial)

Figure A.6. Case 9

(c) Time average velocity
(after 123 hour run)

(d) Turbulence intensity
(after 123 hour run)

Figure A.6. (continued)
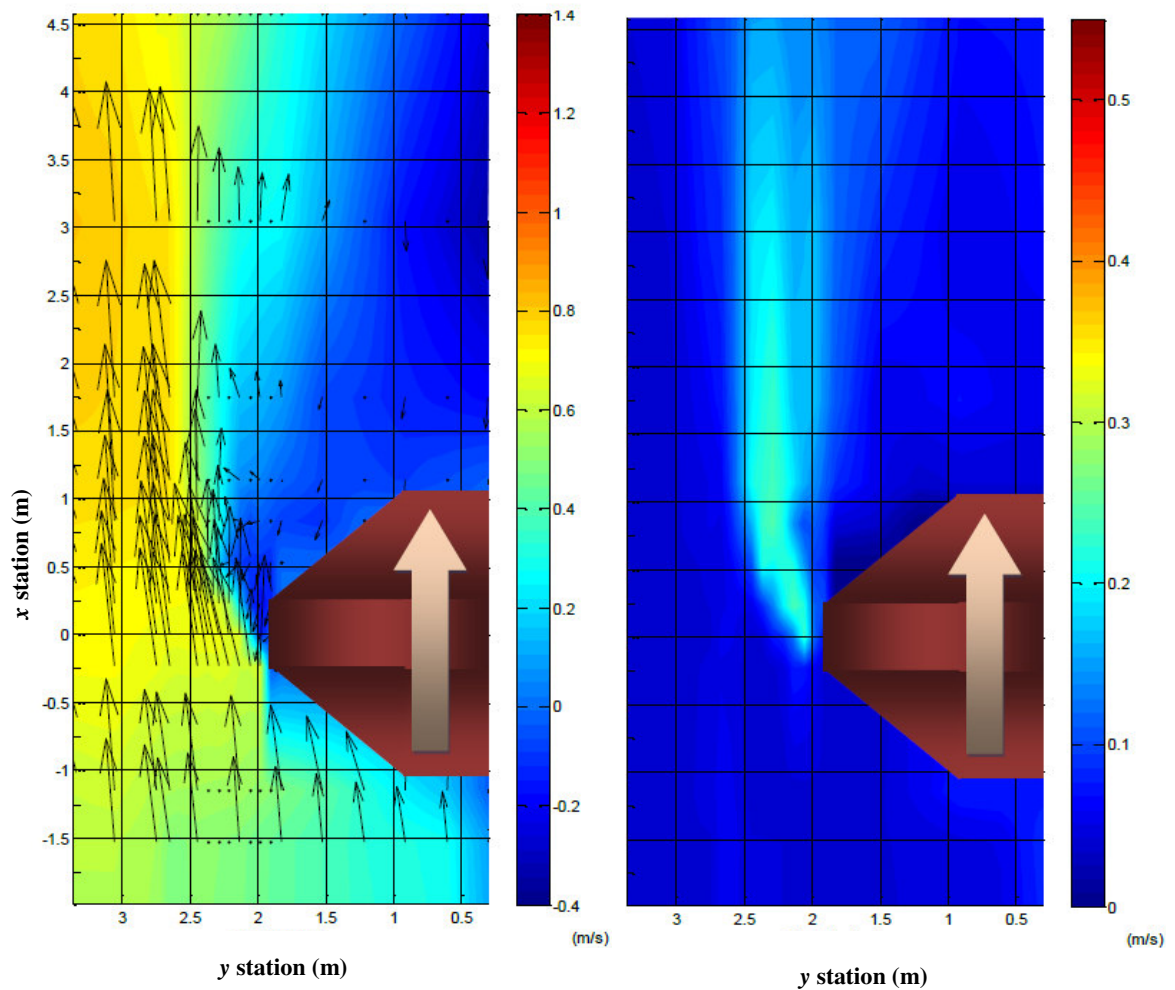
(e) Time average velocity
(after 250 hour run)

(f) Turbulence intensity
(after 250 hour run)

Figure A.6. (continued)
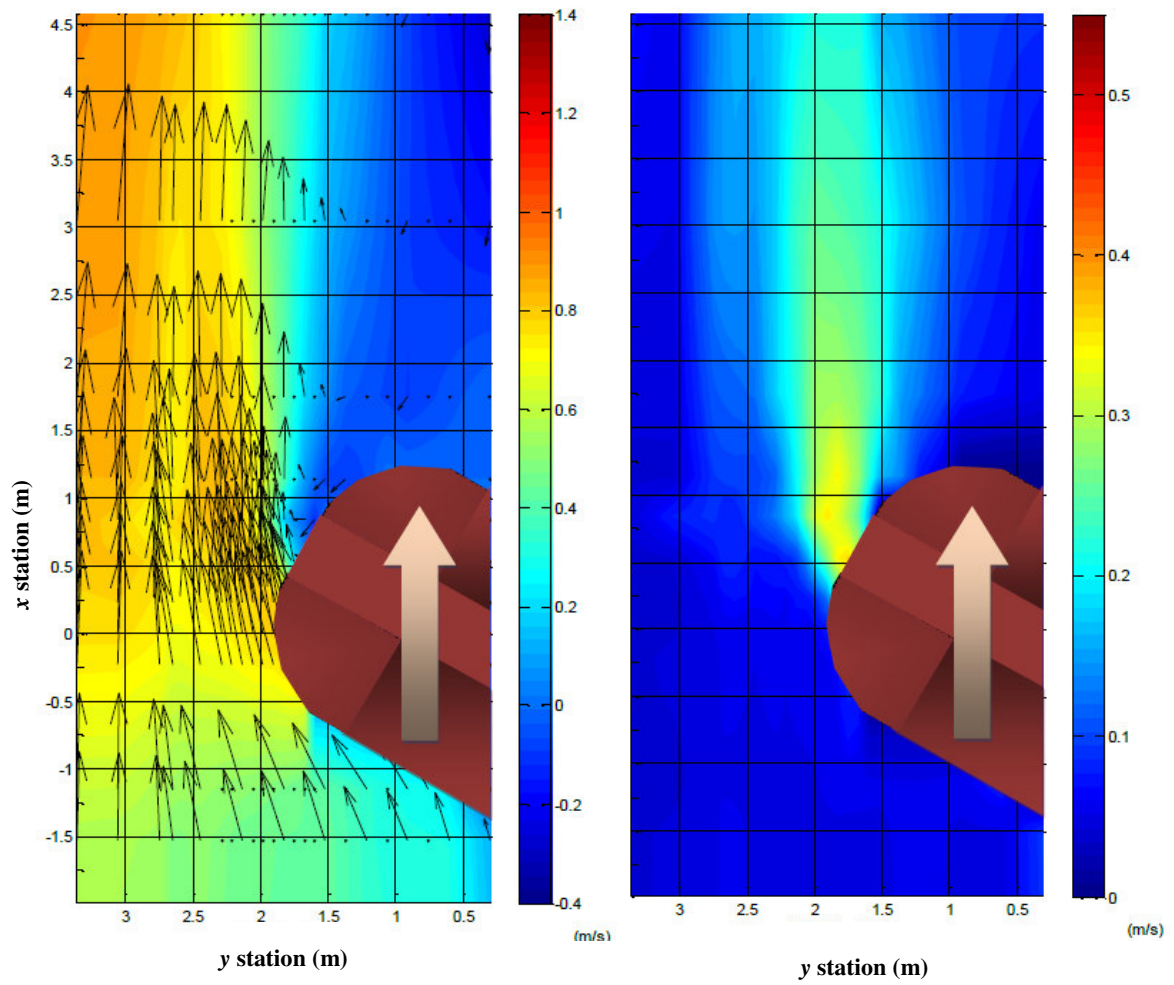
(a) Time average velocity
(initial)

(b) Turbulence intensity
(initial)

Figure A.7. Case 10
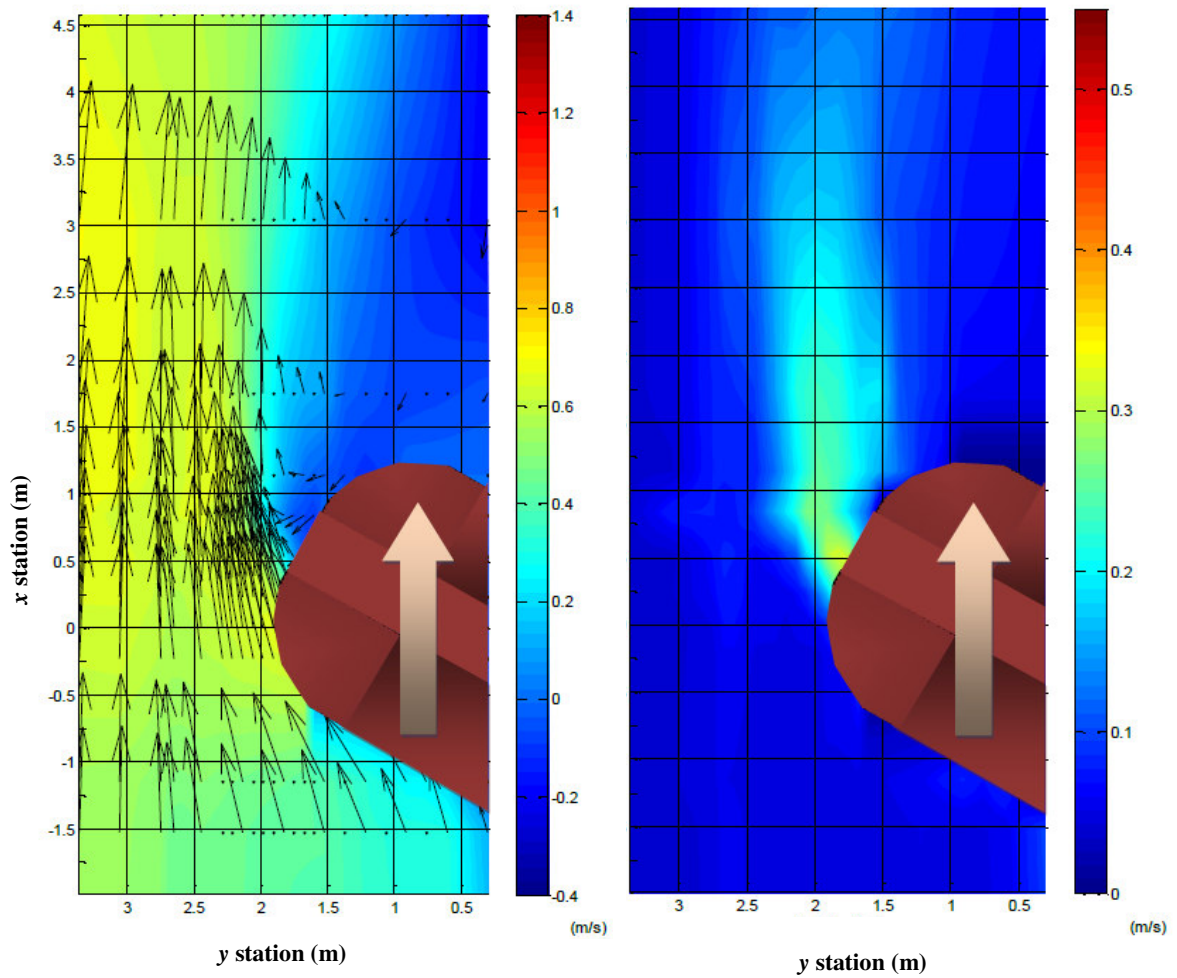
(c) Time average velocity
(after 120 hour run)

(d) Turbulence intensity
(after 120 hour run)

Figure A.7. (continued)
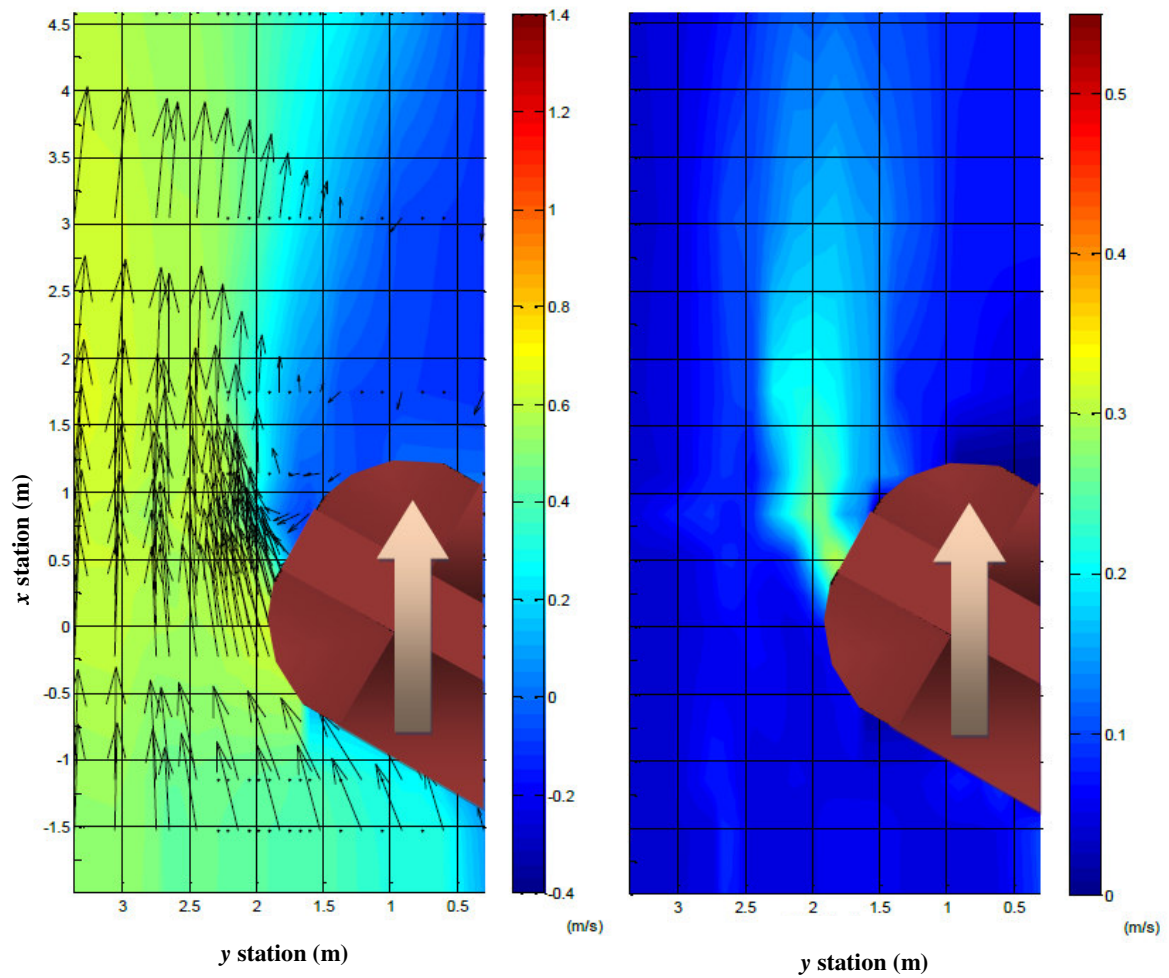
(e) Time average velocity
(after 296 hour run)

(f) Turbulence intensity
(After 296 hour run)

Figure A.7. (continued)
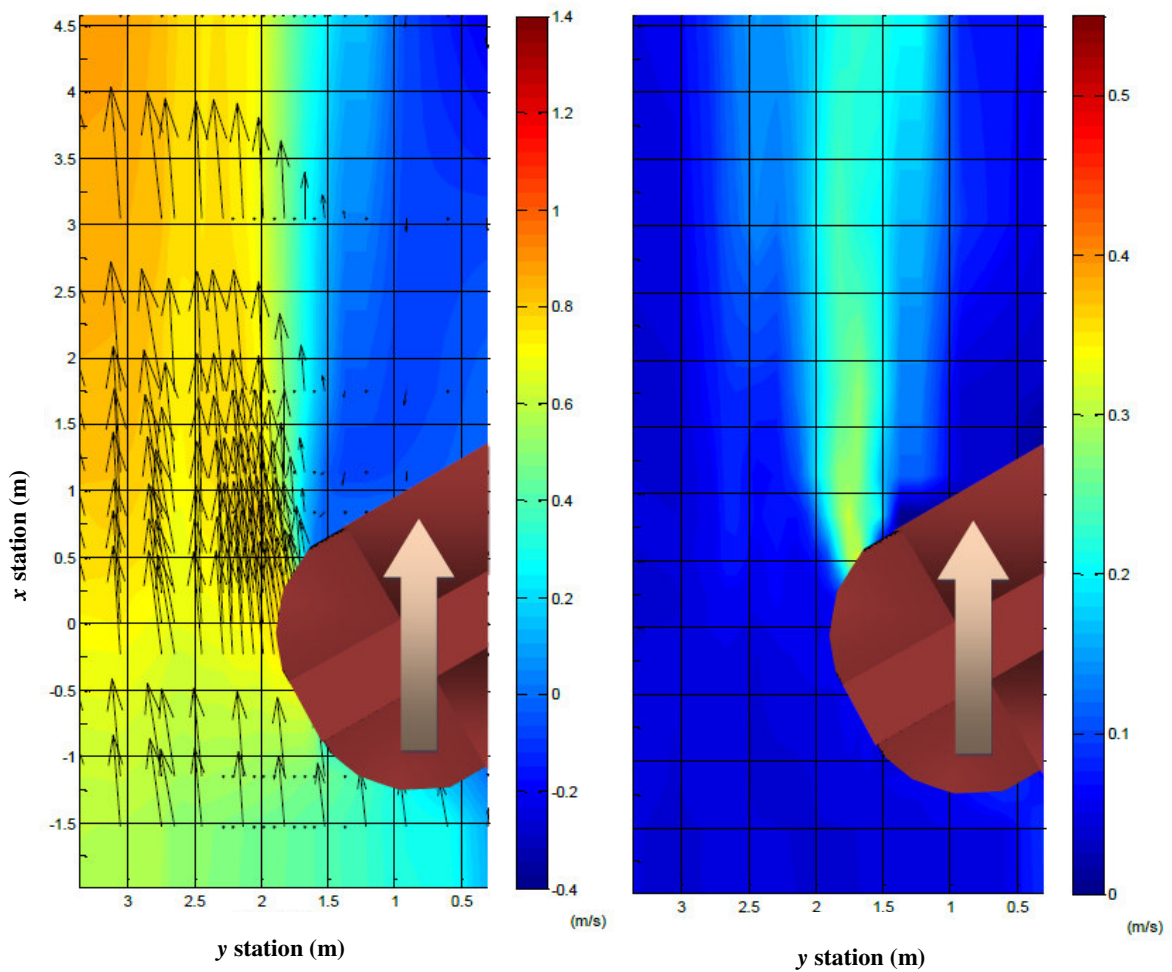
(a) Time average velocity
(initial)

(b) Turbulence intensity
(initial)

Figure A.8. Case 11
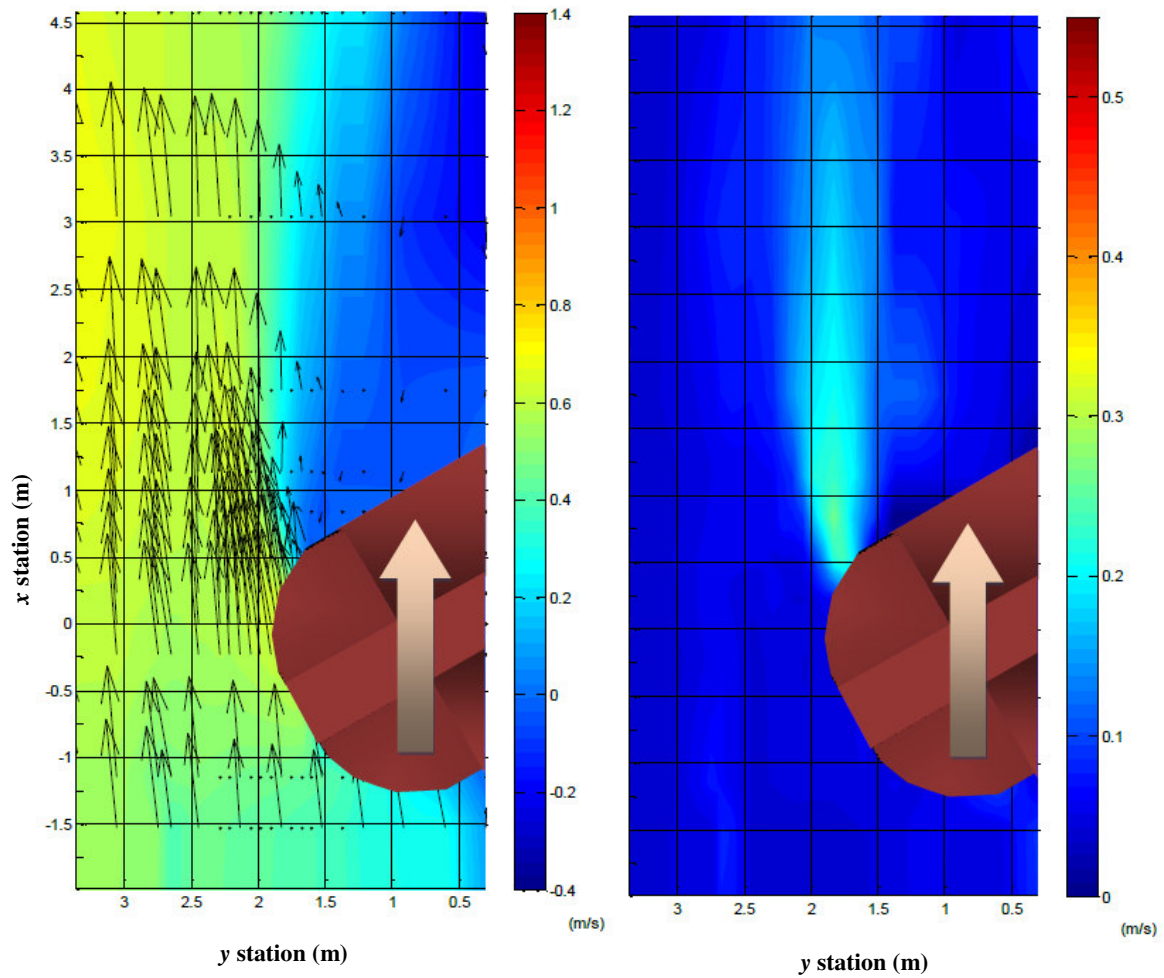
    (c) Time average velocity
       (after 120 hour run)

    (d) Turbulence intensity
       (after 120 hour run)

Figure A.8. (continued)
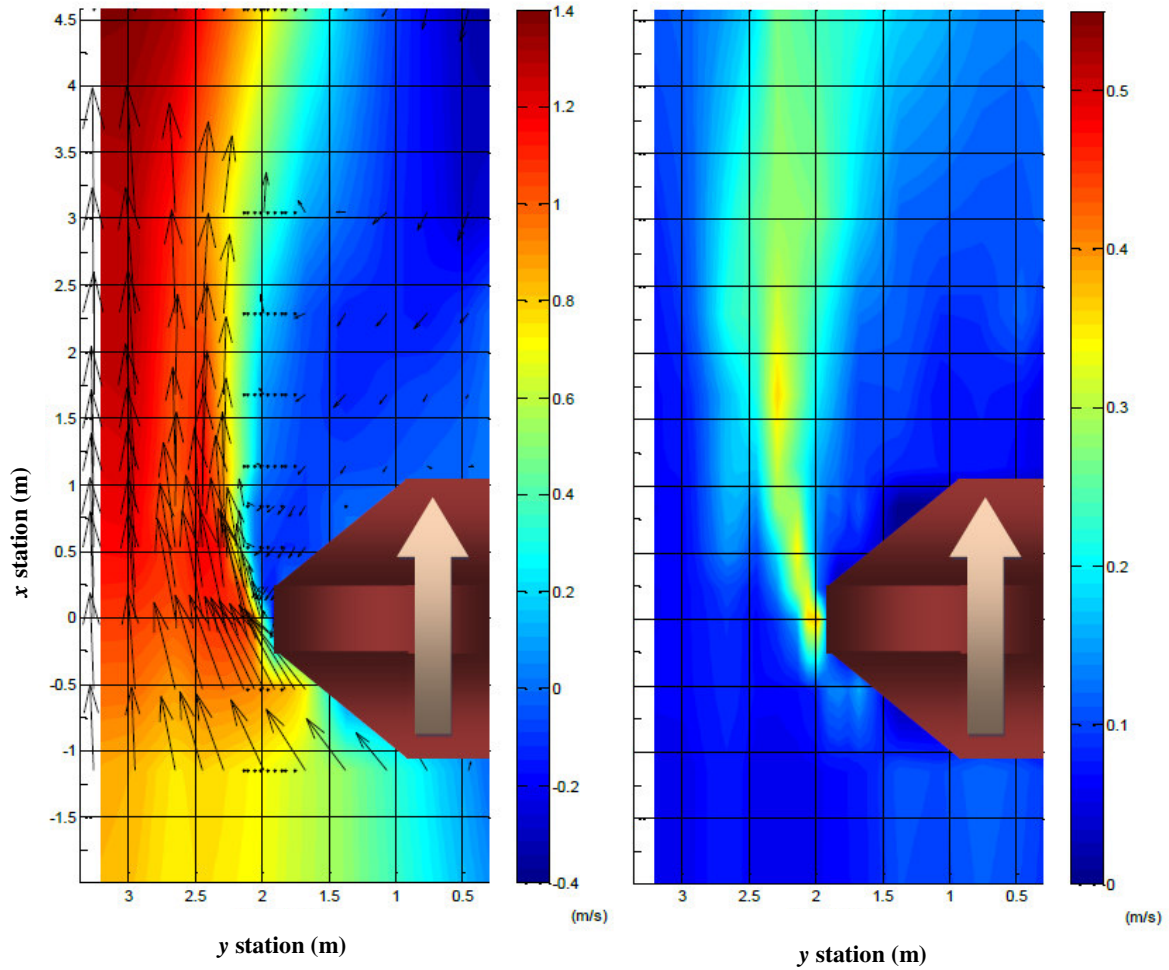
(a) Time average velocity
(initial)

(b) Turbulence intensity
(initial)

Figure A.9. Case 12B
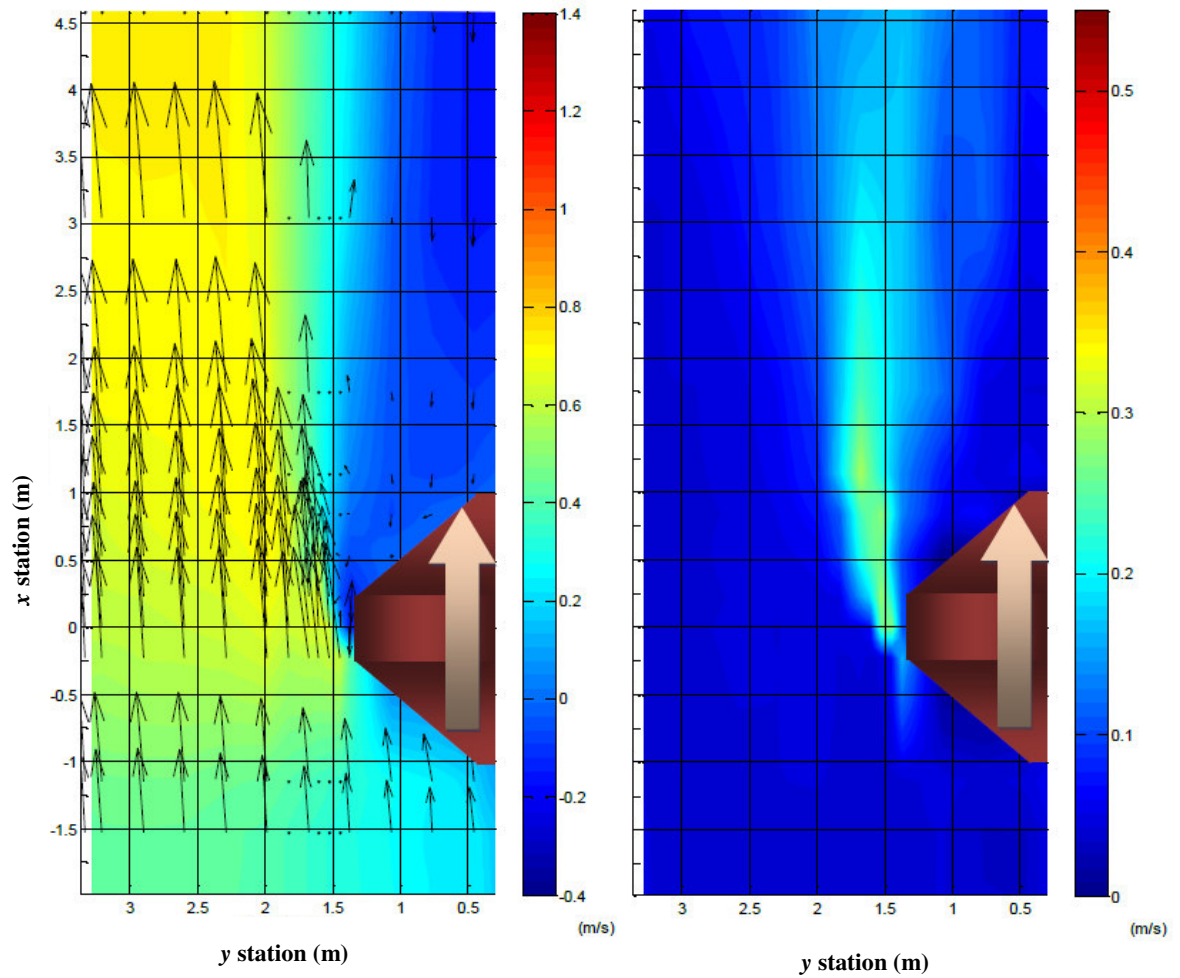
(a) Time average velocity
(initial)

(b) Turbulence intensity
(initial)

Figure A.10. Case 17
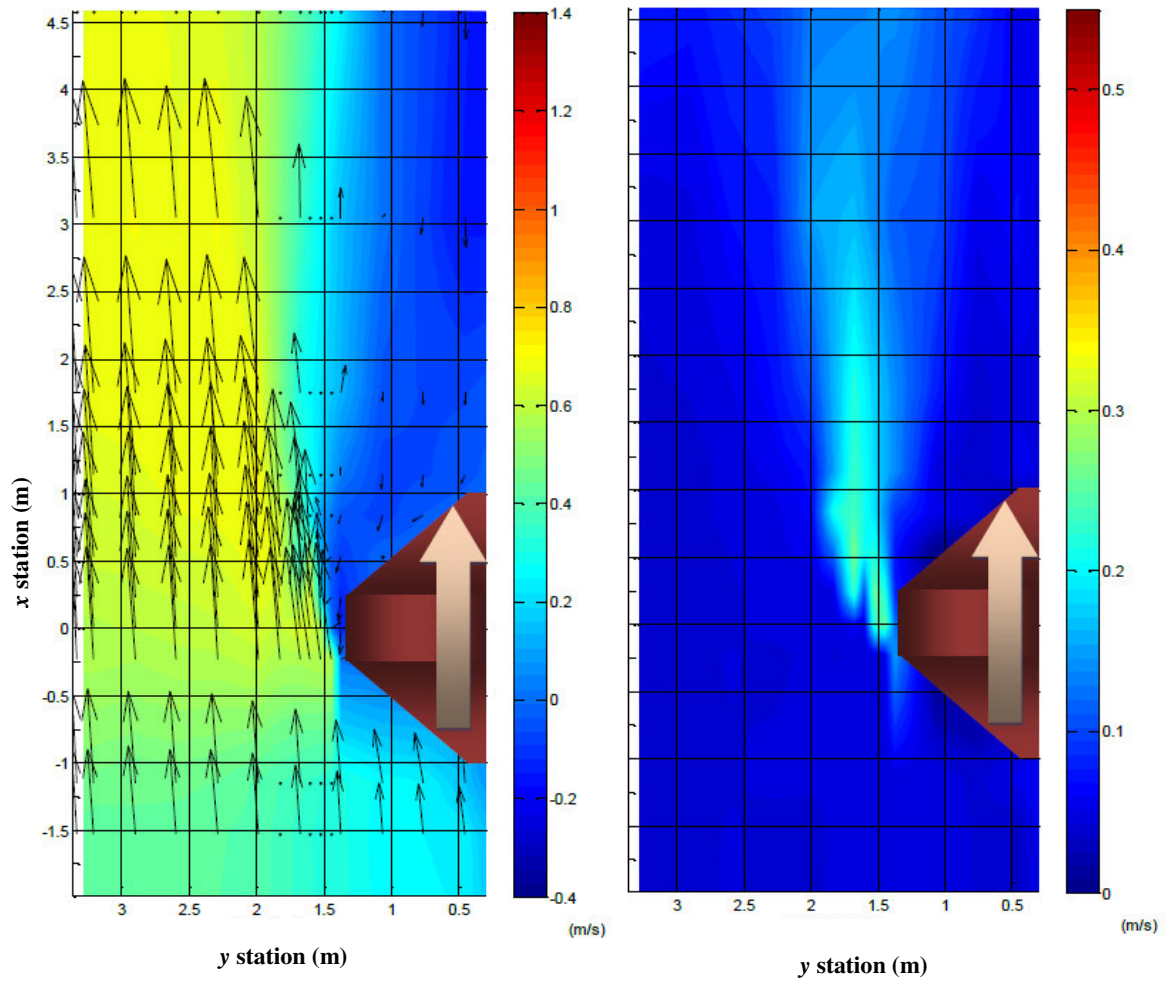
(c) Time average velocity
(after 128 hour run)

(d) Turbulence intensity
(after 128 hour run)

Figure A.10. (continued)
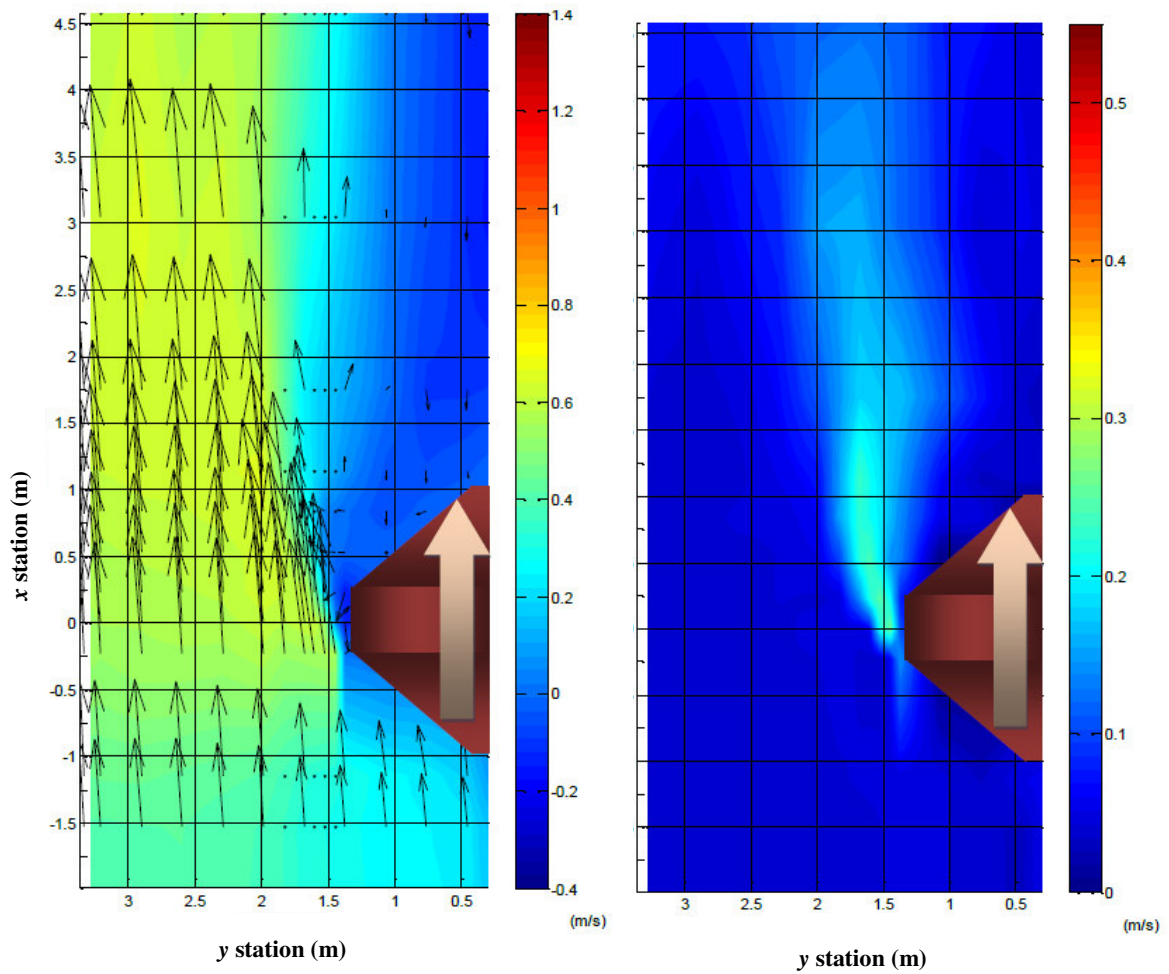
(e) Time average velocity
(after 275 hour run)

(f) Turbulence intensity
(after 275 hour run)

Figure A.10. (continued)

APPENDIX B

SCOUR DEVELOPMENT
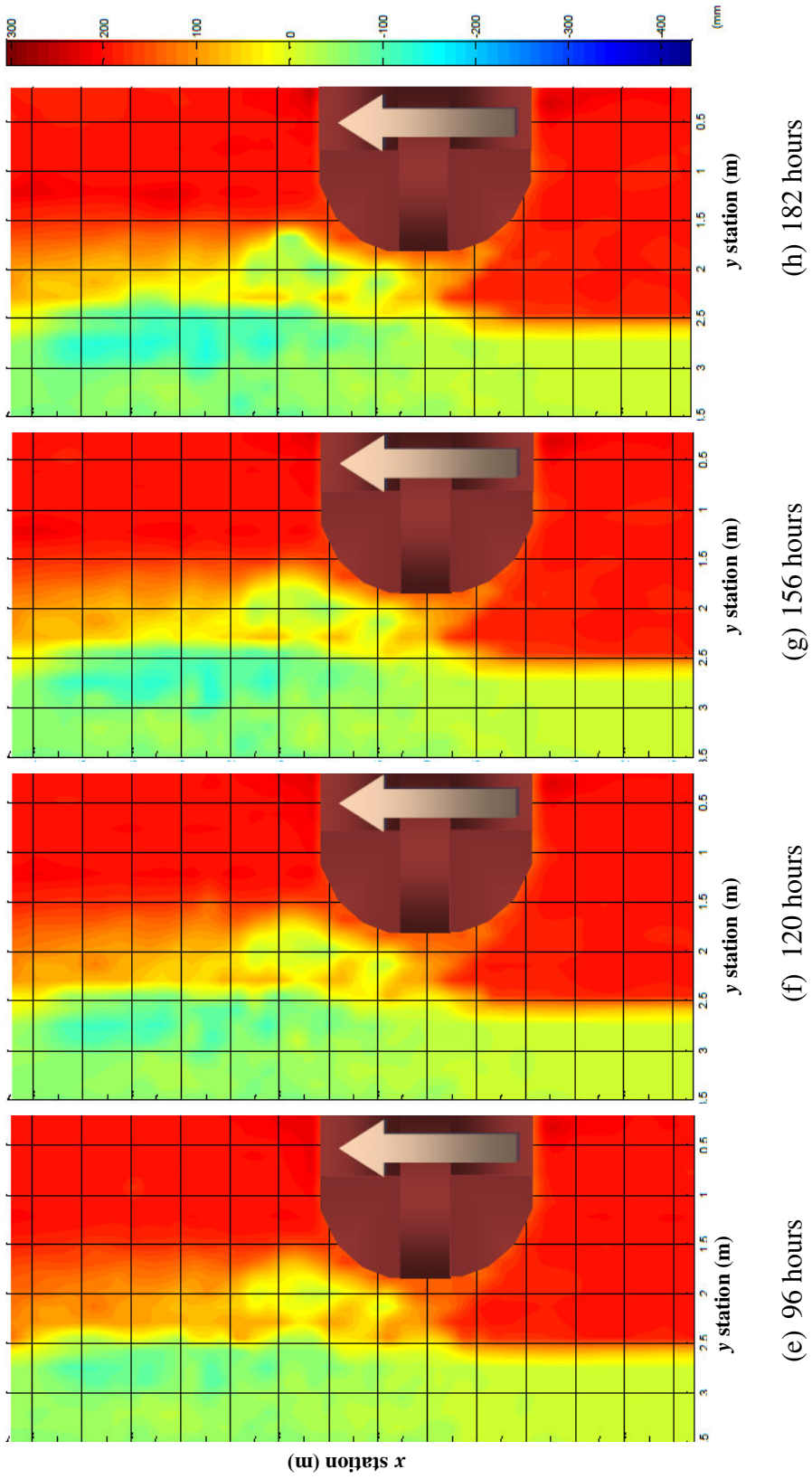
(a) Initial   (b) 24 hours   (c) 48 hous   (d) 72 hours

Figure B.1. Case1

Figure B.1. (continued)
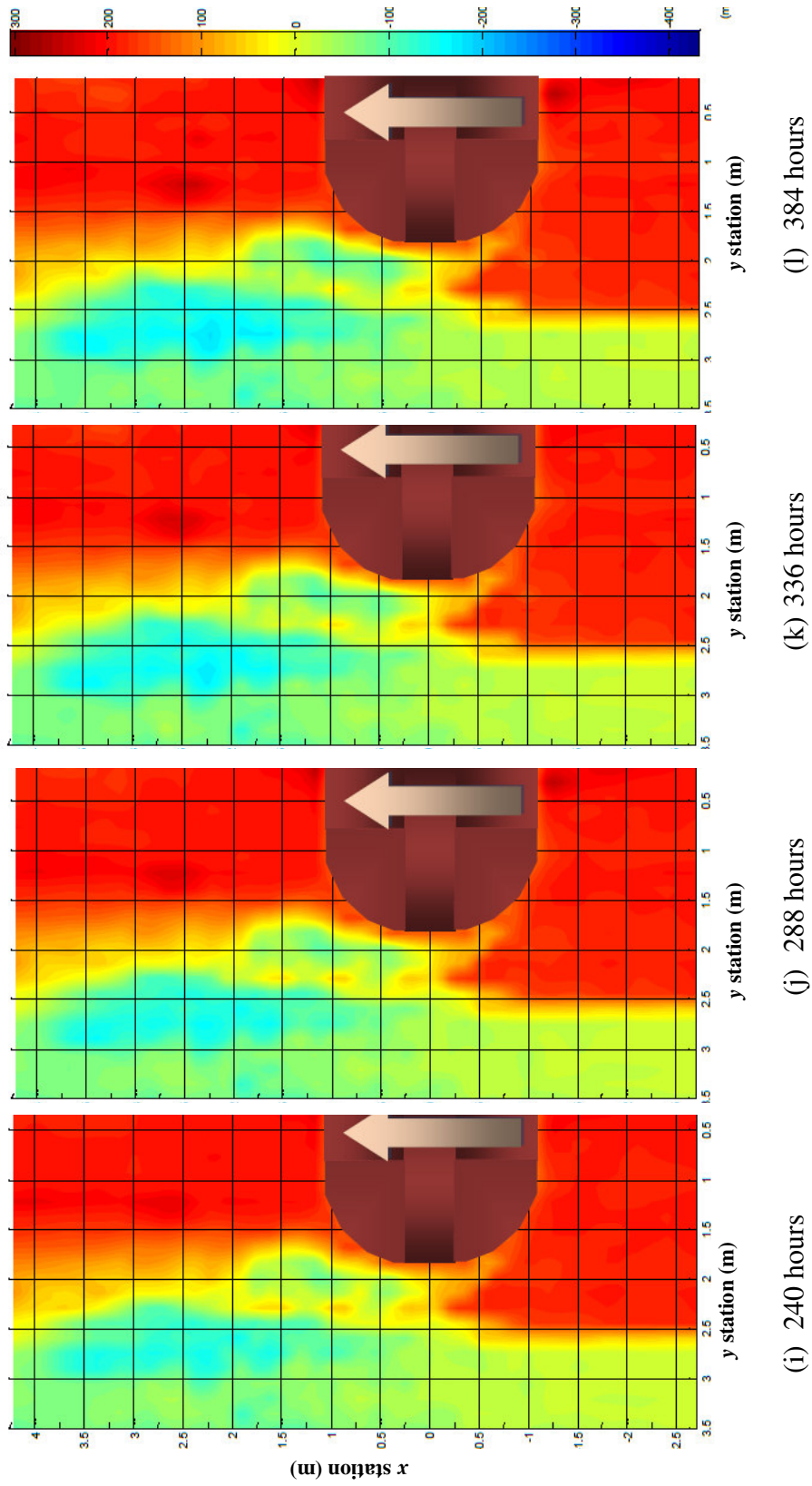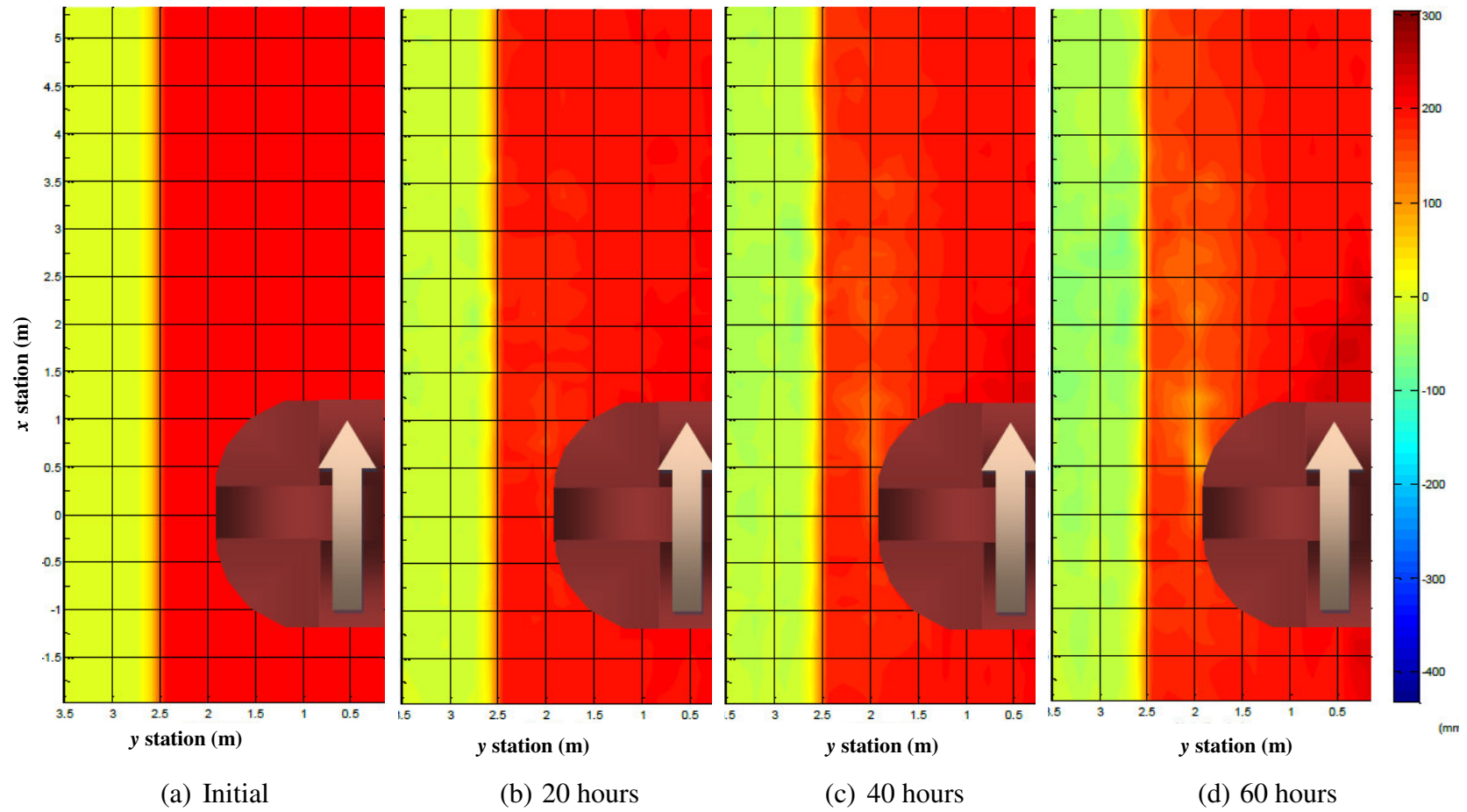
(i) 240 hours   (j) 288 hours   (k) 336 hours   (l) 384 hours

Figure B.1. (continued)

(a) Initial (b) 20 hours (c) 40 hours (d) 60 hours

Figure B.2. Case1II

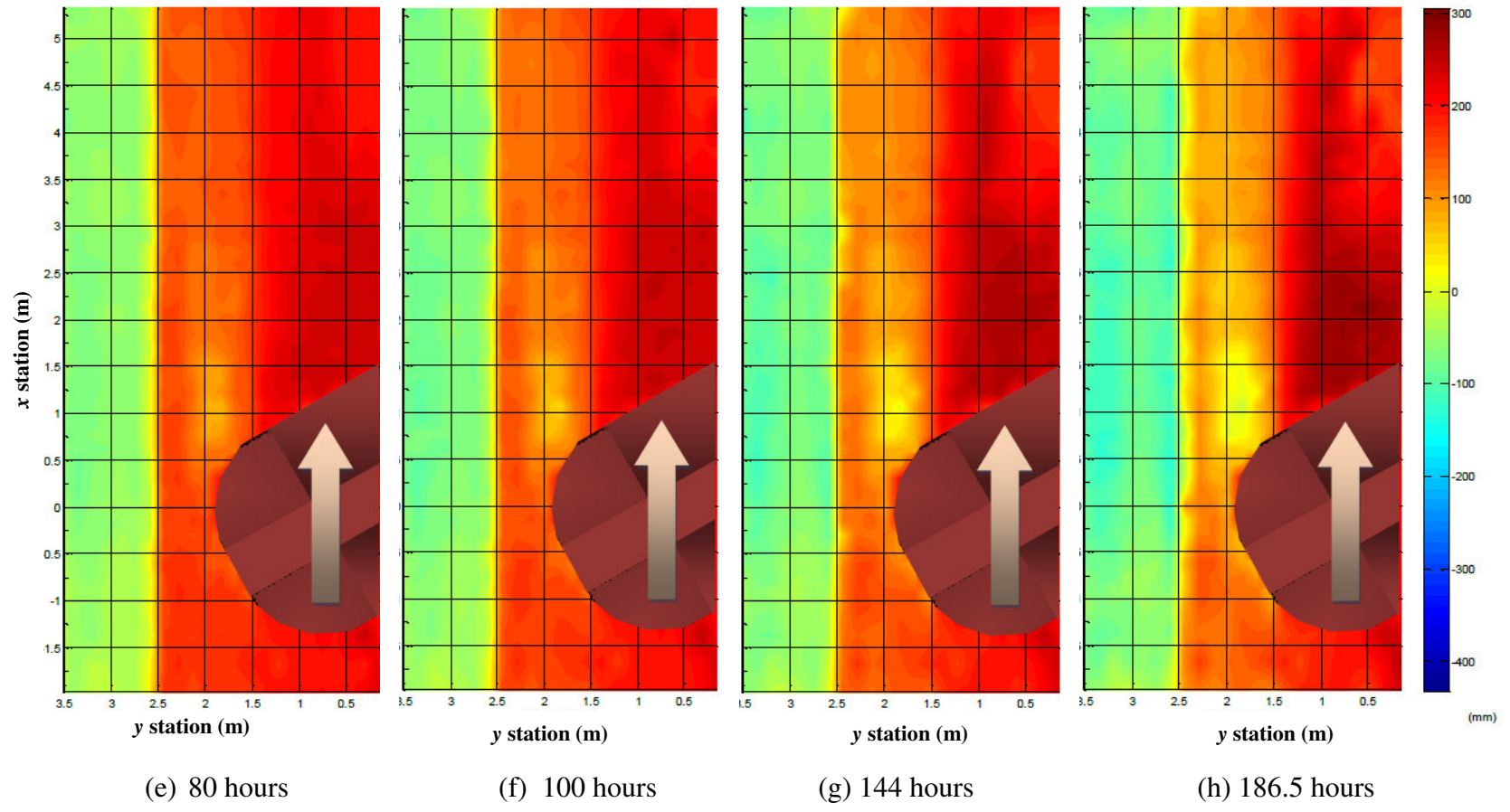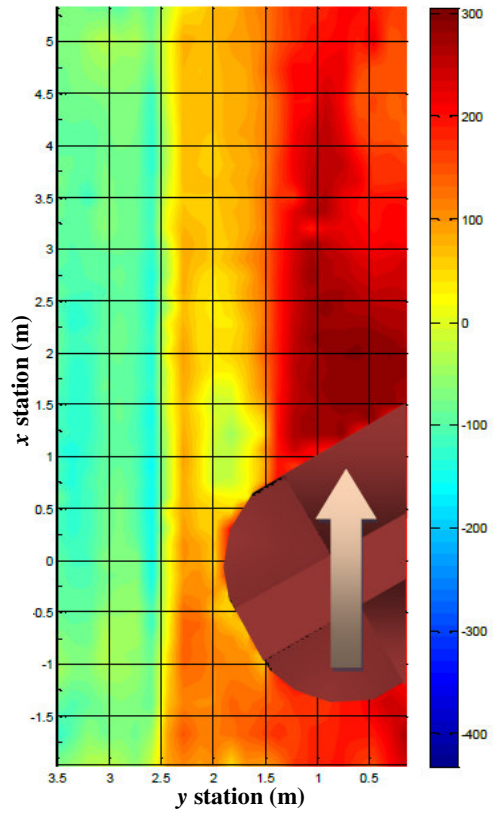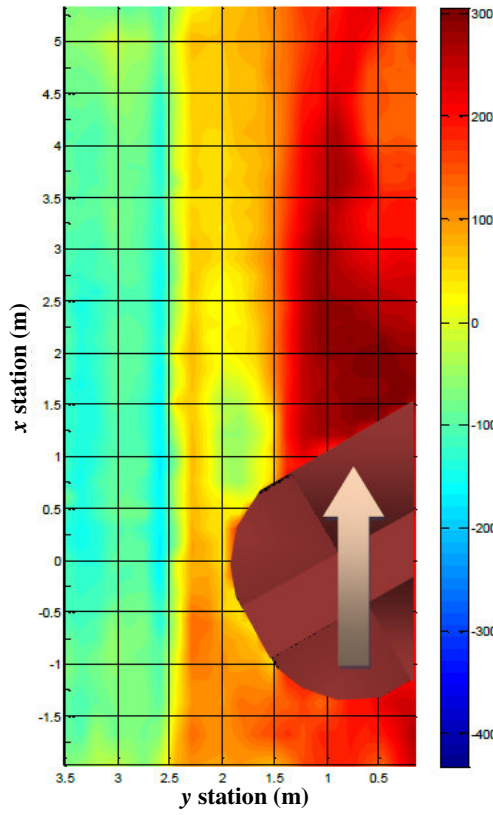(e) 80 hours   (f) 100 hours   (g) 144 hours   (h) 189 hours

Figure B.2. (continued)

(i) 232 hours   (j) 276 hours   (k) 320 hours

Figure B.2. (continued)

(a) Initial   (b) 24 hours   (c) 48 hours   (d) 72 hours

Figure B.3. Case2

(a) 96 hours   (b) 120 hours   (c) 156 hours   (d) 192 hours
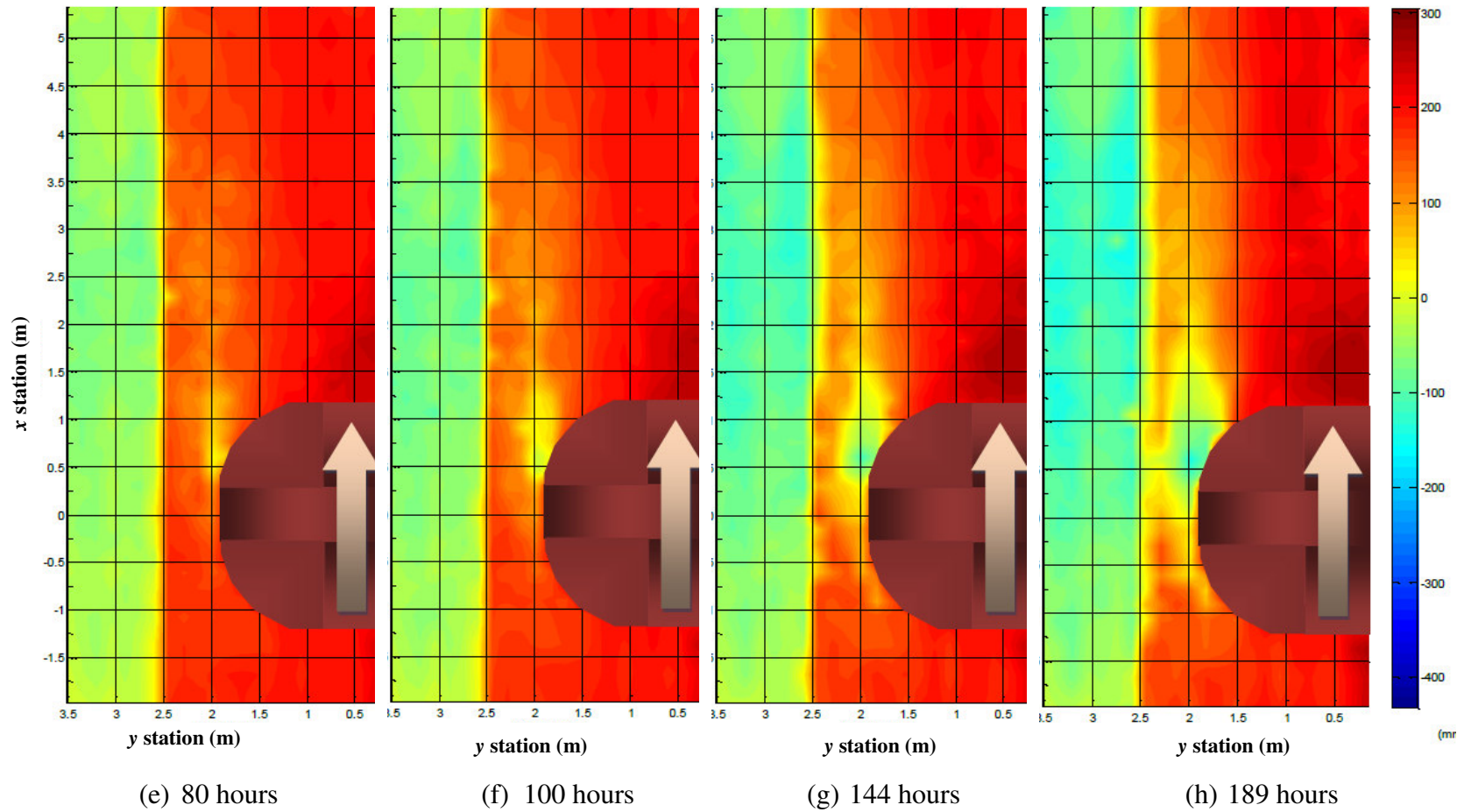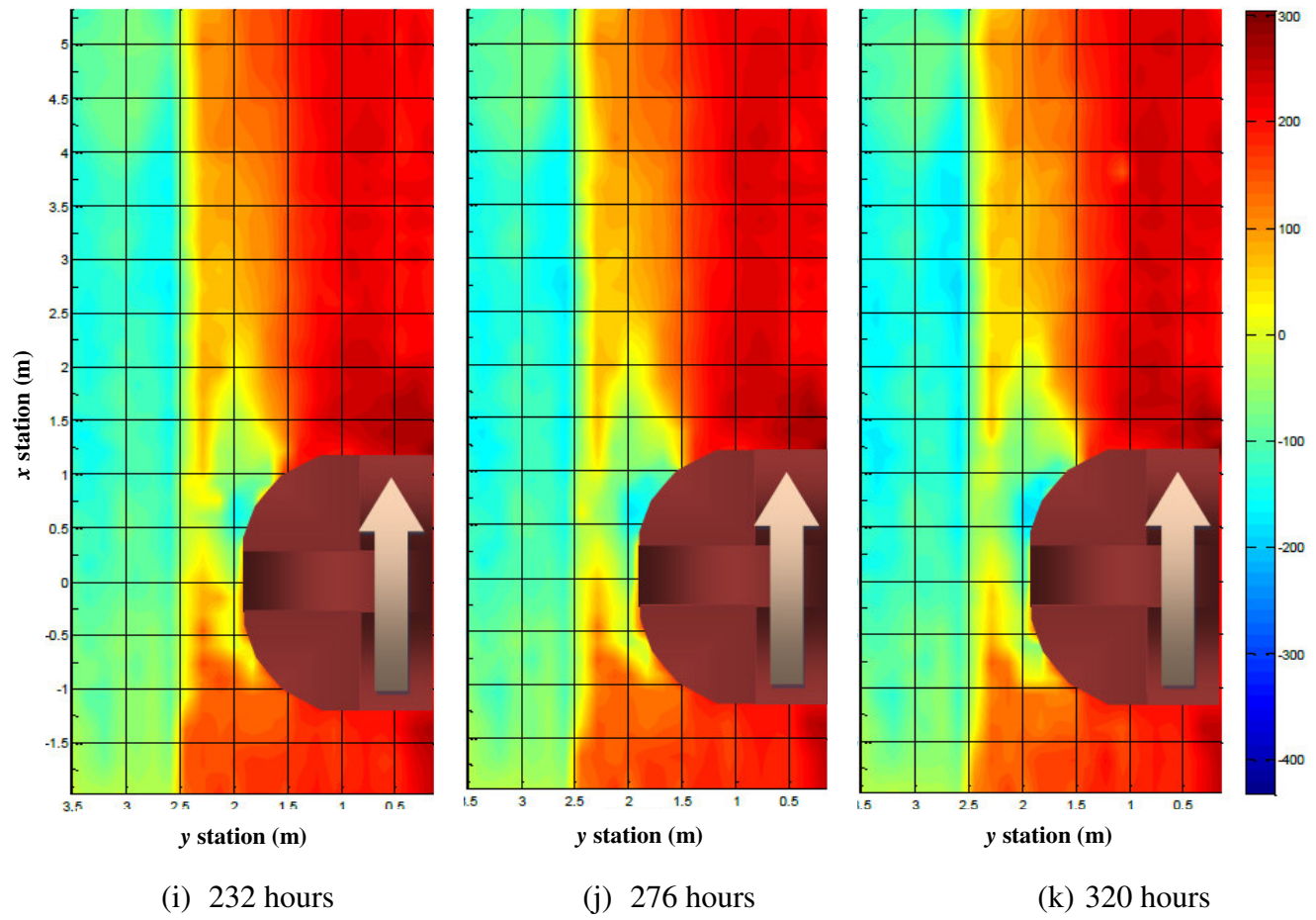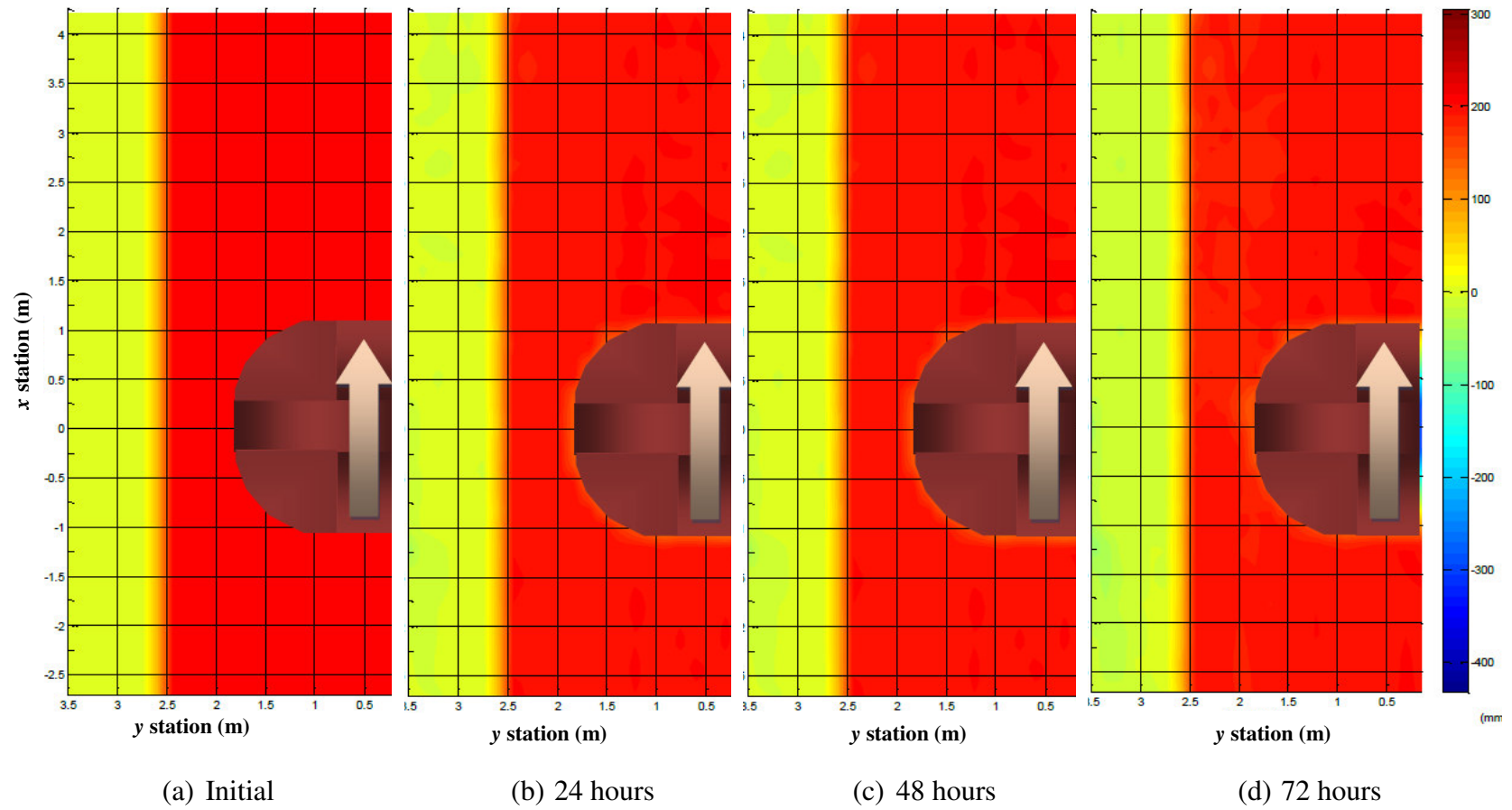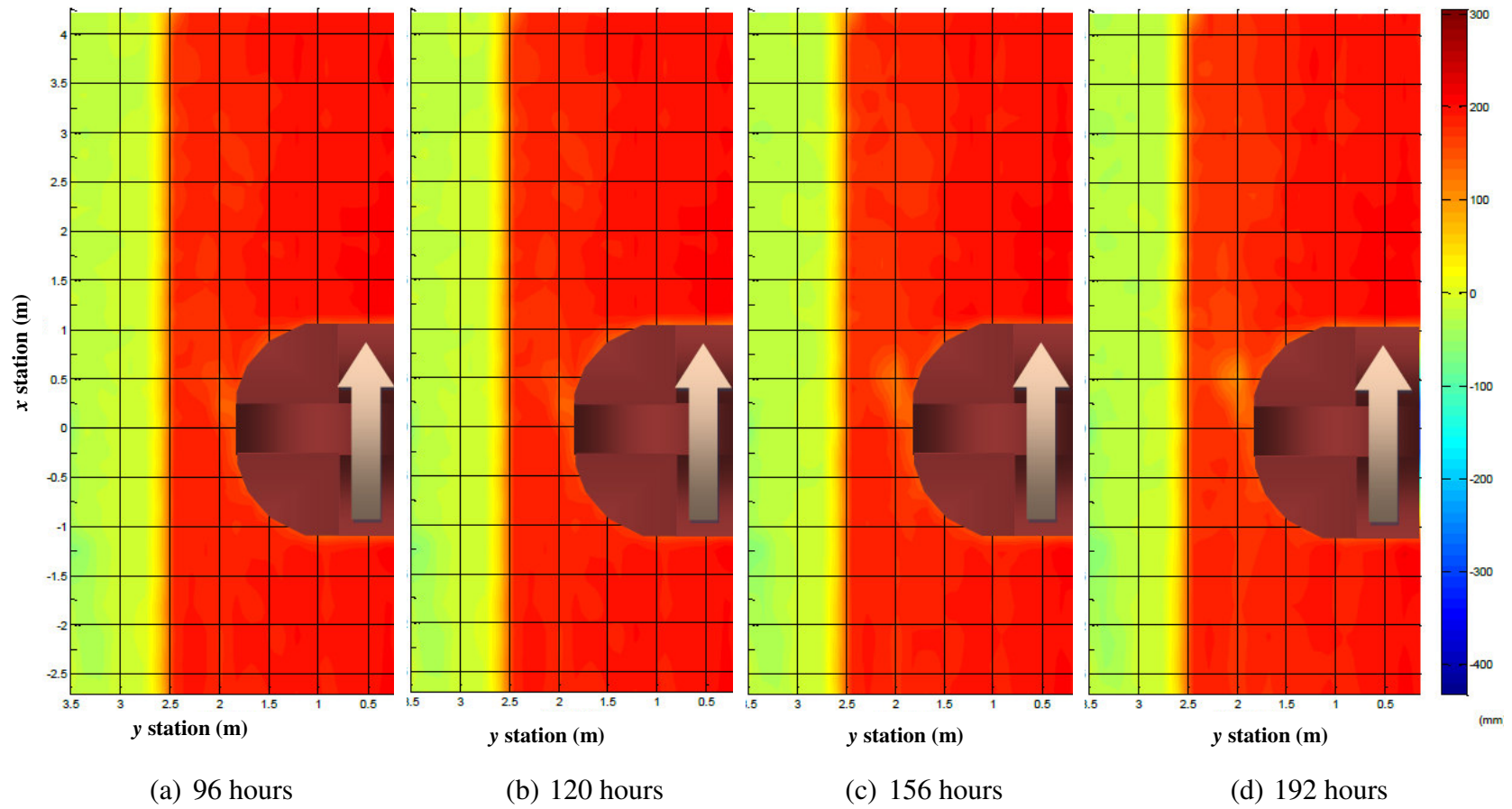
Figure B.3. (continued)
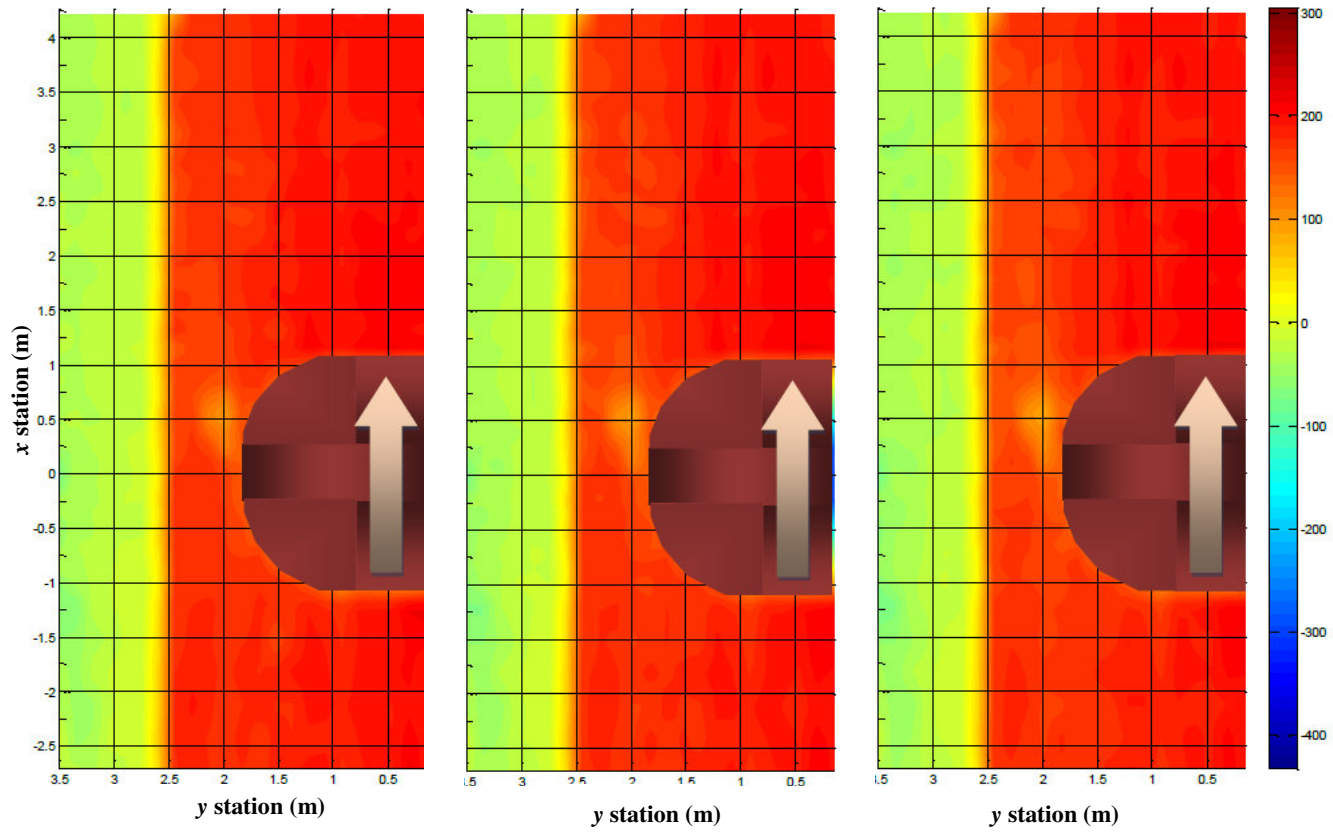
(e) 228 hours   (f) 264 hours   (g) 300 hours

Figure B.3. (continued)

(a) Initial (b) 48 hours (c) 96 hours (d) 156 hours

Figure B.4. Case3

(e) 192 hours   (f) 228 hours   (g) 264 hours   (h) 300 hours

Figure B.4. (continued)

(i) 348 hours   (j) 396 hours   (k) 456 hours   (l) 504 hours

Figure B.4. (continued)

(a) Initial   (b) 48 hours   (c) 72 hours   (d) 96 hours
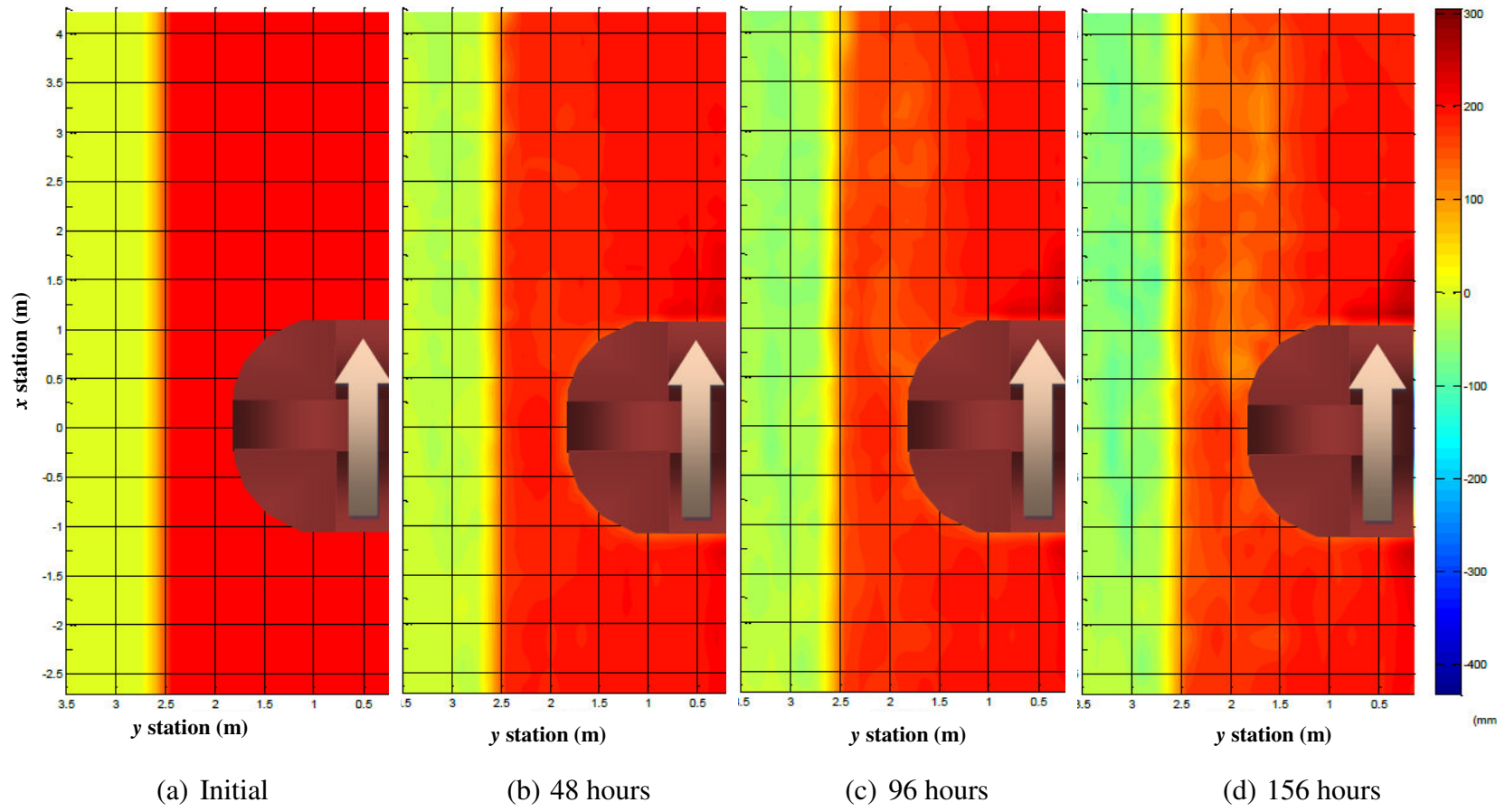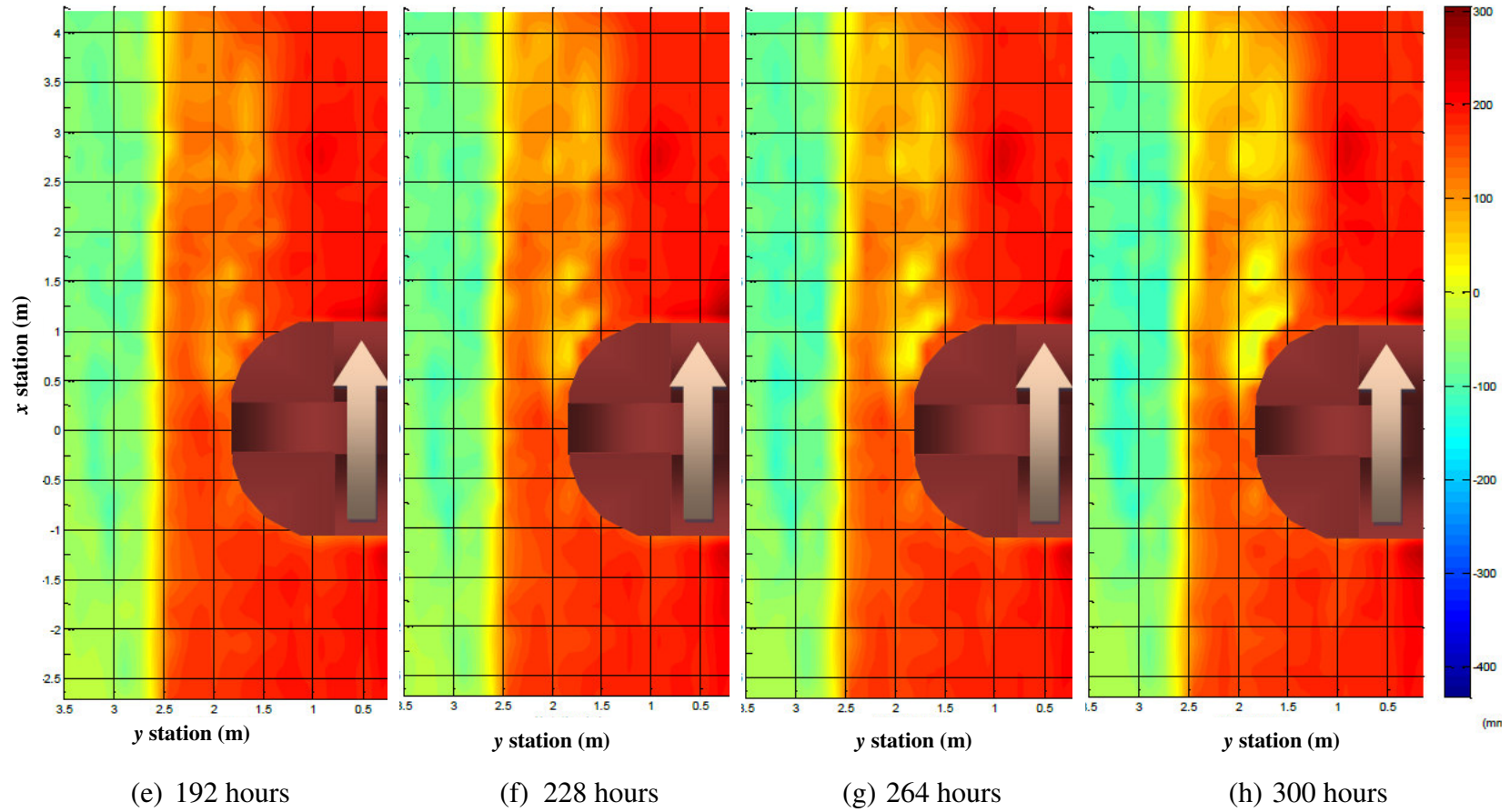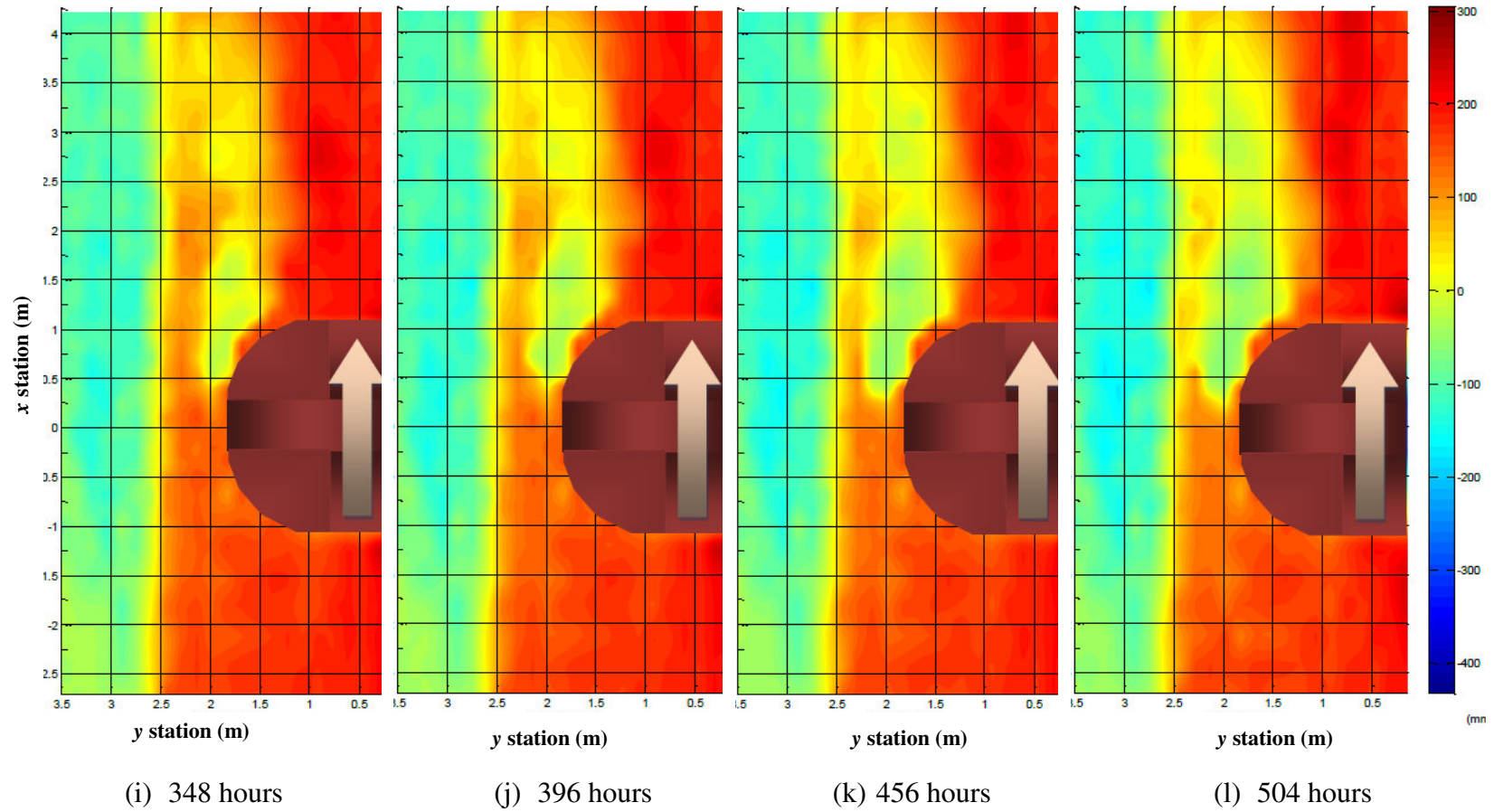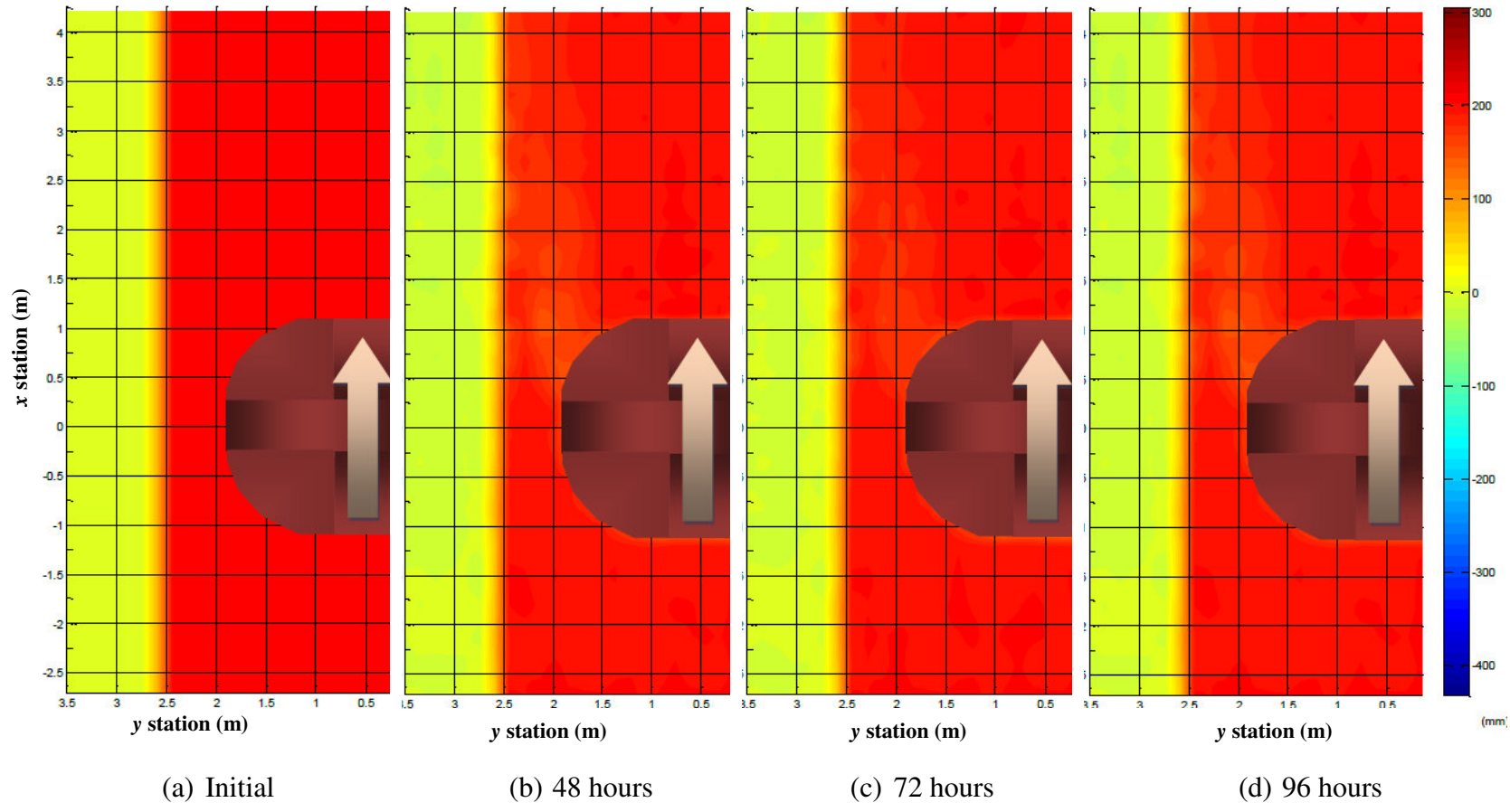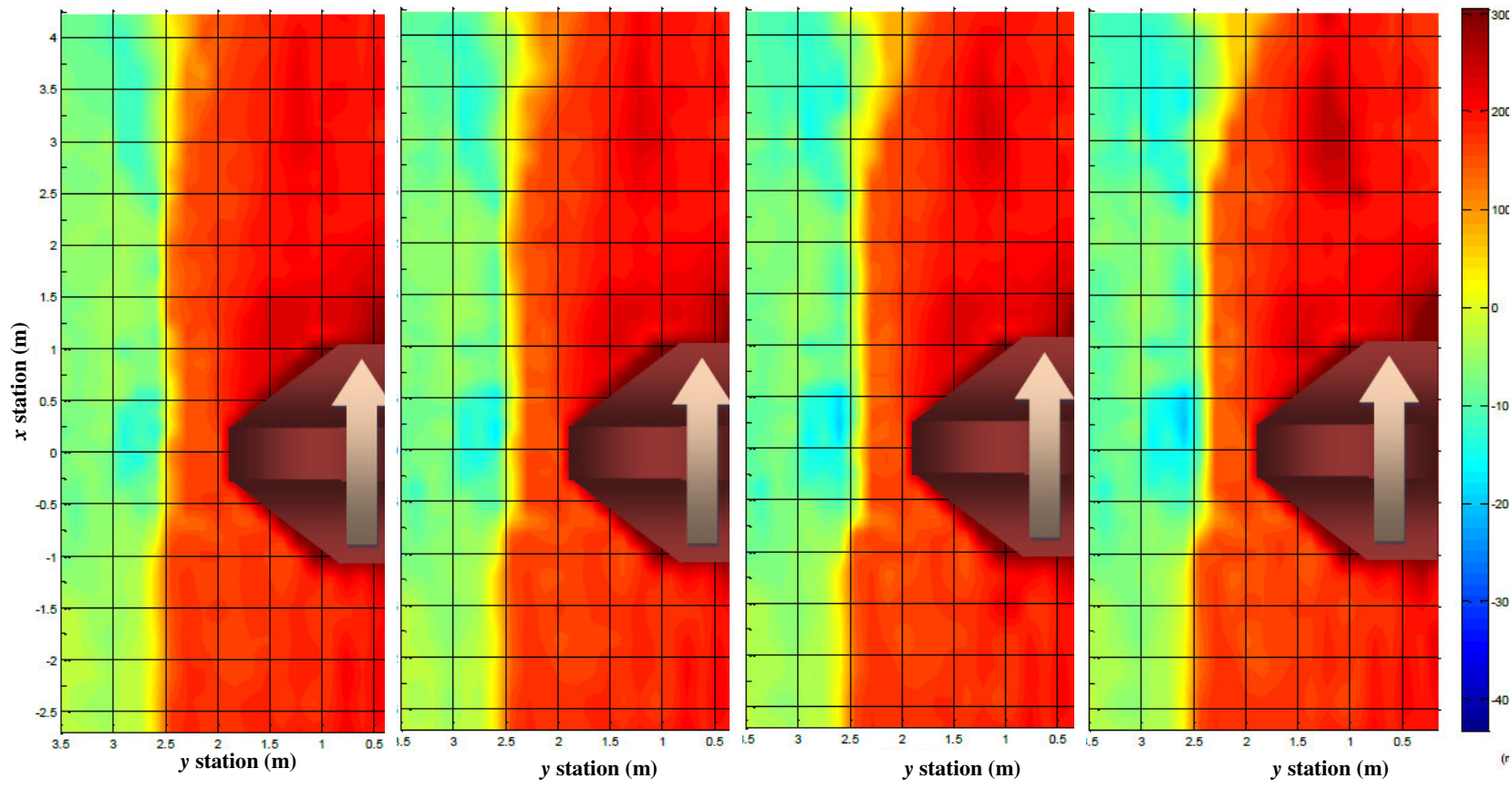
Figure B.5. Case4
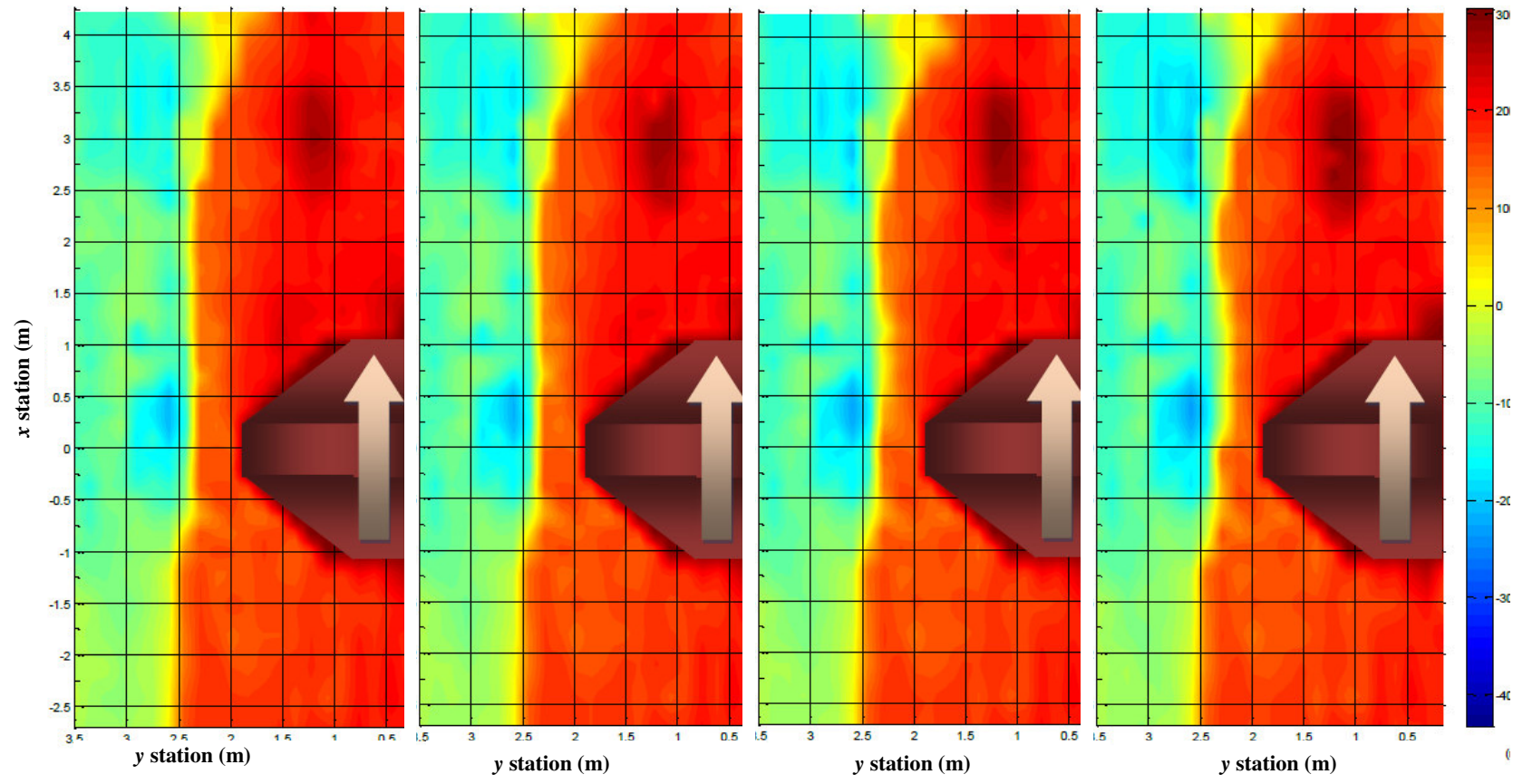
(e) 120 hours   (f) 144 hours   (g) 168 hours   (h) 192 hours
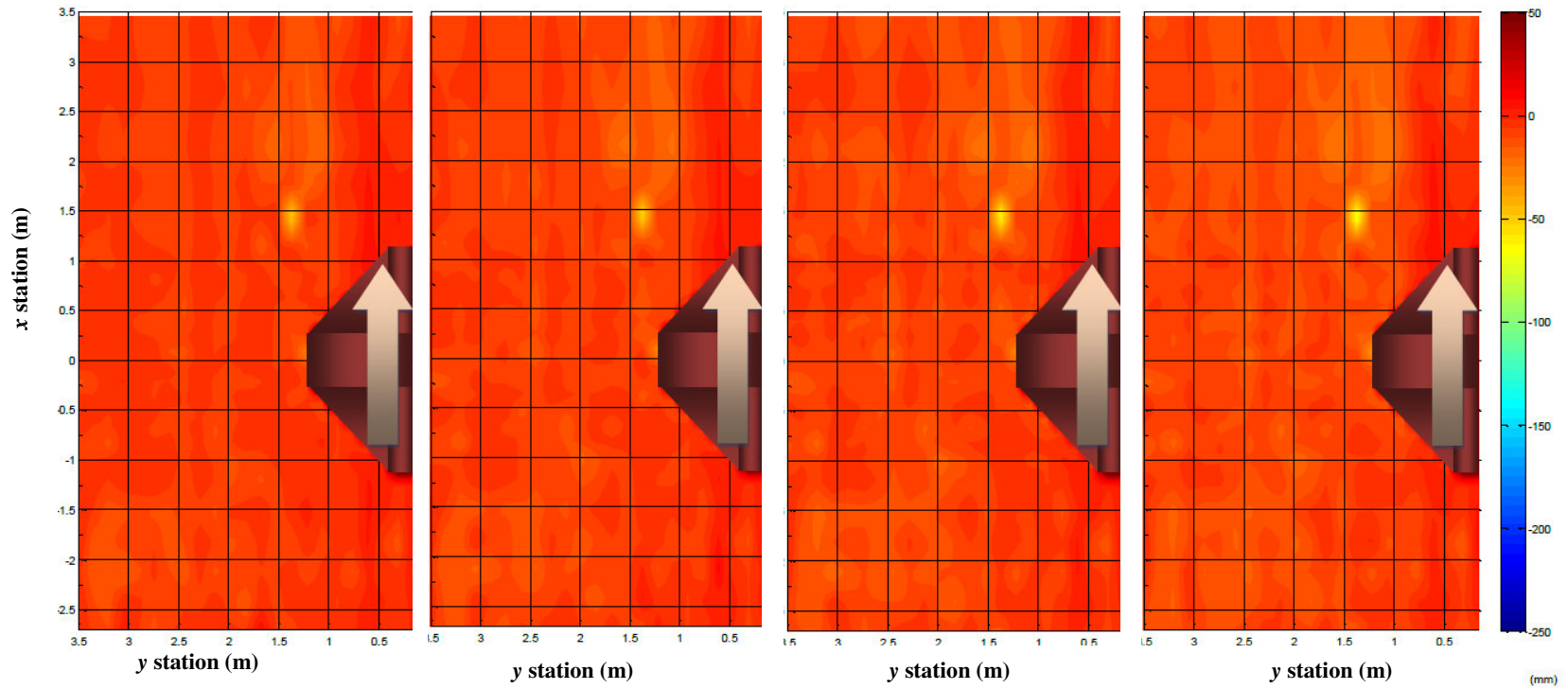
Figure B.5. (continued)

(i) 216 hours   (j) 252 hours   (k) 298 hours   (l) 340 hours

Figure B.5. (continued)

(a) Initial　　　　(b) 24 hours　　　　(c) 48 hours　　　　(d) 72 hours
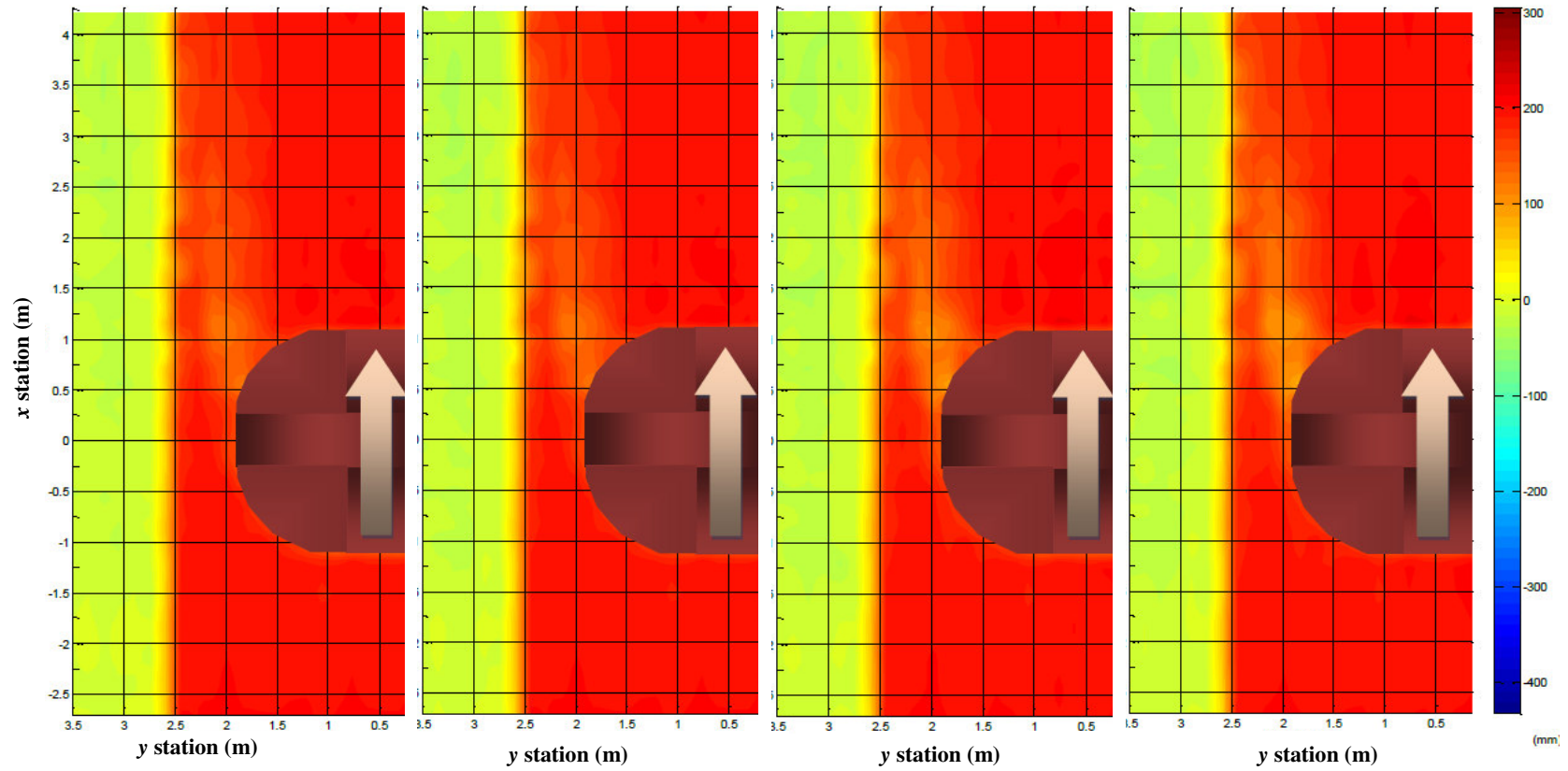
Figure B.6. Case5

(e) 96 hours   (f) 120 hours   (g) 168 hours   (h) 216 hours
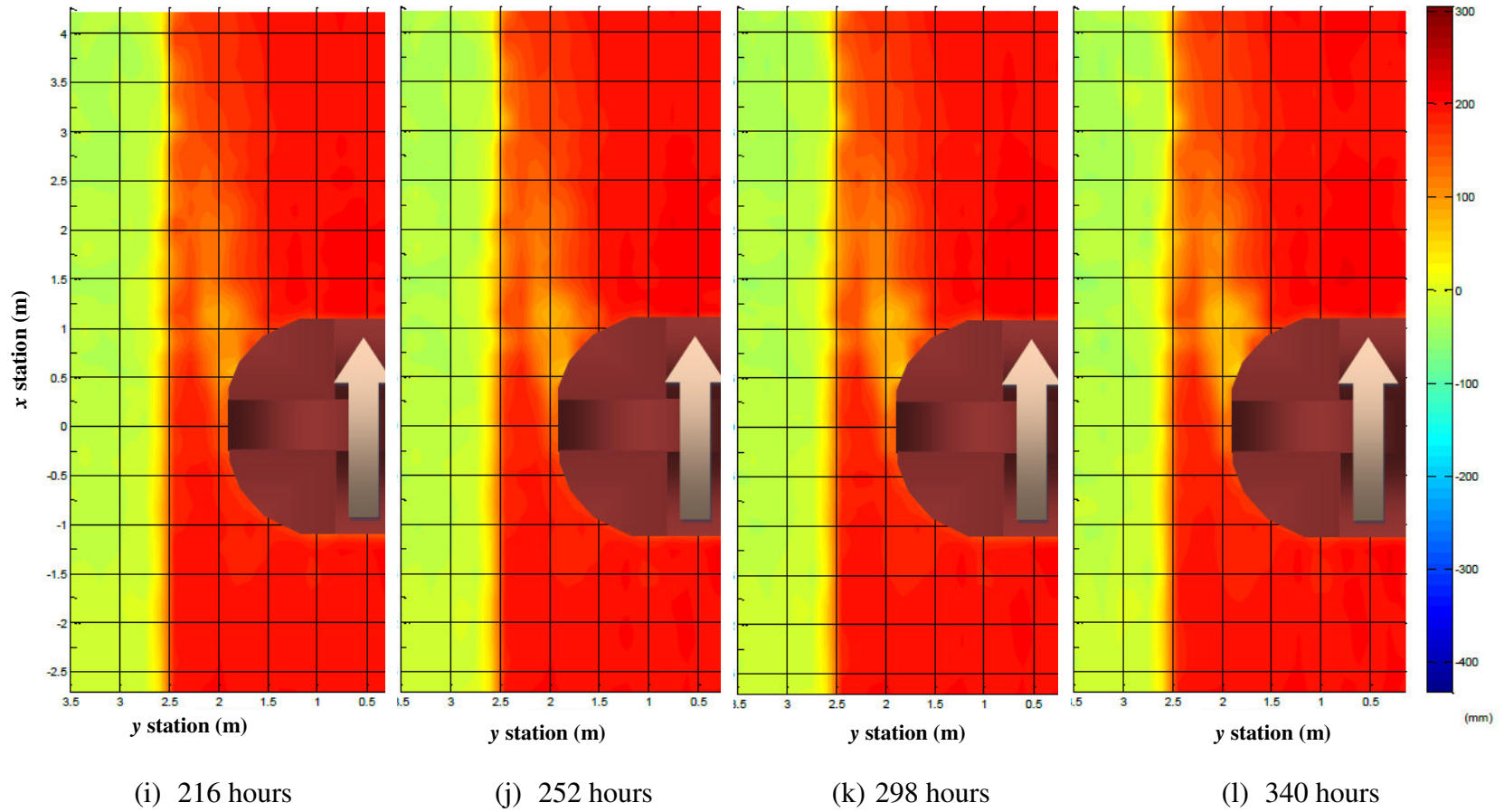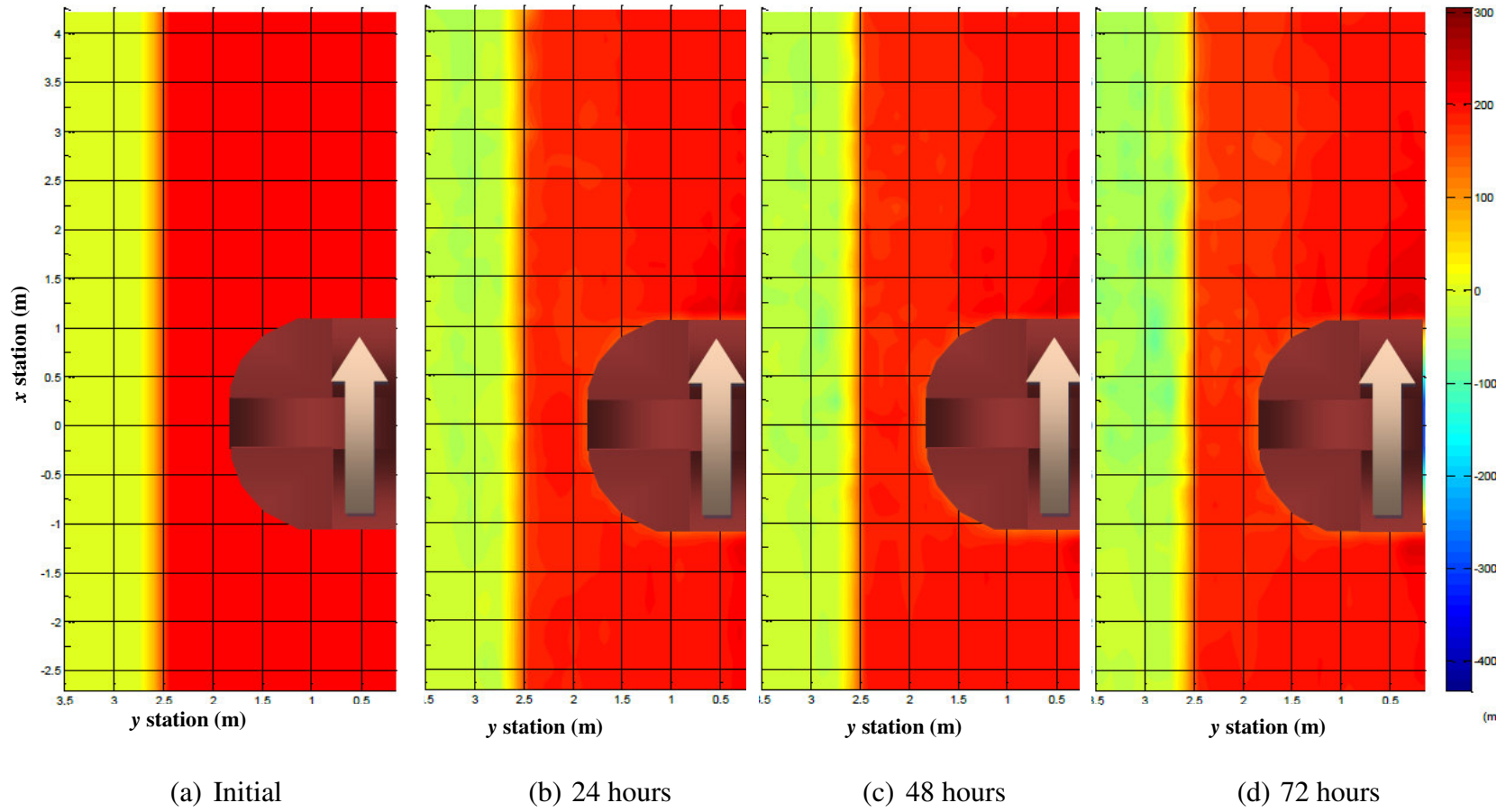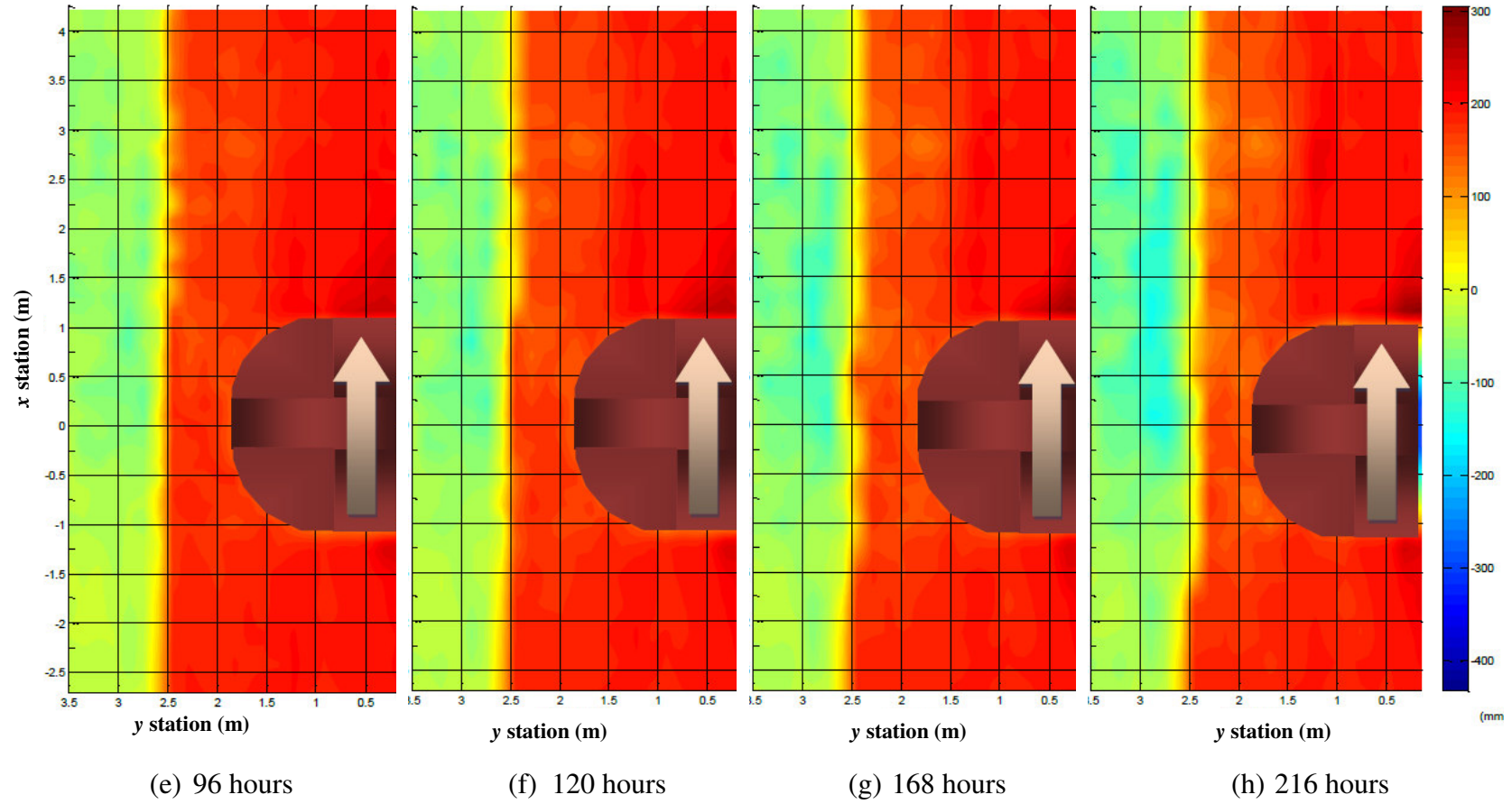
Figure B.6. (continued)
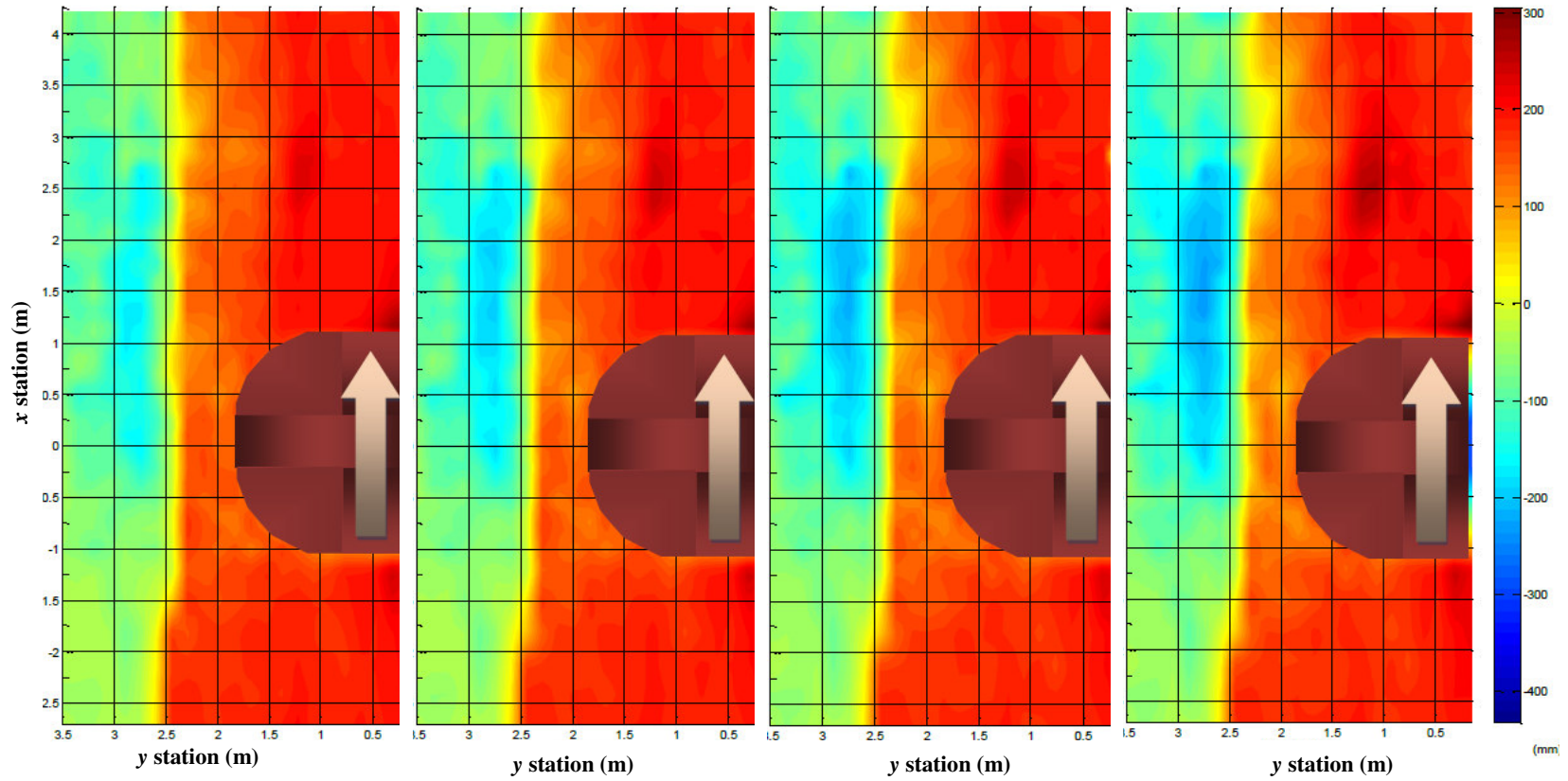
(i) 264 hours   (j) 312 hours   (k) 360 hours   (l) 408 hours

Figure B.6. (continued)

(a) Initial   (b) 20 hours   (c) 40 hours   (d) 60 hours

Figure B.7. Case6

(e) 80 hours (f) 100 hours (g) 144 hours (h) 188 hours
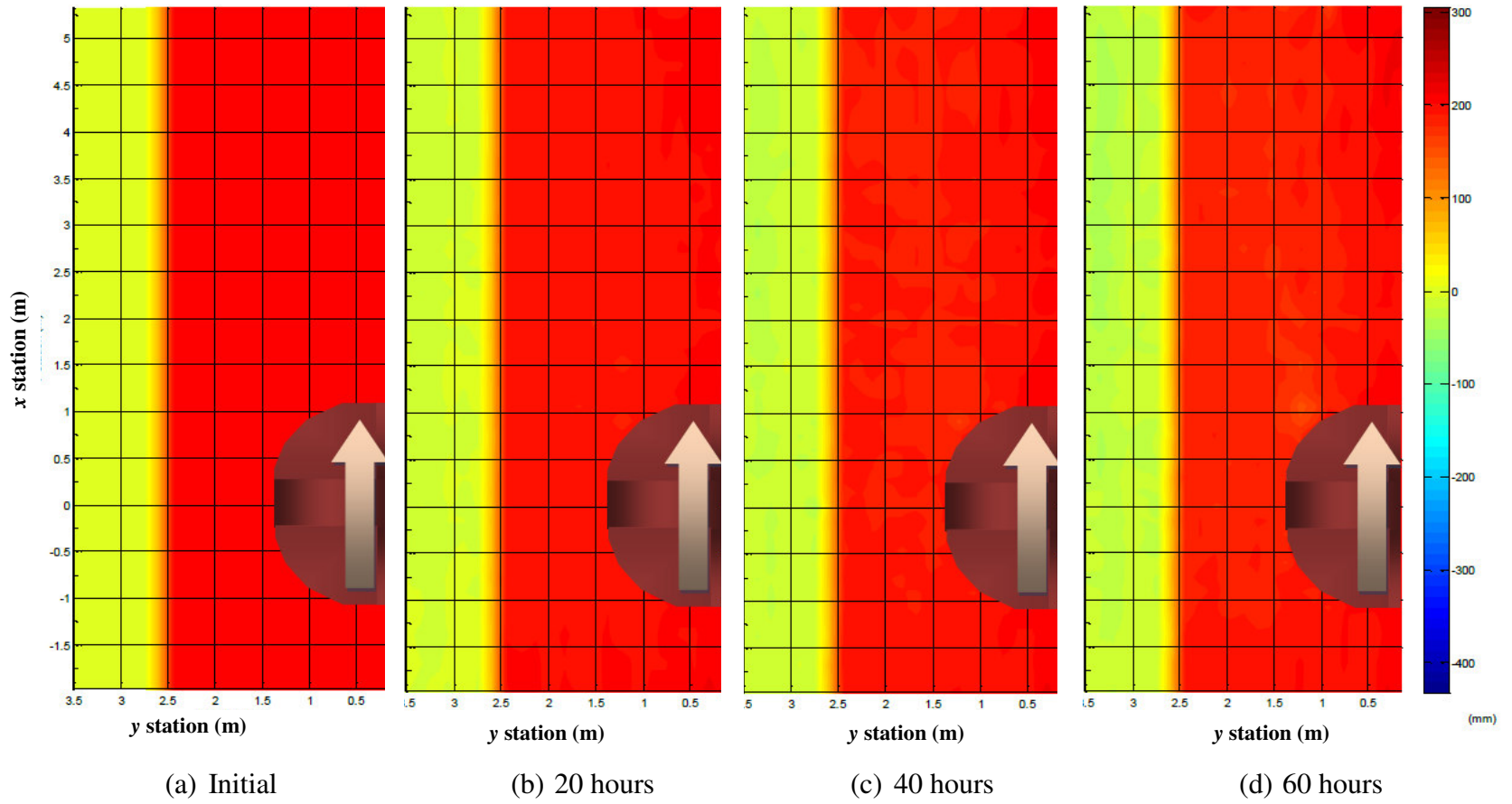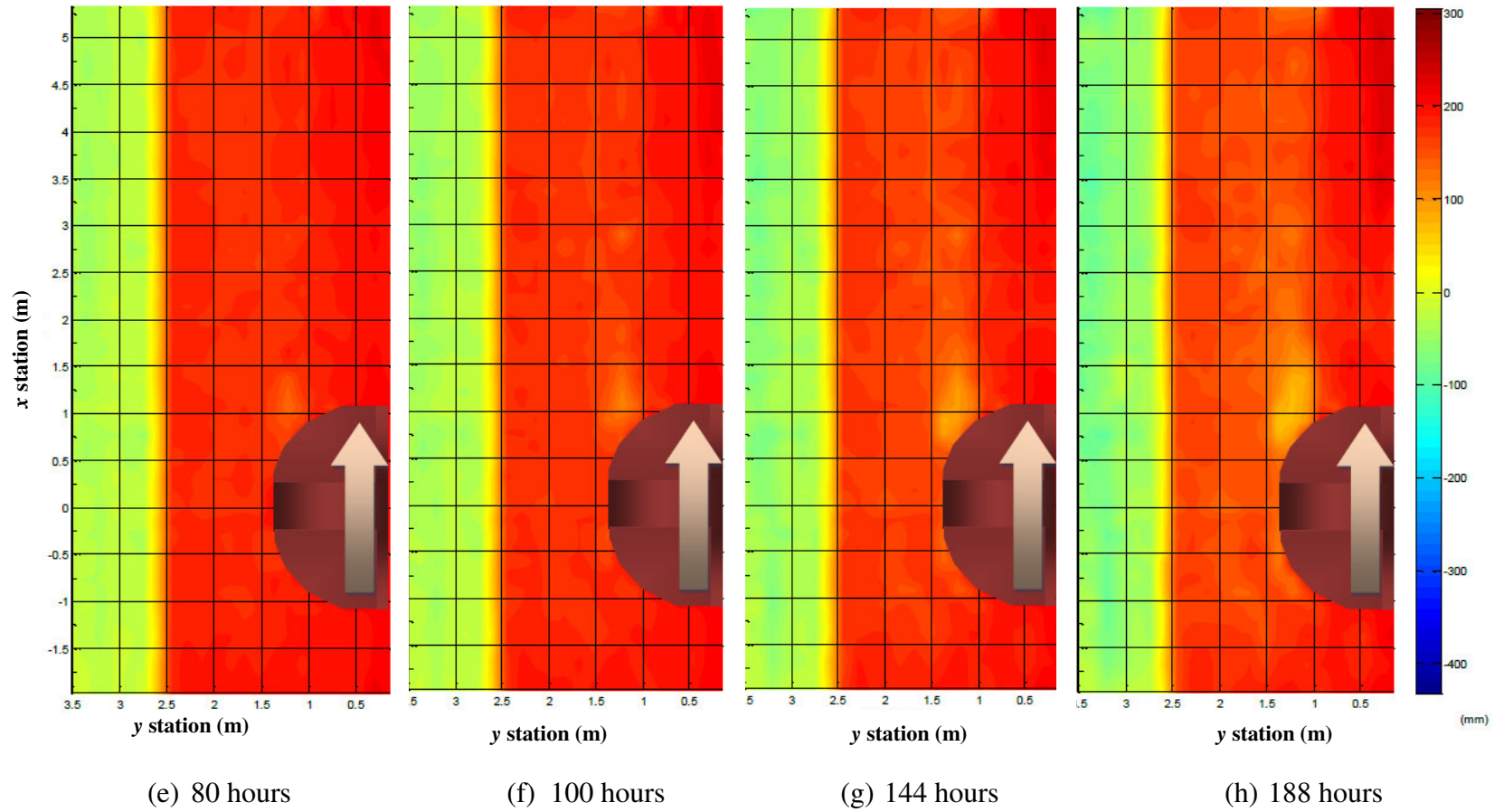
Figure B.7. (continued)

(i) 232 hours   (j) 276 hours   (k) 320 hours

Figure B.7. (continued)

(a) Initial   (b) 20 hours   (c) 40 hours   (d) 60 hours

Figure B.8. Case7

(e) 80 hours   (f) 100 hours   (g) 144 hours   (h) 188 hours
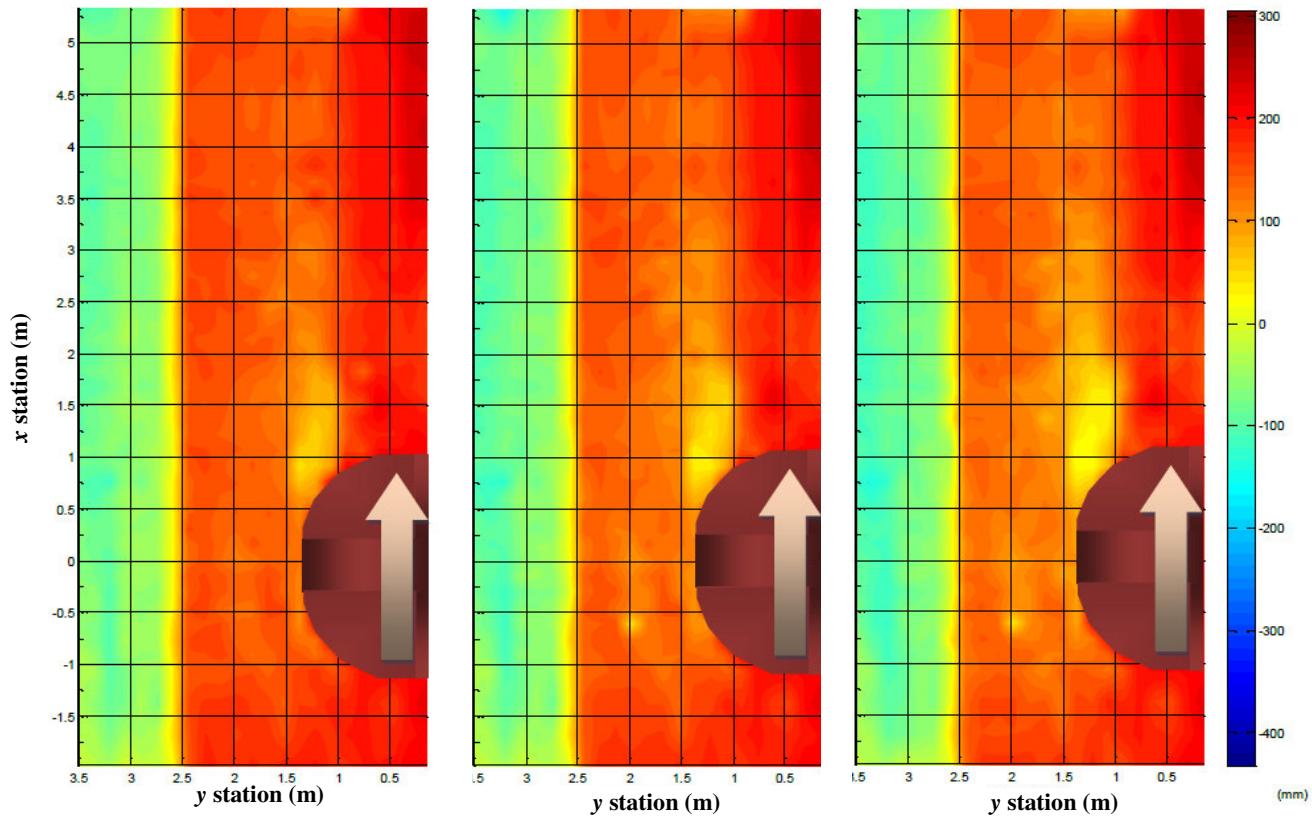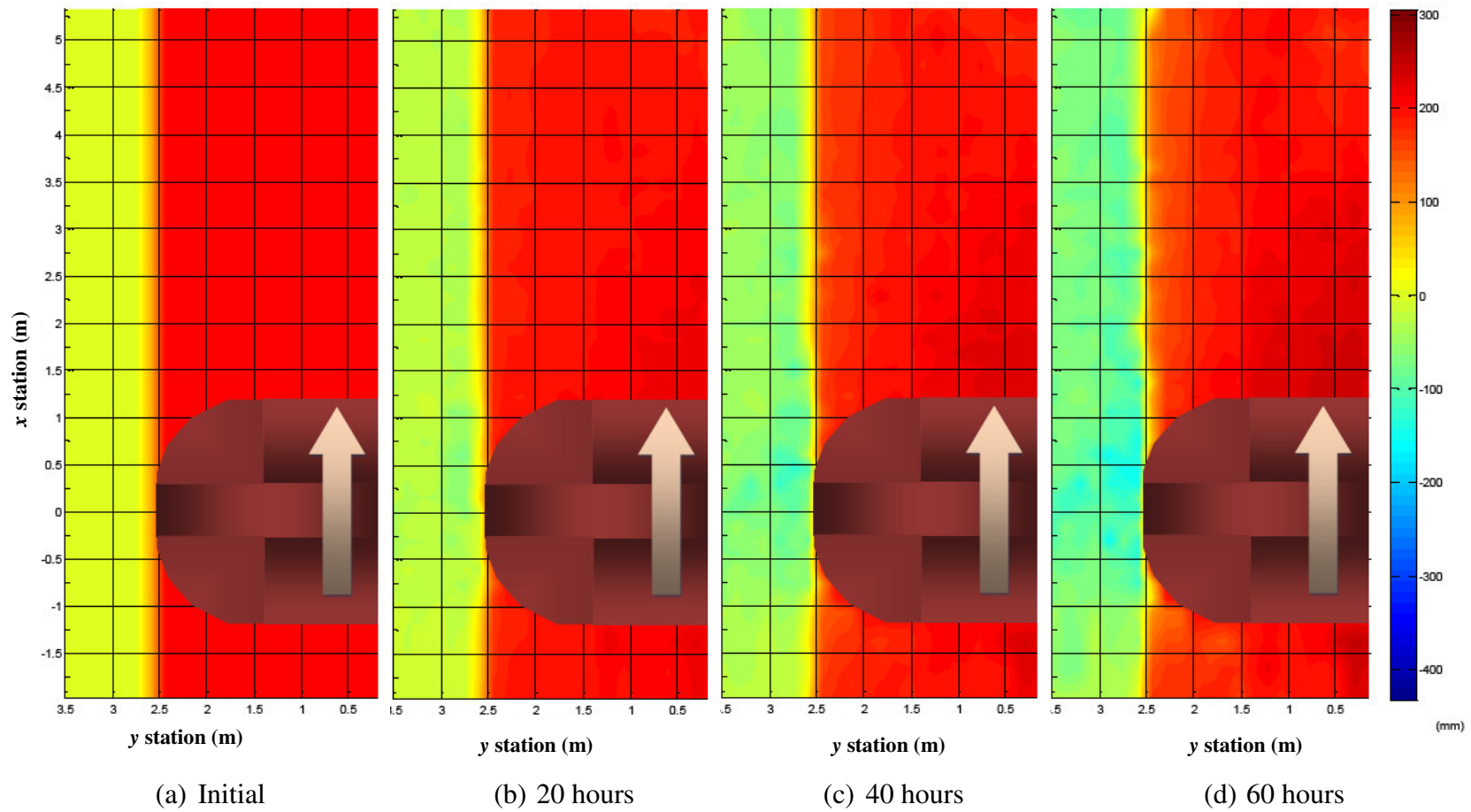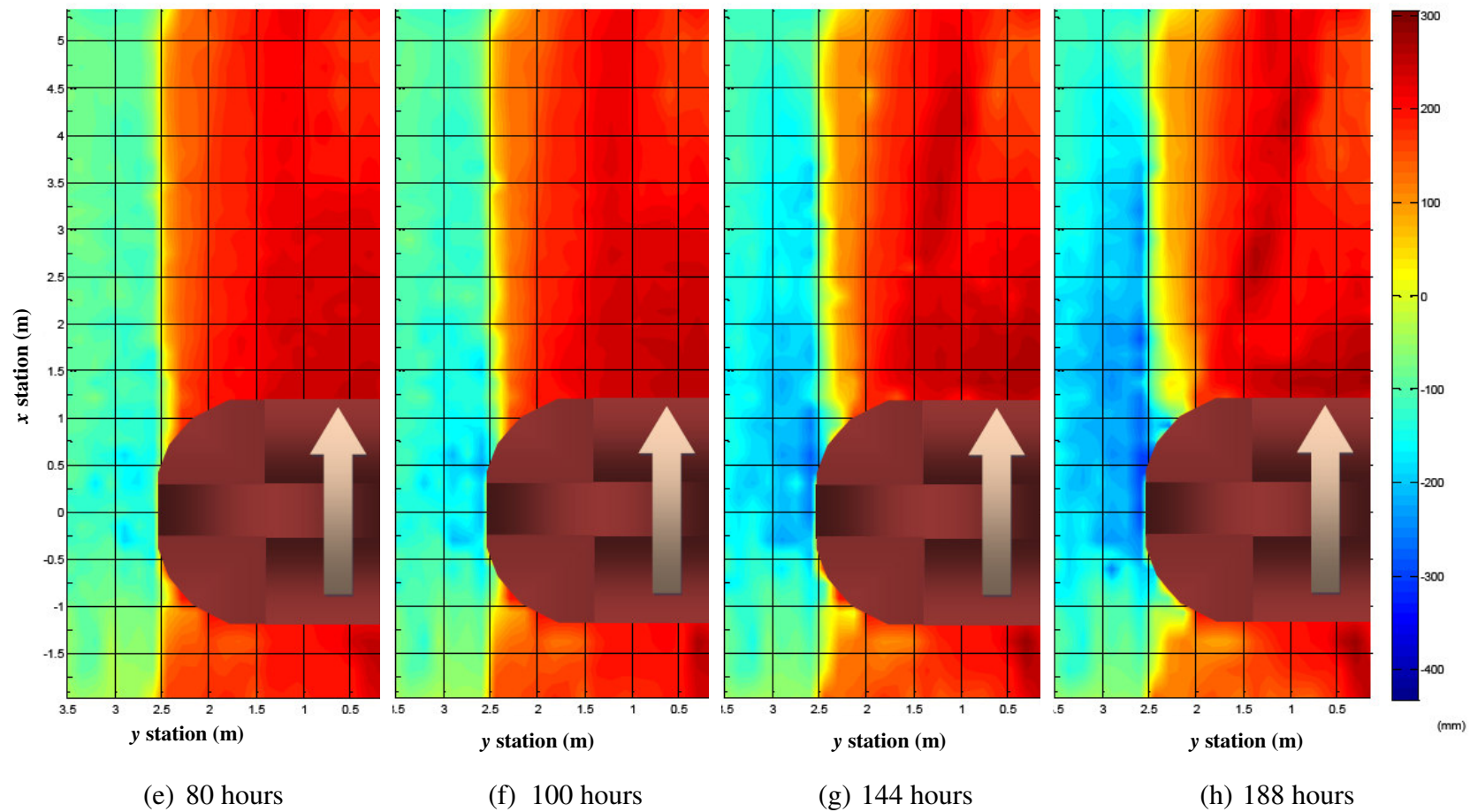
Figure B.8. (continued)
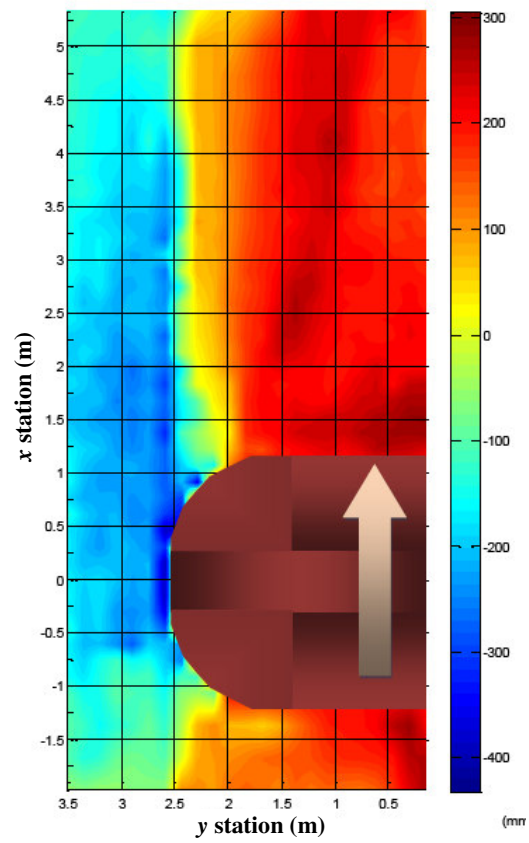
(i) 232 hours   (j) 257 hours

Figure B.8. (continued)

(a) Initial　　　　　(b) 20 hours　　　　　(c) 40 hours　　　　　(d) 60 hours

Figure B.9. Case8

(e) 80 hours   (f) 100 hours   (g) 140 hours   (h) 180 hours
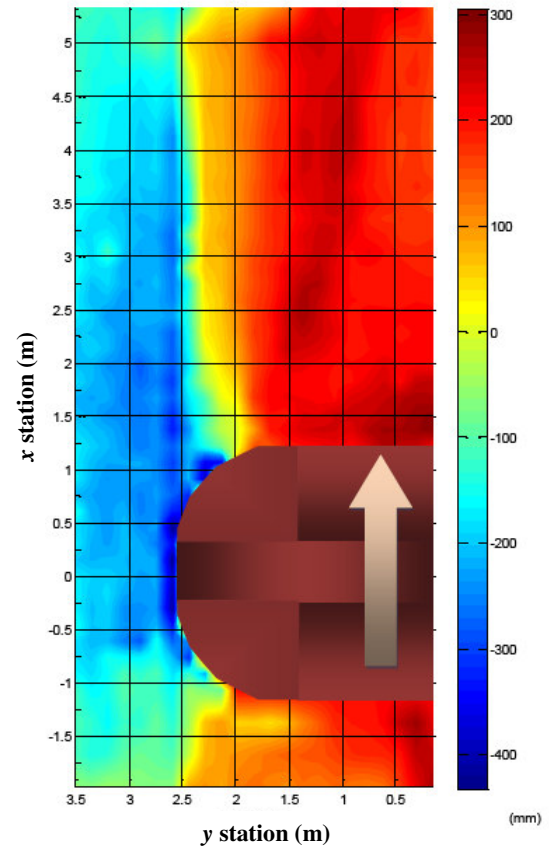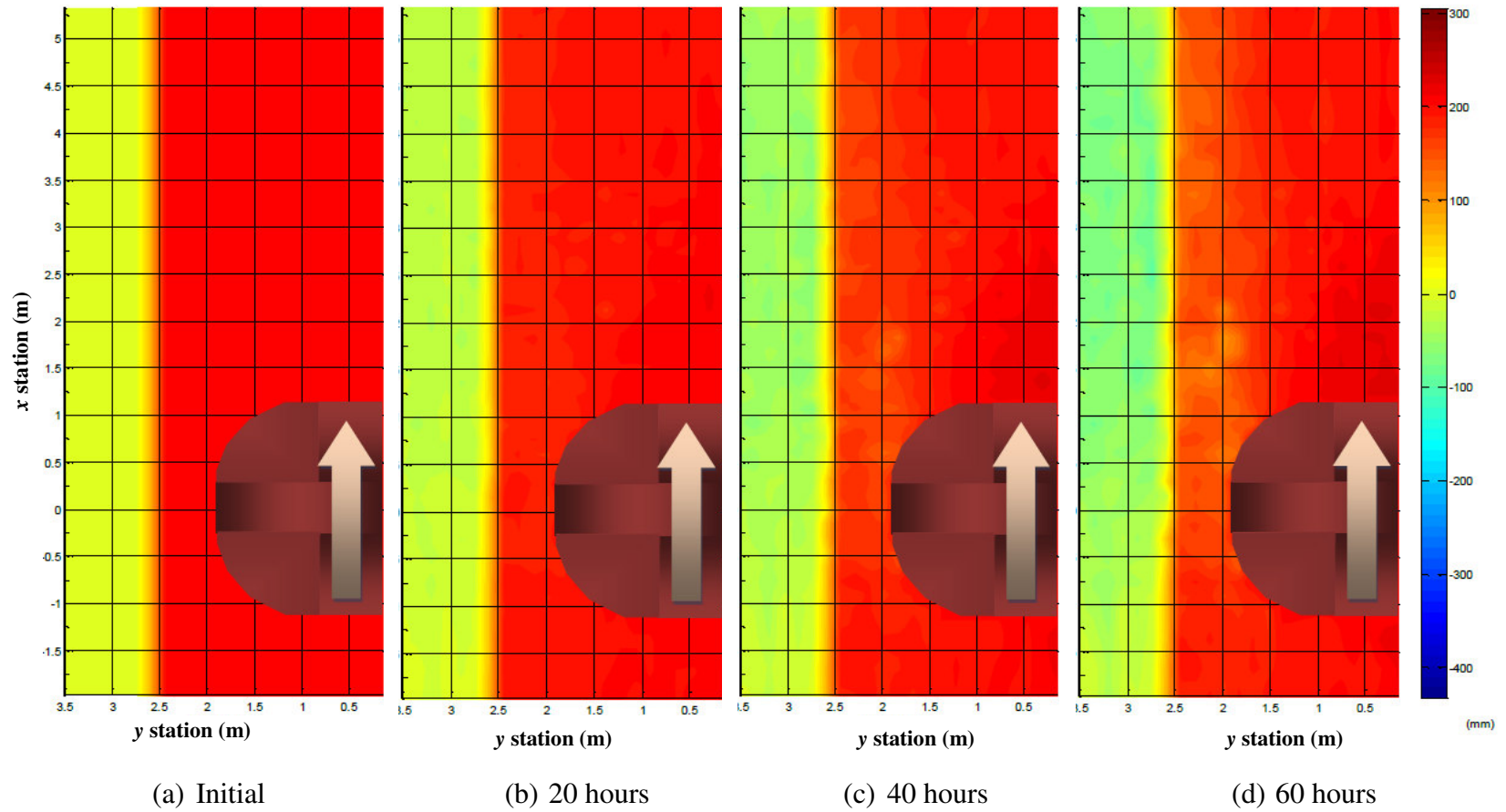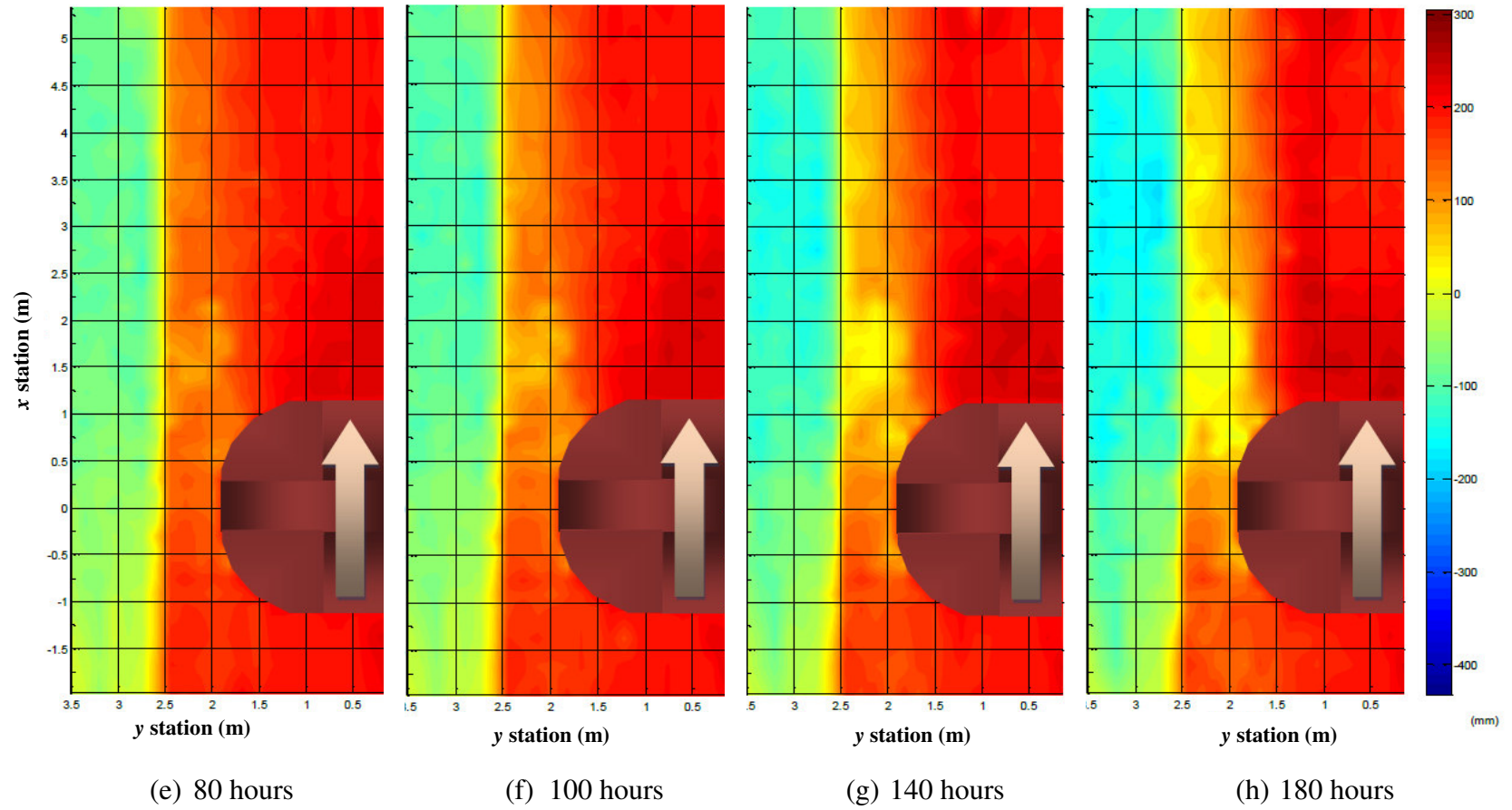
Figure B.9. (continued)
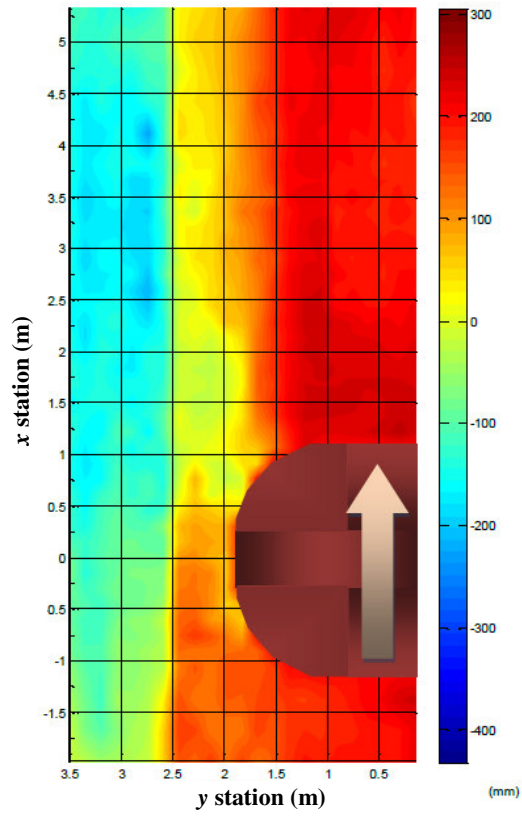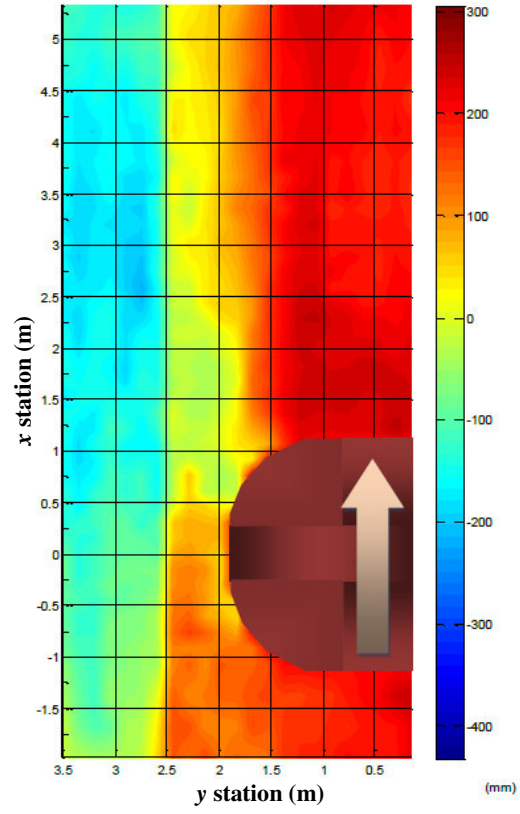
(i) 224 hours   (j) 268 hours   (k) 308 hours

Figure B.9. (continued)

(a) Initial   (b) 20 hours   (c) 40 hours   (d) 60 hours

Figure B.10. Case9

(e) 84 hours   (f) 102 hours   (g) 145 hours   (h) 190 hours
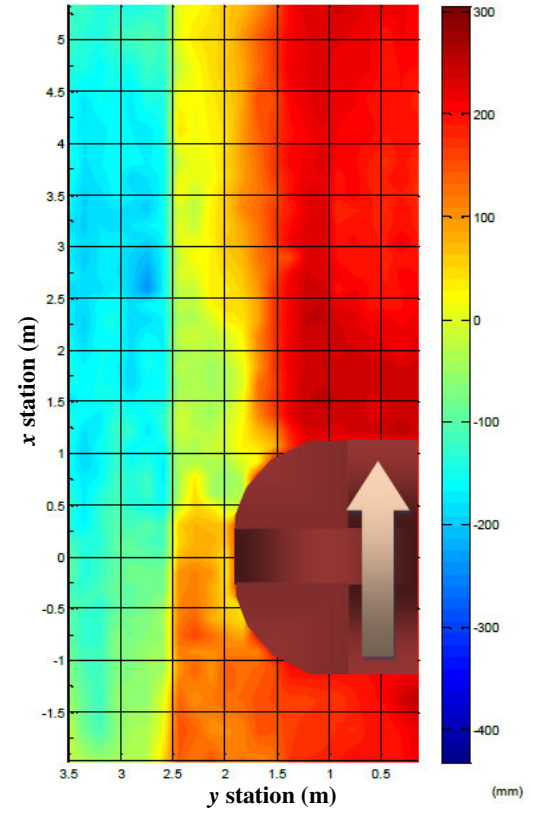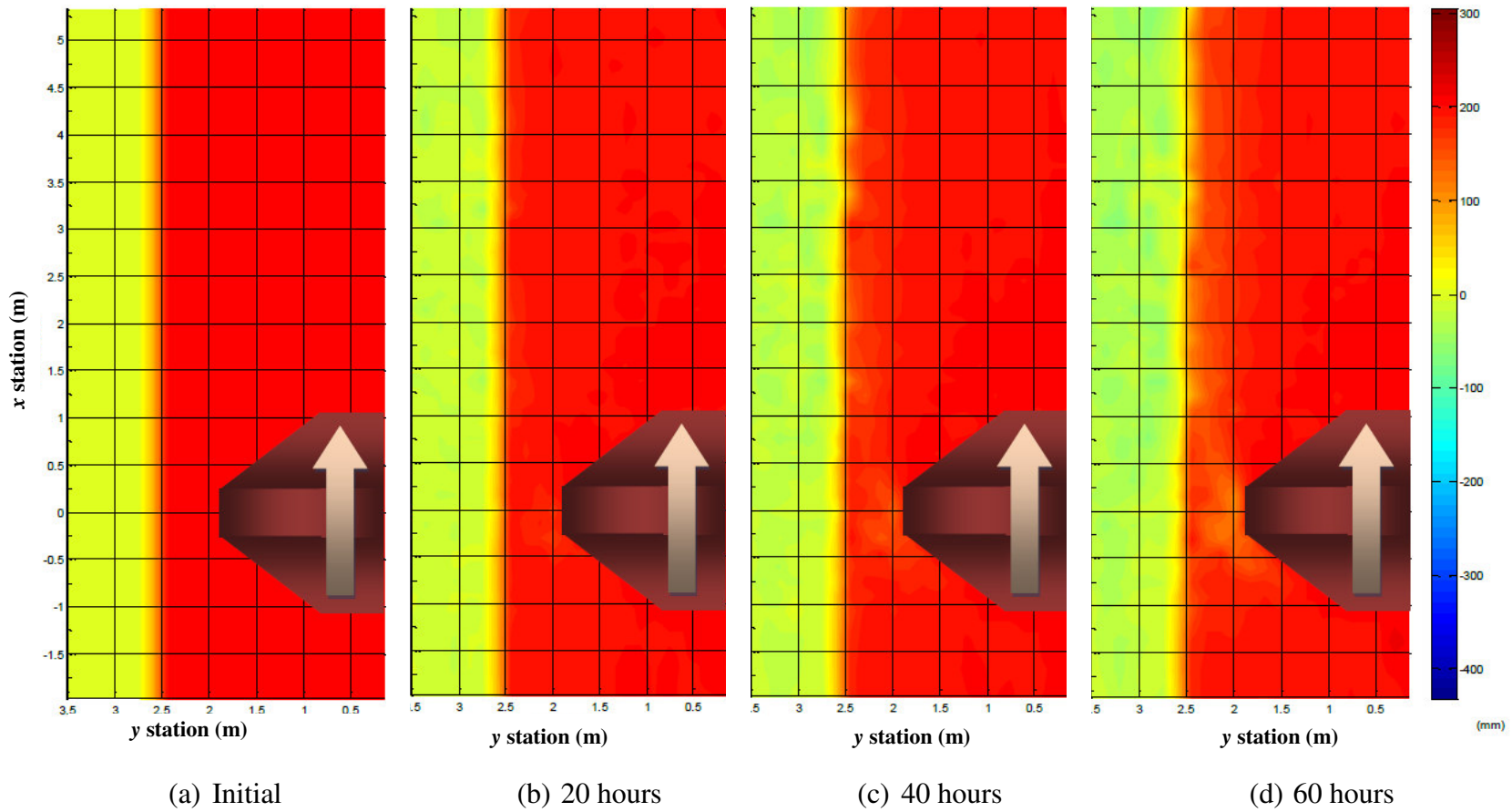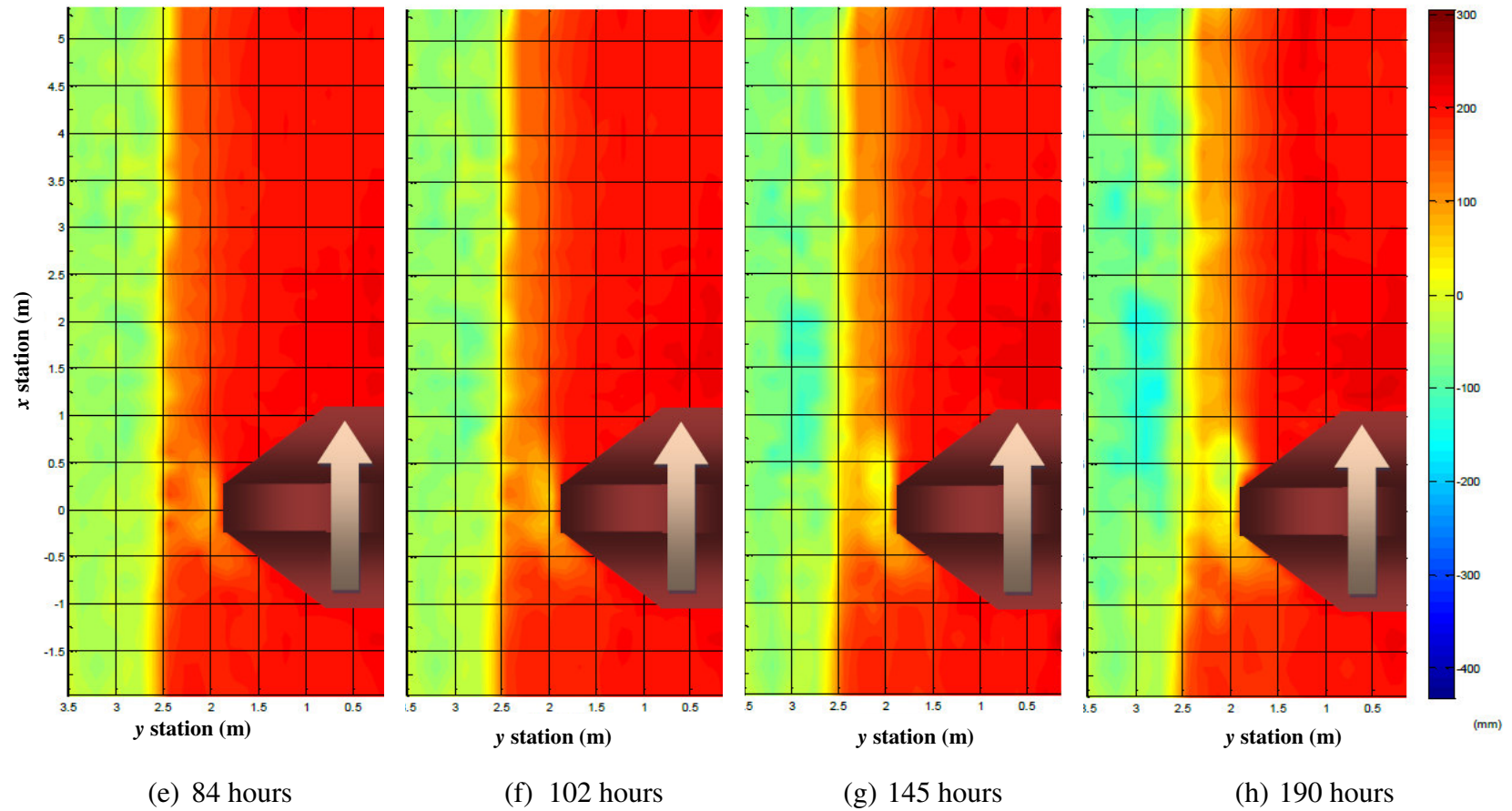
Figure B.10. (continued)
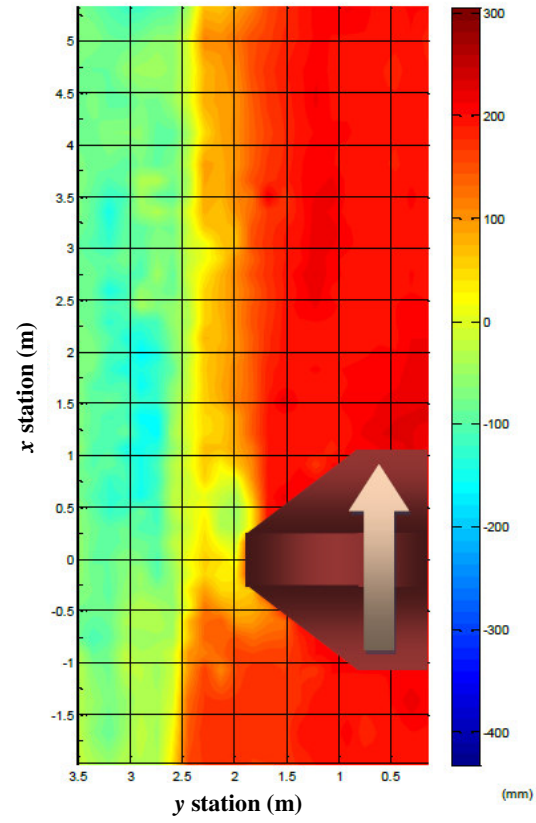
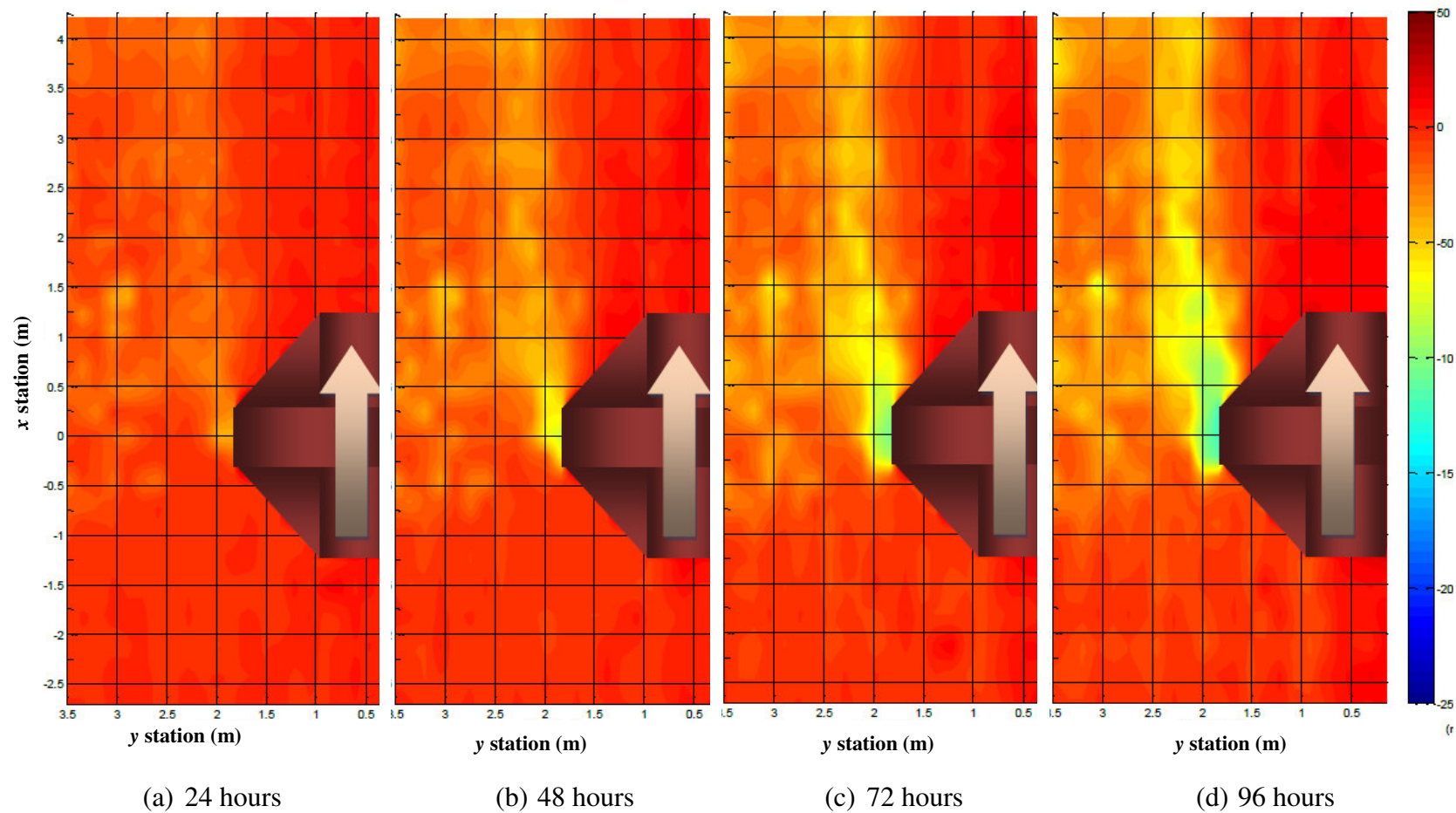(i) 230 hours   (j) 271 hours
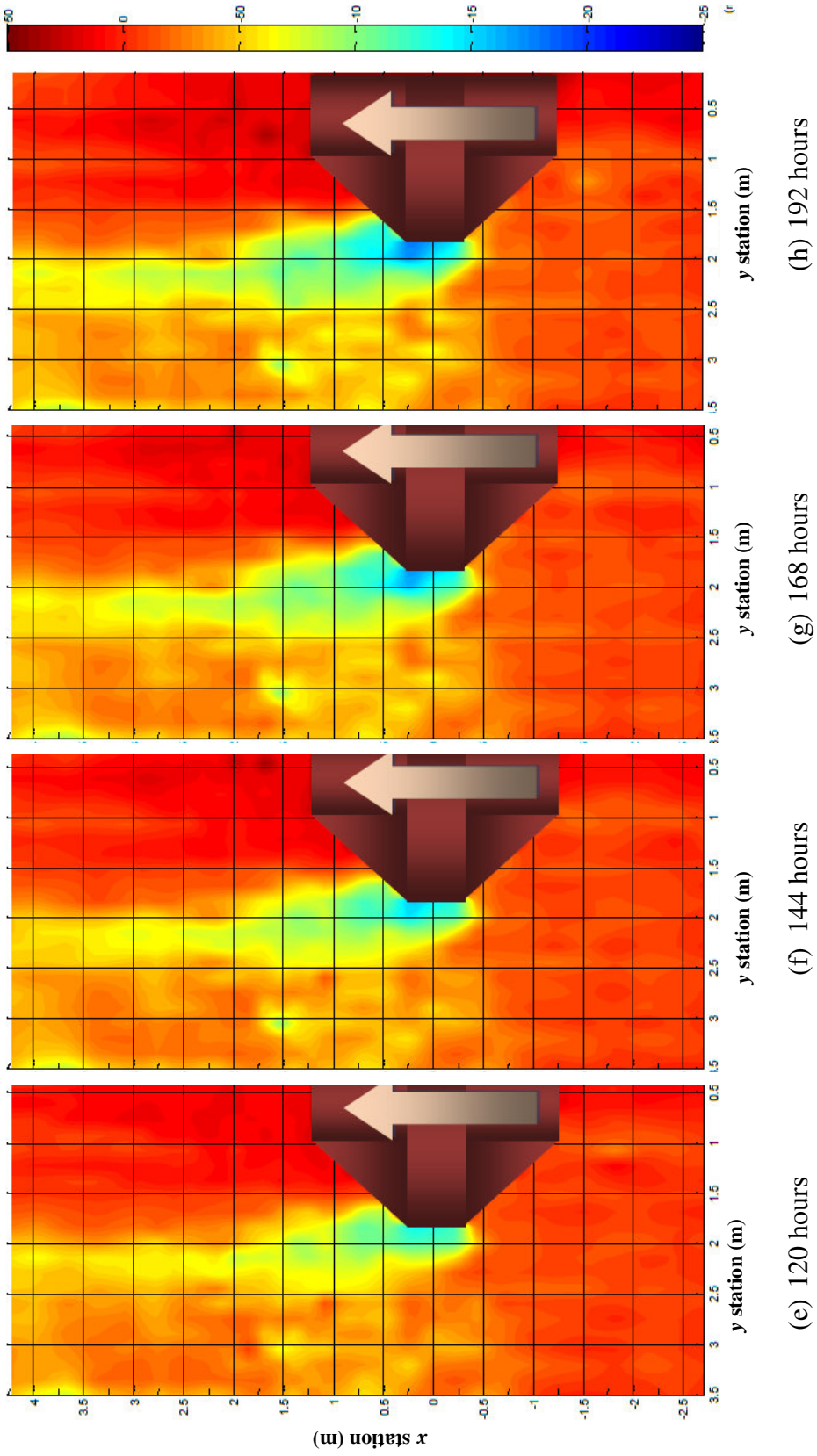
Figure B.10. (continued)

(a) Initial   (b) 20 hours   (c) 40 hours   (d) 60 hours

Figure B.11. Case10

(e) 80 hours   (f) 100 hours   (g) 144 hours   (h) 188 hours
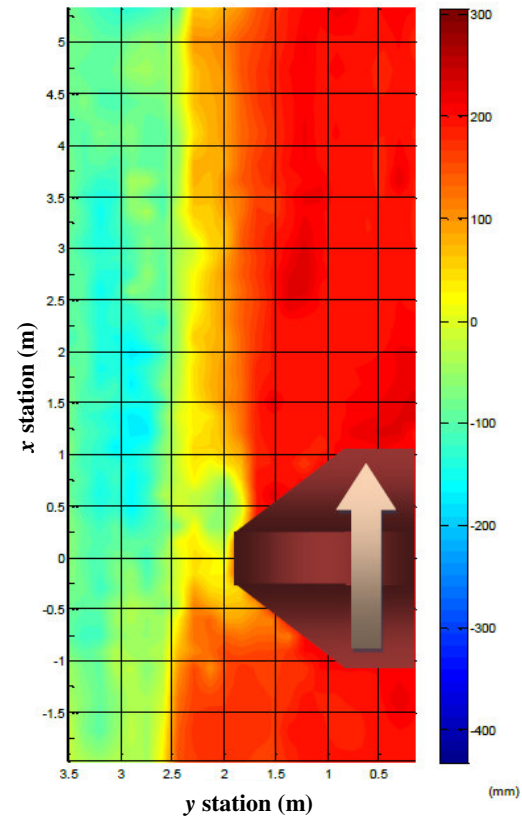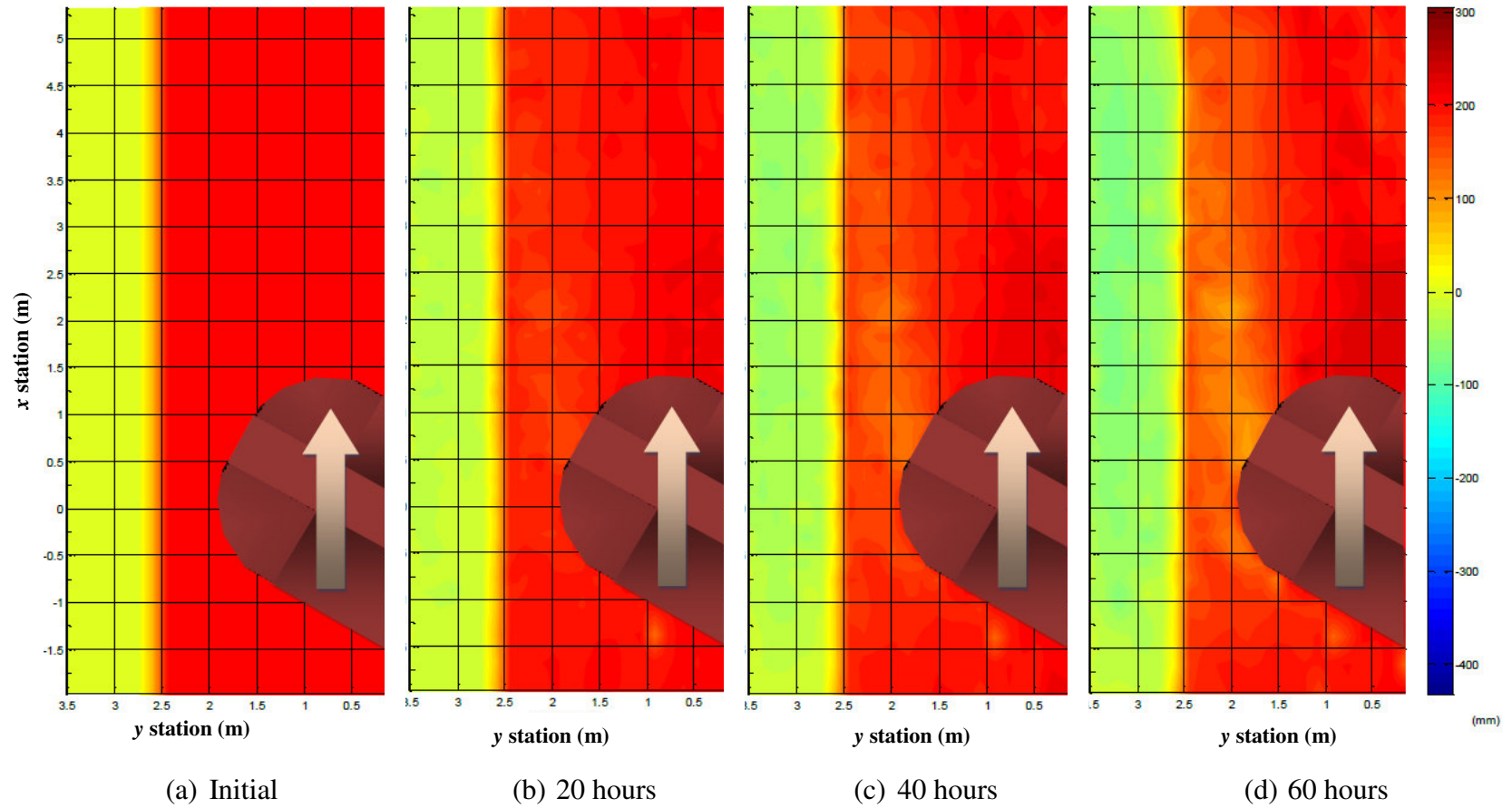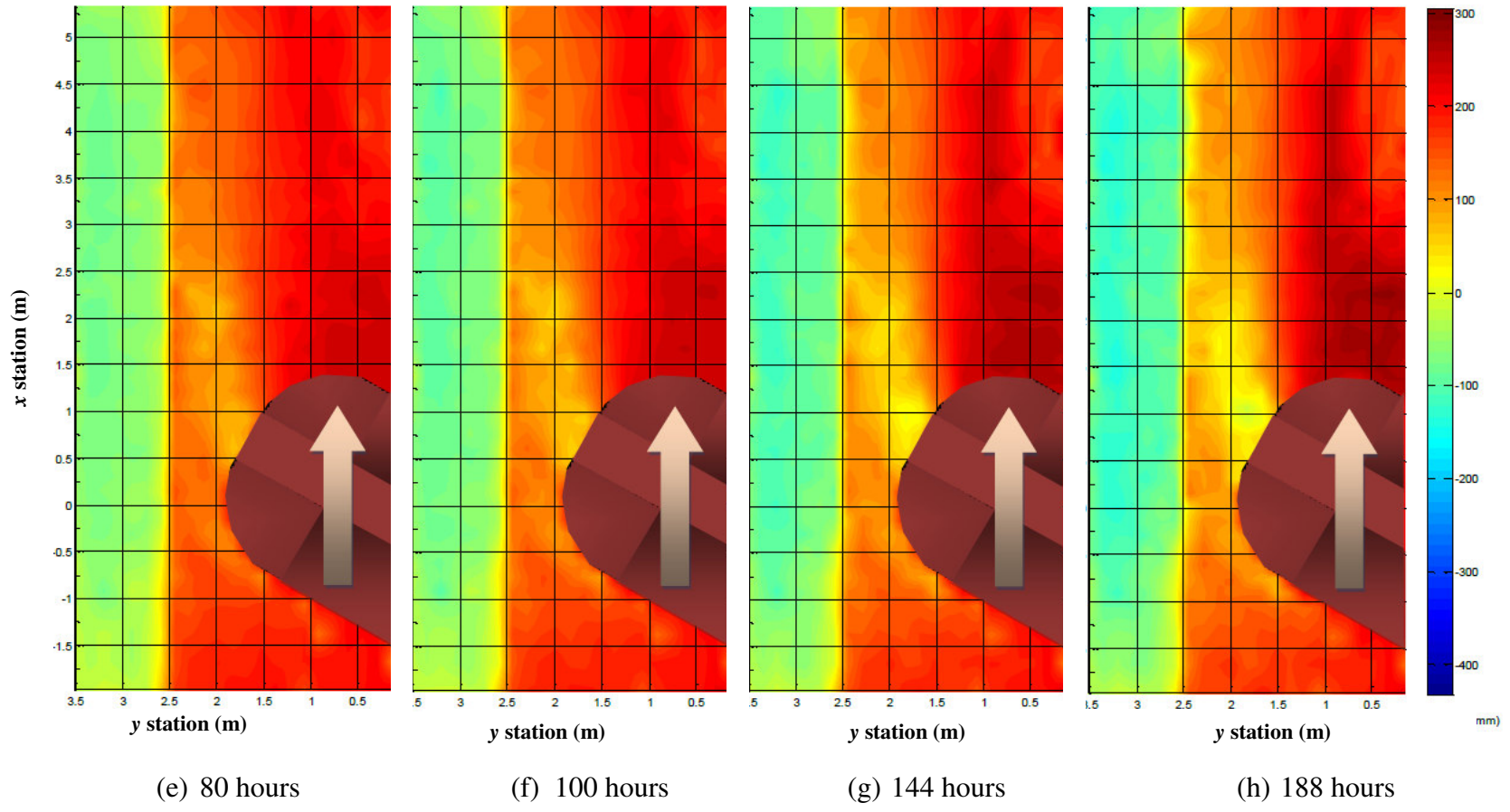
Figure B.11. (continued)

(i) 232 hours   (j) 276 hours   (k) 320 hours

Figure B.11. (continued)

(a) Initial   (b) 20 hours   (c) 40 hours   (d) 60 hours
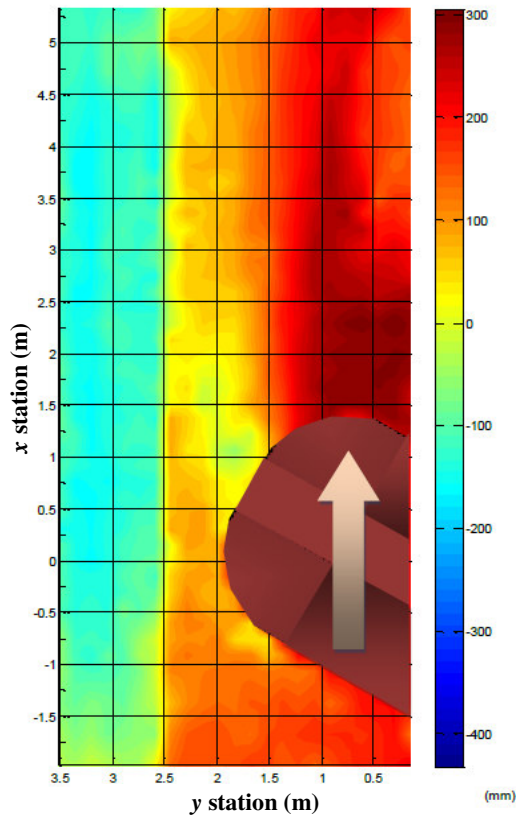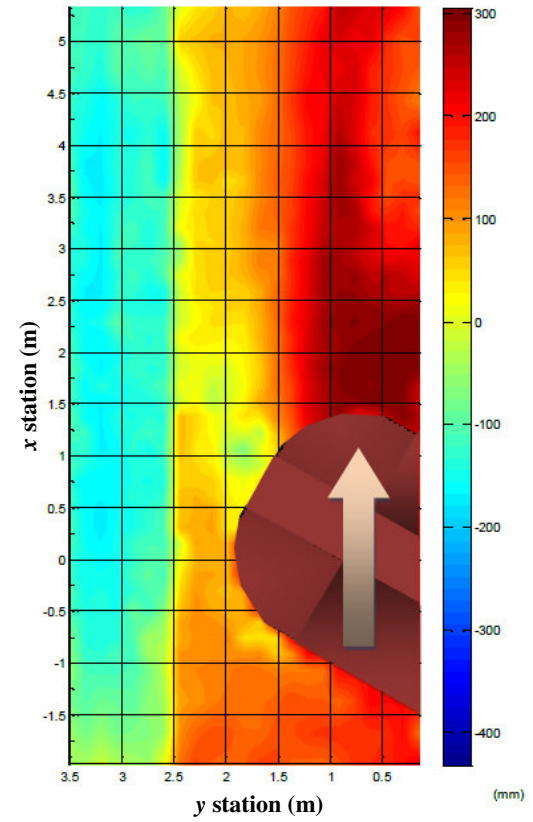
Figure B.12. Case11

(e) 80 hours   (f) 100 hours   (g) 144 hours   (h) 186.5 hours
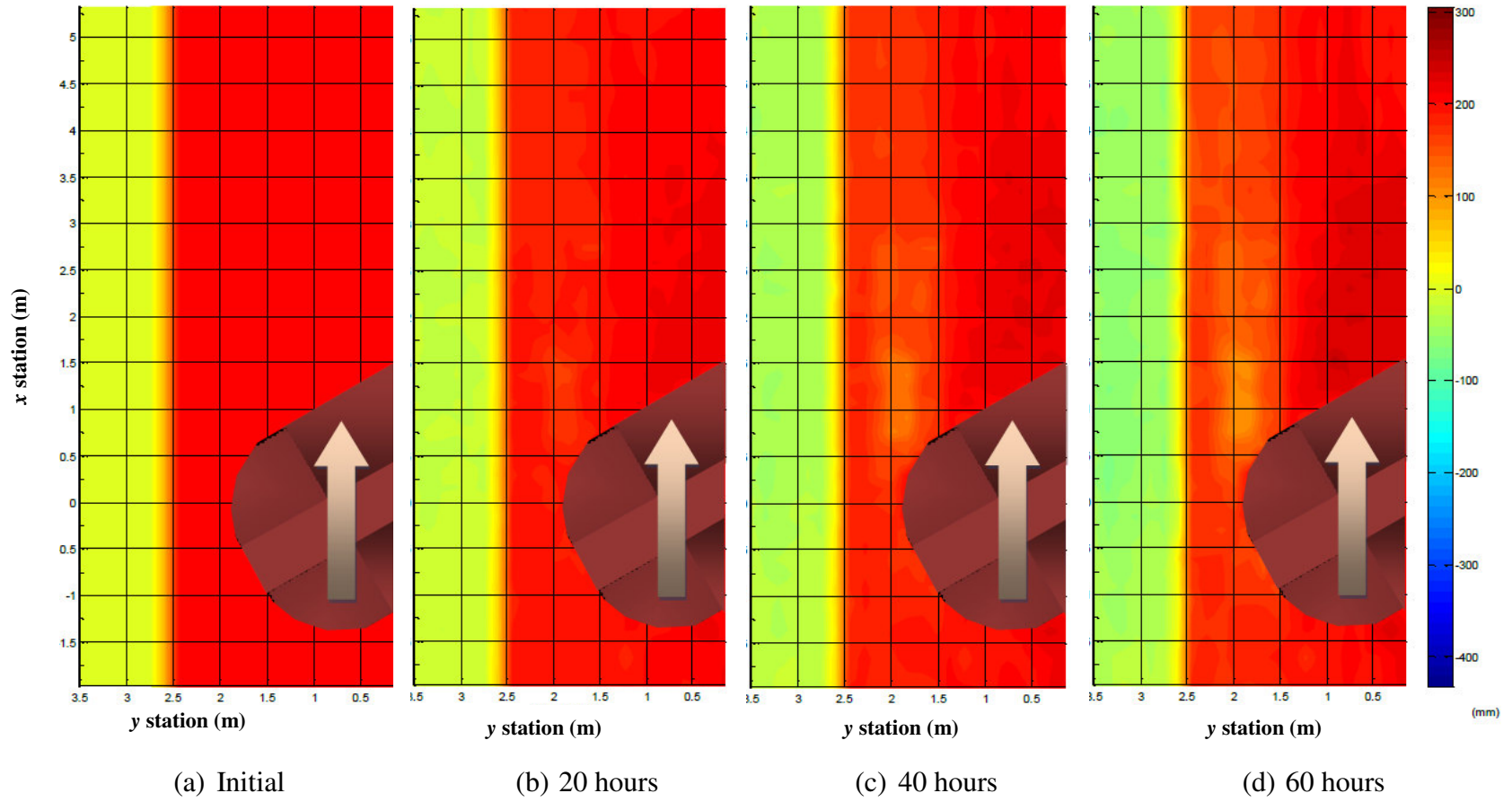
Figure B.12. (continued)

(i) 231.5 hours   (j) 276 hours   (k) 320 hours

Figure B.12. (continued)
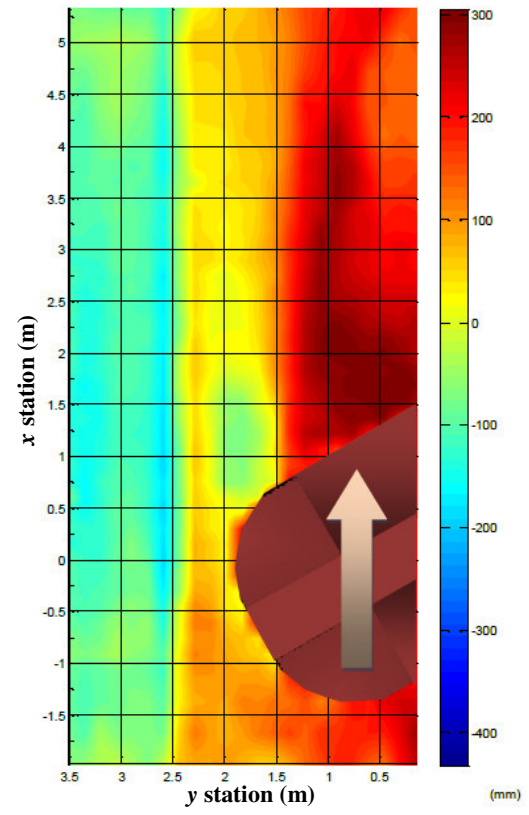
(a) Initial   (b) 48 hours   (c) 72 hours   (d) 96 hours
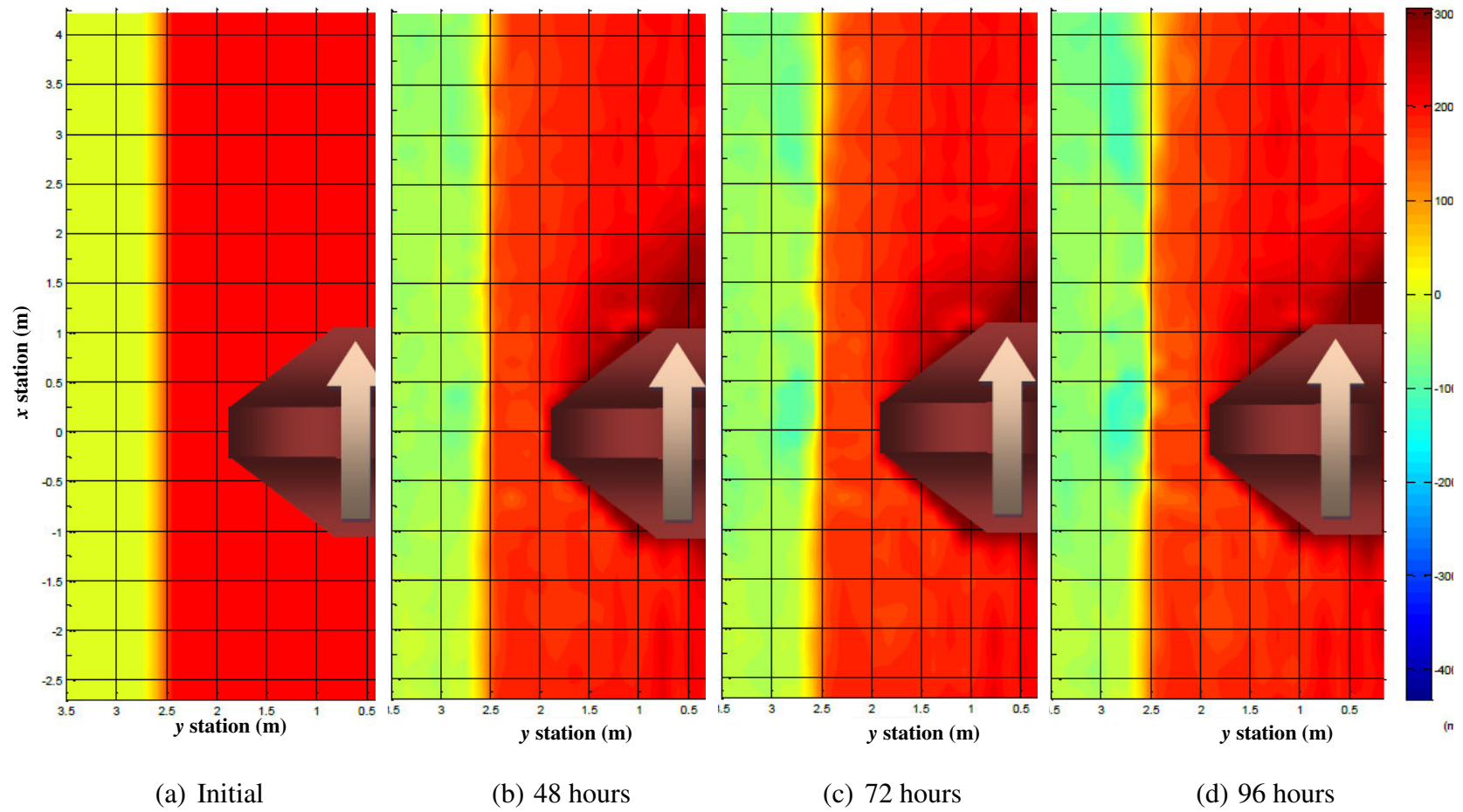
Figure B.13. Case12B

(e) 120 hours   (f) 144 hours   (g) 168 hours   (h) 192 hours

Figure B.13. (continued)

(i) 216 hours   (j) 240 hours   (k) 264 hours   (l) 288 hours

Figure B.13. (continued)
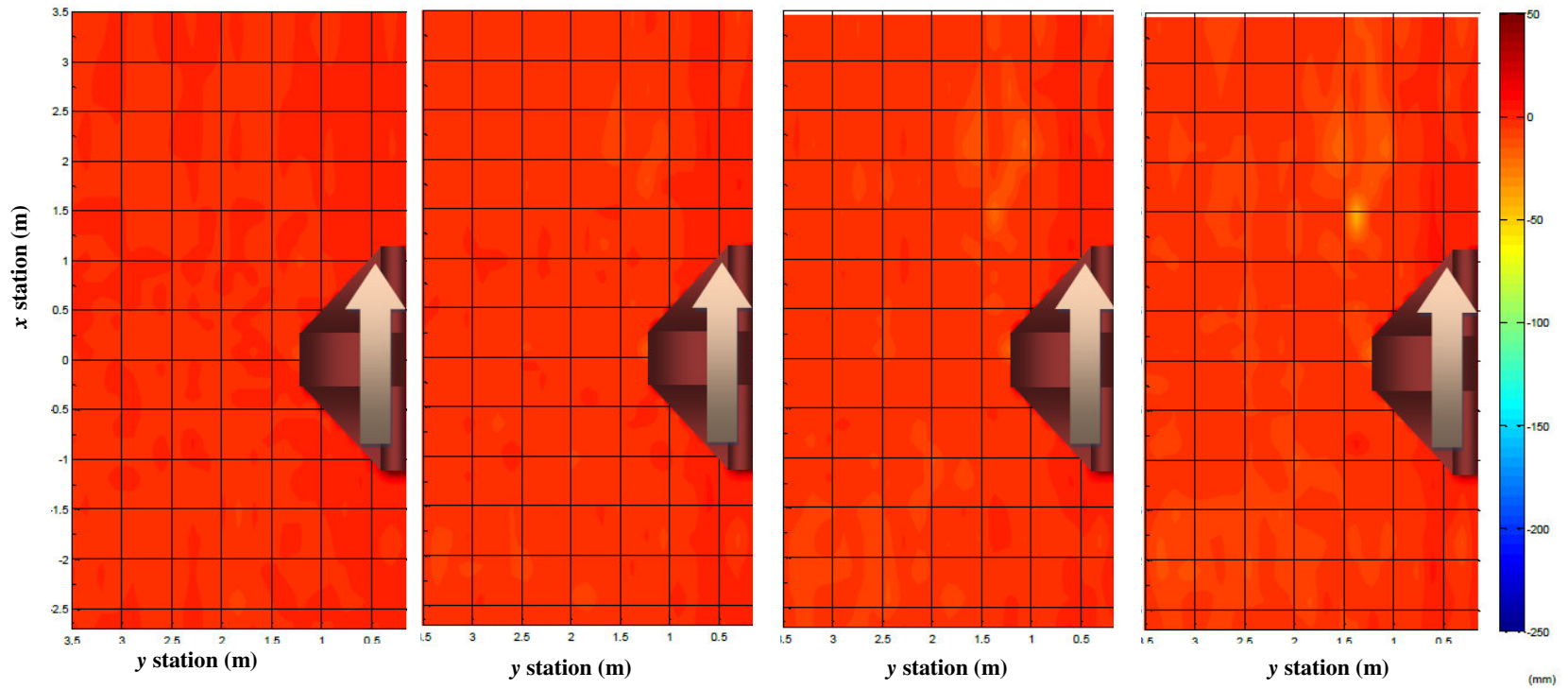
(a) 24 hours   (b) 48 hours   (c) 72 hours   (d) 96 hours

Figure B.14. Case13

(e) 120 hours   (f) 144 hours   (g) 168 hours   (h) 192 hours

Figure B.14. (continued)
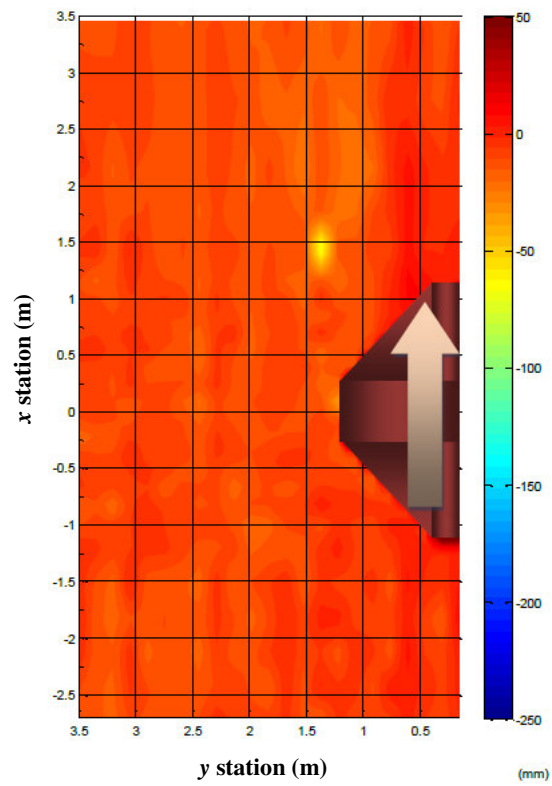
(i) 216 hours   (j) 240 hours
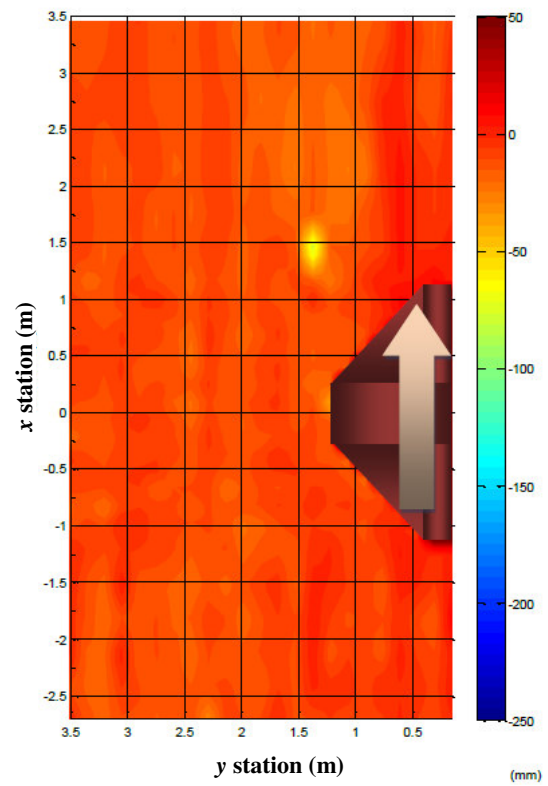
Figure B.14. (continued)

(a) 24 hours   (b) 48 hours   (c) 72 hours   (d) 96 hours

Figure B.15. Case14

(e) 120 hours (f) 144 hours (g) 168 hours (h) 192 hours

Figure B.15. (continued)

318

Figure B.15. (continued)

(i) 216 hours

(j) 240 hours

Figure B.16. Case15

(a) 24 hours   (b) 48 hours   (c) 72 hours   (d) 96 hours

(e) 120 hours   (f) 144 hours   (g) 168 hours   (h) 192 hours
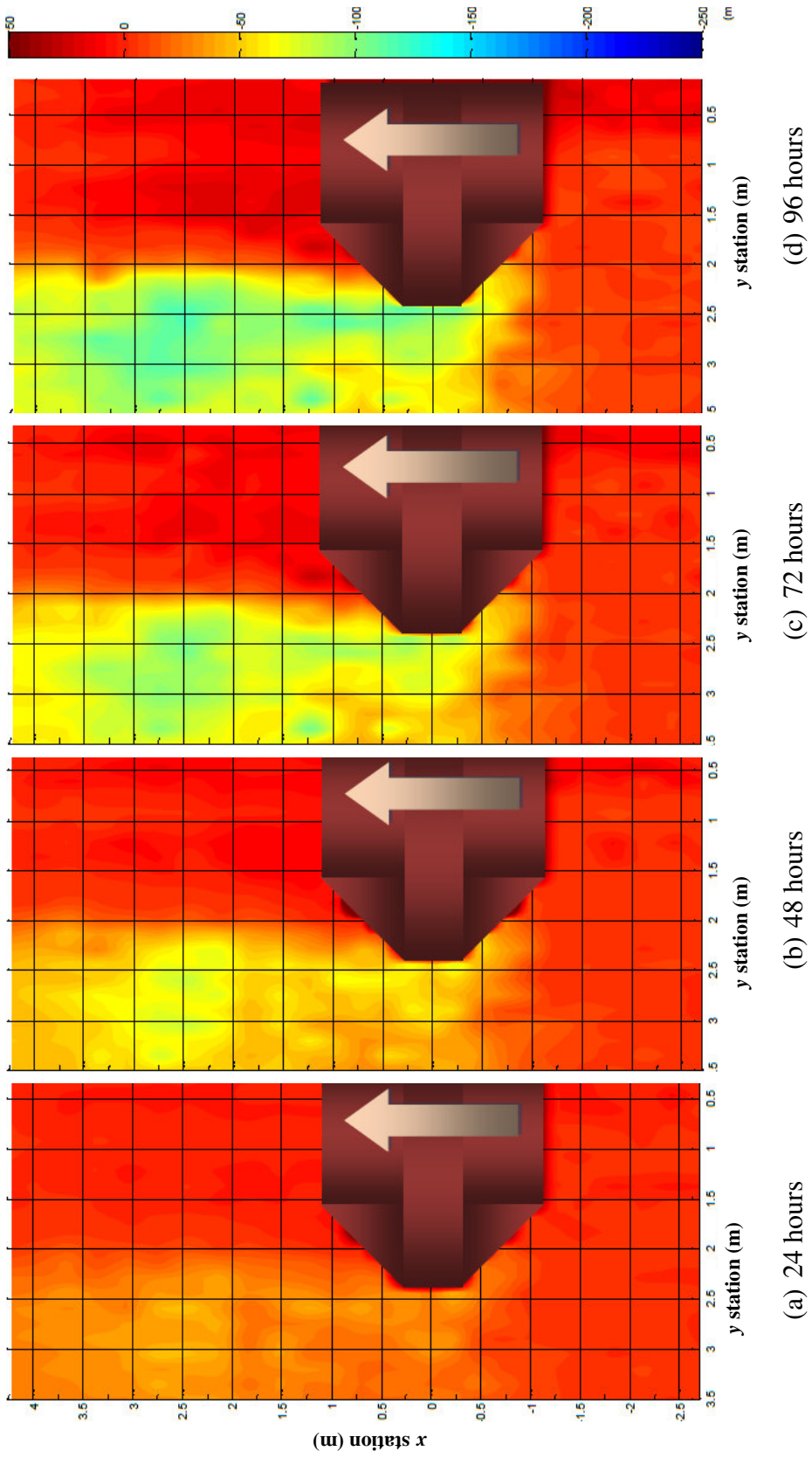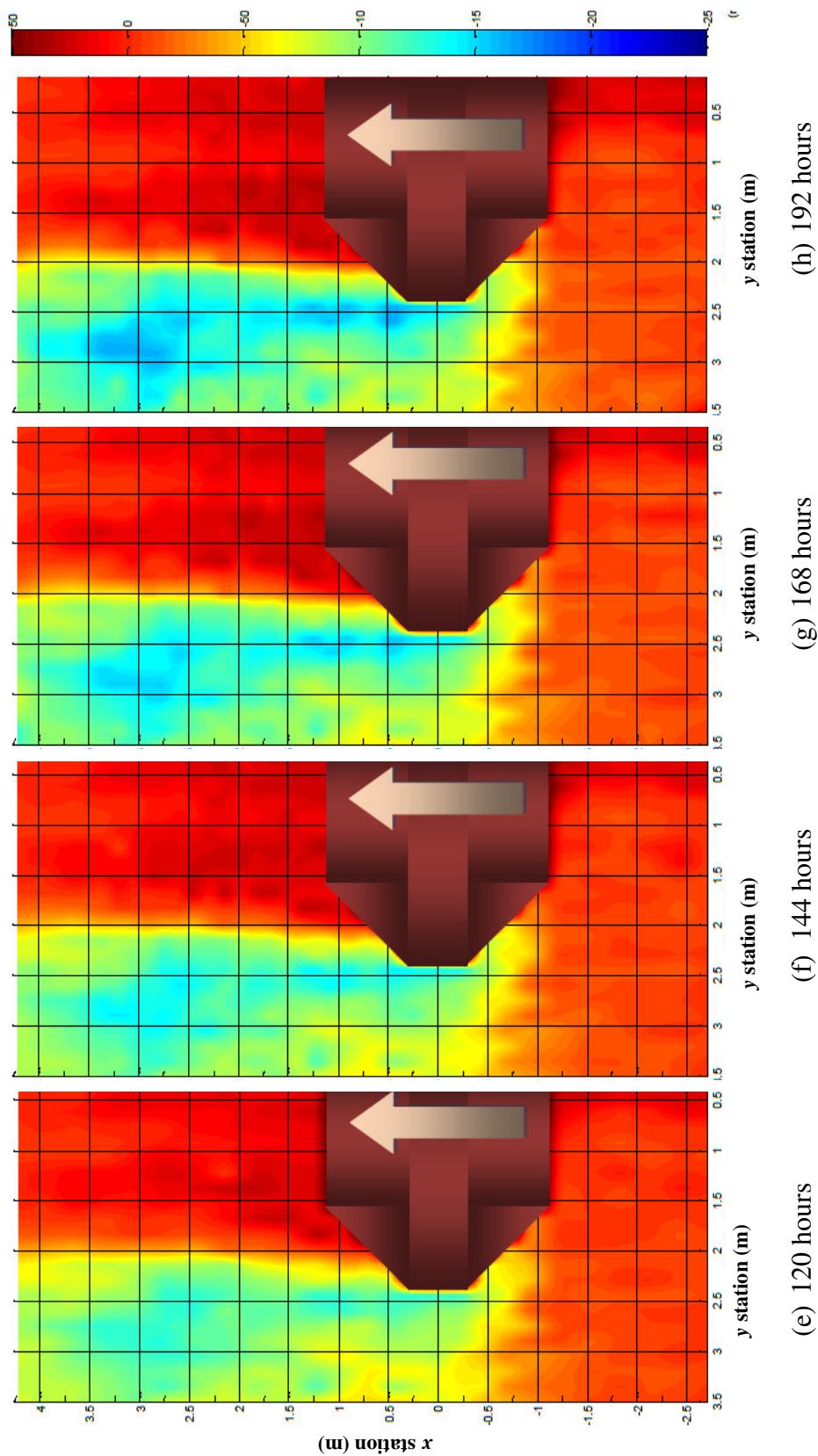
Figure B.16. (continued)
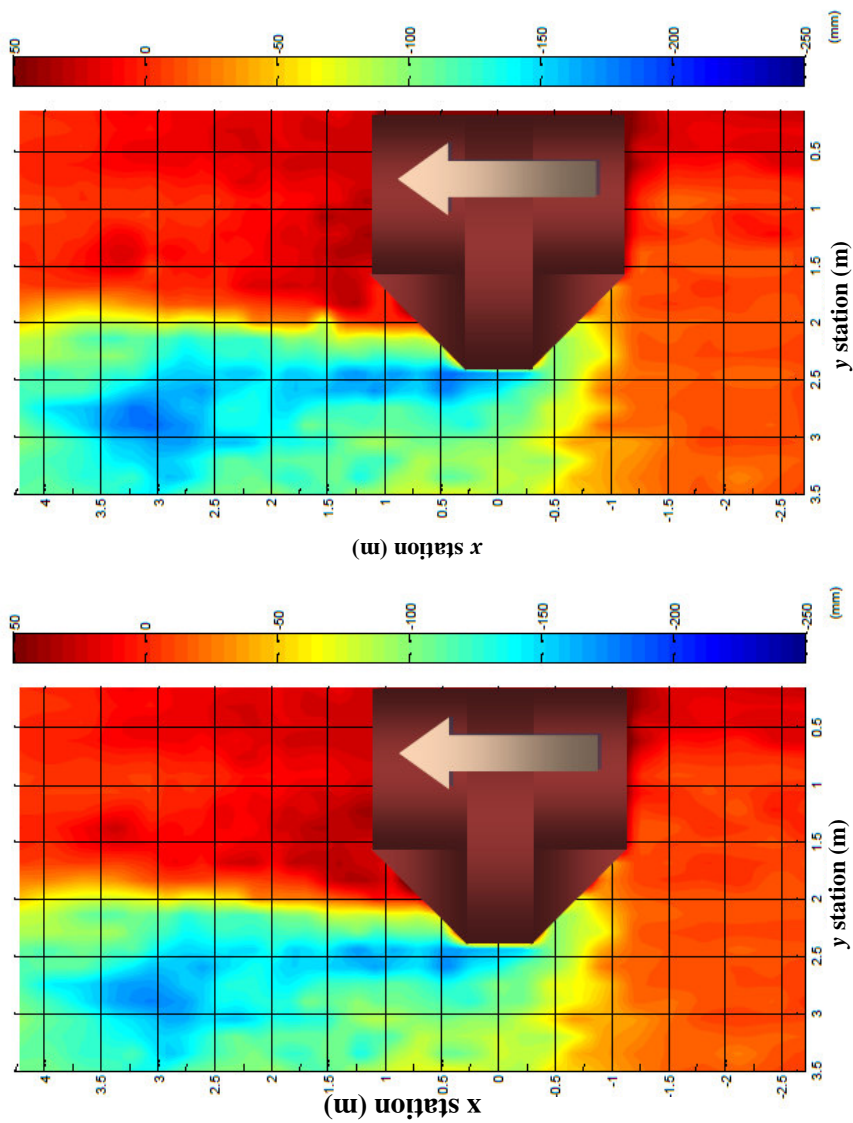
(i) 216 hours   (j) 240 hours

Figure B.16. (continued)

Figure B.17. Case17

(a) 20 hours   (b) 40 hours   (c) 60 hours   (d) 80 hours

(e) 100 hours   (f) 120 hours   (g) 165 hours   (h) 210 hours

Figure B.17. (continued)

(i) 255 hours

(j) 300 hours
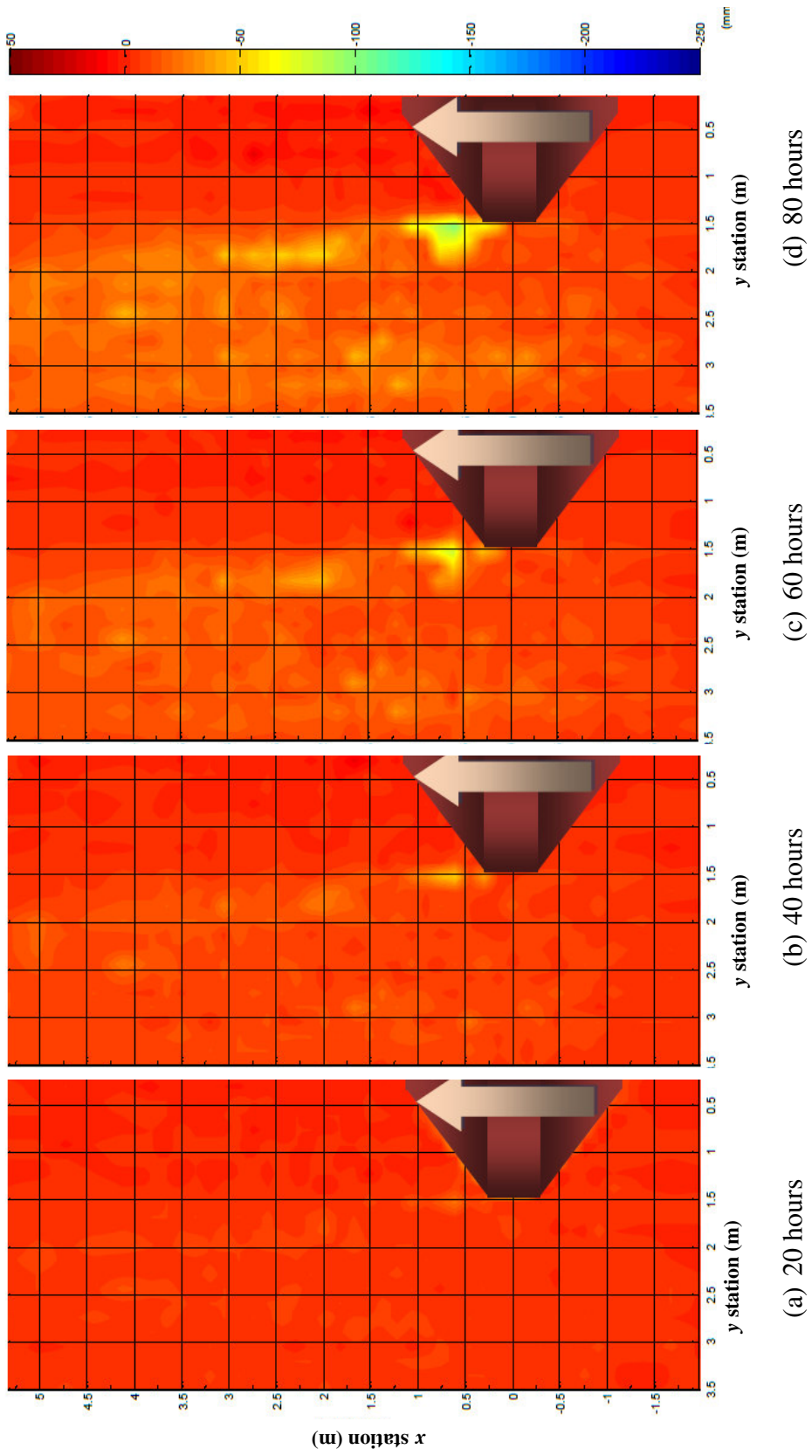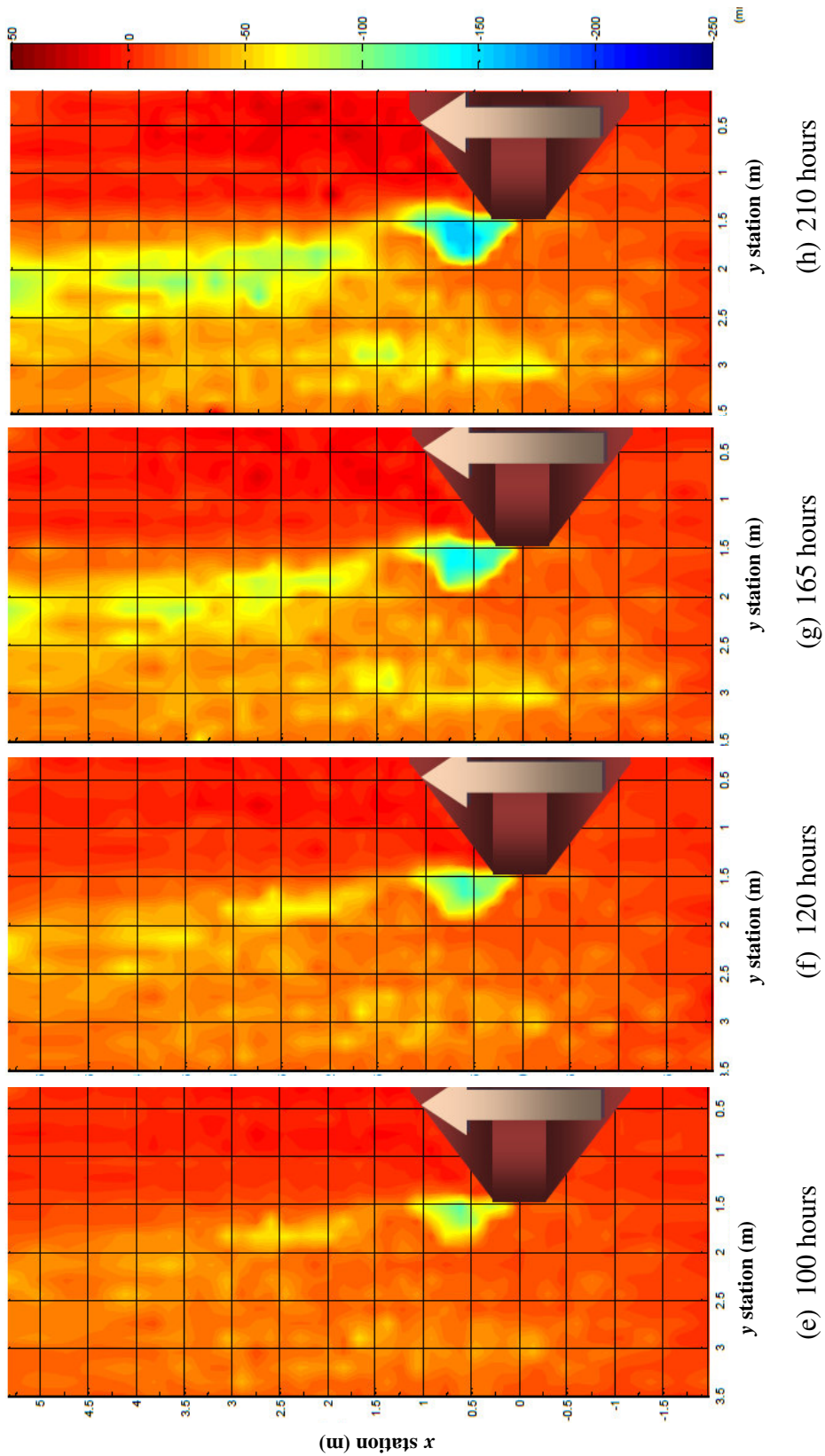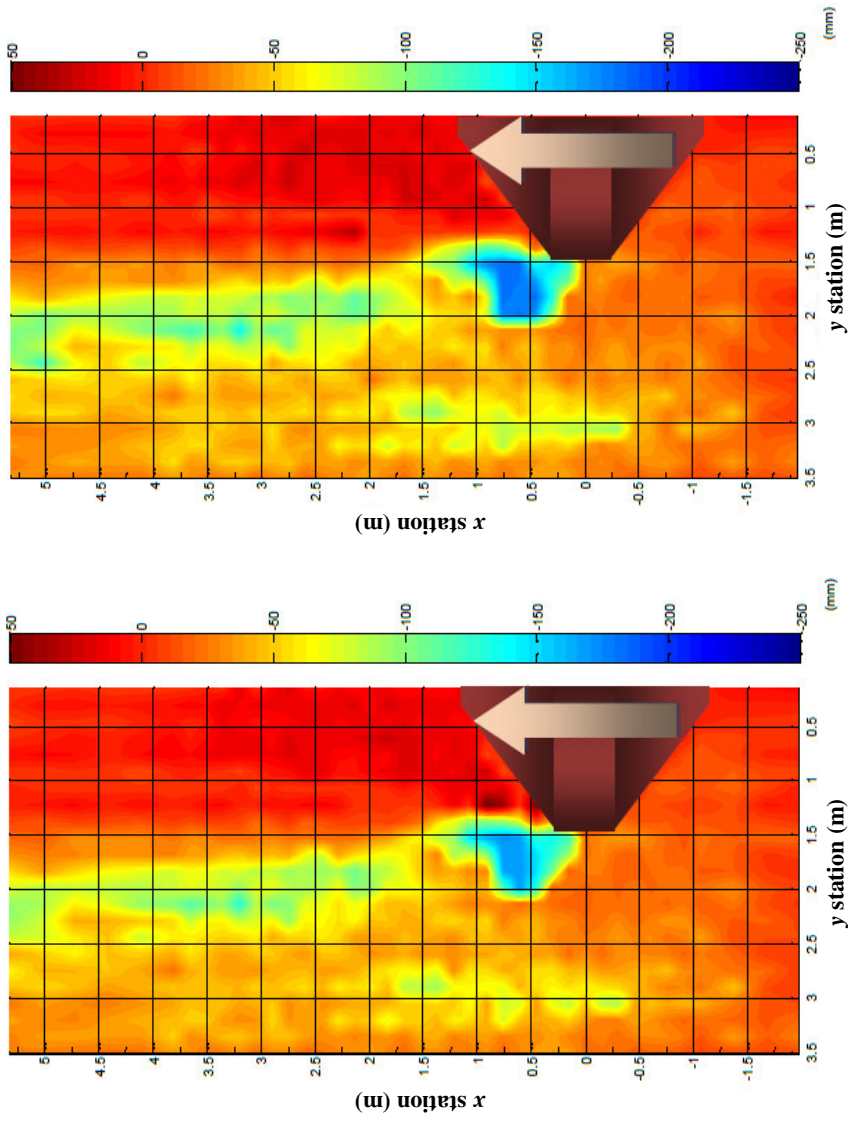
Figure B.17. (continued)

APPENDIX C

PHOTOGRAPHS FROM THE FLUME TESTS

Figure C.1. Flow pattern around abutment of case 1 (flow from right to left)
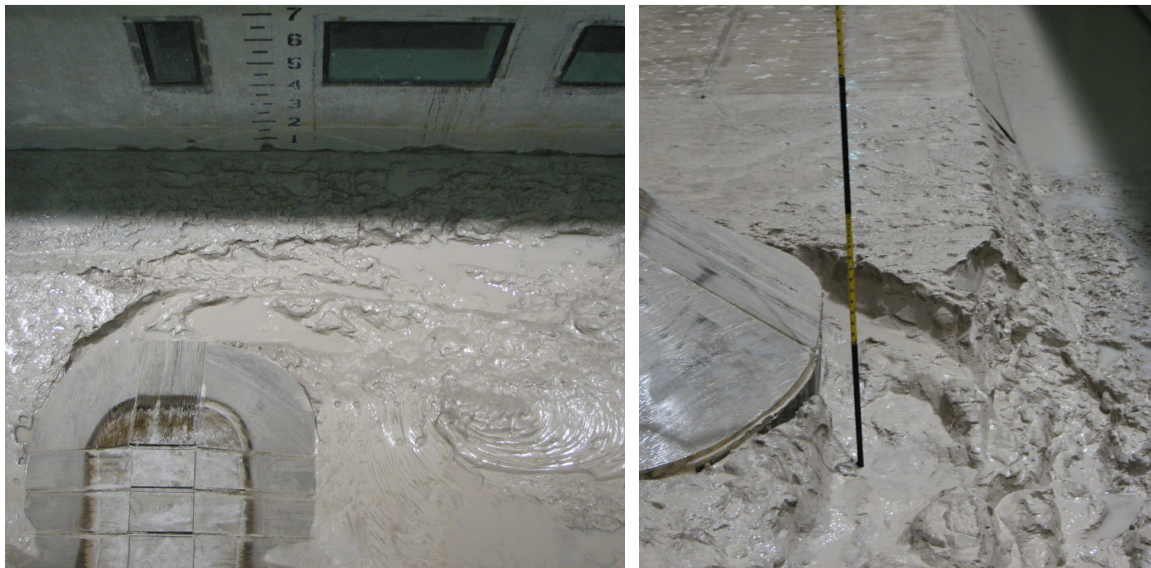
(a) Top view (flow from left to right)   (b) Maximum abutment scour

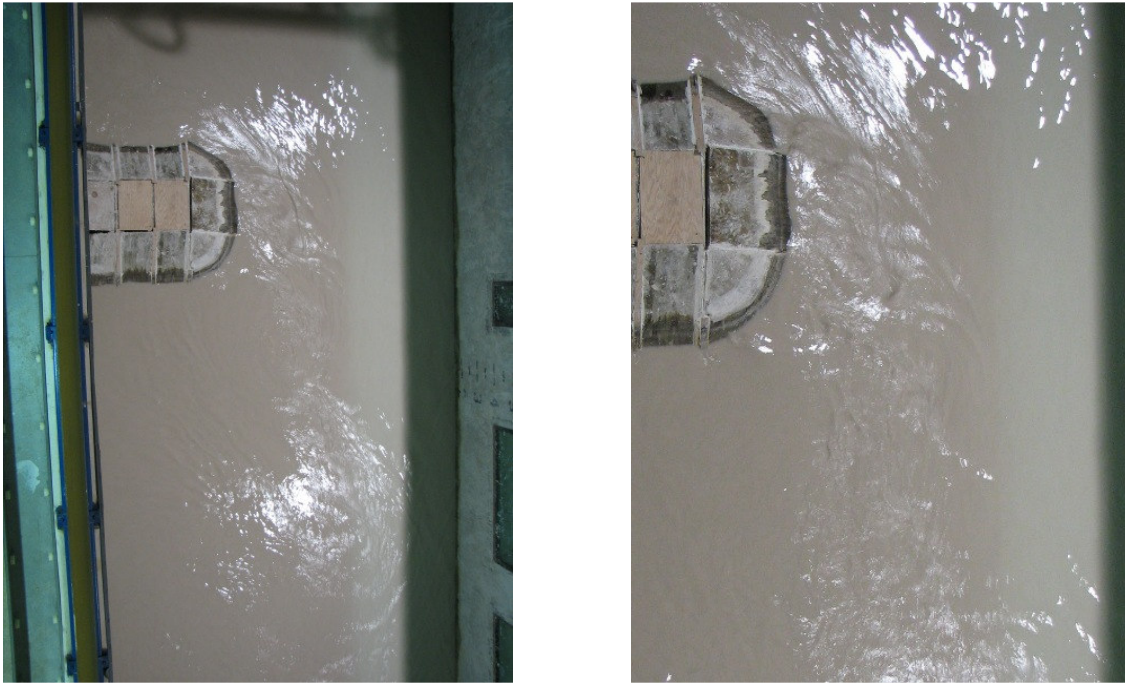Figure C.2. Scour pattern of case 1

Figure C.3. Flow pattern around abutment of case 1II (flow from top to bottom)

(a) Top view (flow from left to right)   (b) Maximum abutment scour
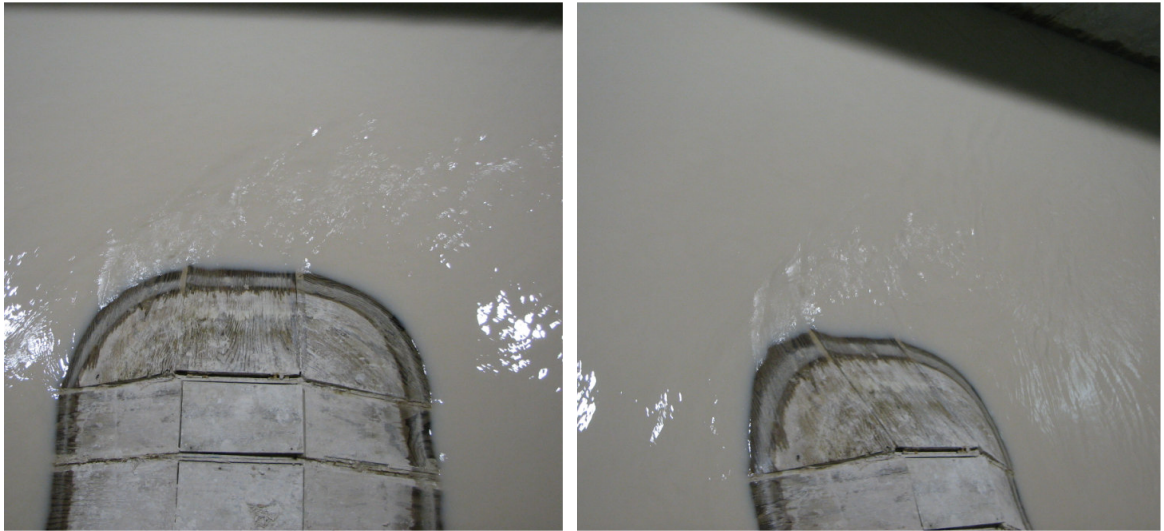
Figure C.4. Scour pattern of case 1II

Figure C.5. Flow pattern around abutment of case 2 (flow from left to right)

(a) Top view (flow from left to right)   (b) Maximum abutment scour
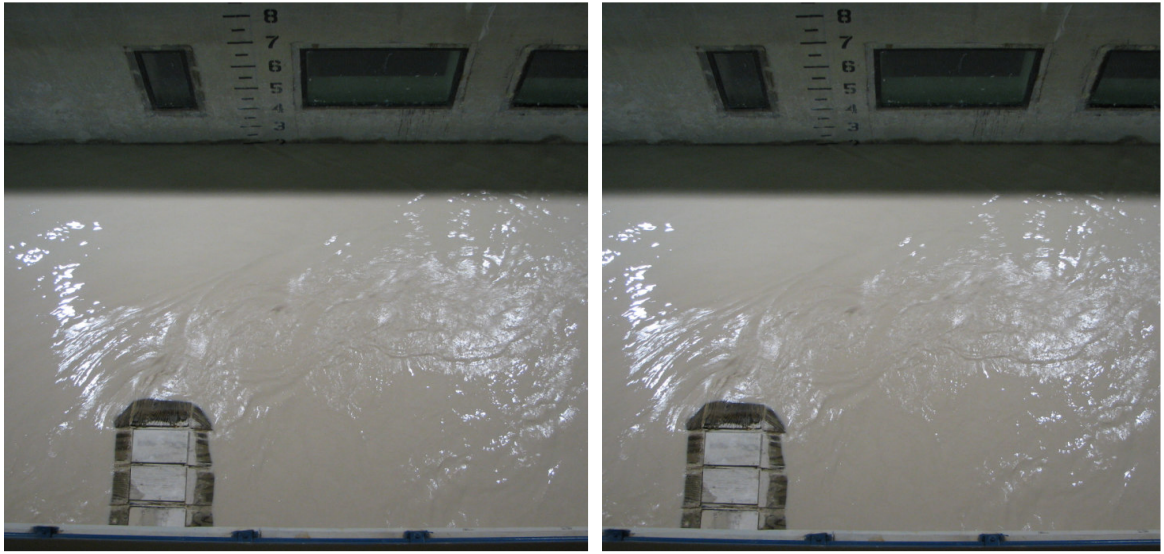
Figure C.6. Scour pattern of case 2

Figure C.7. Flow pattern around abutment of case 3 (flow from left to right)

(a) Top view (flow from left to right)   (b) Maximum abutment scour

Figure C.8. Scour pattern of case 3

Figure C.9. Flow pattern around abutment of case 4 (flow from top to bottom)

    (a) Top view (flow from top to bottom)   (b) Maximum abutment scour

Figure C.10. Scour pattern of case 4

Figure C.11. Flow pattern around abutment of case 5 (flow from top to bottom)

(a) Top view (flow from top to bottom)   (b) Maximum scour
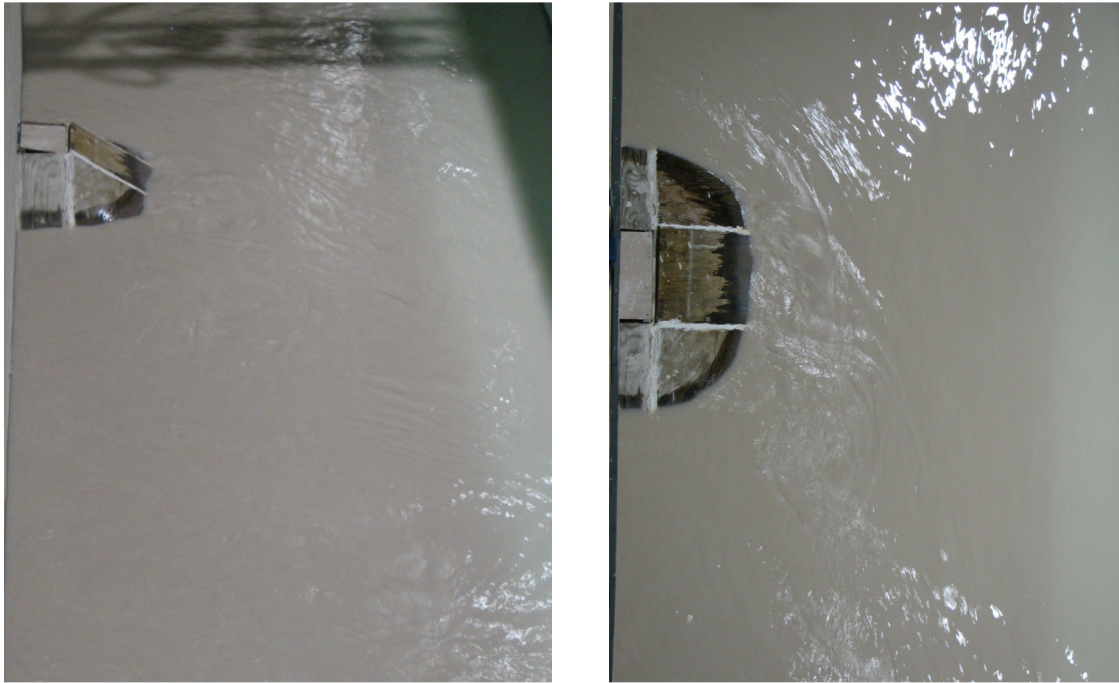
Figure C.12. Scour pattern of case 5

Figure C.13. Flow pattern around abutment of case 6 (flow from top to bottom)

(a) Top view (flow from top to bottom)   (b) Maximum abutment scour

Figure C.14. Scour pattern of case 6

Figure C.15. Flow pattern around abutment of case 7 (flow from top to bottom)

(a) Top view (flow from top to bottom)   (b) Maximum abutment scour

Figure C16. Scour pattern of case 7

Figure C.17. Flow pattern around abutment of case 8 (flow from top to bottom)

(a) Top view (flow from top to bottom) (b) Maximum abutment scour
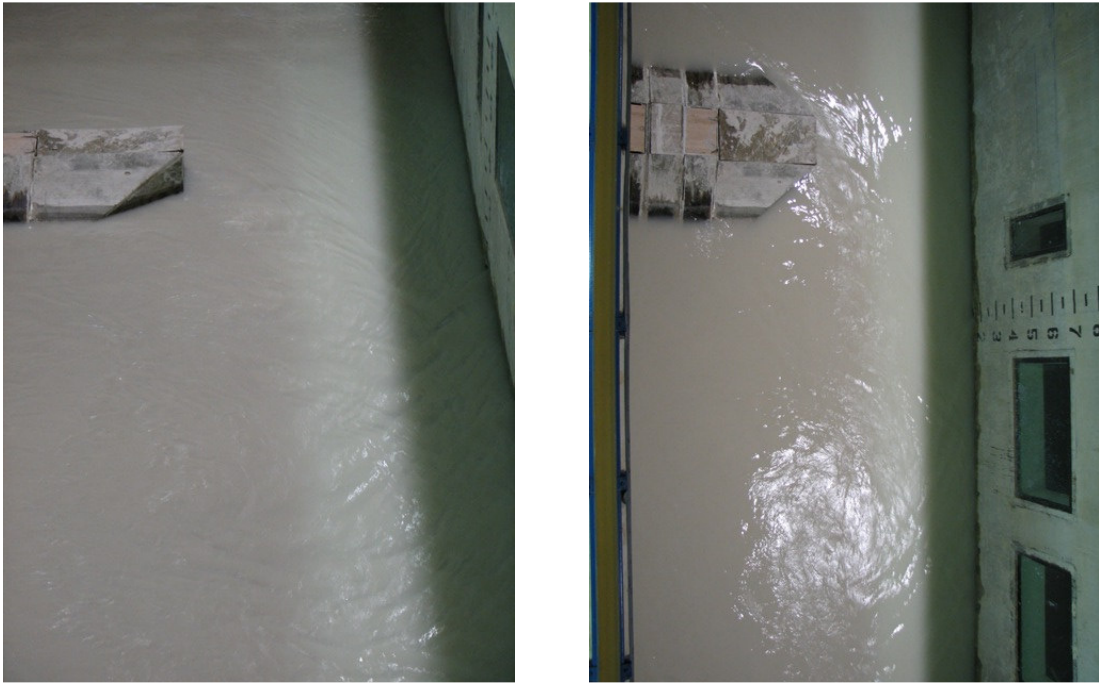
Figure C.18. Scour pattern of case 8

Figure C.19. Flow pattern around abutment of case 9 (flow from top to bottom)

(a) Top view (flow from top to bottom)   (b) Maximum abutment scour

Figure C.20. Scour pattern of case 9

Figure C.21. Flow pattern around abutment of case 10 (flow from top to bottom)

(a) Top view (flow from top to bottom)   (b) Maximum abutment scour

Figure C.22. Scour pattern of case 10

Figure C.23. Flow pattern around abutment of case 11 (flow from top to bottom)

(a) Top view (flow from top to bottom)   (b) Maximum abutment scour

Figure C.24. Scour pattern of case 11

Figure C.25. Flow pattern around abutment of case 12B (flow from top to bottom)

(a) Top view (flow from top to bottom)　　　　(b) Maximum abutment scour

Figure C.26. Scour pattern of case 12B

Figure C27. Flow pattern around abutment of case 13

(a) View from downstream

(b) Maximum scour

Figure C.28. Scour pattern of case 13

Figure C.29. Flow pattern around abutment of case 14

(a) View from upstream   (b) Maximum abutment scour

Figure C.30. Scour pattern of case 14

Figure C.31. Flow pattern around abutment of case 15 (flow from left to right)

(a) Top view (flow from top to bottom)

(b) Maximum abutment scour

Figure C.32. Scour pattern of case 15

Figure C.33. Flow pattern around abutment of case 16 (flow from top to bottom)

(a) Top view (flow from top to bottom)   (b) Maximum abutment scour

Figure C.34. Scour pattern of case 16

Figure C.35. Flow pattern around abutment of case 17 (flow from top to bottom)

(a) Top view (flow from top to bottom)   (b) Maximum abutment scour

Figure C.36. Scour pattern of case 17

VITA

Seung Jae Oh was born in Jinju, Gyeongnam, South Korea. He received his Bachelor of Engineering degree in Civil Engineering in January 1999 from Gyeongsang National University and the Master of Science in Civil Engineering in January 2002 from the Busan National University, South Korea. In August 2003, he went to Texas A&M University, where he served as a research assistant in the Texas Transportation Institute. His research was on bridge scour in cohesive soil. His research interests are soil erosion in cohesive soil and local bridge scours.

He may be reached at: Sueng Jae Oh

Zachry Department of Civil Engineering

Texas A&M University

College Station, Texas 77843-3136, USA

His email address is: seungjaeo@gmail.com.